Regulation of cellular metabolism and intercellular communication by sodium signalling

Alina Lavinia Capatina

PhD

University of York

Biology

September 2023

I. Abstract

The tumour ionic microenvironment is important for tumour cell growth and metastasis but its role on cancer cell/immune cell interactions is poorly explored. Competition for tryptophan (Trp) catabolism is a metabolic immune checkpoint centred around the activity of the enzyme indoleamine 2', 3' – dioxygenase 1 (IDO1). IDO1 works by converting extracellular Trp to the immunosuppressive metabolite kynurenine. This study hypothesises that Trp catabolism and kynurenine levels could be regulated by interfering with the tumour ionic microenvironment. The first part of this study explores the link between Na^+ dynamics, cardiac glycosides, and Trp metabolism, while the second part of the project explores a range of natural products to identify novel regulators of the kynurenine response.

This study identified two Na^+/ K^+ ATPase (NKA) inhibitors, ouabain and digoxin, which downregulated IDO1 activity and expression, also reducing the levels of its transcriptional regulator, phosphorylated signal transducer activator of transcription 1 (pSTAT1). In parallel, proportional elevations in intracellular Na^+ were observed. Similar results were generated also using the Na^+ ionophore monensin. These results show an inverse correlation between intracellular Na^+ levels and IDO1 function. Next, a 630-natural compound screen identified 24 potential IDO1 inhibitors, with the most interesting being artemether and Euphorbia factor L9 (EFL9). Both compounds decreased kynurenine levels independently of IDO1 expression, without affecting intracellular Na^+. Furthermore, EFL9 downregulated the same key Trp metabolites as ouabain and a clinically tested IDO1 inhibitor, Linrodostat, while artemether exhibited a different metabolic profile.

This study proposes a novel association between intracellular Na^+ /NKA integrity and immune checkpoint activity, as a potential mechanism regulating tumour immune evasion, as well as defining a series of chemically diverse compounds with IDO1 inhibitory activity and characterizing their impact on Trp metabolism.

II. Acknowledgements

I would like to thank my PhD supervisors, Dr William Brackenbury and Prof Dimitris Lagos, for all their help, support, and guidance during those 4 years. I would also like to thank Dr Mia Shandell for the guidance and teaching in my first year as a PhD student. Special thanks also go to all the Brackenbury and Lagos lab members, especially Dr Andrew James, Dr Theresa Leslie, Dr Dave Boucher, Dr Ioannis Kourtzelis, Dr Joshua Lee, Dr Katie West and Magnus Gwynne. Many thanks to our CNAP collaborators Dr Tomasz Czechowski, Dr Benjamin R. Lichman, Dr Thierry Tonon, and Prof Ian A. Graham who made possible the natural compound exploratory part of my thesis, as well as to the Metabolomics department at the University of York, and especially to Prof Tony Larson. Furthermore, I would like to thank the funding body and PhD organizers, BBSRC/ UKRI. Last, but not least, I would like to express my gratitude towards my family, my partner and my friends who supported me though this journey.

III. Declaration

I declare that this thesis is a presentation of original work and I am the sole author. This work has not previously been presented for a degree or other qualification at this University or elsewhere. Some of the data presented in Chapter 3 were generated in collaboration with Dr Mia Shandell and were published in *the Journal of Biological Chemistry* in 2022, publication which has been cited throughout this thesis. The data generated by Dr Shandell are indicated in the relevant figure legends. All sources are acknowledged as references.

IV. Table of Contents

V. Table of Figures

VI. Table of Tables

VII. Table of Appendix Figures

VIII. Table of Appendix Tables

1. Chapter 1: Introduction

1.1. Breast Cancer

1.1.1. Incidence and prevalence.

Breast cancer it is the most incident type of cancer and the second cause of cancer fatalities in females in the United States, accounting for 31 % of the newly diagnosed female malignancies in 2023 (Siegel et al., 2023). Worldwide, the number of patients diagnosed with breast cancer exceeds 2 million every year, accounting for about 11.7 % of all cancer diagnoses. Breast cancer is estimated as the 5th cause of global cancer fatalities and the leading cause of cancer death in females world-wide (Sung et al., 2021, Łukasiewicz et al., 2021). The age-adjusted breast cancer incidence, as well as the 5-year survival rate seem to be deeply correlated with the human development index (HDI). In this sense, countries with an elevated HDI seem to have an up to 22 fold increase in age-standardised breast cancer incidence, compared to countries with lower HDI (Sharma, 2021). However, developed countries seem to have better overall 5- year survival, ranging from over 80 % to about 60 % in developed and developing countries, respectively (Sankaranarayanan et al., 2010). This highlights the significant impact of technology, better care systems as well as access to novel therapies, on cancer progression, also revealing the great importance of continuous research in this field.

The majority of breast cancer diagnoses are associated with pre- and post-menopausal women, and about 70-80 % of the cases to date occur in patients over the age of 50 (Łukasiewicz et al., 2021). This is primarily due to the large hormonal changes occurring in women as they age, so that the risk of breast cancer incidence increases linearly with age, from approx. 1.5 % around the age of 40, up to 4 % for females over 70 (Benz, 2008). In males, breast cancer is less incident with approximately 1 % incidence, and it usually occurs

in the late 60s. Alongside age, family history, alcohol intake, smoking and obesity are also important risk factors for breast cancer, whilst pregnancy and physical activity seem to be reducing this risk (Łukasiewicz et al., 2021).

1.1.2. Classification based on pathology.

Breast cancer is a collection of diseases with multiple molecular and clinical features. To allow diagnosis, study and treatment of various breast tumours, a clear classification of the different cancer subtypes is required. Currently, there are three existing systems used for identifying different subtypes of this disease. The oldest and most widely known is the histological classification which divides breast tumours into *in situ* (local, which can be lobular or ductal) and invasive (with high metastatic potential such as infiltrating ductal – 70-80 % incidence, mucinous and lobular ductal carcinomas , as well as others) (Malhotra et al., 2010). Breast carcinoma is histologically classified into ductal/lobular carcinoma *in situ* (DCIS/LCIS) and invasive ductal/lobular carcinoma (IDC/ILC). DCIS is usually not lethal, and it is characterised by local ductal lesions within the breast lobules. It is usually a precursor of invasive carcinoma. LCIS is a multifocal localised carcinoma, which affects both breasts in 30 to 40 % of the cases. Unlike DCIS, LCIS has a more uniform, easy to recognise histological signature and is associated with high expression of E-cadherin, β-catenin, and keratin. LCIS presents a lower risk of development into invasive carcinoma compared to DCIS. IDC is an invasive and heterogeneous type of breast carcinoma, with 75 % of the cases not being histologically classifiable in any of the known subtypes. Some of the IDC histological subtypes include tubular, invasive cribriform, mucinous, medullary, invasive papillary, invasive micropapillary, apocrine, neuroendocrine, metaplastic, lipid-rich, secretory, oncolytic, adenoid cystic and acinic cell carcinoma. ILCs are less prevalent than IDCs, only affecting up to 15 % of the patients and are particularly frequent in post-menopausal women. The main

ILC subtypes include: classic, pleomorphic lobular, histiocytoid, signet ring and tubulolobular carcinoma (Makki, 2015).

The clinical progression of breast cancer is often monitored in order to select the best treatment options. To accurately assess disease progression a system of staging and grading is currently being used clinically. Staging assesses the size and degree of cancer spreading, while grading addresses the abnormal appearance of cancer cells (Koh and Kim, 2019, Taherian-Fard et al., 2015).

The TNM staging system is often used to monitor metastasis. In this system stage T means an isolated tumour, stage N means lymph node spreading and this can vary from N0 to N3, while stage M denominates metastasis (Koh and Kim, 2019, Amin et al., 2017). The stages of breast cancer can also be classified numerically into 5 stages (0 to 4). Stage 0 is usually localised carcinoma. Early breast cancer is classified as stages 1 and 2. Stage 1 can be subdivided into stage 1A, which refers to a tumour that is smaller than 2 cm and is restricted to the breast, and stage 1B, which refers a tumour that is not found in the breast but has formed a small number of micro metastases to axillary lymph nodes. Stage 2 can also be classified as stage 2A and 2B. Stage 2A refers either to a breast localised tumour of 2 – 5 cm, or a tumour that cannot be found in the breast or is smaller than 2 cm but has spread to 1 or 3 axillary lymph nodes or to the bone. Stage 2B refers either to a localised tumour that is larger than 5 cm, or to a tumour that is between 2 and 5 cm long and has spread to 1 or 3 lymph nodes from the axillar region. Stage 3 is classified into 3A, 3B and 3C. Stage 3A refers to a cancer that is either localised to the breast and exceeds 5 cm in length while spreading to up to 3 lymph nodes or near the bone, or to a cancer that is smaller than 5 cm or cannot be detected in the breast but has spread to 4-9 axillary lymph nodes. Stage 3B refers to a cancer that has spread to surrounding tissues, such as skin and muscle, as well as spreading to 1-9 axillary lymph nodes. Stage 3C can refer either to a cancer that has spread to lymph

nodes below the breastbone, or below and above the collar bone and to minimum 4 axillary lymph nodes. Finally, stage 4 is called metastatic breast cancer and refers to a cancer that has spread to other organs such as bone, liver, and lung (Koh and Kim, 2019, Taherian-Fard et al., 2015).

The grading system is based on microscopical examination and comparison of cancer cells with normal cells, and it is used to predict the growth rate of the cancer. Grade 1 (low grade) refers to a cancer where the cells look similar to the normal cells, growth rate is low, and the likelihood of spreading is minimal. Grade 2 is also called moderate or intermediate-grade cancer, and the growth rate is higher than in the case of Grade 1 cancers. Finally, High grade cancer, or Grade 3 and 4, is characterised by highly abnormal cells, when compared to healthy tissue, that might divide faster than Grade 1 and 2 cancers (Taherian-Fard et al., 2015).

1.1.3. Classification based on genetics.

A second and more elaborate system, developed as a necessity to understand the molecular signature of tumours and to predict responsiveness to different therapeutic approaches and recurrence risk, is the molecular classification based on gene profiling. This method was used to identify 6 types of breast cancer: luminal A and B – characterised by their common expression of keratins 8/18, basal like – enriched in keratins 5/6 and 17, normal breast like, human epidermal growth factor receptor 2 (HER2) enriched and claudin low carcinomas (Perou et al., 2000). The profile of each subtype was established by assessing the expression of 4 key markers: the oestrogen receptor (ER), the progesterone receptor (PR), the HER2 receptor, as well as the oncogene p53. As such luminal A and B cancers are both $HER2^{low}$ with A (ER^{high}, $Ki67^{low}$) showing better prognosis than B (ER^{low}, $Ki67^{high}$) (Feeley et al., 2014). Basal and HER2 enriched carcinomas are both ER^{-} and $Ki67^{high}$ and their prognosis is very poor (Cheang et al., 2009, Soliman and Yussif, 2016, Nishimura et al., 2010). Overall, luminal types

of cancer are most incident, occurring in 70 to 80 % of the patients; however, younger patients tend to experience more invasive, therapy-resistant subtypes, like triple negative breast cancer (TNBC), while older females usually develop less aggressive subtypes, such as luminal A (McGuire et al., 2015). TNBC cancers, such as basal-like breast carcinoma, are the most aggressive tumours and they are characterised by high proliferation rates, as supported by elevated expression of the Ki67 marker; in TNBC, Ki67 expression was shown to predict disease severity (Badowska-Kozakiewicz and Budzik, 2016, Keam et al., 2011).

This classification allowed the development of specific therapies, targeted at each specific subtype. The currently in-use therapies for luminal A and B cancers are mostly hormone therapies. Luminal cancers are ER^+, meaning that they grow in response to oestrogen production. Therefore, agents that block the effect of oestrogen, such as tamoxifen, which competes with oestrogen for ER binding, have been developed. In time, non-steroidal aromatase inhibitors, such as Letrozole, which prevent oestrogen synthesis, were developed and shown to be more effective, with less intense side effects. At the moment long-term hormone therapy is usually prescribed for luminal cancers, especially given their lack of responsiveness to chemotherapy (McGuire et al., 2015). $HER2^+$ tumours are usually less responsive to traditional treatments such as chemotherapy, and their prognosis has been massively improved by the development of targeted therapies, such as trastuzumab (monoclonal anti-HER2 antibody) (Slamon et al., 2001). TNBCs are, however, the most aggressive and are best treated by bilateral prophylactic mastectomy. They are often associated with mutations in the BReast CAncer genes 1 and 2 (BRCA 1 and 2) (Greenup et al., 2013). Mutations in BRCA1 and 2 are associated with 40-90% and 50-90% risk of breast cancer development, respectively (Thompson et al., 2002, Hoskins et al., 2008). A series of other mutations have also been associated with severely increased risk of cancer development, such as mutations in the TP53 gene, which is the precursor for the oncogene p53, mutations in the catherin-1 (CDH1) and Phosphatase and Tensin Homolog (PTEN) genes

are also associated with approx. 60-80 and 50-90 % risk of breast cancer development (Børresen-Dale, 2003, Heitzer et al., 2013, Fusco et al., 2020) .

1.1.4. Classification based on cellular origin.

Finally, the third profiling system is based on the origin of the cancer, and it is considered a functional classification. There are 2 existing hypotheses: the first one discusses the idea of breast cancer developing from various mammary stem cell progenitors at various stages in their differentiation process, while the second hypothesis claims that there is only a limited pool of stem cells from which the tumour arises and the surrounding cells have little malignant capacity (Visvader, 2009, Stingl and Caldas, 2007, Al-Hajj et al., 2003). It is thus apparent that the origin, molecular signature, and behaviour of mammary tumours are quite diverse, thus augmenting the need for a better understanding of the underlying processes that lead to these malignancies.

1.1.5. Treatment - targeted therapies.

Currently available treatments for breast cancer range from traditional chemotherapy and hormone therapy treatments to targeted therapies and surgery. Targeted therapies are probably the most diverse collection of treatments, and they are specifically designed to account for the limitations of other approaches, such as hormone therapies. Within the targeted therapies umbrella term, autophagy promoters & proliferation inhibitors, such as inhibitors of mechanistic target of rapamycin (mTOR) and of phosphatidylinositol-3 kinase (PI3K) could be included. Alpelisib was the first PI3K inhibitor FDA approved in 2019 for Hormone receptor $(HR)^{+}HER2^{-}$ breast cancers carrying the *PI3KCA* mutation (Wilhoit et al., 2020). Several clinical trials looked at the efficiency of mTOR inhibitors in treating breast cancer patients. BOLERO-2 is one of the successful clinical trials for mTOR inhibition. It is a phase III clinical trial that led to the FDA approval of Everolimus (mTOR inhibitor) in combination with Exemestane (aromatase inhibitor) for the treatment of post-menopausal

women with HR^+HER^- advanced breast tumours that did not respond to other treatments (Piccart et al., 2014). BOLEO-3 looked at the ability of Everolimus to overcome Trastuzumab resistance in $HER2^+$ cancers and showed a significant improvement on progression-free survival in patients with HR^- tumours (André et al., 2014). BOLERO-1 was a phase III clinical trial that looked at the impact of Everolimus in combination with Trastuzumab and Paclitaxel in HR^-HER2^+ breast cancers. Although BOLERO-1 did not show a significant benefit of mTOR inhibition, it reported a promising effect on progression free survival, with Everolimus prolonging this by 7.2 months (Hurvitz et al., 2015). A less successful trial was the phase III HORIOZN trial, which tested the effect of Temsirolimus (mTOR inhibitor) and Letrozole (aromatase inhibitor, (Bhatnagar, 2007)) on HR^+HER2^- breast cancer, which was stopped due to lack of improvement of progression free survival upon treatment (Wolff et al., 2013).

Tyrosine kinase inhibitors and anti-HER2 monoclonal antibodies are often used for the treatment of $HER2^+$ breast cancer patients. Afatinib, an EGFR tyrosine kinase inhibitor, received global approval for $HER2^+$ positive cancer treatment in 2013 (Dungo and Keating, 2013), other inhibitors such as Lapatinib, Pyrotinib, Tucatinib and Neratinib were also developed, and studies showed that they benefit $HER2^+$ cancer as monotherapies, as well as in combination with other treatments (Ma et al., 2019, Moulder et al., 2017, Kaufman et al., 2009). Trastuzumab is an anti-HER2 monoclonal antibody, FDA-approved as the first targeted therapy for $HER2^+$ breast cancers in 1998 and further developed into antibody-drug conjugates: Ado-Trastuzumab Emtansine and Fam-Trastuzumab Deruxtecan (Jeyakumar and Younis, 2012, Schlam and Swain, 2021). Pertuzumab, another monoclonal antibody targeting HER2, was approved in combination with trastuzumab and docetaxel for $HER2^+$ tumours in 2012 (Blumenthal et al., 2013). Finally, Margetuximab is another recently FDA approved (2020) monoclonal antibody to be used as a combinatorial treatment for metastatic $HER2^+$ tumours (Royce et al., 2022))

For $HER2^-$ and BRCA1/2 mutation carrying tumours Poly (Adenosine Diphosphate (ADP)-Ribose) Polymerase 2 (PARP2) inhibitors, such as Olaparib, are often used. In addition, cyclin-dependent kinase (CDK) 4/6 inhibitors and antibody-drug conjugates are another alternative in $HER2^-$ cancers, with potentially better outcome in patients that do not carry the BRCA1/2 mutation (Schwartzberg and Kiedrowski, 2021, Collins et al., 2021).

For the TNBC subtype cancer vaccines have been developed and tested up to the clinical trials stage, however, none has been approved for TNBC treatment, despite their good safety profiles, because of lack of clinical benefits (Hosseini et al., 2023). Liver kinase B1 (LBK1)/Adenosine Monophosphate (AMP)-activated protein kinase (AMPK) activators have also been used in the treatment of hormone-resistant carcinomas (Lau et al., 2022).

Probably the most popular and extensively explored type of therapy is immunotherapy, in particular the use of immune checkpoint inhibitors, such as anti-Programmed Death 1 (PD-1)/Programmed Death Ligand 1 (PD-L1) therapies (e.g., Pembrolizumab, Nivolumab), used either on their own or in combinations with other drugs. The efficacy of the anti-PD-1/PD-L1 inhibitors in TBNCs varies, with different impact on overall survival, progression free survival and pathological complete response. Atezolizumab (anti-PD-L1) was FDA approved following the IMpassion130 trial (Schmid et al., 2018), due to increased progression free survival, however, the results failed to be validated in a subsequent trial, IMpassion131 (Miles et al., 2021), leading to the withdrawal of Atezolizumab approval for TNBC. Another trial, KEYNOTE-355, showed that Pembrolizumab has superior effects to Nivolumab in terms of progression-free survival (Cortes et al., 2020), while the GeparNuevo trial identified Durvalumab as a neoadjuvant therapy effective at increasing overall survival (Loibl et al., 2022). In fact, Durvalumab is potentially the optimal anti-PD-L1 therapy to be used as a maintenance therapy, according to the SAFIR02-BREAST trial (Bachelot et al., 2021, Elmakaty et al., 2023). However, immune checkpoint therapies are not limited to PD-1/PD-L1 targeted therapies, a

range of other immune checkpoint targets have been investigated over the years, including cytotoxic T-lymphocyte associated protein 4 (CTLA-4), indoleamine 2, 3-dioxygenase 1 (IDO1), lymphocyte activation gene 3 (LAG3), T cell immunoglobulin and mucin domain-containing protein 3 (TIM3) and others, which will be discussed in more detail in section 1.3 (Wang et al., 2022d).

In the UK, immune-checkpoint therapies are clinically used in TNBC patients. Pembrolizumab is the only approved therapy, and it is recommended for stage 2 and 3 breast cancer patients, as well as early-stage TNBC patients. It is administered intravenously as a neoadjuvant therapy pre-surgery, then it is maintained as an adjuvant treatment post-surgery. It can also be used to treat locally recurrent and non-surgery removable breast cancer in combination with paclitaxel or paclitaxel derivatives (Korde et al., 2022). On its own, however, Pembrolizumab did not improve optimal survival compared to chemotherapy in metastatic TNBC patients (Winer et al., 2021); furthermore, in other breast cancer subtypes Pembrolizumab showed best results when combined with paclitaxel and doxorubicin-cyclophosphamide, especially in $HER2^-$ breast cancer. When administered in combination with chemotherapy, in Grade 3 luminal subtypes, Pembrolizumab decreased the pCR, that is the non-invasive residual tumour following neoadjuvant treatment, highlighting a potential benefit for luminal cancers (Cardoso et al., 2019). In metastatic $HER2^+$ breast cancer, Pembrolizumab in combination with trastuzumab also showed promising results with a response rate of 15 % in patients with Trastuzumab-resistant PD-L1-positive tumours (Loi et al., 2019, Debien et al., 2023).

Despite marginally positive responses in other breast cancer subtypes, the TNBC subtype remains the most responsive to immune checkpoint therapies. The main reasons why immune checkpoint therapies work best in TNBC is primarily due to higher tumour immune

infiltration, increased PD-L1 expression, and increased mutation burden given by the high genetic instability occurring in rapidly dividing cells (Abdou et al., 2022).

However, despite the considerable progress that targeted, and immunotherapies have achieved over the years in the treatment of breast cancer, the elevated incidence and complexity of breast cancer subtypes, as well as the constantly changing tumour microenvironment, call for a better understanding of breast tumour biology. Thus, the success and limitations of targeted treatment approaches only highlight the value of and growing necessity for extensive research in cancer biology.

1.2. The tumour microenvironment

The tumour microenvironment is dynamic and complex, rapidly dividing cells require increased vascularization for nutrient and oxygen supply. This high division rate leads to rapid oxygen consumption, thus rendering the tissue hypoxic (Vaupel et al., 2002). The lack of oxygen then triggers a range of metabolic adaptations (discussed in section 1.4). Increased vascularization also leads to increased colloidal pressure in the tumour, causing ionic imbalances, such as a slightly depolarized membrane potential, often associated with cancer cells (discussed in section 1.5). Furthermore, the increased vascularization allows immune infiltration; immune cells in turn attack the tumour exposing intracellular mediators to the extracellular environment, which further triggers activation of more immune cells, thus maintains a pro-inflammatory state in the tumour microenvironment. This pro-inflammatory state can lead to upregulation of immune checkpoint proteins that the tumour then uses to neutralize the immune response. This causes a shift in the type of infiltrating immune cells towards a regulatory phenotype, thus protecting the tumour (Li et al., 2021b, Leslie et al., 2019).

In breast cancer specifically, each subtype has its own unique signature microenvironment. Literature has shown that the luminal B subtype (ER^{low}) is rich in $CD8^+$ T cells, with high tumour cell expression of PD-L1. The $HER2^+$ subtype was also shown to have high PD-L1 expression, as well as elevated levels of the Ki-67 proliferation marker. $HER2^+$ cancers are also associated with infiltration of tumour-protective macrophages. *BRCA1* mutated TBNCs have also been shown to have elevated PD-1/PD-L1 expression, which is correlated with survival outcome (Nolan et al., 2017). Alongside expression of specific biomarkers like PD-1/PD-L1, TNBC tumours exhibit elevations in matrix remodelling, invasion and pro-angiogenetic markers (Kashyap et al., 2023). Studies have shown that, in TNBC, tumour infiltrating lymphocyte numbers directly correlate with tumour immunogenicity, and are in fact anti-correlated with the Ki-67 proliferation marker. Thus, tumour infiltrating lymphocytes are strongly indicative of survival probability for the TNBC subtype (Mao et al., 2016, Adams et al., 2014).

Tumour infiltrating lymphocytes include mostly T and B cells ($CD20^+$ effector B cells and plasma cells, responsible for producing large amounts of antibodies). The T cells can be further classified into effector T cells and $CD4^+$ regulatory T cells (Tregs). Effector T cells can be $CD4^+$ Th cells (responsible for cytokine mediated immune attack) and $CD8^+$ (which target intracellular antigens/oncogenic neoantigens via secretion of granzyme and perforins). Tregs function by producing immunosuppressive signals that protect the tumour (Fan and He, 2022). In TNBC, an elevation in the $CD8^+$ and Treg pools of tumour infiltrating lymphocytes has been reported as a key outcome prediction marker (Liu et al., 2011, Liu et al., 2012b, Zahran et al., 2021, Oshi et al., 2020). Additionally, $CD8^+$ T cells seem to be more active in the TNBC subtype and their high level of PD-1 expression has been correlated with poor outcome (Song et al., 2017a, Sun et al., 2014).

Alongside, lymphocyte infiltration, the immunogenicity of breast tumours is also regulated by tumour associated macrophages. These can be M1 macrophages that enhance the immune attack against the tumour, or M2 tumour protective macrophages. In TNBC, the tumour stimulates differentiation of M2 macrophages, which have been shown to enhance expression of the PD-1 marker on infiltrating lymphocytes (Pu and Ji, 2022, Hao et al., 2023). Other immune cells, as well as cancer associated fibroblasts also contribute to the general immunosuppressive environment in malignant tissue, preventing tumour clearance, remodelling the extracellular matrix and enhancing metastatic behaviour (Li et al., 2021b).

Thus, tumour microenvironment plays a crucial role in dictating the survival outcome. The next three sections will focus on three major aspects of the tumour microenvironment: immunology and immune checkpoints (section 1.3), metabolism (section 1.4) and ionic dynamics (section 1.5).

1.3. Immune checkpoint proteins

1.3.1. Background

Immune checkpoint proteins are molecules that regulate the activity of the immune system, preventing it from being over-active. Immune checkpoints have co-evolved with immune co-stimulatory molecules and share some structural patterns, such as tyrosine-based signalling motifs, which in co-stimulatory proteins play activator function (ITAMs), and in immune checkpoints these are inhibitory (ITIMs); these can also be immunoreceptor tyrosine-based switch motifs (ITSM) (Qi et al., 2020, Xu et al., 2018b). Immune checkpoints can be either membrane expressed or present in the cytoplasm, and some can also be secreted into the extracellular environment.

1.3.2. PD-1/PD-L1

One of the most well-known immune checkpoint pairs is the PD-1/PD-L1/2 set of membrane proteins, which are expressed on effector $CD8^+$ T and tumour cells, respectively. PD-L1 can also be expressed on a variety of non-malignant cells, including antigen presenting cells, and its main function is to interact with the PD-1 molecule on T cells, triggering immunosuppressive signalling events. As both PD-1 and PD-L1 are surface expressed molecules, they are assembled within the endoplasmic reticulum (ER). Both receptors are heavily N-glycosylated, as a means of increasing protein stability, as well as enhancing their immunosuppressive activity. The interaction between PD-1 and PD-L1 leads to phosphorylation of ITIM and TISM on the PD-1 cytoplasmic domain inducing activation of the Src Homology region 2 (SH2)-containing protein tyrosine Phosphatase 2 (SHP2), which is partially responsible for the inhibition of the T cell receptor (TCR)-induced $CD8^+$ T cell activation, through inhibition of the Lymphocyte-specific protein tyrosine Kinase (LCK) and Zeta-chain-Associated Protein kinase 70 (ZAP70) (Bardhan et al., 2016, Simon and Labarriere, 2017). This process ultimately leads to downregulation of key transcription factors such as Nuclear Factor kB (NF-kB), Nuclear Factor of Activated T cells (NFAT) and activating protein 1 (AP-1), preventing expression of genes involved in immune activation (Figure 1.1A) (Wu et al., 2019). PD-1/PD-L1 blockade with monoclonal antibodies has been widely explored in the context of cancer, with several therapies also being used on their own or in combination with other drugs or chemotherapy in patients.

1.3.3. Anti-PD-1/PD-L1 therapies

The most widely known monoclonal antibodies targeting this immune checkpoint include the anti-PD-1 Nivolumab (Opdivo, Bristol-Myers Squibb) and Pembrolizumab (Keytruda, Merck & Co/MSD), as well as the anti-soluble PD-L1 Atezolizumab (Genentech/Rothe), Durvalumab (AstraZeneca) and Avelumab (EMD Serono/Merck&Pfizer) (Wu et al., 2019).

Both Nivolumab and Pembrolizumab are humanized IgG4 monoclonal antibodies, and work by directly interacting with the PD-1 receptor, thus preventing its binding to PD-L1. Nivolumab has received approval from the FDA for the treatment of eight types of cancer, including metastatic melanoma, lung, renal and colorectal cancer (Weber et al., 2015, Brahmer et al., 2015, Motzer et al., 2015, Overman et al., 2017). Pembrolizumab has also been approved for a variety of cancer types, including skin, blood, and lung cancer (Robert et al., 2014, Hui et al., 2016, Reck et al., 2016, Chen et al., 2017a). Atezolizumab, Durvalumab and Avelumab are all IgG1 monoclonal antibodies that bind to the tumour-expressed or tumour-secreted PD-L1 molecule, preventing its interaction with the T cell-expressed PD-1 and thus avoiding T cells exhaustion (Wu et al., 2019). Interestingly, de-glycosylation of PD-L1 was shown to improve the efficacy of monoclonal antibody PD-L1 targeted therapies (Lee et al., 2019). The most common adverse effects of PD-1/PD-L1 inhibitors relate to their pro-inflammatory activity. Such immune-associated adverse effects associated with this type of therapies include type 1 diabetes, renal and cardiac dysfunctions, skin inflammation, as well as damage at the gastrointestinal level (Iwai et al., 2017). However, these are classified as moderate and acceptable, especially when compared with other more severe checkpoint therapies (Constantinidou et al., 2019, Zappasodi et al., 2018, Wu et al., 2019).

Most literature around anti-PD-1/PD-L1 therapies in breast cancer is focused on the TNBC subtype, as this has been reported as the most responsive to immunotherapy (Kwa and Adams, 2018). Literature has reported that anti-PD-1/PD-L1 mono- and combinatorial therapies have a 22 % response rate in metastatic TNBCs, with better results than chemotherapy in terms of progression free survival and objective response rate (Khan et al., 2023). However, while some inhibitors have a consistently good response rate against TNBC (Pembrolizumab), contradictory results across studies for other PD-L1 inhibitors (Atezolizumab) show the limitations of such targeted therapies, which have a much more reduced pool of responsive patients than less targeted approaches such as chemotherapy

(Adams et al., 2019b, Adams et al., 2019a, Schmid et al., 2020, Emens et al., 2019, Miles et al., 2021).

1.3.4. CTLA-4

Another well studied immune check point is the CTLA-4 molecule. CTLA-4 is expressed by effector $CD8^+$ T cells and usually resides in the cytosol. The activated effector T cells start expressing membrane and secreting soluble CTLA-4. Translocation from the cytosol to the membrane is mediated by the T cell receptor interacting molecule (TRIM) (Valk et al., 2006). Additionally, in Tregs, GTPase ADP ribosylation factor-1 and Phospholipase D are required for CTLA-4 secretion (Mead et al., 2005). Once on the surface, CTLA-4 exerts its inhibitory function by interacting with CD80/86 on antigen presenting cells, and thus preventing the costimulatory interaction between CD80/86 and with CD28 (expressed on T cells) (van der Merwe et al., 1997, Qureshi et al., 2011). Interestingly, in a subtype of mouse dendritic cells (DCs), CTLA-4 promotes expression of another immune checkpoint protein, indoleamine 2, 3-dioxygenase, further suppressing the activity of effector T cells through tryptophan depletion (Mellor et al., 2004). While the PD-1/PD-L1 interaction is important for the tumour-immune interaction, CTLA-4 is more important in the initial immune priming step, that occurs between DCs and naive T cells in lymphoid organs (Buchbinder and Desai, 2016). CTLA-4 expression on $CD8^+$ T cells during this type of interaction impairs T cells activation, either by preventing the CD28-CD80/86 interaction, or by inhibiting the CD28/TCR-induced ZAP70 and PI3K signalling, and thus impairing its ability to recognizing and kill the tumour cells (Figure 1.1B) (Rudd et al., 2009).

1.3.5. Anti-CTLA-4 therapies

Ipilimumab is a human IgG1 monoclonal antibody that targets the CTLA-4 molecule and was the first immune checkpoint-targeted therapy to be approved for the treatment of cancer (Hodi et al., 2003). Initially approved for the treatment of melanoma, Ipilimumab has been

used for a range of other cancers since then, including in combination with nivolumab (e.g., renal-cell carcinoma, metastatic non-small lung cancer) (Vellanki et al., 2021, Motzer et al., 2018, Fellner, 2012, Jain and Clark, 2015, Lipson and Drake, 2011).

In breast cancer anti-CTLA4 therapies have also been explored. Pre-clinical mouse studies also highlight the potential of anti-CTLA-4 therapies against breast cancer, showing that combinatorial treatment of HER2/New antibody with Triciribine (Akt inhibitor) and CTLA-4 blockade, synergistically inhibited progression of Trastuzumab resistant $HER2^+$ breast tumours (Wang et al., 2012a). An ongoing clinical trial for breast cancer brain metastasis highlighted the value of using Tremelimumab (anti-CTLA-4 therapy) in combination with Tarstuzumab and radio therapy for $HER2^+$ cancers (Page et al., 2022). Other ongoing clinical trials investigating CTLA-4 blockade in breast cancer include, the NIMBUS trial looking at a combination of Nivolumab and Ipilimumab in hyper mutated $HER2^-$ breast cancer, or the NCT03546686 trial studying Nivolumab and Ipilimumab in combination with cryoablation in HR^-HER2^- breast cancer patients. A third clinical trial, NCT03409198, currently in phase IIb is looking at the combined effect of chemotherapeutic agents such as Doxorubicin and Cyclophosphamide with the Ipilimumab/Nivolumab combination in breast cancer (Kooshkaki et al., 2020). Thus, this ongoing research highlights the strong therapeutic potential of CTLA-4 blockade in breast cancer, especially in combination with PD-L1 blockade, however, the lack of FDA approval for any CTLA-4-targeted therapies in breast cancer also shows that there is still need for further optimization and understanding of how to target this immune checkpoint in breast cancer patients.

1.3.6. IDO1

Indoleamine 2,3-dioxygenase 1, or IDO1, is an immune checkpoint protein highly expressed in breast cancer cells and other solid tumours in response to pro-inflammatory stimulation (e.g., IFNγ and Tumour Necrosis Factor (TNF)). IDO1 inhibits T cell-mediated tumour killing

by metabolizing the tryptophan within the tumour microenvironment and thus inducing T cell starvation, as well as by producing an immunosuppressive metabolite, called kynurenine, which triggers differentiation of tumour-protective Tregs (Figure 1.1C) (Feng et al., 2020, Takikawa et al., 1988, Robinson et al., 2005). This immune checkpoint will be discussed in more detail in section 1.4.3.

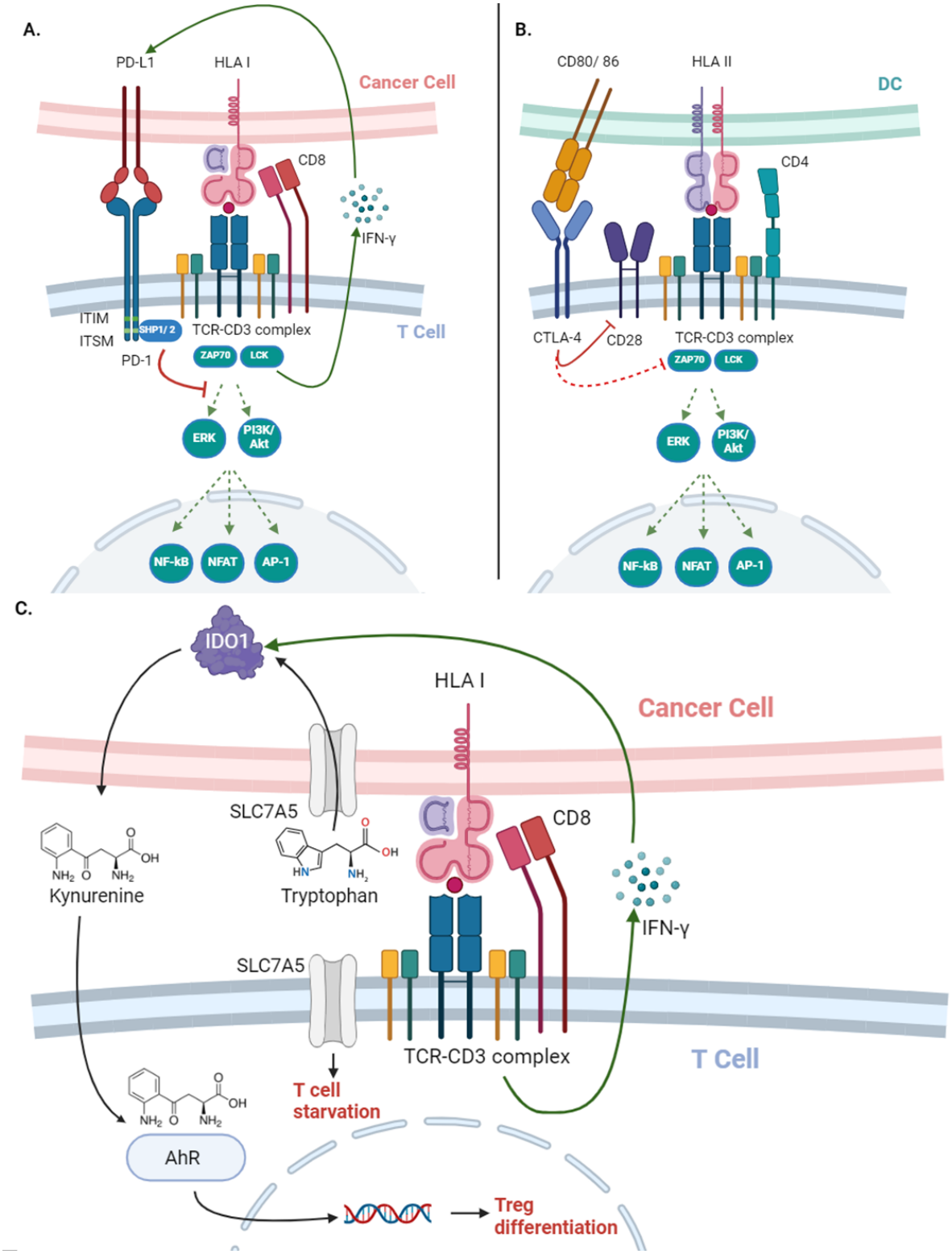
A.
PD-L1
HLA I
Cancer Cell
CD8
IFN-γ
ITIM
ITSM
SHP1/ 2
TCR-CD3 complex
T Cell
PD-1
ZAP70
LCK
ERK
PI3K/ Akt
NF-kB
NFAT
AP-1
B.
CD80/ 86
HLA II
DC
CD4
CTLA-4
CD28
TCR-CD3 complex
ZAP70
LCK
ERK
PI3K/ Akt
NF-kB
NFAT
AP-1
C.
IDO1
HLA I
Cancer Cell
SLC7A5
CD8
Kynurenine
Tryptophan
IFN-γ
SLC7A5
TCR-CD3 complex
T Cell
T cell starvation
AhR
Treg differentiation

Figure 1.1 Summary of the most widely studied immune checkpoints and their mechanisms of action. A. PD-1/PDL1 – cytotoxic T cells recognize tumours via the TCR interaction with the HLA I molecule presenting cancer-specific antigens this interaction is further strengthened by the CD8 co-stimulatory molecule expressed by T cells and it triggers a series of signalling events including activation of kinases downstream of the TCR, such as ZAP70 and LCK, through PI3K/Akt and ERK activation, these lead to expression of different pro-inflammatory transcription factors such as NF-kB, NFAT and AP-1; when the PD-1/PD-L1 interaction occurs as well, this recruits a set of protein tyrosine phosphatases, such as SHP1/2 which inhibit the LCK/ZAP70 signalling, thus preventing T cell activation (Wu et al., 2019). B. CTLA-4 – before cytotoxic T cells can recognise tumour antigens, they need to be primed by DCs in lymphoid organs; this interaction requires both HLA-TCR binding and stimulation via CD28 (on T cells) and CD80/86 on DCs; if CTLA-4 is expressed, this will prevent CD28 signalling, by competing for CD80/86 interaction; additionally CTLA-4 directly inhibits CD28-induced signalling inhibiting ZAP70 activation (Rudd et al., 2009). C. IDO1 – cancer cells express IDO1 in response to pro-inflammatory stimulation, such as IFN-γ; IDO1 metabolises tryptophan from the tumour microenvironment leading to effector T cell starvation and subsequent inhibition; Tryptophan catabolism produces the metabolite kynurenine, which is secrete in the tumour microenvironment and taken up by surrounding T cells; kynurenine then binds the AhR and travels to the nucleus where it triggers differentiation of regulatory T cells (Robinson et al., 2005). AhR – aryl hydrocarbon receptor; Akt – Ak strain transforming; AP-1 – adaptor protein 1; CD8/3/28/80/86 – cluster differentiate 8/3/28/80/86; CTLA4 – cytotoxic T-lymphocyte-associated antigen; ERK - extracellular signal-regulated kinase; DC – dendritic cells; HLA I – human leukocyte antigen I; IDO1 – indoleamine 2,3 dioxygenase; IFN-γ – interferon gamma; ITIM - immunoreceptor tyrosine-based inhibitory Motif ; ITSM - immunoreceptor tyrosine-based switch motif; Lck - lymphocyte-specific protein tyrosine kinase; NFAT - nuclear factor of activated T-cells; NF-kB - nuclear factor kappa B; PI3K - phosphoinositide 3-kinase; SLC7A5 – L-type amino acid transporter (tryptophan transporter); TCR – T cell receptor, ZAP70 - zeta-associated protein 70.

1.3.7. Other immune checkpoints

There are various other immune checkpoints that have been studied in the literature. Some of these are Lymphocyte Activation Gene 3 (LAG3), T cell immunoglobulin mucin 3 (TIM3), T-cell immunoglobulin and ITIM domain (TIGIT) and B And T Lymphocyte Associated (BTLA). LAG3 is primarily expressed on T cells, and it is a competitive inhibitor of the interaction between CD4 and Human Leukocyte Antigen II (HLA II), thus preventing T cell activation, while also triggering CD4-independent inhibitory signals (Maruhashi et al., 2018, Xu et al., 2014). In $CD8^+$ T cells, LAG3-mediated inhibition is triggered by its interaction with lectin ligands (Xu et al., 2014, Kouo et al., 2015). Despite its name, TIM3 is not only expressed on T cells, but also on a variety of other immune cells and can regulate both adaptive and innate responses. T cell activation induces expression and glycosylation of TIM3, which are dependent on carcinoembryonic antigen cell adhesion molecule 1 (CEACAM1) co-expression. The two molecules form a heterodimer and mediate T cell exhaustion (Huang et al., 2015). On $CD8^+$ DCs, TIM3 was shown to mediate phagocytosis, by recognizing apoptotic particles via its fragment crystallizable (FC) loop, and inhibition of TIM3 completely abrogated this process, reducing antigen presentation and thus immune recognition (Nakayama et al., 2009). TIGIT is expressed on T and NK cells and triggers inhibitory signals by preventing co-stimulation through CD226. TIGIT competes with CD226 for CD155 and CD112 on DCs, and this interaction leads to T/NK cell and DC inhibition (Yu et al., 2009, Stanietsky et al., 2009, Johnston et al., 2014) . Finally, BTLA is activated upon binding a subset of receptors within the Tumour Necrosis Factor Receptor (TNFR) family, called Herpes Virus Entry Mediator (HVEM) receptors, and it signals via ITIMs and ITSMs, activating the Src Homology 2 domain-containing protein tyrosine Phosphatase 1 (SHP1) protein and thus inhibiting TCR/CD28 activator signals in T cells, or germinal centre B cell proliferation (Sedy et al., 2005, Marsters et al., 1997, Gavrieli et al., 2003, Xu et al., 2020, Mintz et al., 2019).

Thus, considering the crucial role of immune checkpoints in regulating cancer immune evasion, immune checkpoint blockade therapies are becoming very attractive for modern scientists and clinicians. Immune checkpoint inhibitors are highly specific and effective, showing much longer lasting results compared to non-targeted approaches, particularly given the memory of the adaptive immune system, which serves as a barrier against malignancy and metastasis.

1.4. Tumour metabolism

1.4.1. Background

Alongside the ionic tumour microenvironment, another aspect of crucial importance in understanding cancer biology is the tumour metabolism. Probably the most well-known metabolic change associated with cancer is the Warburg effect, discovered initially by the increased lactate production of cancer cells (~ 2 % of their fresh weight), compared to healthy cells (0.034 % of their fresh weight) (Cori and Cori, 1925). It is now known that this happens due to preferential use of glycolysis by cancer cells, as main energy source, even when oxygen is present, a mechanism also known as aerobic glycolysis (Vander Heiden et al., 2009). This preferential use of glycolysis could be explained by the hypoxic environment often associated with the centre of solid tumours. Interestingly, however, recent studies show an even more specific link between the two, suggesting that the pyruvate produced by glycolysis, might prevent degradation of the hypoxia-induced factor 1 α (HIF-1α), activating its DNA-binding ability and thus mediating expression of HIF-1α-controlled genes (Lu et al., 2002). Glucose metabolism is also the preferred source of energy for activated tumour-infiltrating T cells (Warburg et al., 1958). Given this change of metabolite preference in tumours, infiltrating immune cells need to also reprogramme their metabolite preferences in order to survive, e.g., infiltrating cytotoxic T cells often shift to fatty-acid metabolism to be able to function under glucose starvation (Zhang et al., 2017b). On the other hand, Tregs

also undergo similar adaptations, upregulating the expression of the CD36 lipid transporter, in order to continue suppressing the immune system and protecting the tumour (Field et al., 2020, Wang et al., 2020a). Furthermore, tumours can impact on the immune environment also by secreting suppressive metabolites, such as lactate, which was shown to prevent T cell chemotactic migration and decrease cytotoxic activity by altering the expression of glycolytic enzymes (Haas et al., 2015, Brand et al., 2016).

In fact, a series of metabolites or trace elements have been shown to impact on various immune cells, leading to metabolic reprogramming, with the ultimate purpose of promoting tumour survival. Cholesterol was shown to induce $CD8^+$ T cell exhaustion, which means that T cells become dysfunctional due to overexposure to inflammatory stimuli (Wherry, 2011, Yang et al., 2016b). On the other hand, fatty acids seem to downregulate cytokine production by NK cells (Michelet et al., 2018, Yang et al., 2016b). Prostaglandins, in particular prostaglandin E2 (PGE2), seem to promote differentiation of tumour-protective macrophages (M2), via cAMP-response element binding protein (CREB)-mediated inhibition of pro-inflammatory cytokine production, as well as inducing Treg differentiation and inhibiting NK survival (Luan et al., 2015, Sharma et al., 2005). Methylglyoxal, as well as nitric oxide were also shown to decrease $CD8^+$ T cell proliferation, while high levels of K^+ in the extracellular environment were reported to also inhibit effector and central memory T cell function, for both $CD8^+$ and $CD4^+$ cells (Eil et al., 2016, Bronte et al., 2005, Baumann et al., 2020, Ong et al., 2019). Lastly, tryptophan was shown to promote T cell proliferation, whilst its metabolite, kynurenine, has the opposite effect, inhibiting both effector T and NK cells (Frumento et al., 2002, Munn et al., 2005).

1.4.2. Tryptophan metabolism as an immune checkpoint

Tryptophan (Trp) metabolism is particularly important in cancer, given its impact on energy production (*de novo* NAD^+ synthesis), protein synthesis and immune evasion, via kynurenine

production. Trp is an essential amino acid, taken from dietary sources. In the body 95 % of Trp is metabolised via the kynurenine pathway and 90 % of this goes into the tryptophan dehydrogenase (TDO, mainly in the liver) mediated Trp catabolism. About 1-2% is channelled towards the serotonin pathway, and the remainder is used for the indole pathway and protein synthesis (Bender, 1983, Badawy, 2002, Platten et al., 2019, Li et al., 2022).

The serotonin and kynurenine pathways have been considered complementary: activation of the kynurenine pathway was thought to have inhibitory function on the serotonin metabolism (Oxenkrug, 2013). However, the over-activation of the kynurenine pathway in conditions associated with low serotonin levels, such as depression, is now believed to contribute to this disease directly via kynurenine pathway metabolites with neuroactive properties (Jenkins et al., 2016, Savitz, 2017).

Through the kynurenine pathway, Trp is degraded into metabolites with immunosuppressive potential (e.g., kynurenine and kynurenic acid), neuroactive metabolites (e.g., kynurenic acid, glutamate receptor antagonist; quinolinic acid, excitotoxic for N-methyl-D-aspartate (NMDA) receptors; xanthurenic acid, binds G-protein coupled receptors (GPCR) and modulates cationic transport (Taleb et al., 2012)) and energy carriers (e.g., NAD^+) (Platten et al., 2019). For this reason, the kynurenine metabolic pathway is essential for a range of physiological processes and diseases. The kynurenine to Trp ratio was shown to directly corelate with aging. Although the exact mechanism underlying this observation is not completely understood, literature shows that TDO-depletion can expand the lifespan of *Caenorhabditis elegans*, by preventing protein aggregation otherwise associated with diseases like Alzheimer's and Parkinson's (van der Goot et al., 2012). Other studies point towards mTOR-mediated autophagic response triggered as a result of dysregulation in nutrient availability (Soultoukis and Partridge, 2016, Platten et al., 2019). Additionally, another hypothesis proposes the production of NAD^+ as a potential link between kynurenine

and decreased aging, potentially by enhancing mitochondrial function (Zhang et al., 2016, Fang et al., 2017, Castro-Portuguez and Sutphin, 2020).

The kynurenine pathway is also essential in regulating neurodegenerative diseases. Quinolinic acid was shown to accumulate in Alzheimer's neurological plaques and contribute to disease progression by increasing excitation of NMDA receptors (Guillemin et al., 2003). Furthermore, kynurenic acid was shown to accumulate within the central nervous system in conditions such as Schizophrenia (Plitman et al., 2017).

Lastly, the kynurenine pathway is notorious for its immunoregulatory function, particularly through the activity of the first enzyme of the pathway, IDO1. This enzyme modulates the rate-limiting step of Trp metabolism and converts it to N-formylkynurenine, rapidly metabolized to kynurenine by the formamidase enzyme. Kynurenine as well as other downstream metabolites (kynurenic acid) have immunosuppressive function (Platten et al., 2019). The impact of such metabolites on the immune system has made IDO1 an important therapeutic target in solid cancers (Soliman et al., 2016, Soliman et al., 2014, Berrong et al., 2018). The enzyme uses up the Trp within the tumour microenvironment leading to T cell starvation and subsequent impaired differentiation, as well as producing the immunosuppressive metabolite N-formylkynurenine which promotes T cell differentiation to a tumour-protective regulatory phenotype (Blair et al., 2019, Terness et al., 2002). T cell Trp-starvation leads to activation of the General Control Nonderepressible 2 (GCN2) kinase through accumulation of uncharged Trp transfer-RNA (t-RNA). GCN2 then halts translation by phosphorylation and subsequent inactivation of the eukaryotic initiation factor 2α (eIF2α) kinase. Additionally, Trp depletion induces T cell anergy (inactivation), by repressing mTOR and inducing autophagy (Munn et al., 2005, Ravishankar et al., 2015b, Metz et al., 2012). The immunosuppressive changes triggered by kynurenine on T cells, require its uptake via the Trp/kynurenine transporter solute carrier family 7 member 5 (SLC7A5); once inside the cell,

kynurenine binds the aryl hydrocarbon receptor (AhR), inducing its nuclear translocation; there the AhR regulates expression of various genes, including upregulation of IDO1 and SLC7A5, to allow continuous supply of kynurenine, as well as Transforming Growth Factor β (TGF-β), a known promoter of Treg differentiation (Sinclair et al., 2018, Opitz et al., 2011, Nuti et al., 2014, Kim et al., 2009, Tomblin et al., 2016). Furthermore, kynurenine-induced AhR activation was also shown to upregulate T cell PD-1 expression (Amobi-McCloud et al., 2021). Interestingly, Trp uptake seems to be regulated also by the known oncogene MYC. In colon cancer MYC was shown to enhance expression of SLC5A7, solute carrier family 1 member 5 (SLC1A5), another Trp transporter, as well as upregulating the levels of the enzyme aryl formamidase, involved in the kynurenine pathway (Venkateswaran et al., 2019). In TNBCs, MYC expression was also reported and associated with high glycolytic activity and hypoxia, suggesting that it might regulate a variety of metabolic changes in solid cancers (Gordan et al., 2007, Koboldt et al., 2012, Shim et al., 1997, Koppenol et al., 2011).

The kynurenine pathway, as part of Trp metabolism, thus regulates a multitude of cellular processes and it is, therefore. of particular interest in cancer research. Figure 1.2 summarizes the main steps involved in this pathway.

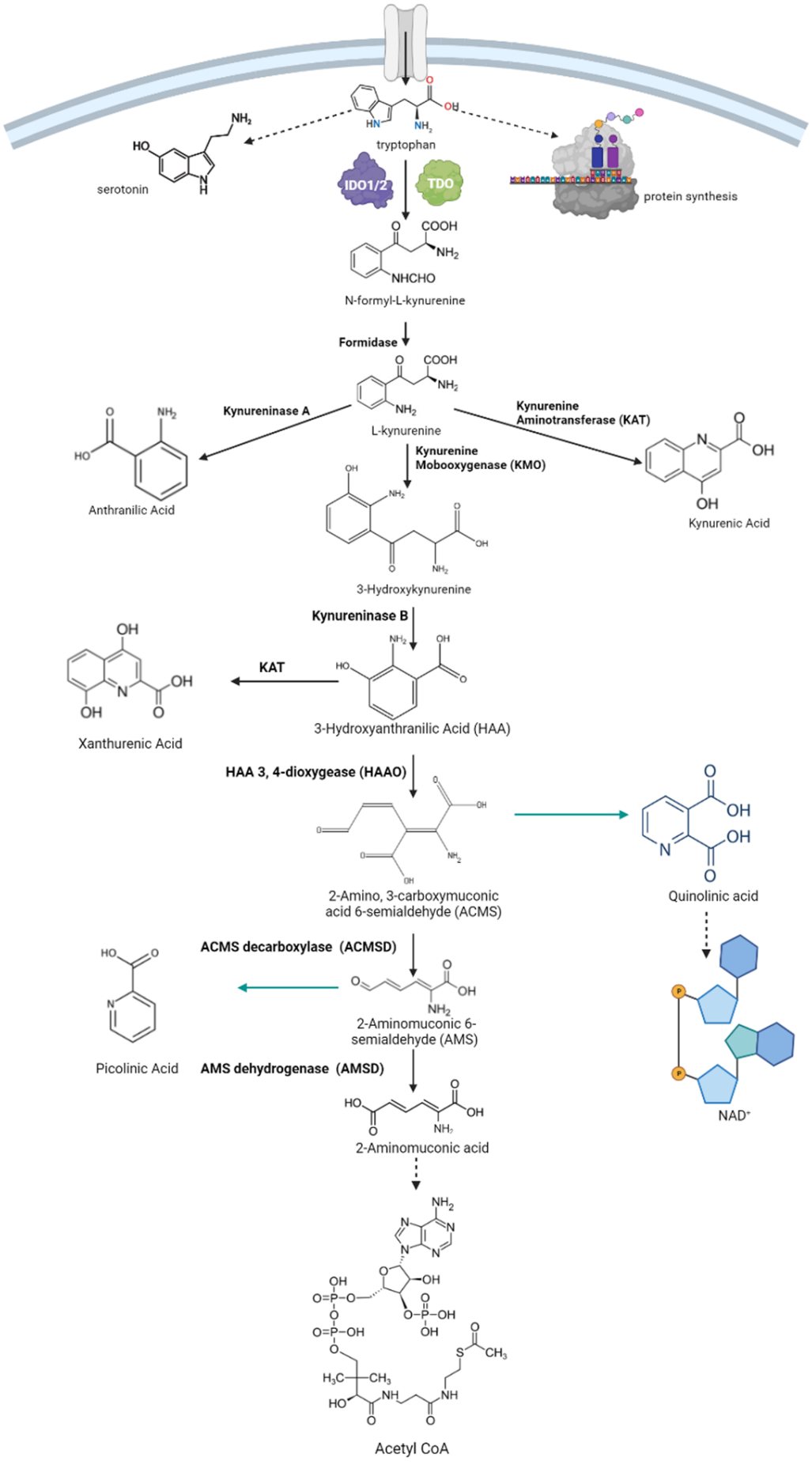
tryptophan
serotonin
IDO1/2
TDO
protein synthesis
N-formyl-L-kynurenine
Formidase
L-kynurenine
Kynureninase A
Kynurenine Aminotransferase (KAT)
Kynurenine Mobooxygenase (KMO)
Anthranilic Acid
Kynurenic Acid
3-Hydroxykynurenine
Kynureninase B
KAT
Xanthurenic Acid
3-Hydroxyanthranilic Acid (HAA)
HAA 3, 4-dioxygease (HAAO)
2-Amino, 3-carboxymuconic acid 6-semialdehyde (ACMS)
Quinolinic acid
ACMS decarboxylase (ACMSD)
Picolinic Acid
2-Aminomuconic 6-semialdehyde (AMS)
AMS dehydrogenase (AMSD)
2-Aminomuconic acid
NAD+
Acetyl CoA

Figure 1.2 The kynurenine pathway. Trp is imported into the cell through the SLC7A5 transporter; once inside the cell Trp can have three potential fates: it can be converted to serotonin, it can be used for protein synthesis (translation), or it can enter the kynurenine pathway. Depending on the cell type the first and rate-limiting step of the pathway can be mediate by TDO or IDO1 (and less often by IDO2), converting Trp to N-formyl-L-kynurenine. A series of enzymatic steps then convert this to the final product: acetyl CoA, as well as producing NAD^+ (Badawy, 2017). ACMS – 2-amino 3-carboxymuconic acid 6-semialdehyde, ACMSD - 2-amino 3-carboxymuconic acid 6-semialdehyde decarboxylase, AMS – 2-aminomuconic 6-semialehide, AMSD - 2-aminomuconic 6-semialehide dehydrogenase, HAA – 3-hydroxyanthranilic acid, HAAO - 3-hydroxyanthranilic acid 3, 4 -dioxygenase, KAT - kynurenine aminotransferase, KMO – kynurenine monooxygenase.

1.4.3. IDO1 as a metabolic and immune regulatory hub.

IDO1 is an intracellular monomeric enzyme of approximately 45 kDa, containing a central haeme group, which mediates the deoxygenise activity. The active IDO1 conformation, is thus complexed with an Fe^{2+} ion. This is one of the two oleophilic IDO1 domains, the second being the substrate binding site. The main IDO1 substrate is the L-stereoisomer of Trp. IDO1 uses oxygen to break the 2, 3- double bond within the indole ring of the Trp molecule, converting it to N-formylkynurenine (Weng et al., 2018, Hornyák et al., 2018). The activity of IDO1 can be regulated post-translationally through phosphorylation of two tyrosine residues, Y115 and Y253, identified in mouse dendritic cells expressing IDO1; through these phospho-tyrosine residues, IDO1 attracts suppressor of cytokine signalling 3 (SOCS3), which targets it for proteasomal degradation (Pallotta et al., 2010). Nitration of Y15, Y345, and Y353, was also associated with inhibition of IDO1 activity (Fujigaki et al., 2006). Nitric oxide can also directly inhibit IDO1 activity by oxidising the Fe^{2+} to Fe^{3+} within its haeme ring (Thomas et al., 2007). Although IDO1 is not normally a constitutively expressed protein, it has been shown to be constantly expressed in specific subtypes of cells. CD123 and CCR6 positive human DCs can express constant levels of IDO1 regardless of stimulation, however, IDO1 is not enzymatically active in these cells, and its activation requires interaction between the DC expressed CD80/86 molecules and the T cell expressed CTLA-4/CD28 markers during antigen presentation (Munn et al., 2004, Munn et al., 2002). This comes to support the idea that tight IDO1 regulation is required for maintaining homeostasis.

IDO1 protein levels can also be transcriptionally regulated. IDO1 expression is usually induced by pro-inflammatory stimulation such as type I IFN (α/β) (often associated with viral infections), lipopolysaccharide (LPS) (associated with bacterial infections) and IFNγ stimulation (mostly associated with IDO1 induction in infections and cancer) (Hoshi et al., 2012, Wang et al., 2010b, Yang et al., 2021). The molecular mechanisms connecting IFNγ

stimulation and IDO1 expression have been investigated over the years. The pathway involves binding of the IFNγ molecule to the Interferon γ Receptor (IFNGR) on tumour cells, which recruits Janus Kinase (JAK1) dimers. These phosphorylate the IFNGR and trans-phosphorylate each other, also recruiting signal transducer and activator of transcription 1 (STAT1) molecules; JAKs phosphorylate STATs (pSTAT), and this leads to pSTAT dimerization. These dimers, in turn, function as transcription regulators for the IDO1 promoter (Moretti et al., 2017). IFNγ stimulation was also shown to activate the IFN regulatory factor 1 (IRF1), which also functions as a regulator of IDO1 expression (Silva et al., 2002, Chon et al., 1996). Studies have shown that combining IFNγ stimulation with TNF treatment enhances the binding of STAT1 to the IFNγ-responsive enhancer domain within the IDO1 promoter gamma activation sequence (GAS), as well as enhancing the interaction between the IRF1 and the IFN-stimulated response elements (ISREs). Both signals contribute to upregulated IDO1 expression either directly, or by increasing the expression of the IFNGR, and thus increasing cellular sensitivity to IFNγ stimulation (Robinson et al., 2003). Other regulators of IDO1 expression have also been identified, such as the oncogenic KIT proteins or the tumour suppressor Bin1 (Balachandran et al., 2011, Muller et al., 2005).

Interestingly, IDO1 expression seems to be regulated also by hormone signalling. In pregnancy oestrogen levels can upregulate placental IDO1 levels by triggering TGFβ signalling (Wang et al., 2020b). Studies indicate that pregnancy-associated increases in oestrogen levels were shown to induce IDO1 expression in DCs, reducing the relapse rate in women suffering from multiple sclerosis (Zhu et al., 2007). In uterine carcinoma, IDO1 levels also correlated positively with oestrogen levels, however, in breast cancer these were inversely correlated (Feng et al., 2020). ER^+ breast cancers are associated with hypermethylation of the IDO1 promoter and subsequent reduced expression of this immune checkpoint (Dewi et al., 2017). These results highlight the clear role that oestrogen plays in regulating IDO1

expression, and further support the idea that TNBC is the most suitable breast cancer subtype to explore the modulation of IDO1.

Tumours that have high expression of IDO1 are associated with a higher immune infiltration and mutation burden in breast and gynaecological cancers, as well as expressing high levels of other immune check points like PD-L1 and LAG3 (Feng et al., 2020). IDO1 was also shown to be a good prognostic marker in prostate cancer patients, where its expression seems to be strongly induced by IFNγ stimulation (Banzola et al., 2018).

Alongside IDO1, IDO2 and tryptophan-2,3-dioxygenase (TDO) are also catabolic enzymes which regulate the rate limiting step of Trp metabolism, as part of the kynurenine pathway, with IDO1 being more catalytically active and preferentially expressed in breast cancer cells (Platten et al., 2012, Ye et al., 2019, Munn and Mellor, 2007, Carvajal-Hausdorf et al., 2017, Wei et al., 2018, Novikov et al., 2016). However, there is evidence to suggest that IDO2 is also expressed in TNBC cell lines such as MDA-MB-231 cells. Recent data also suggests that when expressed on B cells, IDO2 might have pro-inflammatory activity, however, the same study claims that IDO2 can enhance the tolerogenic activity of IDO1, thus contributing to tumour immune evasion (Mo et al., 2023). These data suggest that a comprehensive study of the IDO1/ IDO2 responses in the tumour microenvironment is required in order to allow development of more refined IDO-targeted therapies. Given the association of IDO2 expression with poor prognosis and increased immune infiltration, it might be crucial to analyse the balance between IDO1 and IDO2 expression in various tumours and assess the implications of different IDO1/ IDO2 ratios for response to immunotherapy. Understanding the relationship between IDO1 and IDO2 might help enhance the efficacy of IDO1 targeted therapies, which up to date have had limited clinical success (Fujiwara et al., 2022, Mo et al., 2023). For the scope of this project, however, IDO1 will remain the focus of the research presented here.

Trp metabolism is very important and tightly regulated within cells, with Trp being the precursor for both serotonin and the kynurenine pathway, ultimately producing ATP and biologically active metabolites like NAD^+/NADH, or Trp/kynurenine metabolites (Badawy, 2017). Trp is an essential amino acid, which means that it cannot be synthesized in the body. Shortage of Trp can trigger starvation signalling, ultimately leading to cellular autophagy (Fougeray et al., 2012). Interestingly, the Trp-t-RNA synthetase (WRS) was found to be regulated by IFNγ signalling, so that in cells where more IDO1/2 are expressed, WRS levels also increase, competing with the IDO enzymes for Trp (Frolova et al., 1993). TDO, unlike IDO1, is a constitutively expressed protein, and it is associated with certain types of cells, most commonly found in the liver, but also present in other organs, such as the brain (Haber et al., 1993, Badawy, 2017). TDO is responsible for maintaining basal Trp levels in the blood (Kanai et al., 2009, Lanz et al., 2017, Gostner et al., 2020).

Apart from its metabolic contribution to the energetic needs of the cell, the extra-hepatic kynurenine pathway plays a central role in immune regulation. For this reason IDO1 has been classified as an immune checkpoint protein, being extensively studied in the context of cancer, inflammation/infection, as well as in pregnancy associated foetal tolerance (Schmidt and Schultze, 2014, Li et al., 2021d, Shayda et al., 2009, Sedlmayr et al., 2014, Zong et al., 2016).

The immunosuppressive effect of IDO1 is mediated by multiple mechanisms. High IDO1 expression by tumour cells, leads to Trp depletion in the tumour microenvironment. This then activates the GCN2 kinase through accumulation of uncharged Trp t-RNA. GCN2 then halts translation by phosphorylation and subsequent inactivation of the eukaryotic translation eIF2α kinase. Additionally, Trp depletion induces T cell anergy by repressing mTOR and inducing autophagy (Munn et al., 2005, Ravishankar et al., 2015b, Metz et al., 2012, Yang et al., 2021). Interestingly, IDO1-induced Trp starvation seems to also impact on

less well characterized T cell subsets such as γδT cells. In TNBC patients, IDO1 activity was associated with exhaustion of the γδT cells, however, inhibition of IDO1 enhanced their cytotoxicity and perforin production (Li et al., 2021d). Recent studies have also shown that IDO1-induced Trp depletion can lead to ribosomal stalling during translation at the Trp sites (also known as W-bumps), which leads to frame-shift mutations, giving rise to neoantigens. This in turn, helps the tumour evade the immune system, allowing cancer progression. Therefore, a balance between too little and too much IDO1 expression needs to be achieved to prevent cancer immune evasion (Bartok et al., 2021).

Kynurenine also has immunosuppressive effects. By binding to the AhR on T cells, it induces their differentiation to the $FOXP3^+$ Treg phenotype (Mezrich et al., 2010). Other Trp catabolites produced by DCs: kynurenine, 3-hydroxykynurenine, and 3-hydroxyanthranilic acid were also shown to inhibit activated T cells, as well as killing NKs and B lymphocytes (Terness et al., 2002, Bauer et al., 2005). In mouse T cells, quinolinic and 3-hydroxyanthranilic acids induced caspases 8/cytochrome C mediated apoptosis (Fallarino et al., 2002). Figure 1.3 summarizes the main immune evasion mechanisms employed by IDO1.

Additionally, IDO1 was shown also to be an interesting therapeutic target, as a tumour cell biomarker recognized by effector T cell. Thus, IDO1-primed T cells were reported to be much more effective against clearance of both tumour cells and viral infections, highlighting the essential role of IDO1 in regulating immune evasion (Sørensen et al., 2011).

IDO1 inhibition has also been extensively studied in the context of cancer, and a series of synthetic inhibitors are currently in clinical trials. Indoximod was the first IDO1 inhibitor to enter clinical trials and it is currently tested for relapse brain tumours in combination with chemotherapy and radiotherapy (Qiu et al., 2021). Another example would be Epacadostat which is currently in phase I/II clinical trials or solid cancers, in combination with the anti-PD-1 therapy, Pembrolizumab. BMS-986205/ Linrodostat is also being investigated for advanced

bladder cancer in combination with another anti-PD-1 therapeutic, Nivolumab (Luke et al., 2019). Whereas PF-06840003 is currently being tested in a phase I study for patients with recurrent malignant glioma (Reardon et al., 2020). Furthermore, the Proteolysis Targeting Chimeras (PROTAC) technology has identified a potential compound, IDO1 PROTAC degrader 2c, which seems to be effectively targeting IDO1 for degradation and thus enhancing tumour killing (Hu et al., 2020). However, so far, no IDO1 inhibitors have been FDA approved of clinical use in breast cancer.

All these together highlight the potential of IDO1 as a target for immunomodulatory therapies in cancer patients, as well as in infection or inflammation models.

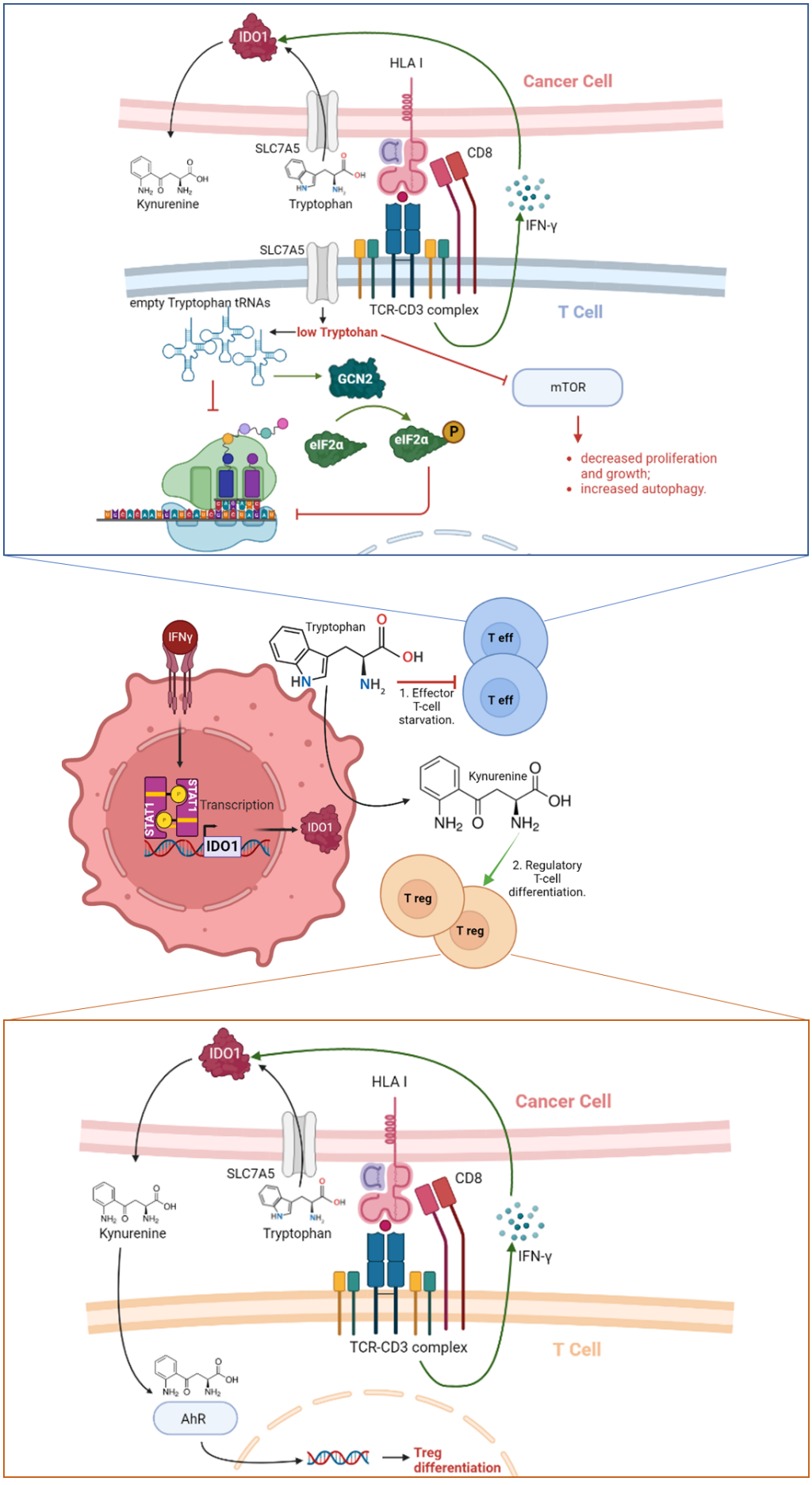
IDO1
HLA I
Cancer Cell
SLC7A5
CD8
Kynurenine
Tryptophan
IFN-γ
SLC7A5
empty Tryptophan tRNAs
TCR-CD3 complex
T Cell
low Tryptohan
GCN2
mTOR
eIF2α
eIF2α
P
decreased proliferation and growth;
increased autophagy.
IFNγ
Tryptophan
T eff
T eff
1. Effector T-cell starvation.
STAT1
STAT1
Transcription
IDO1
IDO1
Kynurenine
2. Regulatory T-cell differentiation.
T reg
T reg
IDO1
HLA I
Cancer Cell
SLC7A5
CD8
Kynurenine
Tryptophan
IFN-γ
TCR-CD3 complex
T Cell
AhR
Treg differentiation

Figure 1.3 IDO1 mode of action. Cancer cells express IDO1 in response to pro-inflammatory stimulation (IFN-γ) this leads to rapid Trp metabolization to N-formylkynurenine, and thus the Trp uptake by cancer cells via SLC7A5 increases, depleting it from the extracellular environment. Effector T cells are thus starved of Trp. This in turn triggers accumulation of empty tRNAs and subsequent activation of the GCN2 kinase, which phosphorylates eIF2α, preventing it from initiating translation. In parallel, empty t-RNA also stall translation of Trp codons. Low Trp levels also inhibit mTOR activation reducing cell growth and proliferation, while initiating autophagy (top diagram) (Munn et al., 2005, Ravishankar et al., 2015b, Metz et al., 2012, Yang et al., 2021). Alternatively, kynurenine is also taken up by T cells, binding to the aryl hydrocarbon receptor (AhR), inducing its nuclear translocation, which leads to transcriptional changes which promote differentiation of the T reg phenotype (bottom diagram) (Mezrich et al., 2010). AhR – aryl hydrocarbon receptor, eIF2α – eukaryotic translation initiation factor 2α, HLA I – human leucocyte antigen I, GCN2 – general control nonderepressible 2, IDO1 – indoleamine 2, 3-dioxygenase, IFNγ – interferon γ, SLC7A5 - Solute carrier family 7 member 5, T eff – effector T cell, T reg – regulatory T cell.

1.5. The tumour ionic microenvironment

1.5.1. Background

One aspect which is insufficiently explored by cancer research is the tumour ionic microenvironment. This is particularly important since variations in the levels and dynamics of multiple ions such as Na^+, K^+, Ca^{2+} and even H^+ have been often associated with solid tumours (Pardo and Stühmer, 2014, Monteith et al., 2017, Webb et al., 2011, Ouwerkerk et al., 2007, Capatina et al., 2022). In breast cancer, elevated intra-tumoral Na^+ levels have been recorded in human patients, suggesting that Na^+ might have a protective effect against tumour clearance (Ouwerkerk et al., 2007, Ianniello et al., 2021). TNBC tumours are primarily associated with such elevations, which have been shown to originate in the intracellular environment. Furthermore, treatment with docetaxel, a drug reported to decrease intra-tumoral Na^+ levels, was shown to reduce cancer growth, tumour volume and expression of the proliferation marker Ki-67 (James et al., 2022). Regulation of Na^+ dynamics occurs through a variety of active and passive transporters, summarised in Table 1.1.

Variations in the concentration of intracellular Na^+ ($[Na^+]_i$), as seen in solid tumours, have severe physiological consequences. The physiological $[Na^+]_i$ is ~10-15 mM, while the extracellular Na^+ concentration ($[Na^+]_e$) is estimated around 145 mM (Leslie et al., 2019). An increase in $[Na^+]_i$, in non-excitable cells, can be associated with depolarisation of the plasma membrane potential, which is otherwise stably kept at ~ -50 to -95 mV. This is common to cells from solid cancers, which tend to have a resting membrane potential of ~ -5 to -40 mV, and it has been suggested in the literature that this might be partially responsible for their increased proliferation capacity (Yang and Brackenbury, 2013, Lan et al., 2014). A depolarised membrane potential has also been associated with cytoskeletal changes and tumorigenesis (Nin et al., 2009, Chernet and Levin, 2014, Szászi et al., 2005, Lobikin et al., 2012). Furthermore, membrane depolarisation has been associated with amplified K-Ras-

dependent MAPK activation (Zhou et al., 2015). Changes in Na^+ dynamics are also likely to impact on the intracellular and extracellular pH, given the antiport of Na^+ and protons, through the Na^+/H^+ exchanger (NHE1), as well as the activity of $Na^+/ HCO3^-$ cotransporter (NBCn1) which co-transports Na^+ and alkaline bicarbonate ions (Boedtkjer et al., 2013, Hulikova et al., 2013). In turn, the altered pH observed in solid tumours, where the extracellular environment is slightly acidic, while the intracellular compartment is more alkaline, might impact on intra-tumoral Na^+ levels (Gerweck and Seetharaman, 1996). Changes in intracellular Na^+ might also impact on metabolism. Cancer cells are known to preferentially utilise glycolysis, even under aerobic conditions, a process called the Warburg effect (Warburg, 1956). Extracellular Na^+ might play a role in controlling that shift, by promoting expression of glycolytic enzymes, whilst intracellular Na^+ might dysregulated metabolic pathways by Na^+/Ca^{2+} exchanger (NCLX) dependent transfer of Ca^{2+} from the mitochondria to the cytosol, leading to enhanced Na^+/ K^+ ATPase (NKA) activity, and consequently enhanced ATP usage, which could justify the need to aerobic glycolysis (Amara et al., 2016, Palty et al., 2010, Leslie et al., 2019, Meyer et al., 2022, Nguyen et al., 2022). Several studies have also associated increases in intracellular Na^+ with proliferation and migration (import via ENaC), as well as invasiveness (import via voltage gated Na^+ channels, VGSCs) (Bondarava et al., 2009, Sparks et al., 1983, Del Mónaco et al., 2009, Roger et al., 2007). Na^+ is also a key regulator of inflammation, as shown by a study which correlated intracellular Na^+ accumulation with different types of lesions occurring in patients diagnosed with multiple sclerosis (Biller et al., 2016). Elevated extracellular Na^+ in tumours has been previously associated with chronic inflammation. This can enhance cancer progression by stimulating proliferation via different cytokines, as well as increasing the chances of malignant mutations through reactive oxygen species (ROS) - induced DNA damage (Coussens and Werb, 2002, Dmitrieva and Burg, 2015, Shapiro and Dinarello, 1995). Conversely, elevated Na^+ levels in the blood have been associated with impaired metastasis

due to anoikis, which is a form of cell death associated with loss of adhesion molecules (Xu et al., 2018c).

The role of intracellular Na^+ in cancer is less well established. Increases in $[Na^+]_i$ have been associated with subsequent increases in intracellular Ca^{2+} levels, which in turn seem to activate a series of signalling events including activation of the calmodulin kinase (CaMK). In cardiac myocytes, these events were shown to regulate expression of differentiation genes NFAT and myocyte-specific enhancer factor (MEF), via activation of salt inducible kinase 1 (SIK1) (Popov et al., 2012). This is particularly interesting given that SIK1 is a known tumour suppressor, of particular interest for breast cancer (Xin et al., 2021). The same SIK1 protein was shown to regulate NKA activity, by inducing phosphorylation of the serine18 within the α subunit, which upregulates Na^+ transport. SIK1 activation also enhances expression of the β subunit of the pump, especially in kidney cells (Taub et al., 2015, Taub et al., 2010). Additionally, actin cytoskeletal changes in myeloid leukaemia cells were shown to increase Na^+ import, suggesting that an elevation in intracellular Na^+ might play a role in migration (Negulyaev et al., 1996, Cantiello, 1995). Therefore, Na^+ dynamics seems to be a crucial factor modulating cancer survival and metastasis, coordinating ionic, metabolic, signalling, and structural changes within the cell.

Channel/Transporter Name	Abbreviation	Type of transporter	Location	Direction of Na^+ transport
Na^+/K^+ ATPase	NKA	Active Antiport system with K^+	Cellular/organelle membranes	Cellular Export
Two-pore Channels/ Transient Receptor Potential Mucolipin 1	TPC/TRPML	Passive	Lysosomal membrane	Lysosomal Export
Voltage Gated Na^+ Channels	VGSC (Na_v)	Passive	Cellular membrane	Cellular Import
Epithelial Na^+ Channel	ENaC	Passive	Cellular membrane	
Acid-sensing ion channels	ASIC	Passive Cotransport system with glutamate	Cellular membrane	
N-methyl D-aspartate	NMDA	Active Cotransport system with Ca2+ and antiport with K+	Cellular membrane	
ATP-gated P2X receptor cation channel family	P2X	Active	Cellular membrane	
Na^+ leak channel, non-selective	NALCN	Passive (ligand dependent)	Cellular membrane	
Sodium-glucose transport proteins	SGLT	Passive Cotransport with glucose	Cellular membrane	
Na^+/H^+ exchanger	NHE1	Passive Antiport with H+	Cellular/organelle membranes	
The Na^+-K^+-Cl^- cotransporter	NKCC	Passive Cotransport with Cl- and K+	Cellular membrane	
Na^+/Ca^{2+} exchanger	NCX NCLX (mitochondrial)	Passive Antiport with Ca2+	Cellular/organelle membrane	
Na^+-$HCO3^-$ co-transporter	NCBn1	Passive Cotransport with HCO3-	Cellular membrane	
Amino Acid transporter/Solute Carrier	SLC - transporters	Passive Cotransport with amino acids	Cellular membrane	

Table 1.1 Summary for the main Na^+ transporters (Wang et al., 2012b, Vangeel and Voets, 2019, Leslie et al., 2019, Suzuki et al., 2006).

1.5.2. The Na^+/K^+ ATPase

The main regulator of intracellular Na^+ homeostasis is the Na^+/K^+ ATPase (NKA). This is a transmembrane molecule, that actively exports 3 Na^+, in exchange for 2 K^+, against their chemical gradients, using ATP (Post et al., 1969). By doing so, the NKA maintains a low intracellular Na^+ concentrations ~10-15 mM (Ianniello et al., 2021).

The NKA consists of 3 subunits, with α being the largest (~110 kDa) and primarily involved in the transport of ions across the plasmalemma. The other two subunits (β and γ) are smaller and less well characterised. The β subunit is approx. 33 kDa and it is highly glycosylated; it is believed to regulate folding and transport of the α subunit to the membrane, potentially stabilising its ion transport function (Sweadner, 1989, Lingrel and Kuntzweiler, 1994). FXYD or the γ subunit is the smallest of the three, with only 7 kDa and 58 amino acids; its function is less clear than for the other two and it is believed to regulate ionic transport through the α subunit (Mercer et al., 1993).

Multiple isoforms of the α subunit are expressed in different tissues, with α1 or the ATP1A1 being the most widespread. The first three subunits: α1, α2 and α3 have about 90 % similarity in structure across multiple species, while α4 is less conserved, with only about 80 % similarity (Clausen et al., 2017). ATP1A1 is also the target for cardiotonic steroids, a class of drugs extensively studied for their inhibitory effect on the activity of the NKA (Spigset et al., 2001, Khajah et al., 2018, Askari, 2019). The α isoforms were discovered given their different kinetic properties, in response to treatment with ouabain (a member of the cardiotonic steroid family). In the late 1970s, researchers recorded a biphasic ouabain-binding response in mouse brains, while other organs only gave monophasic inhibitor responses (Marks and Seeds, 1978). This turned out to be because rodent brains express the α1 subunit of the pump, alongside α2/3, with the former having much lower ouabain affinity compared to the

latter (Edwards et al., 2013). This is, however, different in humans, where the α1 subunit has ~1000-fold higher affinity for ouabain than the rodent α1 (Crambert et al., 2004, Lingrel et al., 1997, Lopina et al., 2020a). In terms of tissue distributions, the α1 subunit is almost ubiquitously expressed, while α2 is primarily found in the heart, muscles and brain, α3 primarily localises to the nervous system and α4 seems to be limited to sperm cells (Clausen et al., 2017). Figure 1.4 presents the crystal structure of the main NKA subunits.

Apart from the ion transport function, the NKA is also involved in signalling events. Studies have shown that ouabain-induced partial NKA inhibition activates the Src kinase (regulating adhesion, motility, proliferation) and enhances NKA association with the epidermal growth factor receptor (EGFR), as well as inducing mitogen-activated protein kinase (MAPK) activation, responsible for myocardial hypertrophy (Haas et al., 2000, Xie and Askari, 2002). Additionally, it has been shown that ouabain also induces protein kinase C (PKC) activation, and impairing this step was demonstrated to prevent the previously reported ouabain-triggered activation of the extracellular signal-regulated kinase 1/2 (ERK1/2), suggesting that PKC is a key signalling element in this pathway (Mohammadi et al., 2001). Although these experiments were carried out in rat cardiac myocytes, rather than human cells, they suggest that the NKA might be a hub of signalling networks, alongside its electrochemical-regulation function, and thus ouabain-induced NKA inhibition might trigger a series of parallel, yet not necessarily connected cellular changes. Ouabain was also shown activate the PI3K/Ak strain transforming (Akt) proliferative pathway, independently of the Src kinase (Wu et al., 2013b). The NKA also directly interacts with various other proteins; an example is the transient receptor potential cation channel subfamily C member 6 (TPC6), which was found to co-immuno-precipitate with the NKA, suggesting that the integrity of the pump might directly alter overall cationic transport, triggering a range of signalling events that are independent of its direct connections (Goel et al., 2005).

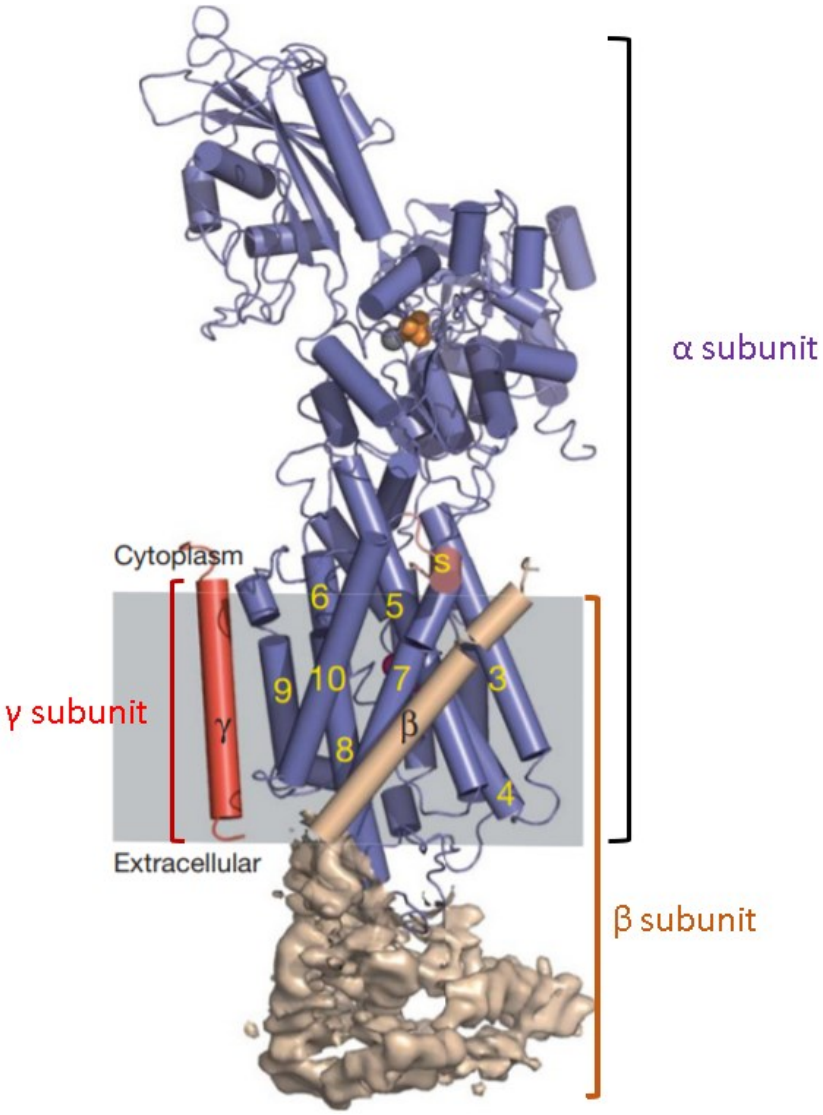

Figure 1.4 Crystal structure of the Na^+/K^+ pump. The α-, β- and γ-subunits were represented in blue, brown, and read. S (switch) marks the C-terminus helix. Ions complexed with the α-subunit were represented in pink (Rb^+), grey (Mg^{2+}) and orange (MgF_4^{2-}). The α-subunit transmembrane helices are labelled 1 t0 10 from the N- to the C-terminus. Source: Morth et al. (2007).

Ouabain-induced NKA inhibition was also shown to trigger transcriptional changes by activating the CREB protein, which further modulates gene expression in a Ca^{2+}/CaMK dependent manner (Desfrere et al., 2009). This is particularly interesting given the indirect effect of ouabain-induced NKA inhibition on intracellular Ca^{2+}. NKA blockade leads to a build-up of intracellular Na^{+}, this in tun activates the reverse function of the NCX, leading to intracellular accumulation of Ca^{2+} (Blaustein and Lederer, 1999). Ca^{2+}, in turn, is a well-known regulator of gene expression, inducing what is known as immediate early genes (IEGs), such as Jun and Fos; the short spike of Ca^{2+} increase has also been associated with the IFNγ signalling and associated genes. Furthermore, Ca^{2+} seems to be able to initiate transcription by phosphorylating proteins that bind to the cAMP response element (CRE) and serum response element (SRE), as well as initiating transcription elongation (van Haasteren et al., 1999). These observations broaden even more the spectrum of effects that ouabain-induced NKA inhibition might have on cells.

Another interesting implication of the ouabain-induced NKA inhibition comes from its metabolic impact. The NKA is an active Na^{+} transporter, which means that it requires ATP to fulfil its function; in astrocytes NKA uses 20 % of the total ATP produced per cell. Inhibition of NKA with ouabain, was shown to reduce ATP-usage and shift the preferred metabolic pathway from glycolysis or oxidative phosphorylation (OXPHOS), to the (phospho-)creatine pathway (Silver and Erecińska, 1997). Furthermore, in lung and breast cancer cell lines, ouabain-induced NKA inhibition seems to inhibit OXPHOS, as well as later glycolytic behaviour, also depleting ATP production. The same study shows that ouabain induced AMPK and Src signalling, potentially leading to autophagic cancer cell death (Shen et al., 2020a, Wang et al., 2012c). Whether these effects are modulated through the ATP1A1 or not, it is yet to be investigated.

Interestingly, NKA activity can be modulated by a variety of other factors. Studies have shown that releases of reactive oxygen species by squamous cancer cells can in fact increase NKA expression and function, suggesting that cancer cells might need a disrupted ionic balance to survive and proliferate (Toledo et al., 2021). Ouabain was also shown to upregulate ATP1A1 expression in rat astrocytes (Hosoi et al., 1997). A series of other agents/ factors were reported to increase ATP1A1 expression, such as aldosterone, corticosterone, dexamethasone (synthetic glucocorticoid), growth factors, glucose, elevated intracellular Na^+ or Ca^{2+} concentrations, as well as decreased K^+ levels, or drugs that increase intracellular Na^+ levels such as veratridine. Some of the ATP1A1 transcriptional inhibitors are tetrodotoxin (TTX) (inhibitor of Na^+ import) and nitric oxide as reviewed by (Li and Langhans, 2015). The ATP1A1 gene incorporates a series of regulatory elements, including the sterol response element (mineralo- and glucocorticoid response element), a few CCAAT box-binding transcription factor (CTF)/nuclear factor 1 (NF-1) binding sites, as well as binding elements for activator proteins 1 to 3 (AP-1 to 3). The ATP1A1 promoter also incorporates a TATA box, specific for housekeeping genes (Kolla et al., 1999, Shull et al., 1990). While hormone/steroid regulation of ATP1A1 expression is easily explained through interaction with the mineralo-/glucocorticoid response element, the mechanism that links ionic imbalances with ATP1A1 expression is not fully understood. Low K^+ seems to enhance ATP1A1 expression by increasing expression of CREB-1, as well as some additional specificity proteins (Sp-1 to 3), inducing their binding to the GC box, instead of the CRE/activating transcription factor (ATF) element in rat cells (Wang et al., 2007b). Additionally, low K^+-mediated ATP1A1 expression, is also dependent on protein kinase A (PKA) and ERK1/2 activation. This suggest that low K^+ triggers a similar response to ouabain, which was also reported to activate the ERK1/2 pathway and to upregulate ATP1A1 levels, further supporting that hypothesis that the ouabain-induced signalling changes occur due to ATP1A1 inhibition and not due to off-target effects (Wang et al., 2007a, Mohammadi et al., 2001, Li and Langhans, 2015).

This range of transcriptional regulators highlights the complexity of factors that might contribute to modifying the molecular mechanisms within cells, but also suggests that the NKA, in particular the ATP1A1, serves as a key component of regulating cellular homeostasis.

1.5.3. Pharmacological Inhibitors of Na^+ transport

A class of compounds known to have an inhibitory effect on the NKA via the ATP1A1 is represented by cardiac glycosides such as ouabain, digoxin, digitoxin, oleandrin or bufalin (Khajah et al., 2016, Spigset et al., 2001, Karlish et al., 1979, Askari, 2019, Ni et al., 2002). Cardiac glycosides are naturally derived compounds, produced by different plants or animals. They are organic molecules consisting of a central sterol structure which consists of 17 carbon atoms forming 4 6-carbon rings, bound to a glycone structure and a lactone ring (Prassas and Diamandis, 2008, Schönfeld et al., 1985). Variations in the sugar moiety structure or the lactone ring are mostly responsible for different kinetics and toxicities of the class members, with digoxin and digitoxin being the best characterised compounds in this sense (Brown et al., 1986, Kanji and MacLean, 2012). Digoxin is in fact FDA approved for the treatment of arrhythmia, and also approved for veterinary use (Atkins et al., 2009, Currie et al., 2011). Of all the compounds digoxin has a relatively long half-life in humans approx. 48 h, while digitoxin as a half-life of up to 6 days, and ouabain only 21 h (Smith, 1985, Selden and Smith, 1972).

Although the specificity of cardiac glycosides has been long considered a dogma of the NKA physiology, there are studies which are currently questioning this hypothesis by identifying additional targets for these compounds, such as the steroid receptor co-activators 1 and 3 (SRC1/3) (Wang *et al*., 2014). Yet, cardiac glycosides have been extensively used as tools in investigating the activity of the NKA, and therefore its contribution to tumorigenesis.

In cancer, treatment with cardiac glycosides was shown to inhibit proliferation and metastasis, reducing inflammation as well as improving patient survival (Zhang et al., 2008,

Kepp et al., 2012, Gould et al., 2018, Khajah et al., 2018). Their effect on intracellular Na^+ accumulation is bound to trigger changes in gene expression, primarily by altering the overall intracellular ionic homeostasis. Elevations in Na^+ often lead to an increase in Ca^{2+} achieved via the NCX, which in turn alter Ca^{2+} signalling (Blaustein and Lederer, 1999). This can impact on gene expression (e.g., SIK1 kinase), as well as altering signalling pathways, such as the cellular response to IFNγ, which is a Ca^{2+}-dependent response (Koide et al., 1988, Popov et al., 2012). Furthermore, increases in intracellular Na^+ can often lead to the acidification of the cytosolic environment mediated by the NHE. Consequently, this might lead to cytoskeletal changes, altered protein folding, as well as metabolic changes (Hulikova et al., 2013). Cardiac glycosides, and ouabain in particular (as one of the most intensively studied representative of the class), are also able to trigger cellular changes via NKA-mediated signalling, activating the Src kinase, as well as enhancing NKA association with the EGFR, thus leading to MAPK activation and subsequent transcriptional changes (Haas et al., 2000, Xie and Askari, 2002). Ouabain also induces ERK1/2 activation in a PKC-dependent manner (Mohammadi et al., 2001). Ouabain has also been shown to be produced endogenously in humans and rodents, at different levels, in different individuals (Manunta et al., 2009, Delva et al., 1989). This leads to individual differences in ouabain sensitivity. Endogenous ouabain also inhibits the NKA ionic function and triggers Src-mediated ERK1/2 and MAPK activator signalling events. Interestingly, an antihypertensive compound, PST 2238, also known as Rostafuroxin, was shown to function as a competitive inhibitor of endogenous ouabain (Ferrari, 2010). Rostafuroxin binds the NKA, destabilising the ion transport, but has no effect on the signalling function of the pump, and it could thus serve as a potential tool, to separate the impact of ionic disbalances and that of NKA-mediated signalling on cellular physiology (Ferrandi et al., 2004). Rostafuroxin was also shown to downregulate the pump activity in cells that present adducin-α hypertension-associated mutations ((mut)Y316F(WT) – in rat).

This is interesting given that such mutations are usually associated with increased expression and activity of the NKA (Torielli et al., 2008, Ferrandi et al., 2004, Ferrari, 2010)

Exogenous ouabain was reported to have cell type dependent effects. In most human cells ouabain is highly cytotoxic, inducing cell death. In rat cardiac myocytes, however, ouabain enhances survival by activating early response genes. This happens due to Na^+-dependent, yet Ca^{2+} independent, activation and dimerization of c-Jun and c-Fos, into the activator protein 1 (AP-1), which functions as transcriptional regulator of survival genes (Taurin et al., 2002). This occurs due to the fact that rat cardiac myocytes express ouabain insensitive NKA (NKAi) (Peng et al., 1996). Interestingly, some papers report upregulation of c-Jun/c-Fos also in human cells, which express ouabain sensitive NKAs (Fedorov et al., 2021, Klimanova et al., 2017). The activation of the AP-1 pathway by ouabain in specific cell types is particularly interesting given that fact that AP-1 has been reported to interfere with IFNγ-induced, STAT1-mediated gene expression, by recruiting the CREB-binding protein (CBP)/P300 complex to the AP-1 promoter, and preventing its association with phosphorylated STAT1 (pSTAT1) dimers (Ramana et al., 2000, Horvai et al., 1997, Peng et al., 1996). Cardiac glycosides were also shown to impact on cellular metabolism, activating the AMPK, decreasing oxygen consumption, as well as inhibiting OXPHOS and glycolysis in breast and lung cancer cells (Shen et al., 2020a). All these diverse and intertwined effects of cardiac glycosides suggest that apart from regulating Na^+ transport, these drugs are able to induce Na^+ independent changes within the cell, making them particularly difficult to study and understand.

Intracellular Na^+ levels can also be altered pharmacologically by either increasing Na^+ import, e.g., via VGSC openers, or by inhibiting Na^+ uptake with VGSC blockers. Na^+ import can also be regulated by inhibiting other types of channels, like ENaC – a known promoter of tumour cell proliferation and apoptosis inhibitor (Sparks et al., 1983, Vila-Carriles et al., 2006,

Bondarava et al., 2009), Na^+ co-transporters (e.g., SGLTs), or Na^+ anti-porters (e.g., NHE, NXC etc.) (Wright et al., 1997, Blaustein and Lederer, 1999, Bobulescu et al., 2005).

Tetrodotoxin (TTX) is a VGSC blocker, which was initially discovered in pufferfish, mostly located within ovaries and liver. It is considered a lethal marine substance with no known antidote to date. TTX has been reported to decrease proliferation of ER^+ and ER^- breast cancer cells, partially by preventing ERK1/2 phosphorylation (Mohammed et al., 2016). Furthermore, it was shown to reduce metastasis, while promoting survival in rats diagnosed with lung cancer (Yildirim et al., 2012). Alongside modulating cancer invasiveness by altering Na^+ dynamics, TTX has also been investigated in clinical trials for its ability to inhibit neuronal firing and thus stop transmission and detection of nociceptive signals in moderate and severe cancer patients, therefore, alleviating pain (Hagen et al., 2017, González-Cano et al., 2021).

Another VGSC-targeted drug is veratridine (VTD). Unlike TTX, VTD enhances the Na^+ transport function of VGSCs, by locking them in an open conformation. VTD is a C-nor-D homo-steroidal alkaloid that belongs to the *Veratum genus* found in *Liliaceae* plants. VTD was shown to induce reversible Na_v channel opening, and its activity seems to be inhibited by divalent ions, but also by TTX. It has been suggested that VTD interacts with the action-potential-regulated Na_v activation site (Catterall, 1975). Further studies showed that VTD binds within the Na_v vestibule and locks it in a persistent open conformation, reducing its single-channel conductance to ~ 25 % (Wang and Wang, 2003). More recent studies propose that VTD might be binding at alternative sites, interacting with Na_v channels allosterically, with the proposed site being the cytoplasmic mouth of the channel pore (Gulsevin et al., 2022).

Apart from preventing Na_v inactivation and thus prolonging persistent Na^+ currents, VTD was shown to also increase the intracellular Na^+ concentration, when applied acutely, with a subsequent rise in intracellular Ca^{2+}, followed by specific cellular responses, such as

neurotransmitter production by neurons (Gulsevin et al., 2022). In pancreatic cells, VTD was shown to promote insulin production in a Ca^{2+} dependent manner. This phenomenon was also shown to occur in Ca^{2+} free media, and it was suggested that a raise in intracellular Na^{+} might be mediating this effect, potentially by triggering release of Ca^{2+} from cellular stores (Lowe et al., 1976). In the context of cancer, some studies show that VTD might have anti-tumour properties, by inhibiting oncogenic proteins such as motalin-2 in colon cancer (Abdullah et al., 2015, Freeling et al., 2022). However, most studies show the complete opposite, suggesting that constant activation of VGSCs with VTD can increase colon cancer invasiveness by leading to constant activation of the MAPK pathway, as well as upregulating transcription of invasive genes via PI3K/ERK activation; this effect seemed to be reversed by TTX (House et al., 2015). In TNBC, as well, VTD was shown to promote invasiveness by inducing proteolytic activation of cysteine cathepsins B and S, via VGSC activity (Gillet et al., 2009b). Additionally, C-terminal domain-induced $Na_v1.5$ activation was also shown to induced epithelial to mesenchymal transition of breast cancer cells (Gradek et al., 2019).

Another class of drugs that can be used to alter intracellular Na^{+} levels is represented by ionophores. These are substances that are able to disrupt the ionic gradient across the membrane by transporting ions in and out of the cell (David and Rajasekaran, 2015). They can be synthetic or naturally produced (Kevin Ii et al., 2009, De Riccardis et al., 2013). Mechanistically these drugs can be classified as either channel or mobile ionophores (David and Rajasekaran, 2015). Mobile carriers can insert themselves into the lipid bilayer and form electrostatic interactions with ions, carrying them through the membrane and then releasing them on the other side. The two most widely studied such ionophores are monensin and salinomycin (Mollenhauer et al., 1990, Naujokat and Steinhart, 2012, Wang et al., 2018). They have been shown to have anti-tumour activity, preventing proliferation and drug resistance, as well as inhibiting oncogenesis in cancer stem cells and causing metabolic dysregulation (Naujokat and Steinhart, 2012, Huczyński, 2012). Monensin has been widely

studied for its ability to increase the intracellular Na^+ concentration. Monensin is a proton and cation electroneutral transporter, which means that negatively charged monensin radicals form a neutral molecule by complexing with either protons or positively charged metal ions, such as Na^+ (Inabayashi et al., 1995, Filipek et al., 1994, Hoogerheide and Popov, 1978, Pinkerton and Steinrauf, 1970). However, some studies reported that monensin might also form electrogenic complexes with Na^+, by complexing initially with a proton to form monensin acid, and then binding one Na^+ ion to form a molecule with an overall charge of +1 (Nakazato and Hatano, 1991, Huczyński et al., 2012a). Monensin is not specific for Na^+ in any way, and it can in fact carry a variety of mono-cations cross the membrane such as Li^+, K^+, Rb^+ and Ag^+ (Filipek et al., 1994, Huczyński et al., 2008, Pinkerton and Steinrauf, 1970). The ion-monensin complex is stabilised by intramolecular H-bond interactions between the carboxylate group of the molecule and two hydroxyl groups, often referred to in the literature as “head-to-tail” alignment (Turner, 1995).

Monensin was shown to impact on the overall ionic balance of the cells, by inducing a short action potential, decreasing Ca^{2+} current and activating the NCX, as well as activating the NKA, by elevating the intracellular Na^+ concentration (Tsuchida et al., 2021). Interestingly, in renal cells, the rate of monensin-induced increase in intracellular Na^+ was dependent on the concentration of extracellular Ca^{2+}. Furthermore, monensin-induced increases in cytosolic Na^+ in kidney cells were reported to interfere with dopamine-induced regulation of the NKA, suggesting that monensin can indirectly impact on NKA integrity (Efendiev et al., 2002). In breast cancer monensin was shown to inhibit expression of matrix metalloproteases 7 and 9, required for invasion, increase apoptosis of tumour cells and downregulate upstream binding protein 1 associated protein 2A (UB2A) protein, which is a receptor that mediates growth of pluripotent cells, preventing proliferation (Gu et al., 2020).

However, despite it being widely used in the literature for modulating intracellular Na^+ levels, the limitation of using monensin for mechanistic studies comes from its effects on cellular trafficking. Monensin is not only disrupting the plasmalemma, but also the Golgi membrane interfering with post-translational modifications, such as protein glycosylation, as well as trafficking; furthermore monensin is also able to trigger phenotypical and behavioural cellular changes via pH variations triggered by the transfer of H^+ across the membrane (Tsuchida et al., 2021, Gao et al., 2022, Efendiev et al., 2002, Mollenhauer et al., 1990, Huczyński et al., 2012a).

Changes in the dynamics of ions across the membrane and within the cell, particularly Na^+, can thus have severe consequences on physiological functions, with potential impact on cancer progression. Therefore, a better understanding of how ions impact on signalling events within the cell, could be a step forward in understanding and treating malignancies.

1.6. Linking everything together

Several studies report a possible connection between ionic transport and cancer immune evasion, as well as tumour metabolism (Djamgoz et al., 2019, Pardo and Stühmer, 2014). Na^+ channels have been linked to metastasis in several cancer types, and thus inhibitors of these channels were often shown to have beneficial effect on tumour progression (Djamgoz et al., 2019). Phenytoin, a VGSC inhibitor, was reported to inhibit metastasis in breast, lung, and prostate cancer (Yang et al., 2012, Nelson et al., 2015a, Abdul and Hoosein, 2001, Fraser et al., 2003, Onganer and Djamgoz, 2005). Other well documented VGSC inhibitors such as carbamazepine and ranolazine have been found to have similar effects particularly against breast cancer (Teichmann et al., 2014, Driffort et al., 2014). Interestingly, these drugs have also been shown to impact on the activity of the immune system, having mostly inhibitory

activity, which suggests that they might have applications also in the treatment of hypersensitivity or autoimmunity (Sorrell and Forbes, 1975).

The hub protein that is likely to connect ionic transport with metabolic regulation and cell signalling is however, the NKA. Specific inhibition of the NKA with drugs belonging to the cardiac glycoside class (e.g., digoxin, ouabain), was shown to impact not only on glycolysis and the Krebs cycle in tumour cells, but also on immune infiltration and cancer survival in mice (Sanderson et al., 2020, Shen et al., 2020a). Cardiac glycoside-dependent NKA inhibition might also be able to induce apoptosis and autophagy in glioma and hepatocellular carcinoma cancer cells, as well as in lung cancer cells, thus impairing cancer cell growth (Felippe Gonçalves-de-Albuquerque et al., 2017, Wang et al., 2012c). Interestingly, the NKA was also reported to regulate immune cell signalling. Increased NKA expression and elevated ion transport function were associated with interleukin-2 (IL-2) induced proliferation of T lymphocytes (Karitskaya et al., 2010, Redondo et al., 1986). In macrophages, the pump seems to have an immunosuppressive function, as its inhibition by cardiac glycosides induces activation of the proinflammatory master transcription factor, NF-kB. This response, however, is dependent on the simultaneous signalling from NKA, the Toll-like receptor 4 (TLR4) and the low-density lipoprotein (LDL) scavenged receptor CD36, suggesting a possible interaction amongst the three (Chen et al., 2017b). The immune implications of intracellular Na^+ variations are particularly interesting, given the predominant immunosuppressive microenvironment in breast tumours. Thus, in breast cancer, the NKA activity has been shown to promote resistance and metastasis, while inhibition of Na^+ import through VGSC blockage seems to prevent the metastatic phenotype (Khajah et al., 2018, Khajah et al., 2016).

Thus, literature supports a link between Na^+ dynamics via the NKA, metabolism and the immune response in cancer. A key regulator of tumour metabolism and immune evasion is

the kynurenine pathway. Studies have linked upregulation of kynurenine pathway enzymes (kynurenine monooxygenase and kynurinase) with the $HER2^+$ and TNBC breast cancer subtypes. These argue that upregulation of kynurenine pathway enzymes contributes to an immunosuppressive tumour microenvironment through metabolites like anthranilic acid and 3-hydroxyanthranylic acid (Heng et al., 2020). Other studies have shown that kynurenine 3-monooxygenase (another kynurenine pathway enzyme) induces expression of pluripotent genes, as well as upregulating the β-catenin pathway to promote progression of TNBC (Huang et al., 2020). Furthermore, IDO1-centered literature has also shown the importance of the kynurenine pathway in metabolic and immune regulation of breast cancer progression (e.g., IDO1 pharmacological inhibition in combination with chemotherapy was shown to decrease tumour size by 30 % in mouse $HER2^+$ breast cancer models (Muller et al., 2005); while IDO1-mediated Treg differentiation was associated with metastatic behaviour in breast tumours (Mansfield et al., 2009)). Overall, literature points toward an essential role of the kynurenine pathway and IDO1 regulation in breast cancer progression (Girithar et al., 2023)

The link between Na^+ dynamics, NKA activity, metabolic reprogramming, and cancer immune evasion, as well as the key role that the IDO1-centric kynurenine pathway plays in metabolic and immune regulation, suggest that these aspects of the tumour microenvironment might be intertwined. This work explores the connections between the ionic microenvironment, tumour metabolism and immune gene expression, by focusing on the IDO1-centric Trp metabolism.

1.7. Hypothesis and aims.

Given the elevated intracellular Na^+ levels associated with human breast tumours, as well as the complex physiological implications associated with functional integrity of the main intracellular Na^+ exporter, the NKA, this study aimed to investigate whether dysregulations in Na^+ physiology might impact on the ability of TNBC cells to evade the attack of the immune system, by interfering with the activity and expression of the immune checkpoint protein IDO1. The study was preceded by a 31-ion transport-targeted drug screen, carried out by Dr Mia Shandell, which identified the cardiac glycoside and NKA inhibitor, ouabain, as a potent IDO1 inhibitor.

Based on these preliminary data, the hypothesis for the first part of this study (Chapters 3 and 4) was formulated. It was hypothesized that fluctuations in intracellular Na^+ levels impact on the activity and/or expression of IDO1.

In the first part of the study, the aims were to understand how ouabain exerts its effects on IDO1 and the kynurenine response, unravel a potential mechanism, as well as investigate the effect of Na^+ on kynurenine production and IDO1 expression using a different, NKA-independent, mechanism of increasing intracellular Na^+ levels.

The hypothesis of the second part of this study (Chapters 5 and 6) was built on the results of the first part. It was hypothesized that, given the impact of cardiac glycosides (natural compounds) on the kynurenine response, other natural compounds might be able to interfere with IDO1-mediated immune evasion by disturbing Trp metabolism.

In this sense, the present study aimed to adapt the IDO1 activity assays for low-to-mid throughput purposes and use it to screen a library of 630 natural compounds for potential inhibitors of the kynurenine response, with lower toxicity that ouabain; it also aimed to investigate the mechanism of action and the impact on the Trp metabolism of potential hits,

as well as compare their metabolic effects to those of ouabain and a clinically tested selective IDO1 inhibitor (Linrodostat).

By completing this study, the ultimate goal was to better understand not only the connection between ionic dynamics and Trp metabolism, but also to unravel potential natural compound candidates to be investigated for breast cancer therapy.

2. Chapter 2: Materials and Methods

2.1. Cell culture

All materials were summarised in Appendix Table 8. 1.

2.1.1. Culture conditions (MDA-MB-231, A549 and HMEC cells)

Human triple-negative metastatic breast cancer MDA-MB-231 cells were provided by our collaborator, Mustafa Djamgoz, while the lung cancer cell line A549 was kindly gifted by the Tyson Sharp group. MDA-MB-231 cells are a TNBC cell line isolated from pleural effusion from a breast cancer patient in the 1970s; A549 cells originate from a type II pneumocyte lung tumour and were isolated around the same time (Cailleau et al., 1974, Swain et al., 2010). Thus, experiments were carried out in parallel in these cell lines due to their similar origin, similar culture conditions as well as due to both of these being reported in the literature as excellent study models for metastatic cancer (Liu et al., 2019a, Shindo-Okada et al., 2002); furthermore, lung is one of the primary sites for breast cancer metastasis alongside bone, brain and liver, thus justifying a comparison between MDA-MB-231 and A549 physiology (Jin et al., 2018, Patanaphan et al., 1988). Human primary mammary epithelial (HMEC CC-2551) cells from 2 donors were purchased from Lonza. All experiments with MDA-MB-231, A549 and HMEC cells were cultured at 37 °C, 5 % CO_2. MDA-MB-231 and A549 cells were cultured in Dulbecco's Modified Eagle's Medium (DMEM) (21969035, Gibco) supplemented with 10 % heat-inactivated Foetal Bovine Serum (FBS) (10439024, Gibco), 1 % L-glutamine (25030081, Gibco), and 1 % penicillin/streptomycin (15070063, Gibco). MDA-MB-231 and A549 cells were used for experiments for no longer than 10 passages from thawing (stock passage 16), the identity of the MDA-MB-231 cells was last checked on 13th February 2017 via short tandem repeat DNA profiling. The A549 cell line was acquired from the Barts Cancer Institute in 2017 and their identity has not been verified since then. HMECs were cultured using Mammary Epithelial Cell Growth Medium Bullet Kit (MEGM) (CC-3150,

Lonza), passaging was caried out using the Reagent Pack Subculture Reagents for primary cell subculturing (CC-5034, Lonza). HMEC cells were used for experiments on passages 3 to 7.

2.1.2. Seeding densities for MDA-MB-231, A549 and HMEC cells.

Knock down and pharmacology experiments were carried out using MDA-MB-231 or A549 cells, in 12-well plates at a density of 2.5 x 10^5/well. For pSTAT1 time-point experiments cells were seeded in T75 flasks to be about 80 % confluent on the day of the experiment. Only MDA-MB-231 cells were used for all experiments measuring intracellular Na^+ levels, seeded at 0.5 x 10^6 (unless otherwise specified in the figure legend) in a total volume of 100 µL/well in flat-bottom 96-well tissue culture-treated (GREINER 96 F-BOTTOM) plates. For the natural compounds screen described in Chapter 5, MDA-MB-231 cells were seeded at 0.7 x 10^5/well in flat-bottom 96-well tissue culture-treated plates. For the primary cell data in Chapter 5 (Figure 5.9), cells were seeded at 0.5 x 10^5/well in 100 µL media in clear 96-well flat-bottom plates. For the metabolomics experiments described in Chapter 6, cells were seeded at 4 x 10^6 in 10 cm tissue culture-treated dishes.

2.2. Pharmacology

For the data in Chapters 3 and 4, a number of small molecules that alter Na^+ transport or target downstream signalling elements responsive to ionic imbalances were studied. Table 2.1 summarizes the main compounds and concentrations used in Chaters 3 and 4, as well as one clinically studied IDO1 inhibitor, used in Chapters 5 and 6 (Linrodostat). Drug concentrations were selected based on previously determined or literature reported I/EC_{50} values, as well as literature reported effective concentrations for the specified cell lines.

Generally, cells were pre-treated with drugs (Table 2.1) for 18 - 24 h. For some experiments, siRNA or plasmid DNA transfection was carried out prior to drug treatment. Next, cells were washed once with PBS and treated with media containing drug and cytokine stimulation for

another 24 h. In the case of monensin experiments looking at IDO1 activity, the drug was added for 8 h prior to the cytokine stimulation and then removed, or for 8 h prior to cytokine stimulation and further kept in culture with the stimulation for another 24 h, or the drug was only added for the last 8 h of the cytokine stimulation. For monensin SBFI experiments the drug was applied acutely (immediately before data collection) or for 2, 4 or 8 h, without cytokine stimulation. For veratridine SBFI experiments the rug was applied for 1 min or 24 h, without cytokine stimulation. Exact details of the treatment protocols were specified in figure legends. For MDA-MB-231 and A549 cells the IFNγ (1 U/mL)/TNF (6.25 ng/mL) cytokine stimulation was used. For HMEC cells, cytokines were supplemented to the culture medium to give a final well concentration of IFN-γ (100 U/mL)/TNF (6.25 ng/mL).

For the screen results in Chapter 5, details of the compounds used were summarised in the Appendix Table 8. 2. All compounds were used at 10 µM in 0.1 % DMSO, with the exception of ouabain which was used at 200 nM in 0.1 % DMSO.

Drug	Concentration						I/ EC_{50}/ Literature recommended concentration	Cell line used in this study
Ouabain	50 nM		100 nM		200 nM		88.9 nM*	MDA-MB-231
Digoxin	75 nM		150 nM		300 nM		164.1 nM*	MDA-MB-231
Ouabain	10 nM		25 nM		50 nM		16.9 nM*	A549
Digoxin	25 nM		50 nM		100 nM		39. 9 nM*	A549
Veratridine	25 µM						10 - 50 µM	MDA-MB-231
Monensin	50 nM	1 µM	10 µM	50 µM	100 µM	500 µM	10 µM	MDA-MB-231
HG-9-91-01	500 nM			1 µM			0.92 µM (Determined *in vitro*)	MDA-MB-231
Linrodostat (Chapters 5 and 6)	1 nM		10 nM		100 nM		1.1 nM (Determined in HEK293 cells)	MDA-MB-231

*Table 2.1. Key drugs and corresponding concentrations – Summary. Concentrations marked with a * were determined experimentally as shown in Figure 3.1, all other concentrations were taken from literature reports (Gillet et al., 2009a, James et al., 2022, Clark et al., 2012, Siu et al., 2017, Tang et al., 2021).*

2.3. Natural compound screen (MDA-MB-231 cells)

2.3.1. Set-up

A 630-natural compound screen was carried out using MDA-MB-231 cells. Drug plates were prepared in advance, all at once, by aliquoting 1 µL per well of 10 mM drug solution in 100 % DMSO in 700 µL 96-well v-bottom plates (LABPRO services, SKU: DP11VR-9-GC100-CS). For ouabain controls 4 µL of 50 µM ouabain 1 % DMSO topped up with 0.96 µL 100 % DMSO were added to corresponding wells. While for the DMSO controls 1 µL DMSO per well was added. The plates were then stored at -80 ˚C until the day of the screen. On the day of the screen, compounds were topped up with complete DMEM and added to the cells to give a final well volume of 250 µL, with a final well concentration for natural compounds of 10 µM in 0.1 % (v/v) DMSO. The well concentration for ouabain was 200 nM, in 0.1 % (v/v) DMSO, chosen based on previous experiments (Shandell et al., 2022) (plate layout presented in Figure 5.4B). Drug pre-treatment was carried out for 18 h, cytokine stimulation was then added straight into the culture media for another 24 h to give a final well concentration of IFNγ (1 U/mL)/TNF (6.25 ng/mL). Supernatants were then collected for the kynurenine assay and remaining cells were used to measure viability.

2.3.2. Analysis: Compounds of Interest (COIs) and Hits Selection

Two selection criteria based on the effect of compounds on kynurenine were used for the screen. The standard deviation (SD) method was applied by firstly calculating the SD for the vehicle control. Next the following formula was applied to calculate variation in the kynurenine levels:

$$X=\frac{Sample\ Kyn-Mean\ Vehicle\ Kyn}{Vehicle\ SD}.$$

A second method looking at fold change in kynurenine compared to the vehicle control was also applied, using the following formula:

$$Y=\frac{Sample\ Kyn}{Mean\ Vehicle\ Kyn}.$$

In addition to the kynurenine-based selection criteria, the following formula was used to calculated viability fold change:

$$Z=\frac{Sample\ Viability\ (570\ nm-600\ nm)}{Mean\ Vehicle\ Unstimulated\ Viability\ (570\ nm-600\ nm)}.$$

For the first round of screening compounds that gave a fold change in kynurenine levels (Y) $\leq \mathbf{0.5\ or} \geq \mathbf{1.4}$ OR a change in kynurenine equivalent to (X) $\geq \mathbf{3\ or} \leq \mathbf{-3}$ SDs away from the vehicle control, while maintaining viability fold change (Z) ≥ **0.7,** were considered COIs. Both replicate plates were included in the fold change and viability analyses. For the SD analysis a quality control was applied, so that only plates where the controls were separated by least 3 SDs were included in this analysis; replicate plates that did not pass this quality control were only used to verify patterns for potential COI exclusion.

For the validation round, the same type of analysis was applied as for COIs, with the exception of the fact that hits had to give a fold change in kynurenine levels (Y) $\leq \mathbf{0.5\ or} \geq \mathbf{1.4}$ AND a change in kynurenine equivalent to (X) $\geq \mathbf{3\ or} \leq \mathbf{-3}$ SDs away from the vehicle control while maintaining viability fold change (Z) ≥ **0.7.**

The intra assay coefficient of variation (CV) was calculated for all the controls and all the treatment conditions included in the initial screen. For each sample, CV was calculated using the following formula, also documented by Schultheiss and Stanton (2009):

$$CV_{sample}=\frac{SD\ of\ technical\ replicates}{Mean\ of\ technical\ replicates * No\ of\ technical\ replicates} * 100.$$

Each control from the two replicate plates corresponding to one set of 63 drugs was treated as one sample. The average of all $CV_{samples}$ gave the CV of the entire screen.

2.4. Metabolomics experiments (MDA-MB-231 cells)

2.4.1. Set-up

For metabolomics experiments, cells were treated with 200 nM ouabain 0.1 % DMSO, or 100 nm Linrodostat (Generon, M6248) in 0.1% DMSO or 10 µM of the corresponding natural comound (artemether and Euphorbia factor L9, ChemFaces, CFN99184 and CFN92887, respectively) in 0.1 % DMSO for 18 h; a DMSO-only control was also set up. Cytokines were supplemented directly into the culture media for another 24 h, to a final concentration of IFNγ (1 U/mL)/TNF (6.25 ng/mL). Kynurenine assays were performed on the supernatants. Supernatant and cell lysates were collected using the freeze-thaw protocol described in Rushing et al. (2022).

2 µL of sample were injected onto a Thermo Vanquish Flex Liquid Chromatography (LC) system fitted with a Waters High Strength Silica T3 column (100 x 2.1 mm). Mobile phases were A: water + 0.1% formic acid (v/c) and B: methanol + 0.1% formic acid (v/v). Samples were eluted over a 10 min gradient as follows: 0-16 min 2-100 % B; 16-20 min isocratic 100 % B; 20-20.1 min to 2 % B; 20.1-30 min re-equilibrate at 2 % B. The column was held at 50 °C and flow rate was 0.4 mL/min. The eluate was sent to a Thermo Orbitrap Fusion instrument between 0.6 and 28 min, fitted with a Heated Electrospray Ionization source operating in positive ion mode (sheath gas 50 units, auxiliary gas 10 units, sweep gas 1 unit, spray voltage 3500V, vaporizer 325°C, ion transfer tube 275°C). The mass spectra (MS) 1 and MS2 data were completed at an orbitrap resolution of 60,000 full width at half maximum (FWHM), with a 0.4 s cycle time. MS1 data was collected between 70 - 1050 m/z. Easy internal calibration was used to achieve mass accuracy < 1 parts per million (ppm). MS2 data was collected alternating between Higher Collisional Dissociation mode with stepped collision energies (35, 40, 45 %) and Collision-Induced Dissociation Mass Spectrometry mode with a fixed collision energy of 40 %. Dynamic exclusion was set for n = 1 over 4s. Once

collected, all files were converted to centroided. mzML and mgf formats using ProteoWIzard msconvert.

2.4.2. Analysis

For metabolomics analysis data were processed through bespoke XCMS scripts, provided by the Metabolomics department at the University of York, looking for exact MS1 matches to the Trp pathway metabolites, with annotations verified and additional annotations added using high-resolution MS2 data processed through Sirius.

The raw data files were converted to centroided. mzML and mgf formats using ProteoWIzard msconvert. The. mzML format files were used as inputs for feature detection using bespoke scripts written in R with functions from the XCMS (Smith et al., 2006, Tautenhahn et al., 2008, Kuhl et al., 2012). Features were detected with the centWaveWithPredictedIsotopeROIs method, with the following function parameters: ppm = 10, signal to noise threshold (snthresh) = 3, range of peak elution times (s) (peakwidth) = c (2, 10), peak definition: number of data points exceeding a set intensity threshold (prefilter) = c (3, 1000), integration method for peak quantification (integrate) = 2 (real data), accepted closeness of two signals in m/z dimension (mzdiff) = -0.1. Duplicate features and features outside the time between 0.7 and 28 min were removed using custom scripts. Features were subsequently grouped using a modified scms group () function. Adducts and isotopes were detected using CAMERA. Feature MS1 values were matched to a custom database comprising predicted [M+H]+ or [M+H]+ ions of the Trp pathway as defined by pathway ID SMP0000063 in the HMDB (Wishart et al., 2007). The best representative MS2 spectra (defined as nearest to the MS1 precursor feature apex) were extracted with custom scripts from the .mgf files and converted to .ms2 format using custom scripts for input into Sirius. Feature tables were initially filtered to: 1) only retain features found at least once in any sample with an area value greater than the mean + 3 x the SD value of blank samples; then 2) retain any features with a HMDB

database hit; then 3) retain features that are probably monoisotopes (as calculated by CAMERA). Sirius matching was then performed on available initially filtered features, using Sirius 5.8.2 (Dührkop et al., 2019, Dührkop et al., 2021) all default databases and instruments were set to Orbitrap with 5 ppm tolerance. Sirius outputs were merged with feature tables. These were manually further edited to remove redundant and near-baseline features and reconcile HMDB and Sirius annotated features.

2.5. siRNA transfections

All transfections were performed in 12-well tissue culture-treated plates, using the 12 µL/reaction mix of TransIT-siQUEST Transfection Reagent in 87 µL OptiMEM; 99 µL of the TransIT-siQuest-OptiMEM mix were then added to 981 µL of siRNA-OptiMEM solution (final siRNA concentration: 25 nM); 160 µL of the TransIT-siQuest-OptiMEM-siRNA reaction mix were added to 640 µL OptiMEM to each well. Untransfected wells were kept in 800 µL Opti-MEM. Appendix Table 8.1 summarizes the details about the transfection reagents and siRNAs used. Transfections were allowed to proceed for 5 h then cells were washed once with PBS and transfection media was replaced with either culture media (supplemented DMEM) alone, or culture media containing drug (section 2.2)

2.6. DNA plasmid transformations

A pCMV6-Entry-Myc-ATP1A1 (NM_000701, PS100001) (Origene, RC201009) plasmid and a pcDNA3.1 +/C-(K) DYK – ATP1A1-FLAG (NM_000701.8) were used for ATP1A1 overexpression experiments. A pCMV3-C-Flag-NCV (SinoBiological, CV012) empty vector was used as a negative control form both plasmids for optimised transfections. A pcDNA3.1 plasmid was kindly supplied by the Hitchcock group at the University of York.

For each plasmid, 30 µL competent E. coli (DH5α) were transformed with 50 ng DNA, and kept on ice for 30 min, cells were then heat-shocked for 45 s at 42 °C and transferred on ice for 2 min. 700 µL of warm LB broth (antibiotic-free, prepared as per manufacturer protocol, Thermo Fisher, L3022) were added to the cells, followed by 1 h incubation at 37 °C. Cells were then seeded on kanamycin (50 µg/mL) LB agar (Lennox LB Agar, Thermos Fisher 22700025) plates and incubated over night at 37 °C.

2.7. DNA plasmid prep

MiniPrep

A single bacterial colony was collected using a sterile tip and transferred to 5 mL of LB broth with kanamycin (50 µg/mL). The culture was kept shaking at 37 °C over night. Plasmid isolation was carried out using the QIAprep Spin Miniprep Kit, following the supplier protocol (QIAgen, 27104).

Midiprep

A single bacterial colony was collected using a sterile tip and transferred to 5 mL of LB broth with kanamycin (50 µg/mL). The culture was kept shaking at 37 °C for 8 h. 200 µL of this pre-culture were transferred into 50 mL of LB broth (50 µg/mL kanamycin) and incubated shaking at 37 °C over night. Plasmid isolation was carried out following the HiSpeed Plasmid Midi Kit, according to the supplier protocol (QIAgen, 12643).

2.8. DNA transfections

JetPrime

pCMV6-MYC-ATP1A1 transfections were carried out using JetPRIME transfection reagent (Polyplus, 114-01). 1 µg DNA and transfection buffer were first mixed, then transfection reagent was added to keep a 2/1 v/w ratio with DNA. The total reaction volume per sample was 75 µL. Following a 10-min room temperature (RT) incubation, the reaction mix was

added to the cells growing in complete growth media. The transfection was allowed to proceed for a minimum of 4 h. Cells were then washed with PBS and left over night in complete growth media. On the next day, either ouabain or media was added for 24 h. For pCMV6-MYC-ATP1A1 transfection, 24 h post ouabain treatment, cytokine stimulation was added for another 24 h. Samples were then collected for western blots, or kynurenine assays.

Lipofectamine™ 3000 Transfection Reagent

pcDNA3.1-ATP1A1-FLAG transfection were carried out using Lipofectamine 3000 transfection reagent (L3000001, Thermo Fisher). 2.5 µg DNA per sample was mixed with P3000 in 1/2 w/v (µg/µL) ratio; the mix was diluted in 125 µL OptiMEM reagent. Separately, 10 µL Lipofectamine was diluted in 125 µL OptiMEM. Next the DNA and Lipofectamine solutions were mixed into 1/1 v/v ratios and incubated for 15 min RT. Next 250 µL of the DNA-Lipofectamine transfection mix were added dropwise to cells in complete media (2 mL). The transfection was allowed to proceed for a minimum of 4 h. Cells were then washed with PBS and left overnight in complete growth media. On the next day, either ouabain or media was added for 24 h. Next, cytokine stimulation was added for another 24 h. Samples were then collected for western blots, or kynurenine assays.

2.9. The kynurenine assay.

2.9.1. Set-up

All kynurenine assays were carried out on culture supernatants in 96-well tissue culture plates. For each kynurenine assay a set of 8 standards, ranging from 0 to 100 µM, was prepared. 150 µL supernatants/standards were transferred to a U-bottom 96-well plate. These were treated with 10 µL 30 % 6.1 N Trichloroacetic acid for 30 min at 50 °C. 100 µL of each sample/standard were then transferred to a new 96-well flat-bottom plate and topped up with 100 µL 1.2 % Ehrlich's reagent in glacial acetic acid. Following a 10 min RT incubation,

absorbance at 492 nm was measured using either a CLARIOstar (BGM Labtech) or VersaMax (Molecular devices) plate reader(Grant et al., 2000, Takikawa et al., 1988) (Figure 2.1).

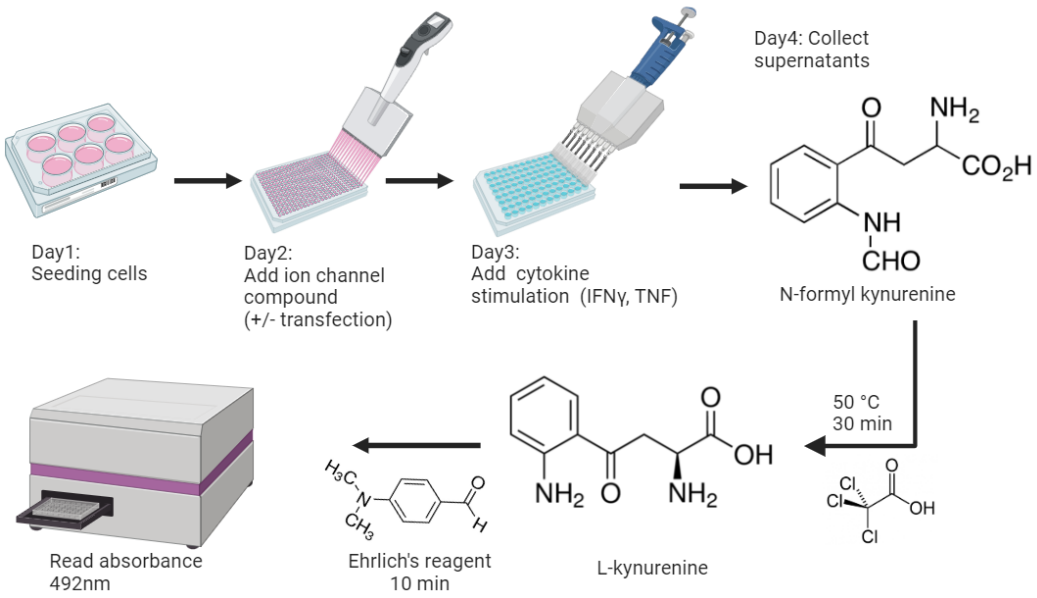

Figure 2.1 The kynurenine assay. N-formylkynurenine from the supernatants is converted to L-kynurenine using trichloro acetic acid (50°C, 30 min), then Ehrlich's reagent is used to allow detection of an absorbance signal at 492 nm[5]. Absorbance was detected using either a CLARIOstar (BGM Labtech) or a VersaMax (Molecular devices) plate reader.

2.9.2. Analysis

A set of calibration wells were used to generate a standard curve (simple-linear regression analysis) which was then used to calculate kynurenine concentrations. Concentrations were plotted in GraphPad Prism v9.0.0 as means and SD. Figure 2.2 shows a representative calibration curve for they kynurenine assay and the associated equation used to convert absorbance values into concentrations (µM).

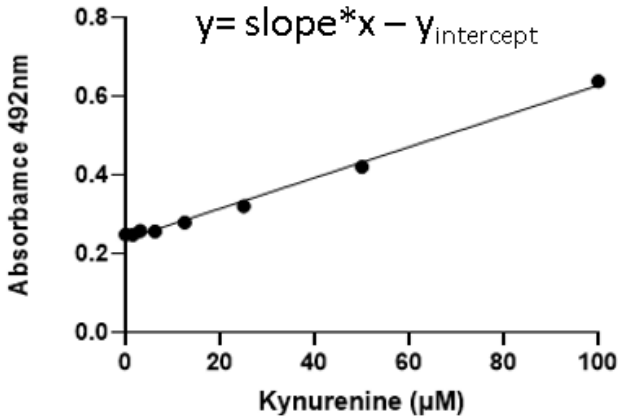

Figure 2.2 Representative kynurenine assay calibration curve and associated equation. Y – corresponds to the absorbance values, x – corresponds to the concentration.

2.10. Viability

Viability was mainly assessed through automatic cell counting. Cells were lifted with 0.05 % Trypsin-EDTA (25300054, Gibco) and stained with trypan blue (T10282, ThemoFisher Scientific), counting was done automatically using a Countess II FL Automated Counter (C10283, Thermo Fisher Scientific).

A plate-based measurement was used to assess viability for experiments where counting individual cells was considered detrimental, either due to large number of samples, or in order to reduce the stress to which cells were exposed (e.g., the natural compound screen, for primary HMECs experiment). The method of choice for assessing cell viability was specified in each figure/figure legend. For plate-based measurements, the Deep Blue Viability dye was added to the cell cultures at a 1:10 ratio with the supernatant volume. Cells were incubated at 37 °C, 5 % CO_2 for 4 h and viability was then measured by reading optical density (OD) at 570 and 600 nm, using either a CLARIOstar (BGM Labtech) or VersaMax (Molecular Devices) plate reader. The absorbance value recorded at 600 nm was then subtracted from the 570 nm absorbance value, to give a measure of cell viability. The given numbers were then normalized (fold change calculations) to the corresponding control (the most viable condition, according to the experimental design) to give a ratio corresponding to sample viability.

2.11. Measurement of cytosolic sodium concentration using Sodium-binding Benzofuran Isophthalate Acetoxymethyl Ester (SBFI-AM)

2.11.1. Set-up

A 10x stock of 144 mM Na^+ physiological saline solution (PSS) and a 10x K^+ saline solution were prepared, no D-glucose was added. These were kept at 4 °C for further use. The 10x stocks were diluted in double-distilled water to 1x and the corresponding amount of D-glucose was added (*1x Na^+ PSS composition:* NaCl 144 mM, KCl 5.4 mM, $MgCl_2$ 1 mM, HEPES

5 mM, $CaCl_2$ 2.5 mM, D-glucose 5.6 mM; *1xK^+ PSS composition:* KCl 149.4 mM, $MgCl_2$ 1 mM, HEPES 5 mM, $CaCl_2$ 2.5 mM, D-glucose 5.6 mM). The pH was adjusted to 7.2 and the solutions were then filtered. These were kept at 4 °C for no longer than 7 days before use. To make up the calibration solutions, Na^+ and K^+ saline solutions were mixed in the corresponding ratio to dilute the 1x Na^+ PSS from 144 mM Na^+ to 0, 25, 50, 75 and 100 mM Na^+.

MDA-MB-231 cells were seeded as described in section 2.1 and treated with the corresponding drugs (Table 2.1). For experiments that included cytokine stimulation, IFNγ (1 U/mL) and TNF (6.25 ng/mL) were also added at the same time with the drugs. Calibration wells were set-up and kept in fully supplemented growth media. 22 h post treatment all samples were washed once with drug/drug-cytokine solutions made up in DMEM (no supplements). Samples were then left for 2 h in 10 µM SBFI-AM and 0.1 % Pluronic acid drug/drug-cytokine solutions made up in DMEM (no supplementation). Calibration wells and samples that did not receive drug treatment were also treated with an SBFI-AM - Pluronic acid DMEM solution. Blank wells were kept in un-supplemented DMEM. After 2 h of SBFI incubation samples were washed twice with drug/drug-cytokine solutions made up in 144 mM Na^+ PSS and left in 200 µL/well of these solutions. Calibration wells were washed with PSS solutions of different Na^+ concentrations: 0, 25, 50, 75 and 100 mM and were left in 200 µL of these solutions supplemented with 20 µM Gramicidin. A CLARIOstar (BGM Labtech) plate reader was used to quantify intracellular Na^+ by exciting samples at 340 and 380 nm and recording fluorescence at 510 nm, every 5 min for 20-30 min.

For 12-well plate siRNA transfections, cells were transferred to a 96-well plate on day 2 post transfection via trypsinisation and SBFI staining was carried out 24 h post transfer.

2.11.2. Analysis

Fluorescence data in response to excitation at 340 and 380 nm were collected for all samples. 340 and 380 fluorescence values were blank corrected by subtracting the average value of

the blank wells (no SBFI) at each excitation wavelength from the value of each sample at the same excitation wavelength. Then 340/380 ratios were then calculated for each sample. Based on the 340/380 values for the calibration wells, the timepoint at which the intracellular Na^+ concentration stabilised was identified for each experiment. The rest of the analysis was carried out with the data corresponding to the identified timepoint. Signal to noise ratios (SNR) were also calculated for each excitation wavelength using the formula:

$$SNR\ wavelength\ 1 = \frac{blank\ corrected\ fluorescence\ at\ wavelength\ 1}{average\ blank\ fluorescence\ at\ wavelength\ 1} \times 100.$$

All samples/calibration wells that had a signal to noise ratio at 380 nm < 20 were excluded. A calibration curve was then plotted using a Pade (1,1) Approximant analysis in GraphPad Prism v9.0.0 and was used to convert fluorescence ratios into Na^+ mM concentrations. Figure 2.3 shows a representative example of timepoint selection (A) and calibration curve representation (B).

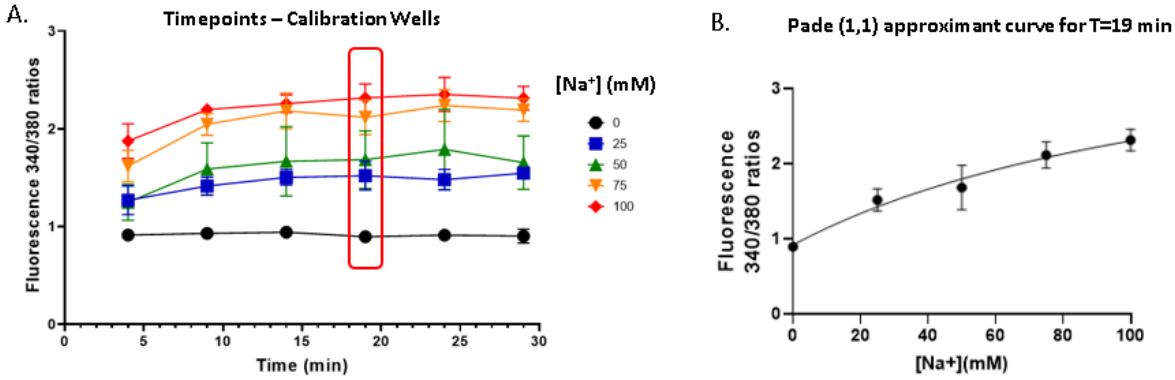

*Figure 2.3 Representative SBFI analysis. A. 340/380 fluorescence ratios for calibration wells at multiple timepoints; B. Pade (1,1) approximant calibration curve for the selected timepoint (T=19 min in A). The equation associated with the curve in B was used to convert fluorescence ratios to concentration values. The equation corresponding to the curve in B is Y= (A0 + A1*X)/ (1 + B1*X), where A0, A1 and B1 were calculated automatically by Graph Pad Prism, y – corresponds to the fluorescence ratio, x – corresponds to the concentration.*

2.12. Protein extraction

Cells were harvested using radioimmunoprecipitation assay (RIPA: 5 mM EDTA, 150 mM NaCl, 10 nM Tris-HCl pH 7.2, 0.1% SDS, 0.1% Triton X-100, 1% sodium deoxycholate) lysis buffer supplemented with protease inhibitory complexes P8340, P5726, and P0044 (1 in 100 dilution). Samples were centrifuged for 10 min at 4 °C 10 000xg. To determine the protein concentration of each sample, 2 µL sample supernatant were diluted in 10 µL PBS; 5 µL of the dilution were added to a 96-well plate, topped up with 95 µL Bicinchoninic Acid Assay (BCA) Reagent A/Reagent B mixture (49/1 v/v ratio) and incubated at 37 °C for 30 min. Absorbance values were recorded at 562 nm. A set of bovine serum albumin (BSA) standards, serially diluted 1 in 2, with concentrations ranging from 1 or 0.031 mg/mL were used to convert the absorbance values to concentrations, by plotting a simple linear regression curve. These were then used to calculate the required volume of sample equivalent to 10 µg of protein, to be used for western blot assays.

2.13. Western Bolt

Samples for western blot were collected using RIPA lysis buffer supplemented with protease inhibitory complexes P8340, P5726, and P0044 (1 in 100 dilution). Most experiments were carried out without boiling the samples, unless otherwise specified in figure legends; for SRC3 KD westerns (section 8.2.2.) the samples were boiled for 5 min at 90 °C. For the western blot electrophoresis, 10-20 µg of protein per sample were loaded on a 10 % SDS-PAGE gel and run for 1 h and 30 min at 120 Volts on a Bio-Rad PowerPac HC. The resolving (Acrylamide 9.9 %, Tris Buffer 4.5 % pH 8.8, SDS 0.1 %, ammonium persulfate 0.1 % and TEMED 0.04 %) and staking (Acrylamide 4.18 %, Tris Buffer 1.28 % pH 6.8, SDS 0.083%, ammonium persulfate 0.083 %, TEMED 0.083 %) gels were made in house. Running buffer (UltraPure Tris 3 g/L, SDS 1 g/L, Glycine 14.4 g/L, pH 8.3) was also made up in house.

Semi-dry transfer was carried out for 1.5 h at 25 V (Chapter 3) using a Trans-Blot SD Cell machine (BioRad), and for 10 min at 25 V using a Trans-Blot Turbo fast-transfer machine (BioRad) (Chapters 4, 5 and 6) on polyvinylidene difluoride (PVDF) membranes. Membranes were blocked with 2 % (w/v) BSA for 30-60 min. Primary antibody incubations were carried out overnight at 4 °C, apart from GAPDH which was incubated for 1 h at RT. A list of all the primary antibodies used can be found in Appendix Table 8.1. Secondary antibody incubations were carried out for 30-60 min at RT. Imaging was carried out using ECL™ Blotting Reagents (GE Healthcare, GERPN2109) and X-ray 100ST Amersham Hyperfilm ECL (Life Science products Cytiva, 15497394) on a Medical Film Processor SRX-101A (Konica Minolta). Between each step 3x 5-minute Tris-buffer saline -Tween (TBS-T) washes were performed.

2.14. Real-Time Quantitative Reverse Transcription PCR (qRT-PCR)

2.14.1. Set-up

Samples were collected using QIAzol lysis reagent and RNA was isolated by chloroform extraction and purified using the QIAgen RWT and PE RNA extraction buffers; RNA was then eluted in 30 µL nuclease-free water, according to recommendations from the manufacturer (QIAzol Lysis protocol and QIAgen RNeasy protocol). For cDNA synthesis two PCR master mixes (MM) were prepared. MM1 consisted of random hex primers (50 ng/mL), deoxynucleotide triphosphates (dNTP) and nuclease-free water in a 1:1:9 ratio. 11 µL of MM1 were added to each sample containing 1.5 µL RNA. These were transferred to a MicroAmp Fast Optical 96 well plate PCR Thermal Cycler (Applied Biosystem) and kept for 1 min at 4 °C, followed by denaturation for 5 min at 65 °C and cooling for 1 min at 4 °C. Once denaturation was complete, the samples were topped up to 20 µL with MM2, consisting of 5x FS Buffer, 0.1 M Dithiothreitol (DTT), RNase OUT 40 U/µL and Super Script II RT 200 U/µL in an 8:4:2:1 ratio. Annealing and polymerization were achieved by sequentially keeping samples for 10 min at 25 °C, followed by 50 min at 50 °C; the polymerase enzyme was then

denatured by increasing the temperature to 85 °C for another 5 min, once the reaction was complete, the samples were stored at 4 °C.

qRT-PCR was performed using Fast SYBR Green (Applied Biosystems, 4385610). All targets were amplified using forward and reverse primers (Sigma Aldrich), except for ATP1A1 and IDO1 which were amplified using QIAgen QuantiTect primers (sequences were included in Appendix Table 8. 1). Forward and reverse primers were mixed as follows: 0.6 µL of each type of primer were added to 7.8 µL water and 10 µL SYBR Green. QuantiTect primers were mixed as follows: 2 µL primers were added to 7 µL water and 10 µL SYBR Green for each reaction. The working primer concentration was 10 µM. 1.5 µL cDNA was added to the 19 µL of primer mix. qRT-PCR was run on a StepOne FASTPlus qPCR machine, by warming up the samples to 95 °C for 20 s, then completing 40 cycles of samples held at 95 °C for 3 s and cooled to 60 °C for 30 s, according to the manufacturer instructions (Applied Biosystems StepOne™ and StepOnePlus™ Real-Time PCR Systems User Bulletin).

2.14.2. Analysis

The threshold for qPCR was set at 0.1. Data were then analysed by calculating the $2^{(-\Delta CT)}$ value in Microsoft Excel, with GAPDH or β-actin normalisation, as specified in figure legends (Livak and Schmittgen, 2001). Fold change was calculated by normalising to the average value for the given gene, across all conditions, or by normalising to the value for the given gene in the positive control, as specified in figure legends. These values were then plotted in GraphPad Prism v9.0.0.

2.15. IDO1 enzyme activity assay

2.15.1. Set-up

An assay buffer was prepared by making up a 50 mM solution of 2-Morpholinoethanesulphonic acid (MES) in water. The assay buffer solution was split in two

tubes for the experiment described in this study (Figure 6.1) and the solution in each tube was adjusted to pH 6.5 using either NaOH or KOH, to verify if the presence of Na^+ in the assay buffer directly interferes with IDO1 activity.

A 96-well tissue culture plate was loaded with the corresponding compounds/DMSO to give the final concentrations described in Table 2.2, for a final assay volume of 100 µL. Then, the recombinant human IDO1 enzyme was diluted in assay buffer to ~16 ng/µM.

Next, a substrate mixture was prepared by making up two intermediate solutions. Firstly, an 80 mM ascorbic acid solution was made up in 0.405 M Tris (pH 8). Secondly, L- Trp, catalase and Methylene Blue were diluted in assay buffer to 800 µM, 9000 units/mL and 40 µM, respectively.

The two intermediate solutions were combined in a 1:1 ratio, immediately before addition to the enzyme, to give a final substrate mixture solution consisting of 40 mM ascorbic acid, 400 µM Trp, 4500 units/mL catalase and 20 µM Methylene Blue. Then, the enzyme was added to the compound plate (50µL enzyme mix, equivalent to 0.8 µg enzyme/well), and 50 µL of substrate mixture was added immediately to the enzyme. The plate was then transferred into a CLARIOstar (BGM Labtech) plate reader and absorbance at 321 nm was recorded every 30 seconds for 30-40 min.

COMPOUND	FINAL COMPOUND CONCENTRATION/WELL
DMSO	0.1 %
LINRODOSTAT	10 µL
	100 nM
ARTEMETHER	10 µL
EUPHORBIA FACTOR L9	10 µL

Table 2.2 Final concentrations of compounds for the IDO1 activity assay.

2.15.2. Analysis

The raw data at each timepoint was blank corrected (blank subtraction) then plotted for each condition. The linear restriction of the enzyme activity Vs time curve for all conditions was selected (timepoints 0 to 1000 s). A simple linear regression curve was then fitted for each condition and the slope of each curve was then in GraphPad Prism v9.0.0 This analysis was completed for each individual replicate. The slopes were then plotted as bar graphs (mean and SD) and statistical analysis was carried out to evaluate any significant changes across conditions.

2.16. Statistical analysis

For all data (except for the *in silico* and metabolomics analysis) statistical analysis was carried out in Graph Pad Prism v9.0.0. All experiments were carried out with an n=1, 2, 3 or 4 biological repeats; therefore, the sample size was too small to perform normality analysis confidently, and normal distribution was assumed for all data. All data were thus plotted as means and SD, and statistical analysis was performed using an ordinary one-way ANOVA, or for more complex data sets with more than one variable, treatment conditions were compared using a two-way ANOVA. The following multiple comparisons tests were used:

Tukey's (coupled with a one-way or two-way ANOVA when all conditions were compared to each other), Bonferroni's (coupled with a one-way or two-way ANOVA when specific pairs of conditions were compared). A two -way ANOVA was also paired with a with a two-stage linear step-up procedure of Benjamini, Krieger and Yekutieli, to account for multiple comparisons (false discovery rate), for experiments that combined a large number of variable conditions (transfection combined with drug titration). For comparisons of two groups an unpaired, two-tailed t-test was used.

For the *in silico* analysis (Figure 4.7) TCGA and METABRIC data sets were merged using RStudio 1.4.1717. A list of STAT1-regulated genes and SIK1-cooexpressed or targeted genes was compiled from the Harmonizome tool (CHEA Transcription Factor Targets; NCBI Entrez Gene Database, 6772; GeneRIF Biological Term Annotations; PhosphoSitePlus Substrates of Kinases), (Brown et al., 2015, Mitchell et al., 2003, Hornbeck et al., 2004, Hornbeck et al., 2015, Lachmann et al., 2010). Bivariate Pearson correlations were calculated in R Studio using the rcorr() function; heatmaps were plotted using the corrplot package. Kaplan Meier (KM) survival plots were generated using the ggsurvplot() function.

For statistical analysis of the metabolomics data (Chapter 6), the Metaboanalyst software was used. Metaboanalyst applied a data integrity check to each set of data uploaded, excluding metabolite entries that exhibited constant or no value for all the treatment conditions included in the data set. All data sets were median normalized and $\log_{10}$ transformed. Principal component analysis was used to verify correct clustering of the data based on treatment conditions. Statistical analysis was carried out using an unpaired t-test and fold change analysis. The data was plotted as a volcano plot and metabolites of interest were selected based on the following thresholds: p value (false discovery rate corrected, FDR) ≤ 0.1 and fold change value ≥ 1.5.

3. Chapter 3: Results. Connecting Na^+/K^+ transport to tryptophan catabolism: a novel pathway in breast cancer cell immune escape.

3.1. Introduction

3.1.1. Background

The elevated intracellular Na^+ levels within the central hypoxic core of breast tumours have led researchers to question whether ionic dynamics, and in particular Na^+ accumulation, might play an active role in tumour cell survival, metastasis, and immune evasion (Ouwerkerk et al., 2007). One important mechanism through which cancer cells preserve their integrity is via immune checkpoints. These are proteins involved in cancer-immune interaction, which function as suppressors of the immune response against tumours, via different mechanisms (Pisibon et al., 2021). This chapter focuses on the immune checkpoint protein IDO1, described in more detail in sections 1.3.6 and 1.4.3. IDO1 is a metabolic enzyme expressed by cancer cells in response to IFNγ stimulation, which converts the amino acid tryptophan (Trp) from the tumour microenvironment to N-formylkynurenine. In this way, IDO1 triggers effector T cell Trp starvation and it induces differentiation of the naïve T cells into an immunosuppressive phenotype, called regulatory T cells (Tregs) (Hornyák et al., 2018).

3.1.2. Hypothesis and aims.

Multiple studies have linked Na^+ dynamics and cancer immune evasion, as described in more detail in sections 1.5 and 1.6 (Djamgoz et al., 2019, Leslie et al., 2019). This chapter investigates the link between the main Na^+ exporter, the NKA and IDO1 activity. It was hypothesized that the integrity of Na^+ dynamics is required for physiological IDO1 activity and expression, and dysregulations in intracellular Na^+ levels, primarily by interfering with NKA activity, might impair the IDO1 response.

To test this hypothesis, this chapter aims to present the NKA as an important target for regulating IDO1 activity, as well as validate the role of IDO1 in kynurenine production in MDA-MB-231 cells. This chapter then explores the impact of pharmacological inhibition of the NKA alone or in combination with knockdown (KD) of the α1 NKA subunit (ATP1A1) on the activity and expression of IDO1 and its upstream regulators. Finally, this chapter explores the effect of ATP1A1 overexpression on IDO1 activity and studies the relationship between intracellular Na^+ levels and kynurenine production in MDA-MB-231 cells.

3.2. Results

3.2.1. Identification of ion transport-modulating compounds that affect kynurenine production in breast cancer cells.

The kynurenine assay was first described by Takikawa et al. (1988), as an *in vitro* method of quantifying IDO1 activity, from cellular extracts, which involved high performance liquid chromatography (HPLC)-based kynurenine quantification. The method was refined by Littlejohn et al. (2000), to include a chemical modification triggered by the reaction of N-formylkynurenine with the Ehrlich reagent, leading to conversion to kynurenine.

The later optimised assay set-up was used for a preliminary screen, analysing the effect of 31 ion transport-targeted compounds on IDO1 activity. Figure 3.1A highlights the results of the drug screen in MDA-MB-231 cells, with the main IDO1 inhibitors identified being diclofenac and ouabain. The stronger inhibitor, the cardiac glycoside ouabain, was taken forward for further testing alongside another member of the class, digoxin. Figure 3.1B and C, show the concentration-dependent effect of ouabain and digoxin on IDO1 activity in MDA-MB-231 breast cancer and A549 lung cancer cells. Figure 3.1D summarizes the IC_{50} value for ouabain and digoxin in each of the 2 cell lines tested.

In summary, a 31-ion transporter-targeted compound screen allowed the identification of the cardiac glycoside ouabain as a strong IDO1 inhibitor in MDA-MB-231 breast cancer cells. This result was validated by a titration of the compound in both MDA-MB-231s and A549s. Furthermore, a second member of the cardiac glycoside class, digoxin, showed similar behaviour to ouabain in both cell lines. The IC_{50} values corresponding to each drug, for each of the 2 cell lines, were experimentally determined and provide the basis for the future experiments listed below.

A.

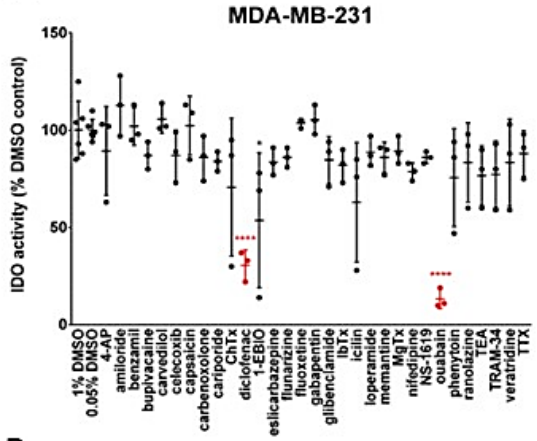

B.

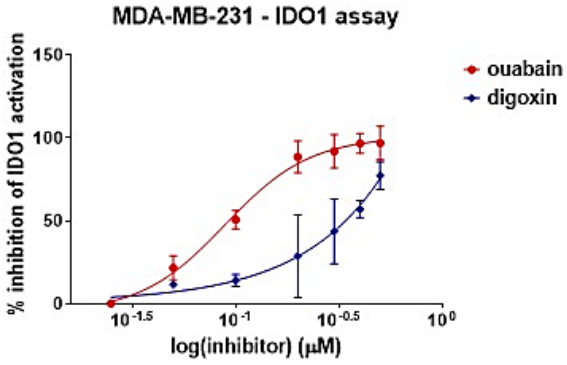

C.

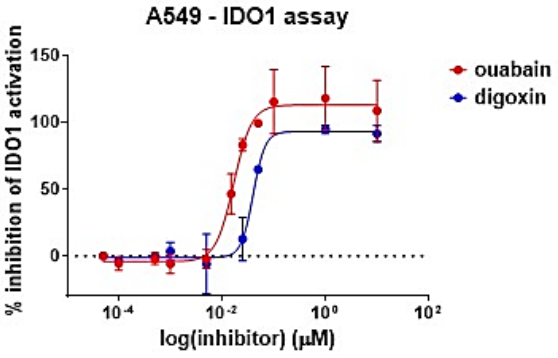

D.

	MDA-MB-231		A549	
	ouabain	digoxin	ouabain	digoxin
IC50	88.9 nM	164.1 nM	16.9 nM	39.9 nM

*Figure 3.1 Effect of 31-ion transport targeted compounds on IDO1 activity (Preliminary data). A. Drug screen results – effect on IDO1 kynurenine production (n=3 biological replicates). B. Titration of ouabain and digoxin in MDA-MB-231s and their effect on IDO1 activation (n=3 biological replicates). C. Titration of ouabain and digoxin in A549s and their effect on IDO1 activation (n=3 biological replicates). D. Summary of the IC_{50} for ouabain and digoxin in MDA-MB-231 and A549 cells. For Figure A, cells were pre-treated with 10 µM of the corresponding drug for 18 h, then stimulation with 1 U IFNγ/6.25ng/mL TNF was applied for another 24 h, as described in more detail in section 2.2. For B and C, cells were treated with a range of ouabain/digoxin concentrations prior to cytokine stimulation, following the timepoints explained in A. The kynurenine assay was carried out as detailed in section 2.9. The IC_{50} for each drug in each of the cell lines were determined from the graphs shown in Figures B and C, using a Nonlinear fit log(inhibitor) vs. response, variable slope (four parameters). Schematics were designed in Biorender.com, data were plotted as mean and SD in GraphPad Prism v9.0.0. Statistical analysis was carried out using a one-way ANOVA, coupled with a Tukey's multiple comparison test, **** p< 0.0001. Data presented in this figure were generated and analysed by Dr Mia Shandell and were included in this thesis for setting the context of the project.*

3.2.2. IDO1 is necessary for kynurenine production.

IDO1 is the enzyme that catalyses the rate-limiting step in the catabolism of Trp to N-formylkynurenine, in MDA-MB-231 breast cancer cells (Novikov et al., 2016). Preliminary data showed that treatment of MDA-MB-231 cells with the NKA cardiac glycoside inhibitor, ouabain, downregulated IDO1 expression and kynurenine production. To verify whether the kynurenine reduction observed by treatment with ouabain is due to IDO1 activity, siRNA KD of IDO1 was carried out, followed by ouabain treatment.

The efficacy of the IDO1 KD was assessed via western blot. Figure 3.2A shows a representative image of the IDO1 band intensities, whilst Figure 3.2B includes densitometry data from n=3 biological replicates showing a statistically significant reduction in IDO1 expression in the KD DMSO-treated cells, compared to the non-targeting control (NTC) DMSO of 46.18 %. Further reduction of IDO1 expression occurred at high ouabain concentrations.

The kynurenine production in the presence of DMSO also dropped by more than 50 % in the IDO1 KD cells compared to the NTC. Addition of ouabain had little to no further impact on the kynurenine response in the IDO1 KD cells, while significantly reducing the kynurenine levels in the NTC and Untransfected controls at high concentrations (200 nM) (Figure 3.2C). Viability data showed no difference in cell survival across the three conditions (IDO1 KD, NTC, Untransfected).

It was thus shown that IDO1 KD reduces the kynurenine response, independently of viability, and addition of ouabain does not impact on kynurenine in the absence of IDO1.

A.

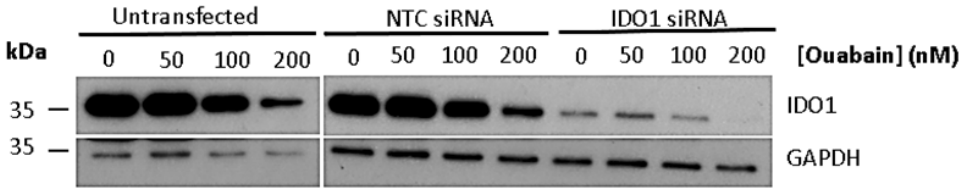
Untransfected
NTC siRNA
IDO1 siRNA
kDa
0 50 100 200 0 50 100 200 0 50 100 200
[Ouabain] (nM)
35
35
IDO1
GAPDH

B.

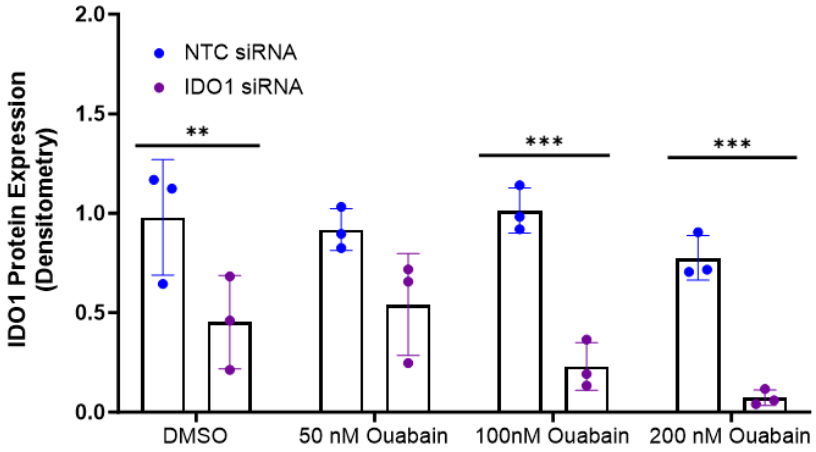
IDO1 Protein Expression (Densitometry)
2.0
1.5
1.0
0.5
0.0
NTC siRNA
IDO1 siRNA
**
***
***
DMSO
50 nM Ouabain
100nM Ouabain
200 nM Ouabain

C.

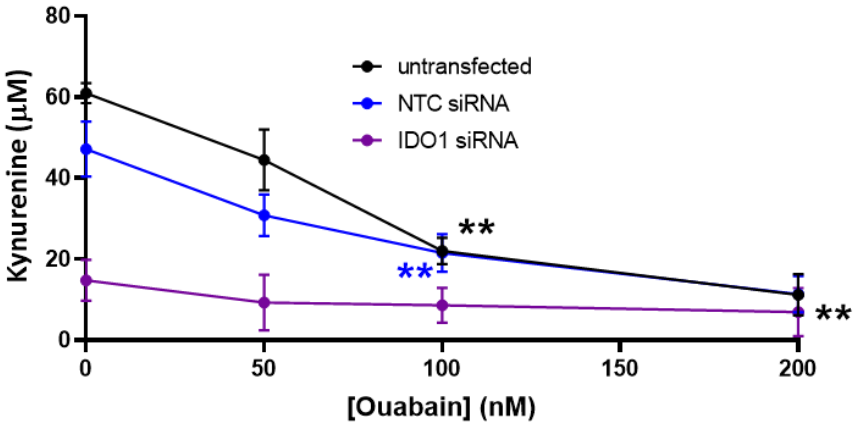
Kynurenine (µM)
80
60
40
20
0
untransfected
NTC siRNA
IDO1 siRNA
**
**
**
0
50
100
150
200
[Ouabain] (nM)

D.

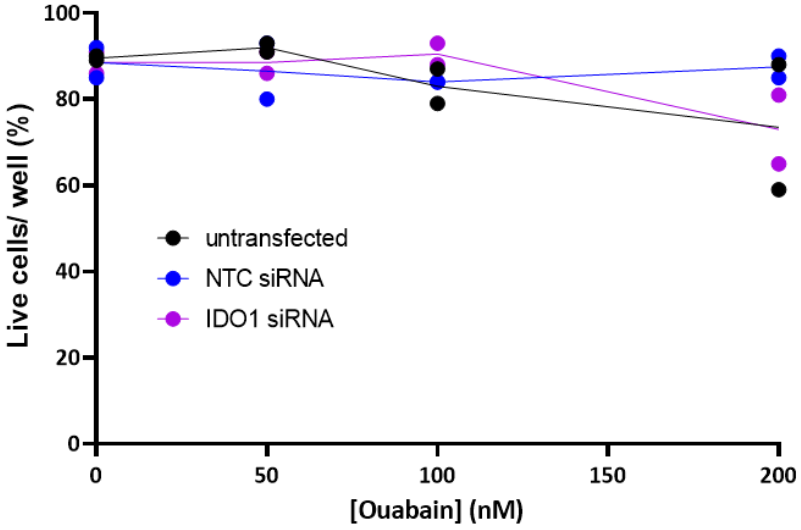
Live cells/ well (%)
100
80
60
40
20
0
untransfected
NTC siRNA
IDO1 siRNA
0
50
100
150
200
[Ouabain] (nM)

*Figure 3.2 IDO1 knockdown abolishes kynurenine production in MDA-MB-231 cells. A. IDO1 KD representative western blot showing IDO1 expression. B. IDO1 protein levels, western blot densitometry data (n=3 biological replicates). C. Kynurenine production in response to ouabain in Untransfected, NTC and IDO1 KD cells in response to ouabain (n=3 biological replicates). D. Percentage viability of Untransfected, NTC and IDO1 KD cells in response to ouabain (n=2 biological replicates). Cells were pre-treated with ouabain for 42 h and IFNγ (1 U)/ TNF(6.25ng/ mL) stimulation was added for another 24 h. Data in B and C were plotted as mean and SD in GraphPad Prism v9.0.0. Data in D were plotted as individual values with a connecting line marking the average due to the low n number. A parametric ordinary one-way ANOVA, coupled with a Bonferroni's multiple comparisons test was used to assess differences in IDO1 protein levels, pairwise for each ouabain concentration (B), and a two-way ANOVA coupled with a Bonferroni's multiple comparisons test was used to assess the changes in kynurenine in response to ouabain treatment, data were compared to the corresponding DMSO condition (Untransfected DMSO, NTC DMSO, ATP1A1 DMSO), *p < 0.05, **p < 0.01, ***p < 0.001. GAPDH – glyceraldehyde 3-phosphate dehydrogenase, IDO1 – indoleamine 2,3-dioxygenase, NTC- non targeting control, siRNA - silencing RNA.*

3.2.3. IDO1 overexpression is sufficient to induce kynurenine production.

Having confirmed that IDO1 is necessary for kynurenine production, the next step was to evaluate whether it is also sufficient to sustain the kynurenine response. To do that, IDO1 was overexpressed in MDA-MB-231 cells and the effect on kynurenine, in the presence or absence of ouabain, or cytokine stimulation, was assessed.

The individual effect of ouabain and cytokine stimulation on exogenous IDO1 was next assessed. Figure3.3A shows a representative western blot, indicating no impact of either ouabain or IFNγ/TNF stimulation, on exogenous IDO1 expression. Densitometry data revealed a similar trend for n=3 biological replicates. A significant increase in IDO1 levels was seen in all IDO1 transfected samples, compared with the empty vector controls, while addition of ouabain, or cytokine stimulation had no impact on the exogenous IDO1 protein levels (Figure 3.3B). The kynurenine response increased by 3-fold upon IDO1 transfection, although this was not statistically significant (Figure 3.3C pCMV3-C-FLAG DSO Vs pCMV3-C-FLAG-IDO1 DMSO). Addition of cytokines did not increase the kynurenine response.

This section thus shows that exogenous IDO1 expression is insensitive to ouabain, and it is sufficient for the upregulation of the kynurenine response.

A.

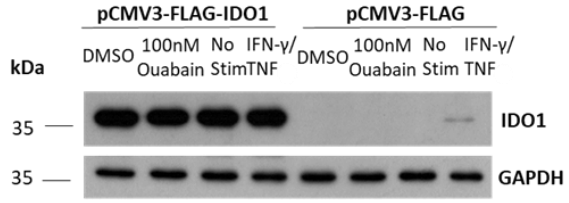
pCMV3-FLAG-IDO1
pCMV3-FLAG
kDa
DMSO
100nM Ouabain
No Stim
IFN-γ/TNF
DMSO
100nM Ouabain
No Stim
IFN-γ/ TNF
35
IDO1
35
GAPDH

B.

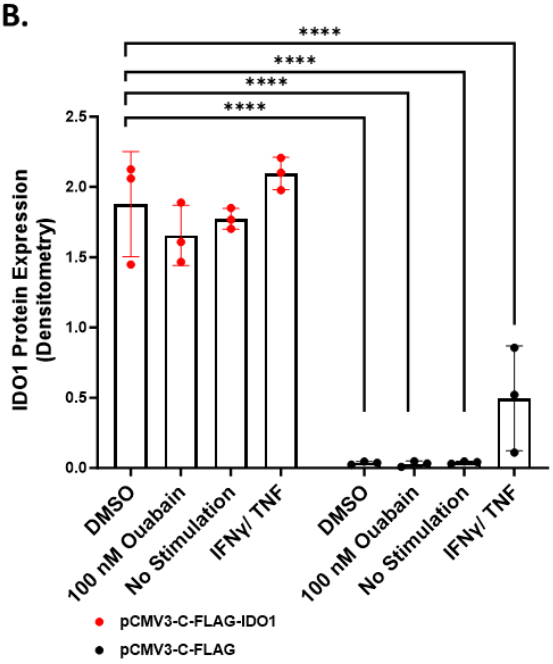
IDO1 Protein Expression (Densitometry)
****
****
****
****
2.5
2.0
1.5
1.0
0.5
0.0
DMSO
100 nM Ouabain
No Stimulation
IFNγ/ TNF
DMSO
100 nM Ouabain
No Stimulation
IFNγ/ TNF
pCMV3-C-FLAG-IDO1
pCMV3-C-FLAG

C.

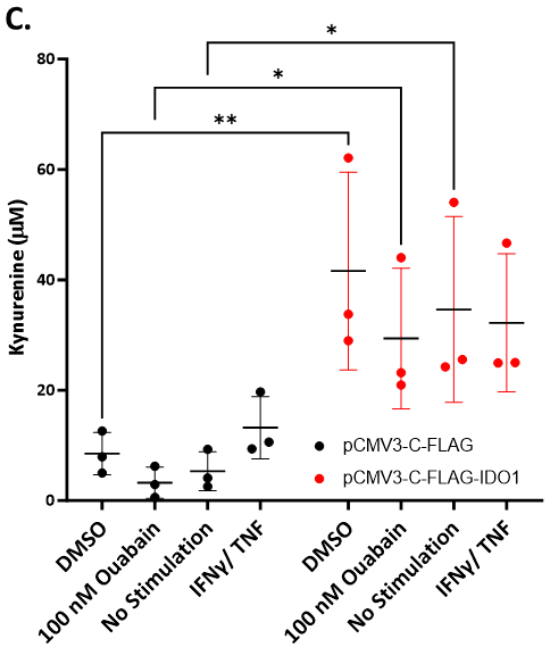
Kynurenine (μM)
*
*
**
80
60
40
20
0
pCMV3-C-FLAG
pCMV3-C-FLAG-IDO1
DMSO
100 nM Ouabain
No Stimulation
IFNγ/ TNF
DMSO
100 nM Ouabain
No Stimulation
IFNγ/ TNF

*Figure 3.3 Impact of IDO1 overexpression on kynurenine production in MDA-MB-231 cells. A. IDO1 overexpression +/- ouabain or +/- cytokine stimulation – representative western blot for n=3 biological replicates (JetPRIME transfection); B. IDO1 overexpression, +/- ouabain or +/- cytokine stimulation, protein expression densitometry data, fold change from average IDO1 expression across all conditions (JetPRIME transfection) (n=3 biological replicates); C. Impact of IDO1 overexpression +/- ouabain or +/- cytokine stimulation on kynurenine levels (JetPRIME transfection) (n=3 biological replicates). Cells were treated with 10 nM ouabain in 0.05% DMSO, 0.05% DMSO or IFNγ (1 U)/ TNF(6.25ng/ mL) for 24 h. Data were represented as men and SD in GraphPad Prism v9.0.0. A parametric ordinary one-way ANOVA, coupled with a Bonferroni's multiple comparison test was used to compare the IDO1 protein levels (B), and a two-way ANOVA coupled with a Bonferroni's multiple comparisons test was used to assess significant differences in kynurenine levels (C), *p < 0.05, **p < 0.01, ***p < 0.001, ****p < 0.0001. DMSO - dimethyl sulfoxide, GAPDH – glyceraldehyde 3-phosphate dehydrogenase, IDO1 – indoleamine 2,3-dioxygenase, IFNγ – interferon gamma, TNF – tumour necrosis factor.*

3.2.4. Cardiac glycosides +/- ATP1A1 KD decrease kynurenine production in MDA-MB-231 breast cancer cells.

Having confirmed that kynurenine levels are a direct representation of IDO1 activity, the next step was to validate the preliminary drug screen results, as well as test whether the observed effect on IDO1 is drug dependent, or whether it is a result of NKA inhibition.

The kynurenine assay was used to assess the impact of two NKA inhibitors ouabain, and the related cardiac glycoside digoxin, as well as that of knocking down the target of these inhibitors, the ATP1A1, on IDO1 activity in MDA-MB-231 cells.

Both cardiac glycosides achieved concentration-dependent reduction in kynurenine production (Figure 3.4A, C). The drop in kynurenine was only statistically significant upon ouabain treatment (Figure 3.4A). However, the digoxin data confirmed the same trend Figure 3.4C). The ATP1A1 KD did not affect IDO1 activity on its own, but in combination with ouabain or digoxin it caused a sharper decrease in kynurenine compared to drug-treated Untransfected and NTC samples, even at low cardiac glycoside concentrations (Figure 3.4A: 50 nM ouabain˜100 % drop, C: 75 nM digoxin˜75 % drop). This kynurenine reduction was much greater than the drop in viability in the same samples (Figure 3.4B: 50 nM ouabain˜15 % decrease, D: 75 nM digoxin˜5 % decrease).

In conclusion, both drugs caused concentration-dependent inhibition of IDO1, and their effects were augmented in ATP1A1 KD cell, with moderate impact on viability in MDA-MB-231 cells.

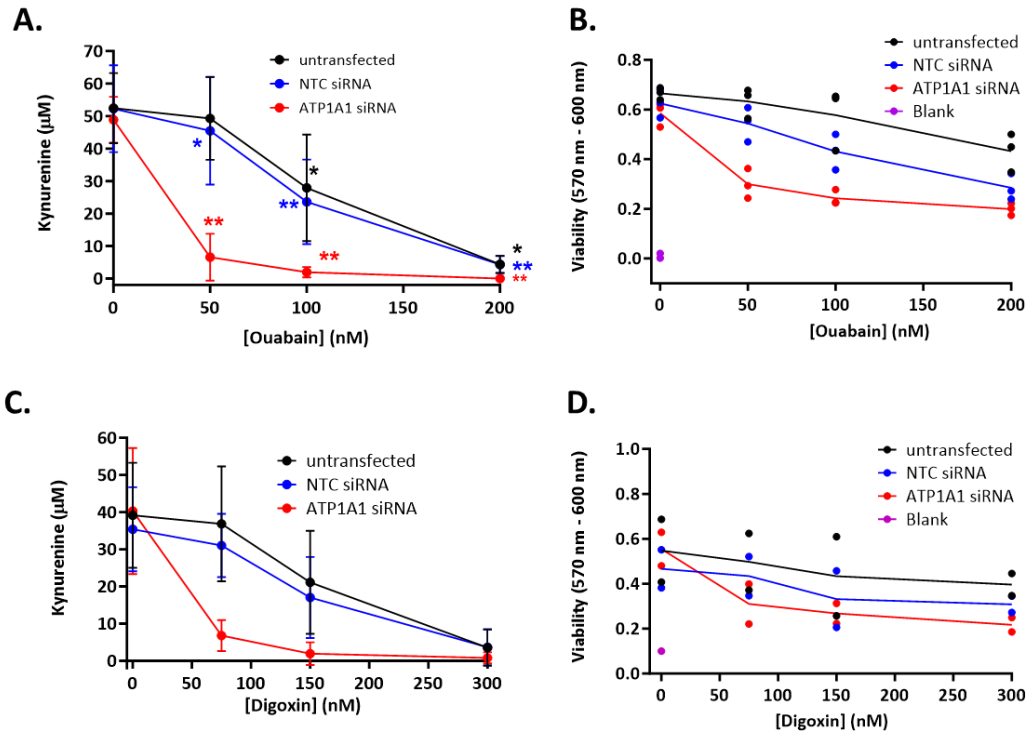

*Figure 3.4 Cardiac glycosides +/- ATP1A1 KD decrease kynurenine production in MDA-MB-231 cells. Kynurenine production (n=3 biological replicates) (A) and viability variation (n=2 biological replicates) (B) in MDA-MB-231 cells in response to ouabain; kynurenine production (n=3 biological replicates) (C) and viability variation (n=2 biological replicates) (D) in MDA-MB-231 cells in response to digoxin. Cells were pre-treated with ouabain/ digoxin for 42 h and IFNγ (1 U)/ TNF(6.25ng/ mL) stimulation was added for another 24 h. Data were plotted as mean and SD. Statistical analysis was performed on kynurenine data only, using a two-way ANOVA, coupled with a two-stage linear step-up procedure of Benjamini, Krieger and Yekutieli, comparing for each transfection condition the effect of different drug concentrations Vs DMSO, * p<0.05, ** p<0.01. Data in figures B and C represent an n=2 biological replicates and were plotted as individual values, with a line connecting the average values for each drug concentration, within each transfection condition; no statistical analysis was performed for these data given the low n number. ATP1A1 – knock down samples of the Na^+/K^+ pump α1 subunit, NTC – non-targeting control, UT - Untransfected, KD – knock down. Replicate experiments were carried out in parallel by Alina Capatina and Mia Shandell.*

3.2.5. Cardiac glycosides +/- ATP1A1 KD decrease kynurenine production in A549 lung cancer cells.

Titration of ouabain and digoxin, in the presence or absence of the ATP1A1 KD was then carried out in A549 lung cancer cells, to verify the robustness of the IDO1 response across different cell/cancer types.

Figure 3.5A and C show a similar response to ouabain and digoxin, as observed in MDA-MB-231s. Both drugs caused a concentration-dependent drop in kynurenine, which was accentuated in ATP1A1 KD samples and ouabain only showed a significant decrease in kynurenine (Figure 3.5A), while digoxin confirmed the pattern (Figure 3.5C). The augmentative effect of the ATP1A1 KD was particularly important at lower drug concentrations, giving an ~100 % reduction in kynurenine in cells treated with either 25 nM ouabain or 50 nM digoxin. Viability was mildly affected by either of the drugs. Ouabain and digoxin caused about ~20 % and 40-50 % drop in viability, respectively, at the highest concentrations (200 nM ouabain and 100 nM digoxin) in ATP1A1 KD cells (Figure 3.5B, C).

In conclusion, both drugs caused concentration-dependent inhibition of IDO1, and their effects were augmented in ATP1A1 KD cells, with moderate impact on viability in A549 cells.

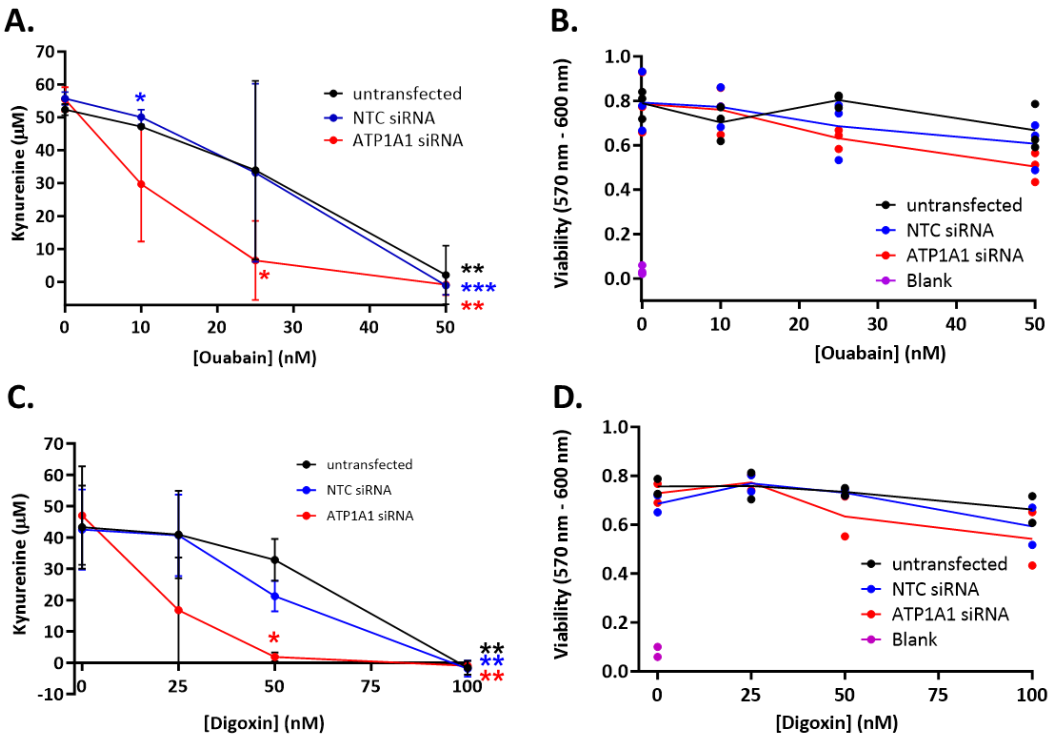

Figure 3.5 Cardiac glycosides +/- ATP1A1 KD decrease kynurenine production in A549 cells. Kynurenine production (n=3 biological replicates) (A) and viability variation (n=2 biological replicates) (B) in A549 cells in response to ouabain; kynurenine production (n=3 biological replicates) (C) and viability variation (n=2 biological replicates) (D) in A549 cells in response to digoxin. Cells were pre-treated with ouabain/ digoxin for 42 h and IFNγ (1 U)/ TNF(6.25ng/ mL) stimulation was added for another 24 h. Data were plotted as mean and range. Statistical analysis was performed on kynurenine data only, using a two-way ANOVA coupled with a two-stage linear step-up procedure of Benjamini, Krieger and Yekutieli, comparing for each transfection condition the effect of different drug concentrations Vs DMSO, * $p<0.05$, ** $p<0.01$, *** $p< 0.001$. Data in figures B and C represent an n=2 biological replicates and were plotted as individual values, with a line showing the average values for each drug concentration, within each transfection condition. ATP1A1 – knock down samples of the Na^+/K^+ pump α1 subunit, NTC – non-targeting control, UT - Untransfected, KD – knock down. Replicate experiments were carried out in parallel by Alina Capatina and Mia Shandell.

3.2.6. Cardiac glycosides +/- ATP1A1 KD inhibit STAT1 signalling in MDA-MB-231 and A549 cells.

Having validated the effect of the cardiac glycosides in combination with the ATP1A1 KD on IDO1, the next step was to investigate the mechanism behind this response. In cancer IDO1 is not constitutively expressed and it requires IFNγ stimulation and STAT1 phosphorylation in order to be produced. For that reason, the effects of cardiac glycosides and of the ATP1A1 KD on the protein levels of phosphorylated STAT1 (pSTAT1) and IDO1 were investigated next (Moretti et al., 2017, Robinson et al., 2003). PD-L1, another immune checkpoint regulated by IFNγ stimulation was also investigated, to verify the specificity of this mechanism to IDO1 function (Garcia-Diaz et al., 2017).

Firstly, the efficiency of the ATP1A1 KD in both MDA-MB-231s and A549 was verified (Figure 3.6A, B, C, D). The ATP1A1 KD was confirmed in both cell lines, also showing a concentration-dependent increase in ATP1A1 levels in response to ouabain/digoxin (Figure 3.6A, B, C, D). IDO1 expression was reduced in response to both drugs in a concentration dependent manner, in both cell lines. A more apparent reduction even at lower drug concentrations was observed in combination with the ATP1A1 KD. Total STAT1 and its activated form, pSTAT1 showed reduced expression with increasing drug concentration, which was augmented in the ATP1A1 KD samples, in both cell lines and with both drugs. PD-L1 showed decreased expression in a drug concentration-dependent manner in A549 cells, with a stronger effect observed in the ATP1A1 samples treated with ouabain and digoxin (Figure 3.6B, D). In MDA-MB-231 cells, PD-L1 expression was irregular, with no apparent pattern (Figure 3.6A, C).

To better understand the effect of these drugs on pSTAT1 and IDO1, a time course experiment was set up. Cells were pre-treated with ouabain and stimulated with IFNγ/TNF for 30 min, 2 h, 8 h and 24 h. The expression levels of total STAT1, pSTAT1 and IDO1 were evaluated at each timepoint. Similar levels of pSTAT1 and total STAT1 in the presence and

absence of ouabain at early timepoints were recorded. However, at 24 h a visible decrease in pSTAT1 was observed upon ouabain treatment, compared to the DMSO control, as highlighted through the red arrow heads in Figure 3.6E. Additionally, IDO1 expression was only visible at 24 h, with lower IDO1 levels in ouabain treated cells (Figure 3.6E). Densitometry showed a small, but not statistically significant decrease in pSTAT1 levels at 24 h (Figure 3.6F). Total STAT1 seemed to decrease at 24 h in response to ouabain according to Figure3.6E, however, densitometry analysis showed no difference between the ouabain and DMSO conditions at that timepoint (Figure 3.6G). Figure 3.6H summarises the ratio of pSTAT1 to TSTAT1 in all conditions, showing no significant change between the DMSO and ouabain treatments at any of the timepoints; however, a small drop in the ratio is visible upon 8 and 24 h ouabain treatment.

In conclusion, IDO1, total and pSTAT1 had similar expression patterns, with protein levels decreasing in response to ouabain/digoxin, but with a much stronger decrease upon combining the ATP1A1 KD with either of the drugs. The ATP1A1 KD was confirmed by western blot, also showing a drug concentration-dependent increase in ATP1A1 expression. In addition, experimental data show that the effect of ouabain and digoxin on pSTAT1, might occur in the late activation phase (24 h), however this remains to be statistically confirmed.

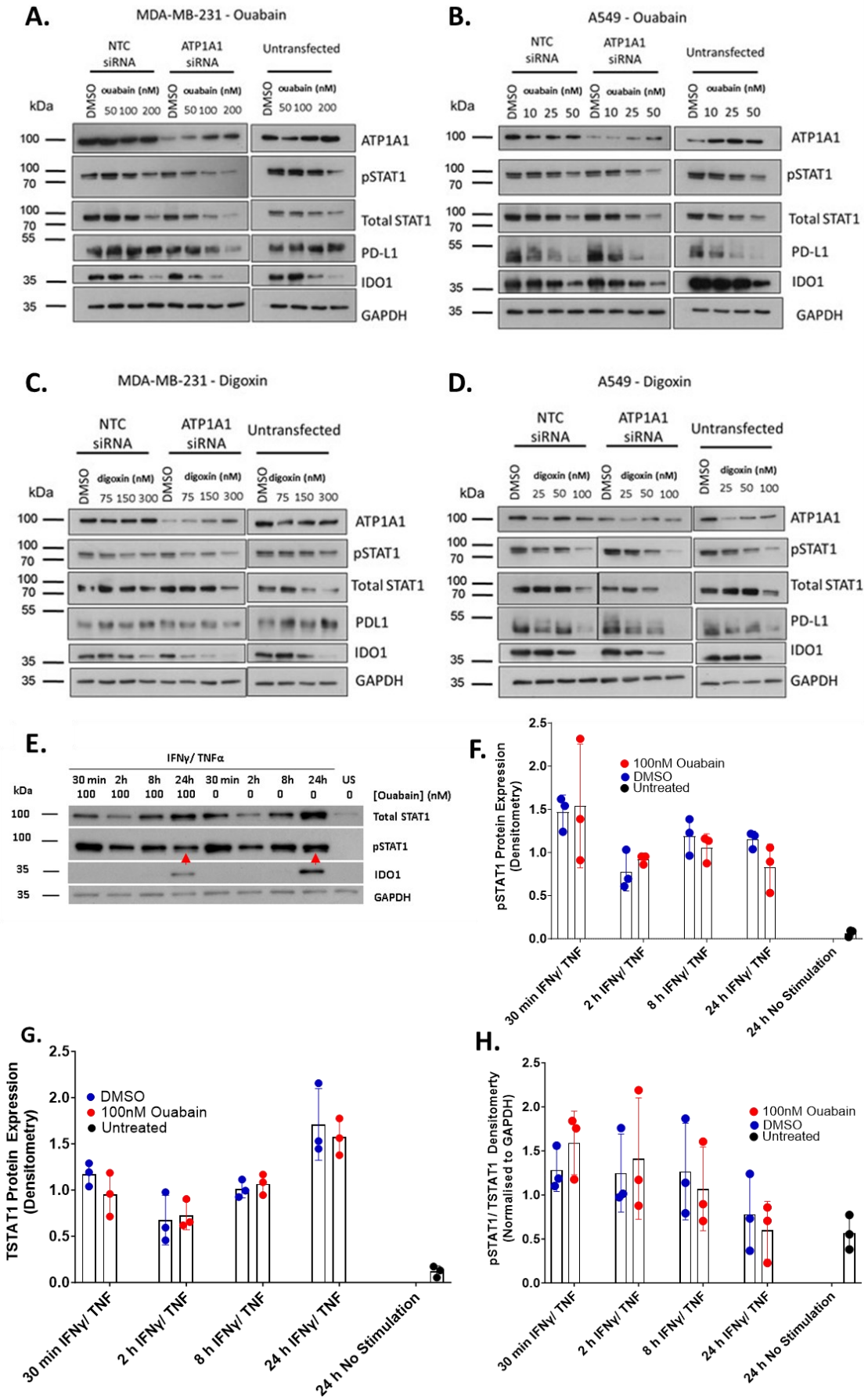
A.
MDA-MB-231 - Ouabain
NTC siRNA
ATP1A1 siRNA
Untransfected
DMSO
ouabain (nM)
50 100 200
kDa
100
70
55
35
ATP1A1
pSTAT1
Total STAT1
PD-L1
IDO1
GAPDH
B.
A549 - Ouabain
10 25 50
C.
MDA-MB-231 - Digoxin
digoxin (nM)
75 150 300
PDL1
D.
A549 - Digoxin
25 50 100
E.
IFNγ/ TNFα
30 min 2h 8h 24h 30 min 2h 8h 24h US
100 100 100 100 0 0 0 0 0
[Ouabain] (nM)
F.
pSTAT1 Protein Expression (Densitometry)
100nM Ouabain
DMSO
Untreated
30 min IFNγ/ TNF
2 h IFNγ/ TNF
8 h IFNγ/ TNF
24 h IFNγ/ TNF
24 h No Stimulation
G.
TSTAT1 Protein Expression (Densitometry)
H.
pSTAT1/ TSTAT1 Densitometry (Normalised to GAPDH)

Figure 3.6 Protein expression in response to siRNA knock down of ATP1A1 +/- ouabain/digoxin. A. Protein expression in MDA-MB-231 cells treated with ouabain (n=1 representative western blot); B. Protein expression in A549 cells treated with ouabain (n=1 representative western blot); C. Protein expression in MDA-MB-231 cells treated with digoxin (n=1 representative western blot); D. Protein expression in A549 cells treated with digoxin (n=1 representative western blot); E. Variation in total STAT1, pSTAT1 and IDO1 protein expression +/- ouabain at 30 min, 2 h, 8 h and 24 h post cytokine stimulation (representative western blot for n=3 biological replicates); F. pSTAT1 expression +/- ouabain at 30 min, 2 h, 8 h and 24 h post cytokine stimulation – densitometry (n=3 biological replicates); G. Total STAT1 expression +/- ouabain at 30 min, 2 h, 8 h and 24 h post cytokine stimulation – densitometry (n=3 biological replicates) H. pSTAT1/ TSTAT1 expression ratios +/- ouabain at 30 min, 2 h, 8 h and 24 h post cytokine stimulation – densitometry (n=3 biological replicates) For A, B, C and D cells were pre-treated with ouabain/ digoxin for 42 h and IFNγ (1 U)/ TNF(6.25ng/ mL) stimulation was added for another 24 h. For E, F and G cells were under ouabain treatment for 42 h, for the last 24, 2, 8 h or 30 min of this treatment IFNγ (1 U)/ TNF(6.25ng/ mL) stimulation was also added. Data were represented as mean and SD. A parametric ordinary one-Way ANOVA, coupled with a Bonferroni's multiple comparison test, was used to assess significant differences between DMSO and ouabain treatments for each time point. ATP1A1 – α1 subunit of the Na^+/K^+ pump, GAPDH - glyceraldehyde 3-phosphate dehydrogenase, IDO1 – indoleamine 2,3-dioxygenase 1, IFNγ – interferon gamma, NTC – non-targeting control, (p)STAT1 – (phosphorylated) signal transduction activator of transcription, PD-L1 – programmed death ligand -1, TNF – tumour necrosis factor, UT – Untransfected. Western blots were prepared and imaged in parallel by Alina Capatina and Mia Shandell.

3.2.7. Cardiac glycosides +/- AT1A1 KD impact on IDO1 mRNA in MDA-MB-231 and A549 cells.

Having confirmed the impact of NKA integrity on IDO1 protein levels, it was next necessary to verify whether these changes are triggered by transcriptional changes.

QPCR analysis revealed a similar pattern in IDO1 mRNA levels, compared to the kynurenine response, particularly in MDA-MB-231 cells in response to ouabain (Figure 3.7A). The trend was less well conserved in A549 cells treated with ouabain or digoxin and in MDA MB 231 cells treated with digoxin. However, ATP1A1 KD significantly enhanced the effect of the drugs on IDO1 mRNA levels in both cell lines (Figure 3.7B, D, C) and ouabain showed a consistently decreasing trend in IDO1 expression in both cell lines (Figure 3.7A, B), while digoxin was more potent in A549s (Figure 3.7D).

In conclusion, the cardiac glycoside effect on IDO1 in the presence of the ATP1A1 KD, but also on their own might be partially mediated through IDO1 transcriptional regulation.

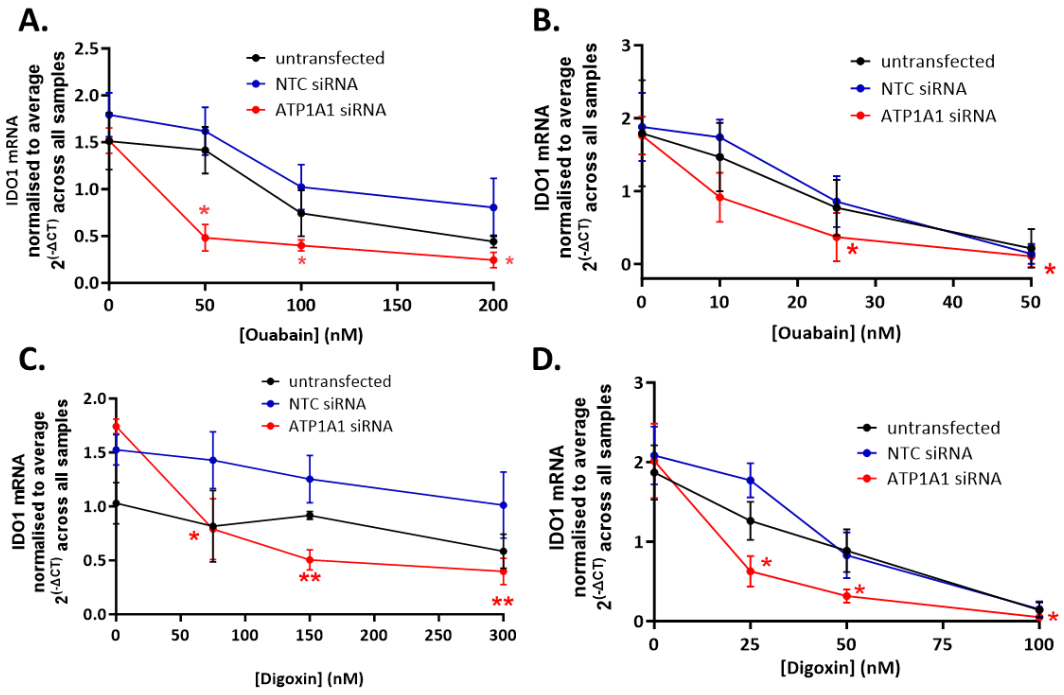
A.
B.
C.
D.
untransfected
NTC siRNA
ATP1A1 siRNA
IDO1 mRNA normalised to average 2^(-ΔCT) across all samples
[Ouabain] (nM)
[Digoxin] (nM)

*Figure 3.7 Effect of cardiac glycosides and the ATP1A1 KD on IDO1 mRNA expression in MDA-MB-231 and A549 cancer cells. A. IDO1 mRNA levels in MDA-MB-231 cells treated with ouabain +/- ATP1A1 KD, samples were normalized to GAPDH, fold change from average expression value across all the samples was calculated using $2^{(-\Delta CT)}$ values (n=3 biological replicates); B. IDO1 mRNA levels in A549 cells treated with ouabain +/- ATP1A1 KD, samples were normalized to GAPDH, fold change from average expression value across all the samples was calculated using $2^{(-\Delta CT)}$ values (n=3 biological replicates); C. IDO1 mRNA levels in MDA-MB-231 cells treated with digoxin +/- ATP1A1 KD, samples were normalized to GAPDH, fold change from average expression value across all the samples was calculated using $2^{(-\Delta CT)}$ values (n=3 biological replicates); D. IDO1 mRNA levels in A549 cells treated with digoxin +/- ATP1A1 KD, samples were normalized to GAPDH, fold change from average expression value across all the samples was calculated using $2^{(-\Delta CT)}$ values (n=3 biological replicates). Cells were pre-treated with ouabain/ digoxin for 42 h and IFNγ (1 U)/ TNF(6.25ng/ mL) stimulation was added for another 24 h. The qPCR protocol was described in section 2.14. Data were plotted as mean and SD; statistical analysis was completed using a two-way ANOVA coupled with a Two-stage linear step-up procedure of Benjamini, Krieger and Yekutieli, comparing for each transfection condition the effect of different drug concentrations Vs DMSO, *p<0.05, **p<0.01, ***p<0.001. ATP1A1 – the Na^+/K^+ pump α1 subunit, IDO1 – indoleamine 2,3-dioxygenase 1, NTC – non-targeting control, UT - Untransfected. Cell seeding/treatment, sample collection and cDNA synthesis were carried out together by Alina Capatina and Mia Shandell.*

3.2.8. ATP1A1 overexpression in MDA-MB-231 cells.

Literature reports the ATP1A1 subunit of the NKA as the primary target of ouabain (Lingrel et al., 1997, Lopina et al., 2020b, Robinson et al., 2003). In order to understand whether the effect of the cardiac glycosides on IDO1 is mediated by the ATP1A1, the next aim was to test whether ATP1A1 overexpression could rescue the previously observed inhibitory effect of ouabain on IDO1.

MDA-MB-231 cells were transfected using a pCMV6-MYC-ATP1A1 plasmid as described in section 2.8. However, as seen in Figure 3.8A and B the transfection did not achieve an increase in ATP1A1 protein levels (non-denatured samples) and did not influence kynurenine production, regardless of IFNγ/TNF stimulation or ouabain treatment.

Transfection with a second plasmid, pcDNA3.1-ATP1A1-FLAG, also did not achieve an upregulation in ATP1A1 protein levels (+/- denaturation). A small increase in pcDNA3.1-ATP1A1-FLAG transfected samples compared to the empty vector control, was visible with denatured samples, however, this did not appear to exceed the ATP1A1 levels in Untransfected samples (Figure 3.8C). These observations were confirmed by densitometry data for both non-denatured and denatured samples (Figure 3.8D, E). Despite undetectable changes in ATP1A1 protein levels, weak FLAG expression as well as a small upregulation in ATP1A1 mRNA were detected in pcDNA3.1-ATP1A1-FLAG transfected samples (Figure 3.8C, F). Nonetheless, the pcDNA3.1-ATP1A1-FLAG transfection did not impact on IDO1 protein levels or on the kynurenine response (Figure 3.8G, H)

Viability data showed similar cell numbers in empty vector controls and pcDNA3.1-ATP1A1-FLAG transfected samples, and percentage viability confirmed over 80 % viability in all samples, regardless of transfection status (Figure 3.8I, J).

In summary, FLAG expression as well as increased ATP1A1 mRNA levels showed low efficiency of the ATP1A1 transfection in MDA-MB-231 cells. The ATP1A1 transfection efficiency was insufficient to elicit a detectable increase in ATP1A1 protein levels and had no effect on IDO1 protein levels or activity, as well as having little impact on viability compared to the empty vector control transfections.

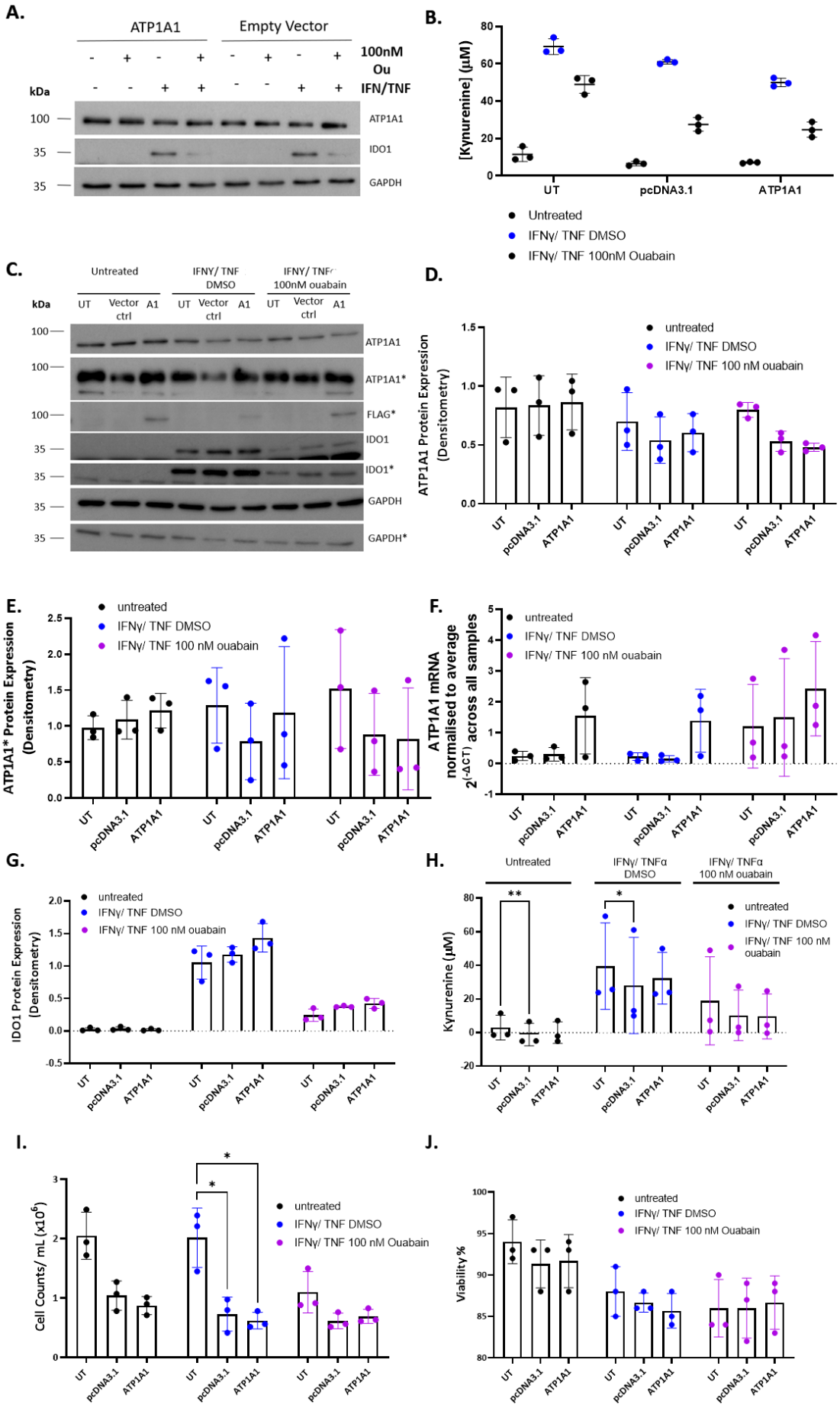
A.
ATP1A1
Empty Vector
100nM Ou
IFN/TNF
kDa
100
35
35
ATP1A1
IDO1
GAPDH
B.
[Kynurenine] (µM)
UT
pcDNA3.1
ATP1A1
Untreated
IFNγ/ TNF DMSO
IFNγ/ TNF 100nM Ouabain
C.
Untreated
IFNγ/ TNF DMSO
IFNγ/ TNF 100nM ouabain
kDa
UT
Vector ctrl
A1
ATP1A1
ATP1A1*
FLAG*
IDO1
IDO1*
GAPDH
GAPDH*
D.
ATP1A1 Protein Expression (Densitometry)
untreated
IFNγ/ TNF DMSO
IFNγ/ TNF 100 nM ouabain
E.
ATP1A1* Protein Expression (Densitometry)
F.
ATP1A1 mRNA normalised to average 2(-ΔCT) across all samples
G.
IDO1 Protein Expression (Densitometry)
H.
Kynurenine (µM)
IFNγ/ TNFα DMSO
IFNγ/ TNFα 100 nM ouabain
I.
Cell Counts/ mL (x10^6)
J.
Viability %

*Figure 3.8. ATP1A1 overexpression in MDA-MB-231 cells. A. ATP1A1 and IDO1 protein levels upon transfection with pCMV6-ATP1A1-MYC +/- IFNγ/TNF stimulation, +/- 100 nM ouabain (representative western blot for n=3 biological replicates); B. The kynurenine response upon transfection with pCMV6-ATP1A1-MYC+/- IFNγ/TNF stimulation, +/- ouabain (n=3 technical replicates); C. ATP1A1, FLAG and IDO1 protein levels upon transfection with pcDNA3.1-ATP1A1-FLAG +/- IFNγ/TNFα stimulation, +/- ouabain (representative western blot for n=3 biological replicates); D. ATP1A1 densitometry data upon transfection with pcDNA3.1-ATP1A1-FLAG +/- IFNγ/TNF stimulation, +/- ouabain (non-denatured samples) (n=3 biological replicates); E. ATP1A1 densitometry data upon transfection with pcDNA3.1-ATP1A1-FLAG +/- IFNγ/TNF stimulation, +/- ouabain (denatured samples) (n=3 biological replicates); F. ATP1A1 mRNA fold change upon transfection with pcDNA3.1-ATP1A1-FLAG +/- IFNγ/TNF stimulation, +/- ouabain, samples were normalized to GAPDH, fold change from average expression value across all the samples was calculated using $2^{(-\Delta CT)}$ values (n=3 biological replicates); G. IDO1 densitometry upon transfection with pcDNA3.1-ATP1A1-FLAG +/- IFNγ/TNF stimulation, +/- ouabain (non-denatured samples) (n=3 biological replicates);H. The kynurenine response upon transfection with pcDNA3.1-ATP1A1-FLAG +/- IFNγ/TNF stimulation, +/- ouabain (n=3 biological replicates); I. Viability (cell counts) upon transfection with pcDNA3.1-ATP1A1-FLAG +/- IFNγ/TNF stimulation, +/- ouabain (n=3 biological replicates); J. Viability percentages upon transfection with pcDNA3.1-ATP1A1-FLAG +/- IFNγ/TNF stimulation, +/- ouabain (n=3 biological replicates). Note: * marks samples that have been denatured for western blot and densitometry analysis, absence of * means that samples have not been denatured. For A and B JetPrime transfections were performed; 24 h after transfection cells were treated with 100 nM ouabain 0.05 % DMSO +/- IFNγ (1 U/mL)/TNF (6.25 ng/mL) and 100 nM ouabain 0.05 % DMSO for another 24 h. The kynurenine assay, western blot and qPCR protocols were described in sections 2.9, 2.13 and 2.14. For C-I Lipofectamine 3000 transfections were performed, as described in section 2.8. Data were plotted as mean and SD; statistical comparison was completed on D-I, using a two-way ANOVA coupled with a Two-stage linear step-up procedure of Benjamini, Krieger and Yekutieli. No statistics was carried out for figure B, given the fact that all replicate points correspond to one biological repeat, * $p< 0.05$, ** $p<0.01$.*

3.2.9. Cardiac glycosides +/- ATP1A1 KD increase intracellular Na^+ levels.

The data presented above showed a consistent decrease in IDO1 expression and kynurenine production in response to cardiac glycoside treatment combined or not with the NKA KD (Figure 3.1 and 3.2). To verify whether this mechanism correlates with changes in the intracellular Na^+ concentration, the effect of the ATP1A1 KD on the intracellular Na^+ concentration was measured using the SBFI-AM technique.

Figure 3.9A shows a significant increase in Na^+ levels in the ATP1A1 KD MDA-MB-231 cells compared to the NTC. Figure 3.9B shows a western blot confirmation of the ATP1A1 KD.

The effect of the two cardiac glycosides: ouabain and digoxin in the presence of cytokine stimulation (needed to induce IDO1 expression) on intracellular Na^+ was also assessed. Figure 3.9C shows a significant increase in intracellular Na^+ levels upon treatment with either ouabain or digoxin. However, digoxin showed lower potency than ouabain in terms of altering Na^+ dynamics.

Figure 3.9D shows that the increase in intracellular Na^+ in response to ouabain is concentration dependent. Furthermore, Figure 3.9E shows an inverse relationship between the kynurenine and the intracellular Na^+ responses, as confirmed by the Pearson correlation coefficient of -0.98, p=0,0188 (Figure 3.9E).

In conclusion, the data indicate that both knockdown of the ATP1A1 subunit and treatment of MDA-MB-231 cells with cardiac glycosides cause an increase in intracellular Na^+, which has an inverse relationship with the kynurenine response. Further experiments would need to be carried out to establish whether the kynurenine and Na^+ responses are co-dependent on NKA.

In this chapter it was thus shown that the kynurenine response is IDO1-dependent, and the experimental data indicated that inhibition of the NKA with cardiac glycosides alone, or in

combination with ATP1A1 KD, decreases the kynurenine response by downregulating IDO1 expression and destabilizing late STAT1 activation. Furthermore, it was confirmed here that cardiac glycosides and the ATP1A1 KD can increase intracellular Na^+ levels, with the former having considerably stronger impact than the ATP1A1 KD. Finally, a potential link between Na^+ dynamics and inhibition of the kynurenine response has been revealed, by showing that the two events have complementary directionality.

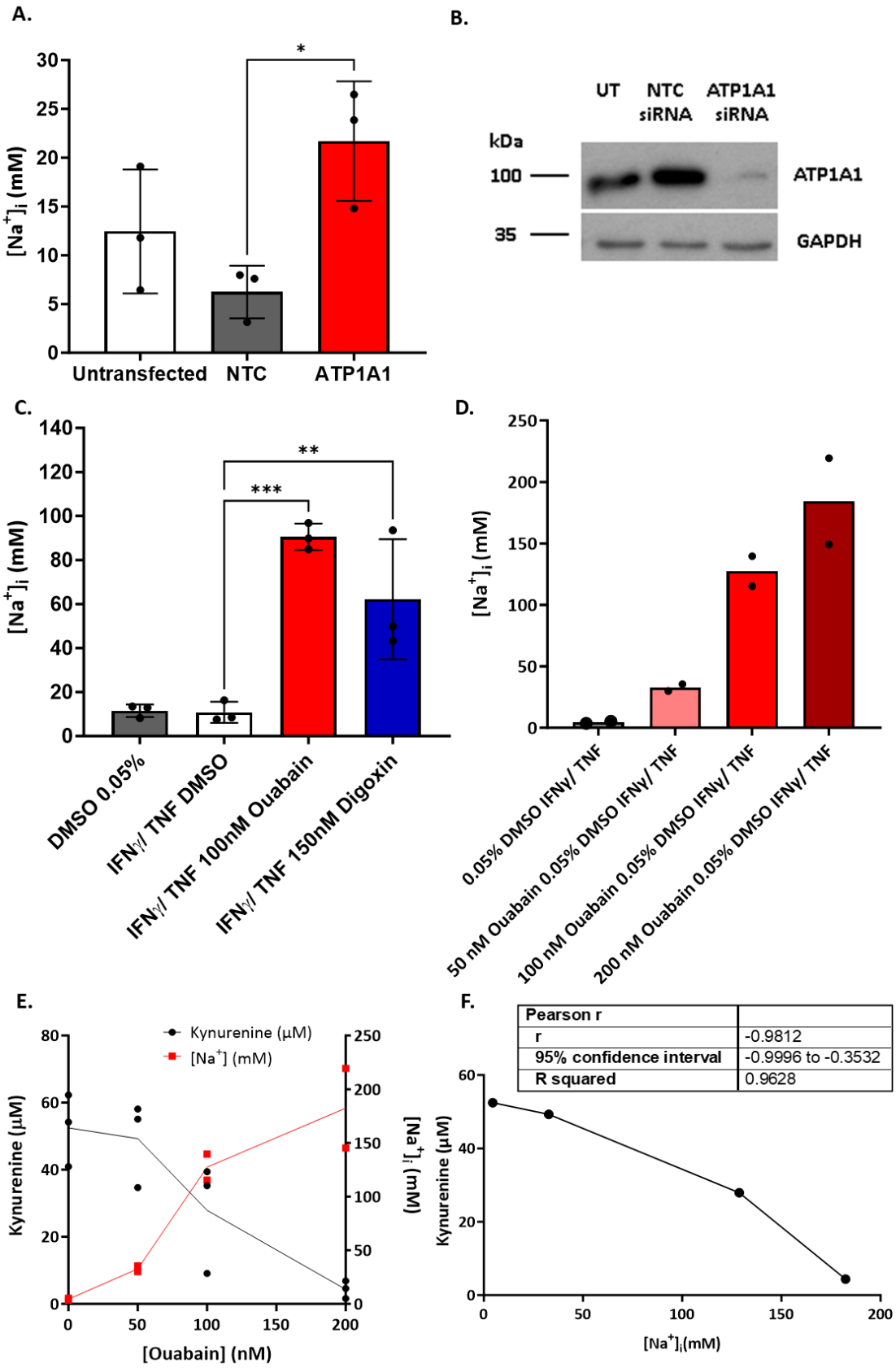
A.
B.
C.
D.
E.
F.
[Na+]i (mM)
Untransfected
NTC
ATP1A1
UT
NTC siRNA
ATP1A1 siRNA
kDa
100
35
ATP1A1
GAPDH
DMSO 0.05%
IFNγ/ TNF DMSO
IFNγ/ TNF 100nM Ouabain
IFNγ/ TNF 150nM Digoxin
0.05% DMSO IFNγ/ TNF
50 nM Ouabain 0.05% DMSO IFNγ/ TNF
100 nM Ouabain 0.05% DMSO IFNγ/ TNF
200 nM Ouabain 0.05% DMSO IFNγ/ TNF
Kynurenine (μM)
[Na+] (mM)
[Ouabain] (nM)
Pearson r
r
-0.9812
95% confidence interval
-0.9996 to -0.3532
R squared
0.9628
[Na+]i(mM)

*Figure 3.9 Effect of the ATP1A1 KD or cardiac glycoside treatment on intracellular Na^+ in MDA-MB-231 cells. A. Effect of the ATP1A1 KD on the intracellular Na^+ concentration (n=3 biological replicates); B. Representative western blot showing the ATP1A1 KD; C. Na^+ response to ouabain or digoxin treatment (n=3 biological replicates); D. Intracellular Na^+ response to ouabain titration (n=2 biological replicates); E. Comparison between kynurenine and Na^+ levels upon ouabain treatment; F. Pearson Correlation between intracellular Na^+ and kynurenine production (p=0,0188, r=-0,9812). For A transfections were performed as described in section 2.8 and cells were seeded for SBFI 48 h post transfection. For C and D drug treatment was carried out for 24 h, and the IFNγ (1 U/ mL)/ TNF (6.25 ng/ mL) stimulation was added at the same time with the drug treatment. Data in A and C was represented as means and SD, a one-way ANOVA coupled with a Bonferroni's post-test were used to assess changes amongst conditions, * p< 0.05, ** p<0.01, *** p<0.001. For D data were plotted as individual values with bars marking the mean, no error bars were added given the small sample size. Data were plotted as individua values with a line marking the average for each condition, to account for the low n number of the $[Na^+]_I$ data (n=2). ATP1A1 – α1 subunit of the Na^+/K^+ ATPase, IFNγ – interferon gamma, TNF – Tumour necrosis factor.*

3.3. Discussion

3.3.1. Summary of the main findings

This chapter presented a set of data that identified the ATP1A1 inhibitor, ouabain as a potential IDO1 regulator (Figure 3.1) and explored multiple approaches on understanding the mechanism behind this phenomenon. Firstly, this chapter validated the fact that the kynurenine response is an accurate quantification of IDO1 activity (Figure 3.2 and 3.3). The reduction in kynurenine was then shown to not be restricted to ouabain inhibition; instead, it occurs also in the presence of digoxin, a second cardiac glycoside. These results were reproduced in both breast and lung cancer cell lines (MDA-MB-231s and A549s) and indicate that the mechanism through which kynurenine is reduced might be ATP1A1-dependent, rather than drug dependent (Figure 3.4 and 3.5). To better understand the role of ATP1A1 in IDO1 regulation, protein expression in response to pharmacological ATP1A1 inhibition and ATP1A1 KD were assessed. Figure 3.6 shows that ouabain and digoxin decrease IDO1 protein levels in a concentration-dependent manner and ATP1A1 KD enhances this effect. Furthermore, the upstream regulator of IDO1 expression, pSTAT1 follows a similar expression pattern with IDO1, indicating that ATP1A1 integrity might be required for IFNγ signalling. These results were reproduced in both MDA-MB-231s and A549s. A second IFNγ-regulated immune checkpoint, PD-L1 was also investigated. PD-L1 protein levels seem to follow the trend of IDO1 expression in A549 cells, but not in MDA-MB-231s. This is interesting and suggests that although ATP1A1 integrity might interfere with IFNγ-induced pSTAT1 signalling, its effect might be specific to IDO1, rather than other IFNγ-regulated genes, in MDA-MB-231s. This chapter also investigated whether the effect of ouabain on pSTAT1 occurs during early pSTAT1 activation or whether ouabain might interfere with pSTAT1 stability. The data in Figure 3.6E show that the reduction in pSTAT1 levels is observed at 24 h IFNγ stimulation, and might thus occur through de-stabilization of pSTAT1, or through

impaired late-stage activation. Furthermore, Figure 3.7 reveals that the IDO1 protein levels might decrease due to transcriptional inhibition and the drop in protein levels is paralleled by a concentration dependent decreasing trend in IDO1 mRNA, particularly in MDA-MB-231s in response to ouabain, that seems to also follow the kynurenine response. All these data indicate that ATP1A1 expression and functional integrity might regulate IDO1 expression and activity.

To better understand the role of the ATP1A1 in this mechanism, two experimental directions were pursued. Firstly, it was aimed to verify whether changes in ATP1A1 expression alone could impact on kynurenine production and IDO1 expression. Secondly, it was investigated whether impaired ATP1A1 ion transport activity could correlate with the effects seen on IDO1.

To test the effect of ATP1A1 expression on IDO1, overexpression of the ATP1A1 protein was attempted, followed by a kynurenine assay to verify whether the effect of ouabain on IDO1 could be rescued. Figure 3.8 shows, however, that ATP1A1 overexpression could not be achieved in MDA-MB-231s, despite multiple transfection reagents being tested, as well as 2 different DNA vectors. This might indicate that ATP1A1 expression might be tightly regulated in MDA-MB-231s. The potential causes for the limited success of the ATP1A1 overexpression experiments were discussed in more detail in section 3.3.5.

Next, to verify if the ion transport activity of the ATP1A1 was related to IDO1 activity, intracellular Na^+ levels upon ATP1A1 inhibition with ouabain and digoxin were measured. Both drugs induced an increase in intracellular Na^+ levels. ATP1A1 KD also increased intracellular Na^+, however, the magnitude of the AT1A1 KD effect was much lower than that of ouabain (Figure 3.9). Interestingly, the decrease in kynurenine was shown to correlate with the increase in intracellular Na^+ levels, suggesting that, ionic dynamics might play a role in IDO1 regulation.

The following sections discuss in more detail all the observations described above.

3.3.2. IDO1 is necessary and sufficient for kynurenine production.

Literature reports three main enzymes involved in kynurenine production: IDO1, IDO2 and TDO (Platten et al., 2012, Ye et al., 2019, Munn and Mellor, 2007, Carvajal-Hausdorf et al., 2017, Wei et al., 2018). IDO1 is particularly important in triple negative breast cancer, where it is upregulated, while in oestrogen receptor positive (ER^+) patients, IDO1 downregulation has been reported. Interestingly, the ER-mediated IDO1 downregulation seems to be independent of the main transcriptional pathway otherwise regulating IDO1 levels, the JAK/STAT pathway; instead ER^+ expression seems to be associated with hypermethylation and thus inactivation of the IDO1 promoter, which appears to be specific to breast tumours (Dewi et al., 2017, Noonepalle et al., 2017). IDO1 is abundantly expressed in MDA-MB-231 triple negative breast cancer cells, and it is the main kynurenine-producing enzyme in these cells (Novikov et al., 2016). This is consistent with the finding that IDO1 expression was necessary and sufficient for kynurenine production (Figure 3.2 and 3.3).

This study reports over 50 % efficacy of the IDO1 KD, which was sufficient to reduce kynurenine levels below 20 µM, in the absence of ouabain (Figure 3.2). Furthermore, the IDO1 KD cells had similar viability counts to the Untransfected and NTC controls, suggesting that the drop in kynurenine was a consequence of the IDO1 KD and not a side effect of transfection toxicity. This, therefore, confirms that IDO1 is necessary for the production of kynurenine in MDA-MB-231 cells, which is in agreement with literature reports (Dewi et al., 2017, Heng et al., 2020).

Next, IDO1 overexpression was performed in MDA-MB-231 cells. A commercially available pCMV3-C-FLAG vector, carrying the IDO1 gene was used. Figure 3.3A shows an over 2-fold upregulation in IDO1 protein levels in transfected cells, corresponding to an almost 4-fold

increase in kynurenine levels (IDO1 DMSO, Vs empty vector DMSO). This is consistent with literature data, which show co-dependence between IDO1 expression and the kynurenine response (Dewi et al., 2017, Heng et al., 2020). Interestingly, ouabain did not impact on exogenous IDO1 expression (Figure 3.3A, B), suggesting that its mechanism of action does not involve direct interaction with IDO1, but rather targets the upstream regulators of endogenous IDO1 expression. Having already shown that IDO1 is the only kynurenine producer in the cell (Figure 3.2), and that its exogenous expression is not affected by ouabain (Figure 3.3), it is likely that small reductions in kynurenine, in IDO1-overexpressig cells could occur due to ouabain toxicity (Winnicka et al., 2007). To verify this assumption, however, viability studies would need to be carried out.

3.3.3. The Na^+/K^+ ATPase integrity is required for IDO1 function.

The role of ions and ion transporters in the context of cancer-immune interaction is an area of growing interest, given the reported ionic disbalances associated with the tumour microenvironment (Nagy et al., 1981, Gradek et al., 2019). This study is investigating the mechanisms underlying an observed correspondence between inhibition/reduced expression of the ATP1A1 and the decreased activity and expression of the immune checkpoint protein IDO1.

Experimental data showed lower levels of kynurenine in response to treatment with ouabain and digoxin, and a stronger inhibitory effect was observed upon drug treatment in cells that had been knocked down for ATP1A1, in a viability independent manner (Figure 3.4 and Figure 3.5). This effect on activity was also reflected in IDO1 mRNA and protein data (Figure 3.6 and 3.7). Total STAT1 and its active phosphorylated form, followed a similar expression pattern to IDO1. Furthermore, time course experiments showed that the cytokine induced IDO1 expression only occurs 24 h after cytokine stimulation. Interestingly, PD-L1, another immune checkpoint protein, was also upregulated after 24 h of stimulation and despite it showing no

sensitivity to ouabain in MDA-MB-231 cells, its expression seemed to be slightly inhibited by the ATP1A1 KD. These observations suggest that there might be key role that ATP1A1 plays in the IFNγ/JAK/STAT1 induced signalling (Figure 3.6). Yet, the exact mechanism is not clear.

IDO1 is an immune-suppressive checkpoint protein employed by cancer cells to deplete the cytotoxic T cell pool within the tumour, thus facilitating cancer survival and metastasis. Pro-inflammatory cytokine stimulation, like IFNγ/TNF, is known to induce IDO1 expression as a negative feedback mechanism (Mailankot and Nagaraj, 2010, Banzola et al., 2018). The IFNγ receptor is a dimeric molecule which becomes activated upon ligand binding, recruiting JAKs which phosphorylate the receptor and trans-phosphorylate each other, further recruiting a second set of signalling molecules called STATs, of which STAT1 has been mostly associated with IDO1 expression (Robinson et al., 2003). Upon their phosphorylation by JAKs, STATs are recruited to the nucleus where they regulate the expression of specific genes, including IDO1. STATs are also activators of suppressor of cytokine signalling proteins (SOCS), which are inhibitors of the JAK/STAT pathway (Federici et al., 2002) (Appendix Figure 8. 1). It is thus possible that the observed impact of NKA inhibition/reduction on IDO1 might occur via interfering directly with STAT1 activation, or via upregulation of SOCS1/3, known inhibitors of pSTAT1 signalling; however, this hypothesis could not be validated experimentally. Appendix Figure 8. 1 shows the impact of ouabain treatment and/or ATP1A KD at different timepoints post cytokine stimulation on SOCS3 protein expression. No change was observed in the experimental setup with any of the conditions. This is, however, not an exhaustive experimental approach, as other members of the class (e.g., SOCS1) or other JAK/STAT regulators such as Protein Inhibitors of Activated STATs (PIAS) and Protein Tyrosine Phosphatases (PTPs) might be mediating the effect of ouabain and ATP1A1 KD on pSTAT1 and IDO1 (Dai et al., 2006, Song and Shuai, 1998, Qin et al., 2012). For the scope of this project, however, this work was not pursued further, drawing the ultimate conclusion that

ouabain exerts a pSTAT1-mediated IDO1 inhibition. In the next chapter the focus was shifted towards the question of whether and how Na^+ mediates this response.

Furthermore, literature shows that ouabain and ATP1A1 KD can induce activation of a series of master kinases such as Src and Akt, as well as inducing association of the pump with EGFR (Wu et al., 2013b, Yu et al., 2019). Both Src and EGFR have been reported to promote STAT3, and STAT1 activation (Garcia et al., 2001, Chang et al., 2004). However, this is in contradiction with the experimental observations herein which show a decrease in STAT1, suggesting that the mechanism leading to ouabain-induced IDO1 inhibition might not involve Src and EGFR-dependent signalling. Other studies reported that IFNγ stimulation reduces NKA activity (measured as phosphate production) in a STAT1 dependent manner (Sugi et al., 2001, Vieira-Coelho et al., 2000). It is thus possible that the reduction in pSTAT1 observed in the presence of ouabain +/- ATP1A1 KD is triggered as a cellular mechanism to rescue NKA activity and allow survival. This is plausible especially since a compensatory mechanism is also seen at protein level, where ATP1A1 expression increases with ouabain (Magro et al., 2004).

Another important aspect that needs to be considered is the steroid structure on the ouabain molecule and the well-established anti-inflammatory action of steroids (Aizman et al., 2001). It is thus possible that the effect of ouabain on IDO1 might be NKA-independent and in fact it might occur through a different target. Several literature reports suggested that cardiac glycosides (e.g., bufalin) might have additional targets within the cell, apart from the NKA. Such a target was reported to be SRC3, as well as several other nuclear receptors (Wang et al., 2014, Zhang et al., 2018b). To test the involvement of SRC3 in the ouabain-IDO1 pathway, SRC3 was knocked down in MDA-MB-231 cells (as confirmed by western blot) and treated with a series of ouabain concentrations (Appendix Figure 8. 2). The kynurenine response in the SRC3 KD upon ouabain treatment was similar to that of the Untransfected cells, suggesting that SRC3 does not impact on IDO1 activity. A variation in the baseline kynurenine

levels between the SRC3, Untransfected and mock transfected cells was observed, which could be explained by a difference in viability across the conditions. Data, therefore, suggest that the ouabain-IDO1 pathway is not related to SRC3 signalling.

The work presented in this chapter shows a synergistic relationship between cardiac glycosides and the ATP1A1 KD, on IDO1 activity and expression. This can potentially be explained when looking at the effect of the ATP1A1 KD Vs ouabain and digoxin on $[Na^+]_i$. While ouabain increases $[Na^+]_i$ up to 100 mM, the ATP1A1 KD only increases the levels to 20 mM. This leads to the speculation that the small change in Na^+ caused by the ATP1A1 KD is not enough to trigger a physiological response resulting in IDO1 inhibition. This supposition also explained why combining ouabain and the ATP1A1 KD has an enhanced effect on IDO1, potentially explained by an enhanced effect on Na^+ (this could not be tested experimentally due to technical limitations). Furthermore, such speculations open the question of an intracellular Na^+ threshold required to have an impact on IDO1, which Figure 3.9.E is briefly addressing, suggesting that a detectable IDO1 inhibition might occur between 20 and 60 mM $[Na^+]_i$. Further experiments would, however, be required to identify the exact $[Na^+]_i$ equivalent to a drop in kynurenine. It is important to specify that the data presented here do not show causality between changes in $[Na^+]_i$ and IDO1 inhibition; instead, a potential correlative link is observed, and remains to be further studied. Figure 3.10 summarizes the main findings linking the NKA and IDO1.

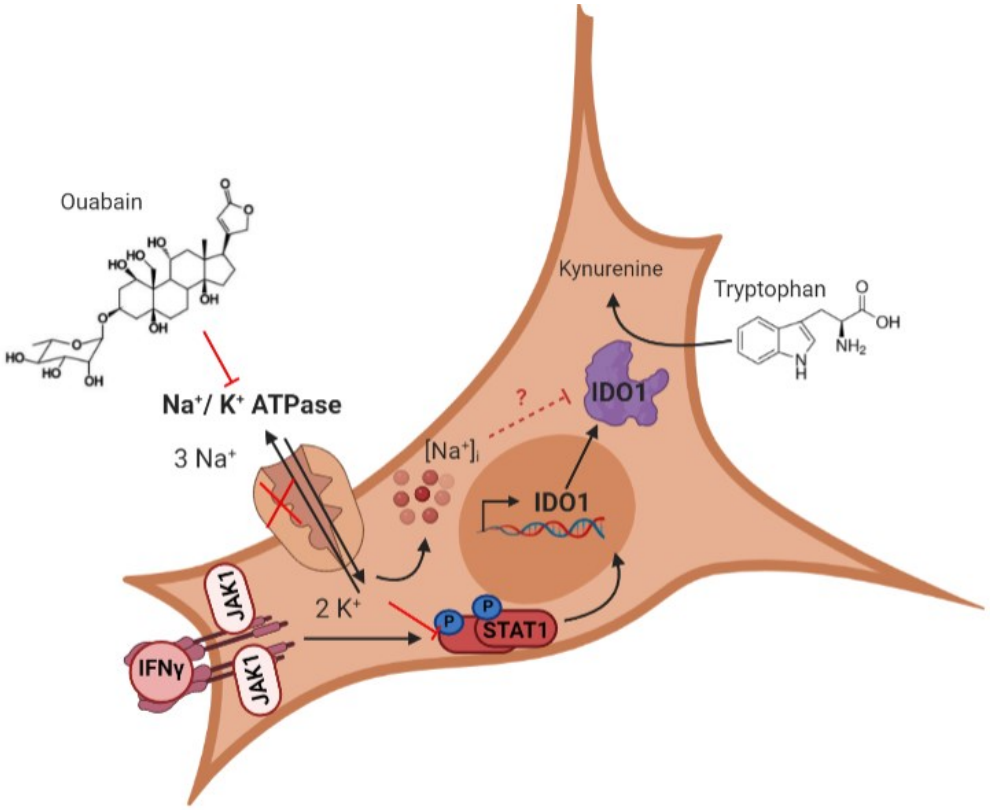

Figure 3.10 Overview of the signalling mechanism showing the IDO1 - Na^+/K^+ pump interdependence. A combination of ATP1A1 KD and ouabain treatment triggers a reduction in IDO1 expression and activity, probably by interfering with the JAK/STAT pathway (the exact mechanism is yet to be discovered). IDO1 – indoleamine 2,3-dioxygenase 1, STAT1 – signal transduction activator of transcription, JAK – Janus Kinase, IFNGR – interferon-γ receptor, Treg – regulatory T cells.

3.3.4. Ouabain might impact on late STAT1 activation, or pSTAT1 stability.

Having confirmed that ouabain regulates endogenous IDO1 expression, the next step was to assess the effect of ouabain on the main transcription factor that regulates IDO1 expression - STAT1 in its active phosphorylated form (pSTAT1). To achieve this, a time course of STAT1 expression and phosphorylation in response to cytokine stimulation was set up, evaluating the time taken for ouabain to have an impact on STAT1 expression and phosphorylation.

The data showed upregulation of STAT1 levels at later timepoints post cytokine stimulation, while the pSTAT1 levels were highest at 30 min, decreasing at later timepoints (Figure 3.6 E, F, G). Both patterns have been previously described in the literature (Cheon and Stark, 2009, Lehtonen et al., 1997, Robinson et al., 2003).

In terms of ouabain activity, at 24 h, a small decrease in band intensity for pSTAT1 (red arrow heads, Figure 3.6E) was observed in ouabain treated samples, compared to the DMSO control, which was visually supported by densitometry data (Figure 3.6E, F), but further repeats would be needed in order to increase the statistical power of the data. Total STAT1 also seems to be decreasing at 24 h in response to ouabain, according to Figure 3.6E, but the densitometry data do not support this observation (Figure 3.6G). Thus, it is hypothesized that the mechanism of action of ouabain might be through inhibition of late STAT1 phosphorylation events, especially since the decrease in pSTAT1 at 24 h correlates with IDO1 downregulation in response to ouabain, but further experiments would have to be carried out before any conclusion can be drawn. It is also possible that the ouabain effect on pSTAT1 and IDO1, is just a consequence of the protein synthesis inhibitory effect of cardiac glycosides, previously reported in the literature (Perne et al., 2009).

3.3.5. ATP1A1 overexpression in MDA-MB-231 cells.

To further assess the relationship between the ATP1A1 and IDO1, overexpression of ATP1A1 in the presence of ouabain was attempted, aiming to assess whether this could rescue the ouabain effect on IDO1. If such a hypothesis were true, it would mean that the ouabain effect on IDO1 is dependent on the function of the ATP1A1.

In the experiments presented here, ATP1A1 overexpression could not be accomplished in MDA-MB-231 cells with either of the two expression vectors tested. Using two different transfection reagents also did not achieve ATP1A1 protein overexpression (Figure 3.8A, C). Despite the lack of change in protein levels, a 10-20-fold increase in ATP1A1 mRNA levels was observed upon transfection (Figure 3.8F). This did not translate, however, in any changes in IDO1 expression or the kynurenine response (Figure 3.8B, G). Previous studies have shown that ATP1A1 overexpression was strongly correlated with apoptosis and decreased proliferation of cancer cells (Zhang et al., 2017a). To verify if that was the reason why ATP1A1 could not be expressed in MDA-MB-231 cells, viability was assessed both as cell counts and as percentage viability (Figure 3.8H, I). Although a drop in live cell numbers was observed in all transfected cells compared to Untransfected, the samples receiving the ATP1A1 plasmid had similar viability counts with the empty vector control samples, indicating that the lack of ATP1A1 overexpression is probably not a consequence of cell death.

ATP1A1 overexpression was previously reported in the literature using viral vectors in A549 lung cancer cells, as well as *in vivo* in cardiac cells of transgenic mice (Correll et al., 2014, Factor et al., 1998). However, no records of ATP1A1 overexpression in MDA-MB-231 cells could be found. It is possible that ATP1A1 expression might be tightly regulated at translational level, which would explain the increase in ATP1A1 mRNA, otherwise not seen at protein level. Given the tight connection between ATP1A1 and metabolism, the NKA being a key ATP consumer, it is likely that the metabolic capacity of the cell might be a limiting

factor in ATP1A1 expression (Post et al., 1969). Interestingly, studies have reported that increased expression of exogenous ATP1A1 is sometimes associated with decreased expression of endogenous ATP1A1, so that overall protein levels of the ATP1A1 remain unchanged; the downregulation in endogenous ATP1A1 levels is believed to be due to a translational repression mechanism (Clifford and Kaplan, 2009). This could explain the disconnection between mRNA and protein levels upon trying to overexpress the ATP1A1 in MDA-MB-231 cells (Figure 3.8C-F).

On the other hand, the lack of efficiency of the ATP1A1 overexpression could indicate either that the transfection reagent, or the transfection conditions are not compatible with the plasmid used for ATP1A1 overexpression (Kim and Eberwine, 2010), or it could mean that overexpression of the ATP1A1 gene in MDA-MB-231 cells is not compatible with survival. Although exogenous ATP1A1 overexpression has been reported in the literature in certain cell lines, it is often associated with apoptosis and high toxicity (Zhang et al., 2017a). Further optimization experiments would need to be carried out in order to confirm whether ATP1A1 overexpression is possible in MDA-MB-231 cells. However, for the scope of this project these experiments were not pursued further.

3.3.6. Cardiac glycosides +/- ATP1A1 KD increase intracellular Na^+ levels.

Given that ATP1A1 overexpression was unsuccessful, and thus it could not be tested whether the ouabain effects on IDO1 are indeed mediated by the ATP1A1, the next step was to verify if these effects are mediated by Na^+ dynamics.

Changes in intracellular Na^+ were measured using the SBFI-AM technique. SBFI, or sodium benzofuran isophthalate, is a ratiometric dye that binds to intracellular Na^+ ions. The SBFI molecule is conjugated with an acetoxymethyl (AM) ester group which is membrane permeable and allows cellular uptake of the dye. A second reagent, Pluronic acid, acts as a

carrier and helps dispersing the dye within the cell. Once inside, the SBFI molecule binds to intracellular Na^+ and the AM group is cleaved to prevent leakage out of the cell. The excitation of the SBFI molecule happens at two wavelengths: 340 (Na^+-bound) and 380 (Na^+-free), while detection is recommended within the 450 – 550 window (Minta and Tsien, 1989, Negulescu and Machen, 1990). For the experiments described here emission was recorded at 500 – 520 nm, based on the quality control experiment presented in Appendix Figure 8. 3 which showed good separation of the 340 and 380 signals at these wavelengths.

Experimental data showed that treatment with either of the two NKA cardiac glycoside inhibitors, ouabain and digoxin, caused a significant elevation in the intracellular Na^+ concentration. IFNγ/TNF stimulation, however, had no impact on Na^+ accumulation on its own (Figure 3.9C). The knockdown of the ATP1A1 subunit of the pump seemed to have an upregulating effect on intracellular Na^+, however, not as strong as the impact observed with cardiac glycoside treatment (Figure 3.9A, B, C). Interestingly, the pattern of intracellular Na^+ changes was complementary to that of kynurenine in the same cells (kynurenine goes down while intracellular Na^+ goes up) (Figure 3.9A, B).

The role of Na^+ in cancer has been often discussed given the characteristic hypernatremia of the tumour microenvironment and the depolarized membranes of cancer cells, which point towards a functional role of ionic imbalances in metastasis and growth (Nagy et al., 1981, Leslie et al., 2019). Studies have also associated expression of cancer biomarkers, such as the human EGFR2, with elevated Na^+ import, as well as suggesting a role of these ions in cytoskeletal rearrangements, growth and motility (Gorbatenko et al., 2014, Bondarava et al., 2009, Popov et al., 2012, Nelson et al., 2015b). It is thus expected that changes in intracellular Na^+ levels could result in changes in gene expression or protein interactions, which could be responsible for the reduced activity of IDO1, upon NKA dysregulation. Another hypothesis is

that Na^+ level fluctuations could have a metabolic impact on the cells, which could impact on IDO1, given its function in Trp catabolism. Increases in intracellular Na^+ are bound to increase the intracellular concentration of Ca^{2+} ions through the reverse function of the NCX, leading to internal stores Ca^{2+} release (Blaustein and Lederer, 1999). Ca^{2+} is a key regulator of mitochondrial metabolism, as well as paying a role in signalling events (Gunter et al., 1998). The IFNγ pathway, is also associated with an acute and sharp Ca^{2+} spike, which is required for downstream signalling events (Popov et al., 2012, Koide et al., 1988). It is thus possible that impaired Ca^{2+}-dependent IFNγ signalling might play a role in ouabain-induced IDO1 downregulation. However, this would require in-depth electrophysiological and signalling analyses. Another possibility is that the NKA inhibition might lead to decreased ATP usage, and thus cause a metabolic switch within the cell. Seahorse experiment would be able to shed some light on that possible mechanism. However, for the scope of this project, the focus was kept on investigating the direct role of Na^+ ions in IDO1 inhibition. Chapter 4 describes the approach taken to study the impact of Na^+ dynamics and subsequent findings in more detail.

3.3.7. Further research on the NKA-Na^+_IDO1 axis

Studying the co-dependency relationship between NKA/ Na^+ and IDO1 signalling is particularly difficult due to the large effect that NKA activity has on cellular physiology, from regulating ion transport and pH to metabolism and cell cycle control (Silva et al., 2021). One interesting approach would be to assess the impact of high Na^+ on IDO1 activity *in vitro*, in a purified enzyme assay. In cells, a Rb^+ uptake assay coupled with Inductively Coupled Plasma Mass Spectrometry (ICPMS) could allow close monitoring of NKA activity under different conditions (e.g., with pharmacological inhibitors, IDO1/ ATP1A1 siRNA knockdown or low K^+ media)(Wilschefski and Baxter, 2019, Clemente et al., 2023, Clausen and Kjeldsen, 1987, Amemiya et al., 1999). By measuring NKA activity and IDO1 kynurenine production, the two

enzymatic activities could be correlated, thus answering the question as to whether it is the expression or the activity of the pump that regulates IDO1. Furthermore, a combined proteomics/ phosphor-proteomics study could shed light on the pathways that are upregulated simultaneously upon NKA inhibition and IDO1 activation, thus providing a starting point for investigating the signalling events that might link NKA and IDO1. Another interesting approach to further build on the currently known steps of this pathway could be to assess the impact of NKA inhibition/ knockdown on the efficacy of IDO1-targeted immune checkpoints *in vitro* and *in vivo*. Such an experiment would provide information on the mechanism of action of the NKA in regulating IDO1. A synergistic effect of NKA inhibition combined with a tryptophan mimetic IDO1 inhibitor would suggest that NKA regulation does not target the enzymatic function of IDO1. Such a result would have clinical value, opening up potential combinatorial treatment regime options (Duarte and Vale, 2022). However, in the absence of further experimental evidence, such hypotheses remain speculative.

Overall, the link between the NKA and IDO1 is complex and difficult to dissect. Further work is required to understand and characterise this pathway. However, the data presented in this thesis justifies the need to further explore this topic, highlighting a clear functional link between the two.

3.4. Conclusion

This chapter showed that regulation of IDO1 activity and expression can be achieved using NKA-inhibitors belonging to the cardiac glycoside class (ouabain and digoxin). It showed that combining cardiac glycosides with ATP1A1 KD can enhance IDO1 inhibition, as well as causing a stronger drop in IDO1 expression and pSTAT1 protein levels. Finally, the drop in kynurenine was shown to be paralleled by a proportional increase in intracellular Na^+. It can therefore be speculated that there might be a correlation between intracellular Na^+ levels and IDO1 activity/expression and this will be further explored in Chapter 4.

4. Chapter 4: Results. Na^+ dynamics and the Na^+/K^+ ATPase regulation of the IDO1 immune checkpoint in breast cancer cells

4.1. Introduction

4.1.1. Background

Chapter 3 identified a correlative link between increases in intracellular Na^+ induced through cardiac glycoside mediated NKA inhibition (Shandell et al., 2022). The wide range of effects of cardiac glycosides on cell function included NKA-PI3K/Akt or NKA-EGFR-Src mediated signalling, steroid-receptor interaction and transcriptional regulation of downstream effector genes, as well as metabolic dysregulations (e.g., through AMPK interactions)(Wu et al., 2013a, Tian et al., 2006, Haas et al., 2002, Shen et al., 2020b, Wu et al., 2015). Furthermore, the NKA is not only a Na^+ exporter, but also an active K^+ importer, which means that inhibiting it would alter the ionic equilibrium of more than one electrolyte (Post et al., 1969). Additionally, the NKA ATP consumption is a significant driver of metabolic activity, therefore, inhibition of NKA function would mean a decrease demand for glycolytic ATP, potentially leading to a switch in the preferred metabolic pathways in the cell; in turn, cellular processes that consume ATP, such as proliferation, decrease the activity of the pump and can thus lead to an altered ratio of intracellular and extracellular Na^+ levels (Mercer and Dunham, 1981, Leslie et al., 2019, Madelin and Regatte, 2013). All these observations indicate that simply looking at cardiac glycoside induced NKA inhibition might be an approach with low discriminative power among different potential mediators of the observed IDO1 response.

To try and study in isolation the effect of Na^+ on IDO1 activity and expression, a different system needed to be designed. One limitation associated with the study of the effect of intracellular ions on cellular function comes from the need to maintain constant physiological osmolarity. That means that the overall electrolyte concentration inside and outside the cell needs to be maintained within physiological parameters. For that to be possible, export of a specific ion is often compensated by the import of another, thus making it particularly difficult to study the effect of one ion in isolation (Finan and Guilak, 2010). Furthermore, the transport of Na^+ ions across the membrane is often associated with proton transport, thus leading to changes in intracellular pH (Harvey and Ehrenfeld, 1988). Such changes can have a wide range of effects on cellular function, including inhibition of enzymatic activity, which would have significant impact on this study, given the fact that IDO1 is a Trp catabolic enzyme (Robinson, 2015).

Taking all these into consideration, a method of assessing the effect of intracellular Na^+ levels on IDO1 activity would be the use of an NKA-independent pharmacological agent. One possibility to increase intracellular Na^+ levels, would be by applying a VGSC opener, such as veratridine (VTD). VTD treatment would lock Na^+ channels in open conformation allowing Na^+ to pass into the cytosol according to its concentration gradient (Wang and Wang, 2003, Ulbricht, 1998). Another possibility to increase intracellular Na^+ levels would be by using an ionophore. Ionophores are chemical compounds that mediate the transport of ions across the membrane and are conventionally grouped in 2 categories: channel or pore forming ionophores and mobile or carrier ionophores (Roy and Talukdar, 2021). Channel ionophores are molecules that can insert themselves within the phospholipid bilayer and create a passage for ions carrying a certain charge. An example of a channel forming ionophore is gramicidin, which was used in Chapter 3 for Na^+ imaging assays to accommodate the intracellular and extracellular Na^+ concentrations. The limitation with channel forming ionophores comes from their rapid effect on ionic concentration, and long term treatment

with channel forming ionophores can often result in cell death due to the continuous flux of ions inside the cell, thus disrupting the membrane (Wang et al., 2019b, David and Rajasekaran, 2015). Carrier ionophores are molecules that insert themselves into the phospholipid membrane as well, and travel from the extracellular to the cytosolic edge. They can form a complex with water molecules as well as with ions and thus transfer them across the membrane. An example of a carrier ionophore is the drug monensin. This is a cation transporter and can complex both mono and divalent ions, forming either an electroneutral complex or an electrogenic complex (Antonenko et al., 2015). Various studies have shown that acute monensin treatment can be used to increase intracellular Na^+ levels, however, longer treatments with monensin are not common for ionic dynamics experiments (Tsuchida et al., 2021, Erecińska et al., 1991, Huczyński et al., 2012a, Pinkerton and Steinrauf, 1970). For this study, longer drug treatments are required to be able to monitor changes at transcriptional level and to quantify overall protein levels of IDO1. Therefore, the effects of acute and longer term monensin treatments on intracellular Na^+ levels and IDO1 activity and expression are described here. This thus represents an alternative, ouabain and NKA-independent, method of increasing intracellular Na^+ and should be a good correlative indicator of the effect of intracellular Na^+ on IDO1 activity.

However, this study system is also not ideal, given the well documented effect of monensin as a Golgi inhibitor, thus interfering with post-translational protein modifications, such as glycosylation (Machamer and Cresswell, 1984, Sbodio et al., 2018). Even though IDO1 is not a significantly post-translationally modified protein, and has no sugar moieties attached, the impact of monensin on protein production could have indirect effects on IDO1 activity, either by affecting the IDO1 transcriptional/translational machinery or by interfering with Trp transport (Fujigaki et al., 2006, Fujigaki et al., 2012). Therefore, the monensin derived data, just as in the case of ouabain, can only be a correlative indication of the link between Na^+ and IDO1 activity and not a clear conclusion of their interdependence.

To further build on the Na^+ - IDO1 co-dependency hypothesis, inhibition of a Na^+ activated kinase, involved in Ca^{2+}-dependent signalling, a known component of the IFNγ response, SIK1 could be tested (Popov et al., 2012). SIK1 is a documented tumour suppressor molecule in breast cancer and also a regulator of NKA integrity, mediating the transcription of the β1 subunit of the NKA, ATP1B1 (Taub, 2018, Taub et al., 2015, Taub et al., 2010, Xin et al., 2021).

4.1.2. Hypothesis and aims.

This chapter was built on the hypothesis that elevations in intracellular Na^+, independent of ouabain or NKA inhibition, can inhibit IDO1 activity, and this effect might be mediated through SIK1 activation.

To assess this hypothesis, this chapter firstly investigates the acute and long-term effect of two ionic modulators, the VGSC opener VTD and the ionophore monensin, on intracellular Na^+ levels. The effect of monensin on kynurenine, as well as IDO1 and pSTAT1 expression is then tested. Furthermore, this chapter will then ask the question of SIK1 involvement in the Na^+-IDO1 pathway, by verifying whether pharmacological inhibition of SIK1 can enhance the kynurenine response to IFNγ/TNF, as well as investigating whether SIK1 inhibition could rescue the inhibitory effect of ouabain on IDO1 function and/or expression.

4.2. Results

4.2.1. Increasing intracellular Na^+ in an NKA-independent manner in MDA-MB-231 cells.

Chapter 3 showed that inhibition of the NKA through cardiac glycoside treatment could elevate intracellular Na^+ as well as inhibit IDO1 expression and activity. To separate the effect of intracellular Na^+ from the NKA or possible off-target effects of cardiac glycoside, the VGSC opener VTD and the ionophore monensin were investigated (Gillet et al., 2009a, Brackenbury and Djamgoz, 2006, Gradek et al., 2019).

VTD, a voltage gated Na^+ channel opener, was previously reported to impact on Na^+ currents in MDA-MB-231 cells at concentrations ranging between 10 and 50 nM (Gillet et al., 2009a, Gradek et al., 2019). Monensin was also widely documented in the literature for acutely increasing the intracellular Na^+ concentration (Brackenbury and Djamgoz, 2006, Russo-Abrahão et al., 2018, Cheng et al., 2019, Xin, 2005). This section investigated the ability of VTD and monensin to increase intracellular Na^+ at different timepoints.

A time course experiment was set up to assess the effect of VTD added 1 min and 24 h prior to the first SBFI reading. Figure 4.1A shows no difference in the Na^+ concentrations at either timepoint between the VTD treatment and DMSO, 10 min after the first SBFI read (actual timepoints: 11 min, and 24 h and 10 min post VTD treatment). Instead, the 2.5% DMSO concentration significantly increased intracellular Na^+ at 24 h compared to the 1 min timepoint, which was recapitulated by the 25 µM VTD 2.5% DMSO condition at 24 h.

Given the lack of response recorded with VTD, monensin was tested next. Acute monensin treatment showed a significant increase in intracellular Na^+ levels at the 100 µM concentration. A small, yet not significant, elevation was also observed with the 10 µM concentration (Figure 4.1.B). The trend persisted at all timepoints, as illustrated by

fluorescence ratios (Figure 4.1C). A lower concentration of monensin, 1 µM, was also evaluated at longer timepoints: 2 h, 4 h and 8 h, and a significant increase in intracellular Na^+ was observed at the 8 h timepoint (Figure 4.1D). To verify whether better consistency could be achieved by higher monensin concentrations, the effects of 1, 10 and 50 µM drug concentration, upon 2 and 8 h treatments were tested. A clear trend of drug concentration-dependent intracellular Na^+ increase could be observed at both timepoints with a significant increase observed at the 10 and 50 µM concentrations after an 8 h treatment, as shown in Figure 4.1E.

In conclusion, monensin, but not VTD, induced acute increases in intracellular Na^+, as well as elevating intracellular Na^+ levels in a concentration dependent manner upon 8 h treatments in MDA-MB-231 cells.

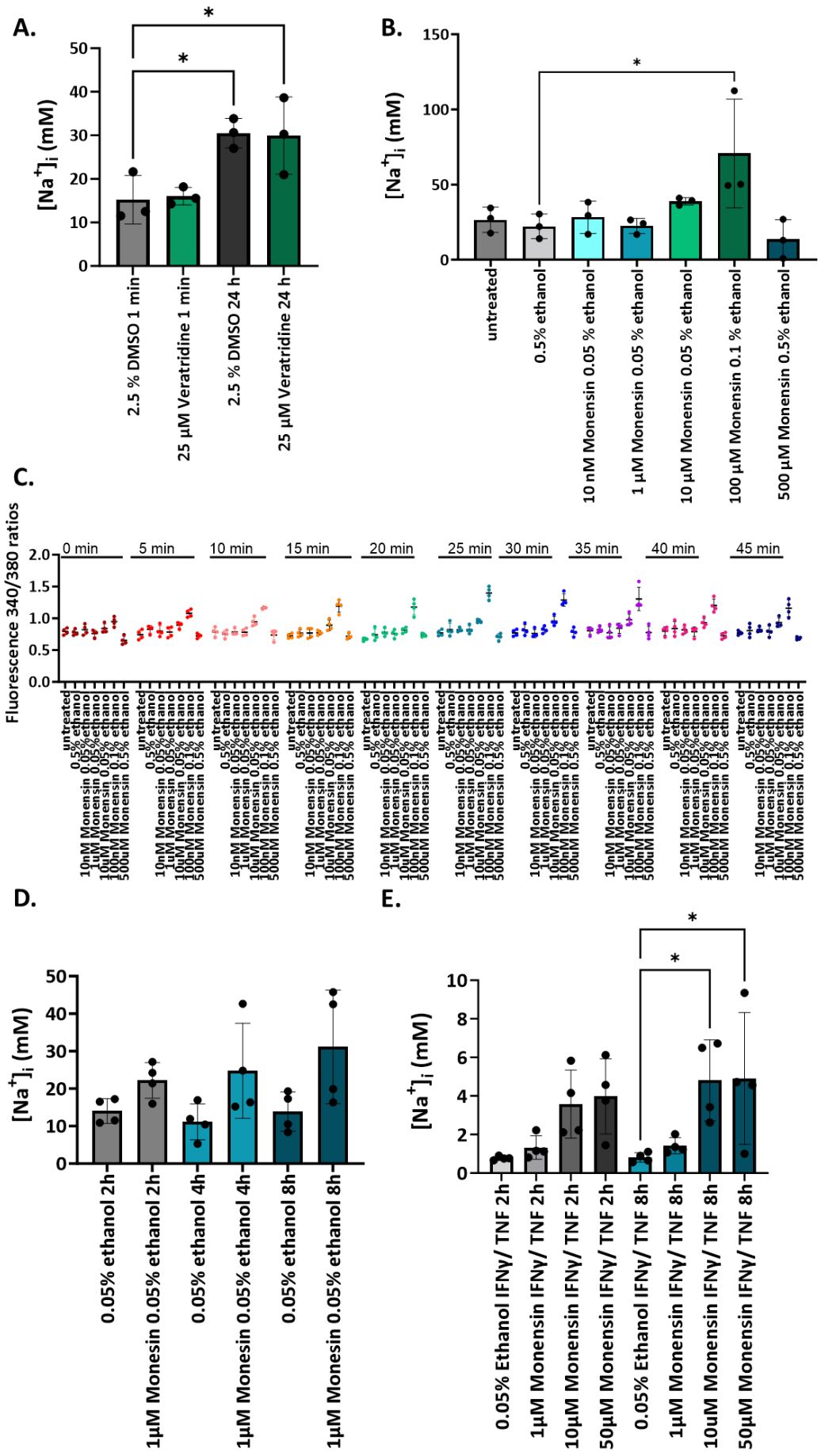
A.
[Na+]i (mM)
2.5 % DMSO 1 min
25 µM Veratridine 1 min
2.5 % DMSO 24 h
25 µM Veratridine 24 h
B.
[Na+]i (mM)
untreated
0.5% ethanol
10 nM Monensin 0.05 % ethanol
1 µM Monensin 0.05 % ethanol
10 µM Monensin 0.05 % ethanol
100 µM Monensin 0.1 % ethanol
500 µM Monensin 0.5% ethanol
C.
Fluorescence 340/380 ratios
0 min
5 min
10 min
15 min
20 min
25 min
30 min
35 min
40 min
45 min
D.
[Na+]i (mM)
0.05% ethanol 2h
1µM Monesin 0.05% ethanol 2h
0.05% ethanol 4h
1µM Monesin 0.05% ethanol 4h
0.05% ethanol 8h
1µM Monesin 0.05% ethanol 8h
E.
[Na+]i (mM)
0.05% Ethanol IFNγ/ TNF 2h
1µM Monensin IFNγ/ TNF 2h
10µM Monensin IFNγ/ TNF 2h
50µM Monensin IFNγ/ TNF 2h
0.05% Ethanol IFNγ/ TNF 8h
1µM Monensin IFNγ/ TNF 8h
10uM Monensin IFNγ/ TNF 8h
50µM Monensin IFNγ/ TNF 8h

*Figure 4.1 Increasing intracellular Na^+ in an NKA-independent manner in MDA-MB-231 cells. A. Effect of VTD on intracellular Na^+ after 11 min and 24 h treatment (n=3 biological replicates); B. Acute effect of monensin on intracellular Na^+ levels (10 min treatment) (n=3 biological replicates); C. Acute effect of monensin on intracellular Na^+ levels, time course over 45 min (one representative graph for n=3 biological replicates); D. Effect of 1 µM monensin after 2, 4, and 8 h treatment (n=4 biological replicates); E. Concentration-dependent effect of monensin on intracellular Na^+ levels after 2 and 8 h treatment (n=4 biological replicates). SBFI staining was achieved as described in section 2.11. The specified VTD (A) or monensin (B, C) concentrations were added to cells immediately prior to the first SBFI reading. Na^+ concentrations at 10 min post veratridine or monensin treatment were plotted in A and B, respectively. 340/380 fluorescence ratios were plotted for the monensin time course treatment (C). For D cells were treated with 1 µM monensin for 2, 4 and 8 h prior to SBFI reading. For E, cells were pre-treated with IFNγ/TNF for 24h and the specified monensin concentration was added for 2 or 8 h prior to SBFI reading; data were normalized to the highest replicate of the 0.05 % ethanol control of the 2 h treatment. All data were plotted as mean and SD. Statistical analysis was conducted in GraphPad Prism v9.0.0 using a one-way ANOVA coupled with Tukey's multiple comparisons test (A), a Bonferroni's multiple comparisons test (B, D, E), *p< 0.05.*

4.2.2. Monensin decreases IDO1 activity and expression in response to IFNγ/TNF stimulation in MDA-MB-231 cells.

Having observed a trend of increase in Na^+ levels in response to monensin, the effect of monensin on the IDO1 pathway and the kynurenine response was evaluated next.

A monensin-concentration-dependent decreasing trend in kynurenine (Figure 4.2A), without impacting on cell growth and viability (Figure 4.2B, C), was observed upon 8 h drug treatment. Additionally, 50 µM monensin significantly decreased IDO1 protein levels (Figure 4.2D, E). PD-L1 levels although not significantly changing according to densitometry (Figure 4.2F), exhibited a shift to lower molecular weight in response to monensin, as seen in Figure 4.2D; this is representative for n=3 biological replicates. The upstream regulator of IDO1 and PD-L1, pSTAT1 did not change in response to monensin and total STAT1 levels also remained constant in response to monensin (Figure 4.2G, H, I).

In summary, monensin seemed to decrease the kynurenine response in a concentration-dependent manner, and higher monensin concentration also downregulated IDO1 protein levels, without impacting on viability and cell growth. Additionally, a shift in PD-L1 molecular weight, but not expression, in response to monensin was observed.

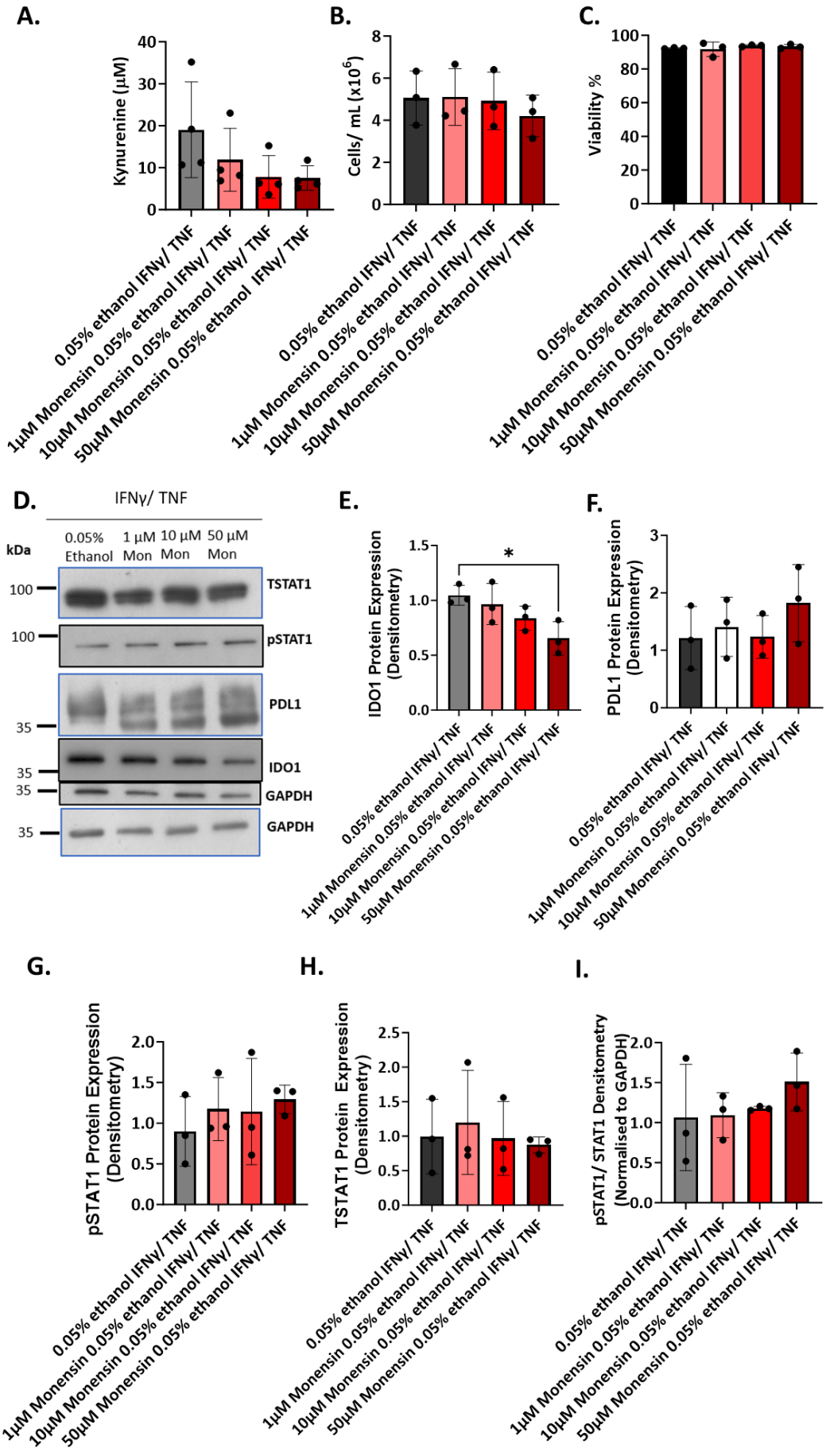
A.
Kynurenine (µM)
B.
Cells/ mL (x10^6)
C.
Viability %
0.05% ethanol IFNγ/ TNF
1µM Monensin 0.05% ethanol IFNγ/ TNF
10µM Monensin 0.05% ethanol IFNγ/ TNF
50µM Monensin 0.05% ethanol IFNγ/ TNF
D.
IFNγ/ TNF
kDa
0.05% Ethanol
1 µM Mon
10 µM Mon
50 µM Mon
100
TSTAT1
100
pSTAT1
PDL1
35
IDO1
35
35
GAPDH
35
GAPDH
E.
IDO1 Protein Expression (Densitometry)
*
F.
PDL1 Protein Expression (Densitometry)
G.
pSTAT1 Protein Expression (Densitometry)
H.
TSTAT1 Protein Expression (Densitometry)
I.
pSTAT1/ STAT1 Densitometry (Normalised to GAPDH)

*Figure 4.2 Effect of monensin on the kynurenine response and IDO1 pathway in MDA-MB-231 cells. A. Concentration-dependent effect of monensin (1, 10 and 50 µM) on the kynurenine response (n=4 biological replicates); B. As in A but for cell growth (n=3 biological replicates); C. As in A but for viability (n=3 biological replicates); D. As in A but for protein expression (representative western blot); E. As in A but for IDO1 protein expression, fold change from GAPDH-normalized average IDO1 expression over all conditions (n=3); F. As in E but for PD-L1 (n=3 biological replicates); G. As in E but for pSTAT1 (n=3); H. As in E but for TSTAT1 (n=3 biological replicates); I. As in E but for pSTAT1/ STAT1 expression ratio (n=3 biological replicates). Cells were stimulated with IFNγ (1 U/ mL)/ TNF (6.25 ng/ mL) for 24 h, and for the last 8 h of the cytokine stimulation, monensin was added to the cultures. Data were plotted as mean and SD in GraphPad Prism v9.0.0. Comparisons were made using an ordinary one-way ANOVA with a Bonferroni's multiple comparisons test (A, E, F, G, H) or a Tukey's post-test (B, C), *p< 0.05.*

4.2.3. Monensin treatment prior to IFNγ/TNF decreases the kynurenine response, but not IDO1 expression, in MDA-MB-231 cells.

To better understand the mechanism of action of monensin, its effect on the initial activation events triggered the IFNγ/TNF stimulation was measured.

Pre-treatment with monensin for 8 h prior to IFNγ/TNF stimulation showed a decreasing trend in kynurenine with drug concentration. Keeping monensin in culture throughout the IFNγ/TNF stimulation (32 h condition) had a significant inhibitory effect on the kynurenine response, especially at the higher concentrations (10 and 50 µM) (Figure 4.3A). Monensin had little or no effect on viability in both the 8 and 32 h conditions (Figure 4.3B). Interestingly, when monensin was added prior to the IFNγ/TNF stimulation, regardless of it being kept in culture with the cytokines, no significant effect on IDO1 protein levels was observed (Figure 4.3C, D). PD-L1 was also not affected at protein level, with either of the two treatment regimes, but monensin induced a drop in the PD-L1 molecular weight, potentially associated with insufficient glycosylation (Figure 4.3C, E) (Li et al., 2016). Pre-treatment with monensin had no effect on pSTAT1 levels (Figure 4.3C, F). A decreasing trend in TSTAT1 expression was observed in response to increasing monensin concentration, particularly in the 32 h conditions. This was, however, not confirmed statistically (Figure 4.3C, G). Figure 4.3H shows the ratio of pSTAT1 to TSTAT1, under the given conditions. No significant changes in the ratio are observed; however, 32 h treatment with 50 µM monensin, leads to a potential increase in pSTAT1 relative to TSTAT1. IDO1 mRNA levels were also measured, and a significant increase in IDO1 mRNA was observed with both treatment conditions (Figure 4.3I).

In conclusion, a decoupling between the effects of monensin on kynurenine and those on IDO1 protein and mRNA levels was observed. A different expression pattern was also seen for IDO1, pSTAT1 and TSTAT1, with the first two being unaltered by monensin, while TSTAT1

might be mildly downregulated. In contrast, the PD-L1 immune checkpoint seemed to be affected through altered post-translational modifications by monensin.

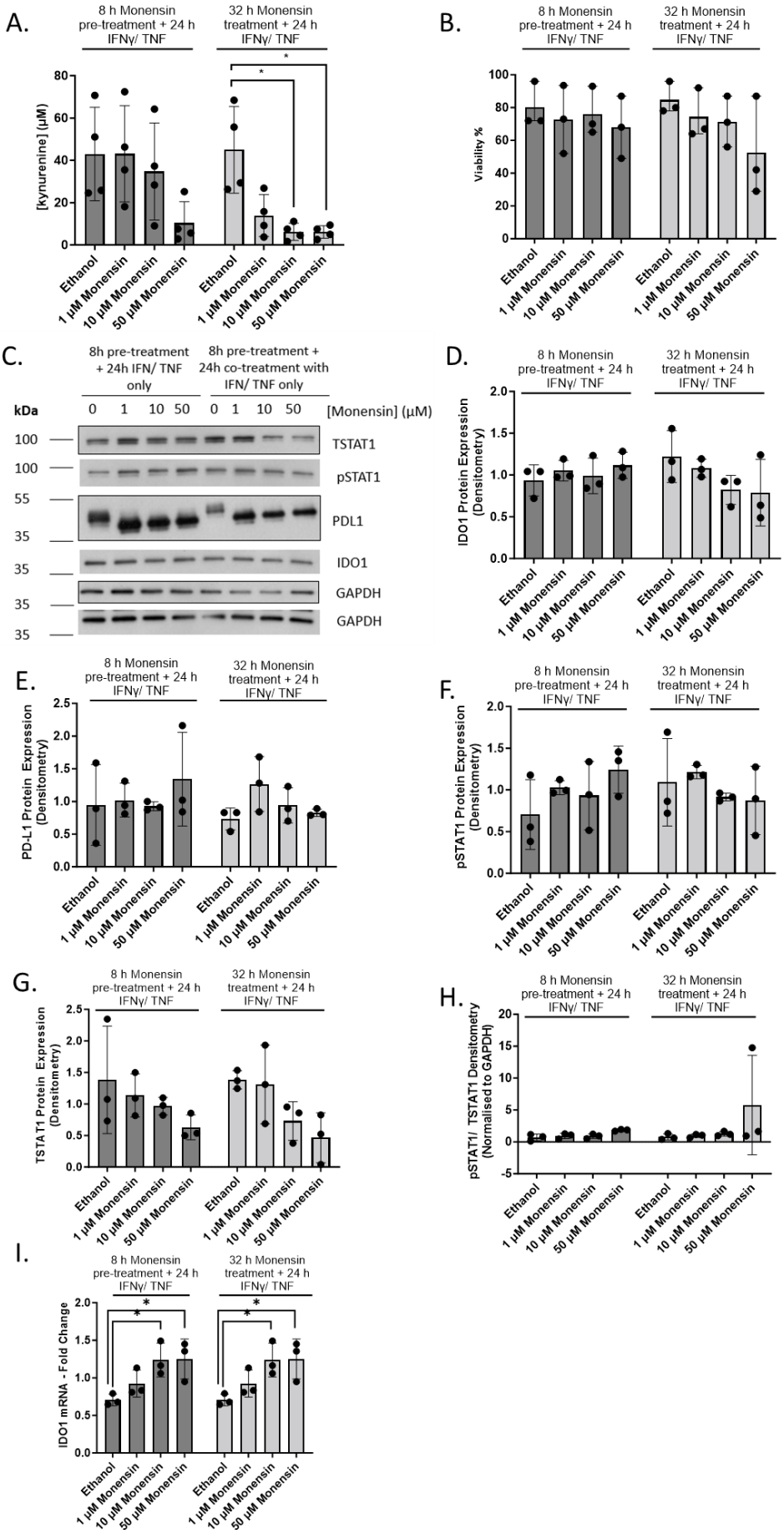
A.
8 h Monensin pre-treatment + 24 h IFNγ/ TNF
32 h Monensin treatment + 24 h IFNγ/ TNF
[kynurenine] (μM)
Ethanol
1 μM Monensin
10 μM Monensin
50 μM Monensin
B.
Viability %
C.
8h pre-treatment + 24h IFN/ TNF only
8h pre-treatment + 24h co-treatment with IFN/ TNF only
kDa
0 1 10 50 0 1 10 50 [Monensin] (μM)
100 TSTAT1
100 pSTAT1
55 PDL1
35
35 IDO1
35 GAPDH
35 GAPDH
D.
IDO1 Protein Expression (Densitometry)
E.
PD-L1 Protein Expression (Densitometry)
F.
pSTAT1 Protein Expression (Densitometry)
G.
TSTAT1 Protein Expression (Densitometry)
H.
pSTAT1/ TSTAT1 Densitometry (Normalised to GAPDH)
I.
IDO1 mRNA - Fold Change

*Figure 4.3 Effect of monensin pre-treatment on the IDO1 response to IFNγ/TNF in MDA-MB-231 cells. A. The kynurenine response (n=4 biological replicates); B. Viability (n=3 biological replicates); C. Representative western blot; D. IDO1 densitometry data, fold change from GAPDH-normalized average IDO1 expression over all conditions (n=3 biological replicates); E. As in C for PD-L1 (n=3 biological repeats); F. As in C for pSTAT1 (n=3 biological repeats); G. As in C for TSTAT1 (n=3 biological repeats); H. As in C for pSTAT1/ TSTAT1 expression ratio (n=3 biological repeats); I. IDO1 mRNA expression, samples were normalized to GAPDH, fold change from average expression value across all the samples was calculated using $2^{(-\Delta CT)}$ values (n=3 biological replicates). For this experiment, monensin was kept in culture for either 8 h prior to the IFNγ/TNF treatment, and removed after cytokine stimulation (24 h), or it was added for 8 h prior cytokine stimulation and for another 24 h with IFNγ/TNF treatment. Data were plotted as mean and SD in GraphPad Prism v9.0.0. Comparisons were made using an ordinary one-way ANOVA with a Bonferroni's multiple comparisons test (A, B, D, E, F, G, H, I), *p< 0.05.*

4.2.4. HG-9-91-01 upregulates IDO1 and kynurenine levels when combined with IFNγ/TNF in MDA-MB-231 cells.

Given the consistent downregulatory effect of Na^+ elevating drugs on IDO1, the mechanism responsible for this effect was investigated in more detail by looking at the SIK1, which has been shown to be activated in response to Na^+ elevations (Sjöström et al., 2007, Taub et al., 2015). HG-9-91-01 has been documented in the literature to be a highly specific SIK1 inhibitor with an IC_{50} of 0.92 µM (Clark et al., 2012) .

Firstly, several pilot experiments were completed to investigate the effect of HG-9-91-01 on kynurenine production and IDO1 expression. HG-9-91-01 slightly upregulated kynurenine levels when combined with IFNγ/TNF but had no effect when added on its own (Figure 4.4A). Higher drug concentrations also severely reduced cell counts and viability (Figure 4.4B, C). Additionally, HG-9-91-01 upregulated IDO1 protein levels in the presence of IFNγ/TNF in a concentration-dependent manner (Figure 4.4D, E). The increase in kynurenine was reproducible while combining HG-9-91-01 with two different IFNγ concentrations, and it was proportional to the initial IFNγ concentration (Figure 4.4F). HG-9-91-01 decreased cell numbers and viability at higher concentrations mostly (Figure 4.4G, H), while increasing IDO1 levels in comparison to the IFNγ/TNF-only treatment, in a concentration-dependent manner. The increase in IDO1 was proportional to the starting IFNγ concentration (Figure 4.4I, J).

In summary, HG-9-91-01 had no effect on IDO1 activity and expression on its own. However, it was able to enhance both the kynurenine response and IDO1 protein levels when combined with IFNγ/TNF. These results were used as guidance for identifying a suitable experimental set-up (0.5 and 1 µM HG-9-91-01 + 1 U IFNγ/TNF stimulation) to assess the effect of monensin on IDO1 activity and expression.

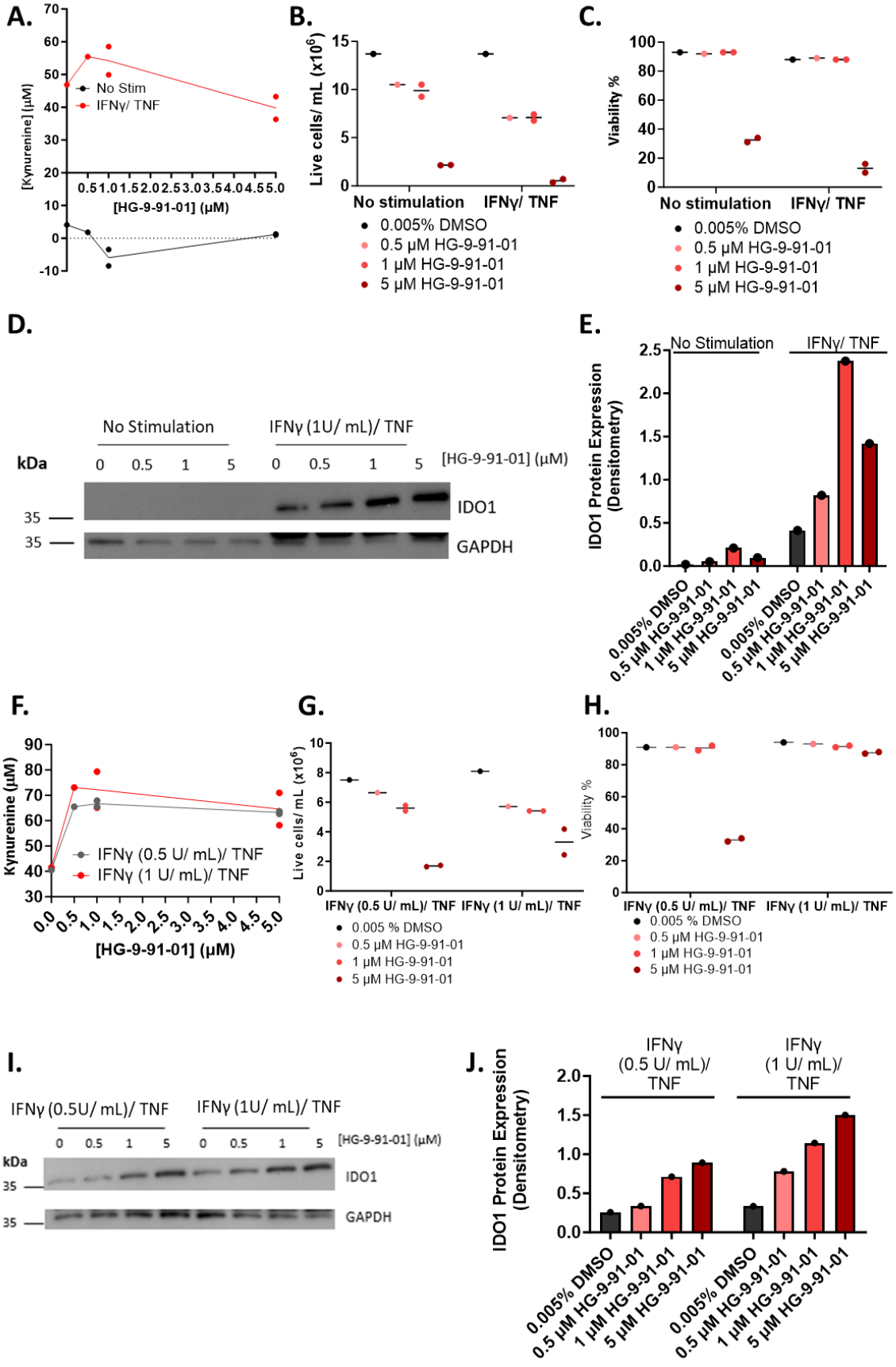
A.
[Kynurenine] (µM)
No Stim
IFNγ/ TNF
[HG-9-91-01] (µM)
B.
Live cells/ mL (x10^6)
No stimulation
IFNγ/ TNF
0.005% DMSO
0.5 µM HG-9-91-01
1 µM HG-9-91-01
5 µM HG-9-91-01
C.
Viability %
No stimulation
IFNγ/ TNF
0.005% DMSO
0.5 µM HG-9-91-01
1 µM HG-9-91-01
5 µM HG-9-91-01
D.
No Stimulation
IFNγ (1U/ mL)/ TNF
kDa
[HG-9-91-01] (µM)
IDO1
GAPDH
E.
No Stimulation
IFNγ/ TNF
IDO1 Protein Expression (Densitometry)
0.005% DMSO
0.5 µM HG-9-91-01
1 µM HG-9-91-01
5 µM HG-9-91-01
F.
Kynurenine (µM)
IFNγ (0.5 U/ mL)/ TNF
IFNγ (1 U/ mL)/ TNF
[HG-9-91-01] (µM)
G.
Live cells/ mL (x10^6)
IFNγ (0.5 U/ mL)/ TNF
IFNγ (1 U/ mL)/ TNF
0.005 % DMSO
0.5 µM HG-9-91-01
1 µM HG-9-91-01
5 µM HG-9-91-01
H.
Viability %
IFNγ (0.5 U/ mL)/ TNF
IFNγ (1 U/ mL)/ TNF
0.005 % DMSO
0.5 µM HG-9-91-01
1 µM HG-9-91-01
5 µM HG-9-91-01
I.
IFNγ (0.5U/ mL)/ TNF
IFNγ (1U/ mL)/ TNF
[HG-9-91-01] (µM)
kDa
IDO1
GAPDH
J.
IDO1 Protein Expression (Densitometry)
IFNγ (0.5 U/ mL)/ TNF
IFNγ (1 U/ mL)/ TNF
0.005% DMSO
0.5 µM HG-9-91-01
1 µM HG-9-91-01
5 µM HG-9-91-01

Figure 4.4 Effect of the SIK1 inhibitor, HG-9-91-01, on IDO1 function and expression in MDA-MB-231 cells. A. Effect of HG-9-91-01 +/- 1 U/mL IFN-γ/TNF on the kynurenine response (n=1); B. As in A but for cell growth (n=1 biological replicate); C. As in A but for viability (n=1); D. As in A but for IDO1 expression – western blot (n=1); E. As in A but for IDO1 expression - densitometry data, GAPDH-normalized (n=1); F. Effect of HG-9-91-01 in combination with 0.5 or 1 U/mL IFN-γ/TNF on the kynurenine response (n=1); G. As in F but for cell growth (n=1); H. As in F but for viability (n=1); I. As in F but for IDO1 expression – western blot (n=1); J. As in F but for IDO1 expression - densitometry data, GAPDH-normalized (n=1). Cells were pre-treated with HG-9-91-01 for 18 h then IFNγ (1 U/ mL)/ TNF (6.24 ng/ mL) stimulation was added for another 24 h. Data were represented as individua values, with A, B, C F, G and H also marking the average of these points. All data for this figure were an n=1 biological repeat, therefore, no statistical analysis was conducted.

4.2.5. HG-9-91-01 does not impact on kynurenine or IDO1 protein levels in ouabain-treated MDA-MB-231 cells.

Given the observed upregulation of kynurenine upon combining IFN-γ treatment with HG-9-91-01, it was considered of interest to test whether ouabain would still have an inhibitory effect on the IDO1 response in the presence of the SIK1 inhibitor, or whether SIK1 inhibition using HG-9-91-01 would rescue the IDO1 activity.

Firstly, the effects of ouabain alone versus ouabain combined with different HG-9-91-01 concentrations were compared, to see if SIK1 inhibition could counteract the effect of ouabain on IDO1 activity. Ouabain caused a significant drop in kynurenine, which was not rescued by the combination of ouabain and HG-9-91-01 at either concentration (Figure 4.5A). While cell numbers significantly decreased in the samples receiving ouabain or ouabain and 1 µM HG-9-91-01 (below Figure 4.5B), viability percentages stayed the same across all conditions (Figure 4.5C). Figure 4.5D shows a western blot representative for 3 biological replicates. A small upregulation in IDO1 seemed to occur with both HG-9-91-01 concentrations, in comparison to ouabain treatment, however, this was not validated statistically (Figure 4.5D, E). No significant difference in the protein levels of the PD-L1 immune checkpoint or the upstream regulators of IDO1 and PD-L1 and pSTAT1 could be seen (Figure 4.5F, G). Total STAT1, although not significantly changing upon addition of either HG-9-91-01 concentration to ouabain, was significantly decreased by ouabain compared to DMSO and this difference was no longer recapitulated in samples treated with both ouabain and HG-9-91-01 (Figure 4.5H). When plotting the ratio of pSTAT1 and TSTAT1 protein levels, no changes were observed upon any of the treatments (Figure 4.5I).

In conclusion, HG-9-91-01 treatment did not rescue the effect of ouabain on the kynurenine response. The SIK1-inhibitor moderately upregulated IDO1 and TSTAT1 protein expression in comparison with ouabain treatment, however, the amplitude of this effect was not enough

to be confirmed statistically with the given number of replicates (n=4). SIK1 inhibition also did not alter the effect of ouabain on the expression of other immune IFNγ-regulated proteins such as PD-L1 and (p)STAT1.

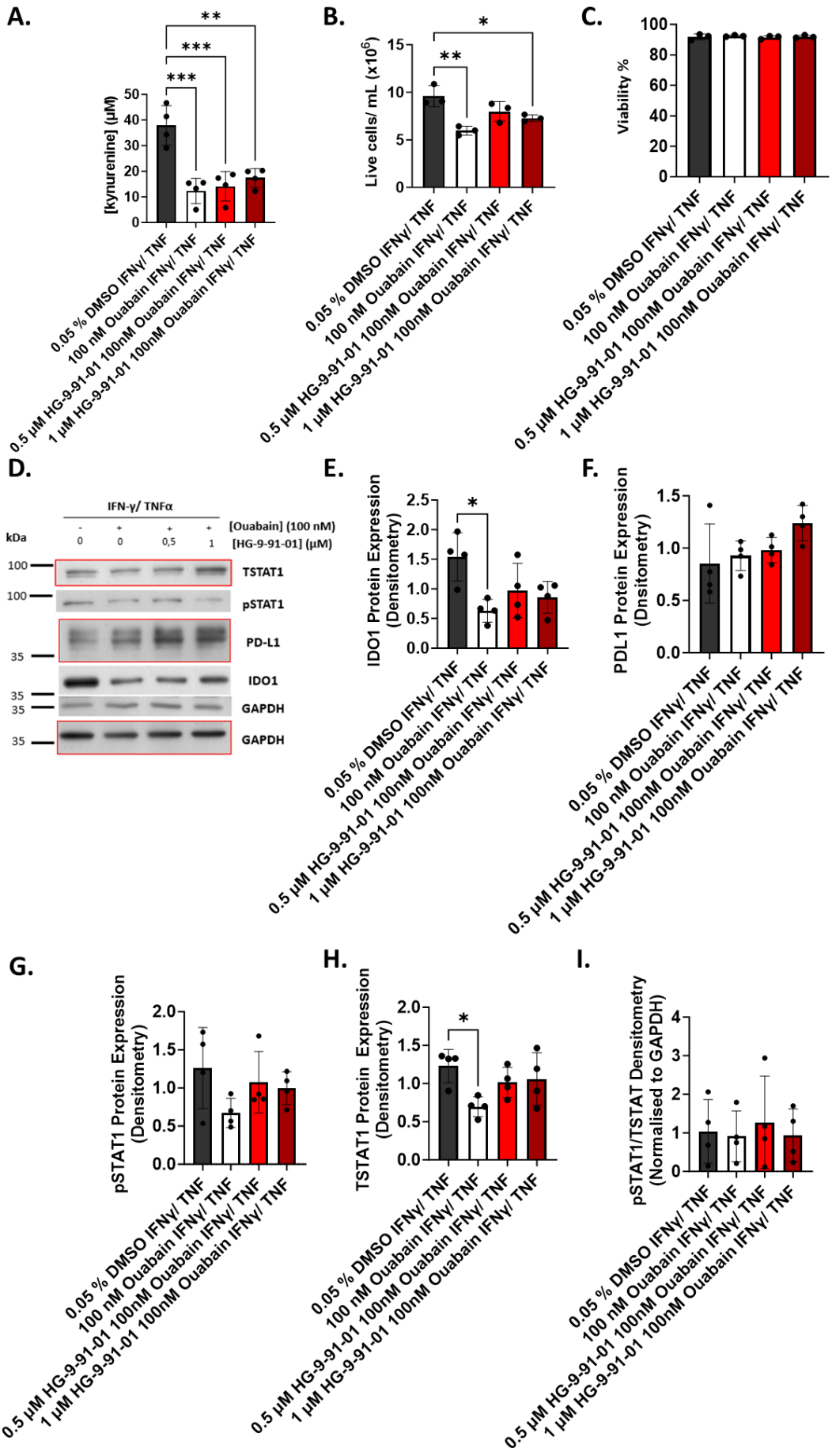
A.
[kynurenine] (µM)
0.05 % DMSO IFNγ/ TNF
100 nM Ouabain IFNγ/ TNF
0.5 µM HG-9-91-01 100nM Ouabain IFNγ/ TNF
1 µM HG-9-91-01 100nM Ouabain IFNγ/ TNF
B.
Live cells/ mL (x10^6)
C.
Viability %
D.
IFN-γ/ TNFα
[Ouabain] (100 nM)
[HG-9-91-01] (µM)
kDa
TSTAT1
pSTAT1
PD-L1
IDO1
GAPDH
GAPDH
E.
IDO1 Protein Expression (Densitometry)
F.
PDL1 Protein Expression (Dnsitometry)
G.
pSTAT1 Protein Expression (Densitometry)
H.
TSTAT1 Protein Expression (Densitometry)
I.
pSTAT1/TSTAT Densitometry (Normalised to GAPDH)

*Figure 4.5 Effect of HG-9-91-01 and ouabain on the IDO1 response and expression in MDA-MB-231 cells. A. Effect of ouabain and HG-9-91-01 compared to ouabain alone on the kynurenine response (n=4 biological replicates); B. Same as A but for cell growth (n=3 biological replicates); C. Same as A but for viability (n=3 biological replicates); D. Same as A but for protein expression – example western blot for n=4 biological replicates; the western blot boxes for each protein were color-coded with their corresponding GAPDH control in red and black; E. Same as A but for IDO1 protein expression, fold change from GAPDH-normalized average IDO1 expression over all conditions (n=4 biological replicates); F. Same as E but for PD-L1 (n=4 biological replicates); G. Same as E but for pSTAT1 (n=4); H. Same as E but for TSTAT1 (n=4 biological replicates); I. Same as E but for pSTAT1/TSTAT1 expression ratio (n=4 biological replicates). Cells were pre-treated with HG-9-91-01 and/ or ouabain for 18 h then IFNγ (1 U/ mL)/ (6.25 ng/ mL) TNF stimulation was added for another 24 h. Data were plotted as mean and SD. Statistical analysis was carried out using an ordinary one-way ANOVA paired with a Tukey's multiple comparison post-test, * p<0.05, ** p<0.01, ***p<0.001.*

4.2.6. HG-9-91-01 does not impact on IDO1 mRNA levels, in ouabain-treated MDA-MB-231 cells.

Next, the effect of HG-9-91-01 in combination with ouabain on IDO1 mRNA expression was tested. qPCR was used to assess the impact of ouabain versus ouabain and HG-9-91-01 on gene expression. In agreement with densitometry data (Figure 4.5E), ouabain caused a significant drop in IDO1 levels, which was not rescued by co-treatment with ouabain and 0.5 µM HG-9-91-01. Treatment with 1µM HG-9-91-01 increased IDO1 expression enough to abolish the statistically significant difference from the DMSO control, however, the magnitude of this effect was not enough to be picked up statistically when comparing it to the ouabain only condition (Figure 4.6A). The addition of ouabain also significantly increased PD-L1 levels in ouabain-treated samples, and HG-9-91-01 did not caused further changes (Figure 4.6B). mRNA expression of other immune markers such as the HLA-A, B and C complexes was also tested. No difference was observed between ouabain only and ouabain and HG-9-91-01-treated samples in HLA-B and C, while HLA-A was significantly upregulated by ouabain, without further significant changes upon treatment with HG-9-91-01 (Figure 4.6C-E). Additionally, to validate the efficacy of HG-9-91-01 as a SIK1 inhibitor, its effect on expression of the ATP1B1, previously reported to be transcriptionally regulated by SIK1, was assessed (Taub, 2018). However, in the experiments presented here, HG-9-91-01 had no effect on ATP1B1 expression (Figure 4.6F).

In summary, HG-9-91-01 did not significantly alter the ouabain effect on expression of IDO1 and other immune genes such as PD-L1, HLA-A, B and C. However, ouabain was able to upregulate PD-L1 and HLA-A mRNA levels, while reducing IDO1 expression in MDA-MB-231 cells. Additionally, it was not possible to validate the efficacy of the HG-9-91-01 as a SIK1 inhibitor since the drug did not affect expression of the canonical target, ATP1B1.

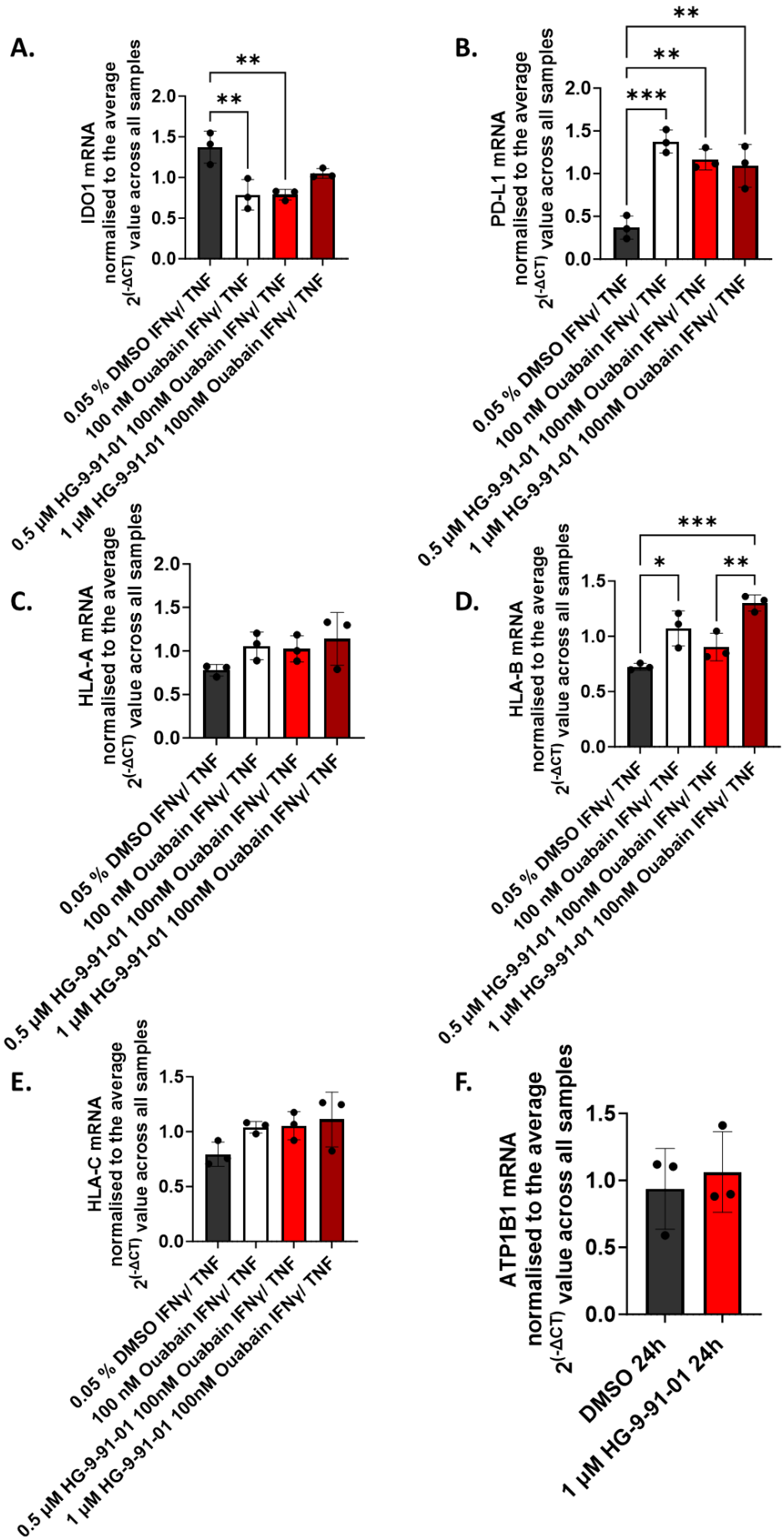
A.
IDO1 mRNA normalised to the average 2(-ΔCT) value across all samples
2.0
1.5
1.0
0.5
0.0
**
**
0.05 % DMSO IFNγ/ TNF
100 nM Ouabain IFNγ/ TNF
0.5 µM HG-9-91-01 100nM Ouabain IFNγ/ TNF
1 µM HG-9-91-01 100nM Ouabain IFNγ/ TNF
B.
PD-L1 mRNA normalised to the average 2(-ΔCT) value across all samples
2.0
1.5
1.0
0.5
0.0
***
**
**
0.05 % DMSO IFNγ/ TNF
100 nM Ouabain IFNγ/ TNF
0.5 µM HG-9-91-01 100nM Ouabain IFNγ/ TNF
1 µM HG-9-91-01 100nM Ouabain IFNγ/ TNF
C.
HLA-A mRNA normalised to the average 2(-ΔCT) value across all samples
2.0
1.5
1.0
0.5
0.0
0.05 % DMSO IFNγ/ TNF
100 nM Ouabain IFNγ/ TNF
0.5 µM HG-9-91-01 100nM Ouabain IFNγ/ TNF
1 µM HG-9-91-01 100nM Ouabain IFNγ/ TNF
D.
HLA-B mRNA normalised to the average 2(-ΔCT) value across all samples
1.5
1.0
0.5
0.0
***
*
**
0.05 % DMSO IFNγ/ TNF
100 nM Ouabain IFNγ/ TNF
0.5 µM HG-9-91-01 100nM Ouabain IFNγ/ TNF
1 µM HG-9-91-01 100nM Ouabain IFNγ/ TNF
E.
HLA-C mRNA normalised to the average 2(-ΔCT) value across all samples
1.5
1.0
0.5
0.0
0.05 % DMSO IFNγ/ TNF
100 nM Ouabain IFNγ/ TNF
0.5 µM HG-9-91-01 100nM Ouabain IFNγ/ TNF
1 µM HG-9-91-01 100nM Ouabain IFNγ/ TNF
F.
ATP1B1 mRNA normalised to the average 2(-ΔCT) value across all samples
1.5
1.0
0.5
0.0
DMSO 24h
1 µM HG-9-91-01 24h

*Figure 4.6 Effect of HG-9-91-01 and ouabain on the IDO1, PD-L1 and HLA A/B/C gene expression in MDA-MB-231 cells. A. Effect of ouabain on IDO1 mRNA levels in the presence of HG-9-91-01, samples were normalized to GAPDH, fold change from average expression value across all the samples was calculated using $2^{(-\Delta CT)}$ values (n=3 biological replicates). B. Same as A but for PD-L1 mRNA expression (n=3 biological replicates); C. Same as A but for HLA-A mRNA expression (n=3 biological replicates); D. Same as A but for HLA-B mRNA expression (n=3 biological replicates); E. Same as A but for HLA-C mRNA expression (n=3 biological replicates); F. ATP1B1 expression in response to 24 h treatment with 1 µM HG-9-91-01, fold change from GAPDH-normalized normalized average ATP1B1 expression over all conditions (n=3 biological replicates). Cells were pre-treated with HG-9-91-01 and/ or ouabain for 18 h then IFNγ (1 U/ mL)/ TNF (6.25 ng/ mL) stimulation was added for another 24 h. Data were plotted as mean and SD. Statistical analysis was conducted using a one-way ANOVA coupled with a Tuckey's multiple comparisons test (A-E), or a two-tailed unpaired t-test (F, p= 0,6359), *** p< 0.001.*

4.2.7. SIK1 enhances overall survival in breast cancer patients, without correlating on a transcriptional level with STAT1-regulated genes.

SIK1 is a tumour suppressor molecule particularly important in breast cancer (Sun et al., 2020). To investigate any clinical connections between SIK1 expression and STAT1-regulated genes, in particular IDO1, an *in silico* study was conducted using the METABRIC and TCGA data sets. The merged datasets covered multiple breast cancer subtypes; the number of patients associated with each subtype are as follows: 20 Breast, 1582 Breast Invasive Ductal Carcinoma, 148 Breast Invasive Lobular Carcinoma, 24 Breast Invasive Mixed Mucinous Carcinoma, 208 Breast Invasive Mixed Ductal and Lobular Carcinoma, 15 Invasive Breast Carcinoma, 1 Metaplastic Breast Cancer. This study chose to analyse all breast cancer subtypes together, in an attempt to assess the impact of SIK1 and STAT1-controled genes, in particular IDO1, in breast cancer progression regardless of subtype. The reason why all subtypes were pulled together was due to literature reports that show no significant differences in SIK1 expression across various breast cancer types (Xin et al., 2021). This study looked at SIK1 and SIK1 co-expressed/targeted proteins, and their correlation with STAT1-controlled proteins in breast cancer. The impact of SIK1 on survival was also assessed.

Figure 4.7A shows mRNA z-score correlations across all patients within the two data sets, indicating no relationship between SIK1 and STAT1-controlled genes. Interestingly, however, patients with higher SIK1 levels had a better survival probability (Figure 4.7 B). The data sets were then split based on IDO1 mRNA z-scores into top and bottom quartiles (corresponding to high and low IDO1 expression respectively). Correlation and survival analyses were conducted again within the top quartile (Figure 4.7C, D) and bottom quartile (Figure 4.7E, F) populations; however, no strong SIK1 correlations were found in either of these populations, and SIK1 expression also did not significantly associate with survival (Figure 4.7D, F). A Cox Proportional Hazards Regression was run in GraphPad Prism comparing the impact of SIK1

high and SIK1 low expression, as well as that of breast cancer subtype on survival. However, SIK1 expression had no impact on survival (p=0.0573) in the selected groups; similarly the breast cancer subtype did not impact on overall survival (Figure 4.7G).

Overall, SIK1 expression was not correlated with any of the selected STAT1-controlled genes, regardless of the IDO1 expression status of the patients. However, SIK1 expression associated positively with enhanced overall survival in breast cancer patients, which is consistent with literature reports (Sun et al., 2020).

A.

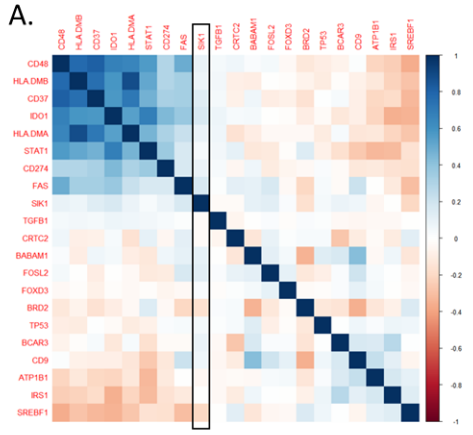

B.

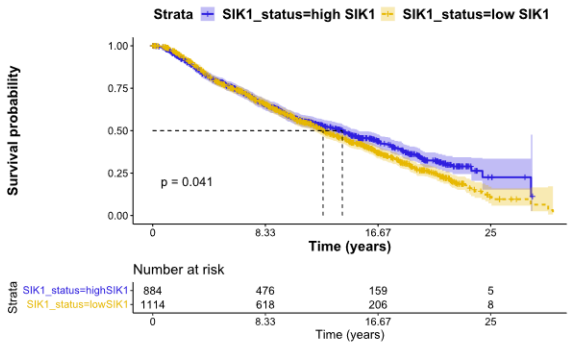

C.

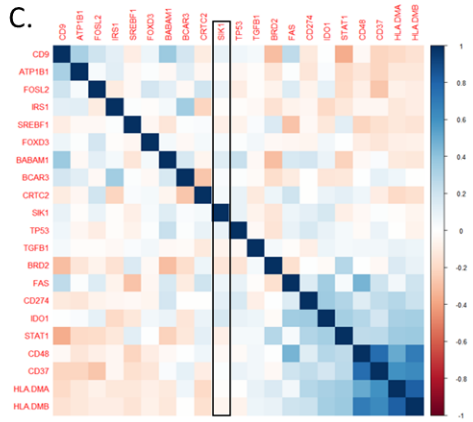

D.

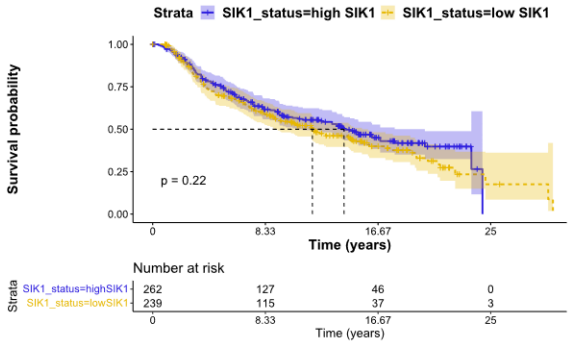

E.

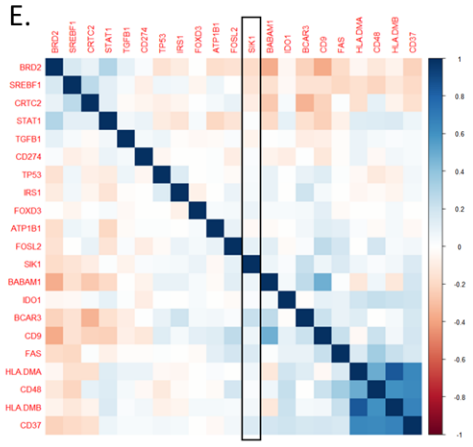

F.

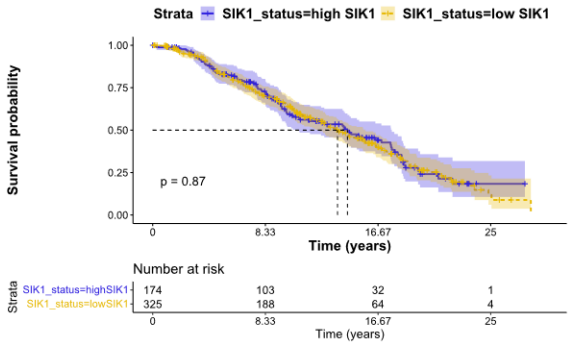

G.

Variables	Hazard ratios (95% CI)	P value
SIK1.status		
High SIK1	1	
Low SIK1	1,124 (0,9968 to 1,268)	0,0573
Cancer.Type.Detailed		
Breast	1	
Breast Invasive Ductal Carcinoma	2,283 (1,059 to 6,380)	0,0657
Breast Mixed Ductal and Lobular Carcinoma	2,263 (1,030 to 6,388)	0,0732
Breast Invasive Lobular Carcinoma	2,283 (1,027 to 6,487)	0,073
Breast Invasive Mixed Mucinous Carcinoma	1,575 (0,5439 to 5,127)	0,4156
Invasive Breast Carcinoma	2,68 (0,8938 to 8,871)	0,0839
Metaplastic Breast Cancer	4,024 (0,2099 to 25,01)	0,2041

Figure 4.7 SIK1 and STAT1-controlled genes in breast cancer patients. A. Correlation analysis for all patients in the METABRIC and TCGA data set (n=1998); B. Survival analysis for all patients in the METABRIC and TCGA data set (n=1998); C. Correlation analysis for patients in the top quartile based on IDO1 expression METABRIC and TCGA data set (n=501); D. Survival analysis for patients in the top quartile based on IDO1 expression METABRIC and TCGA data set (n=501); E. Correlation analysis for patients in the bottom quartile based on IDO1 expression METABRIC and TCGA data set (n=499); F. Survival analysis for patients in the bottom quartile based on IDO1 expression METABRIC and TCGA data set (n=499). G. Results of the COX Proportional Hazards Regression analysis, including breast cancer subtypes for all patients in the METABRIC and TCGA data set (n=1998). For A-E data were analysed using R studio, while figure G was generated using Graph Pad Prism 10.1.2.

4.3. Discussion

This chapter focused on optimizing experimental conditions for achieving an increase in intracellular Na^+ levels, in an NKA and cardiac glycoside-independent manner, via the ionophore monensin. Experimental data showed that treatment with monensin for 8 h after cytokine stimulation inhibits the kynurenine response in a concentration-dependent manner, as well as reducing IDO1 expression. This confirmed the trend observed with cardiac glycoside-induced intracellular Na^+ elevations in Chapter 3. Figure 4.2 and Figure 4.3 show that the effect of monensin on the kynurenine response occurs regardless of whether it is added before or after IFNγ-induced IDO1 expression, suggesting that Na^+ might play a role in both pre and post-transcriptional regulation of IDO1. To better understand the signalling pathway between Na^+ and IDO1, this chapter also investigated the role of a downstream Na^+ effector, SIK1, known to be activated by increased cellular Na^+ and Ca^{2+} levels (Taub et al., 2015, Taub, 2019). An increase in kynurenine was observed upon combining SIK1 inhibition and IFNγ/TNF stimulation. However, the combination of ouabain with a SIK1 inhibitor, HG-9-91-01, gave no significant increase in kynurenine levels compared to ouabain alone, suggesting that SIK1 might not mediate the effect of increased intracellular Na^+ levels on IDO1 activity. This conclusion could not be fully validated, since data did not confirm that HG-9-91-01 has an inhibitory effect on SIK1, given that no changes in the SIK1-regulated gene ATP1B1 could be picked up by qPCR.

4.3.1. Monensin affects intracellular Na^+, kynurenine and IDO1 expression in different ways.

Monensin has been extensively reported in the literature to acutely increase intracellular Na^+ (Russo-Abrahão et al., 2018, Cheng et al., 2019, Efendiev et al., 2002). Based on previously reported concentrations of monensin used in a variety of cell types, an initial acute titration was set up (Russo-Abrahão et al., 2018, Cheng et al., 2019, Efendiev et al., 2002). This

chapter confirmed that acute application of monensin (100 µM) on MDA-MB-231 cells can cause a significant increase in intracellular Na^+(Figure 4.1B). Interestingly, higher monensin concentrations, such as 500 µM did not cause a similar elevation in intracellular Na^+ (Figure 4.1B, C). A possible explanation for that could come from the mode of action of the ionophore. Monensin is a carrier ionophore that forms complexes with monovalent cations such as Na^+, but also H^+, transporting them across the membrane (Huczyński et al., 2012b). By doing so, monensin is likely to disturb both intra and extracellular pH. This could potentially impact on the efficacy of the Na^+ binding dye, SBFI-AM, used in these experiments, as suggested by previous literature reports (Diarra et al., 2001). This highlights the limitations of the SBFI-AM method of quantifying intracellular Na^+ and suggests the need for an alternative detection mechanism (e.g., CoroNa™ Green or Asante NaTRIUM Green-2) (Iamshanova et al., 2016). Additionally, high monensin concentrations, such as 500 µM could also be cytotoxic, leading to disrupted cellular homeostasis which could be responsible for the drop in the intracellular Na^+ signal.

Longer monensin treatments (8 h) significantly increased intracellular Na^+, at 10 and 50 µM (Figure 4.1E). Therefore, given the consistent, concentration-dependent increase in intracellular Na^+ with 8 h monensin treatment, it is justified to conclude that the data presented in this chapter confirms the documented role of monensin as a tool to raise the intracellular Na^+ concentration.

Additionally, the effect of monensin, added for 8 h on MDA-MB-231 cells post cytokine stimulation with IFNγ/TNF, on the kynurenine response and IDO1 expression was tested next. The same monensin concentrations shown to increase intracellular Na^+ (Figure 4.1), seemed to cause a decreasing trend in IDO1 activity, in a concentration dependent manner, while also dropping IDO1 protein levels at the higher 50 µM concentration (Figure 4.2A, D, E). Cell survival was not affected by any monensin concentration (Figure 4.2B, C). IDO1

transcriptional regulators, total and pSTAT1, did not seem to be affected by monensin (Figure 4.2G, H), also supporting the hypothesis of kynurenine changes being triggered by modulation of IDO1 enzymatic activity, either directly through Na^+ changes, via an unknown mechanism, or through pH changes (Littlejohn et al., 2000, Arisaka et al., 1988). Interestingly, PD-L1, while not significantly affected by monensin in terms of expression, seemed to undergo a mild transition towards a lower molecular weight, potentially less glycosylated, isoform, suggesting that intracellular Na^+ changes might affect more than one immune checkpoint protein (Figure 4.2F) (Li et al., 2016). These changes are, however, expected and further confirm the efficacy of monensin, which was documented in the literature to impact on a series of cellular processes including disruption of the Golgi apparatus, which is often associated with defects in post-translational processing, including glycosylation (Machamer and Cresswell, 1984, Sbodio et al., 2018). Although de-glycosylation effects of monensin on PD-L1 specifically have not been reported before, monensin has been known to impair N and O glycosylation of proteins, particularly the HLA molecules (Machamer and Cresswell, 1984). Therefore, this reduction in PD-L1 molecular weight (likely due to impaired glycosylation) confirms the literature-reported effect of monensin and serves as a good positive control to confirm drug activity.

Overall, monensin, just like the cardiac glycosides in Chapter 3, increased intracellular Na^+ levels and dropped IDO1 expression at higher drug concentrations; it also moderately decreased kynurenine production showing a concentration-dependent trend. However, unlike ouabain, monensin did not impact on pSTAT1 levels.

The observations presented above suggest that although there is some overlap in terms of the starting (changes in intracellular Na^+) and ending point (IDO1 activity and/or expression) of the changes triggered by monensin and ouabain, the drugs might be operating through completely different mechanisms.

To better understand the mechanism of action of monensin, its effect on the kynurenine response was investigated, in response to two treatment conditions: (1) 8 monensin pre-treatment, followed by removal of drug and 24 h stimulation with IFNγ/TNF; (2) 8 monensin pre-treatment, followed by 24 h of co-treatment with monensin and IFNγ/TNF stimulation. Pre-treatment of MDA-MB-231 cells with monensin prior to IFNγ/TNF stimulation seemed to reduce kynurenine in a concentration dependent manner, but monensin only caused a significant drop when kept in culture during the IFNγ/TNF stimulation (Figure 4.3A). IDO1 protein levels were, however, not significantly affected with either treatment condition (Figure 4.3C, D). This is particularly unexpected, especially since co-treatment of monensin with IFNγ/TNF, when monensin was added after the cytokine stimulation, did drop IDO1 protein levels (Figure 4.2). This is an observation that is difficult to explain, however, it is possible that adding monensin at the same time with the IFNγ/TNF stimulation, might provide a shock on the transcriptional and post-transcriptional machinery of the cell, while priming the cells with monensin before the cytokine stimulation might interfere with this initial shock. Alternatively, monensin pre-treatment might affect other transcriptional/translational pathways which in turn could enhance the IFNγ/TNF-mediated IDO1 expression. However, further proteomics/171hosphor-proteomics and/or RNAseq experiments would need to be conducted to analyse the exact pathways upregulated within cells upon monensin treatment, before or concomitantly with cytokine stimulation. This kind of in-depth mechanistic analysis of monensin is, however, beyond the scope of this project and was not pursued further.

The clear uncoupling between the IDO1 protein levels and IDO1 activity further suggests that monensin might not be enforcing its effects on IDO1 via transcriptional regulation only. A way to explain this could be that the effect on kynurenine might occur due to defects in IDO1 trafficking, or integrity, given the well-established function of monensin as a disruptor of the Golgi membrane, resulting in defects in protein trafficking, secretion and post-translational

modification (Mollenhauer et al., 1990). Another possible explanation could be that monensin might be able to impact on IDO1 function only, rather than its expression. This could occur as a result of potential intracellular pH changes, often associated with ionic imbalances such as the increase in intracellular Na^+ measured with monensin. Monensin is a cation transporter and could thus import both Na^+ and H^+ ions inside the cell, as well as export H^+ in exchange for Na^+, thus altering the intracellular pH. Furthermore, accumulation of intracellular Na^+ could lead to subsequent activation of the Na^+/H^+ exchanger and thus further alter cytosolic pH (Smallridge et al., 1992, Tapper and Sundler, 1990, Boss et al., 1984, Vanneste et al., 2019). Changes in intracellular pH could interfere with protein folding, as well as the enzymatic function of IDO1, or upstream regulatory proteins and could thus explain the effect seen on kynurenine. However, further experiments would be needed to fully elucidate the mechanism of action of monensin.

Another interesting observation is also the fact that IDO1 and pSTAT1 seem to be responding to monensin in a different way than TSTAT1 (Figure 4.3C, D, F, G), which is not consistent with the effect of ouabain-induced Na^+ increases (Shandell et al., 2022). This further supports the idea that the pathways and effectors triggered by the two drugs are completely different, despite the similar endpoint. It might also suggest that the Na^+-induced downregulation of the IDO1 activity is not dependent on STAT1 expression, and the decrease seen in ouabain-treated samples is just a parallel, independent effect (Chapter 3).

Altogether, the data presented in sections 4.2.1 to 4.2.3 indicate a complex mechanism that might be regulated at multiple levels, affecting multiple immune checkpoints, IDO1 and PD-L1 included.

Given the pleiotropic effects of pharmacological approaches to study fluctuations in intracellular Na^+, a variety of different approaches could be used alternatively or complementarily to try and pinpoint a potential mechanism linking ionic dynamics and IDO1

integrity. One such complementary approach could be directly measuring the activity of the NKA in response to pharmacological treatment and/or cytokine stimulation. Multiple studies have been published showing that uptake of radioactive/no-radioactive rubidium (Rb^+) could be used to quantify NKA activity (Gill et al., 2004, Clemente et al., 2023). That is because the NKA has been shown to have similar affinity and binding site of Rb^+ and K^+ (Hakimjavadi et al., 2018). By tracking the activity of the NKA, it would thus be possible to verify whether IDO1 inhibition via ouabain and monensin is directly correlated with a change in NKA activity. Furthermore, changes in intracellular Na^+ independent of the NKA or pharmacological inhibitors would be a clear indicator of the link between IDO1 activity and Na^+ dynamics. One solution to that would be the use of a chemo genetic ligand gated ion channel. In principle, these are channels engineered to be activated by a low dose of an agonist drug, selected as a safe and clinically approved molecule. In the absence of the agonist, the channel remains inactive. The use of a Na^+ -specific chemo genetic ligand gated channel, could allow us to study the effect of intracellular accumulation of Na^+ independently of NKA inhibition, and with more clarity than using a general cation transporter like monensin (Magnus et al., 2011, Magnus et al., 2019).

4.3.2. HG-9-91-01 upregulates IDO1 and kynurenine levels when combined with IFNγ/TNF.

Although pH changes could potentially explain the inhibitory role of Na^+ on IDO1 activity, the decrease in IDO1 expression seen with ouabain (Chapter 3) and monensin (Figure 4.2D, E) would be probably more difficult to justify. One possible hypothesis would be that elevations in intracellular Na^+ might lead to increases in intracellular Ca^{2+} levels either through store mediated Ca^{2+} release, or via extracellular Ca^{2+} import through the NCX. The increase in intracellular Ca^{2+} is known to activate the Ca^{2+}/CaMK pathway which has as downstream effectors canonical kinases, including SIK1, otherwise well-documented in the literature as a

tumour suppressor in breast cancer (Popov et al., 2012, Taub, 2019, Villalobo and Berchtold, 2020). SIK1 is an AMPK which has as downstream phosphorylation substrates, proteins that incorporate the LX(R/K/H) (S/T) XSXXXL, which includes class IIA histone deacetylases (HDACs) (HDAC4, 5, 7, and 9) and CREB-regulated transcription coactivator (CRTC) proteins. Phosphorylated CRTCs cannot translocate to the nucleus, which impacts on gene expression (Taub et al., 2010, Taub et al., 2015).

SIK1 can also function as a negative feedback mediator in response to increases in intracellular Na^+. SIK1 phosphorylates protein phosphatase methylesterase-1 (PME-1), which then dissociates from the PME-1/ Protein phosphatase 2A (PP2A)/NKA complex, leading to PP2A dephosphorylation and amplified NKA activity (Sjöström et al., 2007). Conversely, SIK kinases can downregulate NKA expression by increasing CYP11A and StAR mRNA levels, inducing hormone dependent NKA downregulation (Okamoto et al., 2004, Lee et al., 2017).

This study tested whether SIK1 might mediate the effect of ouabain and monensin on IDO1 expression and function. The data in this chapter show that treatment with the SIK1 inhibitor, HG-9-91-01, moderately upregulated the kynurenine response when combined with IFNγ/TN stimulation, as well as increasing IDO1 protein levels (Figure 4.4A, D, E, F, I, J). These preliminary observations are consistent with the hypothesis that Na^+ increases might mediate their inhibitory effect on IDO1 through SIK1 activation, given that inhibition of SIK1 seems to upregulate the IDO1 response. However, these observations are undermined by the lack of expected effect of HG-9-91-01 on the established controls, which will be discussed in more detail in the next section.

4.3.3. HG-9-91-01 did not significantly increase kynurenine or IDO1 levels, in ouabain-treated MDA-MB-231 cells.

Having observed that inhibition of SIK1 upregulates the IDO1 response to interferon, it was speculated that co-treatment with HG-9-91-01 and IFNγ/TNF might provide resistance to the inhibitory effect of ouabain. This hypothesis is particularly interesting, given the link between SIK1 and Ca^{2+} signalling. It is well documented in the literature that IFNγ stimulation triggers an acute spike in intracellular Ca^{2+} which seems to be required for the downstream signalling events (Aas et al., 1998, Nair et al., 2002, Koide et al., 1988). Therefore, this set of experiments could justify a further interest to test whether upon addition of IFNγ combined with either monensin or ouabain, the initial Ca^{2+} spike might be altered, thus, negatively impacting on the kynurenine pathway.

To further evaluate the role of SIK1 in ouabain-induced IDO1 inhibition, the effect of HG-9-91-01 on the kynurenine response and IDO1 expression was evaluated. Figure 4.5A shows that ouabain downregulated the kynurenine response regardless of SIK1 inhibition, this was, however, partially due to a decrease in cell numbers (Figure 4.5A, B). No significant change was observed in the kynurenine response upon combining HG-9-91-01 and ouabain, compared to ouabain alone, with no significant difference in viability across these conditions (Figure 4.5A, C). The impact on kynurenine was consistent with the HG-9-91-01 effect on IDO1 protein levels (Figure 4.5D, E). IDO1 mRNA levels were also not significantly affected by HG-9-91-01 treatment (Figure 4.6A). These results again suggest that SIK1 might not impact on the kynurenine pathway and IDO1 expression.

Interestingly, PD-L1 protein levels did not significantly change in response to ouabain or HG-9-91-01, while PD-L1 mRNA levels increased approximately 5-fold upon ouabain treatment (Figure 4.5D, F, and 4.6B), supporting a potential role of Na^{+} in PD-L1 regulation. Upstream

IDO1 regulators, total and pSTAT1 were not significantly changed by HG-9-91-01 combined with ouabain, compared to ouabain alone (Figure 4.5G, H).

To try and verify whether the cellular immunological effects of SIK1 inhibition and increases in Na^+ levels are specific to IDO1, expression levels for a variety of immune-related genes including HLA-A, B and C were measured. However, no major alterations in the expression of these markers were observed with in ouabain and HG-9-91-01 samples compared to ouabain alone (Figure 4.6C, D, E). Furthermore, to verify if these results are an accurate representation of SIK1 inhibition in MDA-MB-231 breast cancer cells, the effect of HG-9-91-01 on the expression of the ATP1B1, a well-established target of SIK1, shown to be upregulated upon SIK1 inhibition, was tested (Taub, 2018, Taub, 2019, Taub et al., 2015). However, no change in ATP1B1 mRNA levels upon HG-9-91-01 treatment was observed (Figure 4.6F). This suggests that the HG-9-91-01 treatment, as described in this chapter, was not efficient at inhibiting SIK1 in MDA-MB-231 cells. Therefore, it is not possible to say whether SIK1 participates in the Na^+- IDO1 pathway and further experiments would need to be conducted to verify this hypothesis. It is important to mention that one significant limitation of this study was that SIK1 expression in MDA-MB-231 cells, although reported in the literature, was not experimentally validated and could be part of the reason why the expected impact of HG-9-91-01 on ATP1B1 mRNA could not be confirmed (Gradek et al., 2019).

A way to clarify whether SIK1 is involved or not in Na^+-dependent inhibition of IDO1 could be to look at the effect of monensin and/or ouabain on IDO1 activity in SIK1 KD cells. Furthermore, another possibility would be to directly measure the involvement of Ca^{2+} in the Na^+-IDO1 pathway, by evaluating the impact of ouabain/ monensin on the initial Ca^{2+} spike required for IFNγ signalling (Aas et al., 1998, Nair et al., 2002, Koide et al., 1988). Furthermore, the study of HG-9-91-01 could be pursued further, by trying to look at its effect

on SIK1 activity, by designing an *in vitro* enzyme activity assay. An *in vitro* enzyme activity assay would provide a clear answer as to whether HG-9-91-01 does inhibit SIK1. By answering the question of HG-9-91-01 efficacy, it would be possible to further verify if SIK1 plays a significant role in ouabain-induced IDO1 inhibition. These experiments were, however, too far from the scope of this project and were not further pursued.

4.3.4. SIK1 enhances overall survival in breast cancer, without correlating on a transcriptional level with STAT1-regulated genes.

To investigate the clinical relevance of SIK1 in breast cancer, two large data sets were pulled together: METABIC and TCGA, and correlations in mRNA gene expression were calculated for different population samples. Survival analysis was also conducted. SIK1 did not seem to be correlated on mRNA level with any of the selected genes. This suggests that any potential interaction between SIK1 and the selected genes should be expression independent, and thus rely on SIK1 activity (Figure 4.7). Additionally, the lack of mRNA correlation might also reflect tumour heterogeneity. Consistency was observed between the survival analysis presented in this chapter and literature data, where even higher magnitude differences in relapse-free survival have been reported (Xin et al., 2021). This analysis indicated that higher SIK1 expression is likely to provide an overall survival advantage in breast cancer, which confirms the well-established tumour suppressor function of SIK1 (Popov et al., 2012). Another interesting aspect is that IDO1 expression in patients does not seem to affect the SIK1 pro-survival effect, potentially suggesting that SIK1 might achieve its function through a different mechanism, and a potential effect on IDO1 might only be a collateral consequence of this pathway.

4.4. Conclusion

This chapter validated the Chapter 3 observation that IDO1 activity and expression correlate with changes in intracellular Na^+ levels, by modulating ionic dynamics, independently of ouabain and the NKA, via the ionophore monensin. The potential implication of SIK1 in the intracellular Na^+-IDO1 pathway could not be addressed. Although a deeper mechanistic understanding of the ouabain/ monensin – induced IDO1 inhibition could not be achieved, it is justified to conclude that the data presented in this chapter, as well as in Chapter 3, support a link between elevated intracellular Na^+ and a decrease in the kynurenine response.

5. Chapter 5: Screening for novel IDO1 inhibitors using a natural compound library.

5.1. Introduction

5.1.1. Background

Cancer immunotherapy research has made a considerable contribution to patient survival over the past years. Since the 2018 Nobel Prize for negative regulation of immune checkpoints, a large body of literature and clinical research has focused on studying small molecules and monoclonal antibodies that target those immune regulatory proteins, either alone or in combination with other therapies (Baglini et al., 2022). Monoclonal antibodies are by far the majority of current immunotherapies. This is because these do not target enzymatic activities. Rather they target protein-protein interactions, which involve large interfaces that cannot be blocked by small molecules (Zahavi and Weiner, 2020). The most therapeutically exploited immune checkpoint pathway in cancer is the PD-1/PD-L1 interaction, yet other immune regulators such as CTLA-4, LAG3, and TIM3 have also been extensively investigated (Wang et al., 2022c, Sharmni Vishnu et al., 2022, Rittmeyer et al., 2017, De Silva et al., 2021, Datar et al., 2019). IDO1 is another important immunotherapeutic target in cancer, which is regulated in a similar way to PD-L1 expression, by IFNγ proinflammatory stimulation (Jung et al., 2022). Its cytosolic localization makes it a difficult target for monoclonal antibodies. Instead, a series of synthetic small molecules including the Trp derivatives Indoximod, Epacadostat, Linrodostat mesylate, Navoximod and PF-0684003, as well as peptide vaccines, have been designed for IDO1-targeted therapies (Tang et al., 2021, Prendergast et al., 2018). The large body of research around DO1 and the kynurenine pathway, as well as the modest success of IDO1 therapeutics, highlight its key role in cancer progression, supporting the need for novel approaches for targeting this checkpoint. This

could be achieved by altering physiological processes which directly or indirectly regulate IDO1 and/or Trp/kynurenine metabolism.

In an attempt to pursue one such approach, the link between the IDO1-centric Trp metabolism and ionic dynamics was investigated in breast cancer. Chapter 3 described a 31-ion transport targeted compound screen, which identified the *Strophanthus gratus* and *Acokanthera schimperi*-derivative, ouabain, as an IDO1 inhibitor. Further experiments showed that another related digitalis plant-derivative, digoxin, had a similar effect on IDO1 (Shandell et al., 2022, Botelho et al., 2019, Domingo et al., 2016).

To harness the potential anti-cancer activity of other natural compounds, a library consisting of 630 molecules, mostly of plant origin, was curated by the Centre for Novel Agricultural Products (CNAP) within the University of York. Figure 5.1 summarises the main classes of compounds included. The library was strongly biased towards terpenes with immune-modulatory activity. The selection of the library was completed by the CNAP collaborators and the bias towards terpenes was supported by their interest in terpene compound structure and chemistry, the wide use of the compound plant of origin for medicinal purposes, and the widely researched bioactivities of these compounds.

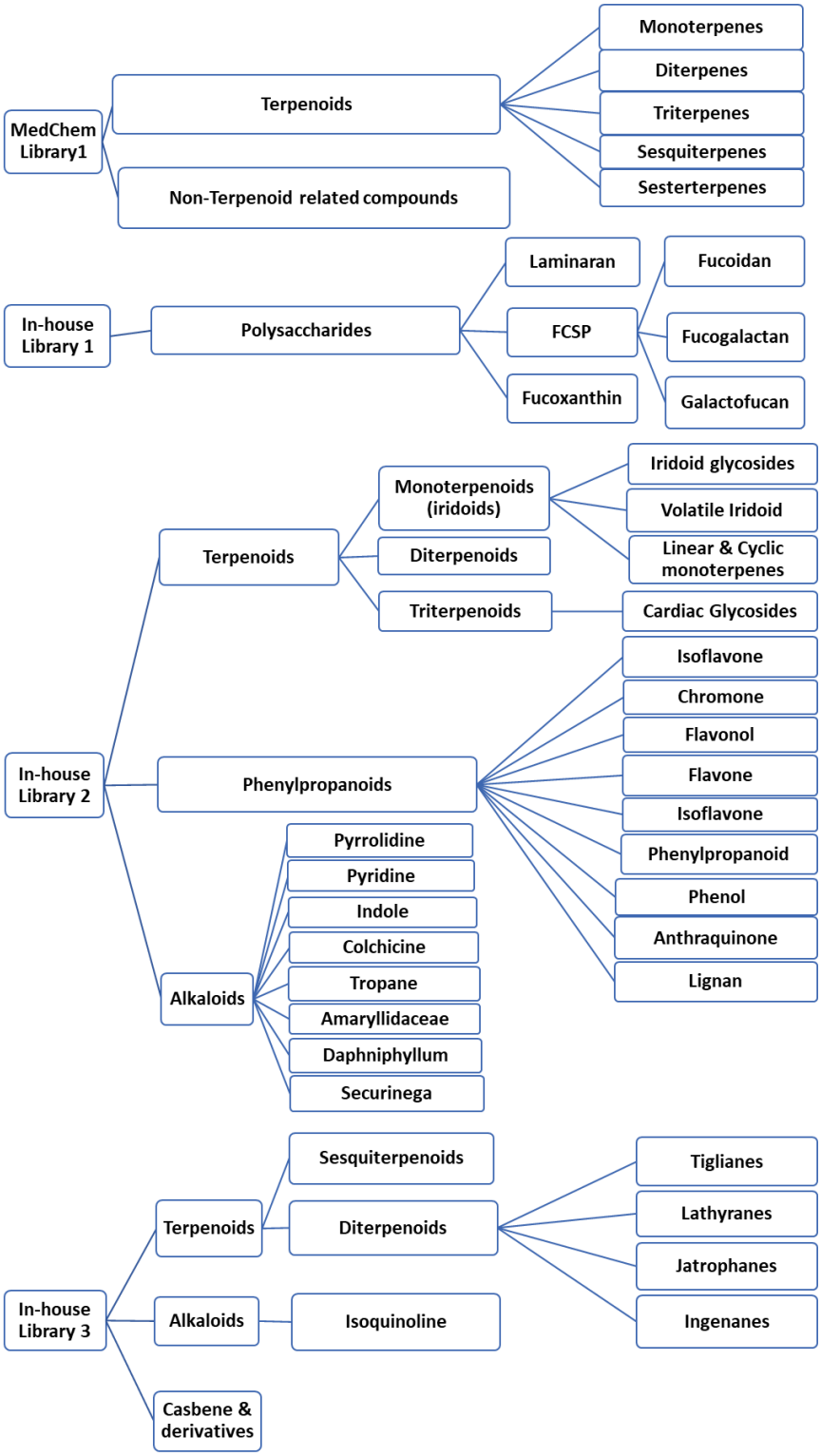

Figure 5.1 Summary of the main classes of compounds within the 630 natural compound library and their sources (MedChem library – commercially available, Internal library 1 – seaweed derivatives, Internal library 2, 3 – compounds of interest for the CNAP collaborators). FCSP – Fucose-containing sulphated polysaccharides.

5.1.2. Terpenes

Terpenes are the most diverse class of natural compounds. In plants, terpenes are responsible for fragrance, taste and colour. Some terpenes, such as squalene and sterols can also be produced by animals. Structurally, terpenes can be classified based on the number of isoprene units into hemi- (1 unit), mono- (2 units), sesqui- (3 units), di- (4 units), sester- (5 units), triterpenes (6 units) and tetraterpenes (8 units) (Evidente et al., 2015). Terpenes that contain oxygen atoms within their molecule in the form of an alcohol, aldehyde, or ketone group, are defined as terpenoids (Brahmkshatriya and Brahmkshatriya, 2013).

Terpenes have been widely studied for medicinal purposes and have been shown to have anti-inflammatory and wound healing activity, as well as being beneficial for cardiovascular diseases (Loreto et al., 1998, Chadwick et al., 2013, Vasas and Hohmann, 2014, Zheljazkov et al., 2015, James and Dubery, 2009). In macrophages some terpenes have been shown to decrease expression of the master signalling kinases MAPK, c-Jun N-terminal kinase (cJNK) and p38, known for regulating a range of cellular functions, including survival and cytokine production, as well as playing a role in tumorigenesis (Wagner and Nebreda, 2009). Terpenes can also regulate inflammatory responses through inhibition of NF-kB nuclear translocation by preventing IkB phosphorylation (Chi et al., 2013, Kim et al., 2015). Furthermore, some terpenes, like borneol, were shown to upregulate expression of nuclear factor erythroid 2–related factor 2 (Nrf2), which is a transcription factor regulating protection against ROS, and therefore reduces oxidative stress (Hur et al., 2013). Terpenes and terpenoids have been found to be particularly good at suppressing neuroinflammation, by preventing microglial production of proinflammatory cytokines such as interleukin 1β (IL-1β) and TNF (Ong et al., 2015, Quintans et al., 2019). Additionally, a range of inflammatory diseases were also shown to benefit from terpene treatment, such as airway inflammation (limonene), autoimmunity in the case of arthritis (β-caryophyllene), or atopic dermatitis (Hirota et al., 2012, Ames-Sibin

et al., 2018, Kang et al., 2019) Terpenes can also cause cell cycle arrest in hepatocarcinoma cells, thus functioning as tumour clearance promoter agents (Xu et al., 2018a).

Interestingly, some terpenes also have ion transport modulating activity. Borneol, 2-methylisoborneol, fenchyl alcohol and camphor are able to modulate Ca^{2+} transport via the TRPA1 channel (Takaishi et al., 2014). Monoterpenes are highly lipophilic molecules, which means that they can easily cross the plasma membrane and have been reported to interfere with ion transport in and out of the cell (Oz et al., 2015). Thymol and menthol were shown to inhibit VGSCs and canonical TRP channels in neurons and muscle cells, thus providing local anaesthetic events (Haeseler et al., 2002, Zheng, 2013). Menthol was shown to also inhibit $Na_v1.8/9$ and TTX-resistant VGSCs in a cumulative manner, thus exerting analgesic effects (Gaudioso et al., 2012). Carvacrol and linalool were shown to inhibit neuronal excitability and action potential firing in rat neurons, while eugenol was reported to inhibit both TTX-sensitive and TTX-resistant VGSCs (Leal-Cardoso et al., 2010, Joca et al., 2012, Gonçalves et al., 2010, Cho et al., 2008). Despite their wide range of biological activities, terpenes are hardly ever administered on their own, and instead they function as adjuvants in combination with other molecules that increase their cellular penetration and stability, particularly because of their increased volatility (El-Hammadi et al., 2021, Aqil et al., 2007).

5.1.3. Polysaccharides

A second class of compounds that can be found in the screening library consists of polysaccharides and pigments derived from marine algae. Literature suggests that marine algae polysaccharides might have antioxidant and anticancer activities (Khan et al., 2019, Chen et al., 2018). A series of *in vivo* and *in vitro* studies identified pro-apoptotic, anti-proliferative activity of marine algae polysaccharides particularly fucan, fucoidan, laminaran, porphyrin and sulphated galactan (Yao et al., 2022). Additionally, several marine algae-derived polysaccharides have also been shown to enhance immunity (Liu et al., 2020b). In

mouse macrophages, the GLP-2 polysaccharide from *Gracilaria lemaneiformis* was shown to induce proliferation as well as promoting production of proinflammatory factors such as nitric oxide (NO), ROS, TNF or interleukin-6 (IL-6) (Ren et al., 2017). Structurally, marine algae polysaccharides can be classified depending on their plant origin, such that the most common chemical compounds derived from green algae are cellulose, mannan, ulvan and sulphated rhamnan; for red algae agar and carrageenan are very abundant; while for brown algae, laminaran and fucoidan are most encountered (Righini et al., 2019, Yao et al., 2022). The pigment fucoxanthin is a highly unsaturated carotenoid produced by brown algae and has also been shown to impact on the immune system, performing anti-inflammatory activities (Bigagli et al., 2021, Pajot et al., 2022). Interestingly, fucoxanthin has also been widely studied in the context of cancer progression, showing the ability to inhibit trans-endothelial migration of breast cancer cells, as well as being documented as an apoptosis inducer and cell cycle blocker in several other types of cancer (Kumar et al., 2013, Wang et al., 2022a).

5.1.4. Alkaloids

Alkaloids represent a large class of naturally occurring secondary metabolites which are characterized by the presence of one or more nitrogen atoms, as well as a heterocyclic ring common for some classes of alkaloids. Alkaloids can also incorporate sulphur, phosphorus, bromide and chloride alongside the carbon-hydrogen backbone. They represent ~20 % of natural secondary metabolites and are usually low molecular weight compounds. Alkaloids have also been extensively studied for therapeutic purposes. Vinflunine has been investigated on its own and as a combinatorial treatment with the anti-HER2 trastuzumab monoclonal antibody for the treatment of $HER2^{+}$ breast cancer (Yardley et al., 2010). Other alkaloids have also been shown to have anti-cancer activity. Based on the chemical structure multiple mechanisms of action were identified. Indole alkaloids, like vinblastine, inhibit proliferation by interfering with tubulin polymerization, or promote apoptotic or necrotic

cell death, as well as inducing autophagy (Adiseshaiah et al., 2013). Isoquinoline alkaloids also induce Autophagy Related 5 (ATG5)-mediated autophagy in hepatocarcinoma cell lines, and some, e.g. berberine, were shown to interfere with the activity of cyclooxygenase 2 (COX-2), preventing colon cancer survival (Fukuda et al., 1999, Wang et al., 2010a, Mondal et al., 2019). Pyrrole and pyrrolizidine alkaloids are also known to exert anti-cancer activity by promoting cell cycle arrest, apoptosis, necrosis and autophagy (Cheng et al., 2017, Sun et al., 2017, Philipp et al., 2015). Phenanthroindolizidine alkaloids and indoquinoline alkaloids are known for cell cycle arrest and apoptotic cell death induction (Dassonneville et al., 2000, Ahmed et al., 2011, Min et al., 2010, Wu et al., 2009). B-carboline-benzoquinolizidine alkaloids are mainly known to interfere with topoisomerase activity and therefore impair proliferation by interfering with DNA replication, additionally some members of this class were shown to inhibit the proinflammatory JAK1/2 / STAT5 pathway in lung cancer cell lines (Jung et al., 2019, Nafisi et al., 2010). Miscellaneous alkaloids have a range of mechanisms of action, including apoptosis promotion, topoisomerase inhibition as well as inhibition of proliferation, metastatic inhibition by interference with matrix metalloproteinases (Canals et al., 2005, Manu and Kuttan, 2009, Ito et al., 2006, Li et al., 2014, Mondal et al., 2019).

5.1.5. Phenylpropanoids

Phenylpropanoids are often secondary metabolites of the amino acid phenylalanine or tyrosine in plants, bacteria or fungi. Structurally, phenylpropanoids consist of a propane group attached to a 6- carbon aromatic ring (Seigler, 1998). Several types of phenylpropanoids have been reported to have therapeutic properties. Prenylated phenylpropanoids have been shown to have cancer preventive function, reducing proliferation and activation in the lymphoma Raji cell line (Itoigawa et al., 2004). A series of other phenylpropanoids such as Apigenin, Curcumin, Resveratrol and Quercetin have been shown to have antioxidant activity, while others such as caffeic acid phenethyl ester have been reported to reduce inflammation by inhibiting the transcription factor NF-kB, as well as

have anti-cancer activity (Grunberger et al., 1988, Natarajan et al., 1996, Kim et al., 2011). However, the impact of these compounds on Trp metabolism has not previously been explored.

5.1.6. Hypothesis and Aims

Given the impact of cardiac glycosides on the kynurenine response reported in Chapter 3, it was hypothesized that other natural compounds might affect kynurenine production in cancer cells possibly through direct effects on IDO1/2 and/or TDO enzymes, impairing Trp metabolism in breast cancer, and these could form the basis of immune checkpoint therapeutics. The aim of this chapter is to describe the design and optimization of a medium to high throughput screening assay, based on the set-up of the previously described kynurenine assay, for evaluating the impact of 630 natural compounds on kynurenine production.

5.2. Results

5.2.1 Kynurenine assay optimization.

The kynurenine assay was previously described in the literature as a method to assess IDO1/2 and/or TDO activity based on supernatant concentration of the Trp metabolite, kynurenine (Shandell et al., 2022, Peng et al., 2016, Takikawa et al., 1988). In this section the optimisation steps performed to explore and reduce assay variation and thus allow its usage for medium to high throughput applications are described.

Typically, the assay is run in a 96-well plate format. Edge-well effects are a common issue with such assays (Mansoury et al., 2021). The type of the plate is also an important factor. To measure background and variability across the plate, several different parameters were sequentially tested.

Figure 5.2A summarizes the main testing conditions. Samples were prepared in either clear or black-walled flat-bottom 96-well plates. Samples from each plate were analysed using 2 different data acquisition instruments: a BMG Labtech CLARIOstar plate reader and a VersaMax microplate reader (Molecular Devices). For each plate reader absorbance values at 492 nm and at 650 nm were recorded. For analysis, values corresponding to absorbance at 492 nm only and values corresponding to the 492 nm absorbance minus the background 650 nm absorbance were plotted and compared.

The accuracy of kynurenine detection at different locations across the plate was tested. Kynurenine standards were plated in the first column and the last two columns of the plate. The standards in column 1 were set up with the highest concentration at the top (A1 – 100 µM) and the lowest at the bottom (G1 – 0 µM), while in columns 11 and 12 the top kynurenine concentration was at the bottom (G11 and G12 – 100 µM) and the lowest concentration at the top (A11 and 12 – 0 µM). The same set-up was prepared for clear and

black-well 96-well plates, and recordings were taken at 492 nm alone and at 492 nm with background subtraction of the 650 nm absorbance reading. Results showed no change in absorbance reading regardless of plate type, well location, background subtraction or plate reader instrument (Figure 5.2B).

A.

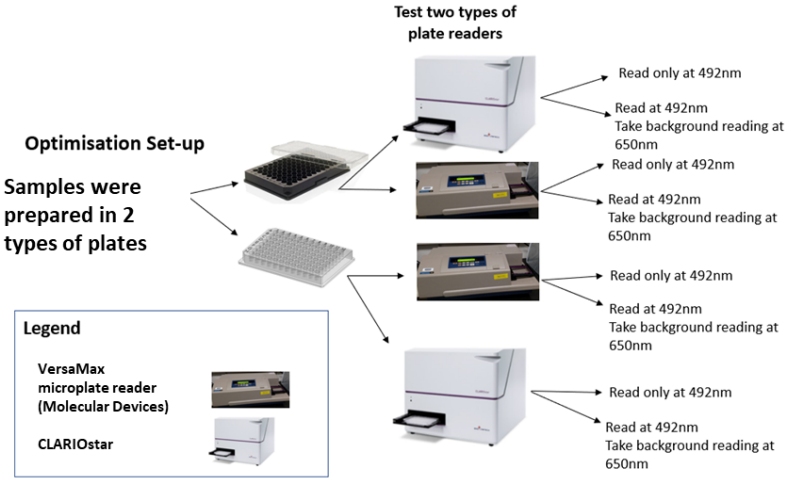

B.

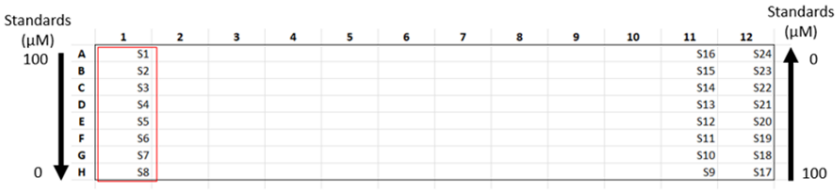

CLARIOstar

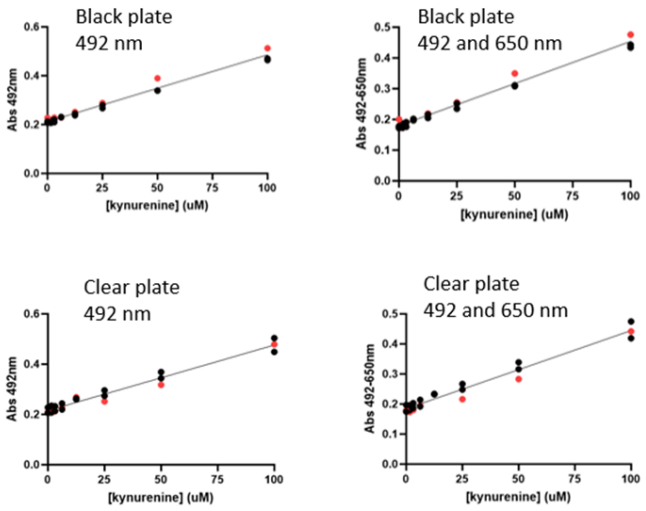

VersaMax microplate reader

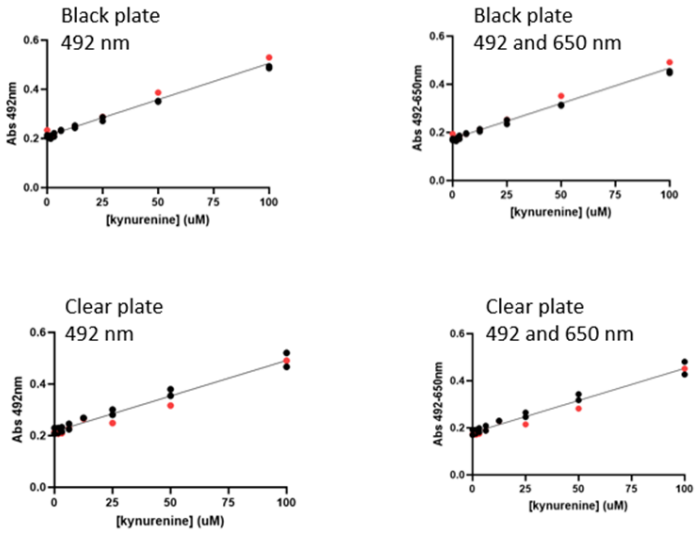

Figure 5.2 Kynurenine assay optimization. A. Schematic of parameters tested for assay optimization; B. Testing plate effect using kynurenine standards (no cells), red dots correspond to data in column 1, S1-24: standards 1 to 24 (n=1 biological replicate). The kynurenine assay, described in more detail in section 2.9, was then performed on culture supernatants. Readings from clear and dark 96-well plates, using the CLARIOstar and the Versamax microplate reader at 492 nm and at 650 nm were taken and data were labelled accordingly.

5.2.2 Mock drug screen: the kynurenine assay.

Next, the consistency of the kynurenine assay was tested in a mock-screen experiment. Cells were seeded using the same layout as planned for the screen at 70 000 cells/well. Nine controls were set up: three vehicles unstimulated (0.1 % DMSO only), three vehicles (0.1 % DMSO stimulated with IFNγ/TNF) and three ouabain treated samples (200 nM ouabain 0.1 % DMSO, stimulated with IFNγ/TNF) (Shandell et al., 2022). All other samples were only stimulated with IFNγ/TNF. Figure 5.3A shows the plate set-up for the mock screen experiment. For these experiments, cells were seeded in all wells, and all were stimulated with IFNγ/TNF.

As described in Figure 5.2A, the absorbance signal for the samples was measured using 2 different types of plate (clear and black), two different plate readers (CLARIOstar and Versamax). Absorbance readings were taken at 492 nm as well as at 492 and 650 nm, for background subtraction. Figure 5.3B shows the results of the mock screen experiment, comparing the different conditions. Acceptable levels of variance in kynurenine levels were observed between the two plate types or the two plate readers, with and without the 650 nm background subtraction, which means that in all IFNγ/TNF-stimulated samples the kynurenine levels were between 40 and 60 µM, unstimulated samples had almost no kynurenine (highlighted b square boxes), while ouabain dropped kynurenine levels below 20 µM (highlighted by round boxes), regardless of plate type, plate reader or background subtraction. While limited variation across different plates/ plate readers or analysis modalities was observed, row variability was recorded with all different measurement conditions (row B gave consistently higher kynurenine levels). This was attributed to pipetting issues and to prevent that in the future, a mechanical multichannel pipette was used for the completion of the screen.

In conclusion, the assay results were shown to be consistent regardless of plate type, plate reader, or background subtraction. Therefore, for the following experiments, the initial published assay conditions: clear plate, Vresamax microplate reader and 492 nm absorbance only, were used for data acquisition (Shandell et al., 2022).

A. Mock screen set-up

	1	2	3	4	5	6	7	8	9	10	11	12
A				vehicle unstimulated	IFNγ/ TNF	IFNγ/ TNF	IFNγ/ TNF	vehicle	IFNγ/ TNF	IFNγ/ TNF	IFNγ/ TNF	Ouabain
B				IFNγ/ TNF	IFNγ/ TNF	IFNγ/ TNF	IFNγ/ TNF	IFNγ/ TNF	IFNγ/ TNF	IFNγ/ TNF	IFNγ/ TNF	IFNγ/ TNF
C				IFNγ/ TNF	IFNγ/ TNF	IFNγ/ TNF	IFNγ/ TNF	IFNγ/ TNF	IFNγ/ TNF	IFNγ/ TNF	IFNγ/ TNF	IFNγ/ TNF
D				Ouabain	IFNγ/ TNF	IFNγ/ TNF	IFNγ/ TNF	vehicle unstimulated	IFNγ/ TNF	IFNγ/ TNF	IFNγ/ TNF	vehicle
E				IFNγ/ TNF	IFNγ/ TNF	IFNγ/ TNF	IFNγ/ TNF	IFNγ/ TNF	IFNγ/ TNF	IFNγ/ TNF	IFNγ/ TNF	IFNγ/ TNF
F				IFNγ/ TNF	IFNγ/ TNF	IFNγ/ TNF	IFNγ/ TNF	IFNγ/ TNF	IFNγ/ TNF	IFNγ/ TNF	IFNγ/ TNF	IFNγ/ TNF
G				IFNγ/ TNF	IFNγ/ TNF	IFNγ/ TNF	IFNγ/ TNF	IFNγ/ TNF	IFNγ/ TNF	IFNγ/ TNF	IFNγ/ TNF	IFNγ/ TNF
H				vehicle	IFNγ/ TNF	IFNγ/ TNF	IFNγ/ TNF	Ouabain	IFNγ/ TNF	IFNγ/ TNF	IFNγ/ TNF	vehicle unstimulated

B.

CLARIOstar

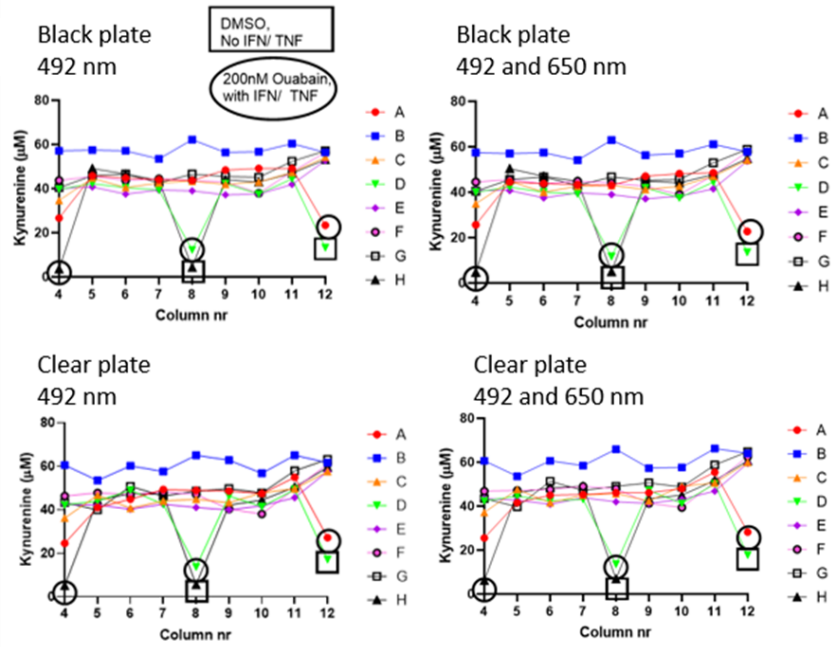

Versamax microplate reader

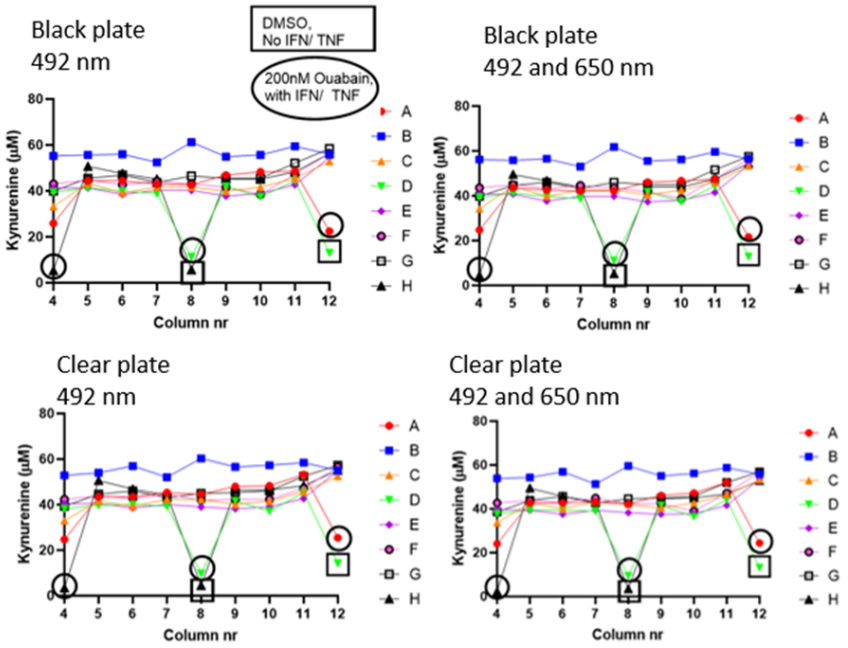

Figure 5.3 Mock drug screen: the kynurenine assay. A. Plate set-up for the mock screen (representative for the layout of all plates in the actual screen); B. Mock screen results. Cells were pre-treated with ouabain for 18 h and IFNγ (1 U/ mL)/ TNF (6.25 ng/ mL) stimulation was added for another 24 h. The kynurenine assay, described in more detail in section 2.9, was then performed on culture supernatants. Readings from clear and dark 96-well plates, using the CLARIOstar and the Versamax microplate reader at 492 nm and at 650 nm were taken and data were labelled accordingly. Square boxes represent DMSO unstimulated samples, while circles highlight samples treated with 200 nM ouabain. Colours A-H represent the plate rows. Legend: vehicle unstimulated (0.1 %DMSO only), vehicle (0.1 % DMSO stimulated with IFNγ/TNF), Ouabain (200 nM ouabain 0.1 % DMSO, stimulated with IFNγ/TNF).

5.2.3 Natural compound screen set-up and raw data example.

Having identified the optimal conditions for the kynurenine assay, the next step was to design a protocol that could accommodate screening the effect of 630 natural compounds on kynurenine production and cellular toxicity, in order to identify modulators of the kynurenine response that do not impact on viability.

Figure 5.4A highlights the workflow of the screen. For each plate of compounds, the duration of the screen was 4 days, including an 18 h drug pre-treatment, followed by another 24 h of drug treatment in the presence of IFNγ/TNF stimulation. Next supernatants were collected for the kynurenine assay, described in the section 2.9, while the remainder cells were treated with Deep Blue viability die for 4 h and absorbance at 570 and 600 nm was used to assess survival (section 2.10).

The 630 compounds were split in 10 plates, each with a similar set-up, as in Figure 5.4B. Details on all the drugs included in the screen were specified in Appendix Table 8. 2. All plates had 3 unstimulated controls (blue), 3 positive controls consisting of cells treated with IFNγ/TNF (bright yellow) and 3 negative controls of cells treated with IFNγ/TNF and 200 nM ouabain (light yellow). Drug plates were all prepared at the same time, as detailed in section 2.3. On the day, the drugs were added to the cells to a final well concentration of 10 µM, in a final well volume of 250 µL. From each drug plate, enough drug solution was prepared for two replicate experimental plates. 18 h later the IFNγ/TNF was added directly to the cells treated with drugs to give a final well concentration of 1 U/mL and 6.25 ng/mL, respectively. Supernatants were then collected for the kynurenine assay (2 plates for each set of drugs) and the remaining cells were used for viability assay. Figure 5.4C shows representative plots for the kynurenine and Deep Blue viability raw data.

A.

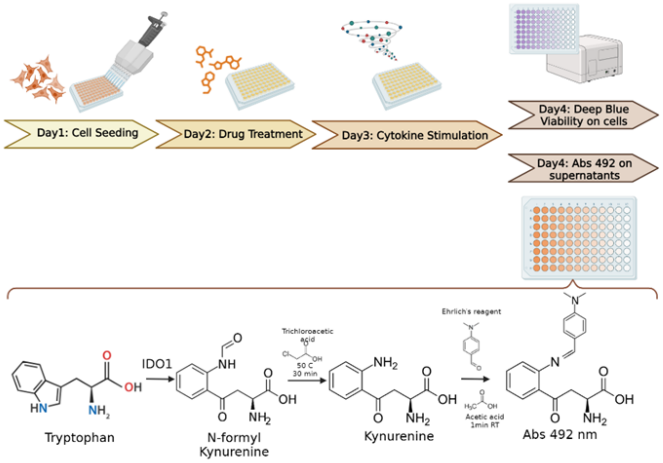

B. **Drug plate**

	1	2	3	4	5	6	7	8	9	10	11	12
A				vehicle unstimulated	1	2	3	vehicle	4	5	6	Ouabain
B				7	8	9	10	11	12	13	14	15
C				16	17	18	19	20	21	22	23	24
D				Ouabain	25	26	27	vehicle unstimulated	28	29	30	vehicle
E				31	32	33	34	35	36	37	38	39
F				40	41	42	43	44	45	46	47	48
G				49	50	51	52	53	54	55	56	57
H				vehicle	58	59	60	Ouabain	61	62	63	vehicle unstimulated

	1	2	3	4	5	6	7	8	9	10	11	12
A	100	100	100	vehicle unstimulated	1	2	3	vehicle	4	5	6	Ouabain
B	50	50	50	7	8	9	10	11	12	13	14	15
C	25	25	25	16	17	18	19	20	21	22	23	24
D	12,5	12,5	12,5	Ouabain	25	26	27	vehicle unstimulated	28	29	30	vehicle
E	6,25	6,25	6,25	31	32	33	34	35	36	37	38	39
F	3,13	3,13	3,13	40	41	42	43	44	45	46	47	48
G	1,56	1,56	1,56	49	50	51	52	53	54	55	56	57
H	0	0	0	vehicle	58	59	60	Ouabain	61	62	63	vehicle unstimulated
	Kynurenine standards											

	1	2	3	4	5	6	7	8	9	10	11	12
A	100	100	100	vehicle unstimulated	1	2	3	vehicle	4	5	6	Ouabain
B	50	50	50	7	8	9	10	11	12	13	14	15
C	25	25	25	16	17	18	19	20	21	22	23	24
D	12,5	12,5	12,5	Ouabain	25	26	27	vehicle unstimulated	28	29	30	vehicle
E	6,25	6,25	6,25	31	32	33	34	35	36	37	38	39
F	3,13	3,13	3,13	40	41	42	43	44	45	46	47	48
G	1,56	1,56	1,56	49	50	51	52	53	54	55	56	57
H	0	0	0	vehicle	58	59	60	Ouabain	61	62	63	vehicle unstimulated
	Kynurenine standards											

C.

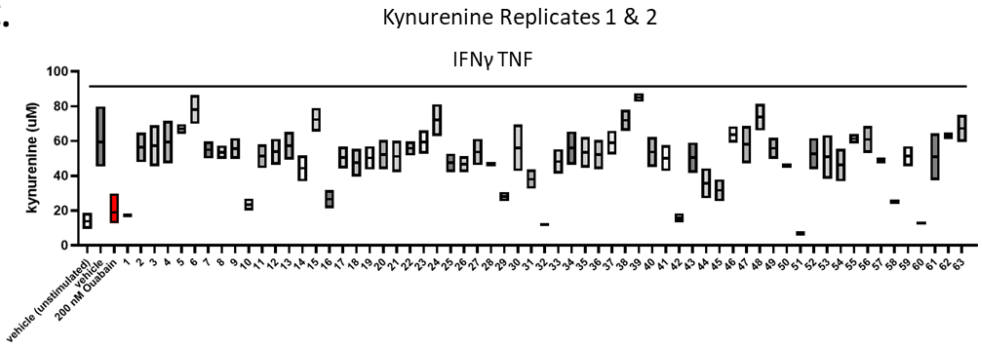

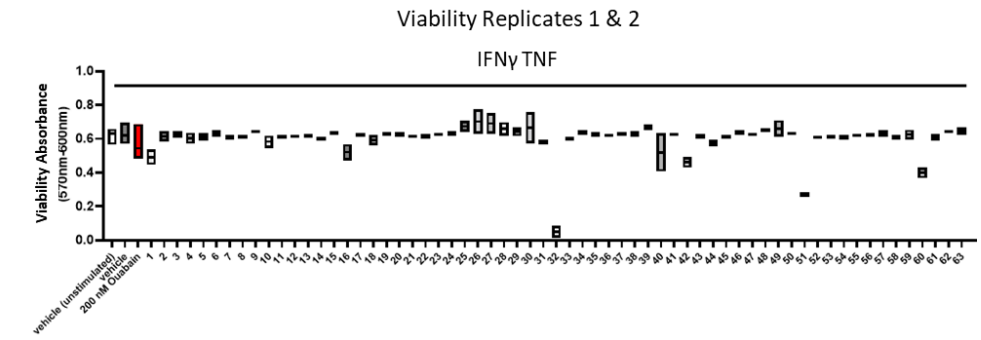

Figure 5.4 Natural compound screen set-up. A. Drug screen workflow: the kynurenine assay and deep blue viability; B. Drug plate and kynurenine plate maps for each set of compounds; C. Representative raw data for the first set of compounds. Cells were seeded and treated as described in sections 2.1and 2.3. Cells were pre-treated with drugs for 18 h and IFNγ (1 U/ mL)/ TNF (6.25 ng/ mL) stimulation was added for another 24 h. The kynurenine assay, described in more detail in section 2.9, was then performed on culture supernatants. The Deep Blue viability assay was carried out as described in section 2.10. Readings from clear 96-well plates, using the Versamax Pro plate reader at 492 nm were taken and data were labelled accordingly. Legend: vehicle (unstimulated) – 0.1 % DMSO; vehicle - 0.1 % DMSO IFNγ/TNF; 200 nM ouabain – 200 nM ouabain 0.1 % DMSO IFNγ/TNF, numbers 1 to 63 correspond to the first 63 compounds from the 630-compound library, their full names and details are found in Appendix Table 8.2.

5.2.4 Natural compound screen – Results.

The first round of screening identified a series of compounds of interest (COIs), these were compounds that decreased or increased kynurenine below or above the selected thresholds, without impacting on viability; the kynurenine response and viability thresholds were specified in 2.3.2. (and briefly explained below). Given the fact that the drug screen was only run in duplicate, due to the large number of compounds for a manual procedure, no statistical analysis could be performed. Therefore, thresholds for identifying compounds with potential effects on kynurenine production were defined.

Inhibitory COIs were defined as compounds that could decrease kynurenine by at least 50 % compared to the vehicle control, or compounds that gave a decrease in kynurenine at least 3 SD away from the kynurenine levels in the vehicle control. The 3 SD threshold was selected based on the statistical principle which states that 99.7 % of the observations within a normally distributed population should lie within 3 SD from the control (Lee et al., 2015). A third selection threshold was applied for viability, so that compounds of interest had to give a viability value of at least 70 % of the vehicle unstimulated control value, to clearly separate active compounds from compounds with high toxicity. In Figure 5.5A, inhibitory COIs correspond to the points highlighted in red in the lower left quadrant (44 inhibitory COIs).

Six enhancer COIs were also identified, and these were characterized by either an increase in kynurenine fold change above 1.4 or a kynurenine concentration 3 SD away from that of the vehicle control, while maintaining viability over the 0.7 threshold. In Figure 5.5A, enhancer COIs correspond to the points highlighted in red in the top right quadrant.

In Figure 5.5B fold change was plotted against viability and all COIs highlighted in red exceeded the 0.7 viability threshold. Amongst the compounds of interest defined according to section 2.3.2. , an arbitrarily selected set of 9 borderline compounds (*e.g.,* gave a 0.51 decrease in kynurenine, or had a viability of 0.69) was also selected for further validation.

These borderline COIs were included in the red point pool from Figure 5.5A, B. Raw data for the first round of screening were included in the Appendix Table 8. 2. Figure 5.5C summarizes all the COIs identified in the first round of screening.

In conclusion, the screen identified 50 inhibitory and enhancer COIs and 9 borderline COIs selected for further validation. In total, 59 compounds were selected for further testing.

A.

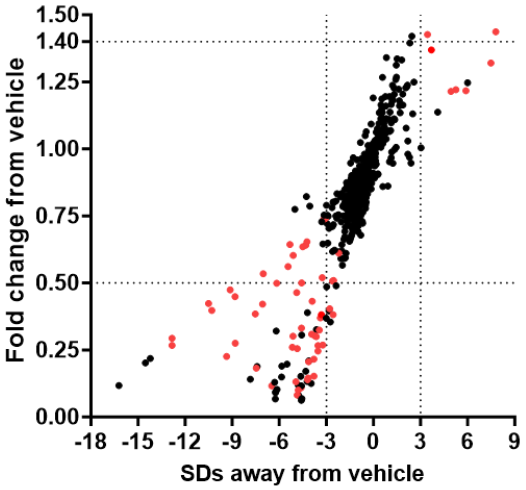

B.

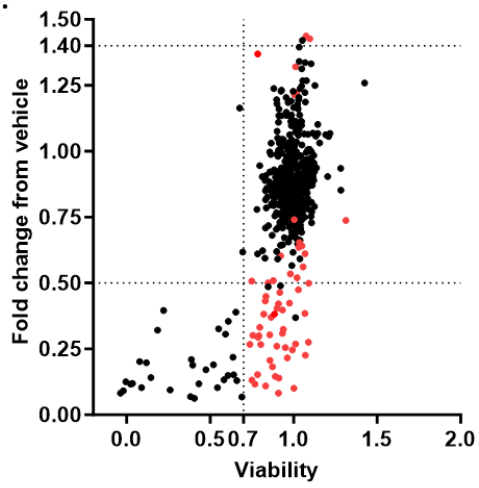

C.

Inhibitory COI	Enhancer COI	Selection of Borderline COI
1 - Demethylzeylasteral	6 - Ruscogenin	42 - Cephalomannine
10 - Dehydrocostus Lactone	15 - Scopolin	67 - Forskolin
16 - Pseudolaric Acid A	24 - Morroniside	243 - Ponicidin
29 - Costunolide	38 - (-)-α-Pinene	256 - Tubeimoside I
31 - Deapioplatycodin D	39 - (R)-(+)-Citronellal	301 - Deoxyingenol
44 - Saikosaponin D	204 - Gymnemic acid I	343 - Lasalocid
45 - Andrographolide		578 - Phorbol 12,13-didecanoate 20
58 - Hinokitiol		586 – Prostratin
91 - Deoxyelephantopin		
92 - Platycodin D2		
116 - Isoalantolactone –		
123 - Eupalinolide B		
127 - Artemether		
167 - Scabertopin		
182 - Euphorbia Factor L2		
197 - Ergolide		
206 - Arnicolide D		
214 - Britannin		
229 - Polygalacin D		
269 - Glaucocalyxin A		
328 - Guggulsterone		
332 - Alantolactone		
337 - Lasalocid (sodium)		
348 - Punicalagin		
349 - 7-epi-Taxol		
352 -Cryptotanshinone		
359 - Paclitaxel		
361 - Parthenolide		
366 - Toosendanin		
390 - Brevilin A		
452 - Colchicine Alkaloid		
468 - Securinine Alkaloid		
473 - CFN97008 Alkaloid		
485 - Flueggea suffructicosa		
530 - Paclitaxel Diterpene Commercial pure		
556 - Dicentrine		
560 - Laudanosine		
577 - Ingenol 3,20-dibenzoate		
580 - Phorbol 13-myristate		
583 - Phorbol 13-acetate		
592 - Euphorbia factor L2		
600 - Euphorbia factor L9		
618 – Artemisinin		
619 – Artemether		
620 – Artesunate		
622 - Dihydroartemisinin		

Figure 5.5 Natural compound screen – Results. A. First screening round: Kynurenine results – Fold Change in kynurenine levels normalized to the vehicle stimulated positive control Vs number of SDs away from the vehicle control (explained in section 2.3.2.) (mean values for fold change and SD variation were plotted for n=2 technical replicates, for drugs where one replicate was excluded from the SD analysis due to missing quality control threshold (see section 2.3.2.), only one SD value was used); B. First screening round: Kynurenine results – Fold Change in kynurenine levels normalized to the vehicle stimulated positive control Vs Viability – fold change normalized to the vehicle control (explained in section 2.3.2.) (mean values for kynurenine fold change and viability were plotted for n=2 technical replicates); C. Annotation of selected compounds of interest (COIs), numbers represent order in the 630-compound screen. Cells were seeded and treated as described in sections 2.1and 2.3. Cells were pre-treated with drugs for 18 h and IFNγ (1 U/ mL)/ TNF (6.25 ng/ mL) stimulation was added for another 24 h. The kynurenine assay, described in more detail in section 2.9, was then performed on culture supernatants. The Deep Blue viability assay was carried out as described in section 2.10. For A and B: red dots represent compounds selected for further validation (COIs), black dots indicate compounds that did not fulfil the COI criteria.

5.2.5 Natural compound screen validation – Results.

To verify the results of the first round of screening, a second validation experiment was then carried out on the 59 COIs identified in the first round of screening (44 inhibitors, 6 enhancers and 9 borderlines, Figure 5.5). The validation was used to identify hits. A hit was defined as a compound that increased or decreased kynurenine levels at least 3 SD away from the vehicle control AND gave a fold change in kynurenine either ≤ 0.5 or ≥ 1.4 from the vehicle control, while maintain viability at least 0.7 of the vehicle unstimulated control.

Figure 5.6A summarizes the kynurenine results of the validation screen, showing kynurenine fold change versus SD. Compounds classified as hits are highlighted in green. The validation screen identified 24 inhibitory hits (lower left quadrant) and 1 enhancer hit (top right quadrant). All hits had a viability score above the 0.7 threshold, as shown in Figure 5.6B, where fold change was plotted against viability. Figure 5.6 C shows the list of hits of the validation screen, ordered by their impact on kynurenine fold change. Raw data for the validation round were included in the Appendix Table 8.3.

In conclusion, out of the 59 COIs included in the validation round, 24 inhibitory compounds and 1 enhancer compound were identified as hits.

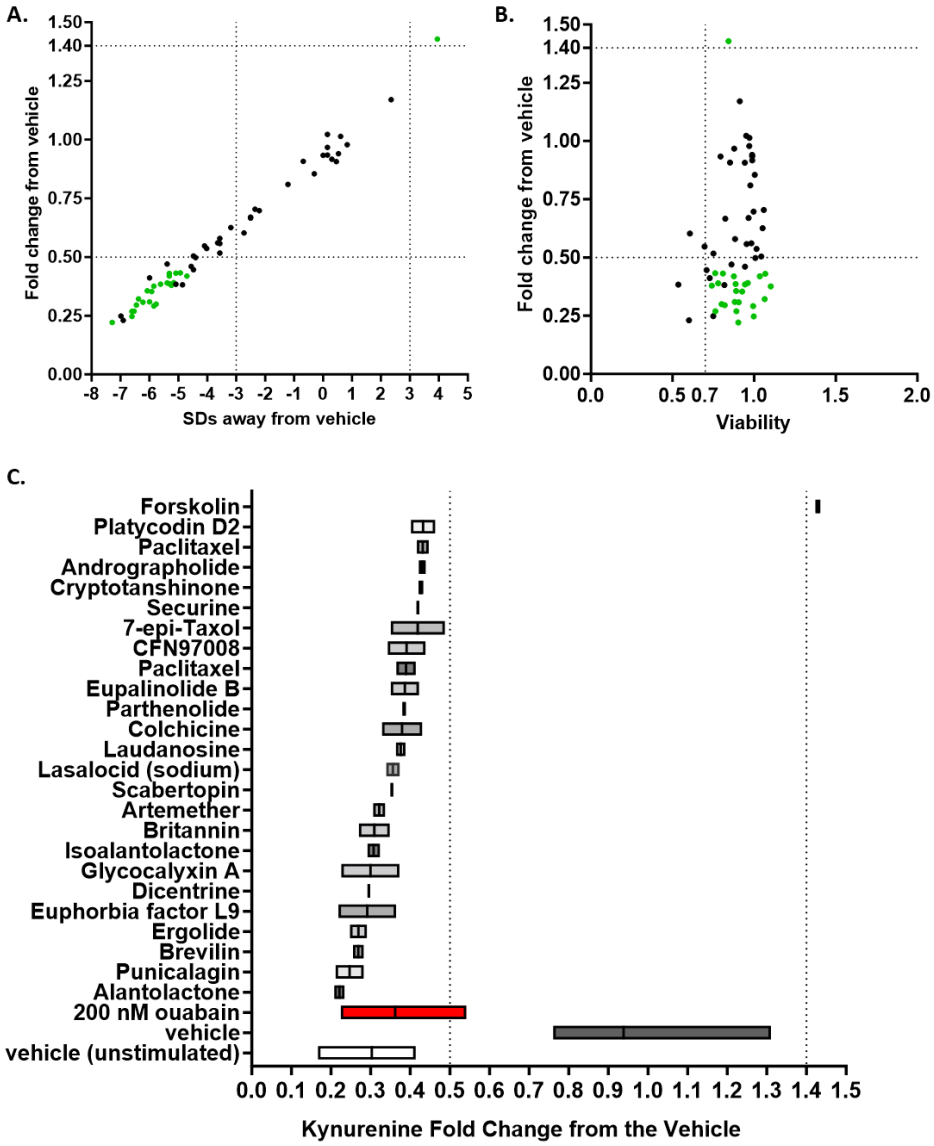
A.
Fold change from vehicle
SDs away from vehicle
B.
Fold change from vehicle
Viability
C.
Forskolin
Platycodin D2
Paclitaxel
Andrographolide
Cryptotanshinone
Securine
7-epi-Taxol
CFN97008
Paclitaxel
Eupalinolide B
Parthenolide
Colchicine
Laudanosine
Lasalocid (sodium)
Scabertopin
Artemether
Britannin
Isoalantolactone
Glycocalyxin A
Dicentrine
Euphorbia factor L9
Ergolide
Brevilin
Punicalagin
Alantolactone
200 nM ouabain
vehicle
vehicle (unstimulated)
Kynurenine Fold Change from the Vehicle

Figure 5.6 Natural compound screen validation – Results. A. Validation round: Kynurenine results – Fold Change in kynurenine levels normalized to the vehicle stimulated positive control Vs number of SDs away from the vehicle control (explained in section 2.3.2.) (mean values for fold change and SD variation were plotted for n=2 technical replicates, for drugs where one replicate was excluded from the SD analysis due to missing quality control threshold (see section 2.3.2.), only one SD value was used); B. Validation Round: Kynurenine results – Fold Change in kynurenine levels normalized to the vehicle stimulated positive control Vs Viability – fold change normalized to the vehicle control (explained in section 2.3.2.) (mean values for kynurenine fold change and viability were plotted for n=2 technical replicates); C. Annotation of validated compounds (hits). Cells were seeded and treated as described in sections 2.1and 2.3. Cells were pre-treated with drugs for 18 h and IFNγ (1 U/ mL)/ TNF (6.25 ng/ mL) stimulation was added for another 24 h. The kynurenine assay, described in more detail in section 2.9, was then performed on culture supernatants. The Deep Blue viability assay was carried out as described in section 2.10. For A and B green dots indicate validated compounds (hits), black dots indicate compounds that did not fulfil the validation criteria.

5.2.6 Natural compound hits – known biological activity.

A non-exhaustive literature search was carried out on the main hits. Five pathways/biological processes were consistently reported as being impacted on by several compounds from the hit list: two inflammatory pathways (NF-kB activation and JAK/STAT signalling) and three pathways/processes regulating survival, metabolism, and general cellular physiology (AKT/PI3K, MAPK/JNK/ERK/p38 and Cell Cycle). In addition to those five pathways, the impact of the hits on ion transport was also researched, given the results from Chapters 3 and 4 which point towards a link between Na^+ transport and IDO1 regulation.

A summary of these pathways and the number of hits affecting them is presented in Figure 5.7. Out of the 24 hits identified, 17 compounds have been documented in the literature to impact on the master immune regulatory transcription factor NF-kB activity, assembly, or expression (Babaei et al., 2021, Xu et al., 2021, Whan Han et al., 2001, Ooppachai et al., 2019, Bailly, 2021, Chae et al., 2008, Saadane et al., 2007, Kampan et al., 2015, Hidalgo et al., 2005, Chun and Kim, 2013, Chiadak et al., 2016, Luo et al., 2020). 10 of the top hits have also been shown to negatively impact on the JAK/STAT pathway (Babaei et al., 2021, Xu et al., 2021, Liu et al., 2019b, Li et al., 2021c, Lou et al., 2019, Kampan et al., 2015, Li et al., 2021a). Other pathways reported to be affected by some of the hits included ERK/JNK/p38/MAPK, PI3K/Akt, ROS production, cell cycle regulation, and ion transport. Appendix Table 8. 4 summarizes the main pathways known to be affected by each one of the hits in detail.

In conclusion, of the 25 hits over 50 % had been shown in the literature to be involved in the regulation of proinflammatory pathways such as NF-kB and JAK/STAT signalling.

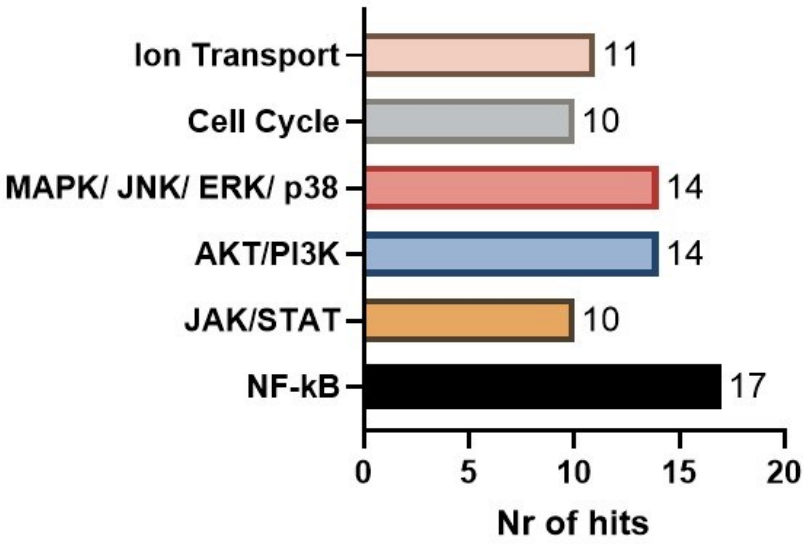

Figure 5.7 Natural compound screen hits – known biological activity. Representation of the main pathways affected by the hits, and number of compounds reported to affect each pathway.

5.2.7 Effect of hit compounds on IDO1 and PD-L1 mRNA levels.

Having identified 25 hits, the next step was to select a small subset of compounds for mechanistic studies. Having confirmed from the validation round of the screen that all hits impact kynurenine production without impacting on viability, the next step was to verify if this occurs, as in the case of ouabain (Chapter 3), through regulation of IDO1 expression, or whether it is an expression independent effect. Furthermore, this chapter aimed to reveal whether the hits are specifically targeting IDO1 expression/activity, or whether they impact on other IFNγ-regulated immune checkpoints, such as PD-L1. To answer these questions, a qPCR was performed on the samples treated with the hit compounds from the validation run, looking at IDO1 and PD-L1 expression. Furthermore, given the common regulatory mechanisms for IDO1 and PD-L1 (via IFNγ) signalling, this work aimed to verify whether the hits might target preferential expression of different PD-L1 isoforms rather than overall PD-L1 mRNA. For that, specific changes in soluble (s) and membrane PD-L1 were assessed. PD-L1 is an immune checkpoint expressed on the surface of tumour cells, however, soluble versions of this checkpoint can be generated either through proteolytic cleavage or via alternative splicing. The exact mechanism regulating alternative splicing is not fully understood yet, however, sPD-L1 levels have been reported as a biomarker of tumour immunogenicity/ responsiveness to anti-PD-1 immunotherapy, as well as being associated with metastasis (Bailly et al., 2021, Larrinaga et al., 2021, Oh et al., 2021). Thus, identifying a compound that can switch the splicing preference from one isoform to the other could contribute to a better understanding of the mechanism that regulates PD-L1 and sPD-l1 splicing, also having positive implications on cancer immunotherapy.

Figure 5.8 summarizes the impact of the hits identified by the drug screen on IDO1, membrane PD-L1 and sPD-L1 expression. Based on their impact on these three parameters four groups of compounds were distinguished (Figure 5.8A): Group1 (red), compounds that decreased both the kynurenine response IDO1 expression; Group 2 (blue), compounds that

decreased kynurenine but did not alter IDO1 mRNA levels by 50 % or more; Group 3 (green), compounds that decreased kynurenine but increased IDO1 expression, Group 4 (orange), compounds that affected membrane and sPD-L1 expression in different ways. Figure 5.8B presents the effects of the hits on IDO1 mRNA levels, highlighting in colours compounds representative for the first 3 groups.

Figure 5.8 C compares the impact of each one of the hits on membrane PD-L1 Vs sPD-L1 expression and identifies members of the 4^{th} group (compounds that do not change membrane PD-L1 levels but decrease sPD-L1 expression.

In conclusion, 4 groups of compounds (summarized in Figure 5.8A) with potential for further mechanistic studies were identified, based on their effects on kynurenine, IDO1 and (membrane and soluble) PD-L1 expression. The following sections will focus on two representative compounds from Group 2. These have been chosen due to similarities between their biological activity and their chemical structures and the rationale for selecting each one of these compounds will be explained in the corresponding sections. One representative compound from Group 4 was also investigated in more detail in section 8.3.1. Group1 compounds were not studied any further due to their presumed similar mechanism of action to ouabain/digoxin (studied in Chapter 3), while Group 3 compounds were also not further studied due to time constraints.

A.

Group 1	Compounds that decrease kynurenine but increase IDO1 mRNA expression
Group 2	Compounds that decrease kynurenine but do not impact on IDO1 mRNA expression
Group 3	Compounds that decrease kynurenine and decrease IDO1 mRNA
Group 4	Compounds that differentially affect membrane and soluble PD-L1 mRNA expression

B.

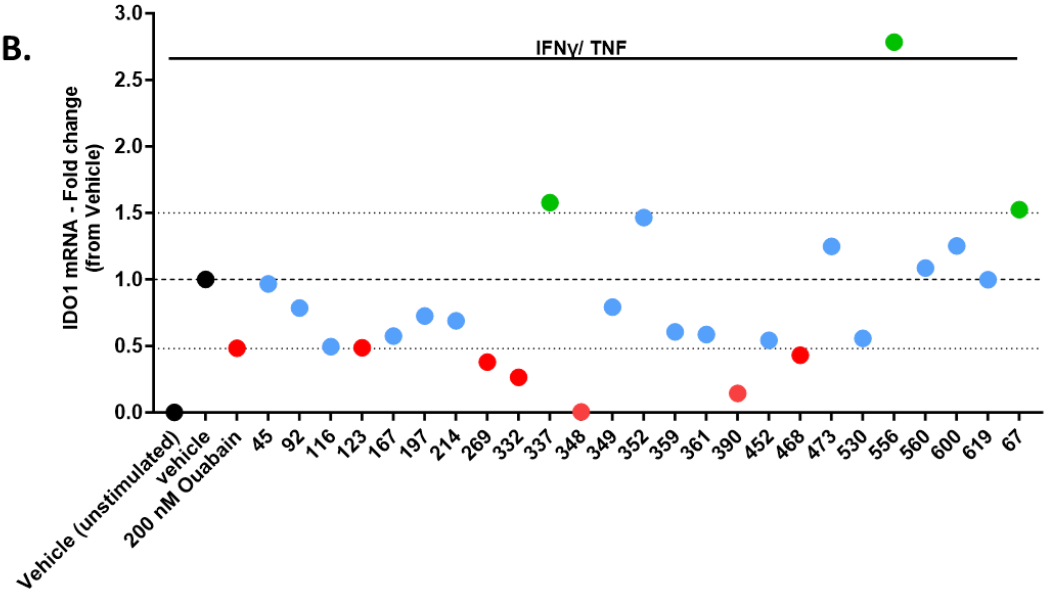

C.

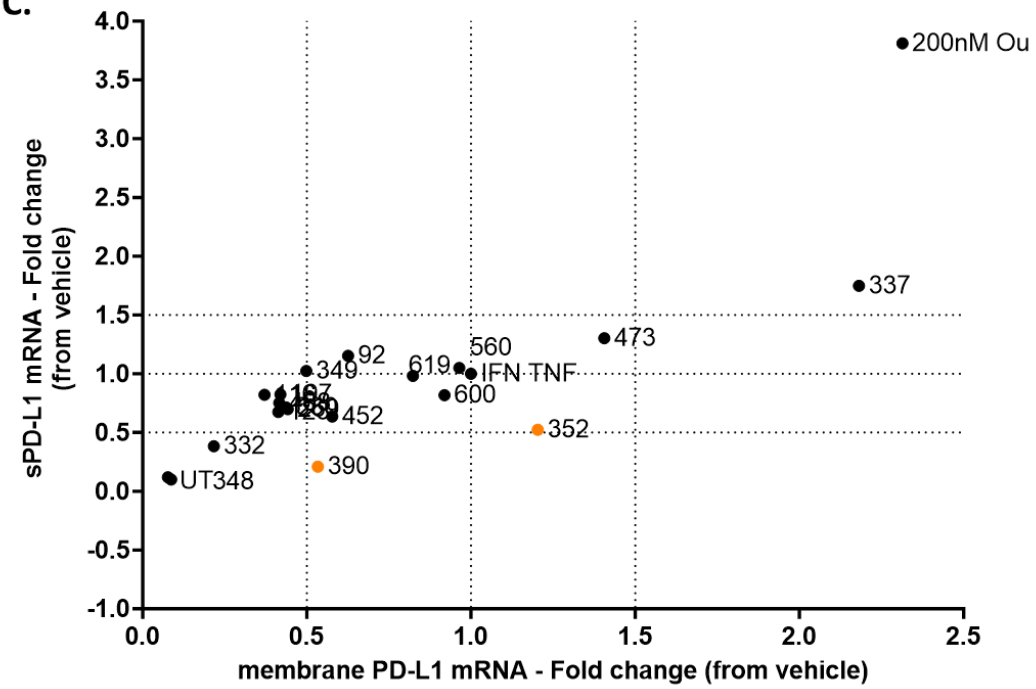

Figure 5.8 Effect of hits on IDO1, membrane and sPD-L1 mRNA levels. A. Summary of groups of compounds based on impact on IDO1, membrane and sPD-L1 gene expression B. Impact of compounds identified as hits on IDO1 mRNA levels, samples were normalized to β-actin, fold change from the vehicle IFNγ/TNF-treated control was calculated using $2^{(-\Delta CT)}$ values (n=1 biological replicate); C. Impact of compounds identified as hits on sPD-L1 Vs membrane PD-L1 mRNA levels, samples were normalized to β-actin, fold change from the vehicle IFNγ/TNF-treated control was calculated using $2^{(-\Delta CT)}$ values (n=1 biological replicate), dotted lines were used to mark 0 % or 50 % decrease (0.5) or 50 % increase (1.5) for any of the genes. Legend: red – compounds corresponding to Group 1; blue- compounds corresponding to Group 2; green - compounds corresponding to Group 3; orange - compounds corresponding to Group 4. Compounds were represented in Figures B and C with their assigned screening number for better visualisation of the data. The name of the compounds corresponding to the assigned numbers are summarised in Appendix Table 8.2.

5.2.8 Artemisinin-derivatives decrease kynurenine production without impacting on pSTAT1/IDO1 expression pathway.

Based on the functional classification of hits in Figure 5.8, Group 2 was the group with the highest number of compounds. Furthermore, Group 2 compounds seemed to behave in a different manner than the control drug, ouabain, discussed in Chater 3, which was classified as a Group 1 compound. For these reasons, a better understanding of the mechanism of action of the compounds in Group 2 could either help us identify potential direct IDO1 inhibitors, or highlight another IDO1/kynurenine regulatory pathway, in addition to the Na^+-correlated IDO1 regulation highlighted in Chapters 3 and 4.

The first representative compound from Group 2 was selected based on its chemical structure, which correlated with biological activity on the kynurenine response. Figure 5.9A, highlights the chemical structures of all artemisinin-derivatives included in the screen (Lu et al., 2019, Fu et al., 2021). All compounds that carried the oxygen endoperoxide bridge highlighted with the red box came up as either COIs or hits (Appendix Table 8.2 and Appendix Table 8. 3). The only member of the class that did not have any activity on kynurenine production, was deoxy artemisinin, which was also the only compound not carrying an oxygen bridge within its molecule. For this reason, the member of the class with the strongest impact on kynurenine (artemether, compound no 619, Appendix Table 8. 3, hit) was selected for further studies, alongside deoxy artemisinin (compound no 621, Appendix Table 8. 2), which was used as a negative control. Figure 5.9B, shows that artemether but not deoxy artemisinin decreases kynurenine levels in a concentration dependent manner in MDA-MB-231 cells. Furthermore, this effect was independent of viability as shown in Figure 5.9C. Confirming the results from the qPCR in Figure 5.8A, artemether had no impact on IDO1 mRNA levels at any of the tested concentrations (Figure 5.9D). The effect of artemether on IDO1 protein levels, as well as on STAT1 expression and activation (pSTAT1), were also tested

via western blot, however the compound did not change the levels of IDO1, STAT1 or pSTAT1 (Figure 5.9E). Densitometry also confirmed the fact that artemether does not impact on IDO1 protein expression or on the ratio between pSTAT1 and TSTAT1 protein levels (Figure 5.9F, G).

In conclusion, artemether decreased kynurenine levels in a concentration dependent manner, via an endoperoxide bridge-dependent mechanism, without impacting on IDO1 mRNA and protein expression, or STAT1 expression and activation.

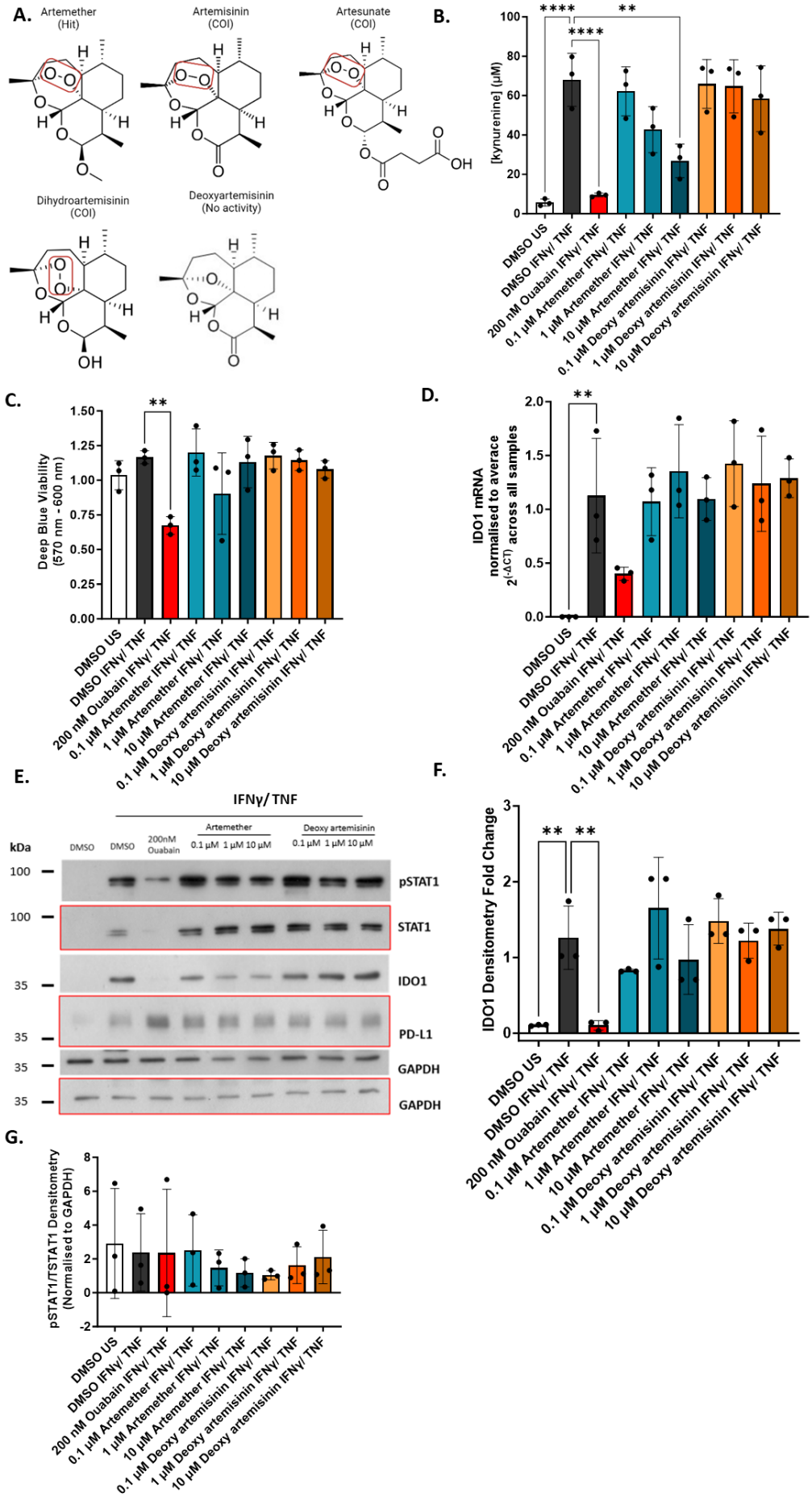
A.
Artemether (Hit)
Artemisinin (COI)
Artesunate (COI)
Dihydroartemisinin (COI)
Deoxyartemisinin (No activity)
B.
[kynurenine] (µM)
C.
Deep Blue Viability (570 nm - 600 nm)
D.
IDO1 mRNA normalised to averace 2(-ΔCT) across all samples
E.
IFNγ/ TNF
Artemether
Deoxy artemisinin
kDa
DMSO
200nM Ouabain
0.1 µM 1 µM 10 µM
pSTAT1
STAT1
IDO1
PD-L1
GAPDH
F.
IDO1 Densitometry Fold Change
G.
pSTAT1/TSTAT1 Densitometry (Normalised to GAPDH)
DMSO US
DMSO IFNγ/ TNF
200 nM Ouabain IFNγ/ TNF
0.1 µM Artemether IFNγ/ TNF
1 µM Artemether IFNγ/ TNF
10 µM Artemether IFNγ/ TNF
0.1 µM Deoxy artemisinin IFNγ/ TNF
1 µM Deoxy artemisinin IFNγ/ TNF
10 µM Deoxy artemisinin IFNγ/ TNF

Figure 5.9 Artemisinin-derivatives suppress kynurenine production in MDA-MB-231 cells without affecting IDO1 expression. A. Chemical structures of artemisinin-derivatives included in the screen; B. Effect of artemether and deoxy artemisinin titration on the kynurenine levels in MDA-MB-231 cells (n=3 biological replicates); C. As in B but for viability (n=3 biological replicates); D. As in B but for IDO1 mRNA levels, samples were normalized to β-actin, fold change from average expression value across all the samples was calculated using $2^{(-\Delta CT)}$ values (n=3 biological replicates); E. Western blot showing the effect of artemether and deoxy artemisinin on (p)STAT1, IDO1 and PD-L1, bands corresponding to the same blot were marked with red margins or no margins (representative for n=3 biological replicates); F. Densitometry fold change for IDO1 protein levels (n=3 biological replicates); G. Densitometry for the pSTAT1/ TSTAT1 expression ratio (n=3 biological replicates). Cells were pre-treated with drugs for 18 h and IFNγ (1 U/ mL)/ TNF (6.25 ng/ mL) stimulation was added for another 24 h. All data were plotted as mean and SD and statistical comparisons were carried out on B, C, D, F and G using a one-way ANOVA coupled with a Bonferroni's multiple comparison test (all conditions were compared to the DMSO IFNγ/TNF). Legend: COI – compound of interest; US – unstimulated.

5.2.9 Euphorbia factor L9 decreases kynurenine production without impacting on pSTAT1/IDO1 expression pathway.

A second set of compounds from Group 2 that was selected for further studies: Euphorbia factor L9 (EFL9) and L2 (EFL2). Eleven members of the Euphorbia factor family and 2 more structurally related molecules (Lathyrol and 7-Beta-Hydroxy Lathyrol) were included in the screen (Figure 5.10A) (Wang et al., 2020c) (PubChem database, PubChem compound CID: 168011854, 101306826, 10627939, 10577938, 74962706, 74962707, 131876111, 102004672, 162639176, 162639174, 162639177, 6443057, 24868376). The only compounds of this class that exerted some activity on the kynurenine response were EFL9 (hit) (compound 600, Appendix Table 8. 3) and EFL2 (COI) (compound 596, Appendix Table 8. 3), which distinguish themselves structurally, by carrying a benzoyl group on C7 (both) and in the case of EFL9 also a nicotinate modification. These C7 modifications, highlighted in red in Figure 5.10A, were therefore hypothesized to play a role in the inhibition of the kynurenine response. For this reason, EFL9, EFL2 were taken forward for detailed studies. The only member of the class the same backbone and side chains as EFL9 and 2, without the C7 modification, EFL3 (compound no 592, Appendix Table 8. 2), was selected as a negative control. Figure 5.10B shows that EFL9 and 2 decrease kynurenine in a concentration-dependent manner, with ELF9 being more potent, while EFL3 had no impact on kynurenine levels. The effect of EFL9 and 2 was not caused by cellular toxicity, as confirmed by the viability measurements in Figure 5.10C, which show no changes in response to any of the drug treatments. Figure 5.10D also supports the qPCR data from Figure 5.8A, suggesting no apparent changes in IDO1 mRNA levels in response to any of the concentrations, for both EFL9 and EFL2 treatments. At protein level, Euphorbia factors did not impact on IDO1 or STAT1 expression and they also do not change the levels of activated pSTAT1 (Figure 5.10E). Densitometry analysis also confirmed the fact that EFL9 and 2 exert their actions on kynurenine independently of IDO1 protein expression (Figure 5.10F).

In conclusion, data suggest that EFL9 and 2 decrease kynurenine levels in a concentration dependent manner, likely via a C7-benzoylation-dependent mechanism, without impacting on IDO1 mRNA and protein expression, or STAT1 expression and activation.

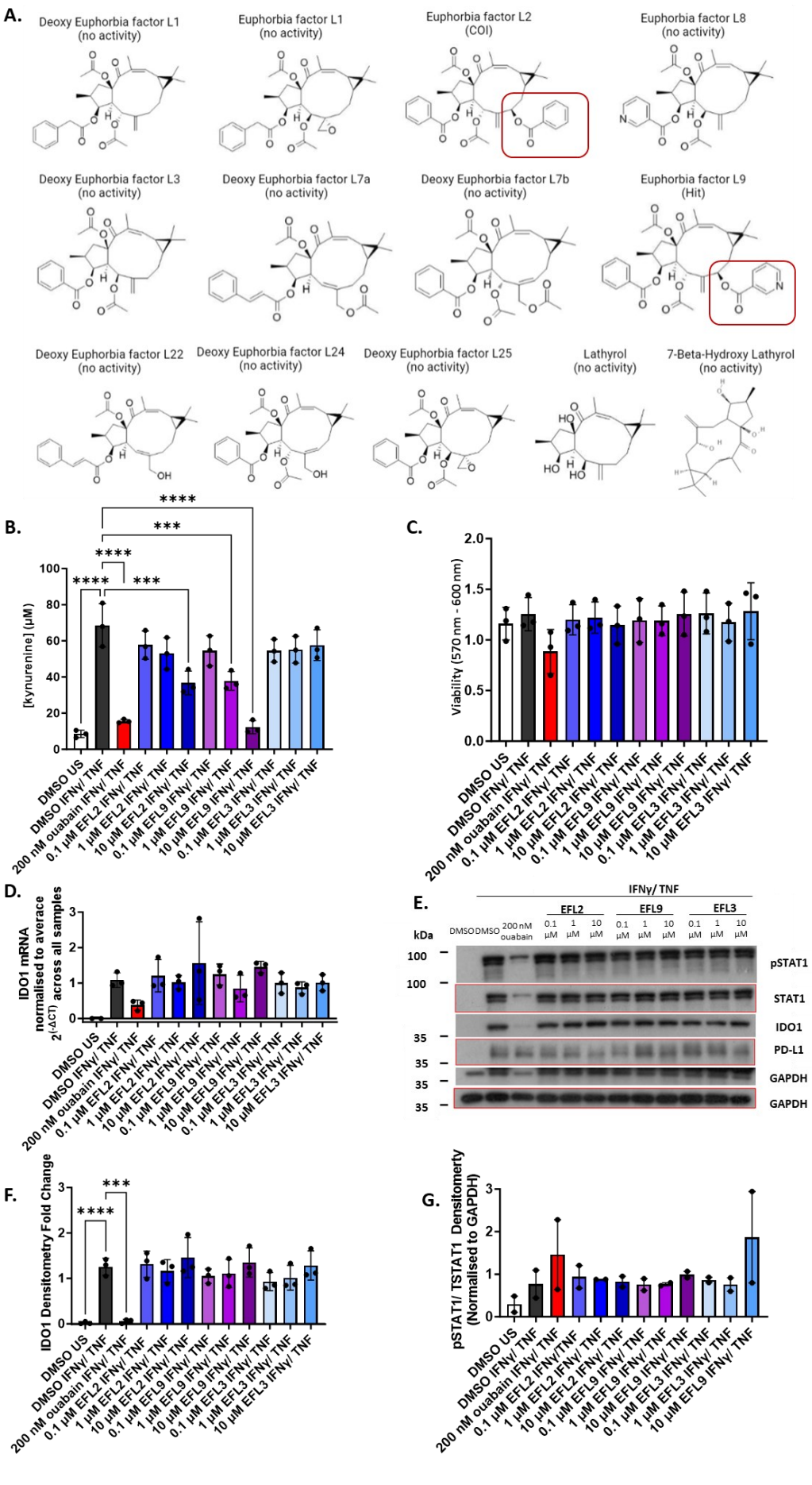
A.
Deoxy Euphorbia factor L1 (no activity)
Euphorbia factor L1 (no activity)
Euphorbia factor L2 (COI)
Euphorbia factor L8 (no activity)
Deoxy Euphorbia factor L3 (no activity)
Deoxy Euphorbia factor L7a (no activity)
Deoxy Euphorbia factor L7b (no activity)
Euphorbia factor L9 (Hit)
Deoxy Euphorbia factor L22 (no activity)
Deoxy Euphorbia factor L24 (no activity)
Deoxy Euphorbia factor L25 (no activity)
Lathyrol (no activity)
7-Beta-Hydroxy Lathyrol (no activity)
B.
[kynurenine] (µM)
C.
Viability (570 nm - 600 nm)
D.
IDO1 mRNA normalised to averace 2^(-ΔCT) across all samples
E.
IFNγ/ TNF
EFL2
EFL9
EFL3
kDa
DMSO
DMSO
200 nM ouabain
0.1 µM
1 µM
10 µM
pSTAT1
STAT1
IDO1
PD-L1
GAPDH
GAPDH
F.
IDO1 Densitometry Fold Change
G.
pSTAT1/ TSTAT1 Densitometry (Normalised to GAPDH)
DMSO US
DMSO IFNγ/ TNF
200 nM ouabain IFNγ/ TNF
0.1 µM EFL2 IFNγ/ TNF
1 µM EFL2 IFNγ/ TNF
10 µM EFL2 IFNγ/ TNF
0.1 µM EFL9 IFNγ/ TNF
1 µM EFL9 IFNγ/ TNF
10 µM EFL9 IFNγ/ TNF
0.1 µM EFL3 IFNγ/ TNF
1 µM EFL3 IFNγ/ TNF
10 µM EFL3 IFNγ/ TNF

Figure 5.10 Euphorbia factors L2 and L9 suppress kynurenine production from MDA-MB-231 cells, without affecting IDO1 expression. A. Chemical structures of Euphorbia Factors included in the screen; B. Effect of Euphorbia factors L9, 2 and 3 titration on the kynurenine response in MDA-MB-231 cells (n=3 biological replicates); C. As in B but for viability (n=3 biological replicates); D. As in B but for IDO1 mRNA levels, samples were normalized to β-actin, fold change from average expression value across all the samples was calculated using $2^{(-\Delta CT)}$ values (n=3 biological replicates, except for the DMSO US which was n=2); E. Western blot showing the effect of Euphorbia factors L9, 2 and 3 on (p)STAT1, IDO1 and PD-L1, bands corresponding to the same blot were marked with red margins or no margins (representative for n=3 biological replicates); F. Densitometry fold change for IDO1 protein levels (n=3 biological replicates); G. Densitometry pSTAT1/ TSTAT1 expression ratio (n=2 biological replicates). Cells were pre-treated with drugs for 18 h and IFNγ (1 U/ mL)/ TNF (6.25 ng/ mL) stimulation was added for another 24 h. All data were plotted as mean and SD and statistical comparisons were carried out on B, C and F using a one-way ANOVA coupled with a Bonferroni's multiple comparison test (all conditions were compared to the DMSO IFNγ/TNF). Legend: COI – compound of interest; EFL9, 2, 3 - 2, 3 – Euphorbia Factors 9, 2, 3; US – unstimulated.

5.2.10 Ouabain, artemether, EFL9 and EFL2 have a similar impact on kynurenine production in primary human mammary epithelial cells (HMECs).

Having shown that artemether and EFL9 and EFL2 decrease kynurenine levels without impacting on IDO1 expression in MDA-MB-231 cells, the next step was to test whether these effects are restricted to cancer cells, or whether they can be reproduced in primary non-transformed breast tissue cells. To do that, the effects of ouabain, artemether (and its control deoxy artemisinin), EFL9 and 2 (and their control EFL3) on kynurenine and IDO1 expression were measured in HMEC cells from 2 donors.

Figure 5.11A shows that ouabain, artemether, EFL9 and EFL2 significantly decreased kynurenine levels, without impacting viability in both donors (Figure 5.11B). Furthermore, only ouabain decreased IDO1 protein levels in both donor 1 (Figure 5.11C) and 2 (Figure 5.11D).

Thus, it was concluded that the effect of ouabain, artemether, EFL9 and EFL2 on kynurenine are not specific to cancer cells.

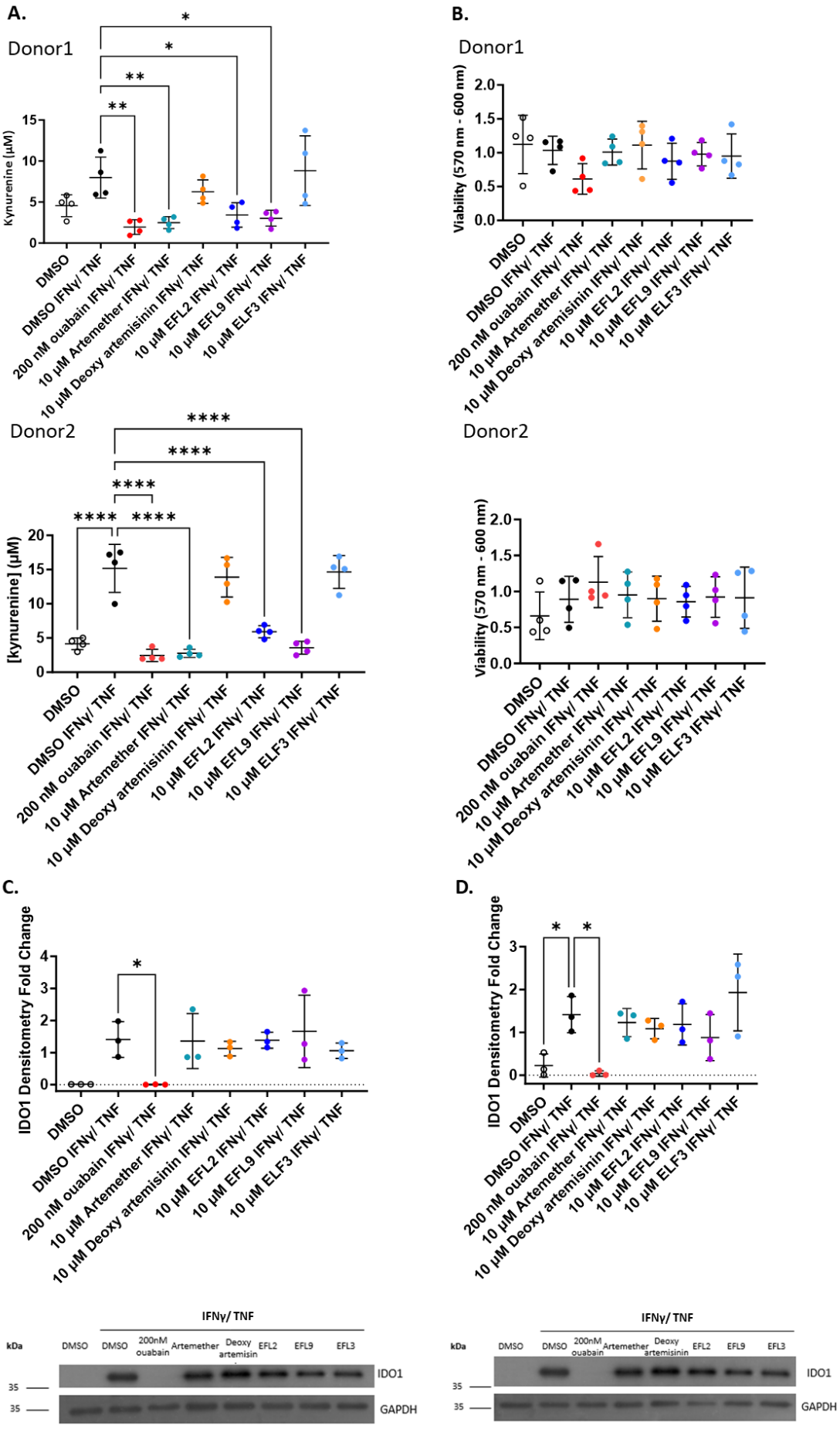
A.
Donor1
Kynurenine (μM)
DMSO
DMSO IFNγ/ TNF
200 nM ouabain IFNγ/ TNF
10 μM Artemether IFNγ/ TNF
10 μM Deoxy artemisinin IFNγ/ TNF
10 μM EFL2 IFNγ/ TNF
10 μM EFL9 IFNγ/ TNF
10 μM ELF3 IFNγ/ TNF
B.
Donor1
Viability (570 nm - 600 nm)
Donor2
[kynurenine] (μM)
Donor2
C.
IDO1 Densitometry Fold Change
D.
IDO1 Densitometry Fold Change
IFNγ/ TNF
kDa
DMSO
200nM ouabain
Artemether
Deoxy artemisin
EFL2
EFL9
EFL3
IDO1
GAPDH
35

Figure 5.11 Effect of ouabain, artemether, and Euphorbia factors L2 and L9 on kynurenine production and IDO1 expression in primary HMECs. A. Effect of ouabain, artemisinin-derivatives and EFL9, 2 and 3 on the kynurenine response in HMECs (n=4 replicates for each donor); B. As in A for viability (n=4 replicates for each donor); C. As in A for IDO1 protein levels in donor 1, one representative western blot as included (n=3 replicates); D. As in A for IDO1 protein levels in donor 2, one representative western blot as included (n=3 replicates). Cells were pre-treated with drugs for 18 h and IFNγ/ TNF stimulation was added for another 24 h. All data were plotted as mean and SD, statistical comparisons were carried out using a one-way ANOVA coupled with a Bonferroni's multiple comparison test (all conditions were compared to the DMSO IFNγ/TNF). Legend: EFL9, 2, 3 – Euphorbia Factor 9, 2, 3; GAPDH – glyceraldehyde-3-phosphate dehydrogenase.

5.3. Discussion

5.3.1 Drug screen results: COIs and Hits.

This chapter highlighted the steps required for designing a medium/high throughput natural compound screen, using the previously documented kynurenine assay (Shandell et al., 2022). It presented the optimization (Figure 5.2 and 5.3), the set-up (Figure 5.4) and results (Figure 5.5 and 5.6) of the screen. The impact of 630 natural compounds on the kynurenine response and viability was tested in the MDA-MB-231 cell line, which allowed identification of 59 COIs selected for further validation (Figure 5.5). Based on the results of the validation screen, 24 inhibitory and 1 enhancer hit were identified (Figure 5.6).

Depending on the assay type and compound library, high throughput screens (HTSs) have different sensitivities for identifying hits. A typical HTS hit rate has been reported to be ranging from 0.5 to 2 % of the total tested compounds (Goodwin et al., 2020). However, studies have also reported rates of 0.3 % in a *C. elegans* motility screen, or 2-3 % in an antagonist assay looking at intracellular Ca^{2+} accumulation, as a readout for GPCR activation (Hughes et al., 2011, Taki et al., 2021). In the compound screen presented in this chapter, the hit rate was 3.97 % (including the enhancer hit). This is above the average literature reported rates for high throughput screening and could be explained by the fact that the screen was only a medium throughput, focused drug screen. This means that the screening library was biased towards compounds with immunological activity. Thus, a higher hit rate than the literature average was expected, given the fact that the target (IDO1) and readout (kynurenine) are well-established immune mediators (Krupa and Kowalska, 2021).

5.3.2 Limitations of the kynurenine assay for medium/high throughput screening.

Various methods for measuring IDO1 activity have been described in the literature. Assays based on fluorescence measurements of N-formylkynurenine have been optimized over time to improve their signal to noise ratio, and have been used in the past for high throughput applications (Matin et al., 2006, Tomek et al., 2015, Seegers et al., 2014). With a similar set-up as the kynurenine assay used in this chapter, absorbance-based measurements of N-formylkynurenine from cellular/tissue lysates were also documented in the literature (Takikawa et al., 1988). Other more complex methods based on high-performance liquid chromatography (HPLC) have been shown to be the most selective and accurate and can be employed to measure a range of metabolites (e.g., both kynurenine and Trp) (Xiao et al., 2008, Ma et al., 2009). Radioactivity based assays that measure incorporation of ^{14}C into the N-formylkynurenine molecule in culture supernatants are also documented as more sensitive that absorbance based kynurenine quantifications (Ozaki et al., 1987).

However, the experimental set-up used for this screen was based on the colorimetric quantification of secreted N-formylkynurenine, by reading absorbance at 492 nm, and it mostly resembles the assay published by Peng et al. (2016) and further described in our publication, Shandell et al. (2022). Unlike the HPLC and radioactivity assays, absorbance measurements are less discriminative and provide more variability in terms of metabolite quantification. In the particular set-up of the screen presented in this chapter, the main assay limitations were low resolution at low kynurenine concentrations, as well as low detection capacity for enhancers. The limited resolving power for the low kynurenine concentrations was not an issue for the purpose of the screen, since the aim of the assay was that of identifying compounds that cause a change in kynurenine, rather than accurately classifying compounds based on their strength. Therefore, when looking at compounds that decreased

kynurenine below 10 µM it is not possible to accurately order them based on strength, but it is possible to confidently state that they are inhibitors of IDO1 activity. The second limitation, regarding the detection of enhancers, comes from the strong effect of the IFNγ/TNF stimulation on the cells, inducing kynurenine values up to 80 µM (Figure 5.3C), close to the top detection limit of the assay which is 100 µM. In this sense, for identification of enhancers a different experimental set-up, separate from that required for identification of inhibitors, should be designed, where lower IFNγ/TNF concentrations could be used, in order to allow a bigger window between the IFNγ/TNF-induced kynurenine levels and the top of the standard curve. However, IDO1 enhancers would be more of a point of interest for autoimmunity research, where the immunoinhibitory activity of this enzyme is required to keep the immune system in check (Lemos et al., 2020, Williams, 2013). In cancer, IDO1 inhibition, equivalent to increased immunogenicity against tumours, is usually the desired outcome (Li et al., 2021d). For these reasons, the assay was considered discriminative enough to identify a series of compounds with potential effect on IDO1 activity, which would have to be further confirmed and mechanistically studied through follow-up experiments.

Another limitation of the kynurenine assay in the context of the drug screen was the variability across replicates of the control conditions. The average intra-assay coefficient of variation (CV) across all controls was 5.42, whereas the CV across all the samples (drugs and controls) was 6.36. These values meet the literature guidelines which suggest that an ideal intra-assay CV should have a value below 10 (Schultheiss and Stanton, 2009). However, variation became more apparent and problematic when applying the 3 SD selection rule for COIs and hits. According to Lee et al. (2015) 99.7% of the members of a normally distributed population lie within 3 SDs of variation from the control, therefore, anything outside that is likely to not be part of the population. For this reason, when carrying out the SD exclusion analysis, the condition that the negative, unstimulated vehicle control should give a kynurenine readout 3SD away from that of the stimulated vehicle control was set as a quality

control. The replicate plates where this condition was not fulfilled were only used to match trends in the effect of compounds on kynurenine, rather than identify COIs or hits. For the kynurenine and viability fold change analyses, due to the lower discriminative power of these analysis methods, both replicates were included. For the first round of screening, the results from the SD and fold change analysis were combined, with the intention of testing a larger number of COIs. For the validation round, however, only compounds that passed both analysis methods were considered as hits, thus applying a more restrictive threshold. To overcome the variability issue, a few measures could be reinforced in the future, including an increase in the number of replicates for each control per compound plate; another source of variation could be human error (e.g., while pipetting), therefore, a fully automated set-up would be likely to decrease variability when screening a library of 630 compounds. Furthermore, literature reports that cell-based assay variation can be decreased by keeping cells at RT for 1 h after seeding, rather than directly transferring those to the 37 °C incubator (Lundholt et al., 2003).

Thus, the experimental set-up used for this drug screen would require significant optimization for future higher throughput applications. However, in the context of the screen presented in this chapter, the technical limitations were overcome through appropriate threshold selection of COIs and hits. This allowed successful identification and validation of 25 hits, of which two sets of compounds (artemisinin-derivatives and Euphorbia factors) were studied in more detail (Figure 5.9, Figure 5.10, Figure 5.11), confirming their inhibitory activity on the kynurenine response.

5.3.3 The biological relevance of hit compounds.

The natural compound library was strongly biased towards molecules that have been shown in the past to have an impact on the immune system. This is further confirmed by the literature reports on the main hits identified by the screen, where 17 compounds were

shown to have an impact on the master immune regulatory transcription factor NF-kB activity, assembly, or expression, with most of the compounds inhibiting its activity (Babaei et al., 2021, Xu et al., 2021, Whan Han et al., 2001, Ooppachai et al., 2019, Bailly, 2021, Chae et al., 2008, Saadane et al., 2007, Kampan et al., 2015, Hidalgo et al., 2005, Chun and Kim, 2013, Chiadak et al., 2016, Luo et al., 2020). The fact that 10 of the top hits have also been shown to negatively impact on the JAK/STAT pathway provides further theoretical support for the findings of the screen (Babaei et al., 2021, Xu et al., 2021, Liu et al., 2019b, Li et al., 2021c, Lou et al., 2019, Kampan et al., 2015, Li et al., 2021a). Given that IDO1 is an enzyme expressed in cancer in response to JAK/STAT activation, inhibition of this pathway could explain why its activity, measured as kynurenine production, is therefore reduced (Iwasaki et al., 2021). The subsequent qPCR data further support this hypothesis for some of the compounds, as it is the case for the top hit of the screen, alantolactone. Figure 5.8B shows a decrease in IDO1 mRNA in response to alantolactone (332) treatment. Other interesting pathways affected by some of these drugs include the MAPK signalling, known to regulate survival and apoptosis, as well as the Akt/PI3K signalling cascade mostly known for autophagy regulation. Both of these were the second most frequently targeted pathways by the compounds identified as hits, with 14 compounds being reported to have regulatory function on one or multiple components of each one of these pathways. 10 compounds were also shown to affect cell cycle progression and 11 compounds are known to have an impact on ionic dynamics, as summarized in Figure 5.9 and further elaborated in Appendix Table 8.4.

Thus, literature confirmed that the identified hits are known to have immunological activity, as well as highlighting their biological significance by revealing a range of crucial cellular pathways targeted by a large proportion of hits.

5.3.4 Artemisinin-derivatives and Euphorbia factors.

To better understand the biology of the hits, their impact on IDO1, membrane and soluble PD-L1 (isoforms of PD-L1, IFNγ-regulated immune checkpoint) expression was assessed. This facilitated identification of compounds that behave in a similar manner as ouabain, decreasing kynurenine by interfering with IDO1 expression (Shandell et al., 2022); compounds that seemed to exert their effect on kynurenine in a different manner than cardiac glycosides, as well as compounds that might interfere with the expression of PD-L1. The hits were further classified into 4 groups based on their impact on the kynurenine response and mRNA levels of IDO1, membrane and soluble PD-L1, as summarized in Figure 5.8. This chapter then focused on investigating in more detail the mechanism of action for compounds from Group 2, compounds that decrease the kynurenine response without impacting on IDO1 mRNA levels. In addition to Group 2 compounds, Group 4 was also briefly investigated, however, the observed impact of these compounds on membrane and soluble PD-L1 expression could not be validated, which is why this work was not pursued further (section 8.3.1.).

Compounds from Group 1 were shown to inhibit both IDO1 expression and kynurenine production, thus resembling the effect of cardiac glycosides (Chapter 3) (Shandell et al., 2022). Therefore, this class of compounds was not investigated further. However, there is value in studying the mechanism of action for each one of the compounds in Group 1. That is firstly because concomitant reduction in IDO1 expression and kynurenine levels, does not imply a single mechanism of action. It is possible that the reduction in kynurenine observed in cell supernatants might not be just a consequence of decreased IDO1 levels; instead, it could signal impaired kynurenine secretion or enhance kynurenine metabolism. Additionally, investigating this class of compounds might have exploratory value, as it could help identify other JAK/STAT-independent regulators of IFNγ-induced IDO1 expression, especially since literature reports a range of upstream IDO1 regulators such as Ras/ PKC, Kit or NF-kB

signalling (Liu et al., 2018a). Compounds from Group 3 upregulated IDO1 mRNA levels while downregulating kynurenine. This is potentially one of the most interesting and complex classes of compounds, which was not studied further due to time constraints. However, these compounds pose multiple research questions. One question could be whether the increase in IDO1 mRNA levels is mimicked also at protein level. If so, it would be interesting to verify if these compounds interfere with Trp metabolism, enhancing kynurenine degradation, or interfering with its secretion. Furthermore, it could be tested whether decreased levels of secreted kynurenine could signal back in a positive feed-back loop and enhance IDO1 expression. This would be contradictory with current literature which reports that elevated kynurenine levels enhance IDO1 expression by activating the AhR (Kaiser et al., 2020). Thus, there is value in exploring each one of the compound classes identified by the natural compound screen.

Due to limited time and resources, only two compound classes of interest belonging to Group 2 were investigated in detail: artemisinin-derivatives (artemether) and Euphorbia factors (EFL9, 2). The representative compounds for each class were chosen based on their chemical structures, which seemed to reflect their biological activity on the kynurenine response. Figure 5.9 shows that only members of the artemisinin-derivatives class that carry an endoperoxide bridge had inhibitory effect on kynurenine levels, with artemether being the most potent member of the group. Artemether was also considered of interest due to its historical usage for the treatment of malaria, which is also attributed to the endoperoxide bridge within its molecule, thus identifying and characterizing an inhibitory effect on the kynurenine pathway, in the context of breast cancer, could be a first step in repurposing this compound for immunotherapy use (O'Neill et al., 2010). Similarly, Figure 5.10 illustrates how only members of the Euphorbia factor/lathyrene class that carry a benzoyl modification (EFL9 and 2) on C7 are able to reduce kynurenine levels. Of the Euphorbia factor class, EFL1 and 2 have been studied in the literature, both have been linked to metabolic disruptions,

including amino acid metabolism, EFL1 was also linked to interference with JAK/STAT signalling, while EFL2 was associated with ion transport dysregulation and membrane receptor signalling disruptions (Zou et al., 2022). However, the most potent kynurenine inhibitor from the Euphorbia factor class, EFL9, has not been analysed in depth in the literature, thus the work presented in this chapter adds considerable value as a first step towards understanding to role of this molecule in metabolic and immune regulatory pathways in breast cancer.

A titration of artemether (Figure 5.9), EFL9 and 2 (Figure 5.10) showed that all these compounds decrease kynurenine, independently of viability, without impacting on IDO1 mRNA or protein levels, and without interfering with STAT1 activation (pSTAT1 levels) in breast cancer cell lines. This result indicates a different mechanism of action than for ouabain, which was shown to inhibit the kynurenine response by interfering with pSTAT1-regulated IDO1 expression (Chapter 3). Furthermore, artemether, EFL9 and 2, as well as ouabain were shown to impact IFNγ/TNF-induced IDO1 activity and expression in a similar way in non-transformed human primary mammary epithelial cells, suggesting that their mechanism of action is not cancer specific (Figure 5.11). The lack of cancer specificity opens a range of hypotheses, the compounds could be interfering with IFNγ/TNF signalling, as it was shown for ouabain in Chapter 3 (Shandell et al., 2022), they could directly interact with IDO1, or they could impact on Trp metabolism, upstream or downstream kynurenine production, impairing Trp uptake (upstream), enhancing kynurenine degradation, or preventing kynurenine export (downstream).

Thus, this chapter identifies three novel inhibitors of the kynurenine response in MDA-MB-231 cells: artemether, EFL9 and EFL2. Comparison of the mechanisms of action of these two compounds to that of ouabain shows that their impact on kynurenine is independent of IDO1 expression. Further studies looking at the impact of these compounds on purified IDO1

activity and Trp metabolism would be required to better understand the mechanisms of action of these compounds.

5.4. Conclusions

In conclusion, this chapter summarizes the steps in optimizing the kynurenine assay for medium/high throughput applications. It presents the effects of 630 natural compounds on IDO1 activity and identifies 24 inhibitory and 1 enhancer hit. This chapter also classifies the hits into 4 groups based on their impact on the kynurenine response, IDO1 and PD-L1 isoform expression, focusing on two classes of compounds artemisinin-derivatives (artemether) and Euphorbia factors (EFL9 and 2). Artemether, EFL9 and EFL2 are shown here to inhibit kynurenine production independently of IDO1 and further studies are needed to understand their full mechanism of action.

6. Chapter 6: Mechanistic studies of novel natural inhibitors of the kynurenine response.

6.1. Introduction

6.1.1. Background

IDO1 has been extensively studied as a therapeutic target, however, its clinical success has been limited, with only one IDO1 inhibitor, Indoximod, approved for cancer use, in stage IIb and IV melanoma patients (Tang et al., 2021). There are multiple possible explanations for this outcome, from the localization of this immune checkpoint to its intricate cellular function.

A substantial difference between other immune checkpoints like PD-1/ PD-L1/ CTLA-4 and IDO1 is its enzymatic activity. A large body of literature has highlighted the challenges associated with enzyme inhibitors, as cancer therapies, by looking at kinase inhibitors. The main limitation of such approaches is the fact that cancer cells tend to develop resistance by constantly mutating the targeted enzyme (Bhullar et al., 2018, Wilson et al., 2012). Thus, targeting IDO1 activity could result be particularly challenging due to potential resistance development.

Another limitation of IDO1 inhibition therapy comes from the structural resemblance between IDO1 and the liver TDO enzyme. Therefore, high dug-target specificity is required to avoid off-target liver damage. Additionally, IDO1 and 2 are alternatively or concomitantly expressed depending on tissue (Fukunaga et al., 2012). Inaccurate determination of IDO1 expression, specifically, or differential expression of IDO1 and 2 at different metastatic sites in each patient might be one of the reasons why IDO1 inhibition has not been as successful as other immune checkpoint therapies in cancer patients (Bilir and Sarisozen, 2017).

Additionally, potential compensatory mechanisms can be triggered by IDO1 inhibition, stimulating the tumour cell to switch from IDO1 to IDO2/TDO expression (Tang et al., 2021).

Alongside IDO1 localization and structure, another limitation comes from the complex cellular role of this protein. Apart from its immune checkpoint function, as Trp-depleting and kynurenine-producing enzyme, IDO1 is also indirectly involved in the synthesis of a range of metabolites with impact on cellular homeostasis. The kynurenine pathway produces a range of immunosuppressive metabolites such as kynurenine, kynurenic acid and 3-hydroxyanthanilic acid, as well as metabolites with neurological activities including quinolinic and kynurenic acid (Stone and Williams, 2023, Heylen et al., 2023).

IDO1 is also a signalling hub, being regulated by a range of upstream mediators, including the IFNγ-induced JAK/ STAT signalling pathway, but also the Ras/ PKC or NF-kB pathways. In cancer constitutive IDO1 expression is achieved via COX-2 and PGE2 induced activation of PKC and PI3K signalling. Downstream of IDO1, there are 3 main cellular effectors regulated by its activity. Firstly, Trp depletion leads to accumulation of uncharged Trp-tRNA which activates the GCN2 kinase and prevents translation initiation; GCN2 activation by IDO1 was also shown to promote neovascularization (Dey et al., 2021, Ravishankar et al., 2015a). Furthermore, Trp depletion can interfere with translation efficiency, contribute to ribosomal frameshifting and thus synthesis of neoantigens. These contribute to cancer cell immune evasion, impairing tumour recognition and attack from the immune system (Bartok et al., 2021). Secondly, IDO1 activity has also been linked to mTORC1 suppression in $CD8^+$ T cells, which triggers autophagy and cellular anergy, meaning that the T cells can no longer attack and clear the tumour; this chain of biological evens was shown to be targetable by Indoximod (Metz et al., 2012). Thirdly, kynurenine binds the AhR promoting IDO1 expression and thus sustaining the immunosuppressive tumour immune environment (Opitz et al., 2011, Grohmann and Puccetti, 2015).

Therefore, the enzymatic activity of IDO1, its structural similarity to IDO2 and TDO, as well as its intertwined signalling, metabolic and immunological roles make it a complex target, and its pharmacological inhibition thus raises implications that are difficult to predict.

The majority of clinically tested IDO1 inhibitors can be classified as Trp mimetics (Indoximod, Epacadostat, Navoximod, Norharmane), molecules that interact with the active stie of IDO1 (PF-0684003) or molecules that interfere with the haeme binding pocket (Linrodostat) (Günther et al., 2019, Wen et al., 2019, Balog et al., 2021, Cherney et al., 2021). One of the problems encountered by treatment with small molecules resembling Trp structure is cross-reactivity. Indoximod, Epacadostat, Navoximod and Norharmane were thus reported to bind and activate the AhR, which is known to function as a promoter of IDO1 expression, mediating cancer progression (Moyer et al., 2017). Additionally, in plasmacytoid DCs, Epacadostat was shown to inhibit the enzymatic activity of IDO1, while stimulating its signalling function which mediates differentiation of tolerogenic, tumour promoting DCs (Panfili et al., 2023). Sometimes, however, the similarity in structure between IDO1 inhibitors and Trp can be beneficial, as is the case for Indoximod which was shown to activate mTOR, otherwise inhibited by Trp depletion and thus reverse T cell anergy (Fox et al., 2018).

The limited clinical efficacy of IDO1 inhibitors highlights the need for further research on the subject. Given that immune regulation is not directly achieved by IDO1, but rather through metabolites like Trp and kynurenine, a better understanding of the Trp metabolic pathway could contribute to the development of better IDO1-centred immunotherapies. There are various ways of increasing the levels of Trp in the tumour microenvironment, from IDO1 inhibition to inhibition of Trp import via the SLC7A5 transporter (Scalise et al., 2018, El Ansari et al., 2018). Targeting SLC7A5 might have double beneficial role, as it has been reported as the main kynurenine importer (Sinclair et al., 2018). Another targetable transporter is also SLC7A11, which was also shown to import kynurenine from the extracellular environment

(Fiore et al., 2022). Kynurenine levels can also be regulated by multiple mechanisms, alongside Trp depletion and IDO1 inhibition. Increased kynurenine degradation can be achieved by enhanced activity of downstream kynurenine amino transferase and kynurenine monooxygenase enzymes, promoting its conversion to kynurenic acid or 3-hydroxykynurenine (Neavin et al., 2018). Furthermore, kynurenine secretion could also be one aspect of interest for further research, especially given the fact that no kynurenine exporter has been identified yet. Studies have also liked kynurenine with iron availability showing that kynurenine import protects against iron-induced cell death (ferroptosis), as well as iron accumulation being associated with increased IDO1 activity and subsequent kynurenine production (Fiore et al., 2022, Donley et al., 2021).

These observations suggest that the kynurenine pathway as well as IDO1 are tightly intertwined with a range of elements from the cytosolic and tumour microenvironments. Thus, this chapter presents a broader exploration of IDO1 inhibition by studying natural compounds with activities on the kynurenine levels and trying to pin down a mechanism of action for each one of the compounds studied. This work aims to reveal novel biological regulators of the kynurenine response and expand the IDO1-centered immunotherapeutic approaches from direct IDO1 inhibition to modulation of cellular homeostasis with the ultimate result of Trp replenishment and kynurenine depletion.

6.1.2. Hypothesis and aims.

Building on the limited success of synthetic, targeted IDO1 inhibitors, this chapter is exploring the efficacy of natural compounds with a broad spectrum of biological activities on Trp metabolism. It was hypothesized that by interfering with Trp metabolism, stable and consistent elevation in Trp levels in the tumour microenvironment, as well as decreased secreted kynurenine levels could be achieved. These metabolic changes should be equivalent to increased $CD8^+$ T cell activation and decreased immunosuppressive signalling in the breast tumour microenvironment.

This chapter thus aims to study two novel natural inhibitors of the kynurenine response, artemether and EFL9, previously identified via a natural compound screen (Chapter 5). This work aims to characterize their mechanism of action by investigating their role on direct IDO1 activity, modulation of intracellular Na^+ levels and Trp metabolism. The mechanisms of action of artemether and EFL9 are compared to those of ouabain, and the clinically tested IDO1 inhibitor, Linrodostat, highlighting a unique metabolic profile associated with each compound.

6.2. Results

6.2.1. Impact of artemether and EFL9 on purified IDO1 enzyme activity.

Having shown that artemether and EFL9 affect the kynurenine response independently of IDO1 expression, the next step was to explore whether they directly interfere with IDO1 activity. An absorbance-based enzyme activity assay was thus used to assess IDO1-dependent oxidation of L-Trp to N-formylkynurenine; for this assay purified human recombinant IDO1 protein was used. The methodology for this assay has been previously tested in the literature (Donley et al., 2021, Jonescheit et al., 2020, Bracho-Sanchez et al., 2019). To be able to interpret the assay results, a small molecule IDO1 inhibitor, Linrodostat, was used as a positive control (Cherney et al., 2021, Tang et al., 2021).

Firstly, Linrodostat was shown to decreased kynurenine levels in culture supernatants when applied to MDA-MB-231 cells, in a concentration-dependent manner (Figure 6.1A) and independently of viability (Figure 6.1B). To test whether an *in vitro* IDO1 activity assay could be confidently used to assess IDO1 inhibition, the highest Linrodostat concentration tested on cells (100 nM) and a second higher concentration, 10 µM, were used as positive controls in the *in vitro* assay. The reason for this choice of concentrations was based on the assumption that in cells the ratio of IDO1 to drug is much lower than in a purified enzyme activity assay set-up. Furthermore, Linrodostat was used as a positive control, therefore, a higher concentration would result in stronger inhibition, providing a better assay detection window. Alongside Linrodostat, artemether and EFL9 (10 µM for both) were also included in the *in vitro* assay, as well as a DMSO control only. For each drug and DMSO condition, a no enzyme control was also included; this allowed assessment of the background signal generated by each compound (elevated background is often an indication that the compounds are not compatible with the given assay set-up) (Simeonov and Davis, 2004). The drug and DMSO testing samples and controls were prepared in assay buffer containing

NaOH. Due to previous findings that showed elevated Na^+ might be correlated with IDO1 inhibition (Chapters 3 and 4), an enzyme DMSO condition and DMSO no enzyme control, both prepared with assay buffer containing KOH, were also set up.

In Figure 6.1C, the red curve represents the IDO1 DMSO (in NaOH) control. The 10 µM Linrodostat condition (dark blue) gave a marginally steeper curve, representative for more rapid Trp oxidation, than the IDO1 DMSO control (red). However, the background for this condition was also elevated (dark grey dots). The 100 nM Linrodostat condition gave lower background (purple dots) and a slower reaction rate (light blue) to the IDO1 DMSO control (red). Thus, Linrodostat did not seem to inhibit IDO1 activity in this set-up. Artemether (dark red) and EFL9 (orange) seemed to slightly speed up IDO1 activity in this set up.

Figure 6.1D, clarifies all these trends, showing that Linrodostat did not significantly inhibit the rate (slope) of the IDO1-mediated Trp to N-formylkynurenine conversion at any of the concentrations. Artemether and EFL9 also had no impact on the reaction rate. Interestingly, using KOH instead of NaOH in the reaction buffer, seemed to have an inhibitory effect on the IDO1 reaction. However, given the fact that the negative controls of this experiment (the two Linrodostat conditions) did not work according to prediction, the results of this assay could not be used to draw a clear conclusion.

In summary, a commercially available IDO1 inhibitor, Linrodostat, was selected as a positive control for the IDO1 enzyme activity assay, and its activity was validated in MDA-MB-231 cells. However, Linrodostat did not show IDO1 inhibition in a purified enzyme activity set-up, potentially due to high background at the given absorbance wavelength. For this reason, the results of this activity assay were considered inconclusive. An alternative assay would need to be to be developed to test whether artemether and EFL9 could have direct inhibitory activity on IDO1.

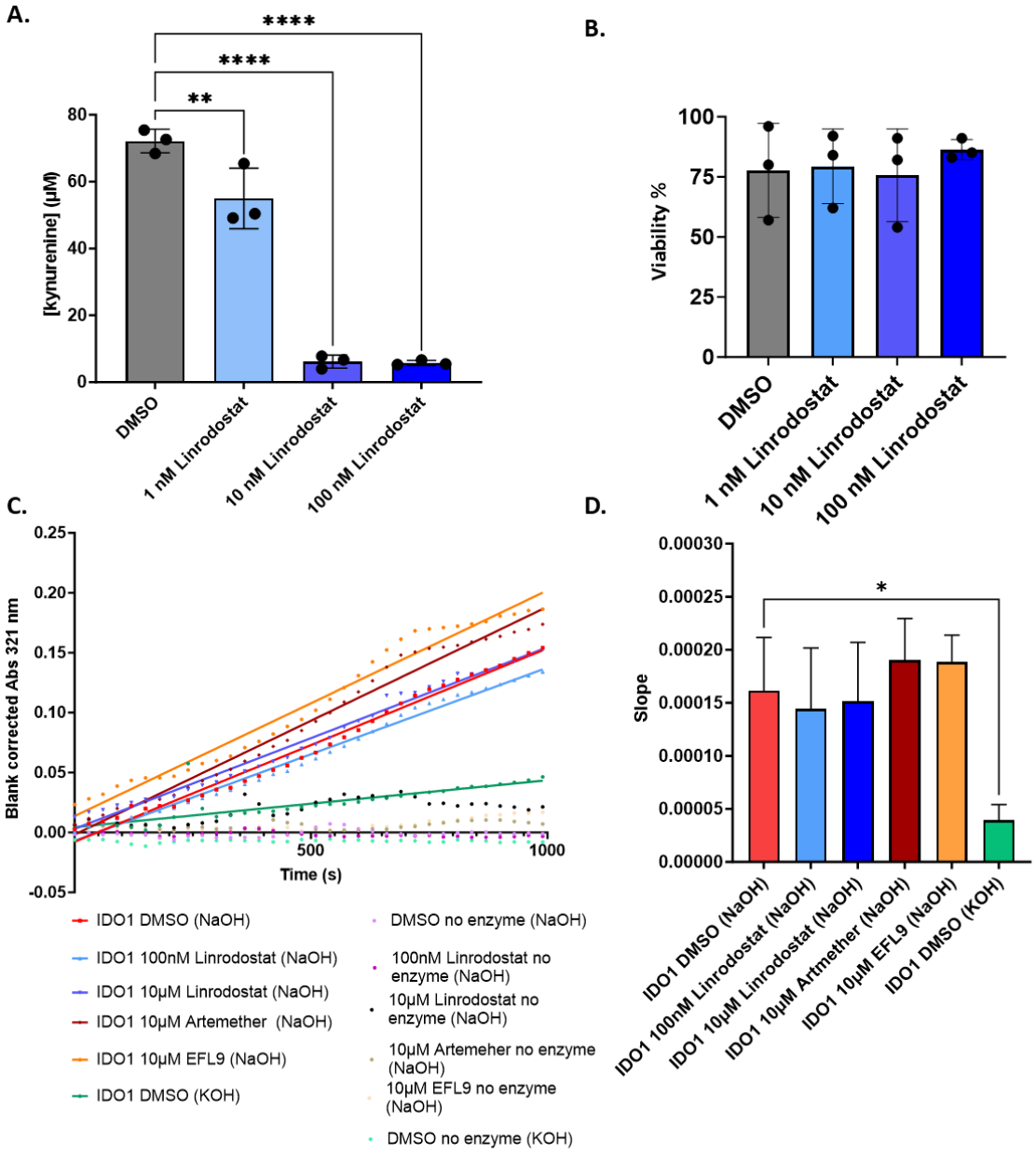
A.
****
****
**
[kynurenine] (μM)
80
60
40
20
0
DMSO
1 nM Linrodostat
10 nM Linrodostat
100 nM Linrodostat
B.
Viability %
100
75
50
25
0
DMSO
1 nM Linrodostat
10 nM Linrodostat
100 nM Linrodostat
C.
Blank corrected Abs 321 nm
0.25
0.20
0.15
0.10
0.05
0.00
-0.05
500
1000
Time (s)
IDO1 DMSO (NaOH)
IDO1 100nM Linrodostat (NaOH)
IDO1 10μM Linrodostat (NaOH)
IDO1 10μM Artemether (NaOH)
IDO1 10μM EFL9 (NaOH)
IDO1 DMSO (KOH)
DMSO no enzyme (NaOH)
100nM Linrodostat no enzyme (NaOH)
10μM Linrodostat no enzyme (NaOH)
10μM Artemeher no enzyme (NaOH)
10μM EFL9 no enzyme (NaOH)
DMSO no enzyme (KOH)
D.
Slope
0.00030
0.00025
0.00020
0.00015
0.00010
0.00005
0.00000
*
IDO1 DMSO (NaOH)
IDO1 100nM Linrodostat (NaOH)
IDO1 10μM Linrodostat (NaOH)
IDO1 10μM Artmether (NaOH)
IDO1 10μM EFL9 (NaOH)
IDO1 DMSO (KOH)

*Figure 6.1 Testing the effect of artemether and EFL9 on purified IDO1 activity Vs a commercially available IDO1 inhibitor, Linrodostat. A. Effect of the commercially available, IDO1 inhibitor, Linrodostat, on kynurenine production in MDA-MB-231s (n=3 biological replicates); B. as in A for viability (n=3 biological replicates); C. Effect of Linrodostat, artemether, EFL9 and NaOH Vs KOH on IDO1 activity in vitro (n=3 biological repeats). D. Quantification of the IDO1 reaction rate/slope upon treatment with DMSO, Linrodostat, artemether, EFL9 in NaOH and KOH (n=3 biological replicate). For A, cells were prepared as described in sections 2.1, 2.2 and a kynurenine assay was carried out on culture supernatants by reading absorbance at 492 nm, as described in section 2.9. For B, viability was measured using a Countess II FL Automated Counter (Thermo Fisher Scientific) (section 2.10). For C, the activity assay was set up as described in section 2.15, absorbance was recorded at 321 nm. For D, the slope of the curve for each one of the conditions in C were calculated using linear regression equation in GraphPad Prism v9.0.0, for each one of the 3 biological repeats; these were then plotted as a bar graph presenting mean an SD. Statistical analysis was carried out on A, B and D using a one-way ANOVA coupled with a Bonferroni's post-test (all conditions were compared to the DMSO control), for specific comparisons, *p<0.05, **p<0.01; ****p<0.0001.*

6.2.2. Impact of artemether and EFL9 on intracellular Na^+.

Having shown in Chapters 3 and 4 that a decrease in kynurenine correlates with an increase in intracellular Na^+ levels, assessment of the impact of artemether and EFL9 impact on ionic homeostasis was considered as the next step in the mechanistic characterization of these compounds. To test that MDA-MB-231 cells were with the highest concentration of artemether and EFL9 seen to reduce kynurenine (10 μM); the same treatment regime as when measuring the kynurenine response was applied (18 h compound pre-treatment, followed by 24 h co-treatment of drug and IFNY/TNF stimulation) (section 2.2).

Figure 6.2 shows that neither artemether, nor EFL9 impacted on the concentration of intracellular Na^+. Ouabain was used as a positive control, elevating intracellular Na^+ levels to a concentration of 95 mM, and thus confirming that the assay can confidently quantify change in the intracellular Na^+ concentration.

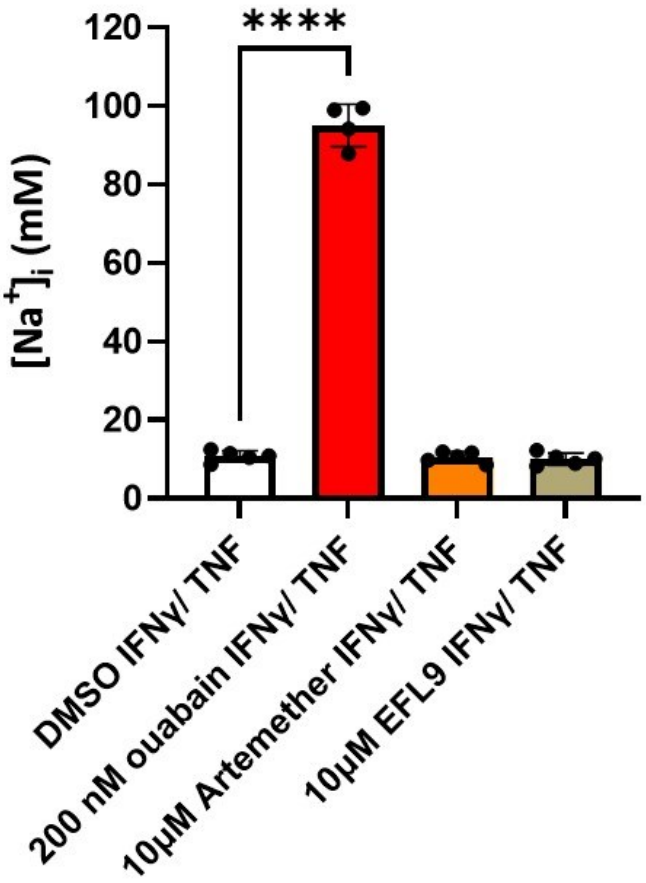

*Figure 6.2 Testing the effect of artemether and EFL9 on intracellular Na^+ levels in MDA-MB-231 cells. One representative of 3 biological repeats was included (n=5 technical replicates, except for the ouabain condition where n=4 technical replicates: one replicate was excluded based on the quality control rule explained in section 2.11). The cells were pre-treated with drugs for 18 h, followed by 24 h co-treatment with drugs and IFNγ (1 U/ mL)/ TNF (6.25 ng/ mL) stimulation; SBFI staining, and analysis were carried out as described in sections 2.11; data was plotted as mean and SD. Statistical analysis was carried out using a one-way ANOVA coupled with a Bonferroni's post-test (all conditions were compared to the DMSO control), for specific comparisons, ****p<0.0001.*

6.2.3. Effects of ouabain, artemether and EFL9 treatment on tryptophan metabolism in MDA-MB-231 cells.

Having shown that artemether and EFL9 affect kynurenine by a different mechanism compared to ouabain (IDO1 expression- and sodium-independent) and having been unable to investigate the impact of those drugs on purified IDO1 activity, due to technical limitations, a deeper mechanistic understanding was sought by assessing their impact (ouabain, artemether and EFL9 Vs DMSO) on Trp metabolism. This experiment aimed to test whether the decrease in kynurenine recorded in the previous experiments was a result of IDO1 inhibition, or whether it is caused by a decrease in Trp uptake, or an increase in kynurenine consumption. For this, a targeted metabolomics analysis was carried out on cell lysates and supernatants, from samples treated with the three compounds, to see how metabolites change upstream and downstream of kynurenine.

Lysates from $4x10^6$ cells/ sample were collected using the freeze-thaw protocol described by Rushing et al. (2022). Samples were run on a Thermo Vanquish Flex LC system. The eluate was sent to a Thermo Orbitrap Fusion instrument and MS1 and data dependent MS2 data were completed at an orbitrap resolution of 60,000 FWHM, as described in section 2.4.1. Bespoke XCMS scripts were use for raw data analysis, looking for exact MS1 matches to the Trp pathway metabolites, with annotations verified and additional annotations added using high-resolution MS2 data processed through Sirius as described in section 2.4.2. 135 metabolites were detected, with 47 of those being confidently annotated. Statistical analysis was carried out using the Metaboanalyst online portal; this applied a data integrity check to each set of data uploaded excluding metabolite entries that exhibited constant or no value for all the treatment conditions included in the data set. All data sets were median normalized and $\log_{10}$ transformed, with no further filtering applied (also explained in section 2.16).

Figure 6.3 shows the results of this analysis. Principal component analysis (PCA) was carried out on all the detected metabolites (135 metabolites) and showed a clear separation of the 4 treatment conditions, with some similarity observed between the artemether and DMSO conditions (Figure 6.3A). The data set was then reduced to the metabolites that could be confidently annotated (47 metabolites), and PCA showed weaker separation of the 4 treatment groups, likely due to reducing the number of included metabolites. Furthermore, the EFL9 condition seemed to be the most heterogenous one, as well as the most distinct from the DMSO group, while artemether-treated samples showed the highest similarity to the DMSO condition (Figure 6.3B).

In summary, differentiation amongst different treatment groups, based on their metabolic impact on intracellular Trp metabolites, was achieved. The separation was more apparent when looking at all detected metabolites than in the data set restricted to known annotations, suggesting that there is overlap in the Trp metabolism specific effects of each one of the treatments.

A.

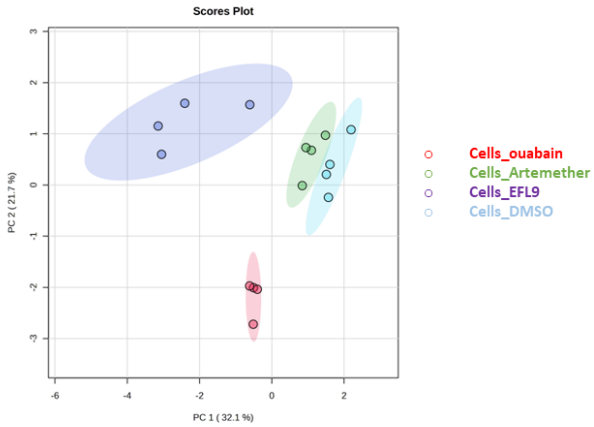

PC1	PC2	PC3	PC4	PC5
32.1%	21.7%	12.1%	9.9%	6.2%

B.

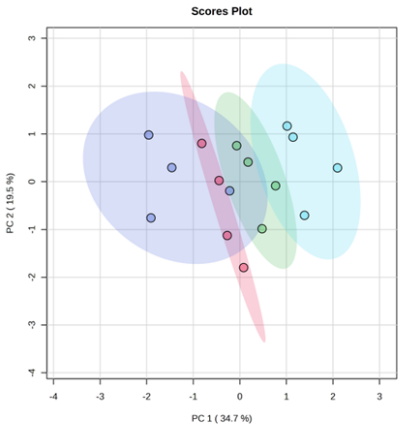

PC1	PC2	PC3	PC4	PC5
34.7%	19.5%	16.2%	8.6%	6%

Figure 6.3 Impact of ouabain, artemether and EFL9 on Trp metabolites in MDA-MB-231 cell extracts. A. PCA analysis of the entire metabolite output data set (135 metabolites), n=4 biological replicates; B. PCA analysis of the annotated metabolite data set (47 metabolites), n=4 biological replicates. For this experiment cells were pre-treated with drugs for 18 h and IFNγ (1 U/ mL)/ TNF (6.25 ng/ mL) stimulation was added for another 24 h. Data were processed and annotated as described in section 2.4 and 2.16. Analysis was carried out using the Metaboanalyst software. Data were median normalized and log_{10} transformed, with no further filtering applied.

6.2.4. Changes in intracellular tryptophan metabolites in response to ouabain, artemether and EFL9 treatment in MDA-MB-231 cells.

The annotated metabolite data set from Figure 6.3 was used for further statistical analysis. The data set was split in 3 files containing paired conditions (File 1: DMSO and ouabain, File 2: DMSO and artemether, File 3: DMSO and EFL9). The files were uploaded in the Metaboanalyst software; this applied a data integrity check to each set of data uploaded excluding metabolite entries that exhibited constant or no value for all the treatment conditions included in the data set. Thus, 2 metabolite entries were excluded from Files 1 and 2. The total number of metabolites included in each file were: 45 (File 1 and 2) and 47 (File 3). Volcano plots were plotted for each file to show changes in metabolites in each respective drug treatment sample Vs the DMSO control. Volcano plots show the FDR corrected p value on the X axis and Fold Change on Y value, as explained in section 2.16.

Figure 6.4A shows the volcano plots representative for each the ouabain Vs DMSO comparison, as wells as summarizing the annotations corresponding to each changing metabolite. Similarly, Figure 6.4B shows the metabolic profile of artemether induced changes with corresponding annotations, while Figure 6.4C presents the changes in intracellular Trp metabolites induced by EFL9.

All drugs increase the Trp levels in the cell, while decreasing the levels of formyl-5-hydroxykynurenamine and 5-hydroxy-L-Trp. Ouabain and EFL9 decreased the levels of N-formylkynurenine. Both artemether and EFL9 decrease the levels of kynurenic acid, however only artemether decreased haeme levels inside the cells. EFL9 also decreased the levels of 5'-methylthioadenosine and L-alanine (Figure 6.4C).

In conclusion, all drugs affected a series of core metabolites in the same way: increasing L-Trp and decreasing formyl-5-hydroxykynurenamine and 5-hydroxy-L-Trp. However, there were also differences in the metabolic profile of each drug, with artemether being the only

one that decreased haeme levels in cellular extracts, EFL9 affected purine and amino acid metabolism in the cell (decreased 5'-methylthioadenosine and L-alanine). Only ouabain and EFL9 decreased the levels of N-formylkynurenine.

A. **Ouabain Vs DMSO**

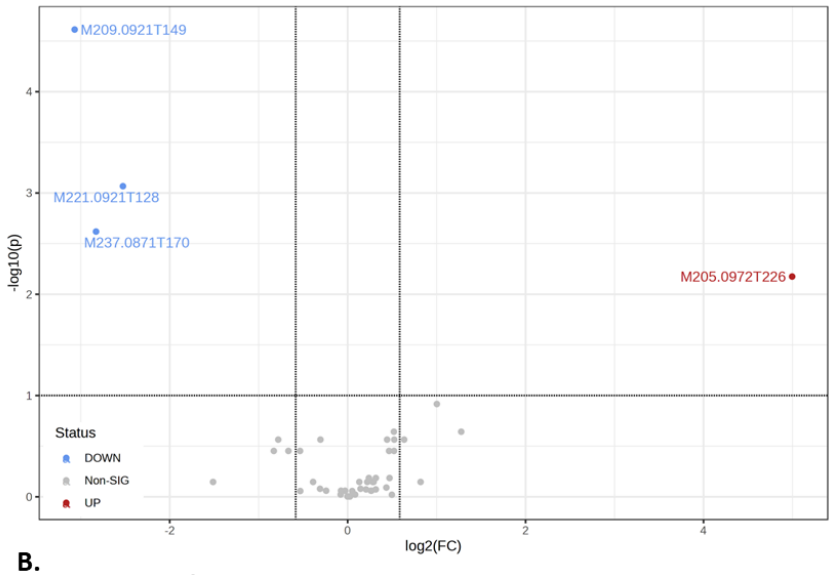

Ouabain Vs DMSO	
UP	• L-Tryptophan
DOWN	• Formyl-5-hydroxykynurenamine • 5-Hydroxy-L-tryptophan • N'-Formylkynurenine

B. **Artemether Vs DMSO**

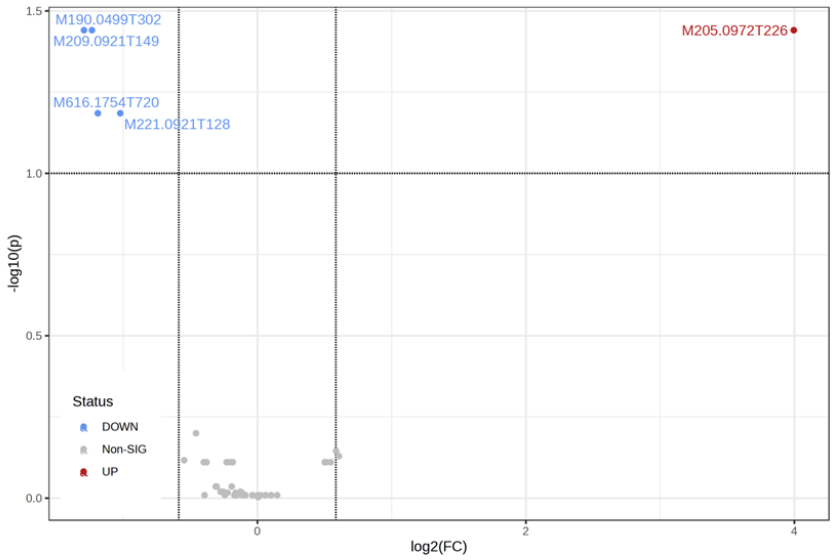

Artemether Vs DMSO	
UP	• L-Tryptophan
DOWN	• Formyl-5-hydroxykynurenamine • Kynurenic acid • Heme • 5-Hydroxy-L-tryptophan

C. **EFL9 Vs DMSO**

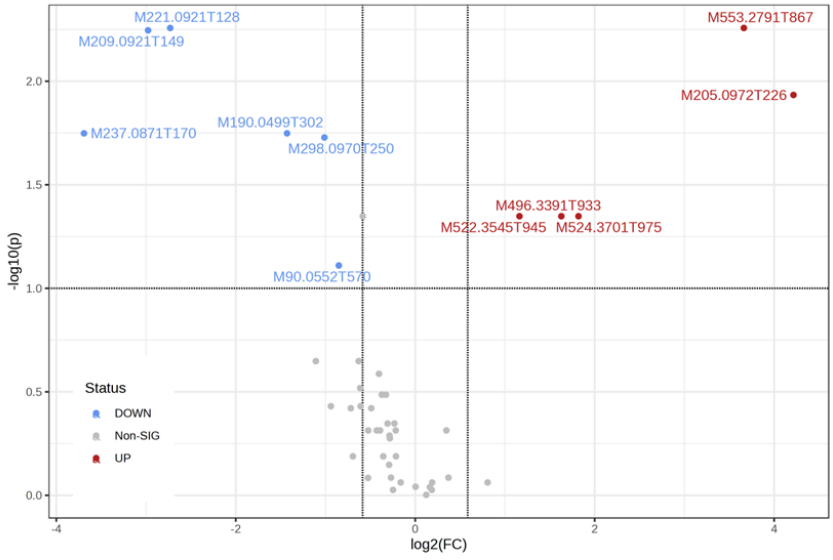

EFL9 Vs DMSO	
UP	• Ambotz28649-59-5 (Euphorbia steroid) • L-Tryptophan • 1-18:0-lysoPC • 1-16:0-lysoPC • Lysolecithin
DOWN	• 5-Hydroxy-L-tryptophan • Formyl-5-hydroxykynurenamine • N'-Formylkynurenine • Kynurenic acid • 5'-Methylthioadenosine • L-Alanine

Figure 6.4 Changes in intracellular Trp metabolites in response to ouabain, artemether and EFL9 treatment in MDA-MB-231 cells. A. Volcano plots of log_{10}(Fold change) Vs log_{10}(p) and looking at changes in metabolites in response to ouabain, and summary of annotated changing metabolites, n=4 biological replicates (47 metabolites of which 2 were automatically excluded by the Metaboanalyst software during the Data Integrity test due to the presence of missing values or features with constant values across all samples); B. As in A for artemether; C. As in A for EFL9. For this experiment cells were pre-treated with drugs for 18 h and IFNγ/ TNF stimulation was added for another 24 h. Data were processed and annotated as described in sections 2.4 and 2.16. Analysis was carried out using the Metaboanalyst software. Data were median normalized and log_{10} transformed, with no further filtering applied. For volcano plots, the Fold change threshold was set at 1.5, while the p value threshold was set at 0.1 False Discovery Rate (FDR), p value was calculated using a parametric, unpaired t-test.

6.2.5. Effects of ouabain, artemether and EFL9 treatment on secreted tryptophan metabolites from MDA-MB-231 cells.

To address whether the tested compounds impact on the export of kynurenine or uptake of Trp, evaluation of the changes in metabolites from MDA-MB-231 cell supernatant was also performed. Supernatants were collected and kept at -80°C until the metabolomics analysis. The data was generated and analysed as described in section 6.2.3, but also in the analysis sections 2.4 and 2.16.

PCA was carried out on all the detected metabolites (135 metabolites, with 19 integrity check exclusions, see section 2.16). Figure 6.5A shows good separation of the DMSO condition from the treatment samples. Just as in the case of cell lysates (Figure 6.3), in supernatant samples, the EFL9 condition was the most distinct from the DMSO control, and the artemether group was the most similar to the DMSO control. Additionally, the ouabain and EFL9 conditions appeared as the most heterogenous, while the artemether condition seemed to be more homogenous, largely overlapping with the ouabain-treated group. The data set was then reduced to the metabolites that could be confidently annotated (47 metabolites with 3 integrity check exclusions, see section 2.16) and a second PCA was used to confirm the separation across the 4 treatment groups. This showed considerable overlap across all 3 drug treatment conditions, with EFL9 and ouabain overlapping the most. The DMSO group, was however, distinctly defined, clearly separating from all 3 drug treatment groups (Figure 6.5B).

In summary, differentiation amongst different treatment groups based on their metabolic impact on secreted Trp metabolites was achieved. There was considerable overlap amongst treatment conditions when looking at all detected metabolites, the DMSO control was however distinctly separated when looking at the annotated restriction of the data set. Large overlap especially between the EFL9 and ouabain conditions, but also between these and the artemether group, was observed especially in the annotated data set.

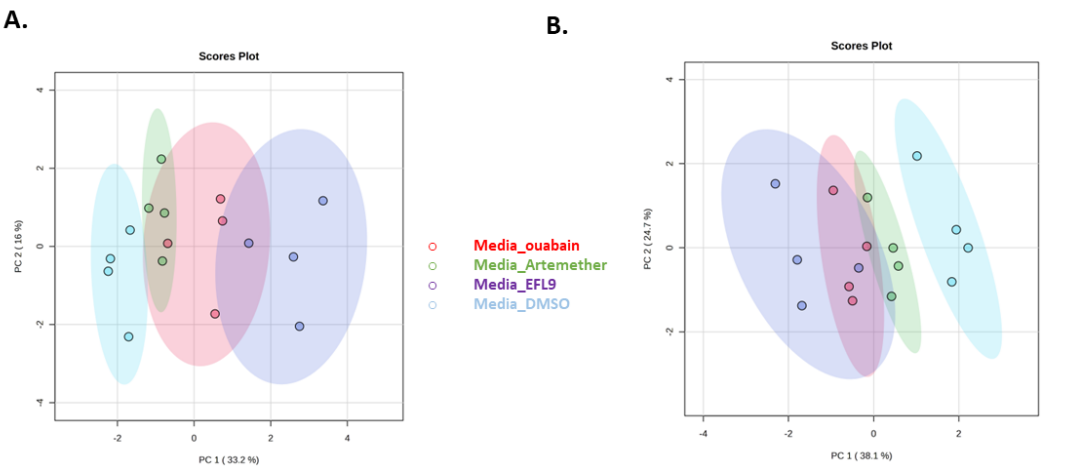

PC1	PC2	PC3	PC4	PC5
33.2%	16%	15%	11.8%	5.9%

PC1	PC2	PC3	PC4	PC5
38.1%	24.7%	12.9%	7.9%	5.5%

Figure 6.5 Effect of ouabain, artemether and EFL9 on secreted Trp metabolites from MDA-MB-231 cells. A. PCA analysis of the entire metabolite output data set (135 metabolites, of which 19 were automatically excluded by the Metaboanalyst software during the Data Integrity test due to the presence of missing values or features with constant values across all samples), n=4 biological replicates; B. PCA analysis of the annotated metabolite data set (47 metabolites, of which 3 were automatically excluded by the Metaboanalyst software during the Data Integrity test due to the presence of missing values or features with constant values across all samples), n=4 biological replicates. For this experiment cells were pre-treated with drugs for 18 h and IFNγ (1 U/ mL)/ TNF (6.25 ng/ mL) stimulation was added for another 24 h. Data were processed and annotated as described in sections 2.4 and 2.16. Analysis was carried out using the Metaboanalyst software. Data were median normalized and log_{10} transformed, with no further filtering applied.

6.2.6. Changes in secreted tryptophan metabolites in response to ouabain, artemether and EFL9 treatment in MDA-MB-231 cells.

The annotated metabolite data set from Figure 6.5 was selected for further statistical analysis, using the Metaboanalyst online portal. The data set was split in 3 files containing paired conditions (File 1: DMSO and ouabain, File 2: DMSO and artemether, File 3: DMSO and EFL9). The total number of metabolites included in each file were: 41 (File 1), 42 (File 2) and 43 (File 3). Volcano plots were generated as described in 2.16.

Figure 6.6A shows the metabolites changing upon treatment with ouabain, as well summarizing their corresponding annotations. Figure 6.6B and C present the impact on secreted Trp metabolites upon treatment with artemether and EFL9, respectively. All drugs increased Trp levels in culture supernatants, while decreasing levels of formyl-5-hydroxykynurenamine, N-formylkynurenine and 5-hydroxy-L- Trp. The profile of artemether had no specific metabolite changes compared to ouabain and EFL9. Ouabain and EFL9 increased the levels of phosphatidylcholine metabolites: 1-18:0-lysoPC and 1-16:0-lysoPC, in the media, while artemether did not. EFL9 also increased levels of a third phosphatidylcholine metabolite, LysoPC. EFL9 caused the highest number of changes in metabolites, suppressing levels of key Trp metabolites such as Kynurenic acid, haeme, 5'-methylthioadenosine, 4,6-dihydroxyquinoline, 4-hydroxyquinoline, and 5-hydroxyindoleaccetaldehyde. EFL9 also decreased levels of antioxidants (didodecyl thiobispropanoate), fatty amides (oleylacetamide), vitamins/energy carrying metabolites (pyridoxine, niacinamide) or amino acids (L-alanine) in culture supernatants (Figure 6.6C).

In summary, all compounds upregulated Trp in the media, downregulating metabolites downstream the IDO1 reaction, such as formyl-5-hydroxykynurenamine and N-formylkynurenine. Artemether and ouabain decreased levels of the same Trp metabolites,

while EFL9 decreased levels of a wider range of key kynurenine pathway metabolites. Both ouabain and EFL9 also increased the levels of phosphatidylcholine derivatives.

A. **Ouabain Vs DMSO**

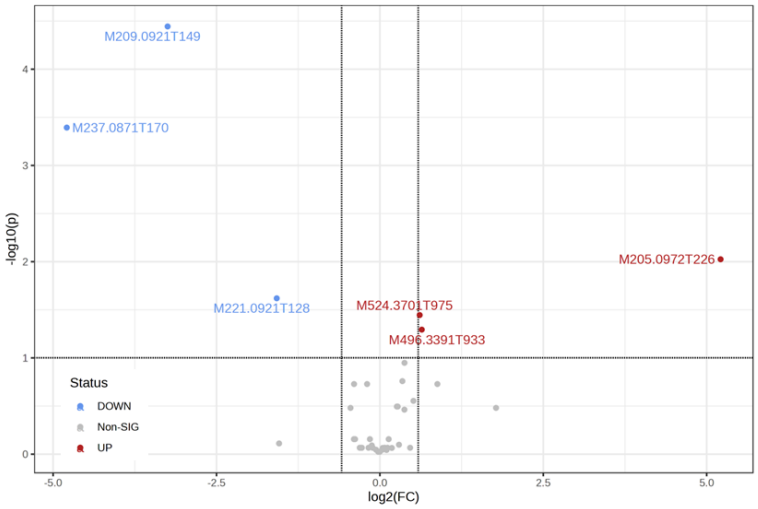

Ouabain Vs DMSO	
UP	• L-Tryptophan • 1-18:0-lysoPC • 1-16:0-lysoPC
DOWN	• Formyl-5-hydroxykynurenamine • N'-Formylkynurenine • 5-Hydroxy-L-tryptophan

B. **Artemether Vs DMSO**

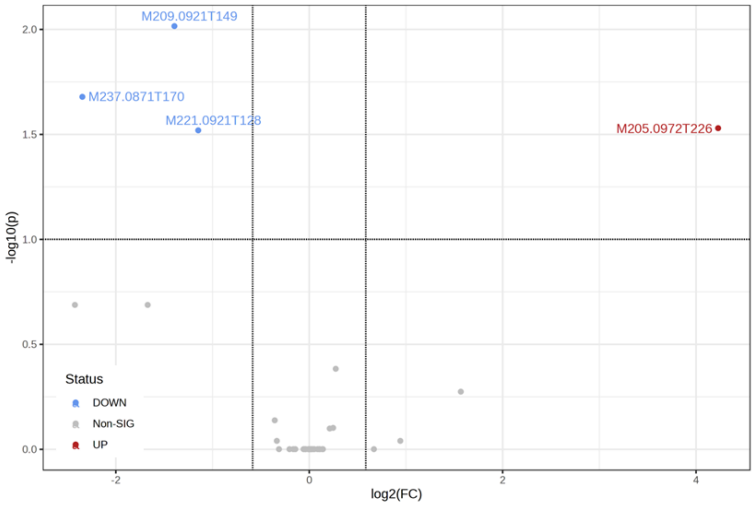

Artemether Vs DMSO	
UP	• L-Tryptophan
DOWN	• Formyl-5-hydroxykynurenamine • N'-Formylkynurenine • 5-Hydroxy-L-tryptophan

C. **EFL9 Vs DMSO**

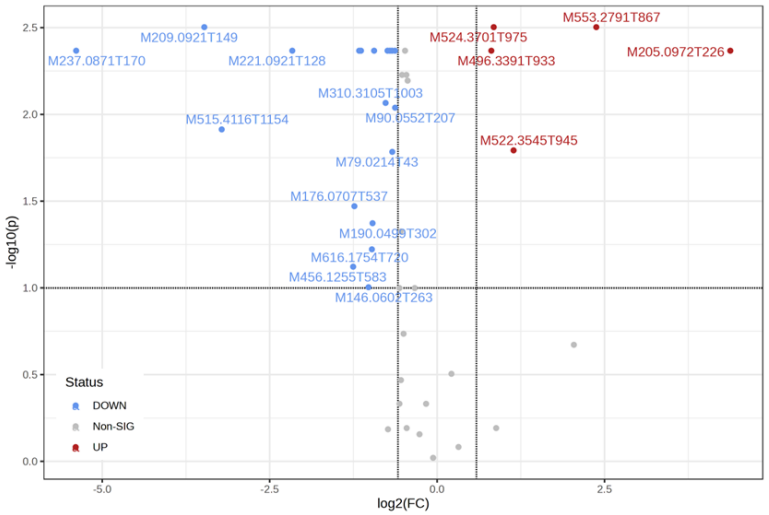

EFL9 Vs DMSO	
UP	• Ambotz28649-59-5 (Euphorbia steroid) • 1-18:0-lysoPC • L-Tryptophan • 1-16:0-lysoPC • Lysolecithin
DOWN	• Formyl-5-hydroxykynurenamine • N'-Formylkynurenine • 5-Hydroxy-L-tryptophan • 4,6-Dihydroxyquinoline • 5'-Methylthioadenosine • Adogen 43 (Linalool 3,6-oxide primeveroside) • Amide 17 (2,4-Dihydroxypyridine) • Adermine/ Pyridoxine (Vitamine B6) • Amide PP/ niacinamide (vitamin B3) • Fenolipuna (phenol red) • cis-11-Eicosenamide (oleylacetamide) • L-Alanine • Milban F (didodecyl thiobispropanoate) • DMSO • 5-Hydroxyindoleacetaldehyde/ Indoleacetic acid • Kynurenic acid • Heme • Epitope ID:150907 (benzylpenicilloyl cysteine) • Kynurine (4-Hydroxyquinoline)

Figure 6.6 Impact of ouabain, artemether and EFL9 on secreted Trp metabolism in MDA-MB-231 MDA-MB-231s. A. Volcano pot of log_{10} (Fold change) Vs log_{10}(p) looking at changes in metabolites in response to ouabain, and summary of annotated metabolites, n=4 biological replicates (47 metabolites of which 6, were automatically excluded by the Metaboanalyst software during the Data Integrity test due to the presence of missing values or features with constant values across all samples); B. As in A for artemether (47 metabolites with 5 Data Integrity test exclusions); C. As in A for EFL9 (47 metabolites with 4 Data Integrity test exclusions). For this experiment cells were pre-treated with drugs for 18 h and IFNγ (1 U/ mL)/ TNF (6.25 ng/ mL) stimulation was added for another 24 h. Data were processed and annotated as described in sections 2.4 and 2.16. Analysis was carried out using the Metaboanalyst software. Data were median normalized and log_{10} transformed, with no further filtering applied. For volcano plots, the Fold change threshold was set at 1.5, while the p value threshold was set at 0.1 False Discovery Rate (FDR), p value was calculated using a parametric, unpaired t-test.

6.2.7. Effect of a selective IDO1 inhibitor (Linrodostat) on tryptophan metabolism in MDA-MB-231 cells.

To better explore whether the metabolic profiles of ouabain, artemether, and EFL9 displayed similarities with that of a direct IDO1 inhibitor, the metabolic changes induced by Linrodostat in MDA-MB-231 cells were assessed. This analysis was only performed in cell extracts. Sample preparation and analysis were summarized in section 6.2.3 and discussed in more detail in the methods section 2.4. 155 metabolites were detected, with 28 of those being confidently annotated. Statistical analysis was carried out using the Metaboanalyst online portal as explained in section 2.16.

A clear separation between control and Linrodostat-treated cells was observed using a PCA carried out in the entire metabolite data set (155 detected metabolites, with 2 integrity check exclusions, see section 2.16) (Figure 6.7A) and on the restricted annotated metabolite data set (28 metabolites) (Figure 6.7B). Pannel C in Figure 6.7 shows the main metabolites being upregulated and downregulated in response to Linrodostat treatment. This analysis was carried out on the annotated dataset. Figure 6.7D summarizes the annotations corresponding to the metabolites that are changing in Linrodostat-treated cells Vs the DMSO control.

All metabolites downregulated by Linrodostat were also downregulated by ouabain and EFL9 in Figure 6.4, with ouabain and Linrodostat having overlapping profiles in terms of downregulated metabolites. Apart from L- Trp, Linrodostat also upregulated a unique range of key Trp metabolites, these include formylanthranilic acid and indole derivatives such as 5-hydroxyindoleacetaldehyde/indole acetic acid and indoleacetaldehyde. In addition, Linrodostat also upregulated other metabolite such as vitamin B6 (pyridoxine), purine/energy carrying metabolites (adenosine monophosphate, isonicotineamide) and amino acid levels (L-valine) (Figure 6.7D).

In conclusion, Linrodostat downregulated metabolites like formyl-5-hydroxykynurenamine, 5-hydroxy Trp and N'-formylkynurenine, some of which were also downregulated by ouabain, artemether and EFL9. However, Linrodostat also upregulated a range of kynurenine pathway metabolites, amino acids, and purine metabolites, thus contributing to a distinct metabolic profile of Linrodostat.

A.

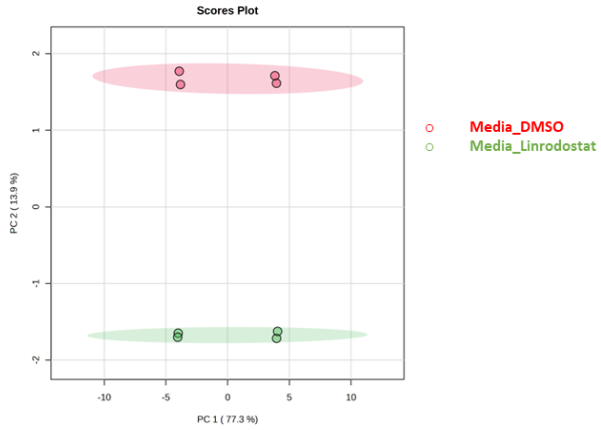

PC1	PC2	PC3	PC4	PC5
77.3%	13.9%	3.1%	1.9%	1.9%

B.

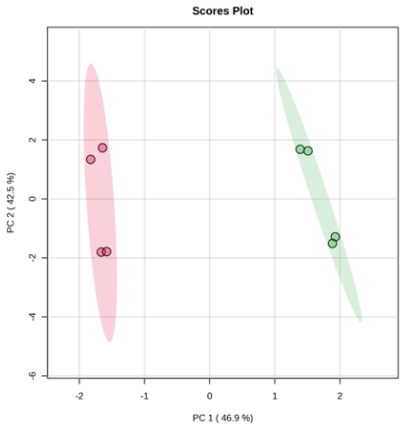

PC1	PC2	PC3	PC4	PC5
46.9%	42.5%	4.6%	2.2%	1.8%

C. **Linrodostat Vs DMSO**

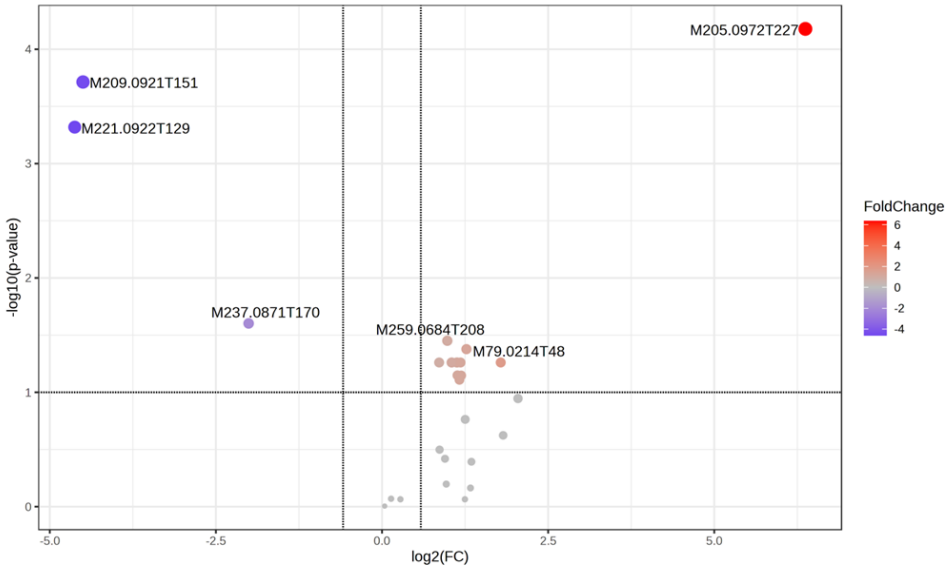

D.

Linrodostat Cells– Annotated Metabolites Data	
	Linrodostat Vs DMSO
UP	• L-Tryptophan • DMSO • Indoleacetaldehyde • Adenosine monophosphate • 5-Hydroxyindoleacetaldehyde/ Indoleacetic acid • 2-Thiazoline-4-carboxylicacid, 5,5-dimethyl- (5CI) • Valinium (L-valine) • Formylanthranilic acid • Isonicotinamide • Adermine/ Pyridoxine • 5-Methoxyindoleacetate
DOWN	• Formyl-5-hydroxykynurenamine • 5-Hydroxy-L-tryptophan • N'-Formylkynurenine

Figure 6.7 Impact of Linrodostat on Trp metabolism in MDA-MB-231 cells. PCA analysis of the entire metabolite output data set (155 metabolites, of which 2 were automatically excluded by the Metaboanalyst software during the Data Integrity test due to the presence of missing values or features with constant values across all samples), n=4 (2 biological replicates, with 2 technical replicates each); B. PCA analysis of the annotated metabolite data set (28 metabolites), n=4 (2 biological replicates, with 2 technical replicates each); C. Volcano pot of log_{10}(Fold change) Vs log_{10}(p) looking at changes in metabolites in response Linrodostat, analysis was carried out using the annotated metabolite data set (28 metabolites), n=4 biological replicates (2 biological replicates, with 2 technical replicates each); D. Summary of annotated metabolites affected by Linrodostat treatment. Data was processed and annotated as described in sections 2.4 and 2.16. Analysis was carried out using the Metaboanalyst software. For this experiment cells were pre-treated with Linrodostat for 18 h and IFNγ/ TNF stimulation was added for another 24 h. Data was median normalized and log_{10} transformed, with no further filtering applied. For volcano plots, the Fold change threshold was set at 1.5, while the p value threshold was set at 0.1 False Discovery Rate (FDR), p value was calculated using a parametric, unpaired t-test.

6.2.8. Summary of the intracellular tryptophan metabolites affected by ouabain, artemether, EFL9 and Linrodostat in MDA-MB-231 cells.

To better understand the specific segment of Trp metabolism targeted by each of the compounds, the next step was to map the identified changing metabolites onto the Trp metabolic pathway for each compound. Figure 6.8 summarizes the changes in intracellular metabolites occurring due to ouabain (A), artemether (B), EFL9 (C) and Linrodostat (D) treatment.

Ouabain downregulates the levels of the immediate IDO1 reaction product, N-formylkynurenine, as expected based on the data from Chapters 3. However, none of the metabolites downstream N-formylkynurenine are affected by this decrease. Ouabain also impacts on the serotonin/indole pathway, reducing metabolites such as formyl-5-hydroxykynurenamine, which is a serotonin-derived IDO-enzyme reaction product, but also upstream metabolites such as 5-hydroxy-L-Trp, which is a direct metabolite of L-Trp produced by Trp hydroxylases 1 and 2 (TPH1/2) (Figure 6.8A).

Artemether decreased the levels of metabolites downstream the TPH1/2 initial reaction and also decreased kynurenic acid and haeme levels. The direct metabolite of the IDO1-mediated conversion of Trp to kynurenine, N-formylkynurenine, was not affected (Figure 6.8B).

EFL9, like ouabain, decreased the levels of the immediate reaction product of the IDO1 reaction, N-formylkynurenine, and the downstream metabolites kynurenic acid and L-alanine (a byproduct from the synthesis of 3-hydroxyanthranilic acid). EFL9 also affected the serotonin pathway, decreasing levels of the TPH1/2 direct reaction product, 5-hydroxy-L-Trp, as well as decreasing IDO-mediated conversion of serotonin to formyl-5-hydroxykynurenamine (Figure 6.8C). Linrodostat had the most distinct metabolic profile. It decreased levels of the direct byproduct of the IDO1-mediated Trp dehydrogenation, N-formylkynurenine, as well as decreasing levels of the IDO-mediated serotonin

dehydrogenation resulting in formyl-5-hydroxykynurenamine. Linrodostat also decreased the levels of 5-hydroxy-L-Trp and kynurenic acid, while upregulating metabolites like 5-hydroxyindoleacetaldehyde and 5-hydroxyindoleacetic acid (Figure 6.8D).

In summary, key changing metabolites in MDA-MB-231 cellular extracts upon treatment with ouabain, artemether and EFL9, were mapped onto the Trp metabolic pathway, allowing comparison of the metabolic profiles of the three drugs with that of a known direct IDO1 inhibitor, Linrodostat. Interestingly, ouabain and Linrodostat showed similar profiles in terms of downregulated metabolites, mirrored most closely by EFL9.

A. Ouabain in cell extracts

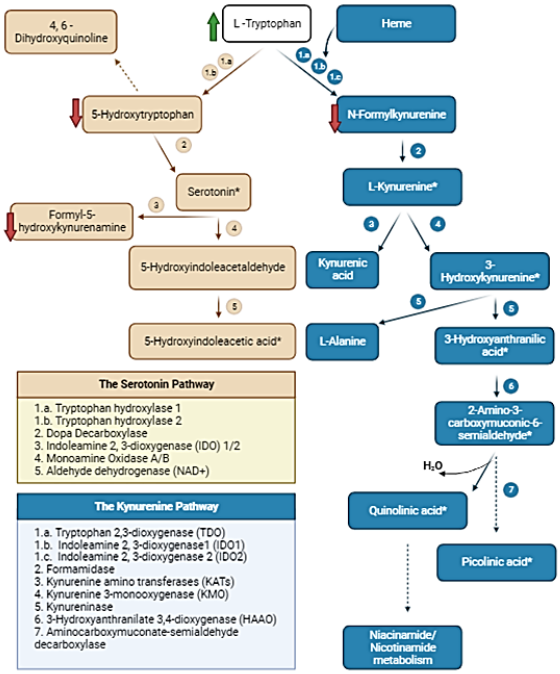

B. Artemether in cell extracts

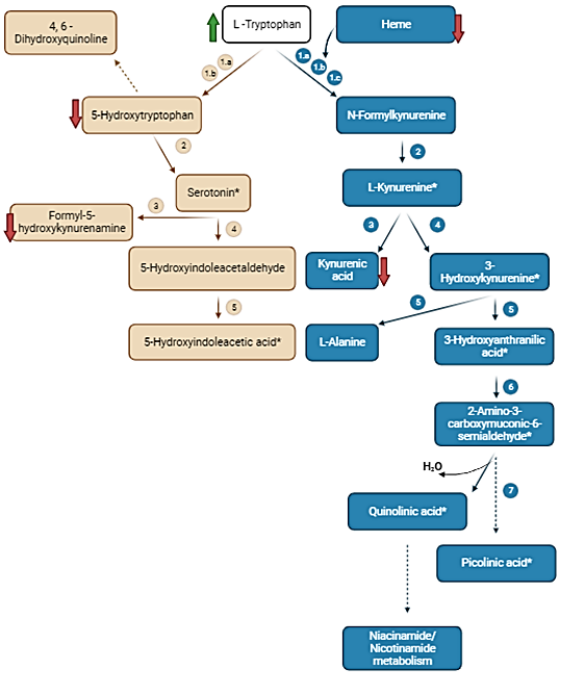

C. EFL9 in cell extracts

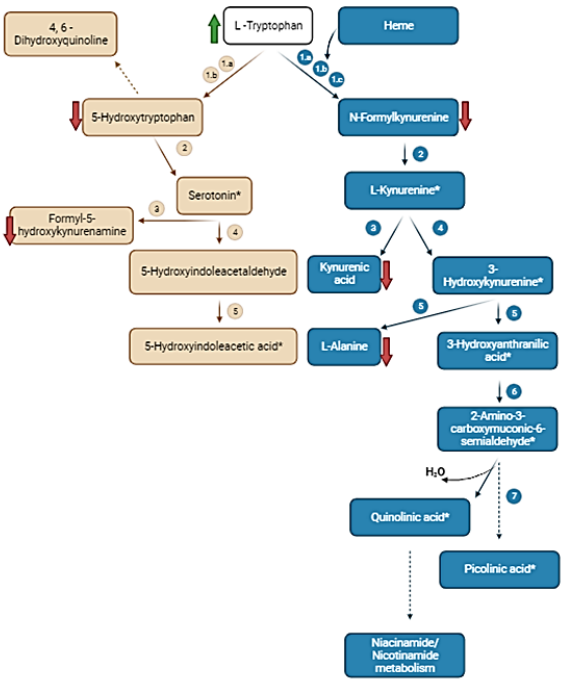

D. Linrodostat in cell extracts

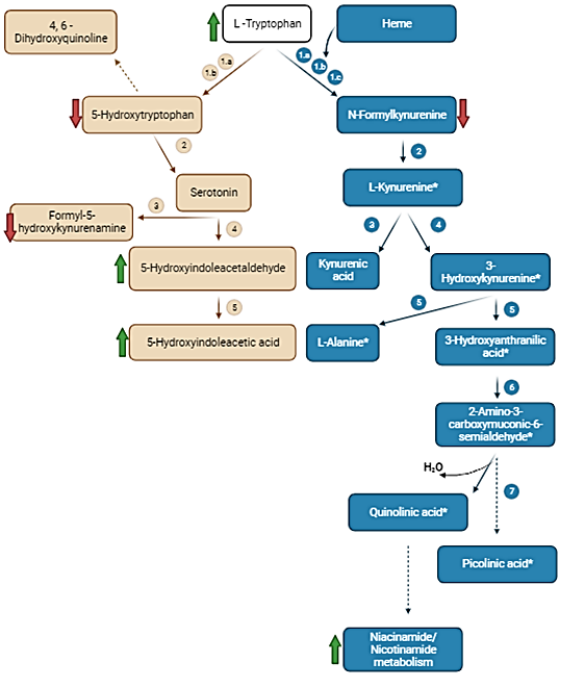

*Figure 6.8 Pathway mapping of intracellular metabolites changing in MDA-MB-231 extracts in response to ouabain, artemether, EFL9 and Linrodostat treatment. A. Change in intracellular metabolites upon ouabain treatment in MDA-MB-231s (based on results in Figure 6.4); B. As in A for artemether; C. As in A for EFL9; D. Change in intracellular metabolites upon Linrodostat treatment in MDA-MB-231s (based on results in Figure 6.7). Diagrams were made in Bio Render, and pathway sequence was created based on Neavin et al. (2018), Stavrum et al. (2013), Song et al. (2017b). Metabolites marked with * were not detected/annotated in the metabolomics file used for analysis.*

6.2.9. Summary of the secreted tryptophan metabolites affected by ouabain, artemether, EFL9 and Linrodostat in MDA-MB-231 cells.

Figure 6.9 maps the changes in secreted Trp metabolites, triggered by treatment with ouabain, artemether and EFL9, onto the Trp metabolic pathway. Figure 6.9A and B shows that ouabain and artemether affect the same metabolites and in the same direction in MDA-MB-231 cell culture supernatants. Both drugs decreased the level of N-formylkynurenine, while decreasing also metabolites from the serotonin pathway including 5-hydroxy-L-Trp and formyl-5-hydroxykynurenamine. In addition to the same changes as those induced by ouabain and artemether, EFL9 also decreases the levels of 5-hydroxyindoleacetaldehyde, 2,4-dihydroxyquinoline, kynurenic acid, haeme, niacinamide and L-alanine (Figure 6.9C). As a quality control, a kynurenine assay was performed (as describe in section 2.9) on the culture supernatants that were used for metabolomics analysis. Figure 6.9D shows that, as expected, N-formylkynurenine levels measured by the kynurenine assay presented in Chapters 3-5 (converted to kynurenine for the assay readout) decreased in the culture supernatants in response to all drug treatments.

In summary the metabolomics data for culture supernatants agreed with the kynurenine assay results, showing a decrease in N-formylkynurenine levels (converted to kynurenine for the kynurenine assay readout). The data show overlapping metabolic signatures for all three drugs in terms of the main kynurenine and serotonin pathway metabolites. However, individual profiles can also be distinguished for all compounds when assessing changes in secreted metabolites.

A. Ouabain in media

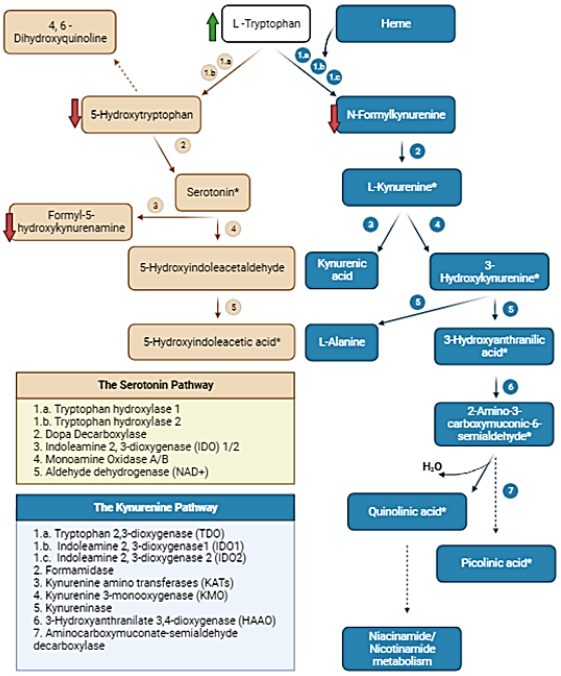

B. Artemether in media

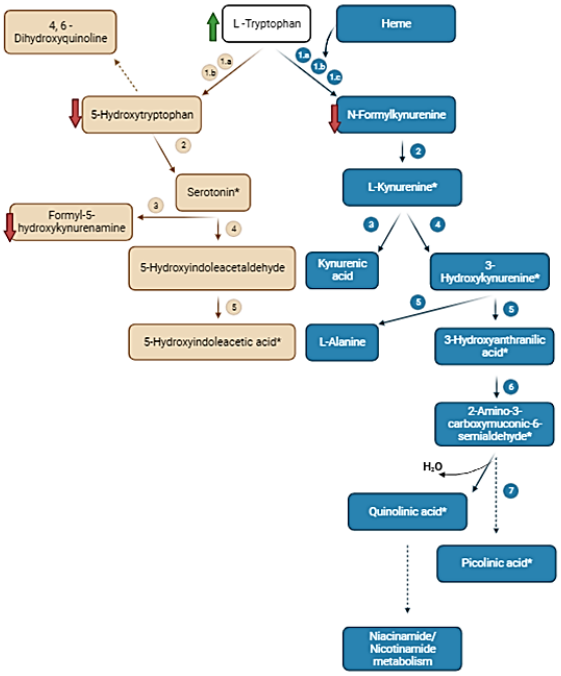

C. EFL9 in media

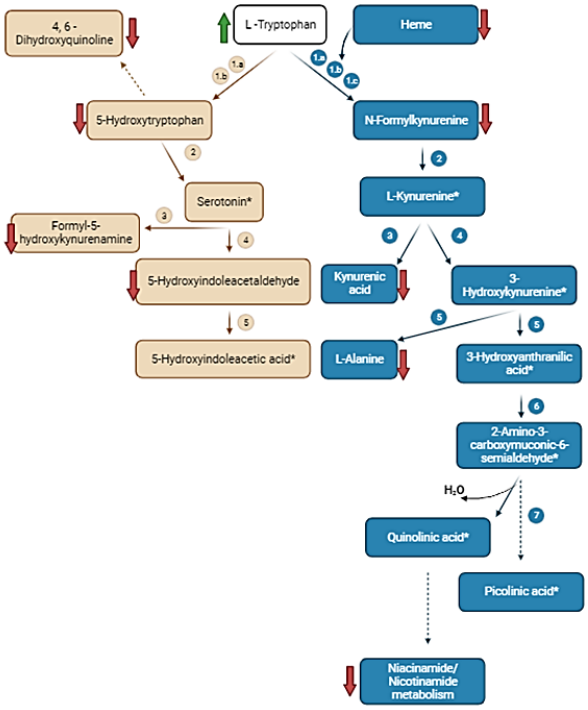

D.

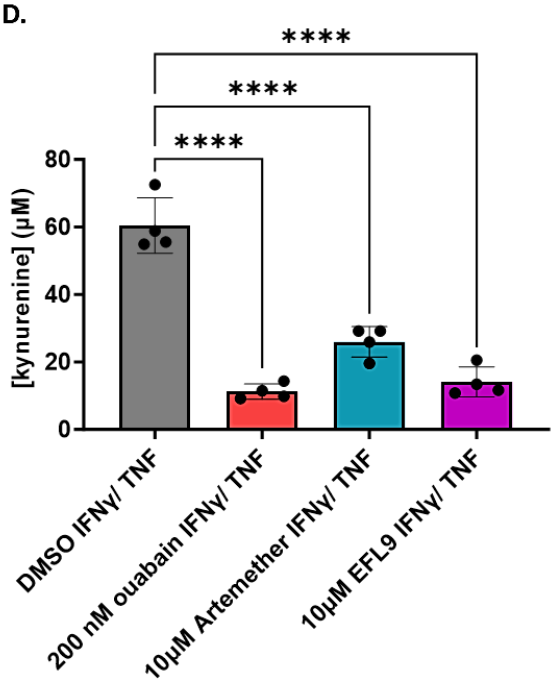

*Figure 6.9 Pathway mapping of metabolites changing in MDA-MB-231 culture supernatants in response to ouabain, artemether and EFL9 treatment. A. Change in secreted metabolites upon ouabain treatment in MDA-MB-231s (based on results in Figure 6.6); B. As in A for artemether; C. As in A for EFL9; D. Quantification of N-formylkynurenine (converted to kynurenine for assay readout) in culture supernatants using the assay described in section 2.9 (n=4 biological replicates). Diagrams were made in Bio Render, and pathway sequence was created based on Neavin et al. (2018), Stavrum et al. (2013), Song et al. (2017b). Metabolites marked with * were not detected/annotated in the metabolomics file used for analysis. For D, data were plotted in GraphPad Prism v9.0.0 as mean and SD; statistical analysis was carried out using a one-way ANOVA coupled with a Bonferroni's post-test for specific comparisons, **** p<0.0001.*

6.3. Discussion

6.3.1. Summary of the main findings.

This chapter aimed to investigate in more detail the mechanism of action of the identified hits, artemether and EFL9, as well as compare their impact on cellular physiology (ionic dynamics, IDO1 enzymatic activity and Trp metabolism) with that of ouabain and the clinically tested IDO1 inhibitor, Linrodostat. To achieve this, the impact of artemether and EFL9 on IDO1 activity in a purified assay set-up was tested. However, the assay did not generate conclusive results, suggesting that further optimization would be needed. Next, this chapter showed that unlike ouabain, artemether and EFL9 do not impact on intracellular Na^+ levels. Consequently, a deeper understanding of the mechanism of action of these compounds was needed. Therefore, the impact of artemether and EFL9 on intracellular and secreted Trp metabolites was measured, and a metabolic signature associated with each one of the compounds was identified. The metabolic impact of ouabain and Linrodostat (in cells only) was also profiled and compared with that of artemether and EFL9, with the ultimate aim of generating a series of hypotheses, that remain to be tested, on how artemether, EFL9 and ouabain might be impacting the physiology of breast cancer cells.

6.3.2. Investigating potential mechanisms of action for artemether and EFL9.

6.3.2.1. Artemether and EFL9 Inhibition of IDO1 enzyme activity.

Having shown in Chapter 5 that artemether and EFL9 decrease kynurenine independently of IDO1 expression, the next question to be answered was whether these drugs might be interfering with the enzymatic activity of IDO1. Thus, the impact of artemether and EFL9 on purified IDO1 activity was compared to that of a commercially available, selective IDO1 inhibitor, Linrodostat (Cherney et al., 2021, Tang et al., 2021). Linrodostat works by

occupying the haeme binding site on the IDO1 molecule thus preventing IDO1 activation (Balog et al., 2021). Experimental data confirmed the inhibitory activity of Linrodostat in a cellular set-up (Figure 6.1A, B). However, when looking at the effect of Linrodostat on purified human IDO1 enzyme, no change in activity was detected with drug concentrations that were ~100-fold or ~10 000-fold above the Linrodostat IC_{50} value (1.1 nM in HEK293 cells)(Siu et al., 2017). Lower Linrodostat concentrations were also tested with a similar result (that data was not included here).

One explanation for this could be the elevated background signal of Linrodostat in the activity assay which could potentially mask a real inhibitory effect. A better approach to look at pharmacologically induced changes in enzyme activity, according to literature, would be developing a fluorescence-based assay, which could limit the signal to noise ratio (Simeonov and Davis, 2004). In high throughput screening set-ups, absorbance assays are not ideal, that is because the sample volume is directly correlated with the pathlength of the light, meaning that for low assay volumes the pathlength is also reduced, leading to a minimization of the signal window (Urban et al., 2008, Simeonov and Davis, 2004). When utilizing fluorescence-based assays these limitations can be reduced using various adaptations. One possibility is the utilization of a high fluorophore concentration, this will increase the signal strength and thus the signal to noise ratio, thus limiting the impact of compound interference (Urban et al., 2008). Additionally, using a fluorescence-based assay to collect data in a kinetic mode, rather than end plate mode, also helps separate the signal from the noise, as with time the fluorescence signal should increase, while the background should stay the same (Jadhav et al., 2010). Finally, the use of radiometric dies, or fluorophores that allow two readings at different wavelengths can also help subtract the background signal from the actual fluorescence readout (Simeonov et al., 2008). However, for this project, the time constraints were decisive towards not pursuing this approach any further.

Another factor contributing to the limited success of the purified IDO1 activity assay could be the choice of positive control, the clinically tested IDO1 inhibitor, Linrodostat. Linrodostat is a haeme displacing molecule, it locks IDO1 in an inactive enzyme form, and prevents its assembly to the holoenzyme (Balog et al., 2021, Cherney et al., 2021). In the enzyme activity assay, the purified IDO1 protein is already in holoenzyme form, which could suggest that Linrodostat might no longer be able to inhibit its activity. This would also explain why Linrodostat has only been studied in cellular assays, rather than in purified enzyme assays (Siu et al., 2017, Balog et al., 2021, Cherney et al., 2021). However, these explanations are speculative and would need to be confirmed experimentally. A future improvement for this assay set-up could be the use of a Trp mimetic compound such as Epacadostat as an alternative to Linrodostat (Günther et al., 2019). Given that the positive control (Linrodostat) did not trigger a change in IDO1 activity, in the assay set-up presented in Figure 6.1, the experiment was considered inconclusive and thus further studies would be needed to clarify whether artemether and EFL9 have any activity against the enzymatic function of IDO1.

6.3.2.2. Artemether and EFL9 and intracellular Na^+ levels

Another mechanistic aspect that needed to be tested was whether the drop in kynurenine induced by artemether and EFL9, is coupled with an increase in intracellular Na^+, as observed with ouabain and monensin in Chapters 3 and 4. Additionally, artemether has been linked with NCX-dependent dysregulated Ca^{2+} cellular import, associated with prolonged Na^+ currents and increased Na^+ import (Moreira Souza et al., 2020). Furthermore, some Euphorbia factors have been associated with ion channel regulation (Zou et al., 2022). Thus, literature evidence justified the intention of this study to verify the direct implication of artemether and EFL9 in intracellular Na^+ accumulation. However, Figure 6.2 shows that neither artemether, nor EFL9 increase intracellular Na^+ levels. This suggests that artemether and EFL9 might have highly distinct impacts on cellular physiology than ouabain and monensin. Furthermore, it could also be speculated that changes in intracellular Na^+ might

rather be associated with changes in IDO1 expression (as observed with ouabain) than just with changes in the kynurenine response. However, all these suppositions would need to be verified experimentally.

6.3.2.3. Artemether and EFL9 and tryptophan metabolism.

Having compared ouabain, artemether, EFL9 and Linrodostat in terms of their impact on secreted kynurenine and/or IDO1 expression (Chapter 5) and intracellular Na^+ levels in MDA-MB-231 (Chapter 6, Figure 6.2), the next step towards building a better understanding of their mechanisms of action in the context of kynurenine production, was to look at how these compounds impact on Trp metabolism. Thus, a metabolomics experiment was carried out on MDA-MB-231 cellular extract and media samples. The effects of artemether and EFL9 were compared directly to those of ouabain in cells (Figure 6.4) and media samples (Figure 6.6); a Linrodostat metabolomics analysis was run separately on cellular extracts only (

Figure 6.7). The changes in key metabolites (specific to the kynurenine or serotonin pathways) were then mapped onto the Trp metabolic pathway (Figure 6.8, cells and 6.9, media).

6.3.3. The effect of artemether on tryptophan metabolism.

Artemether was selected as an interesting compound, based on its chemistry and historical use for malaria treatment. The exact target of artemisinin and its mechanism of action are not fully elucidated, one of the popular current hypotheses is that the endoperoxide structure of the drug interacts with Fe (II) released by the parasite-induced degradation of haemoglobin, which creates a toxic activated oxygen within the artemisinin molecule, that might target different pathways, including hemozyn-dependent haeme detoxification, Ca^{2+} transport across the endoplasmic reticulum membrane via inhibition of the *Plasmodium falciparum* PfATP6 pump, or might disrupt the mitochondrial membrane potential (Krishna et al., 2008). Interestingly, artemisinin-related compounds were shown to also have

antiproliferative and pro-apoptotic activity on cancer cells, as well as inhibiting angiogenesis. The exact mechanism of action is unknow. However, increased iron-depended reactive oxygen species, DNA damage and disrupted mitochondrial membrane are potential factors contributing to these effects (Efferth et al., 2004, O'Neill et al., 2010). In patients, malaria induction with *Plasmodium vivax* was associated with increased kynurenine production and Trp deletion, that could not be abolished by treatment with artemether-lumefantrine. The endoperoxide-haeme interaction proposed as mechanism of action against malaria, could be also how artemether interferes with IDO1. IDO1 is a metalloenzyme carrying a haeme group that enables the oxidation reaction of Trp to N-formylkynurenine. Therefore, artemether could be inhibiting this reaction by blocking the haeme group in the active enzyme, or by hijacking haeme from the cytosol and preventing the activation of IDO1.

To explore this hypothesis, the impact of artemether on Trp metabolism was investigated in cellular lysates and in media (Figure 6.8B and Figure 6.9B). In cells, artemether downregulated one metabolite belonging to the kynurenine pathway, and 2 metabolites belonging to the serotonin pathway. Artemether was also the only compound that decreased haeme levels in cell lysates (Figure 6.8B). This is particularly interesting given the structure of the IDO1 enzyme, which is a haeme-containing dioxygenase and is believed to exert its mechanism of action by subtracting a proton from the substrate using an iron-bound dioxygen (Sugimoto et al., 2006). Given that all the artemisinin derivatives that had an effect on kynurenine production are endoperoxide containing molecules, which are thought to bind haeme-iron, as well as given the fact that artemether seems to decrease the levels of haeme within treated cells, it is safe to hypothesize that artemether might be inhibiting IDO1 activity through direct interference with the enzyme integrity by binding the haeme group. Interestingly, Figure 6.9B shows that artemether did not impact on haeme levels in the supernatants. Furthermore, in culture media, artemether decreases the levels of N-formylkynurenine, even though the intracellular amount of N-formylkynurenine does not

change (Figure 6.9B Vs Figure 6.8B). Thes two observations could be supporting a haeme-dependent inhibition mechanism, thus artemether decreases IDO1 activity in a haeme-dependent manner, therefore less N-formylkynurenine is produced, and to maintain cellular physiology, the cell exports less N-formylkynurenine, thus maintaining its intracellular concentration within optimal levels. This hypothesis would need to be validated and tested in more detail, by docking experiments and crystallography studies which could confirm the exact target of artemether in this mechanism. Further validation could be achieved by detecting N-formylkynurenine levels in cell lysate and supernatants and verifying how different concentrations of Artemether impact on intracellular and extracellular levels of this metabolite.

Furthermore, artemether also decreased the levels of kynurenic acid in cellular lysates. Kynurenic acid is an essential metabolite both for regulating inflammatory activity and for its neuroprotective function. It is produced by Kynurenine amino-transferases (KATs), from L-kynurenine and 2-oxoacid (Baran et al., 1997). Alternatively, it can be synthesized in the presence of ROS from the Trp metabolite, indole-3-pyruvic acid, via pyrrole ring cleavage and spontaneous cyclization (Hardeland, 2008, Blanco Ayala et al., 2015).

Kynurenic acid exerts a variety of actions on the nervous and immune systems. It has been shown to activate M-type K^+ channels as well as bind the G-protein receptor 35 (GPR35), inhibiting N-type Ca^{2+} channels in neurons, as well as reducing Ca^{2+}-cAMP accumulation inside the cells (Guo et al., 2008, Ruddick et al., 2006, Berlinguer-Palmini et al., 2013, Lo et al., 2021). There have been also reports showing that kynurenic acid inhibits the PI3K/Akt and MAPK pathways. High levels of kynurenic acid have been associated with decreased ERK 1/2 and p38 activation, while increasing β-catenin (Walczak et al., 2014). Furthermore, due to its inhibitory effect on Ca^{2+} import, kynurenic acid might also contribute to decreased inflammation by decreasing NF-kB activation and it could prevent T cell activation and

function through decreased cAMP levels (Raker et al., 2016, Yang et al., 2015a). NF-kB inhibition has also been linked to elevated β-catenin (Silva-García et al., 2014). Additionally, literature has reported inhibition of the IL-23/IL-17 pathway in response to kynurenic acid. These observations are particularly interesting, as they would indicate that artemether might in fact promote inflammation, enhance activation of NF-kB and the IL-23/IL-17 pathway, as well as potentially enhancing pathways like PI3K/Akt and MAPK, by downregulating the levels of the immunosuppressive metabolite, kynurenic acid (Salimi Elizei et al., 2017). Kynurenic acid has also been linked with interference with the AhR, this induces dimerization of AhR with AhR nuclear translocator, functioning and an expression regulatory system on genes that control immune response (e.g. increase in IL6 production), but also Trp metabolism (lack of AhR increases levels of kynurenic acid) (DiNatale et al., 2010, García-Lara et al., 2015).

Because artemether only decreases intracellular kynurenic acid, while secreted levels stay the same, this suggests that GPR35 or AhR-mediated kynurenic acid effects are less likely to be affected by artemether. However, a decrease in intracellular kynurenic acid could affect NF-kB activation through the β-catenin pathway, as well as interfere with PI3K/Akt or MAPK activation (Thaker et al., 2013, Ma et al., 2023, Walczak et al., 2020). Although these effects of artemether need to be validated experimentally, these data support a potential link between artemether and these inflammatory, proliferation and survival pathways. Links between artemisinin derivatives and the PI3K/ Akt or MAPK pathways have been reported in the literature before, as supported by Appendix Table 8. 4; however, limited connections have been made with Trp metabolism and kynurenine mediated immune evasion (Bai et al., 2020, Yang et al., 2023).

Alongside kynurenine pathway metabolites, artemether also decreased levels of metabolites from the serotonin pathway. It is important to state that 95 % of the dietary Trp is channelled

towards the kynurenine pathway, whereas the remainder goes to the serotonin pathway, protein synthesis, indole synthesis pathway and others (Haq et al., 2021). This could therefore suggest that small changes in metabolites belonging to the serotonin pathway might be easier to detect than in the case of kynurenine pathway metabolites. 5-Hydroxy-L-Trp and fomyl-5-hydroxyknynurenamine were consistently reduced by artemether in both cell lysates and in media, while 5-hydroxyindoleacetic acid was only decreased in media samples. 5-Hydroxy-L-Trp is produced by TPH1/2. It is then rapidly converted to 5-hydroxytryptamine or serotonin, this can be secreted and impact on the immune system by interfering with the 5-hydroxytryptamine receptor on immune cells. The majority of these receptors belong to the G protein-coupled receptor family and thus their activation triggers increases in intracellular Ca^{2+} which leads to activation of PI3K/Akt and MAPK pathways (Hannon and Hoyer, 2008, Shajib and Khan, 2015, Wan et al., 2020). In this study, however, serotonin could not be detected, instead formyl-5-hydroxykynurenamine levels were decreased. This is particularly interesting because the conversion of hydroxy Trp to formyl-5-hydroxykynurenamine is mediated by IDO enzymes (Fujiwara et al., 1979). This could support the fact that artemether targets IDO1 activity. However, the decrease in hydroxy Trp might also indicate that artemether targets TPH enzymes. These are non-haeme enzymes, that contain iron (Fe II) bound to two histidine and a glutamate residue (Goodwill et al., 1997, Roberts and Fitzpatrick, 2013). This is interesting, as artemether could interfere with this Fe (II) enzymatic core, via the endoperoxide bridge, according to literature (O'Neill et al., 2010). However, this hypothesis would have to be confirmed experimentally.

In conclusion, artemether was shown to decreases cellular haeme, as well as decreasing the activity of iron/haeme containing enzymes, by decreasing cellular and secreted levels of 5-hydroxy Trp, formy-5-hydroxykynurenamine, as well as secreted N-formylkynurenine. Artemether also decreases levels of cellular kynurenic acid which could potentially decrease the immunosuppressive signals produced by the tumour, thus enhancing clearance.

6.3.4. The effect of EFL9 on tryptophan metabolism.

The second class of compounds that were investigated in detail includes Euphorbia factors. Just as in the case of artemisinin derivatives, all compounds that showed activity had a common chemical feature: the addition of a large aromatic residue on the C7 of the core structure (Chapter 5). This chemical specificity suggests a potential direct interaction with IDO1, or other enzymes downstream the kynurenine pathway. Euphorbia factors have not been studied in great detail. The exact function of the C7 modification in terms of physical enzyme interactions can only be speculated upon, in the absence of experimental data. The benzoyl modification could add planar hydrophobic interactions (both EFL9 and 2) and then the nicotinate group could modify the electronic character of this site group (EFL9 only) (O'Neill et al., 2010).

Some studies have linked the L2 factor with decreased NF-kB-mediated lung inflammation, or decreased hepatocarcinoma progression in mice, associated with STAT3 and Akt inhibition (Fan et al., 2019, Zhang et al., 2018a). Euphorbia-derived phytochemicals have also been shown to act as drug resistance modulators, alleviate HIV-1 and bacterial infections or disrupt the mitochondrial respiratory chain (Hezareh, 2005, Geng et al., 2015, Hohmann et al., 2003, Betancur-Galvis et al., 2003). Diterpene ingenol mebutate is a Euphorbia derivative used for the treatment of actinic keratosis, thus working as a prophylactic treatment for skin cancer (Seca and Pinto, 2018). Euphorbia factors have also been associated with intestinal toxicity and transcriptomic studies have shown that factor L2 is likely to achieve that by interfering with membrane receptor signalling, ion transport as well as channel-mediated and passive membrane transport activities; factor L1, on the other hand, seems to be associated with mitochondrial respiration, arachidonic acid metabolism, cAMP and Wnt signalling, as well as protein digestion and absorption and IL17 signalling in colon cancer cells. Protein-protein interaction studies revealed that L1 might also be involved in cell cycle regulation JAK/STAT signalling and K^+/Cl^- transport. Both L1 and L2 were found to interfere

with amino acid metabolism, xenobiotic metabolism, carbohydrate and nucleotide metabolism and the metabolism of cofactors and vitamins. Only L2 seemed to affect energy metabolism (Zou et al., 2022).

This study investigated the role of EFL9, the stronger Euphorbia factor inhibitor of the kynurenine response, on Trp metabolism. EFL9 was shown to downregulate both N-formylkynurenine, the direct product of IDO1 activity, and kynurenic acid in cells. A larger number of serotonin pathway metabolites were affected by EFL9, including formyl-5-hydroxykynurenamine, the reaction product of IDO-mediated serotonin degradation decreased in cellular lysates. Similarly, the TPH 1/2 metabolite 5-hydroxy-L- Trp, a serotonin precursor, was also downregulated in cells. While 5-hydroxyindoleaacetaldehyde, downstream metabolite of serotonin, was also downregulated by FEL9 in media samples. Studies have suggested in the past that increased IDO1 activity is associated with decreased serotonin, justifying the low mood often associated with inflammation (Widner et al., 2002). However, a clear inverse relationship between the kynurenine and serotonin pathway activation has not been confirmed, a more modern view on the subject suggests interconnection between the pathways with some kynurenine metabolites contributing to mood regulation (Arnone et al., 2018). Upon IDO1 inhibition, it would thus be expected to see an upregulation in serotonin pathway metabolites. However, EFL9 seems to downregulate the activity of both kynurenine pathway IDO1, and serotonin degrading IDO-enzymes, thus reducing levels of fromyl-5-hydroxykynurenamine.

The impact of EFL9 on secreted metabolites mimics the observations made on cell lysates. However, a wider range of metabolites were affected by EFL9 in the media. One of the most interesting observations was the upregulation in secreted phosphatidyl choline derivatives (observed both in cells, Figure 6.8D and in media samples, Figure 6.9D). EFL9 increased levels of LysPC (lysophosphatidyl choline), 1-18:0-lysoPC and 1-16:0-lysoPC. Lysophosphatidyl

choline is a signalling phospholipid produced by caspase 3-induced Ca^{2+} independent activation of phospholipase A2 (iPLA2), and functions by recruiting phagocytes (Fogarty and Bergmann, 2015). The elevation in extracellular LysPC suggests that EFL9 treatment might thus promote immune mediated tumour-clearance. This observation is further supported by the decrease in secreted kynurenic acid, otherwise known for its immunosuppressive properties, as well as from the decrease in N-formylkynurenine (Raker et al., 2016, Walczak et al., 2014, Wirthgen et al., 2017). On the other hand, phosphatidylcholine synthesis, via fatty acid metabolism, is often upregulated in cancer cells, and has been linked to cellular proliferation and cell cycle regulation (Ridgway, 2013). Thus, further experimental proof would be required to establish and validate the anti-cancer and anti-inflammatory effects of EFL9 via phosphatidyl choline/lysophosphatidyl choline upregulation. Another observation worth mentioning is that phosphatidyl choline is abundantly present in the cell membrane, therefore elevation of this metabolite in the culture media could also indicate cell death and membrane degradation (van der Veen et al., 2017).

An interesting metabolite downregulated by EFL9 in the media didodecyl thiobispropanoate (PubChem compound CID: 31250) which has antioxidant properties. Two additional antioxidant metabolites, Linalool 3,6-oxide riverside (also anti-inflammatory), and cis-11-Eicosenamide were also downregulated by EFL9 in media samples (Seol et al., 2016, Peana et al., 2002, Downer, 2020, Liu et al., 2012a, Mączka et al., 2022, Johra et al., 2023). Thus, it can be speculated that their downregulation by EFL9 might increase levels of ROS and thus contribute to tumour clearance. One of the main regulators of oxidative stress within the cell is the glutathione pathway. Glutathione is essential in regulating a range of biological processes including proliferation, immune function, apoptosis and xenobiotic detoxification, however, it is also a key redox regulator, preventing oxidative damage during active metabolic processes especially within the mitochondria. Glutathione levels can be replenished by multiple pathways, alongside the pyroglutamic-dependent glutathione

synthesis, this can occur also via transsulfuration. Transsulfuration is a pathway that uses cystathionine, derived from methionine, as a glutathione precursor. The conversion of methionine to cystathionine involves a series of metabolites such as S-adenosylmethionine, one intermediary metabolite in the synthesis of S-adenosylmethionine is methylthioadenosine (He et al., 2006, Lu, 2013). Figure 6.8D and Figure 6.9D show that EFL9 also decreases levels of 5-methylthioadenosine both inside the cell and in media samples. Thus, EFL9 seems to be downregulating a range of metabolites with antioxidant activity, potentially impacting on the glutathione activity, thus increasing tumour oxidative stress, and potentially facilitating tumour clearance.

Furthermore, EFL9 negatively impacted on levels of branched chain amino acids such as 4,6-dihydroxyquinoline, which are known to regulated protein synthesis and glucose metabolism (Xie et al., 2012, Lim et al., 2020). 4-Hydroxyquinoline, another metabolite inhibited by EFL9 is a potent antibacterial. 4-Hydroxyquinoline derivatives have been shown to exhibit toxicity by interfering with the NADH-ubiquinone reductase enzyme and thus impairing cellular respiration (Chung et al., 1989, Sauter et al., 1993). EFL9 also decreased the levels of the amino acid L-alanine, which has been reported as a byproduct of the anthranilic acid synthesis (Phillips, 2014). Since anthranilic acid could not be confidently detected, with the analysis method used in this study, the detection of alanine could be used as an indirect measurement of anthranilic acid production, indicating decreased activity of the kynurenine pathway. Additionally, levels of a range of vitamins such as pyridoxine or vitamin B6 and niacinamide or vitamin B3 were also decreased by EFL9. The former has been linked with Trp metabolism, in such that deficiency of vitamin B6 seems to enhance activation of the kynurenine pathway (Crepaldi et al., 1975, Deac et al., 2015). Thus, an increase in this metabolite validates the inhibitory function of EFL9 on the kynurenine response. Furthermore, a decrease in niacinamide, which is a precursor of NAD^+, the ultimate reaction

product of the kynurenine pathway, further supports the inhibitory effect of EFL9 on this branch of Trp metabolism (Li et al., 2006).

In conclusion, EFL9 seems to be affecting the kynurenine and the serotonin pathway in the same direction, suppressing overall Trp metabolism, and the mechanism of action is yet to be determined. EFL9 seems to increase levels of phagocyte recruiting metabolites in culture supernatants and decrease levels of immunosuppressive molecules such as kynurenic acid. Additionally, EFL9 might mediate tumour clearance by downregulating the production of metabolites with antioxidant properties and there is evidence to suggest interference with the glutathione metabolism.

6.3.5. The effect of ouabain on tryptophan metabolism.

In terms of core Trp pathway metabolites, ouabain exhibited a similar profile with artemether and EFL9. N-formylkynurenine levels decreased both intracellularly and, in the media, which was consistent with the previous observations from Chapter 3, where ouabain was shown to downregulate IDO1 levels and thus inhibits the conversion of L-Trp to N-formylkynurenine. Furthermore, the IDO-mediated conversion of serotonin to formyl-5-hydroxykynurenamine was also inhibited, which is consistent with our published mechanism of action for ouabain (Shandell et al., 2022). The decrease in 5-hydroxy-L-Trp suggests that ouabain might also interfere with TPH 1/2, or upstream regulators of their expression. Given that TPH1/2, just like IDO1, are iron containing enzymes, it could be speculated that ouabain might employ a mechanism of action that involves depletion of cellular iron reserves. Ouabain is involved in regulating the dynamic of Na^+ across the plasma membrane and studies have reported that a disruption in Na^+ transport can also interfere with intracellular iron levels, thus disrupting IDO1-mediated kynurenine production, otherwise upregulated by intracellular iron. An increase in iron is generally associated with increased Na^+ export via the NKA and increased IDO1 activity (Wise and Archdeacon, 1969, Donley et al., 2021, Shandell

et al., 2022, Omar et al., 2017, Sousa et al., 2015). It is thus possible to hypothesize that TPH1/2 might be regulated in the same way by ouabain, via a Na^+ dependent iron depletion mechanism. This hypothesis would need to be tested experimentally. However, ouabain did not impact on intracellular or secreted haeme levels (Figure 6.8D and Figure 6.9D).

When looking at downregulated metabolites, ouabain had a similar effect in cell lysates and in media, however more metabolites were upregulated by this compound in media samples. Thus, in media, ouabain, just like EFL9, upregulated two phosphatidyl choline derivatives, suggesting either increased cell death and membrane degradation, or production of pro-inflammatory mediators that could contribute to tumour clearance (Fogarty and Bergmann, 2015), observations further supported by the decrease in the immunosuppressive metabolite, N-formylkynurenine (Figure 6.9D).

In conclusion, ouabain has a slightly distinct profile from artemether and EFL9, although core Trp metabolites were affected in the same way, as with artemether and EFL9. Ouabain also seemed to stimulate pro-inflammatory signalling.

6.3.6. Comparing the metabolic profiles of artemether, EFL9 and ouabain to that of Linrodostat.

To better understand how these compounds affect Trp metabolism, a comparison between their cellular metabolic profile and that of the clinically used IDO1 inhibitor, Linrodostat, was carried out. Linrodostat was shown to downregulate in cells some of the same key Trp metabolites as ouabain, artemether (in media) and EFL9, 5-hydroxy-L-Trp, N-formylkynurenine and formyl-5hydroxykynurenamine. Interestingly, these three metabolites are generated by two classes of enzymes IDO and TPH. Both of these are iron containing enzymes. While it is known that Linrodostat is a selective IDO1 inhibitor, that binds to the haeme-binding pocket of the enzyme, this data might suggest that Linrodostat might also interfere with TPH enzymes (Balog et al., 2021, Cherney et al., 2021). Alternatively,

that fact that 5-hydroxy-L-Trp was consistently downregulated by all 4 drugs tested here, might indicate some sort of functional link between IDO1/the kynurenine and TPH 1/2 activity.

In terms of upregulated metabolites, Linrodostat exhibits a unique signature, upregulating levels of 5-hydroxyindoleacetaldehyde and indoleacetaldehyde. This is interesting since studies have indicated that an increase in the ratio of downstream serotonin metabolites (e.g., 5-hydroxyindoleacetic acid) to serotonin seems to be an indicator of oxidative stress (Lee et al., 2021). It is, therefore, possible that Linrodostat might interfere with the redox balance in the cell. Alternatively, it is possible that the increase in 5-hydroxyindoleacetaldehyde observed with Linrodostat might be a compensatory mechanism given the inhibition of the IDO enzymes converting serotonin to formyl-5-hydroxykynurenamide. Thus, in order to prevent a build-up of serotonin, the indole synthesis might be upregulated.

Linrodostat also upregulated a range of metabolites that were either not affected or affected in a different direction by the other drugs tested in this study. An increase in vitamin B6 or pyridoxine was reported, this is interesting, as, although a clear link between vitamin B6 and Trp metabolism has not definitively been formulated, studies indicate that vitamin B6 might be able to downregulate an abnormally active kynurenine pathway activity in aged individuals, while other studies show a positive correlation between serum Trp and pyridoxine-derivative levels in young adults (Crepaldi et al., 1975, Deac et al., 2015).

Linrodostat also upregulated intracellular formyl anthranilic acid, downstream of the N-formylkynurenine metabolite, which is otherwise downregulated by Linrodostat. N-formyl anthranilic acid can act as an intermediary metabolite for indole metabolism, thus its upregulation might suggest that Linrodostat enhances other branches of Trp metabolism, while potentially inhibiting the kynurenine pathway (Patel et al., 2023, Dai et al., 2022,

Tsubokura et al., 1961). Finally, Linrodostat upregulated levels of isonicotineamide and adenosine monophosphate, suggesting that there is increased need for energy carriers and thus indicating increased metabolic activity.

In summary, Linrodostat downregulate similar core Trp metabolites as ouabain and EFL9 in cells, while artemether, ouabain and EFL9 downregulate similar metabolites in media. Interestingly, the inhibitory effects of Linrodostat were restricted to IDO1 and TPH 1/2 reaction products, suggesting higher specificity. Linrodostat had opposing effects to those of EFL9 on vitamin B6, nicotinamide-derivatives, hydroxy indole acetaldehyde, thus suggesting that EFL9 does not fit the profile of a selective IDO1 inhibitor.

6.4. Conclusions

In conclusion, this chapter summarised the steps taken in trying to understand the impact of the two hits described in Chapter 5 (artemether and EFL9) on the physiology of triple negative breast cancer cells. The impact of the two kynurenine inhibitory hits on IDO1 enzymatic activity, intracellular Na^+ accumulation and Trp metabolism was investigated. The metabolic impacts of the hits were then compared to those of the previously described IDO1 regulator, ouabain (Chapter 3) and of a clinically used, selective IDO1 inhibitor, Linrodostat. Overall, distinct metabolic profiles were identified for all 4 drugs. These data allow speculative hypotheses about the mechanism of action of each drug, in such that artemether might inhibit the kynurenine response by interfering with intracellular haeme availability, EFL9 might exert its function by suppressing a range of anti-inflammatory and antioxidant metabolites, while ouabain and Linrodostat might interfere with the redox but also ionic balance within the cells. However, future work would be needed to verify these hypotheses and confidently characterize the activity of artemether and EFL9.

7. Chapter 7: Discussion

7.1. Rationale of the project.

Tumour biology is complex and dynamic therefore, researchers are constantly striving to design novel therapeutic approaches. Historically, the most successful therapies have been the ones that are non-specific, have antiproliferative action and exert high toxicity levels, such as chemotherapy (Debela et al., 2021). However, these alone do not always have the potency to improve patient survival, and quite often they present severe side effects (e.g., dysregulation of the gastrointestinal tract, immunosuppression, neurotoxicity etc.) that significantly decrease patient quality of life (Nurgali et al., 2018). These limitations were partially addressed by the development of targeted therapies, such as tyrosine kinase inhibitors, anti-HER2 monoclonal antibodies or immune checkpoint therapies (Dungo and Keating, 2013, Jeyakumar and Younis, 2012, Vanneman and Dranoff, 2012). However, targeted therapies require the patient tumour to express the target molecule, this considerably reduces the pool of responsive patients. Tumours are dynamic systems, which means that resistance mutations can often occur, thus potentially changing a patient from a responder to a non-responder (Alvarado et al., 2014, Engelman et al., 2007, Toy et al., 2013, Vasan et al., 2019). Despite these limitations, targeted therapies in general and, for the scope of this work, immunotherapies, have significantly enhanced our ability to treat cancer and improve patient survival.

This study focuses on one specific immunotherapeutic target, the immune checkpoint protein and Trp catabolic enzyme, IDO1 in TNBC. There are several reasons why this study model and this particular target have been selected for this research. Firstly, TNBC is the only subtype of breast cancer that has been shown to respond to immunotherapy, however, the success of immune checkpoint inhibitors has been limited in comparison with other cancer types (Kwa and Adams, 2018). This highlights the need for improvement and optimization of

current immunotherapies, as well as the importance of designing novel targeted approaches to enhance immune-mediated tumour clearance in TNBC models. Secondly, IDO1 is an immune checkpoint that has been extensively studied, and a number of inhibitors have been investigated in clinical studies, one of which, Indoximod, has also been FDA approved for the treatment of stage IIb and stage IV melanoma(Tang et al., 2021). However, when compared to anti-PD-1/ PD-L1 therapies, IDO1 inhibitors have had limited clinical success and none of them has been approved for breast cancer treatment (Tang et al., 2021, Fujiwara et al., 2022, Jia et al., 2018). Several hypotheses have been formulated around this result. One possibility is that some IDO1 inhibitors, such as the Trp competitor, Epacadostat (INCB024360) might have dual activity, on the one hand inhibiting IDO1 and Trp metabolism, and on the other binding to the AhR receptor and enhancing kynurenine production, as well as immunosuppression (Moyer et al., 2017). Other studies have suggested that the limited clinical success of IDO1 inhibitors might come from the study design. As not all tumours express IDO1, choosing the patient pool is a crucial factor for the outcome of the treatment (Fujiwara et al., 2022, Théate et al., 2015, Eynde et al., 2020). Additionally, IDO1 inhibitors have often been tested in combination with anti-PD-1/ PD-L1 therapies, and recent studies have shown that kynurenine can act as a signalling molecule that triggers PD-1 expression on T cells, in an AhR-dependent manner. Therefore, it is possible that the combined administration of IDO1 and PD-1/ PD-L1 inhibitors might not have the desired effect due to the fact that both have the same ultimate target, and no additional pathways are affected by these inhibitors (Liu et al., 2018a, Amobi-McCloud et al., 2021, Eynde et al., 2020).

Thus, IDO1 and Trp metabolism as therapeutic targets in cancer are an excellent example of targets with promising biological potential but limited clinical success (Fujiwara et al., 2022). This highlights the need to better understand the IDO1-centric Trp metabolism in order to develop novel approaches for targeting this pathway. The potential of this particular immune checkpoint also comes from its dual function as an immune regulator and metabolic enzyme

(as well as having possible signalling activity) (Pallotta et al., 2022, Zhai et al., 2015). The connection between IDO1 activity and Trp metabolism expands the therapeutic spectrum to amino acid availability, transport, and metabolism, as well as other potential cellular mechanisms that are Trp/ amino acid dependent (e.g., translation) (Newman et al., 2021, Kenski et al., 2023, Zhai et al., 2015, Bartok et al., 2021). Thus, given the wide implications of Trp biology for cancer and TNBC in particular, the kynurenine pathway was selected as a core target of this study. Additionally, given the limited success of direct IDO1 inhibition, this study decided to explore interactions between multiple aspects of the tumour microenvironment and Trp metabolism, in an attempt to unravel novel targetable mechanisms regulating the kynurenine pathway.

7.2. Summary of the main findings.

This study showed that alterations in the ionic microenvironment can be linked to Trp metabolism, with intracellular Na^+ levels being negatively correlated with IDO1 expression and activity in TNBC and lung cancer cells (Chapters 3 and 4)(Shandell et al., 2022). This work reports an impact of the NKA inhibitors, ouabain and digoxin on both the kynurenine pathway, decreasing kynurenine levels, and IFNγ-induced JAK/ STAT signalling, decreasing levels of pSTAT1 at 24 h post stimulation as well as decreasing IDO1 expression (Chapter 5)(Shandell et al., 2022). Combined KD of the α1 NKA subunit (ATP1A1) and ouabain/ digoxin treatment had an enhanced inhibitory effect on kynurenine, IDO1 and pSTAT1 (Figure 3.4, 3.5, 3.6), confirming thus that the NKA is essential in this mechanism. Several routes to try and establish which role of the NKA (expression, signalling activity, Na^+ transport) is involved in IDO1 regulation were explored. In Chapter 3, section 3.2.8. describes the efforts of overexpressing the ATP1A1 in MDA-MB-231 cells, with the ultimate purpose of verifying whether increased ATP1A1 expression can rescue the effect of ouabain treatment on IDO1 and the kynurenine response. However, given the tight regulation of the ATP1A1 expression

in the cell, due to its essential role for survival, overexpression was not successful, and the hypothesis could not be verified (Clifford and Kaplan, 2009, Nakamura et al., 2021). Although other studies have reported successful ATP1A1 overexpression, primarily using viral vectors, time constrains and limited resources, as well as the need to progress further with the storyline of the project did not allow further follow up work on this route (Correll et al., 2014, Factor et al., 1998). Chapter 4 (sections 4.2.4. to 4.2.7.) explores one potential signalling mechanism, by looking at the SIK1 kinase, activated in response to intracellular Na^+ elevations (Sjöström et al., 2007, Taub et al., 2015). Experimental work indicated no significant contribution of SIK1 to the ouabain-mediated IDO1 inhibition, however, no clear conclusion could be drawn from the data, given the fact that inhibition of SIK1 with the HG-9-91-01, commercially available SIK1-selective small molecule, could not be validated experimentally. Western blot assessment of changes the levels of SIK1 immediate phosphorylation targets such as cAMP response element-binding protein (CREB), in MDA-MB-231 cells upon HG-9-91-01 treatment, would enable a clear conclusion from the experimental work presented in Chapter 4. This was, however, not pursued due to time constraints. Finally, the role of intracellular Na^+ in regulating the kynurenine response was also investigated in more detail. In Chapter 4, sections 4.2.1. to 4.2.3. show that the ionophore monensin was able to upregulate intracellular Na^+, while decreasing the kynurenine response. Thus, having shown an inverse correlation between intracellular Na^+ levels and kynurenine, in response to NKA inhibition with ouabain/ digoxin, but also in an NKA-independent manner with monensin, it was concluded that intracellular Na^+ and the kynurenine pathway might be indeed interconnected, and there would be great value in pursuing this further, by looking at other non-pharmacological methods of altering intracellular Na^+ levels (discussed in more detail in section 7.3.1). Given the fact that this project aimed to focus on the role of IDO1/ kynurenine and immune evasion in breast cancer, further investigating ionic dynamics was considered beyond the scope of this work. Instead,

the study focused on identifying further connections between the tumour microenvironment and the kynurenine pathway.

Having identified a potential correlation between two distinct aspects of the tumour microenvironment (ionic dynamics and the immune/ metabolic checkpoint IDO1), the next step was to expand the scope of this project towards exploration of different compounds with inhibitory activity of the kynurenine pathway, trying to identify novel potential mechanisms of action. A 630 natural compound screen identified 24 compounds with inhibitory activity on the kynurenine response and 1 compound able to upregulate kynurenine production. Of the 24 kynurenine inhibitors, 4 groups of compounds were defined based on their impact on immune checkpoint activity (IDO1) and expression (IDO1, membrane and sPD-L1). Next, two compounds that decrease the kynurenine response without impacting on IDO1 expression, artemether and EFL9, were selected for further investigation. Data indicated that both compounds decrease the kynurenine response in a concentration-dependent manner, without impacting on pSTAT1 or IDO1 levels (Chapter 5). The impact of these two compounds was then compared with that of ouabain, and a clinically tested IDO1 inhibitor, Linrodostat, on Trp metabolism, to understand the broader spectrum of activity for these compounds (Chapter 6). Ouabain, EFL9 and Linrodostat affected key Trp metabolites in the same way: drop N-formylkynurenine, 5-hydroxy-L-Trp and formyl-5-hydorxykynurenamine in cells (Linrodostat was only tested in cells) and media. This suggests that the IDO1 and the TPH 1/ 2 mediated reactions might be interconnected. This hypothesis is supported by studies which have shown that 5-hydroxy-L-Trp might have immunosuppressive activity, just like N-formylkynurenine (Yang et al., 2015c), while kynurenine and 3-hydroxykynurenine were shown to potentiate the effects of 5-hydroxy-L-Trp on muscular excitation in mouse models (Handley and Miskin, 1977). To validate this hypothesis experimentally, a series of experiments such as sequential knockdown of IDO1 followed by assessment TPH1/ 2 activity/ expression; assessment of correlation between

intracellular iron levels and IDO1, TPH1/ 2 activity (Goodwill et al., 1997, Roberts and Fitzpatrick, 2013); or assessment of a potential synergistic effect on the kynurenine response of concomitant inhibition of IDO1 and TPH1/ 2, could be carried out.

Overall, different metabolic profiles were identified for each one of the 4 compounds tested (ouabain, artemether, EFL9 and Linrodostat). Metabolomics data showed that artemether is the only compound that maintains constant N-formylkynurenine levels in the cell, while dropping the levels of this metabolite in the media. It is also the only compound that interferes with intracellular haeme levels. Thus, artemether might have dual action by causing haeme-dependent IDO1 inhibition, consistent with the currently accepted mechanism of action for this compound (Krishna et al., 2008), and by preventing the transport of kynurenine in the cytosol. Although kynurenine import is known to be mediated by transporters such as SLC7A5, there is no known specific kynurenine exporter (Sinclair et al., 2018). Therefore, understanding the mechanism of action of artemether and identifying its potential target could greatly contribute to understanding Trp and kynurenine pathway biology.

In the case of EFL9, experimental data reported a much broader metabolic effect than for artemether and ouabain, primarily altering the redox balance. EFL9 had the most dissimilar metabolic profile from that of Linrodostat, downregulating metabolites otherwise upregulated by Linrodostat (e.g., 5-hydroxyindoleacetaldehyde). Ouabain had an identical metabolic profile with Linrodostat in terms of downregulated metabolites, however, the Linrodostat-treated cells had a much higher range of upregulated metabolites.

One interesting observation is the limited effect of ouabain on Trp metabolites. By blocking the NKA, which is an active ionic transporter, ouabain is lowering the energetic demands of the cell, which should, in theory, lead to altered metabolic processes (Soltoff and Hedden, 2008). Na^+ import is often coupled with uptake of glucose and glutamine, therefore the

dysregulated ionic balance caused by ouabain could impact on their cellular bioavailability; the deficiency in glutamine and glucose substrates combined with decreased ATP-usage due to NKA inhibition, could impact on glycolysis , the pentose phosphate pathway, as well as glutaminolysis, which can have severe implications for the ability of the cell to maintain the redox balance, as well as interfering with anabolic pathways and proliferation (Leslie et al., 2019). Furthermore, by altering the Na^+ concentration within the cell, ouabain also leads to a release of Ca^{2+} from intracellular stores, as well as extracellular import through the NCX (Blaustein and Hamlyn, 2020). An increase in intracellular Ca^{2+} levels has been associated with increased activity of dehydrogenases enzyme from the tri-carboxylic acid cycle, leading to increased mitochondrial metabolism and thus higher NADH levels (Díaz-Vegas et al., 2019, Rossi et al., 2019). However, despite the expected broad metabolic effect, in the metabolomics experiments described in this study, ouabain seems to be the most specific of the 4 drugs tested, only affecting core Trp metabolites in cell extracts and phosphatidyl choline-derivatives levels in culture media. Phosphatidyl choline accumulation is often a marker of inflammations, oxidative stress of damage (Fogarty and Bergmann, 2015, van der Veen et al., 2017, Ridgway, 2013). Its increase in culture supernatants in response to ouabain is more likely due to signal cell death and membrane degradation given the toxicity of the cardiac glycoside (Tsuji et al., 2023). However, phosphatidyl choline is also known to have an impact on ion channel activity. In fact, lysophosphatidyl choline (16:0), which was upregulated by ouabain the media, has been shown to activate acid-sensing ion channel 3 (ASIC3) (Hung et al., 2020). By doing so, lysophosphatidyl choline (16:0) is likely to promote intracellular buildup of Na^+ thus enhancing the ionic disbalance. Oher Lysophosphatidyl choline derivatives have been shown to activate transient receptor potential (TRP), ligand gated Ca^{2+} channels (Rimola et al., 2020). This could enhance cytosolic Ca^{2+} accumulation and thus impact on a range of Ca^{2+} dependent pathways including IFNγ-induced JAK/ STAT signalling (Tsuji et al., 2023).

Interestingly, however, EFL9 also increased the levels of lysophosphatidyl choline derivatives in culture supernatants and in cellular extracts. EFL9 does not impact on intracellular Na^+-levels, which suggests that in the case of this compound lysophosphatidyl choline might be a marker of cell death, or oxidative/ inflammatory disbalances, rather than an ionic modulator (Tsuji et al., 2023).

Finally, metabolic analysis of the selective IDO1 inhibitor, Linrodostat, revealed upregulation of a range of metabolites some of which are downstream reaction products from kynurenine metabolism. This observation could have multiple implications (Balog et al., 2021, Cherney et al., 2021). Firstly, it might suggest that even though Linrodostat was designed for interacting with IDO1, it might in fact have a range of off-target effects, which could be partially accountable for its limited clinical success. Secondly, it might suggest that IDO1 inhibition could trigger compensatory mechanisms from the downstream pathway increasing production of anthranilic acid and its derivatives. However, in the absence of further experimental data, these speculations cannot be verified.

In summary, although it was not possible to formulate an exact mechanism of action for each one of the compounds studied here, 3 different classes of natural modulators of the kynurenine response and Trp metabolism were studied and characterised in this study. Modulation of kynurenine levels was achieved by interfering with the ionic microenvironment and subsequently with pSTAT1-dependent IDO1 expression and activity (ouabain); by potentially interfering with the intracellular haeme levels and thus altering kynurenine production by the IDO1 holoenzyme (artemether); by interfering with Trp metabolism at different sites, as well as with the cellular redox balance (EFL9). With further studies, there is potential for these compounds to be either developed into future targeted therapies or to be used to better understand the role of Trp biology in TNBC.

7.3. Future plans

The work presented in this study generated a series of hypotheses for future study, including: (1) modulation of Na^+ dynamics might represent a novel therapeutic approach in TNBC, by interfering with IDO1 activation, (2) repurposing artemisinin derivatives for immunotherapy by targeting Trp metabolism might be of value for targeting TNBC and (3) Euphorbia factors could contribute to TNBC clearance by increasing oxidative stress, and enhancing production of immunosuppressive Trp metabolites. Although this study generated experimental evidence to support each one of these hypotheses, time and resources were not sufficient to complete any of these three studies. Future work would need to be carried out to reach a clear response on each one of these questions.

7.3.1. Modulators of Na^+ dynamics might be the future of TNBC immunotherapy by interfering with IDO1 activation.

Chapters 3 and 4 show that pharmacological treatments that alter intracellular Na^+ are likely to interfere with IDO1 activity and expression (Shandell et al., 2022). An inverse correlation between intracellular Na^+ and kynurenine levels was reported and further validated using two different classes of compounds: cardiac glycosides (ouabain and digoxin) and ionophores (monensin).

The data presented in this study, however, only points out a correlation and do not identify a causative relationship between ionic dynamics and IDO1 activity. Establishing such a relationship would be quite challenging, as pharmacological treatments often have a range of off-target effects that make it difficult to pinpoint a mechanism. Alterations in intracellular Na^+ are not singular events, as ionic dynamics are often compensatory. This means that an increase in intracellular Na^+, will trigger a decrease in something else (e.g., K^+), as well as increasing Ca^{2+} import which then leads to signalling alterations (Yu et al., 2010, Barry et al.,

1981). It is therefore very difficult to isolate the effect of altered intracellular Na^+ on cellular physiology.

One essential question that needs to be answered is what happens to Ca^{2+} signalling in response to ouabain/ monensin treatment in IFNγ/ TNF stimulated TNBC cells (the model for this study). Changes in intracellular Ca^{2+} are usually rapid acute events, tightly regulated by the plasma membrane and sarcoplasmic reticulum Ca^{2+} ATPases, as well as the NCX, and would therefore need to be measured by patch clamping methods (Bagur and Hajnóczky, 2017). The next question would then be, how is signalling inside the cell being altered in response to ouabain. Literature already supports a role for ouabain in triggering a series of signalling events which include NKA-mediated activation of the Src kinase; stimulation NKA association with the EGFR, leading to MAPK activation and subsequent transcriptional changes; PKC-dependent ERK1/ 2 activation, as well as activation of the PI3K1A/ Akt pathway (Haas et al., 2000, Xie and Askari, 2002, Mohammadi et al., 2001, Wu et al., 2013a). However, the complete signalling pathway that could connect elevations in intracellular Na^+ with IDO1 has not yet been identified. To try and address this issue, a targeted approach, looking at ouabain/ monensin-triggered changes in molecules associated with IFNγ/ TNF signalling could be taken, alternatively, investigation of all the signalling networks within the cell could be pursued. A combined proteomics and phosphor-proteomics study looking at the changes triggered by ouabain/ monensin, could help trace a potential signalling route, which could be further investigated and validated by western blot and pull-down assays. While this type of analysis would be very demanding in terms of time and resources, it would only be able to reveal a potential signalling pathway associated with ouabain/ monensin treatment. Additionally, this type of analysis assumes a mechanism based on phosphorylation cascade. RNAseq could be used to also assess changes in gene expression, while a Seahorse experiment could be completed to look at changes in metabolic preferences within the cell (Plitzko and Loesgen, 2018). The limitation with such costly and time-demanding analysis

methods is that strong preliminary evidence is required to justify such extensive exploratory work. The fact that no clear direction (phosphorylation cascade, expression changes or metabolic dysregulation) can be inferred from the current data, suggests that more preliminary work is needed before such experiments could be carried out. A good start for the preliminary work would be optimising the ATP1A1 overexpression in MDA-MB-231, potentially by using viral-vector based transfection or electroporation (Fus-Kujawa et al., 2021). Additionally, validation of SIK1 inhibition with HG-9-91-01 in MDA-MB-231s could be a further step in completing the experimental story presented in this study; Validation could be achieved by measuring levels of a direct SIK1 phosphorylation substrate such as CREB/ CREB-regulated transcription co-activator (CRTC), protein phosphatase methylesterase-1 (PME-1) or class IIa histone deacetylases, in response to HG-9-91-01 treatment, via western blot or flow cytometry (Sun et al., 2020). A clear answer to these two questions: (1) is ATP1A1 overexpression able to rescue IDO1 inhibition by ouabain? and (2) is SIK1 modulating the impact of ouabain on IDO1? could greatly contribute to the current understanding of the observations presented in this work and would thus help dictate the next experimental steps. Other approaches would be to look at ouabain/ monensin-induced changes in activation of known signalling hubs such as MAPK, Akt/PI3K in MDA-MB-231s, via western blot; this would be of value especially due to previous literature reports that have shown an impact of ouabain/ monensin in various cell types on MAPK or Akt/ PI3K signalling (Siman et al., 2015, Lopachev et al., 2016, Serter Kocoglu et al., 2023). It would be possible also to evaluate ROS production as an indication of metabolic changes, using 5-(and -6)-carboxy-2',7'-dichlorodihydrofluorescein diacetate (DCFDA) fluorescent labelling, as an indication of metabolic changes (Katerji et al., 2019). Furthermore, an indication of glycolytic rate could be derived from quantification of secreted L-lactate either by ELISA, or using absorbance based lactate-quantification assays described in the literature (Schmiedeknecht et al., 2022). PH measurement using phenol red absorbance at 430 and 560 nm could also be a rapid and

effective indicative of the metabolic changes triggered by each one of the compounds (ouabain/ monensin) (Schmiedeknecht et al., 2022, Ivashkiv, 2020).

Building on the signalling metabolic future work plans, the next step would be to integrate changes in intracellular Na^+ in the study. To answer the question of Na^+ dependency, the impact of low K^+ culture media on IDO1 activity and expression, as well as on the potential signalling network identified to be associated with ouabain/ monensin treatment, could be assessed (Weiss et al., 2017, Kleimaier et al., 2020). Although this type of experiment seems relatively straight forward, a bespoke low K^+ media would need to be designed and the long-term effects on cell survival and growth would also need to be tested prior to the actual experiment. An alternative would be using a Na^+ -specific chemo genetic ligand gated channel. This could allow us to study the effect of intracellular accumulation of Na^+ independently of NKA inhibition, without the challenge of off-target effects often encountered in pharmacology experiments (Magnus et al., 2011, Magnus et al., 2019). The limitations of this approach are, however, coming from cellular mechanisms used to regulate the ionic balance. A Na^+ -specific chemo genetic ligand gated channel would allow constant Na^+ influx, however, this could be compensated by increased NKA activity. Other approaches of regulating NKA activity could also be used. Phospholemman (PLM) is an ion transport regulatory protein belonging to the FXYD family. In cardiac myocytes PLM enhances the activity of the NKA, inhibiting Na^+/ Ca^{2+} exchanger, and upon cardiac glycoside treatment PLM alleviates the stress triggered by intracellular Na^+ accumulation by counteracting the NKA inhibition. It is thus possible to knock down the PLM and this should result in downregulated NKA activity and intracellular Na^+ accumulation. However, given the role of PLM in regulating Ca^{2+} transport , it is likely that the impact of PLM knock down will have a range of effects on intracellular signalling and metabolism (Cheung et al., 2010, Dejos et al., 2020, Berridge et al., 2003). Additionally, because the NKA is an active transporter, increased activity would increase the energetic needs of the cell and thus impact on metabolic function

(Sanderson et al., 2020). Therefore, such changes could be misleading when looking at the activity of a metabolic enzyme like IDO1. However, these limitations are speculative and could be confirmed or denied only experimentally. Finally, an alternative to separating the Na^+ function and the signalling function of the NKA would be to express the rodent ATP1A1 in human cells and compare the impact of ouabain on the kynurenine response in transfected and wild type cells. The rodent ATP1A1 is 1000 less sensitive to ouabain than the human one, and thus could function unimpaired upon treatment (Lopina et al., 2020a). This could provide valuable information on the mechanism of action of ouabain, and the role played by the NKA and Na^+ accumulation.

In summary, there is a large amount of follow-up work that could be completed to better understand the relationship between intracellular Na^+ and Trp metabolism, however, the data presented in this work (Chapters 3 and 4), brings strong evidence to support and justify further research on this topic.

7.3.2. Repurposing artemisinin-derivatives and exploring Euphorbia Factors for immunotherapy by targeting tryptophan metabolism might be a future therapeutic approach for TNBC.

Chater 5 identifies endoperoxide-bearing members of the artemisinin derivative class, and Euphorbia factors with C7 benzoyl modifications as potential inhibitors of the kynurenine response. The chapter focuses on artemether and EFL9 as representatives from each class and show that both of those reduce kynurenine in a concentration dependent manner without impacting on IDO1 expression and without altering intracellular Na^+. In titration experiments, artemether and EFL9 seemed to have identical behaviour, indicating a common mechanism of action. One experiment which could rapidly clarify this hypothesis, would be assessing the kynurenine response upon combined artemether and EFL9 treatment. A synergistic effect would be indicative of different, yet interconnected modes of action, while

an additive effect would indicate a similar mechanism/ target for both drugs. This experiment was not completed due to time constraints, but it would be a priority upon continuing this work.

Having shown that artemether and EFL9 exert their effects independently of IDO1 expression, the next step was to investigate their impact on purified IDO1 activity. However, the assay set-up and control IDO1 inhibitor of choice (Linrodostat) proved to be unsuitable for this type of experiment, and due to time constraints, it was not possible to optimize this set-up. To answer the question of direct IDO1 interaction for both artemether and EFL9, a purified enzyme activity assay would need to be carried out successfully. Literature suggests that a fluorescence-based assay might be a better alternative to an absorbance assay, due to minimized background interference (Simeonov and Davis, 2004). Additionally, an IDO1 inhibitor more likely to function in a purified enzyme set-up, such as a Trp-competitor (e.g., Epacadostat), might be a better control than Linrodostat, otherwise known to interfere with IDO1 holoenzyme assembly (Balog et al., 2021, Cherney et al., 2021).

A way to understand exactly the targets of artemether and EFL9 in MDA-MB-231s would be by using click chemistry (Pang et al., 2022, Fu et al., 2014). Literature reports the design of Activity-Based Protein Profiling Probes (ABPPs), that incorporate the artemisinin pharmacophore (endoperoxide bridge) and are compatible with click chemistry; artemisinin-based click chemistry constructs have also been shown to have therapeutic activity (e.g., working as antiviral agents) (Ismail et al., 2016, Çapcı et al., 2020). The ABPP click chemistry technology uses probes that carry the active site of the compound of interest, thus allowing interaction with the target when added onto cells. Next, a biotin azide or biotin dibenzocyclooctyne is added to the ABPP-target complex via copper free click chemistry. This allows affinity purification and identification of target proteins using liquid chromatography and mass spectrometry (LC-MS/ MS) (Ismail et al., 2016). This approach would firstly help us

understand and validate the interaction between artemether and haeme/ IDO1, and secondly allow us to potentially identify a specific cellular kynurenine exporter. A similar approach where the ABPP is bound to an EFL9-like structure could be used to pinpoint the target of the compound. The limitation of this approach is that EFL9 has not been as widely studied as artemether and information about its active site would have to be determined experimentally. However, even in the absence of such pharmaco-chemical characterization, the click chemistry approach could be used to test whether the C7 benzoylation is indeed responsible for the impact of this compound on the kynurenine response. Additionally, validation of the antioxidant properties of this compound could be achieved by measuring ROS production in TNBC cell cultures upon drug treatment, using DCFDA fluorescent staining.

Once a mechanism of action is validated for both compounds, co-culture studies of cancer and immune cells ($CD8^+$ T cells) would be the first step to validate the biological efficacy of those compounds in a complex set-up. The effect of these compounds would then need to be tested on mouse cell lines, to allow *in vivo* transition to syngeneic mouse models (with an intact immune system).

In conclusion, a range of biochemical, mechanistic, and, later on, safety and efficacy studies would need to be carried out on those compounds to fully characterize their mechanism of action and assess their viability as immunotherapeutic candidates.

7.4. Assessing aims and objectives.

The main goal of the work presented here was to contribute to a better understanding of the role of Trp metabolism in TNBC, and its interaction with other aspects of the tumour microenvironment such as ionic dynamics and immunology. This study focused on the rate-limiting step of Trp conversion to kynurenine (an immunosuppressive metabolite), by looking at the activity and expression of the IDO1 catalytic enzyme. Three different classes

of IDO1/ kynurenine response inhibitors were identified and characterized: ionic modulators (ouabain/ monensin), artemisinin-derivatives and Euphorbia factors. This work established a correlative link between the kynurenine response and intracellular Na^+ levels, highlighting a potential mechanism of action for ouabain-induced IDO1 inhibition. The metabolic effects of ouabain, artemether and EFL9 in TNBC cells were studied and compared to that of the selective IDO1 inhibitor, Linrodostat, identifying unique metabolic profiles for each one of the compounds. Table 7.1 summarizes the main goals of this project and the progress that has been done trying to address each one of those. Thus, a set of experimental studies that enhanced our understanding of TNBC biology were successfully completed, showing complex interactions between the ionic, immune, and metabolic aspects of the tumour microenvironment, all converging towards Trp metabolism. However, the progress towards understanding Trp biology in TNBC presented in this study, only highlights the wide range of implications associated with pharmacological targeting of this pathway, and a large amount of validation work and future mechanistic studies would need to be completed before the full story of how these compounds impact on Trp metabolism in TNBC could be formulated.

General study aims	Status
Investigate the connection between ionic dynamics and Trp metabolism. Unravel potential natural compound candidates to be investigated for breast cancer therapy.	Complete: Chapters 3, 4, 5 and 6.
Na^+ and IDO1 study aims	**Status**
Understand how ouabain exerts its effects on IDO1 and the kynurenine response (mechanism)	Complete: (Chater 3) Inhibition of pSTAT1-mediated IDO1 expression.
Validate the (NKA-independent) effect of Na^+ on kynurenine production and IDO1	Complete (with limitations): (Chapter 4) Validation of correlative relationship between intracellular Na^+ and IDO1 activity, using monensin.
Natural Compounds and IDO1 study aims	**Status**
Adapt the kynurenine assays for low to mid throughput purposes and use it to screen a library of 630 natural compounds for potential inhibitors of the kynurenine response, with lower toxicity that ouabain.	Complete: (Chapter 5) Identification 24 natural compounds with IDO1 inhibitory activity.
Investigate the mechanism of action of selected hits.	Complete (with limitations): (Chapter 5) Confirmation that both artemether and EFL9 inhibit the kynurenine response indepently of IDO1 expression.
Assess the impact of selected hits on Trp metabolism and compare that to the effect of ouabain.	Complete (with limitations): (Chapter 6) Metabolomics study helps us speculate on mechanisms of action: artemether: prevents IDO1 holoenzyme assembly by depleting intracellular haeme. EFL9: impacts on multiple metabolic processes in the cell, interfering with the redox balance and promoting a general immunosuppressive cellular activity.

Table 7.1 Summary of project aims and objectives, and current progress.

8. Appendix

8.1. Chapter 2 Appendix

Appendix Table 8. 1 Summary of the main reagents used in this study.

PRODUCT	SUPPLIER	CATALOG NO
DULBECCO'S MODIFIED EAGLES MEDIUM (DMEM)	Thermo Fisher Scientific (Invitrogen)	21969-035
MAMMARY EPITHELIAL CELL GROWTH MEDIUM BULLET KIT (MEGM)	Lonza	CC-3150
REAGENT PACK SUBCULTURE REAGENTS FOR PRIMARY CELL SUBCULTURING	Lonza	CC-5034
EMBRYONIC STEM-CELL FBS, QUALIFIED, USDA-APPROVED REGIONS	Thermo Fisher Scientific (Gibco)	10439024
PENICILLIN-STREPTOMYCIN (5,000 U/ML)	Thermo Fisher Scientific (Gibco)	15070063
L-GLUTAMINE (200 MM)	Thermo Fisher Scientific (Gibco)	A2916801
PHOSPHATE SALINE BUFFER (PBS), 1X, PH 7.4	Thermo Fisher Scientific (Gibco)	10010023

TRYPSIN-EDTA	Thermo Fisher Scientific (Gibco)	25300054
TRYPAN BLUE	Thermo Fisher Scientific (Invitrogen)	T10282
DEEP BLUE VIABILITY	BioLegend	424702
OPTIMEM (MINIMAL ESSENTIAL MEDIUM)	Thermo Fisher Scientific (Gibco)	11058021
TRANSIT-SIQUEST	Mirus	MIR 2110
SIRNA HUMAN ATP1A1	ON-TARGETplus SMARTpool, GE Dharmacon/Horizon Discovery	L-006111-00-0005
SIRNA NTC	ON-TARGETplus SMARTpool, GE Dharmacon/Horizon Discovery	D-001810-10-05
SIRNA HUMAN NCOA3	ON-TARGETplus SMARTpool, GE Dharmacon/Horizon Discovery	L-003759-00-0005
SIRNA IDO1	ON-TARGETplus SMARTpool, GE Dharmacon/Horizon Discovery	L-010337-01-0005
JETPRIME	Polyplus	101000027

INVITROGEN™ LIPOFECTAMINE™ 3000 TRANSFECTION REAGENT	Thermo Fisher Scientific/Fisher Scientific (Invitrogen)	L3000001
LB BROTH (LENNOX)	Sigma-Aldrich	L3022-250G
LB AGAR, MILLER (USE 40G /1L DISTILLED WATER)	Formedium	LMM0204
SODIUM POTASSIUM ATPASE (ATP1A1) (NM_000701) HUMAN TAGGED ORF CLONE	ORIGENE	RC201009
PCMV6-ENTRY MAMMALIAN EXPRESSION VECTOR (EMPTY VECTOR)	ORIGENE	PS100001
NM_000701.8 HOMO SAPIENS ATPASE NA+/K+ TRANSPORTING SUBUNIT ALPHA 1 (ATP1A1), TRANSCRIPT VARIANT 1, MRNA. PCDNA3.1-C-(K)DYK	GenScript	NM_000701.8
MAMMALIAN PCDNA3.1+/C-(K)-DYK (LENGTH 5444)	GenScript	N/A
IDO CDNA ORF CLONE, HUMAN, C-DYKDDDDK (FLAG®) TAG	SinoBiological	HG11650-CF

PCMV3-C-FLAG VECTOR OVERVIEW (EMPTY VECTOR)	SinoBiological	CV012
QIAPREP SPIN MINIPREP KIT	QIAgen	27104
HISPEED PLASMID MIDI KIT	QIAgen	12643
RECOMBINANT HUMAN IFNΓ	Peprotech	300-02
RECOMBINANT MOUSE IFN-Γ	BioLegend	575304
HUMAN RECOMBINANT TNF	BioTechne	210-TA
MOUSE RECOMBINANT TNF		
OUABAIN OCTAHYDRATE, >=95% (HPLC), POWDER	Sigma-Aldirch	o3125-250mg
DIGOXIN CRYSTALLINE	Sigma-Aldrich	D6003-100MG
VEATRIDINE	BioTechne (Tocris)	2918
MONENSIN SODIUM SALT, 90-95.5% 1G UN3462	Alfa Aesar	J61669-03
HG-9-91-01	APE Bio	B1052
DIMETHYL SULFOXIDE (DMSO)	PanReac AppliChem Lifescience (VWR)	A3672
EHRLICH'S REAGENT (P-DIMETHYLAMINOBENZALDEHYDE)	Sigma-Aldrich	D2004

TRICHLOROACETIC ACID SOLUTION, MP BIOMEDICALS	Thermo Fisher/Fisher Scientific	11462691
PROTEASE INHIBITOR COCKTAIL, PHOSPHATASE INHIBITOR COCKTAIL 2 PHOSPHATASE INHIBITOR COCKTAIL 3	Sigma-Aldrich	P8340-1ML, P5726-1ML, P0044
ECL™ BLOTTING REAGENTS	GE Healthcare, Sigma-Aldrich	GERPN2109
100ST AMERSHAM HYPERFILM ECL 18X24CM, 100SHEETS	Thermo Fisher/Fisher Scientific (Life Science products Cytiva 28-9068-37PR16)	15497394
QIAZOL LYSIS REAGENT (200 ML)	QIAGEN LTD	79306
RNEASY MINI KIT	QIAGEN LTD	74104
SUPERSCRIPT ® III FIRST-STRAND SYNTHESIS SYSTEM FOR RT-PCR (CONTAINS RANDOM HEXAMERS 50 NG/ML)	Invitrogen	18080-051
DNTP MIX, PCR GRADE (200 µL) 10 MM	Qiagen	201900

NUCLEASE-FREE WATER (1 L)	Qiagen	129115
SUPERSCRIPT II REVERSE TRANSCRIPTASE (SS II RT 200 U/ML, 5X FS BUFFER, 0.1 M DTT)	Invitrogen	18064014
RNASE OUT 40 U/ML	Invitrogen	10777019
BUFFER PE (CONCENTRATE, 100 ML)	QIAgen	19065
BUFFER RWT (80 ML)	QIAgen	1067933
HUMAN GAPDH PRIMERS FOR - GGAGTCAACGGATTTGGTCGTA	Sigma-Aldrich	SY200305727-037
HUMAN GAPDH PRIMERS REV - GGCAACAATATCCACTTTACCAGAGT	Sigma-Aldrich	SY200305727-038
HUMAN IDO1 PRIMERS FOR - GGCTTTGCTCTGCCAAATCC	Sigma-Aldrich	SY180324975-083
HUMAN IDO1 PRIMERS REV - TTCTCAACTCTTTCTCGAAGCTG	Sigma-Aldrich	SY180324975-084
HUMAN IDO1 PRIMERS (BOTH FORWARD AND REVERSE)	Qiagen Quanti-Tect	QT00000504
HUMAN PD-L1 PRIMERS FOR – CATCTTATTATGCCTTGGTGTAGCA	Sigma-Aldrich	N/A
HUMAN PD-L1 PRIMERS REV –	Sigma-Aldrich	N/A

GGATTACGTCTCCTCCAAATGTG		
SOLUBLE PD-L1 (FORWARD) - TACAGCTGAATTGGTCATCCCA	Sigma-Aldrich	N/A
SOLUBLE PD-L1 (REVERSE) - AGGCAGACATCATGCTAGGTG	Sigma-Aldrich	N/A
HUMAN ATP1A1 PRIMERS (BOTH FORWARD AND REVERSE)	Qiagen QuantiTect	
ATP1B1 (FORWARD) - CCCAAATGTCCTTCCCGTTCAG	ORIGENE	23223589
ATP1B1 (REVERSE) - GCAGGAGTTTGCCATAGTACGG	ORIGENE	23223586
ATP1B1 (FORWARD) - CCCACATATCAGCGAGT	Primer3Plus	232213588
ATP1B1 (REVERESE) - ATCCCTCTGGGCTGAATCTT	Primer3Plus	232213587
POWERTRACK™ SYBR GREEN MASTER MIX	Sigma-Aldrich	A46109
NULEASE-FREE WATER	Omega Bio-TEK	S173258
HYPURE MOLECULAR BIOLOGY GRADE WATER	HyClone (Cytiva)	SH3053803

SBFI-AM	SantaCruz Biotechnology	sc-215841A
PLURONIC F-127 20% IN DMSO	Biotium	59004
GRAMICIDIN	Sigma-Aldrich	G5002, 1405-97-6
HUMAN PD-L1 ANTIBODIES (WESTERN BLOT) FINAL CONCENTRATION 1:1000	Cell Signaling	E1L3N
HUMAN/MOUSE STAT1 ANTIBODY (WESTERN BLOT) FINAL CONCENTRATION 1:1000	Cell Signaling	9172
HUMAN/MOUSE PSTAT1 TYR-701 ANTIBODY (WESTERN BLOT) FINAL CONCENTRATION 1:1000	Cell Signaling	D4A7
HUMAN IDO1 ANTIBODY (WESTERN BLOT) FINAL CONCENTRATION 1:1000	Cell Signaling	D5J4E
HUMAN ATP1A1 ANTIBODY (WESTERN BLOT) FINAL CONCENTRATION 1:1000 ~ 1µG/ ML	Abcam	ab7671 464.6

HUMAN GAPDH ANTIBODY (WESTERN BLOT) FINAL CONCENTRATION 1:500/ 1:1000 ~ 4/2µG/ ML	Abcam	6C5
POLYCLONAL ANTI-RABBIT IMMUNOGLOBULINE HRP FINAL CONCENTRATION: 1:5000	Dako	P0448-2
POLYCLONAL ANTI-MOUSE IMMUNOGLOBULINE HRP FINAL CONCENTRATION: 1:5000	Dako	P0447
ULTRAPURE PROTOGEL 30 % (W/V) ACRYLAMIDE	National Diagnostics	EC-890
1.5 M TRIS BUFFER (PH 8.8)	Severn Biotech LTD	20-7900-10
1.0 M TRIS BUFFER (PH 6.8)	Severn Biotech LTD	20-7901-10
SODIUM DODECYL SULFATE (SDS), ACS REAGENT, ≥99.0%	Sigma-Aldrich	436143-25G
SKIMED MILK POWDER (500G)	Millipore	70166
BOVINE SERUM ALBUMINE (BSA) (100G)	Sigma-Aldrich (Life Science)	A4378
AMMONIUM PERSULFATE (APS)	Sigma-Aldrich	A3678

ULTRAPURE N, N, N', N'-TETRAMETHYLETHYLENEDIAMINE (TEMED)	Thermo Fisher (Invitrogen)	15524-010
TURBO TRANSFER BUFFER (5X)	BioRad	10026938
ULTRAPURE TRIS	Thermo-Fisher (Invitrogen)	15504-20
RECOMBINANT HUMAN IDO PROTEIN, CF	BioTechne	6030-AO
ASCORBIC ACID	Sigma-Aldrich	A-4544
MORPHOLINOETHANESULPHONIC ACID (MES)	Sigma - Chemical Company	M-8250
METHYLENE BLUE	Fluorochem	F468442
CATALASE (FROM BOVINE LIVER)	Sigma-Aldrich	1003322800
L-TYPTOPHAN, 99 %	Thermo Scientific	A1023014
LINRODOSTAT	Generon	M6248

8.2. Chapter 3 Appendix

8.2.1. Effect of ouabain and ATP1A1 KD on SOCS3 upon 30 min, 4 and 24 h post cytokine stimulation.

Figure 3.6 shows that cardiac glycoside +/- ATP1A1 KD-mediated IDO1 inhibition is mediated by a drop in pSTAT1 levels, potentially occurring at later timepoints post cytokine stimulation (24 h). JAK/STAT signalling is tightly regulated by a series of molecules, including suppressor of cytokine signalling proteins (SOCS), (Federici et al., 2002). For this reason, the effect of ouabain and ATP1A1 KD on one member of the SOCS family, SOCS3, at 30 min, 4 and 24 h post cytokine stimulation was investigated. SOCS3 is one of the most studied molecules of the class and is known to regulate JAK1, JAK2, TYK2 and STAT3 (Babon et al., 2012, Jenkins et al., 2005, Carow and Rottenberg, 2014). JAK1/2 are known downstream mediators of IFNY receptor signalling and STAT1 activation (Kim et al., 2018, Majoros et al., 2017).

Experimental data show that IDO1 expression occurs 4 h post cytokine stimulation (Appendix Figure 8. 1B). While SOCS3 is constitutively expressed, being detected as early as 30 min post cytokine stimulation (Appendix Figure 8. 1A), with no change in at 4 h and 24 h, regardless of transfection status and drug treatment (Appendix Figure 8. 1B, C).

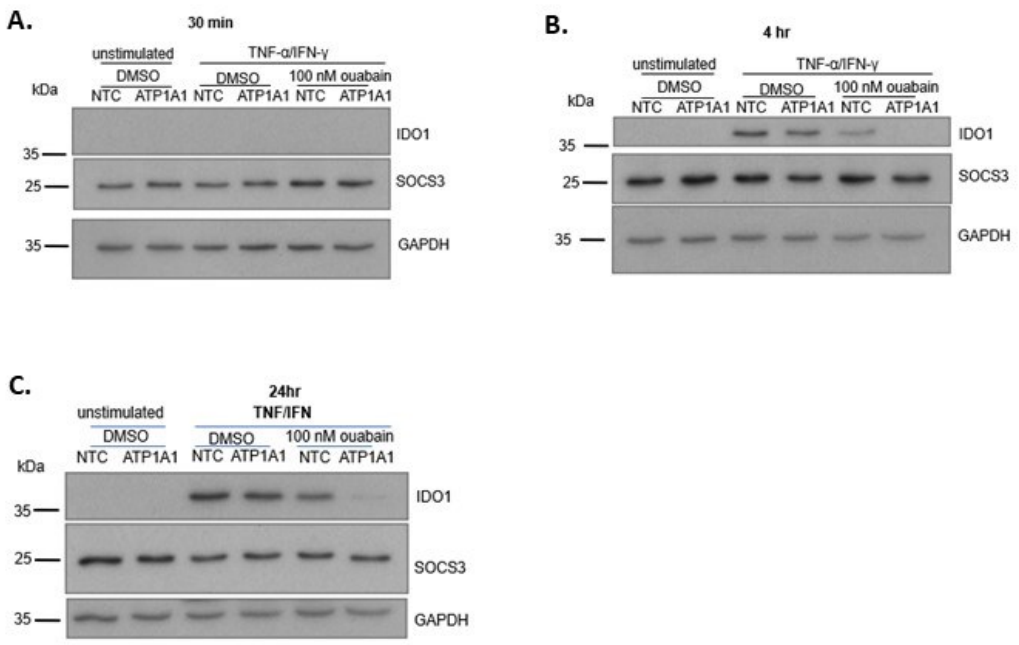

Appendix Figure 8. 1 Effect of ouabain and ATP1A1 KD on SOCS3 upon 30 min, 4 and 24 h post cytokine stimulation. A. Effect of ouabain and ATP1A1 KD on SOCS3 30 post cytokine stimulation (n=1 representative western blot); B. As in A 4 h post cytokine stimulation (n=1 representative western blot); C. As in A post cytokine stimulation (n=1 representative western blot); Note: western blots in A and B came from the same experiment (set up at the same time), western blot in C came from a separate experiment. ATP1A1 – the α1 subunit f the Na^+/K^+ ATPase (knock down samples), NTC – non-targeting control samples.

8.2.2. Alternative ouabain targets – SRC3

Literature records have shown that cardiac glycoside activity is not only restricted to the NKA but can sometimes target additional pathways within the cell. An example of such an alternative target is the steroid receptor coactivator 3 (SRC3) (Wang et al., 2014). To verify if the effects observed on IDO1 expression and activity were a consequence of NKA inhibition or an off-target effect due to ouabain binding SRC3, kynurenine production in response to a range of ouabain concentrations in SRC3 KD (Appendix Figure 8. 2A (red)), mock transfected (blue) and Untransfected (black) MDA MB 231 cells was measured. The experiment showed a similar trend of kynurenine reduction regardless of the presence or absence of SRC3. The efficacy of the SRC3 KD was confirmed by western blot (Appendix Figure 8. 2B). Furthermore, the expression of total and phosphorylated STAT1 proteins, as upstream regulators of IDO1 expression, was tested in response to ouabain in SRC3 KD, mock transfected and Untransfected samples. The same pattern of expression was observed in all sets of samples (Appendix Figure 8. 2B, panels 2 and 3).

In conclusion the effect of ouabain on kynurenine production, as well as on STAT1 expression and phosphorylation was not altered in any way by the knocking down SRC3.

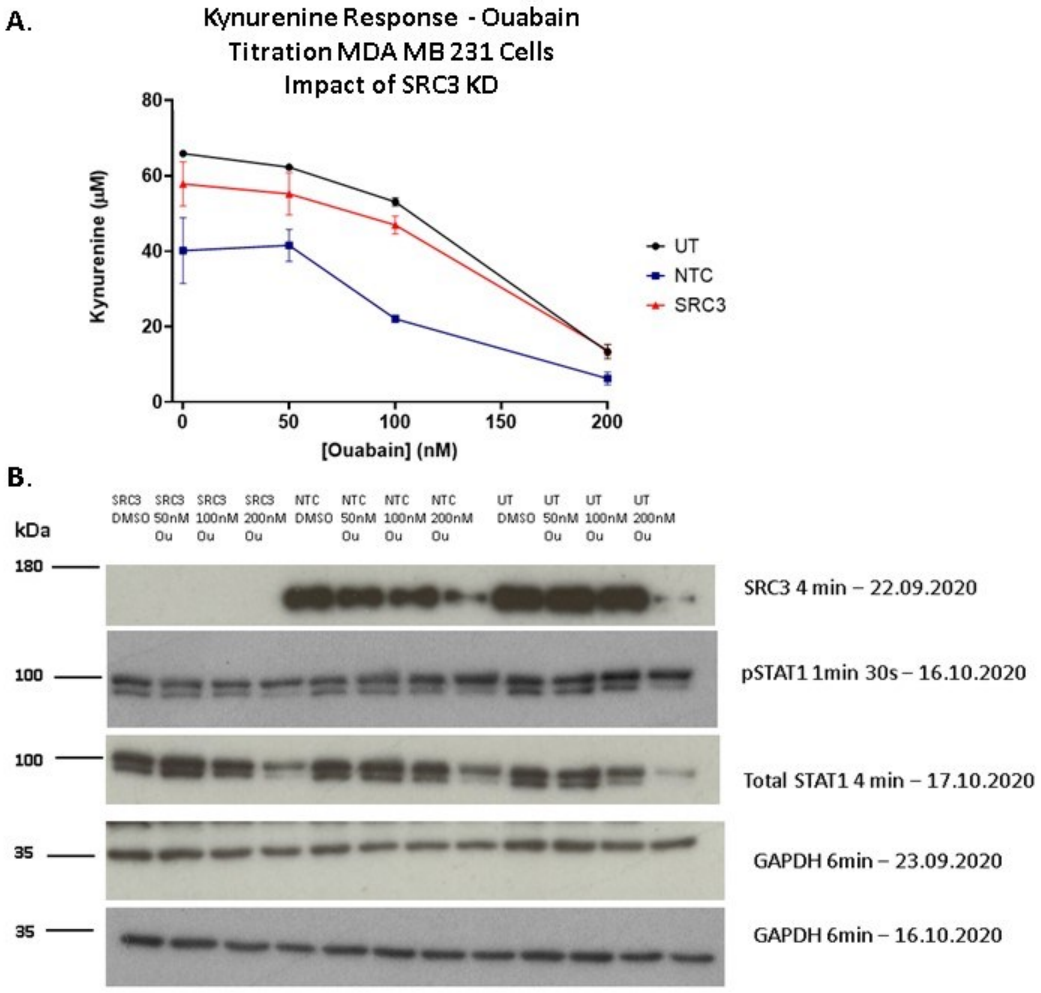

Appendix Figure 8. 2 The role of SRC3 in ouabain-mediated kynurenine production. A. Concentration-dependent kynurenine reduction in MDA MB 231 cells in the presence or absence of SRC3. B. Western blot confirmation of SRC3 knock down and IDO1 pathway protein expression profiles. Two GAPDH controls were included because the data came from 2 western blots: the SRC3 KD data is coupled with GAPDH 23.09.2020, while pSTAt1 and total STAT1 are coupled with GAPDH 16.10.2020. SRC3 – steroid hormone receptor 3, NTC – non-targeting control, Ou – ouabain, STAT1 – signal transducer activator of transcription 1, GAPDH – glyceraldehyde 3-phosphate dehydrogenase.

8.2.3. SBFI quality control

Given the limitations encountered when studying the mechanistic role of the ATP1A1 expression in IDO1 inhibition (Figure 3.8), it was decided to evaluate the effect altered ATP1A1 activity on IDO1. To do that the correlative relationship between the ouabain/digoxin/ ATP1A1-induced IDO1 inhibition and the increase in intracellular Na^+ levels was investigated.

To measure intracellular Na^+ levels the ratiometric dye SBFI-AM was used. A quality control experiment for SBFI-AM imaging was set up to investigate the behaviour of the dye at different emission wavelengths and to establish a protocol that allows accurate detection of the fluorescent signal upon excitation at both 340 and 380 nm. Appendix Figure 8. 3 summarizes the main findings. The recommended detection range for both 340 and 380 nm excitation is between 450 and 550 nm (Minta and Tsien, 1989) – highlighted in red; the blue box shows the noise region where the detection filter overlaps with the excitation wavelength .

Appendix Figure 8. 3A and B compare the emission spectra of unstained (blanks) MDA MB 231 cells (Appendix Figure 8. $3A_1$, B_1) Vs SBFI-treated samples (Appendix Figure 8. $3A_2$, B_2), revealing a visible increase in fluorescence intensity upon SBFI treatment with both excitation wavelengths, as well as a larger separation between the 340 and 380 signals in the SBFI-treated samples compared to the blanks. Appendix Figure 8. 3A and B show that regardless of the number of cells seeded per well the separation between the 340 and 380 nm signal occurs. However, the lower number of cells (30k) seems to give a stronger signal compared to the samples with a higher cell density (120k).

Appendix Figure 8. 3C compares the fluorescence signal in cells that have 0 mM intracellular Na^+ to that of cells that have an intracellular Na^+ concentration of 50 mM. The higher intracellular Na^+ concentration gives a much smaller separation between the 340 and 380

nm signals, thus giving a 340/380 ratio that is closer to 1. The samples with low intracellular Na^+ had a much larger separation of the signals at the two wave lengths thus giving a 340/380 ratio smaller than the samples with 50 mM intracellular Na^+.

Appendix Figure 8. 3D compares the blank corrected signals at 340 and 380 nm with 120 k cell/well (Appendix Figure 8. $3D_1$), 30 k cells/well (D_2) or 30 k cells/well 0 mM Na^+ Vs 50 mM Na^+ (Appendix Figure 8. $3D_3$). The bell-shaped curves in all three figures show that the strongest signal happens within the 500-550 nm window of interest. A stronger fluorescence intensity as well as a bigger separation is seen with 30 k cells/well (Appendix Figure 8. $3D_2$) compared to 120k cells/well (Appendix Figure 8. $3D_1$). Furthermore, Appendix Figure 8. $3D_3$ provides information about expected emission pattens of the dye at each excitation wavelength (340 and 380 nm), showing that the larger separation between the 340 and 380 signals with the higher Na^+ concentration is generated due to an increase in fluorescence intensity upon exciting at 340nm, while the signal at 380 nm excitation stays constant.

Appendix Figure 8. 3E shows the separation of the 340/380 fluorescence ratios for blank corrected values in all 4 samples. The highest signal is observed in the 50 mM Na^+ samples, followed by an overlap between the 120 k and 30 k cells/well (both with a similar intracellular Na^+ concentration ~12 mM) and lastly the cells with 0 mM Na^+.

In conclusion, the quality control experiment showed a clean fluorescence signal, specific for SBFI-treated samples and proportional to the intracellular Na^+ concentration within the 500 – 550 nm emission window, which was used for SBFI detection in all the experiments presented in this thesis. In terms of cell density, no difference was observed in the 340/380 ratios. However, a lower cell density was shown to give a stronger fluorescence signal. Therefore, for the majority of SBFI experiments cells were seeded at ~ 50k/well, unless otherwise stated in the figure legends.

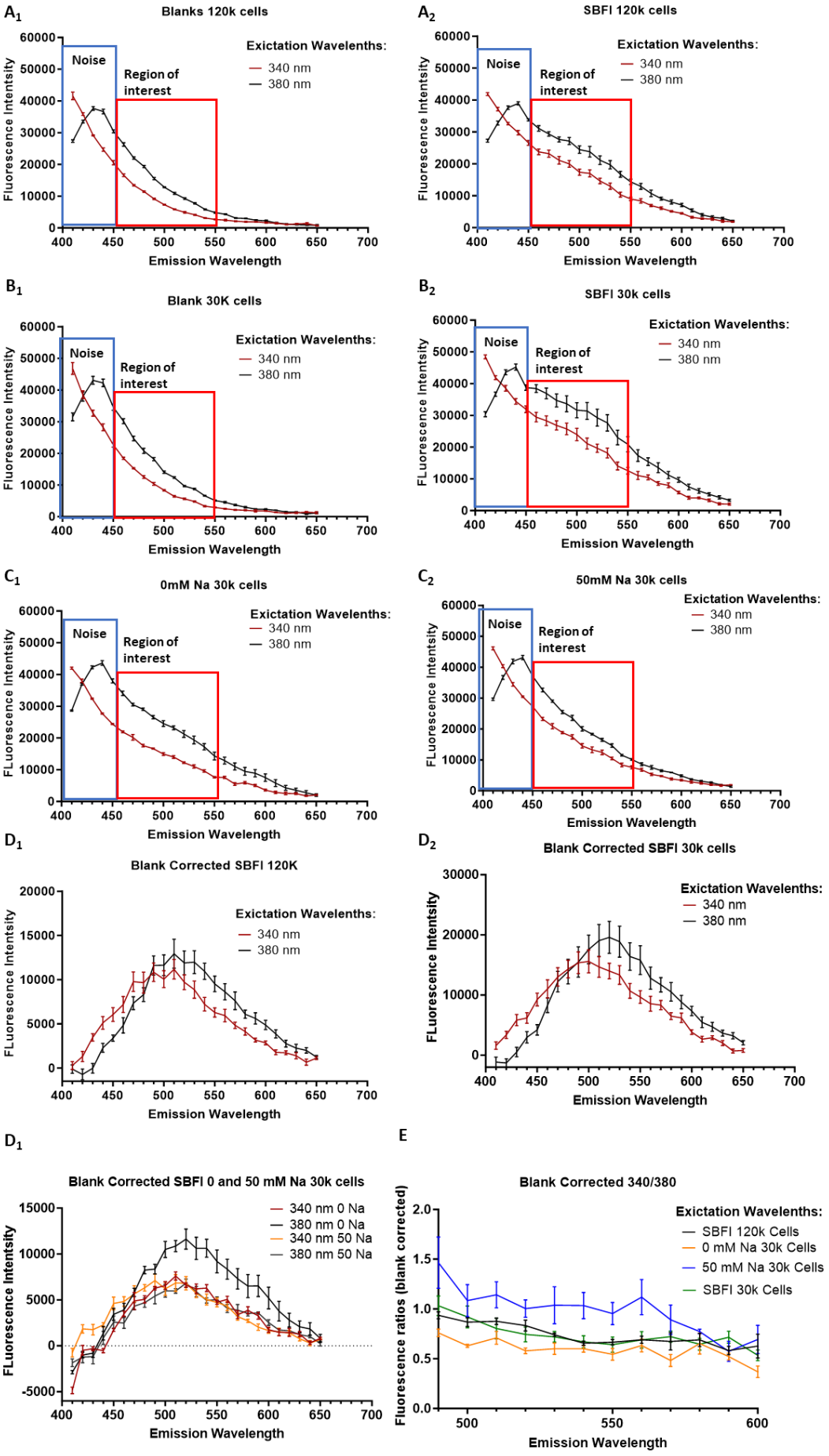
A1
Blanks 120k cells
Noise
Region of interest
Exictation Wavelenths:
340 nm
380 nm
Fluorescence Intentsity
Emission Wavelength
A2
SBFI 120k cells
B1
Blank 30K cells
B2
SBFI 30k cells
C1
0mM Na 30k cells
C2
50mM Na 30k cells
D1
Blank Corrected SBFI 120K
D2
Blank Corrected SBFI 30k cells
D1
Blank Corrected SBFI 0 and 50 mM Na 30k cells
340 nm 0 Na
380 nm 0 Na
340 nm 50 Na
380 nm 50 Na
E
Blank Corrected 340/380
Fluorescence ratios (blank corrected)
SBFI 120k Cells
0 mM Na 30k Cells
50 mM Na 30k Cells
SBFI 30k Cells

Appendix Figure 8. 3 SBFI-AM Staining in MDA MB 231 Cells – Quality Control. A. Emission spectra for 340 and 380 nm excitation for blanks with 120k cells/well (1), for SBFI-AM-treated samples with 120k cells/well (2); B. Emission spectra for 340 and 380 nm excitation for blanks with 30k cells/well (1), for SBFI-AM-treated samples with 30k cells/well (2); C. Emission spectra for 340 and 380 nm excitation for 30k cells/well with 0 mM intracellular Na^+ (1), for SBFI-AM-treated samples with 30k cells/well with 50 mM intracellular Na^+ (2); D. Emission spectra for blank corrected 340 and 380 nm signals with 120k cells/well (1), 30k cells/well (2), 30k cells/well with 0 mM intracellular Na^+ Vs 50 mM intracellular Na^+ (3); E. Comparison of blank corrected fluorescence 340/380 ratios for each sample within the region of interest. Cells were seeded at 0.3 x 10^6 (30k) or 1.2 x 10^6 (120k)/well in a 96-flat bottom plate and left to attach for 24 h. The SBFI staining was performed as described in the Methods section 2.11. Fluorescence was read sequentially at 340 and 380. Readings were taken at 3 timepoints. The figure above shows representative data corresponding to the second timepoint.

8.3. Chapter 5 Appendix

Appendix Table 8. 2 Summary of all compounds included in the drug screen and kynurenine fold change, Kynurenine SD variation and Viability fold change results.

COMPOUND NR - FOR THE FIRST ROUND OF SCREENING	COMPOUND NAME	KYN FOLD CHANGE DATA		KYNURENINE SD VARIATION DATA		VIABILITY	
MCE LIBRARY-DETAILED INFORMATION-HY-LD-000003245-1-MAR 30, 2022		Plate 1	Plate 2	Plate 1	Plate 2	Plate 1	Plate 2
1	Demethylzeylasteral	0,309523	0,278472	-12,8373	-2,05965	0,856914	0,715964
2	Tenuigenin	1,093808	0,810988	1,022751	-0,45987	1,0315	0,935398
3	20(S)-Ginsenoside Rg3	1,165651	0,771904	2,292373	-0,57729	1,034704	0,969034
4	Pedunculoside	1,207559	0,801217	3,032986	-0,48923	1,018687	0,914576
5	Ginsenoside F1	1,177624	1,084574	2,503977	0,362028	1,017085	0,94661
6	Ruscogenin	1,459009	1,182283	7,476664	0,655564	1,037907	0,985051
7	Sesamoside	1,009991	0,845186	-0,45847	-0,35714	0,978644	0,970635
8	Gentiopicroside	0,968083	0,8403	-1,19909	-0,37181	0,97544	0,986652
9	5,15-Diacetyl-3-benzoyllathyrol	1,039926	0,8403	0,070535	-0,37181	1,037907	1,023492

COMPOUND NR - FOR THE FIRST ROUND OF SCREENING	COMPOUND NAME	KYN FOLD CHANGE DATA		KYNURENINE SD VARIATION DATA		VIABILITY	
10	Dehydrocostus Lactone	0,453209	0,341983	-10,298	-1,86885	0,989856	0,876135
11	Phillyrin	0,980057	0,752362	-0,98748	-0,636	0,994661	0,961025
12	Harpagoside	1,033939	0,78656	-0,03527	-0,53326	0,996263	0,978644
13	Mogroside V	1,099795	0,835415	1,128553	-0,38649	1,004271	0,973839
14	Ginsenoside Rf	0,872292	0,62534	-2,89192	-1,01759	0,969034	0,959423
15	Scopolin	1,333284	1,109001	5,254825	0,435412	1,01228	1,017085
16	Pseudolaric Acid A	0,537025	0,361525	-8,81682	-1,81014	0,90977	0,757608
17	Ginsenoside Rh1	0,956109	0,747477	-1,41069	-0,65067	1,017085	0,981847
18	Ziyuglycoside I	0,938148	0,669309	-1,7281	-0,8855	0,994661	0,898558
19	Asiatic acid	0,962096	0,737706	-1,30489	-0,68003	1,020288	0,994661
20	Rosavin	1,021965	0,742591	-0,24687	-0,66535	1,005873	0,999466
21	Pseudoginsenoside RT5	1,015978	0,713278	-0,35267	-0,75341	0,97544	0,997864
22	Linderane	1,009991	0,874499	-0,45847	-0,26907	0,962627	1,007475
23	Loganic acid	1,117755	0,894041	1,445959	-0,21037	0,988254	1,010678

COMPOUND NR - FOR THE FIRST ROUND OF SCREENING	COMPOUND NAME	KYN FOLD CHANGE DATA		KYNURENINE SD VARIATION DATA		VIABILITY	
24	Morroniside	1,369205	1,065032	5,889636	0,303321	1,015483	1,013881
25	Isoescin IB	0,890253	0,713278	-2,57451	-0,75341	1,130806	1,026695
26	Lathyrol	0,866305	0,713278	-2,99772	-0,75341	1,241324	1,007475
27	Rosmarinic acid	1,033939	0,781675	-0,03527	-0,54793	1,206086	1,009076
28	Rebaudioside A	0,806436	0,767018	-4,05574	-0,59196	1,116391	0,991458
29	Costunolide	0,519065	0,429921	-9,13423	-1,60467	1,069941	0,986652
30	Rebaudioside C	1,171638	0,723049	2,398175	-0,72406	1,212493	0,919381
31	Deapioplatycodin D	0,734593	0,552058	-5,32536	-1,23774	0,951415	0,908169
32	Gracillin	0,213733	0,190533	-14,5301	-2,32383	0,134544	0,020822
33	Triptophenolide	0,932161	0,698622	-1,8339	-0,79744	0,954618	0,964229
34	Jujuboside B	1,105782	0,78656	1,234355	-0,53326	1,00267	1,037907
35	Specnuezhenide	1,051899	0,757248	0,282138	-0,62132	0,985051	1,02189
36	Columbin	1,021965	0,742591	-0,24687	-0,66535	0,997864	0,985051
37	Shanzhiside methyl ester	1,111768	0,88427	1,340157	-0,23972	1,004271	1,009076

COMPOUND NR - FOR THE FIRST ROUND OF SCREENING	COMPOUND NAME	KYN FOLD CHANGE DATA		KYNURENINE SD VARIATION DATA		VIABILITY	
38	(-)-α-Pinene	1,315323	1,113887	4,937419	0,450089	1,029899	0,980246
39	(R)-(+)-Citronellal	1,47697	1,397244	7,794069	1,301344	1,049119	1,098772
40	Pectolinarin	1,051899	0,762133	0,282138	-0,60664	1,013881	0,651895
41	10-Deacetylbaccatin III	0,974077	0,723049	-1,09329	-0,72406	1,010678	0,986652
42	Cephalomannine	0,309523	0,224732	-12,8373	-2,22109	0,788041	0,687133
43	Atractylenolide I	0,998017	0,708393	-0,67008	-0,76809	1,00267	0,962627
44	Saikosaponin D	0,746567	0,459234	-5,11376	-1,5166	0,953017	0,89055
45	Andrographolide	0,638803	0,429921	-7,01819	-1,60467	0,993059	0,967432
46	Ginsenoside Rb1	1,153677	1,001521	2,080771	0,112522	1,020288	1,020288
47	(+)-Camphor	1,159664	0,801217	2,186571	-0,48923	0,989856	1,01228
48	Hederacoside C	1,375192	1,118772	5,995438	0,464766	1,029899	1,063534
49	18α-Glycyrrhetinic acid	1,045913	0,8403	0,176336	-0,37181	0,980246	1,13401
50	Bilobalide	0,752554	0,796331	-5,00795	-0,5039	0,999466	1,020288

COMPOUND NR - FOR THE FIRST ROUND OF SCREENING	COMPOUND NAME	KYN FOLD CHANGE DATA		KYNURENINE SD VARIATION DATA		VIABILITY	
51	Brusatol	0,117942	0,117251	-16,2229	-2,54398	0,456487	0,408436
52	Ursolic acid	1,039926	0,742591	0,070535	-0,66535	0,983449	0,962627
53	Limonin	1,069866	0,649767	0,599544	-0,94421	0,986652	0,977042
54	Ginsenoside Rg1	0,938148	0,62534	-1,7281	-1,01759	0,993059	0,957822
55	Patchouli alcohol	1,081834	0,99175	0,811147	0,083169	0,985051	1,00267
56	Pulchinenoside C	1,159664	0,898926	2,186571	-0,19569	0,999466	0,994661
57	Arglabin	0,794462	0,850071	-4,26734	-0,34246	0,980246	1,037907
58	Hinokitiol	0,441235	0,405494	-10,5096	-1,67805	0,97544	0,973839
59	(-)-Cedrene	0,962096	0,771904	-1,30489	-0,57729	1,045916	0,957822
60	Triptonide	0,231693	0,20519	-14,2127	-2,2798	0,685531	0,587827
61	Dipsacoside B	1,087821	0,635111	0,916949	-0,98824	1,005873	0,94661
62	Atractylenolide II	1,093808	1,035719	1,022751	0,215261	1,013881	1,039509
63	(S)-(-)-Citronellal	1,267428	1,006406	4,091005	0,127199	1,001068	1,071543
64	Oridonin	0,768708	0,691566	-1,6877	-0,81655	0,928819	0,904514

COMPOUND NR - FOR THE FIRST ROUND OF SCREENING	COMPOUND NAME	KYN FOLD CHANGE DATA		KYNURENINE SD VARIATION DATA		VIABILITY	
65	Saikosaponin C	1,260209	1,009686	1,702765	0,063793	0,972222	0,883681
66	(-)-Menthol	1,181569	0,795301	1,160291	-0,52948	0,845486	0,953125
67	Forskolin	1,548556	1,189493	3,691836	0,561376	0,840278	0,729167
68	Dihydroartemisinin	0,585214	0,857542	-2,95347	-0,35724	0,892361	0,953125
69	(S)-(−)-Perillyl alcohol	1,011182	1,3693	-0,01507	1,058959	0,970486	0,998264
70	(R)-Citronellol	0,749048	0,899036	-1,82332	-0,24241	1,029514	1,027778
71	Betulinic acid	0,984968	0,912867	-0,19589	-0,20414	0,961806	1,024306
72	cis-Isolimonenol	0,893221	0,73306	-0,82878	-0,70172	0,958333	0,986111
73	β-Elemene	0,880115	0,719228	-0,91919	-0,74	0,888889	0,989583
74	Ammonium glycyrrhizinate	0,945648	0,656988	-0,46713	-0,91224	0,928819	0,975694
75	Eleutheroside E	0,834241	0,73306	-1,23563	-0,70172	0,923611	0,970486
76	Ginsenoside Rc	0,775261	0,712313	-1,64249	-0,75913	0,946181	0,953125
77	Saikosaponin B1	0,676961	0,988939	-2,32058	-0,00637	0,967014	1,060764
78	α-Thujone	0,801475	1,092674	-1,46167	-0,29344	1,005208	1,086806
79	Carvacrol	0,880115	0,829879	-0,91919	-0,43379	1,032986	1,083333

COMPOUND NR - FOR THE FIRST ROUND OF SCREENING	COMPOUND NAME	KYN FOLD CHANGE DATA		KYNURENINE SD VARIATION DATA		VIABILITY	
80	Transcrocetin meglumine salt	0,781814	0,691566	-1,59728	-0,81655	0,993056	1,046875
81	Cynaropicrin	0,10682	0,027663	-6,25352	-2,65378	0,803819	0,576389
82	β-Phellandrene	0,958755	0,705397	-0,37672	-0,77827	0,963542	1,017361
83	Dehydroabietic acid	0,873561	0,553253	-0,9644	-1,1993	1,013889	1,001736
84	Mogroside IV-A	0,880115	0,698481	-0,91919	-0,79741	0,984375	1,001736
85	Soyasapogenol B	0,762154	0,726144	-1,7329	-0,72086	1,010417	1,036458
86	Panaxadiol	0,781814	0,656988	-1,59728	-0,91224	1,029514	1,048611
87	Pseudolaric Acid C2	0,716281	0,739975	-2,04935	-0,68258	1,024306	1,010417
88	Asiaticoside B	0,755601	0,802216	-1,77811	-0,51034	0,998264	1,024306
89	Bacopaside II	0,349293	0,262795	-4,58089	-2,00309	0,637153	0,546875
90	Mogroside II-A	0,749048	0,636241	-1,82332	-0,96965	0,998264	1,095486
91	Deoxyelephantopin	0,074053	0,15906	-6,47955	-2,29016	0,739583	0,796875
92	Platycodin D2	0,270653	0,331952	-5,12336	-1,81171	0,751736	0,760417
93	3-Epiursolic Acid	0,591767	0,705397	-2,90826	-0,77827	0,991319	1,055556
94	α-Terpineol	0,899775	0,89212	-0,78357	-0,26155	0,980903	1,064236

COMPOUND NR - FOR THE FIRST ROUND OF SCREENING	COMPOUND NAME	KYN FOLD CHANGE DATA		KYNURENINE SD VARIATION DATA		VIABILITY	
95	Amarogentin	0,860455	0,871373	-1,05481	-0,31896	0,980903	1,032986
96	Bacoside A3	0,749048	0,594747	-1,82332	-1,08448	0,920139	0,96875
97	Ursolic acid acetate	0,808028	0,73306	-1,41646	-0,70172	1,008681	1,208333
98	(E)-β-Farnesene	0,912881	0,532506	-0,69316	-1,25672	0,967014	0,987847
99	Xanthatin	0,100266	0,15906	-6,29872	-2,29016	0,786458	0,532986
100	Ilexsaponin A	0,873561	0,89212	-0,9644	-0,26155	1,027778	1,005208
101	Calenduloside E	0,899775	1,023517	-0,78357	-0,10206	1,032986	1,109375
102	Momordin Ic	0,827688	1,106505	-1,28084	-0,331722	1,053819	1,086806
103	Astragaloside III	0,834241	0,809132	-1,23563	-0,4912	0,979167	1,076389
104	Cyclogalegenin	0,899775	0,809132	-0,78357	-0,4912	0,96875	1,029514
105	Harpagide	0,794921	0,698481	-1,50687	-0,79741	1,034722	1,012153
106	Diosbulbin B	0,873561	0,68465	-0,9644	-0,83568	0,946181	0,612847
107	Alismoxide	0,834241	0,594747	-1,23563	-1,08448	1,020833	0,994792
108	Isoescin IA	0,860455	0,698481	-1,05481	-0,79741	1,005208	0,996528
109	Dehydroandrographolide	0,794921	0,712313	-1,50687	-0,75913	0,961806	1,006944

COMPOUND NR - FOR THE FIRST ROUND OF SCREENING	COMPOUND NAME	KYN FOLD CHANGE DATA		KYNURENINE SD VARIATION DATA		VIABILITY	
110	Rubusoside	0,834241	0,926698	-1,23563	-0,16586	1,053819	1,081597
111	Stevioside	0,860455	1,058096	-1,05481	0,197757	1,06 25	1,041667
112	Linderalactone	0,827688	0,802216	-1,28084	-0,51034	0,998264	0,998264
113	Barlerin	0,958755	0,809132	-0,37672	-0,4912	1,024306	0,996528
114	Madecassoside	0,886668	0,746891	-0,87399	-0,66344	1,059028	1
115	Astragaloside IV	0,925988	0,829879	-0,60275	-0,43379	1,038194	1,069444
116	Isoalantolactone	0,309973	0,200554	-4,85213	-2,17533	1,008681	0,892361
117	Sweroside	0,952202	0,712313	-0,42192	-0,75913	1,039931	0,951389
118	Aucubin	0,840795	0,899036	-1,19043	-0,24241	1,027778	1
119	Loganin	0,893221	1,154915	-0,82878	-0,465687	1,020833	1,078125
120	Astragaloside I	0,945648	1,182578	-0,46713	-0,542238	1,111111	1,060764
121	Orientin	0,847348	0,988939	-1,14522	-0,006379	0,970486	0,873264
122	Linalool	0,801475	0,809132	-1,46167	-0,4912	0,96875	0,892361
123	Eupalinolide B	0,2641	0,255879	-5,16857	-2,02223	0,939236	0,859375
124	Crocin II	0,998075	0,816048	-0,10548	-0,47207	1,050347	0,923611

COMPOUND NR - FOR THE FIRST ROUND OF SCREENING	COMPOUND NAME	KYN FOLD CHANGE DATA		KYNURENINE SD VARIATION DATA		VIABILITY	
125	Cucurbitacin E	0,1658	0,214385	-5,84666	-2,13706	0,519097	0,520833
126	Alisol B 23-acetate	1,096375	1,438457	0,572611	1,250337	1,078125	1,029514
127	Artemether	0,414419	0,514534	-4,96309	-4,81495	0,866856	0,967293
128	Esculentoside A	0,959329	1,023776	0,088627	-0,23778	0,860675	0,982745
129	Pseudoginsenoside F11	1,174426	1,301545	2,082727	2,258866	0,871491	0,890033
130	Valepotriate	0,292531	0,349195	-6,09308	-6,30105	0,205511	0,165336
131	Pseudolaric Acid C	1,267634	1,195728	2,946837	1,307764	0,860675	0,993562
132	Ginkgolide B	1,203105	1,156047	2,348607	0,951101	0,818954	0,9812
133	Oxypaeoniflorin	0,973669	0,858438	0,221567	-1,72387	1,103271	1,005923
134	Retinyl acetate	0,694044	0,812143	-2,37076	-2,13998	0,954932	0,94257
135	Maslinic acid	0,794422	0,957641	-1,44018	-0,83221	0,93948	0,98429
136	Curdione	0,973669	1,056844	0,221567	0,059444	0,936389	0,914757
137	Asiaticoside	0,973669	0,726167	0,221567	-2,91275	0,760237	0,902395
138	Pachymic acid	0,93782	0,805529	-0,11078	-2,19942	0,791141	0,933299
139	Alisol B	1,031028	1,03039	0,753327	-0,17833	0,771053	0,959567

COMPOUND NR - FOR THE FIRST ROUND OF SCREENING	COMPOUND NAME	KYN FOLD CHANGE DATA		KYNURENINE SD VARIATION DATA		VIABILITY	
140	Notoginsenoside R1	1,031028	0,977481	0,753327	-0,65388	0,86222	0,954932
141	Liriope muscaribaily saponins C	1,152916	1,25525	1,883317	1,842759	0,976565	1,086273
142	Nomilin	0,880461	1,003936	-0,64254	-0,41611	1,047644	1,015194
143	alpha-Boswellic acid	0,93065	0,891505	-0,17725	-1,42665	0,945661	0,961113
144	Neoandrographolide	0,90197	0,884892	-0,44313	-1,4861	0,928663	0,976565
145	Panaxatriol	0,794422	0,898119	-1,44018	-1,36721	0,908576	0,944115
146	Ginsenoside Rh2	0,973669	0,706326	0,221567	-3,09108	0,873036	0,94257
147	8-O-Acetylharpagide	0,959329	0,851824	0,088627	-1,78331	0,852949	0,947206
148	Ginsenoside Rh3	0,837441	0,878278	-1,04136	-1,54554	0,815864	0,967293
149	Ginsenoside Ro	0,980839	1,109752	0,288037	0,534994	0,863765	0,992016
150	Ginsenoside Rg2	0,93065	1,017163	-0,17725	-0,29722	0,94257	1,077002
151	Picroside I	0,887631	0,957641	-0,57607	-0,83221	0,967293	0,961113
152	Ginkgolide J	0,858951	0,891505	-0,84195	-1,42665	0,951841	0,971929
153	Rebaudioside D	0,988009	0,997322	0,354507	-0,47555	0,90394	0,958022

COMPOUND NR - FOR THE FIRST ROUND OF SCREENING	COMPOUND NAME	KYN FOLD CHANGE DATA		KYNURENINE SD VARIATION DATA		VIABILITY	
154	Cucurbitacin B	0,120454	0,256605	-7,68836	-7,13326	0,438836	0,352305
155	Madecassic acid	0,772913	0,904733	-1,63959	-1,30776	0,800412	0,998197
156	Tenuifolin	0,93782	1,017163	-0,11078	-0,29722	0,917847	1,005923
157	Astragaloside II	0,90197	0,924573	-0,44313	-1,12943	0,990471	0,954932
158	Ziyuglycoside II	0,651025	0,640191	-2,76958	-3,68552	0,924028	0,944115
159	Ginkgolide C	1,009519	0,884892	0,553917	-1,4861	0,975019	0,965748
160	Escin IB	0,808762	0,792302	-1,30724	-2,31831	0,899305	0,930209
161	Ecliptasaponin A	0,988009	0,772462	0,354507	-2,49664	0,896214	0,882307
162	Genipin 1-β-D-gentiobioside	0,887631	0,547601	-0,57607	-4,51773	0,839042	0,85913
163	Ganoderic acid A	0,90914	0,805529	-0,37666	-2,19942	0,837497	0,941025
164	Nootkatone	0,880461	0,984095	-0,64254	-0,59444	0,934844	0,931754
165	Wilforgine	0,980839	1,089912	0,288037	0,356663	0,917847	1,115632
166	Araloside VII	0,91631	0,73278	-0,31019	-2,8533	0,922483	0,959567
167	Scabertopin	0,120454	0,243378	-7,68836	-7,25215	0,888488	0,857584
168	Tracheloside	0,90197	0,746008	-0,44313	-2,73442	0,879217	0,886943

COMPOUND NR - FOR THE FIRST ROUND OF SCREENING	COMPOUND NAME	KYN FOLD CHANGE DATA		KYNURENINE SD VARIATION DATA		VIABILITY	
169	Lupenone	1,009519	0,785689	0,553917	-2,37775	0,98429	0,973474
170	Rebaudioside M	0,830272	0,653418	-1,10783	-3,56663	0,947206	0,930209
171	Ingenol	0,815932	0,693099	-1,24077	-3,20997	0,880762	0,893124
172	Ganoderic acid D	0,94499	0,792302	-0,04431	-2,31831	0,890033	0,941025
173	Ginsenoside Rg5	0,794422	0,957641	-1,44018	0,83221	0,883853	0,928663
174	Isosteviol	0,959329	1,037003	0,088627	-0,11889	0,956477	1,075457
175	Atractyloside (potassium salt)	0,959329	0,931187	0,088627	-1,06999	0,672161	0,922483
176	Pulsatilla saponin D	0,091774	0,19047	-7,95424	-7,7277	0,148339	0,142158
177	(20R)-Ginsenoside Rh1	0,90914	0,865051	-0,37666	-1,66443	0,964203	0,958022
178	Betulonic acid	0,837441	0,73278	-1,04136	-2,8533	0,812774	0,85913
179	Bisabolangelone	0,794422	0,626964	-1,44018	-3,80441	0,905485	0,908576
180	Euscaphic acid	0,90914	0,699713	-0,37666	-3,15052	0,919392	0,947206
181	Euphorbia Factor L1	1,117067	1,103139	1,550967	0,475551	0,877672	0,941025
182	Euphorbia Factor L2	0,392909	0,607123	-5,1625	-3,98274	0,877672	0,815864

COMPOUND NR - FOR THE FIRST ROUND OF SCREENING	COMPOUND NAME	KYN FOLD CHANGE DATA		KYNURENINE SD VARIATION DATA		VIABILITY	
183	Farnesol	0,801592	1,076685	-1,37371	0,237775	0,950296	1,038372
184	2,2'-Anhydrouridine	0,988009	0,858438	0,354507	-1,72387	0,880762	0,931754
185	(1R)-α-Pinene	0,701214	0,878278	-2,30429	-1,54554	0,874582	0,988926
186	Citral	0,91631	0,812143	-0,31019	-2,13998	0,908576	0,934844
187	Mogroside I A1	0,772913	1,070071	-1,63959	0,178331	0,832861	0,928663
188	Glycochenodeoxycholic acid (sodium salt)	0,858951	1,05023	-0,84195	0	0,897759	1,013649
189	Isoastragaloside IV	0,995179	1,46027	0,420977	3,685517	0,86531	0,982745
190	Cauloside D	1,093784	1,360151	1,309307	9,333333	1,055606	0,938924
191	Mogroside IV	0,950199	1,281364	0,567367	5,666667	1,075661	0,917046
192	Ginkgolide K	0,781275	1,195414	-0,30551	1,666667	1,101185	0,891522
193	Mogroside I E1	0,730597	1,231227	-0,56737	3,333333	1,015497	0,796718
194	Steviolbioside	0,739043	1,360151	-0,52372	9,333333	1,041021	0,767548
195	Rosamultin	0,907968	1,281364	0,349149	5,666667	1,055606	0,946217
196	Acanthopanaxoside B	0,891075	1,12379	0,261861	-1,66667	1,093892	1,095716

COMPOUND NR - FOR THE FIRST ROUND OF SCREENING	COMPOUND NAME	KYN FOLD CHANGE DATA		KYNURENINE SD VARIATION DATA		VIABILITY	
197	Ergolide	0,156255	0,335919	-3,53513	-38,3333	1,042844	0,940747
198	Incensole Acetate	0,815059	1,06649	-0,13093	-4,33333	1,117593	1,103008
199	Citronellol	0,50255	1,102302	-1,74574	-2,66667	1,110301	0,999088
200	Carboxyatractyloside (dipotassium)	0,519442	1,130952	-1,65846	-1,33333	1,08113	0,980857
201	Geraniol	0,544781	0,980541	-1,52753	-8,33333	1,059253	0,966272
202	Cafestol	0,468765	1,030678	-1,92032	-6	1,077484	0,98268
203	Mogroside III-E	0,781275	1,209739	-0,30551	-2,33333	1,066545	1,084777
204	Gymnemic acid I	1,507649	1,345826	-3,44784	-8,66666	1,108478	1,084777
205	Zingibroside R1	0,958645	1,166764	-0,61101	-0,33333	1,299909	1,082954
206	Arnicolide D	0,105578	0,199833	-3,79699	-44,6667	0,840474	0,727438
207	(-)-Limonene	0,789721	1,080815	-0,26186	-3,66667	1,12124	1,072015
208	Carveol	0,536334	1,06649	-1,57117	-4,33333	1,123063	1,008204
209	Cimigenol	0,561673	0,994865	-1,44024	-7,66667	1,072015	0,979034
210	Ganoderenic acid A	0,595458	1,03784	-1,26566	-5,66667	1,08113	0,984503

COMPOUND NR - FOR THE FIRST ROUND OF SCREENING	COMPOUND NAME	KYN FOLD CHANGE DATA		KYNURENINE SD VARIATION DATA		VIABILITY	
211	Polyporenic acid C	0,663028	1,03784	-0,91652	-5,66667	1,020966	0,986326
212	γ-Terpinene	0,375856	1,12379	-2,4004	-1,66667	1,092069	1,041021
213	Verbenone	1,338725	1,159602	2,574971	9,04E-15	1,126709	1,128532
214	Britannin	0,215378	0,321594	-3,22962	-39	1,041021	0,980857
215	Terpinen-4-ol	0,865737	1,102302	0,130931	-2,66667	1,123063	1,117593
216	Abietic acid	0,646135	0,959053	-1,0038	-9,33333	1,101185	1,066545
217	Perillyl alcohol	0,815059	0,994865	-0,13093	-7,66667	1,039198	1,033728
218	26-Deoxyactein	0,755936	1,06649	-0,43644	-4,33333	0,975387	0,986326
219	Saikosaponin B4	0,772828	1,073652	-0,34915	-4	1,143118	1,106655
220	Mogroside IIA1	0,975537	1,159602	0,698297	9,04E-15	1,325433	1,108478
221	Paederoside	0,85729	1,016353	0,087287	-6,66667	1,117593	1,15588
222	8-Epidiosbulbin E acetate	0,983984	1,130952	0,741941	-1,33333	1,130356	1,134002
223	(-)-Fenchone	0,865737	1,045003	0,130931	-5,33333	1,126709	1,11577
224	Guaiazulene	0,764382	1,06649	-0,39279	-4,33333	1,0866	1,104831
225	Beta-Eudesmol	0,806613	1,002028	-0,17457	-7,33333	1,072015	1,082954

COMPOUND NR - FOR THE FIRST ROUND OF SCREENING	COMPOUND NAME	KYN FOLD CHANGE DATA		KYNURENINE SD VARIATION DATA		VIABILITY	
226	β-Elemonic acid	1,161354	1,159602	1,658456	9,04E-15	1,050137	1,002735
227	Levomenol	1,203585	1,12379	1,876674	-1,66667	1,059253	0,293528
228	Hederacolchiside A1	0,291394	0,500656	-2,83683	-30,6667	0,229717	0,211486
229	Polygalacin D	0,342072	0,421869	-2,57497	-34,3333	0,856882	0,785779
230	Formosanin C	0,071793	0,178345	-3,97157	-45,6667	0	-0,01094
231	Phytol	1,000876	1,12379	0,829228	-1,66667	1,15588	1,113947
232	Erythrodiol	0,739043	0,944728	-0,52372	-10	1,103008	1,059253
233	Agnuside	0,74749	0,980541	-0,48008	-8,33333	1,112124	1,057429
234	Fenchyl alcohol	0,595458	1,03784	-1,26566	-5,66667	1,062899	1,004558
235	Mogroside IIe	0,730597	1,138115	-0,56737	-1	1,04649	0,920693
236	Pseudolaric Acid B	0,451872	0,787154	-2,0076	-17,3333	0,922516	0,873291
237	Carabrone	0,409641	0,822966	-2,22582	-15,6667	1,077484	0,915223
238	Notoginsenoside Fa	0,967091	1,145277	0,654654	-0,66667	1,314494	1,104831
239	Paederosidic acid	1,017768	1,116627	0,916515	-2	1,135825	1,152233

COMPOUND NR - FOR THE FIRST ROUND OF SCREENING	COMPOUND NAME	KYN FOLD CHANGE DATA		KYNURENINE SD VARIATION DATA		VIABILITY	
240	Ganoderic acid G	0,857 29	1,08 7977	0,08728 7	- 3,33333	1,13 9471	1,05 7429
241	20(R)-Ginsenoside Rh2	0,806 613	1,10 9465	- 0,17457	- 2,33333	1,11 577	1,04 2844
242	(-)-α-Terpineol	0,671 474	1,00 919	- 0,87287	-7	1,11 2124	1,02 6436
243	Ponicidin	0,299 841	0,50 7818	- 2,79319	- 30,3333	1,04 8314	0,75 1139
244	Picfeltarraenin IB	0,612 35	0,93 0403	- 1,17838	- 10,6667	1,06 6545	0,97 1741
245	Steviol	0,696 812	1,23 1227	- 0,74194	3,33333 3	1,10 6655	1,08 66
246	Uvaol	0,764 382	1,19 5414	- 0,39279	1,66666 7	1,13 4002	0,92 9809
247	Platycodin D	0,308 287	0,40 0381	- 2,74955	- 35,3333	0,76 0255	0,45 7612
248	Kinsenoside	0,772 828	1,25 2714	- 0,34915	4,33333 3	1,09 9362	0,84 2297
249	Handelin	0,494 103	0,92 3241	- 1,78939	-11	1,03 7375	0,62 3519
250	Gypsogenin-3-O-glucuronide	0,570 119	1,23 1227	- 1,39659	3,33333 3	1,17 5934	0,70 1914
251	Artemisic acid	0,494 103	0,69 4042	- 1,78939	- 21,6667	1,03 9198	0,61 6226
252	Catalpol	0,291 394	1,11 6627	- 2,83683	-2	1,09 7539	0,69 4622
253	Micheliolide	0,669 209	0,51 3229	- 2,71142	- 1,44105	0,85 9451	0,94 8304

COMPOUND NR - FOR THE FIRST ROUND OF SCREENING	COMPOUND NAME	KYN FOLD CHANGE DATA		KYNURENINE SD VARIATION DATA		VIABILITY	
254	Podocarpic acid	0,939096	0,764908	-0,93205	-0,54842	0,896607	0,995153
255	Cucurbitacin IIb	1,016206	0,636601	-0,42366	-1,00348	0,928918	0,957997
256	Tubeimoside I	0,520496	0,493489	-3,69189	-1,51106	0,689822	0,807754
257	Ingenol-5,20-acetonide	1,071285	0,991913	-0,06052	-0,256705	0,901454	0,924071
258	Clinodiside A	1,175935	0,893215	0,629437	-0,09335	0,898223	0,938611
259	7beta-Hydroxylathyrol	0,92808	0,730364	-1,00468	-0,67093	1,003231	0,995153
260	Asperuloside	0,933588	0,715559	-0,96836	-0,72344	0,961228	0,957997
261	Hastatoside	0,884017	0,710624	-1,29519	-0,74094	0,969305	0,993538
262	(20R)-Protopanaxadiol	0,889525	0,69582	-1,25887	-0,79345	0,957997	0,948304
263	Ingenol-5,20-acetonide-3-O-angelate	0,839954	0,636601	-1,5857	-1,00348	0,964459	0,946688
264	Gibberellic acid	0,878509	0,720494	-1,3315	-0,70594	0,959612	0,941842
265	Tubeimoside II	0,212054	0,207265	-5,72545	-2,52621	0,382876	0,390953
266	Macranthoidin A	1,065777	1,085676	-0,09684	-0,589254	0,909532	0,893376

COMPOUND NR - FOR THE FIRST ROUND OF SCREENING	COMPOUND NAME	KYN FOLD CHANGE DATA		KYNURENINE SD VARIATION DATA		VIABILITY	
267	Buddlejasaponin IVb	1,286093	1,386705	1,35571	1,656913	1,021002	1,116317
268	Polygalasaponin V	0,85097	0,755039	-1,51307	-0,58342	1,011309	0,972536
269	Glaucocalyxin A	0,129435	0,088828	-6,27016	-2,94627	0,886914	0,77706
270	Pristimerin	0,079864	0,083893	-6,59698	-2,96377	-0,03231	-0,042
271	Macranthoidin B	0,917064	0,656341	-1,07731	-0,93347	0,988691	0,990307
272	Raddeanin A	0,123928	0,108568	-6,30647	-2,87626	0,04685	0
273	Ganoderic acid B	0,900541	0,646471	-1,18625	-0,96848	0,972536	0,927302
274	Swertiamarin	1,010698	0,814257	-0,45997	-0,37339	0,961228	0,951535
275	Benzoylpaeoniflorin	0,972143	0,814257	-0,71417	-0,37339	0,980614	0,932149
276	Araloside A	1,302617	1,322551	1,464651	1,42938	1,071082	1,025848
277	Chikusetsusaponin Iva	0,889525	0,68595	-1,25887	-0,82846	0,978998	0,993538
278	Parishin	0,884017	0,700755	-1,29519	-0,77595	1,022617	0,946688
279	Furanodienone	0,85097	0,66621	-1,51307	-0,89847	0,995153	0,903069
280	Mogrol	1,010698	0,799453	-0,45997	-0,4259	0,975767	0,903069

COMPOUND NR - FOR THE FIRST ROUND OF SCREENING	COMPOUND NAME	KYN FOLD CHANGE DATA		KYNURENINE SD VARIATION DATA		VIABILITY	
281	11-Keto-beta-boswellic acid	1,027222	0,853736	-0,35103	-0,23337	0,957997	0,940226
282	14-Deoxy-11,12-didehydroandrographolide	0,988667	0,853736	-0,60523	-0,23337	0,890145	0,82391
283	Picfeltarraenin IA	0,977651	0,824127	-0,67785	-0,33838	0,982229	0,995153
284	Nerolidol	0,939096	0,656341	-0,93205	-0,93347	1,038772	0,977383
285	Ginsenoside Rg6	0,873001	0,735299	-1,36781	-0,65343	1,009693	1,017771
286	β-Caryophyllene	0,977651	0,710624	-0,67785	-0,74094	0,996769	0,987076
287	Camphor	0,983159	0,681015	-0,64154	-0,84596	0,988691	0,966074
288	Isoastragaloside I	0,966635	0,883346	-0,75048	-0,12835	0,987076	0,978998
289	Alisol C 23-acetate	0,972143	1,006718	-0,71417	-0,30921 3	0,969305	0,980614
290	AKBA	1,104333	1,016588	-0,15735 9	-0,34421 8	1,050081	1,006462
291	Notoginsenoside R2	1,324648	1,14983	-1,60990 5	-0,81678 8	1,016155	1,059774
292	Pleuromutilin	0,92808	0,794518	-1,00468	-0,4434	0,969305	1,050081
293	Pseudoginsenoside RT1	1,087809	0,888281	-0,04841 8	-0,11085	0,977383	0,974152
294	Shionone	0,856477	0,69582	-1,47676	-0,79345	1,022617	1,017771

COMPOUND NR - FOR THE FIRST ROUND OF SCREENING	COMPOUND NAME	KYN FOLD CHANGE DATA		KYNURENINE SD VARIATION DATA		VIABILITY	
295	Bevirimat	0,884017	0,671145	-1,29519	-0,88096	1,022617	1,012924
296	Kaurenoic acid	0,966635	0,789583	-0,75048	-0,4609	1,001616	1,011309
297	Phorbol	0,900541	0,903085	-1,18625	-0,05834	0,949919	0,974152
298	Isoastragaloside II	0,988667	0,947499	-0,60523	0,099181	0,998384	0,982229
299	Quillaic acid	1,126364	1,100481	0,302614	0,641762	1,022617	1,001616
300	Tussilagone	1,021714	1,021523	-0,38735	0,361721	0,982229	1,030695
301	20-Deoxyingenol	0,53702	0,68595	-3,58295	-0,82846	1,072698	1,063005
302	Ginsenoside Rk3	0,889525	0,730364	-1,25887	-0,67093	0,93538	0,98546
303	Esculentoside H	0,895033	0,755039	-1,22256	-0,58342	0,95315	1,01454
304	Verbenalin	0,922572	0,745169	-1,04099	-0,61843	0,915994	0,990307
305	Ambroxide	0,983159	0,799453	-0,64154	-0,4259	0,927302	1,001616
306	Euphorbiasteroid	0,983159	1,011653	-0,64154	0,326715	0,938611	1,022617
307	Acevaltrate	0,179007	0,162851	-5,94333	-2,68373	0,441034	0,50727
308	Methyl deacetylasperulosidate	1,076793	1,218918	-0,02421	1,061825	0,896607	1,016155

COMPOUND NR - FOR THE FIRST ROUND OF SCREENING	COMPOUND NAME	KYN FOLD CHANGE DATA		KYNURENINE SD VARIATION DATA		VIABILITY	
309	Oleanonic acid	1,137 38	1,13 5025	0,37524 1	0,76428 1	0,93 538	0,97 8998
310	Ginsenoside C-K	1,010 698	0,81 4257	- 0,45997	- 0,37339	0,95 7997	0,98 0614
311	Cucurbitacin D	0,267 133	0,38 4922	- 5,36232	- 1,89612	0,53 4733	0,56 5428
312	3-Dehydrotrametenolic acid	0,889 525	0,76 9843	- 1,25887	- 0,53091	1,04 0388	0,97 7383
313	Polygalaxanthone III	0,988 667	1,04 1262	- 0,60523	0,43173 1	0,96 769	1,03 5541
314	Cedrol	1,049 254	1,07 5807	- 0,20578	0,55424 9	0,93 3764	1,01 9386
315	Cimiracemoside D	1,010 698	1,31 7616	- 0,45997	1,41187 7	0,96 2843	1,08 4006
316	Maoecrystal A	0,863 655	0,86 8096	- 0,70769	-0,3277	0,93 2976	0,93 1367
317	Ursonic acid	0,815 203	0,65 0467	-0,969	- 0,84817	0,92 6542	0,92 0107
318	Cucurbitacin IIa	0,827 316	0,72 9055	- 0,90367	- 0,66022	0,96 5147	0,91 3673
319	Phytolaccagenin	0,942 39	0,80 7643	- 0,28308	- 0,47227	0,95 8713	0,88 9544
320	(20R)-Ginsenoside Rg3	0,912 107	0,75 3236	- 0,44639	- 0,60239	0,94 1019	0,91 0456
321	Hederagenin	1,075 632	1,05 5498	0,43550 4	0,12047 8	0,92 3324	1,20 3217
322	Glycyrrhizic acid	0,881 825	0,80 1598	-0,6097	- 0,48673	0,99 4102	1,10 0268

COMPOUND NR - FOR THE FIRST ROUND OF SCREENING	COMPOUND NAME	KYN FOLD CHANGE DATA		KYNURENINE SD VARIATION DATA		VIABILITY	
323	Mogroside II-A2	0,845486	0,656512	-0,80568	-0,83371	1,032708	0,990885
324	Ingenol Mebutate	0,815203	0,565834	-0,969	-1,05057	1,029491	0,992493
325	alpha-Bisabolol	0,899994	0,680693	-0,51172	-0,77588	0,989276	0,99571
326	Plantamajoside	0,845486	0,511427	-0,80568	-1,18069	1,006971	0,982842
327	Tripterin	0,106594	0,130577	-4,79054	-2,0915	0,041823	0,027346
328	Guggulsterone	0,35491	0,293798	-3,45137	-1,70115	0,941019	0,934584
329	Gynostemma Extract	1,105915	0,934593	0,59881 7	-0,16867	0,934584	0,974799
330	Artemisinin	0,645622	0,680693	-1,88355	-0,77588	0,947453	1,111528
331	Saikosaponin B2	0,766751	0,710919	-1,2303	-0,70359	1,042359	1,052011
332	Alantolactone	0,094481	0,070125	-4,85586	-2,23607	0,924933	0,892761
333	Ginsenoside Rb3	0,863655	0,59606	-0,70769	-0,97828	1,018231	0,997319
334	Ginsenoside F2	0,906051	0,729055	-0,47905	-0,66022	1,015013	0,968365
335	Myricitrin	0,809147	0,577924	-1,00166	-1,02165	0,97319	1,002145
336	Albiflorin	0,930277	0,886231	-0,3484	-0,28433	0,941019	0,98445
337	Lasalocid (sodium)	0,367023	0,372386	-3,38604	-1,5132	0,836461	0,892761

COMPOUND NR - FOR THE FIRST ROUND OF SCREENING	COMPOUND NAME	KYN FOLD CHANGE DATA		KYNURENINE SD VARIATION DATA		VIABILITY	
338	(−)-Myrtenal	0,881825	1,001091	-0,6097	-0,00964	0,949062	1,027882
339	Ginkgolide A	1,136197	1,254991	0,762131	0,597571	0,93941	1,117962
340	Geniposidic acid	0,760695	0,668603	-1,26296	-0,80479	1,027882	1,006971
341	Betulinaldehyde	0,784921	0,608151	-1,13231	-0,94937	0,998928	1,011796
342	Ginsenoside Rd	0,899994	0,656512	-0,51172	-0,83371	0,987668	1,018231
343	Lasalocid	0,524492	0,493291	-2,53681	-1,22406	0,865416	0,889544
344	Geniposide	0,954503	0,922503	-0,21775	-0,19758	0,924933	0,968365
345	Santonin	1,033237	1,001091	0,206864	-0,00964	0,974799	0,968365
346	Curcumol	0,906051	0,759281	-0,47905	-0,58793	0,97319	1,021448
347	Echinocystic acid	0,833373	0,741146	-0,87101	-0,63131	1,016622	1,035925
348	Punicalagin	0,106594	0,094306	-4,79054	-2,17824	1,000536	1,002145
349	7-epi-Taxol	0,318571	0,281708	-3,64734	-1,73007	0,813941	0,768901
350	Oleuropein	0,839429	0,626286	-0,83834	-0,906	0,924933	1,031099
351	Hederacoside D	0,966616	0,7351	-0,15243	-0,64576	0,875067	0,969973
352	Cryptotanshinone	0,379136	0,384477	-3,32071	-1,48429	0,850938	0,918499

COMPOUND NR - FOR THE FIRST ROUND OF SCREENING	COMPOUND NAME	KYN FOLD CHANGE DATA		KYNURENINE SD VARIATION DATA		VIABILITY	
353	Bakuchiol	0,748582	0,72301	-1,32829	-0,67468	0,923324	0,976408
354	Paeoniflorin	1,14831	1,533071	0,827457	1,26261	0,91689	1,148525
355	Orcinol glucoside	0,887881	0,753236	-0,57704	-0,60239	1,031099	1,069705
356	Atractylenolide III	0,869712	0,656512	-0,67503	-0,83371	1,008579	1,021448
357	Saikosaponin A	0,893938	0,753236	-0,54438	-0,60239	1,021448	1,008579
358	Genipin	0,797034	0,72301	-1,06698	-0,67468	0,98445	1,021448
359	Paclitaxel	0,300402	0,305889	-3,74533	-1,67224	0,857373	0,855764
360	Kansuinine A	0,730412	0,686739	-1,42627	-0,76142	0,913673	0,953887
361	Parthenolide	0,264063	0,354251	-3,94131	-1,55658	0,908847	0,957105
362	Euphol	1,009011	1,007136	0,076213	0,004819	0,941019	1,013405
363	Corosolic acid	1,093802	1,279171	0,533492	0,655401	0,958713	1,182306
364	Pulchinenoside A	0,918164	0,837869	-0,41373	-0,39999	1,008579	1,080965
365	Oleanolic Acid	0,827316	0,729055	-0,90367	-0,66022	1,008579	0,958713
366	Toosendanin	0,227724	0,184984	-4,13728	-1,96138	0,897587	0,818767
367	Asperosaponin VI	0,809147	0,686739	-1,00166	-0,76142	0,989276	0,986059

COMPOUND NR - FOR THE FIRST ROUND OF SCREENING	COMPOUND NAME	KYN FOLD CHANGE DATA		KYNURENINE SD VARIATION DATA		VIABILITY	
368	Atractyloside A	0,893938	0,813688	-0,54438	-0,45782	0,965147	1,006971
369	Emodin-8-glucoside	0,972672	0,771372	-0,11976	-0,55902	0,987668	0,981233
370	Triptolide	0,136877	0,166848	-4,62723	-2,00476	0,616086	0,664343
371	alpha-Hederin	0,778864	0,970865	-1,16497	-0,08193	0,884718	0,979625
372	Escin	1,063519	1,206629	0,370178	0,481912	0,834853	0,987668
373	Ganoderic acid N	0,94239	0,771372	-0,28308	-0,55902	0,989276	1,064879
374	Alisol F	0,881825	0,813688	-0,6097	-0,45782	0,968365	1,013405
375	Ginsenoside Rk1	0,809147	0,759281	-1,00166	-0,58793	0,900804	1,039142
376	Gypenoside LI	0,797034	0,650467	-1,06698	-0,84817	0,876676	0,99571
377	Squalene	0,906051	0,868096	-0,47905	-0,3277	0,818767	1,008579
378	18β-Glycyrrhetinic acid	0,966616	1,218719	-0,15243	-0,51082917	0,904021	1,1437
379	Mogroside III	1,089391	0,904512	0,022206	-0,04922	0,86961	0,844675
380	3-O-Acetyl-11-hydroxy-beta-boswellic acid	1,046289	0,928735	-0,24426	-0,073833	0,864935	0,861818
381	Rotundic acid	0,943923	0,914201	-0,87713	-6,75E-16	0,885195	0,880519

COMPOUND NR - FOR THE FIRST ROUND OF SCREENING	COMPOUND NAME	KYN FOLD CHANGE DATA		KYNURENINE SD VARIATION DATA		VIABILITY	
382	Siamenoside I	1,057065	1,146748	-0,17765	1,18132	1,387013	0,902338
383	Dehydroandrographolide succinate	1,132492	1,258177	0,288675	1,74737	0,81974	0,977143
384	Inulicin	1,057065	1,263022	-0,17765	1,771981	0,844675	0,98026
385	β-D-glucopyranosyl-[α-L-rhamnopyranosyl-(1→3)-βD-glucuronopyranosyl-(1→3)]-3β-hydroxyolean-12-ene28-oate	1,008575	0,856064	-0,47742	-0,29533	0,93039	0,952208
386	Picroside II	1,030126	0,807617	-0,34419	-0,54144	0,950649	0,896104
387	Ingenol-3,4,5,20-diacetonide	0,992412	0,793083	-0,57735	-0,61527	1,254545	0,927273
388	1,4-Cineole	0,938535	0,788238	-0,91044	-0,63988	0,888312	0,925714
389	Gypenoside XLVI	0,922372	0,701033	-1,01036	-1,08288	0,838442	1,218701
390	Brevilin A	0,119607	0,143889	-5,97335	-3,91312	0,774545	0,724675
391	Monotropein	0,938535	0,754325	-0,91044	-0,81216	0,833766	0,899221

COMPOUND NR - FOR THE FIRST ROUND OF SCREENING	COMPOUND NAME	KYN FOLD CHANGE DATA		KYNURENINE SD VARIATION DATA		VIABILITY	
392	Rehmanniosid e D	0,992 412	0,88 9977	- 0,57735	- 0,12305	0,84 4675	1,25 1429
393	11-oxo-mogroside V	1,294 123	1,36 9606	1,28793 5	2,31341 9	1,02 0779	1,18 7532
394	Ginsenoside Rb2	0,976 249	0,78 3393	- 0,67728	- 0,66449	0,93 974	0,99 5844
395	Notoginsenosi de Fe	0,960 086	0,77 8549	-0,7772	-0,6891	0,90 0779	0,96 1558
396	Dipotassium glycyrrhizinate	0,954 698	0,66 2275	- 0,81051	- 1,27976	0,94 5974	0,90 2338
397	Sinigrin	1,137 88	0,93 358	0,32198 4	0,09844 3	0,94 2857	0,92 2597
398	Notoginsenosi de Ft1	0,970 862	0,74 948	- 0,71058	- 0,83677	0,88 0519	0,91 7922
399	Wilforlide A	0,927 76	0,73 9791	- 0,97705	- 0,88599	0,84 3117	0,91 013
400	Betulin	0,916 985	0,73 4946	- 1,04367	-0,9106	0,81 3506	0,86 961
401	Lupeol	0,981 637	0,86 0909	- 0,64397	- 0,27072	0,83 2208	0,88 987
402	Kalii Dehydrograph olidi Succinas	1,267 184	1,26 7867	1,12139 2	1,79659 1	0,98 6494	1,16 5714
403	Tanshinone I	0,739 191	0,54 6001	- 2,14286	- 1,87042	0,90 0779	0,94 1299
IN-HOUSE LIBRARY 1-SEAWEED_COMPOUNDS_ 30.05.2022_CNAP-M2							
404	A - Fucoidan - Laminarina	0,987 025	0,73 9791	- 0,61066	- 0,88599	0,96 9351	0,94 4416

COMPOUND NR - FOR THE FIRST ROUND OF SCREENING	COMPOUND NAME	KYN FOLD CHANGE DATA		KYNURENINE SD VARIATION DATA		VIABILITY	
	japonica_non-filtered						
405	FCSP - Cladosiphon Okamuranus	1,003188	0,754325	-0,51073	-0,81216	0,927273	0,933506
406	Fucogalactan - from Undaria pinnatifida	0,960086	0,74948	-0,7772	-0,83677	0,874286	0,914805
407	Fucoidan - Fucus serratus	1,024738	0,778549	-0,3775	-0,6891	0,864935	0,917922
408	Fucoidan - Alaria	0,976249	0,860909	-0,67728	-0,27072	0,933506	0,938182
409	Laminaran - from Laminaria cloustoni	0,9978	0,826996	-0,54404	-0,443	0,936623	0,955325
410	Fucoidan - Durvillea	1,008575	0,75917	-0,47742	-0,78755	0,914805	0,961558
411	Fucoidan - Ecklonia	1,003188	0,754325	-0,51073	-0,81216	0,924156	0,963117
412	Laminaran - from Thallus laminariae	1,003188	0,730101	-0,51073	-0,93521	0,816623	0,938182
413	Laminaran - from Eisenia bicyclis	1,013963	0,705878	-0,44412	-1,05827	0,804156	0,874286
414	Fucoidan - Fucus vesiculosus (crude)	0,911597	0,720412	-1,07698	-0,98443	0,804156	0,858701

COMPOUND NR - FOR THE FIRST ROUND OF SCREENING	COMPOUND NAME	KYN FOLD CHANGE DATA		KYNURENINE SD VARIATION DATA		VIABILITY	
415	Fucoidan - Fucus vesiculosus (pure)	1,024738	0,744635	-0,3775	-0,86138	0,838442	0,866494
416	Fucoidan, macrocystis pyrifera	1,008575	0,797927	-0,47742	-0,59066	0,751169	0,872727
417	Laminaran - from Laminaria digitata	1,283348	1,233953	1,221318	1,624316	1,70026	1,15013
418	Fucoidan - Lessonia nigrescens	0,981637	0,734946	-0,64397	-0,9106	0,950649	0,949091
419	Fucoidan - Ascophyllum nodosum	0,987025	0,74948	-0,61066	-0,83677	0,836883	0,924156
420	Fucoidan - Undaria pinnatifida	0,938535	0,764014	-0,91044	-0,76294	0,91013	0,93974
421	Fucoidan - Macrocystis pyrifera	0,965474	0,773704	-0,74389	-0,71371	0,886753	0,93039
422	Fucoidan - Ascophyllum nodosum, analytical grade	0,933148	0,599293	-0,94375	-1,5997	0,892987	0,900779
423	Fucoidan - Laminaria digitata	0,970862	0,633207	-0,71058	-1,42743	0,858701	0,88987

COMPOUND NR - FOR THE FIRST ROUND OF SCREENING	COMPOUND NAME	KYN FOLD CHANGE DATA		KYNURENINE SD VARIATION DATA		VIABILITY	
424	Fucoidan polysaccharide from Durvillea antarctica	1,019351	0,701033	-0,41081	-1,08288	0,897662	0,914805
425	Fucoidan polysaccharide from Chorda filum	1,008575	0,633207	-0,47742	-1,42743	0,888312	1,277922
426	Fucoidan polysaccharide from Ascophyllum nodosum	1,245634	0,817306	0,988157	-0,49222	0,947532	1,045714
427	Fucoidan polysaccharide from Fucus vesiculosus	1,003188	0,865754	-0,51073	-0,24611	0,966234	0,961558
428	Galactofucan polysaccharide from Undaria pinnatifida	1,003188	0,807617	-0,51073	-0,54144	0,967792	0,958442
429	2 - Fucoidan - Pelagic Sargassum	0,965474	0,793083	-0,74389	-0,61527	0,974026	0,956883
430	3 - Fucoidan - Pelagic Sargassum	0,976249	0,807617	-0,67728	-0,54144	0,956883	0,953766

COMPOUND NR - FOR THE FIRST ROUND OF SCREENING	COMPOUND NAME	KYN FOLD CHANGE DATA		KYNURENINE SD VARIATION DATA		VIABILITY	
431	15 - Fucoidan - Pelagic Sargassum	1,024738	0,783393	-0,3775	-0,66449	1,461818	0,944416
432	10 - Fucoidan - Pelagic Sargassum	0,965474	0,870598	-0,74389	-0,2215	0,883636	0,945974
433	8 - Fucoidan - Pelagic Sargassum	1,013963	0,739791	-0,44412	-0,88599	0,892987	0,931948
434	5 - Fucoidan - Pelagic Sargassum	1,003188	0,754325	-0,51073	-0,81216	0,891429	0,938182
435	18 - Fucoidan - Pelagic Sargassum	1,353387	0,725256	1,654331	-0,95982	0,942857	1,036364
436	Fucoxanthin	1,046289	0,822151	-0,24426	-0,46761	0,897662	1,005195
437	Fucoxanthin	1,030126	0,730101	-0,34419	-0,93521	0,916364	1,231169
438	Fucoxanthin	1,062452	0,807617	-0,14434	-0,54144	0,908571	1,655065
IN-HOUSE LIBRARY 2							
439	Demecolcine (colcemid)	0,41593	0,555691	-4,14138	-1,8212	0,755844	0,938182
440	Cuscohygrine	0,981637	0,943269	-0,64397	0,147665	0,877403	1,076883
441	3-5-pyridinedicarboxylic acid	0,965474	1,001406	-0,74389	0,442995	1,011429	1,073766

COMPOUND NR - FOR THE FIRST ROUND OF SCREENING	COMPOUND NAME	KYN FOLD CHANGE DATA		KYNURENINE SD VARIATION DATA		VIABILITY	
442	Nicotinic acid	1,035919	0,853113	-0,07392	-0,49561	0,947638	0,88617
443	Methyl nicotinate	1,035919	0,712841	-0,07392	-1,22251	1,000569	0,947638
444	Trigonelline hydrochloride	1,016212	0,795729	-0,16896	-0,79298		0,913489
445	6-hydroxynicotinic acid	1,042488	0,904122	-0,04224	-0,23129	0,976665	0,925441
446	(-)-nicotine	1,121315	0,967882	0,33793	0,099123	1,034718	0,922026
447	3-acetylindol	1,009643	1,203795	-0,20065	1,321637	1,06033	0,850313
448	6-hydroxypyridine-3-carboxylic acid	0,884833	0,757473	-0,80258	-0,99123	1,017644	0,963005
449	Nicotinic acid riboside	0,11627	0,610824	-4,50925	-1,75117	0,527604	1,039841
450	Homoharrigtonine	0,096563	0,062485	-4,60429	-4,59269	0,442231	0,36881
451	Homoharringtonine	0,181959	0,068861	-4,19244	-4,55965		0,38247
452	Colchicine	0,201666	0,266518	-4,0974	-3,53538	0,734206	0,870803
453	Atropine sulfate	0,825713	0,763849	-1,08771	-0,95819	0,985202	1,007399
454	Scopolamine hydrobromide	0,858558	0,763849	-0,92931	-0,95819	0,964713	1,000569

COMPOUND NR - FOR THE FIRST ROUND OF SCREENING	COMPOUND NAME	KYN FOLD CHANGE DATA		KYNURENINE SD VARIATION DATA		VIABILITY	
455	Tropine	0,760024	1,044394	-1,40452	0,495614	0,848606	1,027888
456	Pseudotropine	0,851989	1,42058	-0,96099	2,445029	1,0535	1,050085
457	Scopine	0,819144	0,776601	-1,11939	-0,89211	1,000569	1,000569
458	Tropinone	0,766593	0,668208	-1,37284	-1,4538	0,993739	1,041548
459	Hyoscyamine hydrobromide	0,7863	0,700089	-1,2778	-1,2886	1,009106	1,043256
460	Galantamine hydrobromide	0,838851	0,744721	-1,02435	-1,05731		1,041548
461	Lycorine chloride	0,23451	0,132622	-3,93899	-4,22924	0,542971	0,621514
462	Dihydrolycorine	0,707473	0,738345	-1,65797	-1,09035	0,932271	0,990324
463	Galanthaminone	0,779731	0,789353	-1,30948	-0,82602	0,928856	0,976665
464	Daphnicyclidin D	0,700904	0,961506	-1,68965	-0,066082	0,894707	1,002277
465	CFN96776	0,595801	0,859489	-2,19654	-0,46257	1,003984	1,003984
466	CFN98270	0,66149	0,591696	-1,87973	-1,85029	1,022766	1,051793
467	Virosine B	0,799438	0,763849	-1,21443	-0,95819	1,021059	1,07399
468	Securinine	0,280493	0,145374	-3,71723	-4,16316		0,889585
469	Securitinine	0,792869	0,674584	-1,24612	-1,42076	0,957883	1,007399

COMPOUND NR - FOR THE FIRST ROUND OF SCREENING	COMPOUND NAME	KYN FOLD CHANGE DATA		KYNURENINE SD VARIATION DATA		VIABILITY	
470	CFN99608	0,819144	0,74 4721	-1,11939	-1,05731	0,92 3734	0,98 3495
471	CFN98003	0,766593	1,08 2651	-1,37284	0,69386	1,01 5936	1,04 8378
472	CFN98629	0,865127	0,82 7609	-0,89763	-0,62778	1,02 2766	1,02 7888
473	CFN97008	0,241079	0,21 551	-3,90731	-3,79971	0,92 8856	0,99 5447
474	CFN97421	0,838851	0,71 9217	-1,02435	-1,18947	1,02 4474	1,05 1793
475	CFN97436	1,02935	0,77 0225	-0,1056	-0,92515		1,05 35
476	CFN97447	0,858558	0,74 4721	-0,92931	-1,05731	0,89 2999	1,01 2521
477	CFN97448	0,917678	0,80 2105	-0,64418	-0,75994	0,97 325	1,01 5936
478	CFN97484	0,937385	0,75 1097	-0,54914	-1,02427	1,00 5692	0,96 642
479	CFN96450	0,943954	1,18 4667	-0,51745	-1,22251 4	0,91 8611	1,01 5936
480	CFN96778	1,055625	1,39 5076	-0,02112 1	-2,31286 5	1,03 1303	1,03 4718
481	CFN96679	0,812575	0,80 2105	-1,15107	-0,75994	1,00 5692	0,99 5447
482	Daphniphylline	0,806006	0,69 3713	-1,18275	-1,32164	0,99 5447	1,03 3011
483	Yuzurimine	0,806006	0,70 6465	-1,18275	-1,25556	1,02 1059	1,06 2038

COMPOUND NR - FOR THE FIRST ROUND OF SCREENING	COMPOUND NAME	KYN FOLD CHANGE DATA		KYNURENINE SD VARIATION DATA		VIABILITY	
484	Flueggea suffructicosa leaf	0,536681	0,368535	-2,48167	-3,00672		1,010814
485	Flueggea suffructicosa leaf	0,208235	0,138998	-4,06572	-4,1962	0,903244	0,920319
486	Daphniphyllum A mature leaf 2020	0,72061	0,725593	-1,59461	-1,15643	0,937393	1,005692
487	Daphniphyllum C mature leaf 2020	0,851989	0,763849	-0,96099	-0,95819	1,017644	0,957883
488	Daphniphyllum D mature leaf 2020	0,727179	0,827609	-1,56292	-0,62778	0,862265	0,968127
489	Daphniphyllum A mature leaf 2019	0,983367	1,165539	-0,32737	-1,12339 2	1,010814	0,988617
490	Daphniphyllum B mature leaf 2019	0,858558	0,846737	-0,92931	-0,52865	0,927149	0,978372
491	Daphniphyllum D stems 2020	0,668059	0,566192	-1,84805	-1,98246	0,98691	0,992032
492	Daphniphyllum EF ground leaves	0,819144	0,738345	-1,11939	-1,09035	1,005692	1,036426
493	Daphniphyllum G mature leaves	0,924247	0,661832	-0,6125	-1,48684		1,038133

COMPOUND NR - FOR THE FIRST ROUND OF SCREENING	COMPOUND NAME	KYN FOLD CHANGE DATA		KYNURENINE SD VARIATION DATA		VIABILITY	
494	Daphniphyllum H mature leaves	0,812575	0,731969	-1,15107	-1,12339	0,949345	1,012521
495	Daphniphyllum C berries 2019	0,812575	0,751097	-1,15107	-1,02427	0,95959	0,992032
496	Humile berries 2019	0,832282	0,731969	-1,05603	-1,12339	0,956175	0,951053
497	Puerarin	0,950523	0,904122	-0,48577	-0,23129	0,925441	0,963005
498	Naringin	1,127884	1,178291	0,369611	1,189473	1,033011	1,012521
499	5.7-dihydroxychromone	0,851989	0,884994	-0,96099	-0,33041	0,922026	0,923734
500	Kaempferol	0,687766	0,655456	-1,75301	-1,51988	1,024474	0,913489
501	Rutin	0,714042	0,795729	-1,62629	-0,79298		0,867388
502	Naringenin	0,779731	0,763849	-1,30948	-0,95819	0,930563	0,911781
503	Quercetin	0,668059	0,489679	-1,84805	-2,37895	1,002277	0,840068
504	Sarathrin (4',5,7-Trihydroxy-3,6,8-trimethoxylfavone)	1,035919	0,68096	-0,07392	-1,38772	0,918611	0,822994
505	Apigenin	0,824347	0,78792	-1,39847	-1,23752	0,996902	0,922557

COMPOUND NR - FOR THE FIRST ROUND OF SCREENING	COMPOUND NAME	KYN FOLD CHANGE DATA		KYNURENINE SD VARIATION DATA		VIABILITY	
506	Kaempferol 3-rutinoside	0,989707	0,920851	-0,37796	-0,21657	1,197972	0,993523
507	O-coumaric acid	0,995831	0,987317	-0,34017	0,293912	1,044213	0,90735
508	4-methoxythioanisole	0,891716	1,053783	-0,98271	0,804391	1,005351	0,924247
509	Ethyl cinnamate	1,057076	1,216926	0,037796	2,057384	1,047592	0,927626
510	4-deoxypodophyllotoxin	0,487504	0,757708	-3,47727	-1,46956	0,784005	0,843143
511	Formononetin	0,879467	0,86647	-1,0583	-0,63423	0,964799	1,01042
512	Trans-cinnamic acid	0,897841	0,86647	-0,94491	-0,63423	1,01042	1,037454
513	Acetosyringone	0,946836	0,824174	-0,64254	-0,95908	1,025627	1,071248
514	Quercetin	0,940711	0,854386	-0,68034	-0,72705	0,991833	1,062799
515	Hypericin	0,058794	0,147433	-6,12302	-6,15668	0,148691	0,028724
516	Yatein	0,867218	0,818132	-1,13389	-1,00549	0,996902	0,995213
517	Asperuloside	0,989707	1,053783	-0,37796	0,804391	0,993523	1,020558
518	Deacetylasperulosidic acid	1,044827	1,102121	-0,0378	1,175648	0,993523	1,027316

COMPOUND NR - FOR THE FIRST ROUND OF SCREENING	COMPOUND NAME	KYN FOLD CHANGE DATA		KYNURENINE SD VARIATION DATA		VIABILITY	
519	Teucrein	0,781476	0,902724	-1,66304	-0,35579	0,870177	0,90735
520	dolichodial	0,910089	0,884597	-0,86932	-0,49501	1,025627	0,980006
521	Baldrinal	0,830472	0,739581	-1,36067	-1,60878	1,01042	1,001971
522	CFN90622	0,095541	0,093052	-5,89625	-6,57435	0,321036	0,19938
523	Daphylloside	0,922338	0,854386	-0,79373	-0,72705	0,954661	1,042523
524	CFN90205	0,064919	0,117221	-6,08523	-6,38872	0,010138	-0,05069
525	Digoxin	0,05267	0,153475	-6,16082	-6,11028	0,589693	0,496761
526	Digitoxin	0,983582	0,951063	-0,41576	-0,01546 9	0,983385	1,01042
527	Lanatoside C	0,138412	0,159518	-5,63167	-6,06387	0,591383	0,621797
528	Digitonin	0,603868	0,630819	-2,75914	-2,44411	0,709659	0,679245
529	Docetaxel	0,793725	0,721454	-1,58745	-1,748	0,969868	0,875246
530	Paclitaxel	0,328269	0,334745	-4,45998	-4,71806	0,80428	0,789074
531	α terpineol (mixed)	0,934587	0,818132	-0,71813	-1,00549	0,931005	1,022247
532	Geraniol	0,934587	0,854386	-0,71813	-0,72705	0,993523	0,973247

COMPOUND NR - FOR THE FIRST ROUND OF SCREENING	COMPOUND NAME	KYN FOLD CHANGE DATA		KYNURENINE SD VARIATION DATA		VIABILITY	
533	(-+)-lavandillol acetate	1,020329	0,96919	-0,18898	0,154691	0,995213	1,015489
534	Linalool	1,00808	0,884597	-0,26458	-0,49501	0,995213	1,025627
535	(+)-α-pinene	0,995831	0,945021	-0,34017	-0,03094	0,993523	0,990144
536	(r)-(+)-limonene	0,934587	0,878555	-0,71813	-0,54142	0,963109	1,00873
537	Geranyl acetate	0,910089	0,854386	-0,86932	-0,72705	0,95973	1,050972
538	(-)-α-terpineol	0,95296	0,872513	-0,60474	-0,58782	0,947902	1,01042
539	1,8-cineole	0,965209	0,860428	-0,52915	-0,68064	0,931005	1,025627
540	(s)-(-)-limonene	0,910089	0,769793	-0,86932	-1,37675	0,90735	0,980006
541	L(-)-carvone	1,00808	0,938978	-0,26458	-0,07735	0,915798	1,013799
542	(-)-carveol (mixed)	1,032578	1,005444	-0,11339	0,433134	0,924247	1,045903
543	Citronellal	1,191813	1,25318	0,869318	2,335827	1,06111	1,072937
544	Citronellol	0,922338	0,854386	-0,79373	-0,72705	1,015489	0,985075
545	D(+)-carvone	0,879467	0,848343	-1,0583	-0,77345	0,981695	1,018868
546	Myrcene	0,940711	0,793962	-0,68034	-1,19112	0,976626	1,054351
547	(-)-linalool	0,891716	0,800005	-0,98271	-1,14471	0,880315	1,040834

COMPOUND NR - FOR THE FIRST ROUND OF SCREENING	COMPOUND NAME	KYN FOLD CHANGE DATA		KYNURENINE SD VARIATION DATA		VIABILITY	
548	Terpineol	0,946836	0,824174	-0,64254	-0,95908	0,90735	1,030696
549	(1R,2S,5R)-(-)-menthol	0,85497	0,757708	-1,20949	-1,46956	0,910729	0,95973
IN-HOUSE LIBRARY 3							
550	Magnoflorine	0,977458	0,896682	-0,45356	-0,4022	0,931005	1,001971
551	Cycleanine	0,181283	0,213899	-5,3671	-5,64621	0,116587	0,119966
552	Tetrandrine	1,130569	1,096079	0,491354	1,129241	1,040834	1,052661
553	Magnocurarine	0,995831	0,878555	-0,34017	-0,54142	1,030696	1,01042
554	Oblongine	1,081573	0,981275	0,188982	0,247505	0,942833	0,995213
555	Coclaurine	1,087698	0,999402	0,226779	0,386726	0,95635	1,018868
556	Dicentrine	0,438509	0,42538	-3,77964	-4,02195	0,799211	0,860039
557	Dehydrodicentrine	0,891716	0,721454	-0,98271	-1,748	0,931005	0,961419
558	Berberine	0,885592	0,727497	-1,0205	-1,7016	0,882005	0,883695
559	Reserpine	1,0632	0,96919	0,075593	0,154691	0,934385	0,973247
560	Laudanosine	0,493629	0,546227	-3,43948	-3,09381	0,990144	1,050972
561	Nuciferine	1,155066	1,041698	0,64254	0,711577	1,083075	1,01042

COMPOUND NR - FOR THE FIRST ROUND OF SCREENING	COMPOUND NAME	KYN FOLD CHANGE DATA		KYNURENINE SD VARIATION DATA		VIABILITY	
562	Corytuberine	0,965209	0,812089	-0,52915	-1,0519	0,811039	0,846522
563	Curine	0,407887	0,370999	-3,96863	-4,43962	0,680935	0,626866
564	Ingenol	0,965209	0,908767	-0,52915	-0,30938	0,870177	0,981695
565	20-Deoxyingenol	0,818223	0,769793	-1,43626	-1,37675	0,870177	0,892143
566	Ingenol-3-hexanoate	0,928463	0,896682	-0,75593	-0,4022	0,90904	0,941143
567	3-O-(2'E,4'EDecadienoyl)ingenol	0,750854	0,872513	-1,85203	-0,58782	0,969868	0,966488
568	3-O-(2'E,4'ZDecadienoyl) ingenol	1,016531	1,028439	-0,23083	0,976092	1,065471	0,938117
569	Ingenol 3-Angelate	0,866949	1,090096	-1,74168	1,863449	1,036771	0,878924
570	Ingenol-3,4:5,20-diacetonide	1,141182	1,077765	1,028223	1,685977	1,054709	1,024215
571	Ingenol-5,20-acetonide	1,18481	1,040771	1,468891	1,153563	0,986547	0,979372
572	Ingenol-5,20-acetonide-3-O-angelate	1,166112	1,028439	1,280033	0,976092	1,006278	0,966816
573	Jatrophanes 1-7	1,078856	0,979114	0,398699	0,266207	0,984753	1,013453

COMPOUND NR - FOR THE FIRST ROUND OF SCREENING	COMPOUND NAME	KYN FOLD CHANGE DATA		KYNURENINE SD VARIATION DATA		VIABILITY	
574	20-Deoxyingenol 3-angelate	0,854484	0,861965	-1,86759	-1,41977	1,078027	1,008072
575	Dodecanoic acid ingenol ester	0,798391	0,763314	-2,43416	-2,83954	1,106726	0,96861
576	20-O-Acetylingenol-3-angelate	0,835786	0,911291	-2,05645	-0,70989	1,160538	1,03139
577	Ingenol 3,20-dibenzoate	0,642577	0,64	-4,00797	-4,61425	1,092377	1,006278
578	Phorbol 12,13-didecanoate 20-homovanillate	0,7236	0,757148	-3,18959	-2,92828	1,020628	0,986547
579	12-O-tetradecanoyl phorbol-13-acetate	0,873182	0,843468	-1,67873	-1,68598	1,092377	1,03139
580	Phorbol 13-myristate	0,692437	0,578343	-3,50435	-5,50161	1,076233	0,984753
581	Phorbol 12, 13-Dihexanoate	0,935507	0,8558	-1,04921	-1,50851	0,997309	1,104933
582	Phorbol 12-Myristate 13-Acetate	0,860717	1,151753	-1,80464	-2,750805	1,058296	1,112108
583	Phorbol 13-acetate	0,630112	0,492023	-4,13388	-6,74391	1,092377	1,020628
584	Phorbol 12,13-Dibutyrate	0,804624	0,757148	-2,37121	-2,92828	1,13722	1,034978

COMPOUND NR - FOR THE FIRST ROUND OF SCREENING	COMPOUND NAME	KYN FOLD CHANGE DATA		KYNURENINE SD VARIATION DATA		VIABILITY	
585	Phorbol	0,935507	0,837303	-1,04921	-1,77471	1,115695	1,03139
586	Prostratin	0,754763	0,720154	-2,87483	-3,46069	1,06009	1,565919
587	Phorbol 12,13,20-triacetate	0,873182	0,72632	-1,67873	-3,37195	1,049327	0,686996
588	Lathyrol	0,935507	0,880462	-1,04921	-1,15356	1,038565	1,034978
589	7-beta-Hydroxylathyrol	0,96667	0,8558	-0,73445	-1,50851	1,018834	1,047534
590	Deoxy euphorbia factor L1	0,954205	0,948285	-0,86035	-0,17747	1,022422	1,126457
591	Euphorbia factor L1	0,9916	1,145588	-0,48264	-2,66207	1,115695	1,115695
592	Euphorbia factor L2	0,418205	0,350212	-6,27426	-8,78483	1,078027	1,056502
593	Euphorbia factor L22	1,028996	0,89896	-0,10492	-0,88736	1,140807	1,074439
594	Euphorbia factor L24	0,96667	0,8558	-0,73445	-1,50851	1,106726	1,076233
595	Euphorbia factor L25	0,960438	0,861965	-0,7974	-1,41977	1,054709	1,06009
596	Euphorbia factor L3	0,96667	0,81264	-0,73445	-2,12966	1,065471	1,038565
597	Euphorbia factor L7a	0,923042	0,972948	-1,17511	-0,17747 1	1,083408	1,088789

COMPOUND NR - FOR THE FIRST ROUND OF SCREENING	COMPOUND NAME	KYN FOLD CHANGE DATA		KYNURENINE SD VARIATION DATA		VIABILITY	
598	Euphorbia factor L7b	0,910577	0,960617	-1,30102	0	1,086996	1,043946
599	Euphorbia factor L8	0,947972	0,831137	-0,9233	-1,86345	1,149776	1,043946
600	Euphorbia factor L9	0,206298	0,245395	-8,41465	-10,2933	1,13722	1,002691
601	jolkinol C	0,929275	0,806474	-1,11216	-2,21839	1,097758	1,040359
602	jolkinol E	0,817089	0,824971	-2,2453	-1,95218	1,043946	0,724664
603	jolkinol C/epi-jolkinol C/jolkinol E mix (58:31:11)	0,923042	0,917457	-1,17511	-0,62115	1,029596	1,018834
604	jolkinol F	0,954205	0,929788	-0,86035	-0,44368	1,01704	1,040359
605	Jatrophane 2	0,891879	0,960617	-1,48987	0	1,03139	1,119283
606	Jatrophane 3	0,692437	0,948285	-3,50435	-0,17747	1,000897	1,079821
607	Jatrophane 4	0,748531	0,757148	-2,93778	-2,92828	1,115695	1,092377
608	Jatrophane 5	0,904345	0,905125	-1,36397	-0,79862	1,135426	1,097758
609	Pepluanin A	0,848252	0,763314	-1,93054	-2,83954	1,119283	1,095964
610	Jatrophane 1-3 mix (74:13:12)	0,754763	0,701657	-2,87483	-3,7269	1,10852	1,106726

COMPOUND NR - FOR THE FIRST ROUND OF SCREENING	COMPOUND NAME	KYN FOLD CHANGE DATA		KYNURENINE SD VARIATION DATA		VIABILITY	
611	Jatrophanes 1+4 and Pepluanian A mix (62:38)	0,873182	0,794143	-1,67873	-2,39586	1,083408	0,764126
612	6-hydroxy-5-ketocasbene	0,885647	0,8558	-1,55283	-1,50851	1,092377	1,090583
613	6,9-dihydroxy-5-ketocasbene	0,879414	0,818805	-1,61578	-2,04092	1,06009	1,06009
614	9-hydroxy-5-ketocasbene	0,885647	0,905125	-1,55283	-0,79862	1,061883	1,12287
615	5-ketocasbene/9-ketocasbene	0,947972	1,114759	-0,9233	2,218391	1,160538	1,149776
616	Casbene	0,910577	0,831137	-1,30102	-1,86345	1,081614	1,140807
617	Arteannuin X	0,898112	0,880462	-1,42692	-1,15356	1,12287	1,117489
618	Artemisinin	0,555321	0,442698	-4,88931	-7,45379	1,119283	1,061883
619	Artemether	0,287321	0,263892	-7,59626	-10,0271	1,078027	1,097758
620	Artesunate	0,449368	0,393372	-5,9595	-8,16368	1,004484	0,81435
621	Deoxyartemisinin	0,854484	0,849634	-1,86759	-1,59724	1,495964	1,069058
622	Dihydroartemisinin	0,692437	0,615337	-3,50435	-4,9692	1,038565	1,029596
623	Artemisinic acid	0,866949	0,911291	-1,74168	-0,70989	1,004484	1,158744

COMPOUND NR - FOR THE FIRST ROUND OF SCREENING	COMPOUND NAME	KYN FOLD CHANGE DATA		KYNURENINE SD VARIATION DATA		VIABILITY	
624	Dihydroartemisinic acid	0,972903	1,022274	-0,67149	0,887357	1,10852	1,104933
625	Amorpha-4,11-diene	1,097554	0,824971	0,587556	-1,95218	1,049327	0,965022
626	Jatrophanes 1+4,7 and Pepluanian A mix (62:11:17)	0,997833	0,750983	-0,41968	-3,01701	1,000897	0,945291
627	Peplusol (Triterpene purified from E. peplus)	0,854484	0,652331	-1,86759	-4,43678	0,98296	0,907623
628	(R)-Glaucine (Alkaloid purified from Papaver californicum)	1,022763	0,849634	-0,16787	-1,59724	0,95426	0,921973
629	(S)-Glaucine (Alkaloid purified from Papaver somniferum)	0,94174	0,868131	-0,98626	-1,33103	0,975785	0,957848
630	(S)-Glaucine (commercial standard)	0,804624	0,89896	-2,37121	-0,88736	1,020628	1,112108

Appendix Table 8. 3 Summary of COIs included in the screen validation round and their impact on kynurenine fold change, kynurenine SD variation and viability fold change.

VALIDATION ROUND	KYN FOLD CHANG DATA		KYNURENINE SD VARIATION DATA		VIABILITY	
COMPUND NR - COMPOUNDS OF INTEREST	Plate 1	Plate 2	Plate 1	Plate 2	Plate 1	Plate 2
1	0,347816	0,475333	-5,9976	-2,10209	0,771398	0,68299
10	0,413442	0,526601	-5,39025	-1,89829	0,991549	0,729794
16	0,552896	0,541249	-4,09962	-1,84006	0,786999	0,604984
29	0,725163	0,607166	-2,50533	-1,57802	0,887541	0,759263
31	1,250169	1,090555	2,353488	0,343555	0,918743	0,904875
44	0,864618	0,753647	-1,2147	-0,99573	1,012351	0,939545
45	0,421645	0,438712	-5,31433	-2,24766	1,083424	1,052221
58	0,51188	0,497305	-4,47922	-2,01475	1,067822	1,019285
91	0,241174	0,25561	-6,98454	-2,97554	0,807801	0,691658
92	0,462661	0,402092	-4,93473	-2,39324	0,786999	0,734995
116	0,323206	0,292231	-6,22535	-2,82996	0,868472	0,943012
123	0,421645	0,350823	-5,31433	-2,59704	0,823402	0,949946
127	0,503677	0,41674	-4,55514	-2,33501	0,821668	1,066089
167	0,356019	0,350823	-5,92168	-2,59704	0,977681	0,875406
182	0,74157	0,665758	-2,35349	-1,3451	1,073023	1,045287
197	0,290393	0,248286	-6,52903	-3,00465	0,967281	0,814735
206	0,249377	0,211666	-6,90863	-3,15022	0,676056	0,525244
214	0,347816	0,270258	-5,9976	-2,91731	0,908342	0,854605
229	0,51188	0,38012	-4,47922	-2,48058	0,691658	0,726327

269	0,372426	0,226314	-5,76984	-3,09199	0,715926	0,884074
332	0,208361	0,233638	-7,28822	-3,06288	0,92221	0,884074
337	0,339613	0,372795	-6,07352	-2,5097	0,910076	0,868472
343	0,610319	0,548573	-3,56819	-1,81094	0,849404	0,91701
348	0,28219	0,211666	-6,60495	-3,15022	0,96208	1,033153
349	0,48727	0,350823	-4,70698	-2,59704	1,367714	0,702059
359	0,446254	0,41674	-5,08657	-2,33501	0,858072	0,759263
361	0,388832	0,38012	-5,618	-2,48058	0,913543	0,974215
390	0,28219	0,25561	-6,60495	-2,97554	0,71766	0,806067
452	0,429848	0,328851	-5,23841	-2,68439	0,75753	0,72286
468	0,421645	0,41674	-5,31433	-2,33501	0,792199	0,958613
473	0,438051	0,343499	-5,16249	-2,62616	0,906609	1,015818
485	0,470864	0,292231	-4,85881	-2,82996	0,658722	0,975948
530	0,413442	0,365471	-5,39025	-2,53881	0,819935	0,738462
556	0,298597	0,292231	-6,45311	-2,82996	0,844204	0,793933
560	0,364222	0,387444	-5,84576	-2,45147	1,133694	1,069556
577	0,561099	0,511953	-4,0237	-1,95652	0,998483	1,029686
580	0,602115	0,519277	-3,64411	-1,9274	0,986349	0,979415
583	0,610319	0,504629	-3,56819	-1,98563	0,960347	0,946479
592	0,963056	0,746323	-0,30368	-1,02484	0,982882	1,024485
600	0,364222	0,21899	-5,84576	-3,12111	0,936078	1,050488
618	0,651335	0,599842	-3,1886	-1,60714	1,071289	1,031419
619	0,3068	0,336175	-6,37719	-2,65527	1,08169	1,047021
620	0,520083	0,475333	-4,4033	-2,10209	0,986349	1,027952
622	0,757976	0,636462	-2,20165	-1,46156	0,991549	1,00195
6	1,086104	0,870833	0,835109	-0,52989	0,906609	1,033153
15	1,028682	0,804916	0,303676	-0,79192	0,930878	1,045287
24	1,012276	0,856184	0,151838	-0,58812	0,920477	1,055688
38	1,045088	0,768296	0,455514	-0,9375	0,96208	0,923944
39	1,061495	0,966046	0,607352	-0,1514	1,007151	0,934345

204	1,053292	0,826888	0,531433	-0,70458	1,078223	0,896208
42	0,446254	0,321527	-5,08657	-2,7135	0,568581	0,500975
67	1,422436	1,434786	3,947786	1,711952	0,785265	0,901408
243	1,012276	1,031962	0,151838	0,110636	0,799133	1,102492
256	0,700554	0,504629	-2,73308	-1,98563	0,520043	0,691658
301	1,012276	0,922101	0,151838	-0,32609	0,752329	1,00195
328	0,725163	0,61449	-2,50533	-1,54891	0,833803	1,097291
366	0,610319	0,424064	-3,56819	-2,30589	0,610184	0,891008
578	0,995869	0,870833	1,97E-15	-0,52989	0,653521	0,934345
586	0,92204	0,892805	-0,68327	-0,44255	0,705525	0,998483

Appendix Table 8. 4 List of Drug Screen Hits and their Documented Biological Activities

DRUG N0	DRUG NAME	NOTES	NF-KB	JAK/ STAT	AKT/ PI3K	MAPK/JNK/ERK/P38	CELL CYCLE	ION TRANSPORT	REFERENCES
332	Alantolactone	**MDA-MB-231:** ER stress --Bcl-2, cyclin B1, CDC2, pSTAT3, cyclin D1, NF-kB; ++p-c-Jun ; **Other cells:** --AKT, Nrf2; ++p38, ROS; **In myocardial infarction:** --ROS, apoptosis, Ca^{2+} overload, L-type Ca^{2+} current.	yes	yes	yes	yes	yes	yes	(Babaei et al., 2021, Liu et al., 2022)
348	Punicalagin	--NF-kB, ERK/JNK/p38/MAPK, PI3K/AKT/mTOR, JAK/STAT; ++ glutamate uptake in colon cancer cell lines; It binds metal ions such as iron and copper.	yes	yes	yes	yes	no	yes	(Venusova et al., 2021, Xu et al., 2021, Kulkarni et al., 2007, Biolley et al., 2019)
390	Brevilin	--cyclin D, CDC2, p-PI3K/p-AKT/p-mTOR, pSTAT3 ++PARP, cleaved Caspase 9, Bax.	no	yes	yes	no	yes	no	(Liu et al., 2019b)
197	Ergolide	--PGE2, iNOS, COX-2, NF-kB(activity).	yes	no	no	no	no	no	(Whan Han et al., 2001)

600	Euphorbia factor L9	**Generally lathyranes**: --Pglycoprotein-ATPase, NF-kB; Cytotoxic activity against tumour and nontumor epithelial cell lines; **Other properties of general Euphorbia derivatives:** Antioxidant, antibacterial, antiangiogenetic, wound healing, analgesic activity (inhibiting TRPV1 channels)	yes	no	no	no	no	yes	(Huang et al., 2021b, Liu et al., 2020a, Benjamaa et al., 2022, Basu et al., 2019, Yang et al., 2015b)
556	Dicentrine	Na^+ /K^+ channel blocker; --α-adrenoreceptors; TRPA1 (Ca^{2+}) channel; **Anti-inflammatory action:** ++ Caspase 8, 9,3, PARP; --cIAP2, cFLIP, Bcl-XL, TAK1/p38/JNK/AKT/NF-kB/AP-1.	yes	no	yes	yes	no	yes	(Young et al., 1994, Montrucchio et al., 2013, Clapham, 2015, Yodkeeree et al., 2018, Ooppachai et al., 2019)
269	Glycocalyxin A	Impacts PI3K/AKT; ++ATF4/CHOP/CHAC1, BAX, --Bcl-2, ROS, cleaved Caspase 9, 3; ++ purine metabolism; --pSTAT3/IL-6, mitochondrial	no	yes	yes	yes	no	no	(Zhu et al., 2018, Wang et al., 2022b, Xiao et al., 2013, Zhang et al., 2022a, Li et al.,

		membrane potential, amino acid metabolism.							2021c, Liu et al., 2018b)
116	Isoalantolactone	**In prostate cancer:** ++ER stress, ROS, JNK; **In MDA-MB-231:** --p38/MAPK/NF-kB.	yes	no	yes	yes	no	no	(Huang et al., 2021a, Wang et al., 2016)
214	Britannin	-- cyclin D1, CDK4, NF-kB/ROS, Keap1-Nrf2, c-Myc/HIF1α -> --PD-1/PD-L1	yes	no	no	no	yes	no	(Hamzeloo-Moghadam et al., 2019, Bailly, 2021)
619	Artemether	-- nucleic acid synthesis (antimalarial drug), chemotaxis, cytokine production in macrophages and neutrophils; ++ glutamine, glutamic acid, aspartic acid, ornithine, glycine, histidine, phenylalanine and threonine; -- cancer cell proliferation, angiogenesis; ++ apoptosis and ROS. Artemisinin derivatives: ++ apoptosis by inhibiting JAK/ STAT signalling -- TNF induced signalling, including NF-kB activation and expression of downstream genes (c-IAP1, Bcl-2, FLIP, COX-2,	yes	may be	yes	yes	yes	yes	(White et al., 1999, Morad et al., 2022, Schellenberg and Coatney, 1961, Krishna et al., 2008, Beekman et al., 1998, Rong et al., 2022, Bose et al., 2020, Wang et al., 2017, Bai et al., 2020, Moreira Souza et al., 2020)

		cyclinD1, MMP-9, VEGF, TNF, iNOS, and MCP1); ++PI3K/ Akt and AMPK in mouse liver and skeletal muscle, promoting anti-diabetic effects; ++ NCX-dependent lengthening of action potential and interferes with Ca^{2+} currents in mouse cardiac myocytes.							
167	Scabertopin	antitumor, proapoptotic activity.	no	no	no	no	no	no	(Xu et al., 2006, Geetha et al., 2012)
337	Lasalocid (sodium)	++ROS, cytotoxic apoptosis, autophagy; affects cellular trafficking and Golgi integrity; Cationic ionophore antibiotic.	no	no	mayb e	no	no	yes	(Mahtal et al., 2020)
560	Laudanosine	interacts with GABA and opioid receptors	no	no	no	no	no	no	(Katz et al., 1994)
452	Colchicine	--microtubule assembly, inflammasome activation (interferes with P2X7/P2X2 induced NLRP3 activation & pore formation); interferes with RhoA/Rho effector kinase (ROCK) and NF-	yes	no	no	no	no	yes	(Dalbeth et al., 2014, Leung et al., 2015, Sun et al., 2019, Blaghen et al., 1999, Brazaluk et al., 1996,

		kB via tubulin disruption; **++ trans-membrane transport of divalent ions; -- glycine receptor (glycine/amino acid transport).**							Muñoz-Montesino et al., 2020)
361	Parthenolide	--NF-kB, HIF-1α, Th17 cells (in EAE);	yes	no	no	no	no	no	(Saadane et al., 2007, Dawood et al., 2019, Zhang et al., 2022b)
123	Eupalinolide B	--(p-)STAT3, AKT, mitochondrial membrane potential ++G2/M arrest, apoptosis, Caspase3 activity, ROS; Regulates AKT/p38/MAPK	no	yes	yes	yes	yes	no	(Lou et al., 2019, Yang et al., 2016a, Zhao et al., 2022)
530	Paclitaxel	TLR4-ligand ++MyD88/NF-kB/JNK/p38, JAK/STAT, Bad/Bax/Bcl-2s mediated apoptosis, Raf-1/p53/p21 mediated apoptosis, ROS; --microtubule depolymerization -> G2/M arrest, IDO1 in breast cancer, glutamine uptake;	yes	yes	yes	yes	yes	yes	(Akin et al., 2021, Kampan et al., 2015, Wu et al., 2007, Lv et al., 2017, Salvadori et al., 2015)

		Induces amino acid transport-mediated apoptosis in breast cancer.							
473	CFN97008	No info	no						
349	7-epi-Taxol	active metabolite of paclitaxel	see 530						
468	Securine	--GABA receptor A, ++DNA damage cell cycle arrest and cell death, IRAK/JNK/AP-1 mediated cancer cell death (NF-kB INDEPENDENT)	no	no	no	yes	yes	no	(Gupta et al., 2011, Beutler et al., 1985, Gupta et al., 2015)
352	Cryptotanshinone	--PI3K/Akt/mTOR; affects JAK2/STAT3, NF-KB, AMPK pathways; **Anti-inflammatory mechanisms:** interferes with TLR4-MyD88/PI3K/Nrf2 and TLR4-MyD88/NF-κB/MAPK pathway; **organ fibrosis:** interferes with NF-κB, and Nrf-2/HO-1 pathways; **neuroprotective effects:** -- PI3K/AKT-eNOS pathway.	**yes**	**yes**	**yes**	**yes**	**no**	**no**	(Luo et al., 2020, Li et al., 2021a)

45	Andrographolide	--NF-kB, COX-2,TNFα, IL-1β, IL6 production	yes	no	no	no	no	no	(Jayakumar et al., 2013)
359	Paclitaxel		see 530						
92	Platycodin D2	--MAPK/p38/JNK/ERK, PI3K/AKT/NF-kB or mTOR, PGE2, NO, proinflammatory cytokines.	yes	no	yes	yes	no	no	(Li et al., 2015, Chun and Kim, 2013, Jang et al., 2013)
67	Forskolin	++cAMP levels & signalling, cleaved Caspases 3, 9, c-JNK-mediated apoptosis, ERK1/2 JNK1/2 phosphorylation (transient ++survival, constant ++death), Na^+&Cl- transport in epithelium; --β-catenin, cyclin D1, cMyc, NF-kB, TLR4, MCP1, NKA activity (in combination with other drugs)	yes	no	no	yes	yes	yes	(Wang et al., 2019a, Barovsky et al., 1984, Chiadak et al., 2016, Park et al., 2012, Bajnath et al., 1991, Bajnath et al., 1993, Cuthbert and Spayne, 1982, Ono et al., 1995, Fisone et al., 1998)

Abbreviation list: AMPK - AMP-activated protein kinase, AP-1 - adaptor protein 1, ATF4 - activating transcription factor 4, Bax- BCL2-Associated X Protein, Bcl-2 - B-cell leukaemia/lymphoma 2 protein, Bcl-XL - B-cell lymphoma-extra-large, cAMP – cyclic adenosine monophosphate, CDC2 - cell division control 2, CDK4 - Cyclin-dependent kinase 4, (c)FLIP - Cellular FLICE (FADD-like IL-1β-converting enzyme)-inhibitory protein, CHAC1 - catalyses the cleavage of glutathione into 5-oxo-L-proline and a Cys-Gly dipeptide, CHOP - C/EBP Homologous Protein, cIAP2 - cellular inhibitor of apoptosis 2, c-Myc - cellular Myc oncogene, COX-2 – cyclooxygenase 2, EAE - Experimental Autoimmune Encephalomyelitis, ER – endoplasmic reticulum, ERK - extracellular signal-regulated kinase, eNOS - Endothelial nitric oxide synthase, GABA receptor - γ-Aminobutyric acid type A, HIF1α – hypoxia inducible factor 1 α, HO- 1 - haeme oxygenase-1, IAP-1 – inhibitor of apoptosis 1, IDO1 – indoleamine 2,3-dioxygenase, IL- 1β/6 – interleukin 1β/6, iNOS- inducible nitric oxide synthase, IRAK - Interleukin 1 Receptor Associated Kinase 1, JAK – Janus Kinase, JNK - c-Jun N-terminal kinase, MAPK- mitogen activated protein kinase, MCP1 - Monocyte chemoattractant protein-1, MMP9 – matrix metalloprotease 9, MyD88 - Myeloid Differentiation Primary-Response Gene 88, NCX – Na^+/Ca^{2+} exchanger, NF-kB- nuclear factor kB, NKA – Na^+/K^+ ATPase, NLRP3 - NLR family pyrin domain containing 3, NO - nitric oxide, Nrf2 - nuclear factor erythroid 2–related factor 2, p-c-Jun – phosphorylated c-Jun proto- oncogene, (p)-Akt – (phosphorylated) Ak strain transforming, PARP - poly-ADP ribose polymerase, PD-1/PD-L1 – programmed death 1/programmed death ligand 1, PGE2 – prostaglandin E2, PI3K - phosphatidylinositol-3 kinase, (p)-mTOR –(phosphorylated) mechanistic target of rapamycin, (p)STAT(3) – (phosphorylated) signal transducer and activator of transcription (3), P2X7/P2X2 - P2X purinoceptor 7/2, p21 - Cyclin-dependent kinase inhibitor 1, p38 - p38 mitogen-activated protein kinases, p53 – oncogenic protein, Raf1 - Rapidly Accelerated Fibrosarcoma 1, RhoA - RAS homologue gene family member A, ROCK - Rho-associated protein kinases, ROS – reactive oxygen species, TAK1 - TGF-β-activated kinase 1, Th17 – T helper 17, TLR4 – toll-like receptor 4, TRPA1 - Transient receptor potential ankyrin 1 TRPV1 - transient receptor potential vanilloid 1, VEGF – vascular endothelial growth factor.

8.3.1. Group 4 – Validation studies

Having classified the hits into 4 groups based on their impact on IDO1 expression, the next step was to select representative compounds and identify a potential mechanism of action. Group 4 only consisted of 2 compounds. Compound 352, Cryptotanshinone, was selected for further studies, as it was the compound with the lowest impact on membrane PD-L1, while still causing a ~50 % decrease in sPD-L1 levels.

This study aimed to validate the impact of Cryptotanshinone, by testing the effect on soluble and membrane PD-L1 mRNA expression in the presence and absence of the IFNγ/TNF stimulation. Appendix Figure 8.4 shows, however, that the chosen compound, Cryptotanshinone (352), did not impact on either soluble (A) or membrane PD-L1 (B).

Thus, this short set of experiments did not validate the previous observations (Figure 5.8) regarding the impact of Cryptotanshinone on membrane and soluble PD-L1. For this reason, this group of compounds was not further investigated.

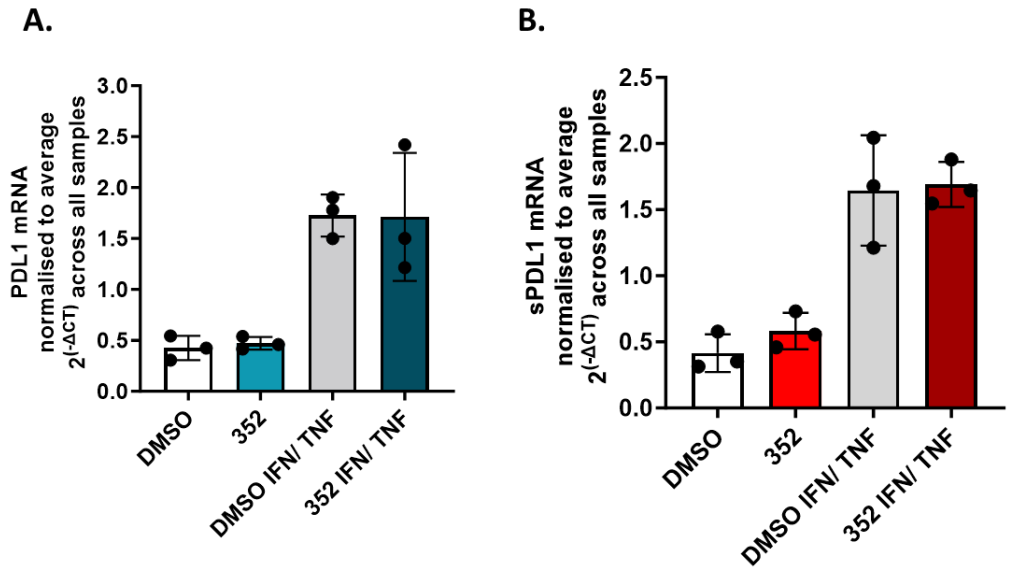

Appendix Figure 8.4 Impact of Cryptotanshinone (352) on soluble (A) and membrane PD-L1(B) mRNA expression. Samples were prepared as detailed in section 2.2 and qRT-PCR was carried out as described in section 2.14, data was normalized to β-actin, and fold change from the average expression levels across all samples was calculated using $2^{(-\Delta CT)}$ values. Statistical analysis was carried out using a one-way ANOVA coupled with a Bonferroni's post-test to compare DMSO Vs 325 +/- IFNγ/TNF stimulation. All experiments were carried out with n=3 biological replicates.

9. Abbreviation List

1-80:0-lysoPC/ 1-16:0-lysoPC - lysophosphatidyl choline derivatives

ABPP - activity-based protein profiling probes

ACMS – 2-amino 3-carboxymuconic acid 6-semialdehyde

ACMSD - 2-amino 3-carboxymuconic acid 6-semialdehyde decarboxylase

ADP – adenosine diphosphate

AhR – aryl hydrocarbon receptor

Akt - Ak strain transforming

AMP – adenosine monophosphate

AMPK – AMP-activated protein kinase

AMS – 2-aminomuconic 6-semialehide

AMSD - 2-aminomuconic 6-semialehide dehydrogenase

AP-1 -adaptor protein 1

AP1-3 – activator proteins 1 to 3

ASIC - acid-sensing ion channels

ATF - activating transcription factor

ATG5 - autophagy related 5

ATP – adenosine triphosphate

ATP1A1 - α1 subunit of the NKA

ATP1B1 - β1 subunit of the NKA

BCA - bicinchoninic acid assay

BRCA 1/ 2 - BReast CAncer genes 1 and 2

BSA – bovine serum albumin

BTLA - B and T lymphocyte associated

CaMK - calmodulin kinase

cAMP – cyclic adenosine monophosphate

CBP - CREB-binding protein

CD4/8/3/28/80/86/ 226/155/112 – cluster differentiate 4/8/3/28/80/86226/155/112

CDH1 - catherin-1

CDK 4/6 - cyclin-dependent kinase 4/6

cDNA – complementary DNA

CEACAM1 - carcinoembryonic antigen cell adhesion molecule 1

cJNK - c-Jun N-terminal kinase

CNAP - Centre for novel agricultural products

COI – compound of interest

COX-2 - cyclooxygenase 2

CRE – cAMP response element

CREB - cAMP-response element binding protein

CRTC - CREB-regulated transcription coactivator 1

CT – cycle threshold

CTF - CCAAT box-binding transcription factor

CTLA-4 - cytotoxic T-lymphocyte associated protein 4

CV – coefficient of variation

DC – dendritic cells

DCIS/LCIS - ductal/lobular carcinoma in situ

DMSO -dimethylsulfoxide

EFL2/3/9 – Euphorbia factor L 2/3/9

EGFR - epidermal growth factor receptor

eIF2α - eukaryotic initiation factor 2α

ENaC - epithelial Na^+ channel

ER - oestrogen receptor

ERK1/2 - extracellular signal-regulated kinase 1/2

FC - fragment crystallizable

FCSP - fucose-containing sulphated polysaccharides

FDA – Food and drug administration

FDR – false discovery rate

FOXP3 - forkhead box P3

FWHM - full width at half maximum

GAPDH - glyceraldehyde dehydrogenase

GAS - gamma activation sequence

GCN2 - general control nonderepressible 2

GLP2 polysaccharide - Ganoderma lucidum polysaccharide

GPR35 - G-protein receptor 35

GTPase - guanosine triphosphate hydrolase

HAA – 3-hydroxyanthranilic acid

HAAO - 3-hydroxyanthranilic acid 3, 4 -dioxygenase

HDAC – histone deacetylase

HER2 - human epidermal growth factor receptor 2

HIF-1α - hypoxia-induced factor 1 α

HLA I/ II – human leucocyte antigen I/ II

HLA-A, B, C – human leukocyte antigen A, B, C

HMDB – human metabolite database

HPLC - high performance liquid chromatography

HR – hormone receptor

HMEC - human primary mammary epithelial cell

HVEM - herpes virus entry mediator

IC/ EC50 - half-maximal inhibitory/ effective concentration

IDC/ILC - invasive ductal/lobular carcinoma

IDO1 - indoleamine 2, 3-dioxygenase 1

IEGs – immediate early genes

IFNGR - Interferon γ Receptor

IFNγ/α/β – interferon gamma/ alpha/ beta

IL - 1β/ 17/2/23/6 - interleukin 1β/ 17/2/23/6

iPLA2 - caspase 3-induced Ca^{2+} independent activation of phospholipase A2

IRF1 - IFN regulatory factor 1

ISREs - IFN-stimulated response elements

ITAM - immunoreceptor tyrosine-based activation motif

ITIM - immunoreceptor tyrosine-based inhibition motif

ITSM - immunoreceptor tyrosine-based switch motif

JAK1 – Janus kinase 1

KAT - kynurenine aminotransferase,

KD – knockdown

KMO – kynurenine monooxygenase.

LAG3 - lymphocyte activation gene 3

LBK1 - liver kinase B1

LC – liquid chromatography

LCK - lymphocyte-specific protein tyrosine kinase

LDL- low density lipoprotein

LPS – lipopolysaccharide

LysPC - lysophosphatidyl choline

MAPK - mitogen-activated protein kinase

MEF - myocyte-specific enhancer factor

METABRIC - Molecular Taxonomy of Breast Cancer International Consortium

MM - master mix

MS - mass spectrum

mTOR - mechanistic target of rapamycin

NAD - nicotinamide adenine dinucleotide

NALCN - Na^+ leak channel, non-selective

NBCn1 - Na^+/ $HCO3^-$ cotransporter

NCLX - Na^+/Ca^{2+} exchanger

NF-1 - nuclear factor 1

NFAT - nuclear factor of activated t cells

NF-kB - nuclear factor kB

NHE1 - Na^+/H^+ exchanger

NK – natura killer cells

NKA - Na^+/ K^+ ATPase

NKAi - ouabain insensitive NKA

NKCC - the Na^+-K^+-Cl^- cotransporter

NMDA - N-methyl-D-aspartate receptor

NO – nitric oxide

Nrf2 - nuclear factor erythroid 2–related factor 2

NTC – non-targeting control

OXPHOS - oxidative phosphorylation

P2X - ATP-gated P2X receptor cation channel family

PARP2 – poly ADP-ribose polymerase 2

PCA - principal component analysis

PD-1 - programmed death 1

PD-L1 - programmed death ligand 1

PGE2 - prostaglandin E2

PI3K - phosphatidylinositol-3 kinase

PIAS - protein inhibitors of activated STATs

PKA/C - protein kinase A/C

PLM – phospholemman

PME-1 - protein phosphatase methylesterase-1

PP2A - protein phosphatase 2A

PR - progesterone receptor

PROTAC - proteolysis targeting chimeras

PSS – physiological saline solution

PTEN - phosphatase and tensin homolog

PTP - protein tyrosine phosphatases

RNAseq - RNA sequencing

ROS - reactive oxygen species

RT - room temperature

SBFI - AM - sodium-binding benzofuran isophthalate acetoxymethyl ester

SD - standard deviation

SGLT - sodium-glucose transport proteins

SHP1 - Src homology 2 domain-containing protein tyrosine phosphatase 1

SHP2 - Src homology region 2 (SH2)-containing protein tyrosine phosphatase 2

SIK1 - salt inducible kinase 1

SLC - amino acid transporter/solute carrier

SLC1A5 - solute carrier family 1 member 5

SLC7A5 – L-type amino acid transporter

SNR – signal to noise ratio

SOCS3 - suppressor of cytokine signalling 3

Sp-1 to 3 -specificity proteins 1 to 3

sPD-L1 - soluble PD-L1

SRE - serum response element

SRK 1/ 3 - steroid receptor co-activators 1 and 3

STAT 1/ 3/ 5 - signal transducer and activator of transcription 1/3/ 5

T eff – effector T cell

TCGA - The Cancer Genome Atlas Program

TCR – T cell receptor

TDO - Trp dehydrogenase

TGF-β – transforming growth factor β

Th cells – T helper cells

TIGIT - T-cell immunoglobulin and ITIM domain

TIM3 - T cell immunoglobulin and mucin domain-containing protein 3

TLR - Toll-like receptor

TNBC - triple negative breast cancer

TNF - tumour necrosis factor

TNFR – TNF receptor

TP53 - tumour protein p53

TPC/TRPML - two-pore channels/ transient receptor potential mucolipin 1

TPC6 - transient receptor potential cation channel subfamily C member 6

TPH1/ 2 - Trp hydroxylases 1 and 2

Treg – regulatory T cells

TRIM - T cell receptor interacting molecule

t-RNA - transfer-RNA

TRP - transient receptor potential

Trp – tryptophan

TTX -tetrodotoxin

UB2A - upstream binding protein 1 associated protein 2A

VGSC (Na_v) - voltage gated Na^+ channel

VTD - veratridine

Wnt - wingless-related integration site

WRS - Trp-t-RNA synthetase

ZAP70 - zeta-chain-associated protein kinase 70

10. References

AAS, V., LARSEN, K. & IVERSEN, J. G. 1998. IFN-gamma induces calcium transients and increases the capacitative calcium entry in human neutrophils. *J Interferon Cytokine Res,* 18**,** 197-205.

ABDOU, Y., GOUDARZI, A., YU, J. X., UPADHAYA, S., VINCENT, B. & CAREY, L. A. 2022. Immunotherapy in triple negative breast cancer: beyond checkpoint inhibitors. *npj Breast Cancer,* 8**,** 121.

ABDUL, M. & HOOSEIN, N. 2001. Inhibition by anticonvulsants of prostate-specific antigen and interleukin-6 secretion by human prostate cancer cells. *Anticancer Res,* 21**,** 2045-8.

ABDULLAH, A., SANE, S., BRANICK, K. A., FREELING, J. L., WANG, H., ZHANG, D. & REZVANI, K. 2015. A plant alkaloid, veratridine, potentiates cancer chemosensitivity by UBXN2A-dependent inhibition of an oncoprotein, mortalin-2. *Oncotarget,* 6**,** 23561-81.

ADAMS, S., DIAMOND, J. R., HAMILTON, E., POHLMANN, P. R., TOLANEY, S. M., CHANG, C. W., ZHANG, W., IIZUKA, K., FOSTER, P. G., MOLINERO, L., FUNKE, R. & POWDERLY, J. 2019a. Atezolizumab Plus nab-Paclitaxel in the Treatment of Metastatic Triple-Negative Breast Cancer With 2-Year Survival Follow-up: A Phase 1b Clinical Trial. *JAMA Oncol,* 5**,** 334-342.

ADAMS, S., GRAY, R. J., DEMARIA, S., GOLDSTEIN, L., PEREZ, E. A., SHULMAN, L. N., MARTINO, S., WANG, M., JONES, V. E., SAPHNER, T. J., WOLFF, A. C., WOOD, W. C., DAVIDSON, N. E., SLEDGE, G. W., SPARANO, J. A. & BADVE, S. S. 2014. Prognostic value of tumor-infiltrating lymphocytes in triple-negative breast cancers from two phase III randomized adjuvant breast cancer trials: ECOG 2197 and ECOG 1199. *J Clin Oncol,* 32**,** 2959-66.

ADAMS, S., LOI, S., TOPPMEYER, D., CESCON, D. W., DE LAURENTIIS, M., NANDA, R., WINER, E. P., MUKAI, H., TAMURA, K., ARMSTRONG, A., LIU, M. C., IWATA, H., RYVO, L., WIMBERGER, P., RUGO, H. S., TAN, A. R., JIA, L., DING, Y., KARANTZA, V. & SCHMID, P. 2019b. Pembrolizumab monotherapy for previously untreated, PD-L1-positive, metastatic triple-negative breast cancer: cohort B of the phase II KEYNOTE-086 study. *Ann Oncol,* 30**,** 405-411.

ADISESHAIAH, P. P., CLOGSTON, J. D., MCLELAND, C. B., RODRIGUEZ, J., POTTER, T. M., NEUN, B. W., SKOCZEN, S. L., SHANMUGAVELANDY, S. S., KESTER, M., STERN, S. T. & MCNEIL, S. E. 2013. Synergistic combination therapy with nanoliposomal C6-ceramide and vinblastine is associated with autophagy dysfunction in hepatocarcinoma and colorectal cancer models. *Cancer Lett,* 337**,** 254-65.

AHMED, F., TOUME, K., OHTSUKI, T., RAHMAN, M., SADHU, S. K. & ISHIBASHI, M. 2011. Cryptolepine, isolated from Sida acuta, sensitizes human gastric adenocarcinoma cells to TRAIL-induced apoptosis. *Phytother Res,* 25**,** 147-50.

AIZMAN, O., UHLÉN, P., LAL, M., BRISMAR, H. & APERIA, A. 2001. Ouabain, a steroid hormone that signals with slow calcium oscillations. *Proc Natl Acad Sci U S A,* 98**,** 13420-4.

AKIN, E. J., ALSALOUM, M., HIGERD, G. P., LIU, S., ZHAO, P., DIB-HAJJ, F. B., WAXMAN, S. G. & DIB-HAJJ, S. D. 2021. Paclitaxel increases axonal localization and vesicular trafficking of Nav1.7. *Brain,* 144**,** 1727-1737.

AL-HAJJ, M., WICHA, M. S., BENITO-HERNANDEZ, A., MORRISON, S. J. & CLARKE, M. F. 2003. Prospective identification of tumorigenic breast cancer cells. *Proceedings of the National Academy of Sciences,* 100**,** 3983-3988.

ALVARADO, Y., KANTARJIAN, H. M., LUTHRA, R., RAVANDI, F., BORTHAKUR, G., GARCIA-MANERO, G., KONOPLEVA, M., ESTROV, Z., ANDREEFF, M. & CORTES, J. E. 2014.

Treatment with FLT3 inhibitor in patients with FLT3-mutated acute myeloid leukemia is associated with development of secondary FLT3-tyrosine kinase domain mutations. *Cancer,* 120**,** 2142-9.

AMARA, S., ZHENG, M. & TIRIVEEDHI, V. 2016. Oleanolic Acid Inhibits High Salt-Induced Exaggeration of Warburg-like Metabolism in Breast Cancer Cells. *Cell Biochem Biophys,* 74**,** 427-34.

AMEMIYA, M., TABEI, K., KUSANO, E., ASANO, Y. & ALPERN, R. J. 1999. Incubation of OKP cells in low-K+ media increases NHE3 activity after early decrease in intracellular pH. *Am J Physiol,* 276**,** C711-6.

AMES-SIBIN, A. P., BARIZÃO, C. L., CASTRO-GHIZONI, C. V., SILVA, F. M. S., SÁ-NAKANISHI, A. B., BRACHT, L., BERSANI-AMADO, C. A., MARÇAL-NATALI, M. R., BRACHT, A. & COMAR, J. F. 2018. β-Caryophyllene, the major constituent of copaiba oil, reduces systemic inflammation and oxidative stress in arthritic rats. *J Cell Biochem,* 119**,** 10262-10277.

AMIN, M. B., GREENE, F. L., EDGE, S. B., COMPTON, C. C., GERSHENWALD, J. E., BROOKLAND, R. K., MEYER, L., GRESS, D. M., BYRD, D. R. & WINCHESTER, D. P. 2017. The Eighth Edition AJCC Cancer Staging Manual: Continuing to build a bridge from a population-based to a more "personalized" approach to cancer staging. *CA Cancer J Clin,* 67**,** 93-99.

AMOBI-MCCLOUD, A., MUTHUSWAMY, R., BATTAGLIA, S., YU, H., LIU, T., WANG, J., PUTLURI, V., SINGH, P. K., QIAN, F., HUANG, R. Y., PUTLURI, N., TSUJI, T., LUGADE, A. A., LIU, S. & ODUNSI, K. 2021. IDO1 Expression in Ovarian Cancer Induces PD-1 in T Cells via Aryl Hydrocarbon Receptor Activation. *Front Immunol,* 12**,** 678999.

ANDRÉ, F., O'REGAN, R., OZGUROGLU, M., TOI, M., XU, B., JERUSALEM, G., MASUDA, N., WILKS, S., ARENA, F., ISAACS, C., YAP, Y. S., PAPAI, Z., LANG, I., ARMSTRONG, A., LERZO, G., WHITE, M., SHEN, K., LITTON, J., CHEN, D., ZHANG, Y., ALI, S., TARAN, T. & GIANNI, L. 2014. Everolimus for women with trastuzumab-resistant, HER2-positive, advanced breast cancer (BOLERO-3): a randomised, double-blind, placebo-controlled phase 3 trial. *Lancet Oncol,* 15**,** 580-91.

ANTONENKO, Y. N., ROKITSKAYA, T. I. & HUCZYŃSKI, A. 2015. Electrogenic and nonelectrogenic ion fluxes across lipid and mitochondrial membranes mediated by monensin and monensin ethyl ester. *Biochim Biophys Acta,* 1848**,** 995-1004.

AQIL, M., AHAD, A., SULTANA, Y. & ALI, A. 2007. Status of terpenes as skin penetration enhancers. *Drug Discov Today,* 12**,** 1061-7.

ARISAKA, H., IKEDA, U., TAKAYASU, T., TAKEDA, K., NATSUME, T. & HOSODA, S. 1988. Ouabain inhibits intracellular pH recovery from acidosis in cultured mouse heart cells. *Journal of Molecular and Cellular Cardiology,* 20**,** 1-3.

ARNONE, D., SARAYKAR, S., SALEM, H., TEIXEIRA, A. L., DANTZER, R. & SELVARAJ, S. 2018. Role of Kynurenine pathway and its metabolites in mood disorders: A systematic review and meta-analysis of clinical studies. *Neurosci Biobehav Rev,* 92**,** 477-485.

ASKARI, A. 2019. The sodium pump and digitalis drugs: Dogmas and fallacies. *Pharmacology Research & Perspectives,* 7**,** n/a-n/a.

ATKINS, C., BONAGURA, J., ETTINGER, S., FOX, P., GORDON, S., HAGGSTROM, J., HAMLIN, R., KEENE, B., LUIS-FUENTES, V. & STEPIEN, R. 2009. Guidelines for the diagnosis and treatment of canine chronic valvular heart disease. *J Vet Intern Med,* 23**,** 1142-50.

BABAEI, G., GHOLIZADEH-GHALEH AZIZ, S., RAJABI BAZL, M. & KHADEM ANSARI, M. H. 2021. A comprehensive review of anticancer mechanisms of action of Alantolactone. *Biomedicine & Pharmacotherapy,* 136**,** 111231.

BABON, J. J., KERSHAW, N. J., MURPHY, J. M., VARGHESE, L. N., LAKTYUSHIN, A., YOUNG, S. N., LUCET, I. S., NORTON, R. S. & NICOLA, N. A. 2012. Suppression of cytokine

signaling by SOCS3: characterization of the mode of inhibition and the basis of its specificity. *Immunity,* 36**,** 239-50.
BACHELOT, T., FILLERON, T., BIECHE, I., ARNEDOS, M., CAMPONE, M., DALENC, F., COUSSY, F., SABLIN, M. P., DEBLED, M., LEFEUVRE-PLESSE, C., GONCALVES, A., REYNIER, M. M., JACOT, W., YOU, B., BARTHELEMY, P., VERRET, B., ISAMBERT, N., TCHIKNAVORIAN, X., LEVY, C., THERY, J. C., L'HARIDON, T., FERRERO, J. M., MEGE, A., DEL PIANO, F., ROULEAU, E., TRAN-DIEN, A., ADAM, J., LUSQUE, A., JIMENEZ, M., JACQUET, A., GARBERIS, I. & ANDRE, F. 2021. Durvalumab compared to maintenance chemotherapy in metastatic breast cancer: the randomized phase II SAFIR02-BREAST IMMUNO trial. *Nat Med,* 27**,** 250-255.
BADAWY, A. A. 2002. Tryptophan metabolism in alcoholism. *Nutr Res Rev,* 15**,** 123-52.
BADAWY, A. A. 2017. Kynurenine Pathway of Tryptophan Metabolism: Regulatory and Functional Aspects. *Int J Tryptophan Res,* 10**,** 1178646917691938.
BADOWSKA-KOZAKIEWICZ, A. M. & BUDZIK, M. P. 2016. Immunohistochemical characteristics of basal-like breast cancer. *Contemp Oncol (Pozn),* 20**,** 436-443.
BAGLINI, E., SALERNO, S., BARRESI, E., MARZO, T., SETTIMO, F. D. & TALIANI, S. 2022. Cancer Immunotherapy: An Overview of Small Molecules as Inhibitors of the Immune Checkpoint PD-1/PD-L1 (2015-2021). *Mini Rev Med Chem,* 22**,** 1816-1827.
BAGUR, R. & HAJNÓCZKY, G. 2017. Intracellular Ca(2+) Sensing: Its Role in Calcium Homeostasis and Signaling. *Mol Cell,* 66**,** 780-788.
BAI, X., PEI, R., LEI, W., ZHAO, M., ZHANG, J., TIAN, L. & SHANG, J. 2020. Antidiabetic Effect of Artemether in Db/Db Mice Involves Regulation of AMPK and PI3K/Akt Pathways. *Front Endocrinol (Lausanne),* 11**,** 568864.
BAILLY, C. 2021. Anticancer Targets and Signaling Pathways Activated by Britannin and Related Pseudoguaianolide Sesquiterpene Lactones. *Biomedicines,* 9.
BAILLY, C., THURU, X. & QUESNEL, B. 2021. Soluble Programmed Death Ligand-1 (sPD-L1): A Pool of Circulating Proteins Implicated in Health and Diseases. *Cancers (Basel),* 13.
BAJNATH, R. B., AUGERON, C., LABOISSE, C. L., BIJMAN, J., DE JONGE, H. R. & GROOT, J. A. 1991. Electrophysiological studies of forskolin-induced changes in ion transport in the human colon carcinoma cell line HT-29 cl.19A: lack of evidence for a cAMP-activated basolateral K+ conductance. *J Membr Biol,* 122**,** 239-50.
BAJNATH, R. B., VAN DEN BERGHE, N., DE JONGE, H. R. & GROOT, J. A. 1993. Activation of ion transport by combined effects of ionomycin, forskolin and phorbol ester on cultured HT-29cl.19A human colonocytes. *Pflugers Arch,* 425**,** 90-9.
BALACHANDRAN, V. P., CAVNAR, M. J., ZENG, S., BAMBOAT, Z. M., OCUIN, L. M., OBAID, H., SORENSON, E. C., POPOW, R., ARIYAN, C., ROSSI, F., BESMER, P., GUO, T., ANTONESCU, C. R., TAGUCHI, T., YUAN, J., WOLCHOK, J. D., ALLISON, J. P. & DEMATTEO, R. P. 2011. Imatinib potentiates antitumor T cell responses in gastrointestinal stromal tumor through the inhibition of Ido. *Nat Med,* 17**,** 1094-100.
BALOG, A., LIN, T. A., MALEY, D., GULLO-BROWN, J., KANDOUSSI, E. H., ZENG, J. & HUNT, J. T. 2021. Preclinical Characterization of Linrodostat Mesylate, a Novel, Potent, and Selective Oral Indoleamine 2,3-Dioxygenase 1 Inhibitor. *Mol Cancer Ther,* 20**,** 467-476.
BANZOLA, I., MENGUS, C., WYLER, S., HUDOLIN, T., MANZELLA, G., CHIARUGI, A., BOLDORINI, R., SAIS, G., SCHMIDLI, T. S., CHIFFI, G., BACHMANN, A., SULSER, T., SPAGNOLI, G. C. & PROVENZANO, M. 2018. Expression of Indoleamine 2,3-Dioxygenase Induced by IFN-γ and TNF-α as Potential Biomarker of Prostate Cancer Progression. *Front Immunol,* 9**,** 1051.
BARAN, H., AMANN, G., LUBEC, B. & LUBEC, G. 1997. Kynurenic acid and kynurenine aminotransferase in heart. *Pediatr Res,* 41**,** 404-10.

BARDHAN, K., PATSOUKIS, N., WEAVER, J., FREEMAN, G., LI, L. & BOUSSIOTIS, V. A. 2016. PD-1 inhibits the TCR signaling cascade by sequestering SHP-2 phosphatase, preventing its translocation to lipid rafts and facilitating Csk-mediated inhibitory phosphorylation of Lck. *The Journal of Immunology,* 196**,** 128.15-128.15.

BAROVSKY, K., PEDONE, C. & BROOKER, G. 1984. Distinct mechanisms of forskolin-stimulated cyclic AMP accumulation and forskolin-potentiated hormone responses in C6-2B cells. *Mol Pharmacol,* 25**,** 256-60.

BARRY, W. H., BIEDERT, S., MIURA, D. S. & SMITH, T. W. 1981. Changes in cellular Na+, K+, and Ca2+ contents, monovalent cation transport rate, and contractile state during washout of cardiac glycosides from cultured chick heart cells. *Circ Res,* 49**,** 141-9.

BARTOK, O., PATASKAR, A., NAGEL, R., LAOS, M., GOLDFARB, E., HAYOUN, D., LEVY, R., KÖRNER, P. R., KREUGER, I. Z. M., CHAMPAGNE, J., ZAAL, E. A., BLEIJERVELD, O. B., HUANG, X., KENSKI, J., WARGO, J., BRANDIS, A., LEVIN, Y., MIZRAHI, O., ALON, M., LEBON, S., YANG, W., NIELSEN, M. M., STERN-GINOSSAR, N., ALTELAAR, M., BERKERS, C. R., GEIGER, T., PEEPER, D. S., OLWEUS, J., SAMUELS, Y. & AGAMI, R. 2021. Anti-tumour immunity induces aberrant peptide presentation in melanoma. *Nature,* 590**,** 332-337.

BASU, P., HORNUNG, R. S., AVERITT, D. L. & MAIER, C. 2019. Euphorbia bicolor (Euphorbiaceae) Latex Extract Reduces Inflammatory Cytokines and Oxidative Stress in a Rat Model of Orofacial Pain. *Oxid Med Cell Longev,* 2019**,** 8594375.

BAUER, T. M., JIGA, L. P., CHUANG, J. J., RANDAZZO, M., OPELZ, G. & TERNESS, P. 2005. Studying the immunosuppressive role of indoleamine 2,3-dioxygenase: tryptophan metabolites suppress rat allogeneic T-cell responses in vitro and in vivo. *Transpl Int,* 18**,** 95-100.

BAUMANN, T., DUNKEL, A., SCHMID, C., SCHMITT, S., HILTENSPERGER, M., LOHR, K., LAKETA, V., DONAKONDA, S., AHTING, U., LORENZ-DEPIEREUX, B., HEIL, J. E., SCHREDELSEKER, J., SIMEONI, L., FECHER, C., KÖRBER, N., BAUER, T., HÜSER, N., HARTMANN, D., LASCHINGER, M., EYERICH, K., EYERICH, S., ANTON, M., STREETER, M., WANG, T., SCHRAVEN, B., SPIEGEL, D., ASSAAD, F., MISGELD, T., ZISCHKA, H., MURRAY, P. J., HEINE, A., HEIKENWÄLDER, M., KORN, T., DAWID, C., HOFMANN, T., KNOLLE, P. A. & HÖCHST, B. 2020. Regulatory myeloid cells paralyze T cells through cell-cell transfer of the metabolite methylglyoxal. *Nat Immunol,* 21**,** 555-566.

BEEKMAN, A. C., WIERENGA, P. K., WOERDENBAG, H. J., VAN UDEN, W., PRAS, N., KONINGS, A. W., EL-FERALY, F. S., GALAL, A. M. & WIKSTRÖM, H. V. 1998. Artemisinin-derived sesquiterpene lactones as potential antitumour compounds: cytotoxic action against bone marrow and tumour cells. *Planta Med,* 64**,** 615-9.

BENDER, D. A. 1983. Biochemistry of tryptophan in health and disease. *Mol Aspects Med,* 6**,** 101-97.

BENJAMAA, R., MOUJANNI, A., KAUSHIK, N., CHOI, E. H., ESSAMADI, A. K. & KAUSHIK, N. K. 2022. Euphorbia species latex: A comprehensive review on phytochemistry and biological activities. *Front Plant Sci,* 13**,** 1008881.

BENZ, C. C. 2008. Impact of aging on the biology of breast cancer. *Crit Rev Oncol Hematol,* 66**,** 65-74.

BERLINGUER-PALMINI, R., MASI, A., NARDUCCI, R., CAVONE, L., MARATEA, D., COZZI, A., SILI, M., MORONI, F. & MANNAIONI, G. 2013. GPR35 activation reduces Ca2+ transients and contributes to the kynurenic acid-dependent reduction of synaptic activity at CA3-CA1 synapses. *PLoS One,* 8**,** e82180.

BERRIDGE, M. J., BOOTMAN, M. D. & RODERICK, H. L. 2003. Calcium signalling: dynamics, homeostasis and remodelling. *Nature Reviews Molecular Cell Biology,* 4**,** 517-529.

BERRONG, Z., MKRTICHYAN, M., AHMAD, S., WEBB, M., MOHAMED, E., OKOEV, G., MATEVOSYAN, A., SHRIMALI, R., ABU EID, R., HAMMOND, S., JANIK, J. E. & KHLEIF,

S. N. 2018. Antigen-Specific Antitumor Responses Induced by OX40 Agonist Are Enhanced by the IDO Inhibitor Indoximod. *Cancer Immunol Res,* 6**,** 201-208.
BETANCUR-GALVIS, L., PALOMARES, E., MARCO, J. A. & ESTORNELL, E. 2003. Tigliane diterpenes from the latex of Euphorbia obtusifolia with inhibitory activity on the mammalian mitochondrial respiratory chain. *J Ethnopharmacol,* 85**,** 279-82.
BEUTLER, J. A., KARBON, E. W., BRUBAKER, A. N., MALIK, R., CURTIS, D. R. & ENNA, S. J. 1985. Securinine alkaloids: a new class of GABA receptor antagonist. *Brain Res,* 330**,** 135-40.
BHATNAGAR, A. S. 2007. The discovery and mechanism of action of letrozole. *Breast Cancer Res Treat,* 105 Suppl 1**,** 7-17.
BHULLAR, K. S., LAGARÓN, N. O., MCGOWAN, E. M., PARMAR, I., JHA, A., HUBBARD, B. P. & RUPASINGHE, H. P. V. 2018. Kinase-targeted cancer therapies: progress, challenges and future directions. *Molecular Cancer,* 17**,** 48.
BIGAGLI, E., D'AMBROSIO, M., CINCI, L., NICCOLAI, A., BIONDI, N., RODOLFI, L., DOS SANTOS NASCIMIENTO, L. B., TREDICI, M. R. & LUCERI, C. 2021. A Comparative In Vitro Evaluation of the Anti-Inflammatory Effects of a Tisochrysis lutea Extract and Fucoxanthin. *Mar Drugs,* 19.
BILIR, C. & SARISOZEN, C. 2017. Indoleamine 2,3-dioxygenase (IDO): Only an enzyme or a checkpoint controller? *Journal of Oncological Sciences,* 3**,** 52-56.
BILLER, A., PFLUGMANN, I., BADDE, S., DIEM, R., WILDEMANN, B., NAGEL, A. M., JORDAN, J., BENKHEDAH, N. & KLEESIEK, J. 2016. Sodium MRI in Multiple Sclerosis is Compatible with Intracellular Sodium Accumulation and Inflammation-Induced Hyper-Cellularity of Acute Brain Lesions. *Sci Rep,* 6**,** 31269.
BIOLLEY, C., TRETOLA, M., BEE, G., JUD, C. & SILACCI, P. 2019. Punicalagin increases glutamate absorption in differentiated Caco-2 cells by a mechanism involving gene expression regulation of an EAAT3 transporter. *Food Funct,* 10**,** 5333-5338.
BLAGHEN, M., LAHLOU, N., DZAIRI, F. Z., MOUTAOUAKKIL, A. & TALBI, M. 1999. Complexation and ionophoric properties of taxol and colchicine: complex formation and transport of sodium, potassium, magnesium and calcium ions across a liquid membrane. *Nat Toxins,* 7**,** 179-85.
BLAIR, A. B., KLEPONIS, J., THOMAS, D. L., MUTH, S., MURPHY, A. G., KIM, V. & ZHENG, L. 2019. IDO1 inhibition potentiates vaccine-induced immunity against pancreatic adenocarcinoma. *Journal Of Clinical Investigation,* 129**,** 1742-1755.
BLANCO AYALA, T., LUGO HUITRÓN, R., CARMONA APARICIO, L., RAMÍREZ ORTEGA, D., GONZÁLEZ ESQUIVEL, D., PEDRAZA CHAVERRÍ, J., PÉREZ DE LA CRUZ, G., RÍOS, C., SCHWARCZ, R. & PÉREZ DE LA CRUZ, V. 2015. Alternative kynurenic acid synthesis routes studied in the rat cerebellum. *Front Cell Neurosci,* 9**,** 178.
BLAUSTEIN, M. P. & HAMLYN, J. M. 2020. Ouabain, endogenous ouabain and ouabain-like factors: The Na(+) pump/ouabain receptor, its linkage to NCX, and its myriad functions. *Cell Calcium,* 86**,** 102159.
BLAUSTEIN, M. P. & LEDERER, W. J. 1999. Sodium/calcium exchange: its physiological implications. *Physiol Rev,* 79**,** 763-854.
BLUMENTHAL, G. M., SCHER, N. S., CORTAZAR, P., CHATTOPADHYAY, S., TANG, S., SONG, P., LIU, Q., RINGGOLD, K., PILARO, A. M., TILLEY, A., KING, K. E., GRAHAM, L., RELLAHAN, B. L., WEINBERG, W. C., CHI, B., THOMAS, C., HUGHES, P., IBRAHIM, A., JUSTICE, R. & PAZDUR, R. 2013. First FDA approval of dual anti-HER2 regimen: pertuzumab in combination with trastuzumab and docetaxel for HER2-positive metastatic breast cancer. *Clin Cancer Res,* 19**,** 4911-6.
BOBULESCU, I. A., DI SOLE, F. & MOE, O. W. 2005. Na+/H+ exchangers: physiology and link to hypertension and organ ischemia. *Curr Opin Nephrol Hypertens,* 14**,** 485-94.

BOEDTKJER, E., MOREIRA, J. M., MELE, M., VAHL, P., WIELENGA, V. T., CHRISTIANSEN, P. M., JENSEN, V. E., PEDERSEN, S. F. & AALKJAER, C. 2013. Contribution of Na+,HCO3(-)-cotransport to cellular pH control in human breast cancer: a role for the breast cancer susceptibility locus NBCn1 (SLC4A7). *Int J Cancer,* 132**,** 1288-99.

BONDARAVA, M., LI, T., ENDL, E. & WEHNER, F. 2009. alpha-ENaC is a functional element of the hypertonicity-induced cation channel in HepG2 cells and it mediates proliferation. *Pflugers Arch,* 458**,** 675-87.

BØRRESEN-DALE, A. L. 2003. TP53 and breast cancer. *Hum Mutat,* 21**,** 292-300.

BOSE, S., BANERJEE, S., MONDAL, A., CHAKRABORTY, U., PUMAROL, J., CROLEY, C. R. & BISHAYEE, A. 2020. Targeting the JAK/STAT Signaling Pathway Using Phytocompounds for Cancer Prevention and Therapy. *Cells,* 9.

BOSS, W. F., MORRÉ, D. J. & MOLLENHAUER, H. H. 1984. Monensin-induced swelling of Golgi apparatus cisternae mediated by a proton gradient. *Eur J Cell Biol,* 34**,** 1-8.

BOTELHO, A. F. M., PIEREZAN, F., SOTO-BLANCO, B. & MELO, M. M. 2019. A review of cardiac glycosides: Structure, toxicokinetics, clinical signs, diagnosis and antineoplastic potential. *Toxicon,* 158**,** 63-68.

BRACHO-SANCHEZ, E., HASSANZADEH, A., BRUSKO, M. A., WALLET, M. A. & KESELOWSKY, B. G. 2019. Dendritic Cells Treated with Exogenous Indoleamine 2,3-Dioxygenase Maintain an Immature Phenotype and Suppress Antigen-specific T cell Proliferation. *J Immunol Regen Med,* 5.

BRACKENBURY, W. J. & DJAMGOZ, M. B. 2006. Activity-dependent regulation of voltage-gated Na+ channel expression in Mat-LyLu rat prostate cancer cell line. *J Physiol,* 573**,** 343-56.

BRAHMER, J., RECKAMP, K. L., BAAS, P., CRINÒ, L., EBERHARDT, W. E., PODDUBSKAYA, E., ANTONIA, S., PLUZANSKI, A., VOKES, E. E., HOLGADO, E., WATERHOUSE, D., READY, N., GAINOR, J., ARÉN FRONTERA, O., HAVEL, L., STEINS, M., GARASSINO, M. C., AERTS, J. G., DOMINE, M., PAZ-ARES, L., RECK, M., BAUDELET, C., HARBISON, C. T., LESTINI, B. & SPIGEL, D. R. 2015. Nivolumab versus Docetaxel in Advanced Squamous-Cell Non-Small-Cell Lung Cancer. *N Engl J Med,* 373**,** 123-35.

BRAHMKSHATRIYA, P. P. & BRAHMKSHATRIYA, P. S. 2013. Terpenes: Chemistry, Biological Role, and Therapeutic Applications. *In:* RAMAWAT, K. G. & MÉRILLON, J.-M. (eds.) *Natural Products: Phytochemistry, Botany and Metabolism of Alkaloids, Phenolics and Terpenes.* Berlin, Heidelberg: Springer Berlin Heidelberg.

BRAND, A., SINGER, K., KOEHL, G. E., KOLITZUS, M., SCHOENHAMMER, G., THIEL, A., MATOS, C., BRUSS, C., KLOBUCH, S., PETER, K., KASTENBERGER, M., BOGDAN, C., SCHLEICHER, U., MACKENSEN, A., ULLRICH, E., FICHTNER-FEIGL, S., KESSELRING, R., MACK, M., RITTER, U., SCHMID, M., BLANK, C., DETTMER, K., OEFNER, P. J., HOFFMANN, P., WALENTA, S., GEISSLER, E. K., POUYSSEGUR, J., VILLUNGER, A., STEVEN, A., SELIGER, B., SCHREML, S., HAFERKAMP, S., KOHL, E., KARRER, S., BERNEBURG, M., HERR, W., MUELLER-KLIESER, W., RENNER, K. & KREUTZ, M. 2016. LDHA-Associated Lactic Acid Production Blunts Tumor Immunosurveillance by T and NK Cells. *Cell Metab,* 24**,** 657-671.

BRAZALUK, A. Z., FEDOROV, A. N. & TKACHENKO, V. P. 1996. [Ca2+ ion transport in the sarcoplasmic reticulum of the gastrocnemius muscles of white rats under treatment of the sciatic nerve with a colchicine solution]. *Ukr Biokhim Zh (1978),* 68**,** 114-9.

BRONTE, V., KASIC, T., GRI, G., GALLANA, K., BORSELLINO, G., MARIGO, I., BATTISTINI, L., IAFRATE, M., PRAYER-GALETTI, T., PAGANO, F. & VIOLA, A. 2005. Boosting antitumor responses of T lymphocytes infiltrating human prostate cancers. *J Exp Med,* 201**,** 1257-68.

BROWN, G. R., HEM, V., KATZ, K. S., OVETSKY, M., WALLIN, C., ERMOLAEVA, O., TOLSTOY, I., TATUSOVA, T., PRUITT, K. D., MAGLOTT, D. R. & MURPHY, T. D. 2015. Gene: a gene-centered information resource at NCBI. *Nucleic Acids Res,* 43**,** D36-42.

BROWN, L., THOMAS, R. & WATSON, T. 1986. Cardiac glycosides with non-rotating steroid to sugar linkages: tools for the study of digitalis structure-activity relationships. *Naunyn Schmiedebergs Arch Pharmacol,* 332**,** 98-102.

BUCHBINDER, E. I. & DESAI, A. 2016. CTLA-4 and PD-1 Pathways: Similarities, Differences, and Implications of Their Inhibition. *Am J Clin Oncol,* 39**,** 98-106.

CAILLEAU, R., YOUNG, R., OLIVÉ, M. & REEVES, W. J., JR. 1974. Breast tumor cell lines from pleural effusions. *J Natl Cancer Inst,* 53**,** 661-74.

CANALS, A., PURCIOLAS, M., AYMAMÍ, J. & COLL, M. 2005. The anticancer agent ellipticine unwinds DNA by intercalative binding in an orientation parallel to base pairs. *Acta Crystallogr D Biol Crystallogr,* 61**,** 1009-12.

CANTIELLO, H. F. 1995. Role of the actin cytoskeleton on epithelial Na+ channel regulation. *Kidney Int,* 48**,** 970-84.

CAPATINA, A. L., LAGOS, D. & BRACKENBURY, W. J. 2022. Targeting Ion Channels for Cancer Treatment: Current Progress and Future Challenges. *Rev Physiol Biochem Pharmacol,* 183**,** 1-43.

ÇAPCI, A., LORION, M. M., MAI, C., HAHN, F., HODEK, J., WANGEN, C., WEBER, J., MARSCHALL, M., ACKERMANN, L. & TSOGOEVA, S. B. 2020. (Iso)Quinoline-Artemisinin Hybrids Prepared through Click Chemistry: Highly Potent Agents against Viruses. *Chemistry,* 26**,** 12019-12026.

CARDOSO, F., BARDIA, A., ANDRE, F., CESCON, D. W., MCARTHUR, H. L., TELLI, M. L., LOI, S., CORTES, J., SCHMID, P., HARBECK, N., DENKERT, C., JACKISCH, C., JIA, L., HIRSHFIELD, K. M. & KARANTZA, V. 2019. KEYNOTE-756: Randomized, double-blind, phase 3 study of pembrolizumab vs placebo combined with neoadjuvant chemotherapy and adjuvant endocrine therapy for high-risk, early-stage estrogen receptor–positive, human epidermal growth factor receptor 2–negative (ER+/HER2−) breast cancer. *Journal of Clinical Oncology,* 37**,** TPS601-TPS601.

CAROW, B. & ROTTENBERG, M. E. 2014. SOCS3, a Major Regulator of Infection and Inflammation. *Front Immunol,* 5**,** 58.

CARVAJAL-HAUSDORF, D. E., MANI, N., VELCHETI, V., SCHALPER, K. A. & RIMM, D. L. 2017. Objective measurement and clinical significance of IDO1 protein in hormone receptor-positive breast cancer. *J Immunother Cancer,* 5**,** 81.

CASTRO-PORTUGUEZ, R. & SUTPHIN, G. L. 2020. Kynurenine pathway, NAD(+) synthesis, and mitochondrial function: Targeting tryptophan metabolism to promote longevity and healthspan. *Exp Gerontol,* 132**,** 110841.

CATTERALL, W. A. 1975. Activation of the action potential Na+ ionophore of cultured neuroblastoma cells by veratridine and batrachotoxin. *J Biol Chem,* 250**,** 4053-9.

CHADWICK, M., TREWIN, H., GAWTHROP, F. & WAGSTAFF, C. 2013. Sesquiterpenoids lactones: benefits to plants and people. *Int J Mol Sci,* 14**,** 12780-805.

CHAE, J. J., WOOD, G., RICHARD, K., JAFFE, H., COLBURN, N. T., MASTERS, S. L., GUMUCIO, D. L., SHOHAM, N. G. & KASTNER, D. L. 2008. The familial Mediterranean fever protein, pyrin, is cleaved by caspase-1 and activates NF-kappaB through its N-terminal fragment. *Blood,* 112**,** 1794-803.

CHANG, Y. J., HOLTZMAN, M. J. & CHEN, C. C. 2004. Differential role of Janus family kinases (JAKs) in interferon-gamma-induced lung epithelial ICAM-1 expression: involving protein interactions between JAKs, phospholipase Cgamma, c-Src, and STAT1. *Mol Pharmacol,* 65**,** 589-98.

CHEANG, M. C., CHIA, S. K., VODUC, D., GAO, D., LEUNG, S., SNIDER, J., WATSON, M., DAVIES, S., BERNARD, P. S., PARKER, J. S., PEROU, C. M., ELLIS, M. J. & NIELSEN, T.

O. 2009. Ki67 index, HER2 status, and prognosis of patients with luminal B breast cancer. *J Natl Cancer Inst,* 101**,** 736-50.

CHEN, R., ZINZANI, P. L., FANALE, M. A., ARMAND, P., JOHNSON, N. A., BRICE, P., RADFORD, J., RIBRAG, V., MOLIN, D., VASSILAKOPOULOS, T. P., TOMITA, A., VON TRESCKOW, B., SHIPP, M. A., ZHANG, Y., RICART, A. D., BALAKUMARAN, A. & MOSKOWITZ, C. H. 2017a. Phase II Study of the Efficacy and Safety of Pembrolizumab for Relapsed/Refractory Classic Hodgkin Lymphoma. *J Clin Oncol,* 35**,** 2125-2132.

CHEN, Y., HUANG, W., YANG, M., XIN, G., CUI, W., XIE, Z. & SILVERSTEIN, R. L. 2017b. Cardiotonic Steroids Stimulate Macrophage Inflammatory Responses Through a Pathway Involving CD36, TLR4, and Na/K-ATPase. *Arterioscler Thromb Vasc Biol,* 37**,** 1462-1469.

CHEN, Y., JIANG, X., XIE, H., LI, X. & SHI, L. 2018. Structural characterization and antitumor activity of a polysaccharide from ramulus mori. *Carbohydr Polym,* 190**,** 232-239.

CHENG, M. F., LIN, C. S., CHEN, Y. H., SUNG, P. J., LIN, S. R., TONG, Y. W. & WENG, C. F. 2017. Inhibitory Growth of Oral Squamous Cell Carcinoma Cancer via Bacterial Prodigiosin. *Mar Drugs,* 15.

CHENG, R.-C., CHENG, P.-C., WANG, Y.-C. & HUANG, R.-C. 2019. Role of Intracellular Na+ in the Regulation of [Ca2+]i in the Rat Suprachiasmatic Nucleus Neurons. *International Journal of Molecular Sciences,* 20**,** 4868.

CHEON, H. & STARK, G. R. 2009. Unphosphorylated STAT1 prolongs the expression of interferon-induced immune regulatory genes. *Proc Natl Acad Sci U S A,* 106**,** 9373-8.

CHERNET, B. T. & LEVIN, M. 2014. Transmembrane voltage potential of somatic cells controls oncogene-mediated tumorigenesis at long-range. *Oncotarget,* 5**,** 3287-306.

CHERNEY, E. C., ZHANG, L., NARA, S., ZHU, X., GULLO-BROWN, J., MALEY, D., LIN, T. A., HUNT, J. T., HUANG, C., YANG, Z., DARIENZO, C., DISCENZA, L., RANASINGHE, A., GRUBB, M., ZIEMBA, T., TRAEGER, S. C., LI, X., JOHNSTON, K., KOPCHO, L., FERESHTEH, M., FOSTER, K., STEFANSKI, K., FARGNOLI, J., SWANSON, J., BROWN, J., DELPY, D., SEITZ, S. P., BORZILLERI, R., VITE, G. & BALOG, A. 2021. Discovery and Preclinical Evaluation of BMS-986242, a Potent, Selective Inhibitor of Indoleamine-2,3-dioxygenase 1. *ACS Med Chem Lett,* 12**,** 288-294.

CHEUNG, J. Y., ZHANG, X. Q., SONG, J., GAO, E., RABINOWITZ, J. E., CHAN, T. O. & WANG, J. 2010. Phospholemman: a novel cardiac stress protein. *Clin Transl Sci,* 3**,** 189-96.

CHI, G., WEI, M., XIE, X., SOROMOU, L. W., LIU, F. & ZHAO, S. 2013. Suppression of MAPK and NF-κB pathways by limonene contributes to attenuation of lipopolysaccharide-induced inflammatory responses in acute lung injury. *Inflammation,* 36**,** 501-11.

CHIADAK, J. D., ARSENIJEVIC, T., VERSTREPEN, K., GREGOIRE, F., BOLAKY, N., DELFORGE, V., FLAMAND, V., PERRET, J. & DELPORTE, C. 2016. Forskolin Inhibits Lipopolysaccharide-Induced Modulation of MCP-1 and GPR120 in 3T3-L1 Adipocytes through an Inhibition of NFκB. *Mediators Inflamm,* 2016**,** 1431789.

CHO, J. S., KIM, T. H., LIM, J. M. & SONG, J. H. 2008. Effects of eugenol on Na+ currents in rat dorsal root ganglion neurons. *Brain Res,* 1243**,** 53-62.

CHON, S. Y., HASSANAIN, H. H. & GUPTA, S. L. 1996. Cooperative role of interferon regulatory factor 1 and p91 (STAT1) response elements in interferon-gamma-inducible expression of human indoleamine 2,3-dioxygenase gene. *J Biol Chem,* 271**,** 17247-52.

CHUN, J. & KIM, Y. S. 2013. Platycodin D inhibits migration, invasion, and growth of MDA-MB-231 human breast cancer cells via suppression of EGFR-mediated Akt and MAPK pathways. *Chem Biol Interact,* 205**,** 212-21.

CHUNG, K. H., CHO, K. Y., ASAMI, Y., TAKAHASHI, N. & YOSHIDA, S. 1989. New 4-hydroxypyridine and 4-hydroxyquinoline derivatives as inhibitors of NADH-ubiquinone reductase in the respiratory chain. *Z Naturforsch C J Biosci,* 44**,** 609-16.

CLAPHAM, D. E. 2015. Structural biology: Pain-sensing TRPA1 channel resolved. *Nature,* 520**,** 439-41.

CLARK, K., MACKENZIE, K. F., PETKEVICIUS, K., KRISTARIYANTO, Y., ZHANG, J., CHOI, H. G., PEGGIE, M., PLATER, L., PEDRIOLI, P. G., MCIVER, E., GRAY, N. S., ARTHUR, J. S. & COHEN, P. 2012. Phosphorylation of CRTC3 by the salt-inducible kinases controls the interconversion of classically activated and regulatory macrophages. *Proc Natl Acad Sci U S A,* 109**,** 16986-91.

CLAUSEN, M. V., HILBERS, F. & POULSEN, H. 2017. The Structure and Function of the Na,K-ATPase Isoforms in Health and Disease. *Frontiers in physiology,* 8**,** 371-371.

CLAUSEN, T. & KJELDSEN, K. 1987. Chapter 18 Effects of Potassium Deficiency on Na,K Homeostasis and Na+,K+-ATPase in Muscle. *In:* GIEBISCH, G. (ed.) *Current Topics in Membranes and Transport.* Academic Press.

CLEMENTE, N., BARONI, S., FIORILLA, S., TASSO, F., REANO, S., BORSOTTI, C., RUGGIERO, M. R., ALCHERA, E., CORRAZZARI, M., WALKER, G., FOLLENZI, A., CRICH, S. G. & CARINI, R. 2023. Boosting intracellular sodium selectively kills hepatocarcinoma cells and induces hepatocellular carcinoma tumor shrinkage in mice. *Commun Biol,* 6**,** 574.

CLIFFORD, R. J. & KAPLAN, J. H. 2009. Regulation of Na,K-ATPase subunit abundance by translational repression. *J Biol Chem,* 284**,** 22905-15.

COLLINS, J. M., NORDSTROM, B. L., MCLAURIN, K. K., DALVI, T. B., MCCUTCHEON, S. C., BENNETT, J. C., MURPHY, B. R., SINGHAL, P. K., MCCREA, C., SHINDE, R. & BRICENO, J. M. 2021. A Real-World Evidence Study of CDK4/6 Inhibitor Treatment Patterns and Outcomes in Metastatic Breast Cancer by Germline BRCA Mutation Status. *Oncol Ther,* 9**,** 575-589.

CONSTANTINIDOU, A., ALIFIERIS, C. & TRAFALIS, D. T. 2019. Targeting Programmed Cell Death -1 (PD-1) and Ligand (PD-L1): A new era in cancer active immunotherapy. *Pharmacol Ther,* 194**,** 84-106.

CORI, C. F. & CORI, G. T. 1925. THE CARBOHYDRATE METABOLISM OF TUMORS: II. CHANGES IN THE SUGAR, LACTIC ACID, AND CO2-COMBINING POWER OF BLOOD PASSING THROUGH A TUMOR. *Journal of Biological Chemistry,* 65**,** 397-405.

CORRELL, R. N., EDER, P., BURR, A. R., DESPA, S., DAVIS, J., BERS, D. M. & MOLKENTIN, J. D. 2014. Overexpression of the Na+/K+ ATPase α2 but not α1 isoform attenuates pathological cardiac hypertrophy and remodeling. *Circulation research,* 114**,** 249-256.

CORTES, J., CESCON, D. W., RUGO, H. S., NOWECKI, Z., IM, S. A., YUSOF, M. M., GALLARDO, C., LIPATOV, O., BARRIOS, C. H., HOLGADO, E., IWATA, H., MASUDA, N., OTERO, M. T., GOKMEN, E., LOI, S., GUO, Z., ZHAO, J., AKTAN, G., KARANTZA, V. & SCHMID, P. 2020. Pembrolizumab plus chemotherapy versus placebo plus chemotherapy for previously untreated locally recurrent inoperable or metastatic triple-negative breast cancer (KEYNOTE-355): a randomised, placebo-controlled, double-blind, phase 3 clinical trial. *Lancet,* 396**,** 1817-1828.

COUSSENS, L. M. & WERB, Z. 2002. Inflammation and cancer. *Nature,* 420**,** 860-7.

CRAMBERT, G., SCHAER, D., ROY, S. & GEERING, K. 2004. New molecular determinants controlling the accessibility of ouabain to its binding site in human Na,K-ATPase alpha isoforms. *Mol Pharmacol,* 65**,** 335-41.

CREPALDI, G., ALLEGRI, G., DE ANTONI, A., COSTA, C. & MUGGEO, M. 1975. Relationship between tryptophan metabolism and vitamin B6 and nicotinamide in aged subjects. *Acta Vitaminol Enzymol,* 29**,** 140-4.

CURRIE, G. M., WHEAT, J. M. & KIAT, H. 2011. Pharmacokinetic considerations for digoxin in older people. *Open Cardiovasc Med J,* 5**,** 130-5.
CUTHBERT, A. W. & SPAYNE, J. A. 1982. Stimulation of sodium and of chloride transport in epithelia by forskolin. *Br J Pharmacol,* 76**,** 33-5.
DAI, C., MA, F., MA, Q., YANG, J., LI, Y., YANG, B. & QU, Y. 2022. Investigation of indole biodegradation by Cupriavidus sp. strain IDO with emphases on downstream biotransformation and indigo production. *Environmental Science and Pollution Research,* 29**,** 8369-8381.
DAI, X., SAYAMA, K., YAMASAKI, K., TOHYAMA, M., SHIRAKATA, Y., HANAKAWA, Y., TOKUMARU, S., YAHATA, Y., YANG, L., YOSHIMURA, A. & HASHIMOTO, K. 2006. SOCS1-negative feedback of STAT1 activation is a key pathway in the dsRNA-induced innate immune response of human keratinocytes. *J Invest Dermatol,* 126**,** 1574-81.
DALBETH, N., LAUTERIO, T. J. & WOLFE, H. R. 2014. Mechanism of action of colchicine in the treatment of gout. *Clin Ther,* 36**,** 1465-79.
DASSONNEVILLE, L., LANSIAUX, A., WATTELET, A., WATTEZ, N., MAHIEU, C., VAN MIERT, S., PIETERS, L. & BAILLY, C. 2000. Cytotoxicity and cell cycle effects of the plant alkaloids cryptolepine and neocryptolepine: relation to drug-induced apoptosis. *Eur J Pharmacol,* 409**,** 9-18.
DATAR, I., SANMAMED, M. F., WANG, J., HENICK, B. S., CHOI, J., BADRI, T., DONG, W., MANI, N., TOKI, M., MEJÍAS, L. D., LOZANO, M. D., PEREZ-GRACIA, J. L., VELCHETI, V., HELLMANN, M. D., GAINOR, J. F., MCEACHERN, K., JENKINS, D., SYRIGOS, K., POLITI, K., GETTINGER, S., RIMM, D. L., HERBST, R. S., MELERO, I., CHEN, L. & SCHALPER, K. A. 2019. Expression Analysis and Significance of PD-1, LAG-3, and TIM-3 in Human Non-Small Cell Lung Cancer Using Spatially Resolved and Multiparametric Single-Cell Analysis. *Clin Cancer Res,* 25**,** 4663-4673.
DAVID, J. M. & RAJASEKARAN, A. K. 2015. Gramicidin A: A New Mission for an Old Antibiotic. *J Kidney Cancer VHL,* 2**,** 15-24.
DAWOOD, M., OOKO, E. & EFFERTH, T. 2019. Collateral Sensitivity of Parthenolide via NF-κB and HIF-α Inhibition and Epigenetic Changes in Drug-Resistant Cancer Cell Lines. *Front Pharmacol,* 10**,** 542.
DE RICCARDIS, F., IZZO, I., MONTESARCHIO, D. & TECILLA, P. 2013. Ion transport through lipid bilayers by synthetic ionophores: modulation of activity and selectivity. *Acc Chem Res,* 46**,** 2781-90.
DE SILVA, P., AIELLO, M., GU-TRANTIEN, C., MIGLIORI, E., WILLARD-GALLO, K. & SOLINAS, C. 2021. Targeting CTLA-4 in cancer: Is it the ideal companion for PD-1 blockade immunotherapy combinations? *Int J Cancer,* 149**,** 31-41.
DEAC, O. M., MILLS, J. L., SHANE, B., MIDTTUN, Ø., UELAND, P. M., BROSNAN, J. T., BROSNAN, M. E., LAIRD, E., GIBNEY, E. R., FAN, R., WANG, Y., BRODY, L. C. & MOLLOY, A. M. 2015. Tryptophan catabolism and vitamin B-6 status are affected by gender and lifestyle factors in healthy young adults. *J Nutr,* 145**,** 701-7.
DEBELA, D. T., MUZAZU, S. G., HERARO, K. D., NDALAMA, M. T., MESELE, B. W., HAILE, D. C., KITUI, S. K. & MANYAZEWAL, T. 2021. New approaches and procedures for cancer treatment: Current perspectives. *SAGE Open Med,* 9**,** 20503121211034366.
DEBIEN, V., DE CALUWÉ, A., WANG, X., PICCART-GEBHART, M., TUOHY, V. K., ROMANO, E. & BUISSERET, L. 2023. Immunotherapy in breast cancer: an overview of current strategies and perspectives. *npj Breast Cancer,* 9**,** 7.
DEJOS, C., GKIKA, D. & CANTELMO, A. R. 2020. The Two-Way Relationship Between Calcium and Metabolism in Cancer. *Front Cell Dev Biol,* 8**,** 573747.

DEL MÓNACO, S. M., MARINO, G. I., ASSEF, Y. A., DAMIANO, A. E. & KOTSIAS, B. A. 2009. Cell migration in BeWo cells and the role of epithelial sodium channels. *J Membr Biol,* 232**,** 1-13.

DELVA, P., CAPRA, C., DEGAN, M., MINUZ, P., COVI, G., MILAN, L., STEELE, A. & LECHI, A. 1989. High plasma levels of a ouabain-like factor in normal pregnancy and in pre-eclampsia. *Eur J Clin Invest,* 19**,** 95-100.

DESFRERE, L., KARLSSON, M., HIYOSHI, H., MALMERSJÖ, S., NANOU, E., ESTRADA, M., MIYAKAWA, A., LAGERCRANTZ, H., EL MANIRA, A., LAL, M. & UHLÉN, P. 2009. Na,K-ATPase signal transduction triggers CREB activation and dendritic growth. *Proc Natl Acad Sci U S A,* 106**,** 2212-7.

DEWI, D. L., MOHAPATRA, S. R., BLANCO CABAÑES, S., ADAM, I., SOMARRIBAS PATTERSON, L. F., BERDEL, B., KAHLOON, M., THÜRMANN, L., LOTH, S., HEILMANN, K., WEICHENHAN, D., MÜCKE, O., HEILAND, I., WIMBERGER, P., KUHLMANN, J. D., KELLNER, K. H., SCHOTT, S., PLASS, C., PLATTEN, M., GERHÄUSER, C., TRUMP, S. & OPITZ, C. A. 2017. Suppression of indoleamine-2,3-dioxygenase 1 expression by promoter hypermethylation in ER-positive breast cancer. *Oncoimmunology,* 6**,** e1274477.

DEY, S., MONDAL, A., DUHADAWAY, J. B., SUTANTO-WARD, E., LAURY-KLEINTOP, L. D., THOMAS, S., PRENDERGAST, G. C., MANDIK-NAYAK, L. & MULLER, A. J. 2021. IDO1 Signaling through GCN2 in a Subpopulation of Gr-1(+) Cells Shifts the IFNγ/IL6 Balance to Promote Neovascularization. *Cancer Immunol Res,* 9**,** 514-528.

DIARRA, A., SHELDON, C. & CHURCH, J. 2001. In situ calibration and [H+] sensitivity of the fluorescent Na+ indicator SBFI. *Am J Physiol Cell Physiol,* 280**,** C1623-33.

DÍAZ-VEGAS, A., EISNER, V. & JAIMOVICH, E. 2019. Skeletal muscle excitation-metabolism coupling. *Archives of Biochemistry and Biophysics,* 664**,** 89-94.

DINATALE, B. C., MURRAY, I. A., SCHROEDER, J. C., FLAVENY, C. A., LAHOTI, T. S., LAURENZANA, E. M., OMIECINSKI, C. J. & PERDEW, G. H. 2010. Kynurenic acid is a potent endogenous aryl hydrocarbon receptor ligand that synergistically induces interleukin-6 in the presence of inflammatory signaling. *Toxicol Sci,* 115**,** 89-97.

DJAMGOZ, M. B. A., FRASER, S. P. & BRACKENBURY, W. J. 2019. In Vivo Evidence for Voltage-Gated Sodium Channel Expression in Carcinomas and Potentiation of Metastasis. *Cancers (Basel),* 11.

DMITRIEVA, N. I. & BURG, M. B. 2015. Elevated sodium and dehydration stimulate inflammatory signaling in endothelial cells and promote atherosclerosis. *PLoS One,* 10**,** e0128870.

DOMINGO, V., QUILEZ DEL MORAL, J. F. & BARRERO, A. F. 2016. Chapter 1 - Recent Accomplishments in the Total Synthesis of Natural Products Through C–H Functionalization Strategies. *In:* ATTA UR, R. (ed.) *Studies in Natural Products Chemistry.* Elsevier.

DONLEY, D. W., REALING, M., GIGLEY, J. P. & FOX, J. H. 2021. Iron activates microglia and directly stimulates indoleamine-2,3-dioxygenase activity in the N171-82Q mouse model of Huntington's disease. *PLoS One,* 16**,** e0250606.

DOWNER, E. J. 2020. Anti-inflammatory Potential of Terpenes Present in Cannabis sativa L. *ACS Chem Neurosci,* 11**,** 659-662.

DRIFFORT, V., GILLET, L., BON, E., MARIONNEAU-LAMBOT, S., OULLIER, T., JOULIN, V., COLLIN, C., PAGÈS, J. C., JOURDAN, M. L., CHEVALIER, S., BOUGNOUX, P., LE GUENNEC, J. Y., BESSON, P. & ROGER, S. 2014. Ranolazine inhibits NaV1.5-mediated breast cancer cell invasiveness and lung colonization. *Mol Cancer,* 13**,** 264.

DUARTE, D. & VALE, N. 2022. Evaluation of synergism in drug combinations and reference models for future orientations in oncology. *Current Research in Pharmacology and Drug Discovery,* 3**,** 100110.

DÜHRKOP, K., FLEISCHAUER, M., LUDWIG, M., AKSENOV, A. A., MELNIK, A. V., MEUSEL, M., DORRESTEIN, P. C., ROUSU, J. & BÖCKER, S. 2019. SIRIUS 4: a rapid tool for turning tandem mass spectra into metabolite structure information. *Nature Methods,* 16**,** 299-302.

DÜHRKOP, K., NOTHIAS, L.-F., FLEISCHAUER, M., REHER, R., LUDWIG, M., HOFFMANN, M. A., PETRAS, D., GERWICK, W. H., ROUSU, J., DORRESTEIN, P. C. & BÖCKER, S. 2021. Systematic classification of unknown metabolites using high-resolution fragmentation mass spectra. *Nature Biotechnology,* 39**,** 462-471.

DUNGO, R. T. & KEATING, G. M. 2013. Afatinib: first global approval. *Drugs,* 73**,** 1503-15.

EDWARDS, I. J., BRUCE, G., LAWRENSON, C., HOWE, L., CLAPCOTE, S. J., DEUCHARS, S. A. & DEUCHARS, J. 2013. Na+/K+ ATPase α1 and α3 isoforms are differentially expressed in α- and γ-motoneurons. *J Neurosci,* 33**,** 9913-9.

EFENDIEV, R., BERTORELLO, A. M., ZANDOMENI, R., CINELLI, A. R. & PEDEMONTE, C. H. 2002. Agonist-dependent regulation of renal Na+,K+-ATPase activity is modulated by intracellular sodium concentration. *J Biol Chem,* 277**,** 11489-96.

EFFERTH, T., BENAKIS, A., ROMERO, M. R., TOMICIC, M., RAUH, R., STEINBACH, D., HÄFER, R., STAMMINGER, T., OESCH, F., KAINA, B. & MARSCHALL, M. 2004. Enhancement of cytotoxicity of artemisinins toward cancer cells by ferrous iron. *Free Radic Biol Med,* 37**,** 998-1009.

EIL, R., VODNALA, S. K., CLEVER, D., KLEBANOFF, C. A., SUKUMAR, M., PAN, J. H., PALMER, D. C., GROS, A., YAMAMOTO, T. N., PATEL, S. J., GUITTARD, G. C., YU, Z., CARBONARO, V., OKKENHAUG, K., SCHRUMP, D. S., LINEHAN, W. M., ROYCHOUDHURI, R. & RESTIFO, N. P. 2016. Ionic immune suppression within the tumour microenvironment limits T cell effector function. *Nature,* 537**,** 539-543.

EL-HAMMADI, M. M., SMALL-HOWARD, A. L., FERNÁNDEZ-ARÉVALO, M. & MARTÍN-BANDERAS, L. 2021. Development of enhanced drug delivery vehicles for three cannabis-based terpenes using poly(lactic-co-glycolic acid) based nanoparticles. *Industrial Crops and Products,* 164**,** 113345.

EL ANSARI, R., CRAZE, M. L., MILIGY, I., DIEZ-RODRIGUEZ, M., NOLAN, C. C., ELLIS, I. O., RAKHA, E. A. & GREEN, A. R. 2018. The amino acid transporter SLC7A5 confers a poor prognosis in the highly proliferative breast cancer subtypes and is a key therapeutic target in luminal B tumours. *Breast Cancer Research,* 20**,** 21.

ELMAKATY, I., ABDO, R., ELSABAGH, A., ELSAYED, A. & MALKI, M. I. 2023. Comparative efficacy and safety of PD-1/PD-L1 inhibitors in triple negative breast cancer: a systematic review and network meta-analysis of randomized controlled trials. *Cancer Cell Int,* 23**,** 90.

EMENS, L. A., CRUZ, C., EDER, J. P., BRAITEH, F., CHUNG, C., TOLANEY, S. M., KUTER, I., NANDA, R., CASSIER, P. A., DELORD, J. P., GORDON, M. S., ELGABRY, E., CHANG, C. W., SARKAR, I., GROSSMAN, W., O'HEAR, C., FASSÒ, M., MOLINERO, L. & SCHMID, P. 2019. Long-term Clinical Outcomes and Biomarker Analyses of Atezolizumab Therapy for Patients With Metastatic Triple-Negative Breast Cancer: A Phase 1 Study. *JAMA Oncol,* 5**,** 74-82.

ENGELMAN, J. A., ZEJNULLAHU, K., MITSUDOMI, T., SONG, Y., HYLAND, C., PARK, J. O., LINDEMAN, N., GALE, C. M., ZHAO, X., CHRISTENSEN, J., KOSAKA, T., HOLMES, A. J., ROGERS, A. M., CAPPUZZO, F., MOK, T., LEE, C., JOHNSON, B. E., CANTLEY, L. C. & JÄNNE, P. A. 2007. MET amplification leads to gefitinib resistance in lung cancer by activating ERBB3 signaling. *Science,* 316**,** 1039-43.

ERECIŃSKA, M., DAGANI, F., NELSON, D., DEAS, J. & SILVER, I. A. 1991. Relations between intracellular ions and energy metabolism: a study with monensin in synaptosomes, neurons, and C6 glioma cells. *J Neurosci,* 11**,** 2410-21.

EVIDENTE, A., KORNIENKO, A., LEFRANC, F., CIMMINO, A., DASARI, R., EVIDENTE, M., MATHIEU, V. & KISS, R. 2015. Sesterterpenoids with Anticancer Activity. *Curr Med Chem,* 22**,** 3502-22.

EYNDE, B. J. V. D., BAREN, N. V. & BAURAIN, J.-F. 2020. Is There a Clinical Future for IDO1 Inhibitors After the Failure of Epacadostat in Melanoma? *Annual Review of Cancer Biology,* 4**,** 241-256.

FACTOR, P., SENNE, C., DUMASIUS, V., RIDGE, K., ARI JAFFE, H., UHAL, B., GAO, Z. & IASHA SZNAJDER, J. 1998. Overexpression of the Na+,K+-ATPase α1Subunit Increases Na+,K+-ATPase Function in A549 Cells. *American Journal of Respiratory Cell and Molecular Biology,* 18**,** 741-749.

FALLARINO, F., GROHMANN, U., VACCA, C., BIANCHI, R., ORABONA, C., SPRECA, A., FIORETTI, M. C. & PUCCETTI, P. 2002. T cell apoptosis by tryptophan catabolism. *Cell Death Differ,* 9**,** 1069-77.

FAN, L., ZHU, H., TAO, W., LIU, L., SHAN, X., ZHAO, M. & SUN, D. 2019. Euphorbia factor L2 inhibits TGF-β-induced cell growth and migration of hepatocellular carcinoma through AKT/STAT3. *Phytomedicine,* 62**,** 152931.

FAN, Y. & HE, S. 2022. The Characteristics of Tumor Microenvironment in Triple Negative Breast Cancer. *Cancer Manag Res,* 14**,** 1-17.

FANG, E. F., LAUTRUP, S., HOU, Y., DEMAREST, T. G., CROTEAU, D. L., MATTSON, M. P. & BOHR, V. A. 2017. NAD(+) in Aging: Molecular Mechanisms and Translational Implications. *Trends Mol Med,* 23**,** 899-916.

FEDERICI, M., GIUSTIZIERI, M. L., SCARPONI, C., GIROLOMONI, G. & ALBANESI, C. 2002. Impaired IFN-gamma-dependent inflammatory responses in human keratinocytes overexpressing the suppressor of cytokine signaling 1. *J Immunol,* 169**,** 434-42.

FEDOROV, D. A., SIDORENKO, S. V., YUSIPOVICH, A. I., PARSHINA, E. Y., TVERSKOI, A. M., ABRAMICHEVA, P. A., MAKSIMOV, G. V., ORLOV, S. N., LOPINA, O. D. & KLIMANOVA, E. A. 2021. Na(+) (i)/K(+) (i) imbalance contributes to gene expression in endothelial cells exposed to elevated NaCl. *Heliyon,* 7**,** e08088.

FEELEY, L. P., MULLIGAN, A. M., PINNADUWAGE, D., BULL, S. B. & ANDRULIS, I. L. 2014. Distinguishing luminal breast cancer subtypes by Ki67, progesterone receptor or TP53 status provides prognostic information. *Modern Pathology,* 27**,** 554-561.

FELIPPE GONÇALVES-DE-ALBUQUERQUE, C., RIBEIRO SILVA, A., IGNÁCIO DA SILVA, C., CAIRE CASTRO-FARIA-NETO, H. & BURTH, P. 2017. Na/K Pump and Beyond: Na/K-ATPase as a Modulator of Apoptosis and Autophagy. *Molecules,* 22.

FELLNER, C. 2012. Ipilimumab (yervoy) prolongs survival in advanced melanoma: serious side effects and a hefty price tag may limit its use. *P t,* 37**,** 503-30.

FENG, X., TANG, R., ZHANG, R., WANG, H., JI, Z., SHAO, Y., WANG, S., ZHONG, T., GU, Y. & MENG, J. 2020. A comprehensive analysis of IDO1 expression with tumour-infiltrating immune cells and mutation burden in gynaecologic and breast cancers. *Journal of cellular and molecular medicine,* 24**,** 5238-5248.

FERRANDI, M., MOLINARI, I., BARASSI, P., MINOTTI, E., BIANCHI, G. & FERRARI, P. 2004. Organ hypertrophic signaling within caveolae membrane subdomains triggered by ouabain and antagonized by PST 2238. *J Biol Chem,* 279**,** 33306-14.

FERRARI, P. 2010. Rostafuroxin: an ouabain-inhibitor counteracting specific forms of hypertension. *Biochim Biophys Acta,* 1802**,** 1254-8.

FIELD, C. S., BAIXAULI, F., KYLE, R. L., PULESTON, D. J., CAMERON, A. M., SANIN, D. E., HIPPEN, K. L., LOSCHI, M., THANGAVELU, G., CORRADO, M., EDWARDS-HICKS, J., GRZES, K. M., PEARCE, E. J., BLAZAR, B. R. & PEARCE, E. L. 2020. Mitochondrial

Integrity Regulated by Lipid Metabolism Is a Cell-Intrinsic Checkpoint for Treg Suppressive Function. *Cell Metab,* 31**,** 422-437.e5.
FILIPEK, S., RZESZOTARSKA, J. & KALINOWSKI, M. K. 1994. Polarographic study of Tl+, Li+, Na+, K+, and Cs+ complexes with monensin anion in dipolar aprotic solvents. *Monatshefte für Chemie / Chemical Monthly,* 125**,** 801-809.
FINAN, J. D. & GUILAK, F. 2010. The effects of osmotic stress on the structure and function of the cell nucleus. *J Cell Biochem,* 109**,** 460-7.
FIORE, A., ZEITLER, L., RUSSIER, M., GROß, A., HILLER, M.-K., PARKER, J. L., STIER, L., KÖCHER, T., NEWSTEAD, S. & MURRAY, P. J. 2022. Kynurenine importation by SLC7A11 propagates anti-ferroptotic signaling. *Molecular Cell,* 82**,** 920-932.e7.
FISONE, G., SNYDER, G. L., APERIA, A. & GREENGARD, P. 1998. Na+,K(+)-ATPase phosphorylation in the choroid plexus: synergistic regulation by serotonin/protein kinase C and isoproterenol/cAMP-PK/PP-1 pathways. *Mol Med,* 4**,** 258-65.
FOGARTY, C. E. & BERGMANN, A. 2015. Chapter Nine - The Sound of Silence: Signaling by Apoptotic Cells. *In:* STELLER, H. (ed.) *Current Topics in Developmental Biology.* Academic Press.
FOUGERAY, S., MAMI, I., BERTHO, G., BEAUNE, P., THERVET, E. & PALLET, N. 2012. Tryptophan depletion and the kinase GCN2 mediate IFN-γ-induced autophagy. *J Immunol,* 189**,** 2954-64.
FOX, E., OLIVER, T., ROWE, M., THOMAS, S., ZAKHARIA, Y., GILMAN, P. B., MULLER, A. J. & PRENDERGAST, G. C. 2018. Indoximod: An Immunometabolic Adjuvant That Empowers T Cell Activity in Cancer. *Front Oncol,* 8**,** 370.
FRASER, S. P., SALVADOR, V., MANNING, E. A., MIZAL, J., ALTUN, S., RAZA, M., BERRIDGE, R. J. & DJAMGOZ, M. B. 2003. Contribution of functional voltage-gated Na+ channel expression to cell behaviors involved in the metastatic cascade in rat prostate cancer: I. Lateral motility. *J Cell Physiol,* 195**,** 479-87.
FREELING, J. L., SCHOLL, J. L., EIKANGER, M., KNOBLICH, C., POTTS, R. A., ANDERSON, D. J., ROWER, J. E., FARJOO, M. H., ZHAO, H., PILLATZKI, A. & REZVANI, K. 2022. Pre-clinical safety and therapeutic efficacy of a plant-based alkaloid in a human colon cancer xenograft model. *Cell Death Discovery,* 8**,** 135.
FROLOVA, L. Y., GRIGORIEVA, A. Y., SUDOMOINA, M. A. & KISSELEV, L. L. 1993. The human gene encoding tryptophanyl-tRNA synthetase: interferon-response elements and exon-intron organization. *Gene,* 128**,** 237-45.
FRUMENTO, G., ROTONDO, R., TONETTI, M., DAMONTE, G., BENATTI, U. & FERRARA, G. B. 2002. Tryptophan-derived catabolites are responsible for inhibition of T and natural killer cell proliferation induced by indoleamine 2,3-dioxygenase. *J Exp Med,* 196**,** 459-68.
FU, C., SHI, H., CHEN, H., ZHANG, K., WANG, M. & QIU, F. 2021. Oral Bioavailability Comparison of Artemisinin, Deoxyartemisinin, and 10-Deoxoartemisinin Based on Computer Simulations and Pharmacokinetics in Rats. *ACS Omega,* 6**,** 889-899.
FU, Y., MI, L., SANDA, M., SILVERSTEIN, S., AGGARWAL, M., WANG, D., GUPTA, P., GOLDMAN, R., APPELLA, D. H. & CHUNG, F. L. 2014. A Click Chemistry Approach to Identify Protein Targets of Cancer Chemopreventive Phenethyl Isothiocyanate. *RSC Adv,* 4**,** 3920-3923.
FUJIGAKI, H., SAITO, K., LIN, F., FUJIGAKI, S., TAKAHASHI, K., MARTIN, B. M., CHEN, C. Y., MASUDA, J., KOWALAK, J., TAKIKAWA, O., SEISHIMA, M. & MARKEY, S. P. 2006. Nitration and inactivation of IDO by peroxynitrite. *J Immunol,* 176**,** 372-9.
FUJIGAKI, H., SEISHIMA, M. & SAITO, K. 2012. Posttranslational modification of indoleamine 2,3-dioxygenase. *Anal Bioanal Chem,* 403**,** 1777-82.
FUJIWARA, M., SHIBATA, M., NOMIYAMA, Y., SUGIMOTO, T., HIRATA, F., TOKUYAMA, T., SENOH, S. & HAYAISHI, O. 1979. Formation of 5-hydroxykynurenine and 5-

hydroxykynurenamine from 5-hydroxytryptophan in rabbit small intestine. *Proc Natl Acad Sci U S A,* 76**,** 1145-9.
FUJIWARA, Y., KATO, S., NESLINE, M. K., CONROY, J. M., DEPIETRO, P., PABLA, S. & KURZROCK, R. 2022. Indoleamine 2,3-dioxygenase (IDO) inhibitors and cancer immunotherapy. *Cancer Treat Rev,* 110**,** 102461.
FUKUDA, K., HIBIYA, Y., MUTOH, M., KOSHIJI, M., AKAO, S. & FUJIWARA, H. 1999. Inhibition by berberine of cyclooxygenase-2 transcriptional activity in human colon cancer cells. *J Ethnopharmacol,* 66**,** 227-33.
FUKUNAGA, M., YAMAMOTO, Y., KAWASOE, M., ARIOKA, Y., MURAKAMI, Y., HOSHI, M. & SAITO, K. 2012. Studies on tissue and cellular distribution of indoleamine 2,3-dioxygenase 2: the absence of IDO1 upregulates IDO2 expression in the epididymis. *J Histochem Cytochem,* 60**,** 854-60.
FUS-KUJAWA, A., PRUS, P., BAJDAK-RUSINEK, K., TEPER, P., GAWRON, K., KOWALCZUK, A. & SIERON, A. L. 2021. An Overview of Methods and Tools for Transfection of Eukaryotic Cells in vitro. *Front Bioeng Biotechnol,* 9**,** 701031.
FUSCO, N., SAJJADI, E., VENETIS, K., GAUDIOSO, G., LOPEZ, G., CORTI, C., ROCCO, E. G., CRISCITIELLO, C., MALAPELLE, U. & INVERNIZZI, M. 2020. PTEN Alterations and Their Role in Cancer Management: Are We Making Headway on Precision Medicine? *Genes (Basel),* 11.
GAO, Y., MACK, A. A., LITTERAL, C., DELAMERE, N. A. & EL-MALLAKH, R. S. 2022. NMDA receptor inhibition prevents intracellular sodium elevations in human olfactory neuroepithelial precursors derived from bipolar patients. *Sci Rep,* 12**,** 10437.
GARCIA-DIAZ, A., SHIN, D. S., MORENO, B. H., SACO, J., ESCUIN-ORDINAS, H., RODRIGUEZ, G. A., ZARETSKY, J. M., SUN, L., HUGO, W., WANG, X., PARISI, G., SAUS, C. P., TORREJON, D. Y., GRAEBER, T. G., COMIN-ANDUIX, B., HU-LIESKOVAN, S., DAMOISEAUX, R., LO, R. S. & RIBAS, A. 2017. Interferon Receptor Signaling Pathways Regulating PD-L1 and PD-L2 Expression. *Cell Rep,* 19**,** 1189-1201.
GARCÍA-LARA, L., PÉREZ-SEVERIANO, F., GONZÁLEZ-ESQUIVEL, D., ELIZONDO, G. & SEGOVIA, J. 2015. Absence of aryl hydrocarbon receptors increases endogenous kynurenic acid levels and protects mouse brain against excitotoxic insult and oxidative stress. *J Neurosci Res,* 93**,** 1423-33.
GARCIA, R., BOWMAN, T. L., NIU, G., YU, H., MINTON, S., MURO-CACHO, C. A., COX, C. E., FALCONE, R., FAIRCLOUGH, R., PARSONS, S., LAUDANO, A., GAZIT, A., LEVITZKI, A., KRAKER, A. & JOVE, R. 2001. Constitutive activation of Stat3 by the Src and JAK tyrosine kinases participates in growth regulation of human breast carcinoma cells. *Oncogene,* 20**,** 2499-513.
GAUDIOSO, C., HAO, J., MARTIN-EAUCLAIRE, M. F., GABRIAC, M. & DELMAS, P. 2012. Menthol pain relief through cumulative inactivation of voltage-gated sodium channels. *Pain,* 153**,** 473-484.
GAVRIELI, M., WATANABE, N., LOFTIN, S. K., MURPHY, T. L. & MURPHY, K. M. 2003. Characterization of phosphotyrosine binding motifs in the cytoplasmic domain of B and T lymphocyte attenuator required for association with protein tyrosine phosphatases SHP-1 and SHP-2. *Biochem Biophys Res Commun,* 312**,** 1236-43.
GEETHA, B. S., NAIR, M. S., LATHA, P. G. & REMANI, P. 2012. Sesquiterpene lactones isolated from Elephantopus scaber L. inhibits human lymphocyte proliferation and the growth of tumour cell lines and induces apoptosis in vitro. *J Biomed Biotechnol,* 2012**,** 721285.
GENG, D., YI, L. T., SHI, Y. & MIN, Z. D. 2015. Structure and antibacterial property of a new diterpenoid from Euphorbia helioscopia. *Chin J Nat Med,* 13**,** 704-6.
GERWECK, L. E. & SEETHARAMAN, K. 1996. Cellular pH gradient in tumor versus normal tissue: potential exploitation for the treatment of cancer. *Cancer Res,* 56**,** 1194-8.

GILL, S., GILL, R., WICKS, D., DESPOTOVSKI, S. & LIANG, D. 2004. Development of an HTS assay for Na+, K+-ATPase using nonradioactive rubidium ion uptake. *Assay Drug Dev Technol,* 2**,** 535-42.

GILLET, L., ROGER, S., BESSON, P., LECAILLE, F., GORE, J., BOUGNOUX, P., LALMANACH, G. & LE GUENNEC, J.-Y. 2009a. Voltage-gated Sodium Channel Activity Promotes Cysteine Cathepsin-dependent Invasiveness and Colony Growth of Human Cancer Cells. *The Journal of biological chemistry,* 284**,** 8680-8691.

GILLET, L., ROGER, S., BESSON, P., LECAILLE, F., GORE, J., BOUGNOUX, P., LALMANACH, G. & LE GUENNEC, J. Y. 2009b. Voltage-gated Sodium Channel Activity Promotes Cysteine Cathepsin-dependent Invasiveness and Colony Growth of Human Cancer Cells. *J Biol Chem,* 284**,** 8680-91.

GIRITHAR, H. N., STAATS PIRES, A., AHN, S. B., GUILLEMIN, G. J., GLUCH, L. & HENG, B. 2023. Involvement of the kynurenine pathway in breast cancer: updates on clinical research and trials. *Br J Cancer,* 129**,** 185-203.

GOEL, M., SINKINS, W., KEIGHTLEY, A., KINTER, M. & SCHILLING, W. P. 2005. Proteomic analysis of TRPC5- and TRPC6-binding partners reveals interaction with the plasmalemmal Na(+)/K(+)-ATPase. *Pflugers Arch,* 451**,** 87-98.

GONÇALVES, J. C., ALVES ADE, M., DE ARAÚJO, A. E., CRUZ, J. S. & ARAÚJO, D. A. 2010. Distinct effects of carvone analogues on the isolated nerve of rats. *Eur J Pharmacol,* 645**,** 108-12.

GONZÁLEZ-CANO, R., RUIZ-CANTERO, M. C., SANTOS-CABALLERO, M., GÓMEZ-NAVAS, C., TEJADA, M. & NIETO, F. R. 2021. Tetrodotoxin, a Potential Drug for Neuropathic and Cancer Pain Relief? *Toxins (Basel),* 13.

GOODWILL, K. E., SABATIER, C., MARKS, C., RAAG, R., FITZPATRICK, P. F. & STEVENS, R. C. 1997. Crystal structure of tyrosine hydroxylase at 2.3 A and its implications for inherited neurodegenerative diseases. *Nat Struct Biol,* 4**,** 578-85.

GOODWIN, S., SHAHTAHMASSEBI, G. & HANLEY, Q. S. 2020. Statistical models for identifying frequent hitters in high throughput screening. *Scientific Reports,* 10**,** 17200.

GORBATENKO, A., OLESEN, C. W., MORUP, N., THIEL, G., KALLUNKI, T., VALEN, E. & PEDERSEN, S. F. 2014. ErbB2 upregulates the Na+,HCO3(-)-cotransporter NBCn1/SLC4A7 in human breast cancer cells via Akt, ERK, Src, and Kruppel-like factor 4. *Faseb j,* 28**,** 350-63.

GORDAN, J. D., BERTOUT, J. A., HU, C. J., DIEHL, J. A. & SIMON, M. C. 2007. HIF-2alpha promotes hypoxic cell proliferation by enhancing c-myc transcriptional activity. *Cancer Cell,* 11**,** 335-47.

GOSTNER, J. M., GEISLER, S., STONIG, M., MAIR, L., SPERNER-UNTERWEGER, B. & FUCHS, D. 2020. Tryptophan Metabolism and Related Pathways in Psychoneuroimmunology: The Impact of Nutrition and Lifestyle. *Neuropsychobiology,* 79**,** 89-99.

GOULD, H. J., 3RD, NORLEANS, J., WARD, T. D., REID, C. & PAUL, D. 2018. Selective lysis of breast carcinomas by simultaneous stimulation of sodium channels and blockade of sodium pumps. *Oncotarget,* 9**,** 15606-15615.

GRADEK, F., LOPEZ-CHARCAS, O., CHADET, S., POISSON, L., OULDAMER, L., GOUPILLE, C., JOURDAN, M. L., CHEVALIER, S., MOUSSATA, D., BESSON, P. & ROGER, S. 2019. Sodium Channel Na(v)1.5 Controls Epithelial-to-Mesenchymal Transition and Invasiveness in Breast Cancer Cells Through its Regulation by the Salt-Inducible Kinase-1. *Sci Rep,* 9**,** 18652.

GRANT, R. S., NAIF, H., THURUTHYIL, S. J., NASR, N., LITTLEJOHN, T., TAKIKAWA, O. & KAPOOR, V. 2000. Induction of indolamine 2,3-dioxygenase in primary human macrophages by human immunodeficiency virus type 1 is strain dependent. *Journal of virology,* 74**,** 4110-4115.

GREENUP, R., BUCHANAN, A., LORIZIO, W., RHOADS, K., CHAN, S., LEEDOM, T., KING, R., MCLENNAN, J., CRAWFORD, B., KELLY MARCOM, P. & SHELLEY HWANG, E. 2013. Prevalence of BRCA mutations among women with triple-negative breast cancer (TNBC) in a genetic counseling cohort. *Ann Surg Oncol,* 20**,** 3254-8.

GROHMANN, U. & PUCCETTI, P. 2015. The Coevolution of IDO1 and AhR in the Emergence of Regulatory T-Cells in Mammals. *Front Immunol,* 6**,** 58.

GRUNBERGER, D., BANERJEE, R., EISINGER, K., OLTZ, E. M., EFROS, L., CALDWELL, M., ESTEVEZ, V. & NAKANISHI, K. 1988. Preferential cytotoxicity on tumor cells by caffeic acid phenethyl ester isolated from propolis. *Experientia,* 44**,** 230-2.

GU, J., HUANG, L. & ZHANG, Y. 2020. Monensin inhibits proliferation, migration, and promotes apoptosis of breast cancer cells via downregulating UBA2. *Drug Dev Res,* 81**,** 745-753.

GUILLEMIN, G. J., WILLIAMS, K. R., SMITH, D. G., SMYTHE, G. A., CROITORU-LAMOURY, J. & BREW, B. J. 2003. Quinolinic acid in the pathogenesis of Alzheimer's disease. *Adv Exp Med Biol,* 527**,** 167-76.

GULSEVIN, A., GLAZER, A. M., SHIELDS, T., KRONCKE, B. M., RODEN, D. M. & MEILER, J. 2022. Veratridine Can Bind to a Site at the Mouth of the Channel Pore at Human Cardiac Sodium Channel Na(V)1.5. *Int J Mol Sci,* 23.

GUNTER, T. E., BUNTINAS, L., SPARAGNA, G. C. & GUNTER, K. K. 1998. The Ca2+ transport mechanisms of mitochondria and Ca2+ uptake from physiological-type Ca2+ transients. *Biochim Biophys Acta,* 1366**,** 5-15.

GÜNTHER, J., DÄBRITZ, J. & WIRTHGEN, E. 2019. Limitations and Off-Target Effects of Tryptophan-Related IDO Inhibitors in Cancer Treatment. *Front Immunol,* 10**,** 1801.

GUO, J., WILLIAMS, D. J., PUHL, H. L., 3RD & IKEDA, S. R. 2008. Inhibition of N-type calcium channels by activation of GPR35, an orphan receptor, heterologously expressed in rat sympathetic neurons. *J Pharmacol Exp Ther,* 324**,** 342-51.

GUPTA, K., CHAKRABARTI, A., RANA, S., RAMDEO, R., ROTH, B. L., AGARWAL, M. L., TSE, W., AGARWAL, M. K. & WALD, D. N. 2011. Securinine, a myeloid differentiation agent with therapeutic potential for AML. *PLoS One,* 6**,** e21203.

GUPTA, K., PARIZHER, G., DE LIMA, M. & WALD, D. N. 2015. Securinine Targets Cancer Cells through an Irak and JNK Dependent Pathway. *Blood,* 126**,** 3791-3791.

HAAS, M., ASKARI, A. & XIE, Z. 2000. Involvement of Src and epidermal growth factor receptor in the signal-transducing function of Na+/K+-ATPase. *J Biol Chem,* 275**,** 27832-7.

HAAS, M., WANG, H., TIAN, J. & XIE, Z. 2002. Src-mediated inter-receptor cross-talk between the Na+/K+-ATPase and the epidermal growth factor receptor relays the signal from ouabain to mitogen-activated protein kinases. *J Biol Chem,* 277**,** 18694-702.

HAAS, R., SMITH, J., ROCHER-ROS, V., NADKARNI, S., MONTERO-MELENDEZ, T., D'ACQUISTO, F., BLAND, E. J., BOMBARDIERI, M., PITZALIS, C., PERRETTI, M., MARELLI-BERG, F. M. & MAURO, C. 2015. Lactate Regulates Metabolic and Pro-inflammatory Circuits in Control of T Cell Migration and Effector Functions. *PLoS Biol,* 13**,** e1002202.

HABER, R., BESSETTE, D., HULIHAN-GIBLIN, B., DURCAN, M. J. & GOLDMAN, D. 1993. Identification of tryptophan 2,3-dioxygenase RNA in rodent brain. *J Neurochem,* 60**,** 1159-62.

HAESELER, G., MAUE, D., GROSSKREUTZ, J., BUFLER, J., NENTWIG, B., PIEPENBROCK, S., DENGLER, R. & LEUWER, M. 2002. Voltage-dependent block of neuronal and skeletal muscle sodium channels by thymol and menthol. *Eur J Anaesthesiol,* 19**,** 571-9.

HAGEN, N. A., CANTIN, L., CONSTANT, J., HALLER, T., BLAISE, G., ONG-LAM, M., DU SOUICH, P., KORZ, W. & LAPOINTE, B. 2017. Tetrodotoxin for Moderate to Severe Cancer-Related Pain: A Multicentre, Randomized, Double-Blind, Placebo-Controlled, Parallel-Design Trial. *Pain Res Manag,* 2017**,** 7212713.

HAKIMJAVADI, H., STINER, C. A., RADZYUKEVICH, T. L., LINGREL, J. B., NORMAN, N., LANDERO FIGUEROA, J. A. & HEINY, J. A. 2018. K^+ and Rb^+ Affinities of the Na,K-ATPase α_1 and α_2 Isozymes: An Application of ICP-MS for Quantification of Na^+ Pump Kinetics in Myofibers. *Int J Mol Sci,* 19.

HAMZELOO-MOGHADAM, M., AGHAEI, M., ABDOLMOHAM MADI, M. H. & FALLAHIAN, F. 2019. Anticancer activity of britannin through the downregulation of cyclin D1 and CDK4 in human breast cancer cells. *J Cancer Res Ther,* 15**,** 1105-1108.

HANDLEY, S. L. & MISKIN, R. C. 1977. The interaction of some kynurenine pathway metabolites with 5-hydroxytryptophan and 5-hydroxytryptamine. *Psychopharmacology (Berl),* 51**,** 305-9.

HANNON, J. & HOYER, D. 2008. Molecular biology of 5-HT receptors. *Behav Brain Res,* 195**,** 198-213.

HAO, M., HUANG, B., WU, R., PENG, Z. & LUO, K. Q. 2023. The Interaction between Macrophages and Triple-negative Breast Cancer Cells Induces ROS-Mediated Interleukin 1α Expression to Enhance Tumorigenesis and Metastasis. *Adv Sci (Weinh)***,** e2302857.

HAQ, S., GRONDIN, J. A. & KHAN, W. I. 2021. Tryptophan-derived serotonin-kynurenine balance in immune activation and intestinal inflammation. *Faseb j,* 35**,** e21888.

HARDELAND, R. 2008. Comparative Aspects of Circadian Rhythms.

HARVEY, B. J. & EHRENFELD, J. 1988. Role of Na+/H+ exchange in the control of intracellular pH and cell membrane conductances in frog skin epithelium. *J Gen Physiol,* 92**,** 793-810.

HE, Q., SUZUKI, H. & SHARMA, R. P. 2006. S-adenosylmethionine or 5'-methylthioadenosine are unable to prevent fumonisin B1 hepatotoxicity in mice despite increased oxidation in liver. *J Appl Toxicol,* 26**,** 509-16.

HEITZER, E., LAX, S., LAFER, I., MÜLLER, S. M., PRISTAUZ, G., ULZ, P., JAHN, S., HÖGENAUER, C., PETRU, E., SPEICHER, M. R. & GEIGL, J. B. 2013. Multiplex genetic cancer testing identifies pathogenic mutations in TP53 and CDH1 in a patient with bilateral breast and endometrial adenocarcinoma. *BMC Med Genet,* 14**,** 129.

HENG, B., BILGIN, A. A., LOVEJOY, D. B., TAN, V. X., MILIOLI, H. H., GLUCH, L., BUSTAMANTE, S., SABARETNAM, T., MOSCATO, P., LIM, C. K. & GUILLEMIN, G. J. 2020. Differential kynurenine pathway metabolism in highly metastatic aggressive breast cancer subtypes: beyond IDO1-induced immunosuppression. *Breast Cancer Res,* 22**,** 113.

HEYLEN, A., VERMEIREN, Y., KEMA, I. P., VAN FAASSEN, M., VAN DER LEY, C., VAN DAM, D. & DE DEYN, P. P. 2023. Brain Kynurenine Pathway Metabolite Levels May Reflect Extent of Neuroinflammation in ALS, FTD and Early Onset AD. *Pharmaceuticals,* 16**,** 615.

HEZAREH, M. 2005. Prostratin as a new therapeutic agent targeting HIV viral reservoirs. *Drug News Perspect,* 18**,** 496-500.

HIDALGO, M. A., ROMERO, A., FIGUEROA, J., CORTÉS, P., CONCHA, II, HANCKE, J. L. & BURGOS, R. A. 2005. Andrographolide interferes with binding of nuclear factor-kappaB to DNA in HL-60-derived neutrophilic cells. *Br J Pharmacol,* 144**,** 680-6.

HIROTA, R., NAKAMURA, H., BHATTI, S. A., NGATU, N. R., MUZEMBO, B. A., DUMAVIBHAT, N., EITOKU, M., SAWAMURA, M. & SUGANUMA, N. 2012. Limonene inhalation reduces allergic airway inflammation in Dermatophagoides farinae-treated mice. *Inhal Toxicol,* 24**,** 373-81.

HODI, F. S., MIHM, M. C., SOIFFER, R. J., HALUSKA, F. G., BUTLER, M., SEIDEN, M. V., DAVIS, T., HENRY-SPIRES, R., MACRAE, S., WILLMAN, A., PADERA, R., JAKLITSCH, M. T., SHANKAR, S., CHEN, T. C., KORMAN, A., ALLISON, J. P. & DRANOFF, G. 2003. Biologic activity of cytotoxic T lymphocyte-associated antigen 4 antibody blockade in previously vaccinated metastatic melanoma and ovarian carcinoma patients. *Proc Natl Acad Sci U S A,* 100**,** 4712-7.

HOHMANN, J., RÉDEI, D., FORGO, P., MOLNÁR, J., DOMBI, G. & ZORIG, T. 2003. Jatrophane diterpenoids from Euphorbia mongolica as modulators of the multidrug resistance of L5128 mouse lymphoma cells. *J Nat Prod,* 66**,** 976-9.

HOOGERHEIDE, J. G. & POPOV, A. I. 1978. Study of monensin complexes with monovalent metal lons in anhydrous methanol solutions. *Journal of Solution Chemistry,* 7**,** 357-372.

HORNBECK, P. V., CHABRA, I., KORNHAUSER, J. M., SKRZYPEK, E. & ZHANG, B. 2004. PhosphoSite: A bioinformatics resource dedicated to physiological protein phosphorylation. *Proteomics,* 4**,** 1551-61.

HORNBECK, P. V., ZHANG, B., MURRAY, B., KORNHAUSER, J. M., LATHAM, V. & SKRZYPEK, E. 2015. PhosphoSitePlus, 2014: mutations, PTMs and recalibrations. *Nucleic Acids Res,* 43**,** D512-20.

HORNYÁK, L., DOBOS, N., KONCZ, G., KARÁNYI, Z., PÁLL, D., SZABÓ, Z., HALMOS, G. & SZÉKVÖLGYI, L. 2018. The Role of Indoleamine-2,3-Dioxygenase in Cancer Development, Diagnostics, and Therapy. *Front Immunol,* 9**,** 151.

HORVAI, A. E., XU, L., KORZUS, E., BRARD, G., KALAFUS, D., MULLEN, T. M., ROSE, D. W., ROSENFELD, M. G. & GLASS, C. K. 1997. Nuclear integration of JAK/STAT and Ras/AP-1 signaling by CBP and p300. *Proc Natl Acad Sci U S A,* 94**,** 1074-9.

HOSHI, M., MATSUMOTO, K., ITO, H., OHTAKI, H., ARIOKA, Y., OSAWA, Y., YAMAMOTO, Y., MATSUNAMI, H., HARA, A., SEISHIMA, M. & SAITO, K. 2012. L-tryptophan-kynurenine pathway metabolites regulate type I IFNs of acute viral myocarditis in mice. *J Immunol,* 188**,** 3980-7.

HOSKINS, L. M., ROY, K., PETERS, J. A., LOUD, J. T. & GREENE, M. H. 2008. Disclosure of Positive BRCA1/2-Mutation Status in Young Couples: The Journey From Uncertainty to Bonding Through Partner Support. *Fam Syst Health,* 26**,** 296-316.

HOSOI, R., MATSUDA, T., ASANO, S., NAKAMURA, H., HASHIMOTO, H., TAKUMA, K. & BABA, A. 1997. Isoform-specific up-regulation by ouabain of Na+,K+-ATPase in cultured rat astrocytes. *J Neurochem,* 69**,** 2189-96.

HOSSEINI, M., SEYEDPOUR, S., KHODAEI, B., LOGHMAN, A. H., SEYEDPOUR, N., YAZDI, M. H. & REZAEI, N. 2023. Cancer Vaccines for Triple-Negative Breast Cancer: A Systematic Review. *Vaccines (Basel),* 11.

HOUSE, C. D., WANG, B. D., CENICCOLA, K., WILLIAMS, R., SIMAAN, M., OLENDER, J., PATEL, V., BAPTISTA-HON, D. T., ANNUNZIATA, C. M., GUTKIND, J. S., HALES, T. G. & LEE, N. H. 2015. Voltage-gated Na+ Channel Activity Increases Colon Cancer Transcriptional Activity and Invasion Via Persistent MAPK Signaling. *Sci Rep,* 5**,** 11541.

HU, M., ZHOU, W., WANG, Y., YAO, D., YE, T., YAO, Y., CHEN, B., LIU, G., YANG, X., WANG, W. & XIE, Y. 2020. Discovery of the first potent proteolysis targeting chimera (PROTAC) degrader of indoleamine 2,3-dioxygenase 1. *Acta Pharm Sin B,* 10**,** 1943-1953.

HUANG, H., LI, P., YE, X., ZHANG, F., LIN, Q., WU, K. & CHEN, W. 2021a. Isoalantolactone Increases the Sensitivity of Prostate Cancer Cells to Cisplatin Treatment by Inducing Oxidative Stress. *Front Cell Dev Biol,* 9**,** 632779.

HUANG, J. D., ZHANG, C., XU, W. J., LIAN, C. L., LIU, X. M., WANG, C. F. & LIU, J. Q. 2021b. New lathyrane diterpenoids with anti-inflammatory activity isolated from the roots of Jatropha curcas L. *J Ethnopharmacol,* 268**,** 113673.

HUANG, T. T., TSENG, L. M., CHEN, J. L., CHU, P. Y., LEE, C. H., HUANG, C. T., WANG, W. L., LAU, K. Y., TSENG, M. F., CHANG, Y. Y., CHIANG, T. Y., UENG, Y. F., LEE, H. C., DAI, M. S. & LIU, C. Y. 2020. Kynurenine 3-monooxygenase upregulates pluripotent genes through β-catenin and promotes triple-negative breast cancer progression. *EBioMedicine,* 54**,** 102717.

HUANG, Y. H., ZHU, C., KONDO, Y., ANDERSON, A. C., GANDHI, A., RUSSELL, A., DOUGAN, S. K., PETERSEN, B. S., MELUM, E., PERTEL, T., CLAYTON, K. L., RAAB, M., CHEN, Q., BEAUCHEMIN, N., YAZAKI, P. J., PYZIK, M., OSTROWSKI, M. A., GLICKMAN, J. N., RUDD, C. E., PLOEGH, H. L., FRANKE, A., PETSKO, G. A., KUCHROO, V. K. & BLUMBERG, R. S. 2015. CEACAM1 regulates TIM-3-mediated tolerance and exhaustion. *Nature,* 517**,** 386-90.

HUCZYŃSKI, A. 2012. Polyether ionophores-promising bioactive molecules for cancer therapy. *Bioorg Med Chem Lett,* 22**,** 7002-10.

HUCZYŃSKI, A., JANCZAK, J., LOWICKI, D. & BRZEZINSKI, B. 2012a. Monensin A acid complexes as a model of electrogenic transport of sodium cation. *Biochim Biophys Acta,* 1818**,** 2108-19.

HUCZYŃSKI, A., JANCZAK, J., ŁOWICKI, D. & BRZEZINSKI, B. 2012b. Monensin A acid complexes as a model of electrogenic transport of sodium cation. *Biochimica et Biophysica Acta (BBA) - Biomembranes,* 1818**,** 2108-2119.

HUCZYŃSKI, A., RATAJCZAK-SITARZ, M., KATRUSIAK, A. & BRZEZINSKI, B. 2008. Molecular structure of rubidium six-coordinated dihydrate complex with monensin A. *Journal of Molecular Structure,* 888**,** 224-229.

HUGHES, J. P., REES, S., KALINDJIAN, S. B. & PHILPOTT, K. L. 2011. Principles of early drug discovery. *Br J Pharmacol,* 162**,** 1239-49.

HUI, R., GANDHI, L., COSTA, E. C., FELIP, E., AHN, M.-J., EDER, J. P., BALMANOUKIAN, A. S., LEIGHL, N. B., AGGARWAL, C., HORN, L., PATNAIK, A., MIDDLETON, G. W., GUBENS, M. A., HELLMANN, M. D., SORIA, J.-C., RAMALINGAM, S. S., LUBINIECKI, G. M., ZHANG, J., PIPERDI, B. & GARON, E. B. 2016. Long-term OS for patients with advanced NSCLC enrolled in the KEYNOTE-001 study of pembrolizumab (pembro). *Journal of Clinical Oncology,* 34**,** 9026-9026.

HULIKOVA, A., HARRIS, A. L., VAUGHAN-JONES, R. D. & SWIETACH, P. 2013. Regulation of intracellular pH in cancer cell lines under normoxia and hypoxia. *J Cell Physiol,* 228**,** 743-52.

HUNG, C. H., LEE, C. H., TSAI, M. H., CHEN, C. H., LIN, H. F., HSU, C. Y., LAI, C. L. & CHEN, C. C. 2020. Activation of acid-sensing ion channel 3 by lysophosphatidylcholine 16:0 mediates psychological stress-induced fibromyalgia-like pain. *Ann Rheum Dis,* 79**,** 1644-1656.

HUR, J., PAK, S. C., KOO, B. S. & JEON, S. 2013. Borneol alleviates oxidative stress via upregulation of Nrf2 and Bcl-2 in SH-SY5Y cells. *Pharm Biol,* 51**,** 30-5.

HURVITZ, S. A., ANDRE, F., JIANG, Z., SHAO, Z., MANO, M. S., NECIOSUP, S. P., TSENG, L. M., ZHANG, Q., SHEN, K., LIU, D., DREOSTI, L. M., BURRIS, H. A., TOI, M., BUYSE, M. E., CABARIBERE, D., LINDSAY, M. A., RAO, S., PACAUD, L. B., TARAN, T. & SLAMON, D. 2015. Combination of everolimus with trastuzumab plus paclitaxel as first-line treatment for patients with HER2-positive advanced breast cancer (BOLERO-1): a phase 3, randomised, double-blind, multicentre trial. *Lancet Oncol,* 16**,** 816-29.

IAMSHANOVA, O., MARIOT, P., LEHEN'KYI, V. & PREVARSKAYA, N. 2016. Comparison of fluorescence probes for intracellular sodium imaging in prostate cancer cell lines. *Eur Biophys J,* 45**,** 765-777.

IANNIELLO, C., MOY, L., FOGARTY, J., SCHNABEL, F., ADAMS, S., AXELROD, D., AXEL, L., BROWN, R. & MADELIN, G. 2021. Multinuclear MRI to disentangle intracellular

sodium concentration and extracellular volume fraction in breast cancer. *Scientific Reports,* 11.

INABAYASHI, M., MIYAUCHI, S., KAMO, N. & JIN, T. 1995. Conductance change in phospholipid bilayer membrane by an electroneutral ionophore, monensin. *Biochemistry,* 34**,** 3455-60.

ISMAIL, H. M., BARTON, V., PHANCHANA, M., CHAROENSUTTHIVARAKUL, S., WONG, M. H., HEMINGWAY, J., BIAGINI, G. A., O'NEILL, P. M. & WARD, S. A. 2016. Artemisinin activity-based probes identify multiple molecular targets within the asexual stage of the malaria parasites Plasmodium falciparum 3D7. *Proc Natl Acad Sci U S A,* 113**,** 2080-5.

ITO, C., ITOIGAWA, M., NAKAO, K., MURATA, T., TSUBOI, M., KANEDA, N. & FURUKAWA, H. 2006. Induction of apoptosis by carbazole alkaloids isolated from Murraya koenigii. *Phytomedicine,* 13**,** 359-65.

ITOIGAWA, M., ITO, C., TOKUDA, H., ENJO, F., NISHINO, H. & FURUKAWA, H. 2004. Cancer chemopreventive activity of phenylpropanoids and phytoquinoids from Illicium plants. *Cancer Lett,* 214**,** 165-9.

IVASHKIV, L. B. 2020. The hypoxia-lactate axis tempers inflammation. *Nat Rev Immunol,* 20**,** 85-86.

IWAI, Y., HAMANISHI, J., CHAMOTO, K. & HONJO, T. 2017. Cancer immunotherapies targeting the PD-1 signaling pathway. *J Biomed Sci,* 24**,** 26.

IWASAKI, T., KOHASHI, K., TODA, Y., ISHIHARA, S., YAMADA, Y. & ODA, Y. 2021. Association of PD-L1 and IDO1 expression with JAK-STAT pathway activation in soft-tissue leiomyosarcoma. *J Cancer Res Clin Oncol,* 147**,** 1451-1463.

JADHAV, A., FERREIRA, R. S., KLUMPP, C., MOTT, B. T., AUSTIN, C. P., INGLESE, J., THOMAS, C. J., MALONEY, D. J., SHOICHET, B. K. & SIMEONOV, A. 2010. Quantitative analyses of aggregation, autofluorescence, and reactivity artifacts in a screen for inhibitors of a thiol protease. *J Med Chem,* 53**,** 37-51.

JAIN, S. & CLARK, J. I. 2015. Ipilimumab for the treatment of melanoma. *Melanoma Manag,* 2**,** 33-39.

JAMES, A. D., LESLIE, T. K., KAGGIE, J. D., WIGGINS, L., PATTEN, L., MURPHY O'DUINN, J., LANGER, S., LABARTHE, M. C., RIEMER, F., BAXTER, G., MCLEAN, M. A., GILBERT, F. J., KENNERLEY, A. J. & BRACKENBURY, W. J. 2022. Sodium accumulation in breast cancer predicts malignancy and treatment response. *Br J Cancer,* 127**,** 337-349.

JAMES, J. T. & DUBERY, I. A. 2009. Pentacyclic triterpenoids from the medicinal herb, Centella asiatica (L.) Urban. *Molecules,* 14**,** 3922-41.

JANG, K. J., KIM, H. K., HAN, M. H., OH, Y. N., YOON, H. M., CHUNG, Y. H., KIM, G. Y., HWANG, H. J., KIM, B. W. & CHOI, Y. H. 2013. Anti-inflammatory effects of saponins derived from the roots of Platycodon grandiflorus in lipopolysaccharide-stimulated BV2 microglial cells. *Int J Mol Med,* 31**,** 1357-66.

JAYAKUMAR, T., HSIEH, C. Y., LEE, J. J. & SHEU, J. R. 2013. Experimental and Clinical Pharmacology of Andrographis paniculata and Its Major Bioactive Phytoconstituent Andrographolide. *Evid Based Complement Alternat Med,* 2013**,** 846740.

JENKINS, B. J., GRAIL, D., NHEU, T., NAJDOVSKA, M., WANG, B., WARING, P., INGLESE, M., MCLOUGHLIN, R. M., JONES, S. A., TOPLEY, N., BAUMANN, H., JUDD, L. M., GIRAUD, A. S., BOUSSIOUTAS, A., ZHU, H. J. & ERNST, M. 2005. Hyperactivation of Stat3 in gp130 mutant mice promotes gastric hyperproliferation and desensitizes TGF-beta signaling. *Nat Med,* 11**,** 845-52.

JENKINS, T. A., NGUYEN, J. C., POLGLAZE, K. E. & BERTRAND, P. P. 2016. Influence of Tryptophan and Serotonin on Mood and Cognition with a Possible Role of the Gut-Brain Axis. *Nutrients,* 8.

JEYAKUMAR, A. & YOUNIS, T. 2012. Trastuzumab for HER2-Positive Metastatic Breast Cancer: Clinical and Economic Considerations. *Clin Med Insights Oncol,* 6**,** 179-87.
JIA, L., ZHANG, Q. & ZHANG, R. 2018. PD-1/PD-L1 pathway blockade works as an effective and practical therapy for cancer immunotherapy. *Cancer Biol Med,* 15**,** 116-123.
JIN, L., HAN, B., SIEGEL, E., CUI, Y., GIULIANO, A. & CUI, X. 2018. Breast cancer lung metastasis: Molecular biology and therapeutic implications. *Cancer Biol Ther,* 19**,** 858-868.
JOCA, H. C., CRUZ-MENDES, Y., OLIVEIRA-ABREU, K., MAIA-JOCA, R. P., BARBOSA, R., LEMOS, T. L., LACERDA BEIRÃO, P. S. & LEAL-CARDOSO, J. H. 2012. Carvacrol decreases neuronal excitability by inhibition of voltage-gated sodium channels. *J Nat Prod,* 75**,** 1511-7.
JOHNSTON, R. J., COMPS-AGRAR, L., HACKNEY, J., YU, X., HUSENI, M., YANG, Y., PARK, S., JAVINAL, V., CHIU, H., IRVING, B., EATON, D. L. & GROGAN, J. L. 2014. The immunoreceptor TIGIT regulates antitumor and antiviral CD8(+) T cell effector function. *Cancer Cell,* 26**,** 923-937.
JOHRA, F. T., HOSSAIN, S., JAIN, P., BRISTY, A. T., EMRAN, T., AHMED, R., SHARKER, S. M., BEPARI, A. K. & REZA, H. M. 2023. Amelioration of CCl4-induced oxidative stress and hepatotoxicity by Ganoderma lucidum in Long Evans rats. *Scientific Reports,* 13**,** 9909.
JONESCHEIT, H., OBERG, H. H., GONNERMANN, D., HERMES, M., SULAJ, V., PETERS, C., KABELITZ, D. & WESCH, D. 2020. Influence of Indoleamine-2,3-Dioxygenase and Its Metabolite Kynurenine on γδ T Cell Cytotoxicity against Ductal Pancreatic Adenocarcinoma Cells. *Cells,* 9.
JUNG, M. Y., AIBAIDULA, A., BROWN, D. A., HIMES, B. T., CUMBA GARCIA, L. M. & PARNEY, I. F. 2022. Superinduction of immunosuppressive glioblastoma extracellular vesicles by IFN-γ through PD-L1 and IDO1. *Neurooncol Adv,* 4**,** vdac017.
JUNG, Y. Y., SHANMUGAM, M. K., NARULA, A. S., KIM, C., LEE, J. H., NAMJOSHI, O. A., BLOUGH, B. E., SETHI, G. & AHN, K. S. 2019. Oxymatrine Attenuates Tumor Growth and Deactivates STAT5 Signaling in a Lung Cancer Xenograft Model. *Cancers (Basel),* 11.
KAISER, H., PARKER, E. & HAMRICK, M. W. 2020. Kynurenine signaling through the aryl hydrocarbon receptor: Implications for aging and healthspan. *Exp Gerontol,* 130**,** 110797.
KAMPAN, N. C., MADONDO, M. T., MCNALLY, O. M., QUINN, M. & PLEBANSKI, M. 2015. Paclitaxel and Its Evolving Role in the Management of Ovarian Cancer. *Biomed Res Int,* 2015**,** 413076.
KANAI, M., FUNAKOSHI, H., TAKAHASHI, H., HAYAKAWA, T., MIZUNO, S., MATSUMOTO, K. & NAKAMURA, T. 2009. Tryptophan 2,3-dioxygenase is a key modulator of physiological neurogenesis and anxiety-related behavior in mice. *Mol Brain,* 2**,** 8.
KANG, N. J., HAN, S. C., YOON, S. H., SIM, J. Y., MAENG, Y. H., KANG, H. K. & YOO, E. S. 2019. Cinnamomum camphora Leaves Alleviate Allergic Skin Inflammatory Responses In Vitro and In Vivo. *Toxicol Res,* 35**,** 279-285.
KANJI, S. & MACLEAN, R. D. 2012. Cardiac glycoside toxicity: more than 200 years and counting. *Crit Care Clin,* 28**,** 527-35.
KARITSKAYA, I., AKSENOV, N., VASSILIEVA, I., ZENIN, V. & MARAKHOVA, I. 2010. Long-term regulation of Na,K-ATPase pump during T-cell proliferation. *Pflugers Arch,* 460**,** 777-89.
KARLISH, S. J. D., BEAUGÉ, L. A. & GLYNN, I. M. 1979. Vanadate inhibits (Na+ + K+)ATPase by blocking a conformational change of the unphosphorylated form. *Nature,* 282**,** 333.

KASHYAP, D., BAL, A., IRINIKE, S., KHARE, S., BHATTACHARYA, S., DAS, A. & SINGH, G. 2023. Heterogeneity of the Tumor Microenvironment Across Molecular Subtypes of Breast Cancer. *Appl Immunohistochem Mol Morphol*.

KATERJI, M., FILIPPOVA, M. & DUERKSEN-HUGHES, P. 2019. Approaches and Methods to Measure Oxidative Stress in Clinical Samples: Research Applications in the Cancer Field. *Oxid Med Cell Longev,* 2019**,** 1279250.

KATZ, Y., WEIZMAN, A., PICK, C. G., PASTERNAK, G. W., LIU, L., FONIA, O. & GAVISH, M. 1994. Interactions between laudanosine, GABA, and opioid subtype receptors: implication for laudanosine seizure activity. *Brain Res,* 646**,** 235-41.

KAUFMAN, B., TRUDEAU, M., AWADA, A., BLACKWELL, K., BACHELOT, T., SALAZAR, V., DESILVIO, M., WESTLUND, R., ZAKS, T., SPECTOR, N. & JOHNSTON, S. 2009. Lapatinib monotherapy in patients with HER2-overexpressing relapsed or refractory inflammatory breast cancer: final results and survival of the expanded HER2+ cohort in EGF103009, a phase II study. *Lancet Oncol,* 10**,** 581-8.

KEAM, B., IM, S. A., LEE, K. H., HAN, S. W., OH, D. Y., KIM, J. H., LEE, S. H., HAN, W., KIM, D. W., KIM, T. Y., PARK, I. A., NOH, D. Y., HEO, D. S. & BANG, Y. J. 2011. Ki-67 can be used for further classification of triple negative breast cancer into two subtypes with different response and prognosis. *Breast Cancer Res,* 13**,** R22.

KENSKI, J. C. N., HUANG, X., VREDEVOOGD, D. W., DE BRUIJN, B., TRAETS, J. J. H., IBÁÑEZ-MOLERO, S., SCHIEVEN, S. M., VAN VLIET, A., KRIJGSMAN, O., KUILMAN, T., POZNIAK, J., LOAYZA-PUCH, F., TERRY, A. M., MÜLLER, J., LOGTENBERG, M. E. W., DE BRUIJN, M., LEVY, P., KÖRNER, P. R., GODING, C. R., SCHUMACHER, T. N., MARINE, J. C., AGAMI, R. & PEEPER, D. S. 2023. An adverse tumor-protective effect of IDO1 inhibition. *Cell Rep Med,* 4**,** 100941.

KEPP, O., MENGER, L., VACCHELLI, E., ADJEMIAN, S., MARTINS, I., MA, Y., SUKKURWALA, A. Q., MICHAUD, M., GALLUZZI, L., ZITVOGEL, L. & KROEMER, G. 2012. Anticancer activity of cardiac glycosides: At the frontier between cell-autonomous and immunological effects. *Oncoimmunology,* 1**,** 1640-1642.

KEVIN II, D. A., MEUJO, D. A. & HAMANN, M. T. 2009. Polyether ionophores: broad-spectrum and promising biologically active molecules for the control of drug-resistant bacteria and parasites. *Expert Opin Drug Discov,* 4**,** 109-46.

KHAJAH, M. A., MATHEW, P. M. & LUQMANI, Y. A. 2018. Na+/K+ ATPase activity promotes invasion of endocrine resistant breast cancer cells. *PLoS One,* 13**,** e0193779.

KHAJAH, M. A., YANG, M., BRACKENBURY, W. J., LUQMANI, Y. A., MOHAMMED, F. H., KHAJAH, M. A., YANG, M., BRACKENBURY, W. J. & LUQMANI, Y. A. 2016. Blockade of voltage-gated sodium channels inhibits invasion of endocrine-resistant breast cancer cells. *International journal of oncology.,* 48**,** 73-83.

KHAN, B. M., QIU, H. M., WANG, X. F., LIU, Z. Y., ZHANG, J. Y., GUO, Y. J., CHEN, W. Z., LIU, Y. & CHEONG, K. L. 2019. Physicochemical characterization of Gracilaria chouae sulfated polysaccharides and their antioxidant potential. *Int J Biol Macromol,* 134**,** 255-261.

KHAN, M., DU, K., AI, M., WANG, B., LIN, J., REN, A., CHEN, C., HUANG, Z., QIU, W., YUAN, Y. & TIAN, Y. 2023. PD-L1 expression as biomarker of efficacy of PD-1/PD-L1 checkpoint inhibitors in metastatic triple negative breast cancer: A systematic review and meta-analysis. *Front Immunol,* 14**,** 1060308.

KIM, D. S., JANG, I. K., LEE, M. W., KO, Y. J., LEE, D. H., LEE, J. W., SUNG, K. W., KOO, H. H. & YOO, K. H. 2018. Enhanced Immunosuppressive Properties of Human Mesenchymal Stem Cells Primed by Interferon-γ. *EBioMedicine,* 28**,** 261-273.

KIM, D. S., LEE, H. J., JEON, Y. D., HAN, Y. H., KEE, J. Y., KIM, H. J., SHIN, H. J., KANG, J., LEE, B. S., KIM, S. H., KIM, S. J., PARK, S. H., CHOI, B. M., PARK, S. J., UM, J. Y. & HONG, S. H. 2015. Alpha-Pinene Exhibits Anti-Inflammatory Activity Through the Suppression

of MAPKs and the NF-κB Pathway in Mouse Peritoneal Macrophages. *Am J Chin Med,* 43**,** 731-42.
KIM, S., DERE, E., BURGOON, L. D., CHANG, C. C. & ZACHAREWSKI, T. R. 2009. Comparative analysis of AhR-mediated TCDD-elicited gene expression in human liver adult stem cells. *Toxicol Sci,* 112**,** 229-44.
KIM, T. K. & EBERWINE, J. H. 2010. Mammalian cell transfection: the present and the future. *Anal Bioanal Chem,* 397**,** 3173-8.
KIM, W., SEONG, K. M. & YOUN, B. 2011. Phenylpropanoids in radioregulation: double edged sword. *Exp Mol Med,* 43**,** 323-33.
KLEIMAIER, D., SCHEPKIN, V., NIES, C., GOTTWALD, E. & SCHAD, L. R. 2020. Intracellular Sodium Changes in Cancer Cells Using a Microcavity Array-Based Bioreactor System and Sodium Triple-Quantum MR Signal. *Processes,* 8**,** 1267.
KLIMANOVA, E. A., TVERSKOI, A. M., KOLTSOVA, S. V., SIDORENKO, S. V., LOPINA, O. D., TREMBLAY, J., HAMET, P., KAPILEVICH, L. V. & ORLOV, S. N. 2017. Time- and dose dependent actions of cardiotonic steroids on transcriptome and intracellular content of Na(+) and K(+): a comparative analysis. *Sci Rep,* 7**,** 45403.
KOBOLDT, D. C., FULTON, R. S., MCLELLAN, M. D., SCHMIDT, H., KALICKI-VEIZER, J., MCMICHAEL, J. F., FULTON, L. L., DOOLING, D. J., DING, L., MARDIS, E. R., WILSON, R. K., ALLY, A., BALASUNDARAM, M., BUTTERFIELD, Y. S. N., CARLSEN, R., CARTER, C., CHU, A., CHUAH, E., CHUN, H.-J. E., COOPE, R. J. N., DHALLA, N., GUIN, R., HIRST, C., HIRST, M., HOLT, R. A., LEE, D., LI, H. I., MAYO, M., MOORE, R. A., MUNGALL, A. J., PLEASANCE, E., GORDON ROBERTSON, A., SCHEIN, J. E., SHAFIEI, A., SIPAHIMALANI, P., SLOBODAN, J. R., STOLL, D., TAM, A., THIESSEN, N., VARHOL, R. J., WYE, N., ZENG, T., ZHAO, Y., BIROL, I., JONES, S. J. M., MARRA, M. A., CHERNIACK, A. D., SAKSENA, G., ONOFRIO, R. C., PHO, N. H., CARTER, S. L., SCHUMACHER, S. E., TABAK, B., HERNANDEZ, B., GENTRY, J., NGUYEN, H., CRENSHAW, A., ARDLIE, K., BEROUKHIM, R., WINCKLER, W., GETZ, G., GABRIEL, S. B., MEYERSON, M., CHIN, L., PARK, P. J., KUCHERLAPATI, R., HOADLEY, K. A., TODD AUMAN, J., FAN, C., TURMAN, Y. J., SHI, Y., LI, L., TOPAL, M. D., HE, X., CHAO, H.-H., PRAT, A., SILVA, G. O., IGLESIA, M. D., ZHAO, W., USARY, J., BERG, J. S., ADAMS, M., BOOKER, J., WU, J., GULABANI, A., BODENHEIMER, T., HOYLE, A. P., SIMONS, J. V., SOLOWAY, M. G., MOSE, L. E., JEFFERYS, S. R., BALU, S., PARKER, J. S., NEIL HAYES, D., PEROU, C. M., MALIK, S., MAHURKAR, S., SHEN, H., WEISENBERGER, D. J., TRICHE JR, T., et al. 2012. Comprehensive molecular portraits of human breast tumours. *Nature,* 490**,** 61-70.
KOH, J. & KIM, M. J. 2019. Introduction of a New Staging System of Breast Cancer for Radiologists: An Emphasis on the Prognostic Stage. *Korean J Radiol,* 20**,** 69-82.
KOIDE, Y., INA, Y., NEZU, N. & YOSHIDA, T. O. 1988. Calcium influx and the Ca2+-calmodulin complex are involved in interferon-gamma-induced expression of HLA class II molecules on HL-60 cells. *Proc Natl Acad Sci U S A,* 85**,** 3120-4.
KOLLA, V., ROBERTSON, N. M. & LITWACK, G. 1999. Identification of a mineralocorticoid/glucocorticoid response element in the human Na/K ATPase alpha1 gene promoter. *Biochem Biophys Res Commun,* 266**,** 5-14.
KOOSHKAKI, O., DERAKHSHANI, A., HOSSEINKHANI, N., TORABI, M., SAFAEI, S., BRUNETTI, O., RACANELLI, V., SILVESTRIS, N. & BARADARAN, B. 2020. Combination of Ipilimumab and Nivolumab in Cancers: From Clinical Practice to Ongoing Clinical Trials. *Int J Mol Sci,* 21.
KOPPENOL, W. H., BOUNDS, P. L. & DANG, C. V. 2011. Otto Warburg's contributions to current concepts of cancer metabolism. *Nature Reviews Cancer,* 11**,** 325-337.
KORDE, L. A., SOMERFIELD, M. R., HERSHMAN, D. L., FOR THE NEOADJUVANT CHEMOTHERAPY, E. T., PANEL, T. T. F. B. C. G. E., FOR THE NEOADJUVANT

CHEMOTHERAPY, E. T. & PANEL, T. T. F. B. C. G. E. 2022. Use of Immune Checkpoint Inhibitor Pembrolizumab in the Treatment of High-Risk, Early-Stage Triple-Negative Breast Cancer: ASCO Guideline Rapid Recommendation Update. *Journal of Clinical Oncology,* 40**,** 1696-1698.

KOUO, T., HUANG, L., PUCSEK, A. B., CAO, M., SOLT, S., ARMSTRONG, T. & JAFFEE, E. 2015. Galectin-3 Shapes Antitumor Immune Responses by Suppressing CD8+ T Cells via LAG-3 and Inhibiting Expansion of Plasmacytoid Dendritic Cells. *Cancer Immunol Res,* 3**,** 412-23.

KRISHNA, S., BUSTAMANTE, L., HAYNES, R. K. & STAINES, H. M. 2008. Artemisinins: their growing importance in medicine. *Trends Pharmacol Sci,* 29**,** 520-7.

KRUPA, A. & KOWALSKA, I. 2021. The Kynurenine Pathway-New Linkage between Innate and Adaptive Immunity in Autoimmune Endocrinopathies. *Int J Mol Sci,* 22.

KUHL, C., TAUTENHAHN, R., BÖTTCHER, C., LARSON, T. R. & NEUMANN, S. 2012. CAMERA: an integrated strategy for compound spectra extraction and annotation of liquid chromatography/mass spectrometry data sets. *Anal Chem,* 84**,** 283-9.

KULKARNI, A. P., MAHAL, H. S., KAPOOR, S. & ARADHYA, S. M. 2007. In Vitro Studies on the Binding, Antioxidant, and Cytotoxic Actions of Punicalagin. *Journal of Agricultural and Food Chemistry,* 55**,** 1491-1500.

KUMAR, S. R., HOSOKAWA, M. & MIYASHITA, K. 2013. Fucoxanthin: a marine carotenoid exerting anti-cancer effects by affecting multiple mechanisms. *Mar Drugs,* 11**,** 5130-47.

KWA, M. J. & ADAMS, S. 2018. Checkpoint inhibitors in triple-negative breast cancer (TNBC): Where to go from here. *Cancer,* 124**,** 2086-2103.

LACHMANN, A., XU, H., KRISHNAN, J., BERGER, S. I., MAZLOOM, A. R. & MA'AYAN, A. 2010. ChEA: transcription factor regulation inferred from integrating genome-wide ChIP-X experiments. *Bioinformatics,* 26**,** 2438-44.

LAN, J. Y., WILLIAMS, C., LEVIN, M. & BLACK, L. D., 3RD 2014. Depolarization of Cellular Resting Membrane Potential Promotes Neonatal Cardiomyocyte Proliferation In Vitro. *Cell Mol Bioeng,* 7**,** 432-445.

LANZ, T. V., WILLIAMS, S. K., STOJIC, A., IWANTSCHEFF, S., SONNER, J. K., GRABITZ, C., BECKER, S., BÖHLER, L. I., MOHAPATRA, S. R., SAHM, F., KÜBLBECK, G., NAKAMURA, T., FUNAKOSHI, H., OPITZ, C. A., WICK, W., DIEM, R. & PLATTEN, M. 2017. Tryptophan-2,3-Dioxygenase (TDO) deficiency is associated with subclinical neuroprotection in a mouse model of multiple sclerosis. *Sci Rep,* 7**,** 41271.

LARRINAGA, G., SOLANO-ITURRI, J. D., ERRARTE, P., UNDA, M., LOIZAGA-IRIARTE, A., PÉREZ-FERNÁNDEZ, A., ECHEVARRÍA, E., ASUMENDI, A., MANINI, C., ANGULO, J. C. & LÓPEZ, J. I. 2021. Soluble PD-L1 Is an Independent Prognostic Factor in Clear Cell Renal Cell Carcinoma. *Cancers (Basel),* 13.

LAU, K. H., TAN, A. M. & SHI, Y. 2022. New and Emerging Targeted Therapies for Advanced Breast Cancer. *Int J Mol Sci,* 23.

LEAL-CARDOSO, J. H., DA SILVA-ALVES, K. S., FERREIRA-DA-SILVA, F. W., DOS SANTOS-NASCIMENTO, T., JOCA, H. C., DE MACEDO, F. H., DE ALBUQUERQUE-NETO, P. M., MAGALHÃES, P. J., LAHLOU, S., CRUZ, J. S. & BARBOSA, R. 2010. Linalool blocks excitability in peripheral nerves and voltage-dependent Na+ current in dissociated dorsal root ganglia neurons. *Eur J Pharmacol,* 645**,** 86-93.

LEE, D. K., IN, J. & LEE, S. 2015. Standard deviation and standard error of the mean. *Korean J Anesthesiol,* 68**,** 220-3.

LEE, H.-S., KIM, S.-M., JANG, J.-H., PARK, H.-D. & LEE, S.-Y. 2021. Serum 5-Hydroxyindoleacetic Acid and Ratio of 5-Hydroxyindoleacetic Acid to Serotonin as Metabolomics Indicators for Acute Oxidative Stress and Inflammation in Vancomycin-Associated Acute Kidney Injury. *Antioxidants,* 10**,** 895.

LEE, H. H., WANG, Y. N., XIA, W., CHEN, C. H., RAU, K. M., YE, L., WEI, Y., CHOU, C. K., WANG, S. C., YAN, M., TU, C. Y., HSIA, T. C., CHIANG, S. F., CHAO, K. S. C., WISTUBA, II, HSU, J. L., HORTOBAGYI, G. N. & HUNG, M. C. 2019. Removal of N-Linked Glycosylation Enhances PD-L1 Detection and Predicts Anti-PD-1/PD-L1 Therapeutic Efficacy. *Cancer Cell,* 36**,** 168-178.e4.

LEE, J., YAMAZAKI, T., DONG, H. & JEFCOATE, C. 2017. A single cell level measurement of StAR expression and activity in adrenal cells. *Mol Cell Endocrinol,* 441**,** 22-30.

LEHTONEN, A., MATIKAINEN, S. & JULKUNEN, I. 1997. Interferons up-regulate STAT1, STAT2, and IRF family transcription factor gene expression in human peripheral blood mononuclear cells and macrophages. *J Immunol,* 159**,** 794-803.

LEMOS, H., MOHAMED, E., OU, R., MCCARDLE, C., ZHENG, X., MCGUIRE, K., HOMER, N. Z. M., MOLE, D. J., HUANG, L. & MELLOR, A. L. 2020. Co-treatments to Boost IDO Activity and Inhibit Production of Downstream Catabolites Induce Durable Suppression of Experimental Autoimmune Encephalomyelitis. *Front Immunol,* 11**,** 1256.

LESLIE, T. K., JAMES, A. D., ZACCAGNA, F., GRIST, J. T., DEEN, S., KENNERLEY, A., RIEMER, F., KAGGIE, J. D., GALLAGHER, F. A., GILBERT, F. J. & BRACKENBURY, W. J. 2019. Sodium homeostasis in the tumour microenvironment. *Biochim Biophys Acta Rev Cancer,* 1872**,** 188304.

LEUNG, Y. Y., YAO HUI, L. L. & KRAUS, V. B. 2015. Colchicine--Update on mechanisms of action and therapeutic uses. *Semin Arthritis Rheum,* 45**,** 341-50.

LI, C.-W., LIM, S.-O., XIA, W., LEE, H.-H., CHAN, L.-C., KUO, C.-W., KHOO, K.-H., CHANG, S.-S., CHA, J.-H., KIM, T., HSU, J. L., WU, Y., HSU, J.-M., YAMAGUCHI, H., DING, Q., WANG, Y., YAO, J., LEE, C.-C., WU, H.-J., SAHIN, A. A., ALLISON, J. P., YU, D., HORTOBAGYI, G. N. & HUNG, M.-C. 2016. Glycosylation and stabilization of programmed death ligand-1 suppresses T-cell activity. *Nature Communications,* 7**,** 12632.

LI, D., YU, S., LONG, Y., SHI, A., DENG, J., MA, Y., WEN, J., LI, X., LIU, S., ZHANG, Y., WAN, J., LI, N. & AO, R. 2022. Tryptophan metabolism: Mechanism-oriented therapy for neurological and psychiatric disorders. *Front Immunol,* 13**,** 985378.

LI, F., CHONG, Z. Z. & MAIESE, K. 2006. Cell Life versus cell longevity: the mysteries surrounding the NAD+ precursor nicotinamide. *Curr Med Chem,* 13**,** 883-95.

LI, H., GAO, C., LIU, C., LIU, L., ZHUANG, J., YANG, J., ZHOU, C., FENG, F., SUN, C. & WU, J. 2021a. A review of the biological activity and pharmacology of cryptotanshinone, an important active constituent in Danshen. *Biomed Pharmacother,* 137**,** 111332.

LI, J. J., TSANG, J. Y. & TSE, G. M. 2021b. Tumor Microenvironment in Breast Cancer-Updates on Therapeutic Implications and Pathologic Assessment. *Cancers (Basel),* 13.

LI, M., CHEN, C., WANG, Q., JIANG, X., TAN, L., HUANG, Y., ZHANG, Y. & ZHANG, Z. 2021c. Glaucocalyxin A suppresses multiple myeloma progression in vitro and in vivo through inhibiting the activation of STAT3 signaling pathway. *Cancer Cell Int,* 21**,** 683.

LI, M., LI, P., ZHANG, M., MA, F. & SU, L. 2014. [Brucine inhibits the proliferation of human lung cancer cell line PC-9 [illegible]via arresting cell cycle]. *Zhongguo Fei Ai Za Zhi,* 17**,** 444-50.

LI, P., WU, R., LI, K., YUAN, W., ZENG, C., ZHANG, Y., WANG, X., ZHU, X., ZHOU, J., LI, P. & GAO, Y. 2021d. IDO Inhibition Facilitates Antitumor Immunity of Vγ9Vδ2 T Cells in Triple-Negative Breast Cancer. *Front Oncol,* 11**,** 679517.

LI, T., XU, X. H., TANG, Z. H., WANG, Y. F., LEUNG, C. H., MA, D. L., CHEN, X. P., WANG, Y. T., CHEN, Y. & LU, J. J. 2015. Platycodin D induces apoptosis and triggers ERK- and JNK-mediated autophagy in human hepatocellular carcinoma BEL-7402 cells. *Acta Pharmacol Sin,* 36**,** 1503-13.

LI, Z. & LANGHANS, S. A. 2015. Transcriptional regulators of Na,K-ATPase subunits. *Front Cell Dev Biol,* 3**,** 66.

LIM, W. F., NASIR, S. M., TEH, L. K., JAMES, R. J., IZHAR, M. H. M. & SALLEH, M. Z. 2020. The methanolic extract of Garcinia atroviridis (MeGa) reduces body weight and food intake, and improves lipid profiles by altering the lipid metabolism: a rat model. *Turk J Biol,* 44**,** 437-448.

LINGREL, J. B., ARGÜELLO, J. M., VAN HUYSSE, J. & KUNTZWEILER, T. A. 1997. Cation and cardiac glycoside binding sites of the Na,K-ATPase. *Ann N Y Acad Sci,* 834**,** 194-206.

LINGREL, J. B. & KUNTZWEILER, T. 1994. Na+,K(+)-ATPase. *J Biol Chem,* 269**,** 19659-62.

LIPSON, E. J. & DRAKE, C. G. 2011. Ipilimumab: an anti-CTLA-4 antibody for metastatic melanoma. *Clin Cancer Res,* 17**,** 6958-62.

LITTLEJOHN, T. K., TAKIKAWA, O., SKYLAS, D., JAMIE, J. F., WALKER, M. J. & TRUSCOTT, R. J. 2000. Expression and purification of recombinant human indoleamine 2, 3-dioxygenase. *Protein Expr Purif,* 19**,** 22-9.

LIU, F., LANG, R., ZHAO, J., ZHANG, X., PRINGLE, G. A., FAN, Y., YIN, D., GU, F., YAO, Z. & FU, L. 2011. $CD8^+$ cytotoxic T cell and $FOXP3^+$ regulatory T cell infiltration in relation to breast cancer survival and molecular subtypes. *Breast Cancer Res Treat,* 130**,** 645-55.

LIU, K., CHEN, Q., LIU, Y., ZHOU, X. & WANG, X. 2012a. Isolation and biological activities of decanal, linalool, valencene, and octanal from sweet orange oil. *J Food Sci,* 77**,** C1156-61.

LIU, K., NEWBURY, P. A., GLICKSBERG, B. S., ZENG, W. Z. D., PAITHANKAR, S., ANDRECHEK, E. R. & CHEN, B. 2019a. Evaluating cell lines as models for metastatic breast cancer through integrative analysis of genomic data. *Nature Communications,* 10**,** 2138.

LIU, M., LIU, P., ZHENG, B., LIU, Y., LI, L., HAN, X., LIU, Y. & CHU, L. 2022. Cardioprotective effects of alantolactone on isoproterenol-induced cardiac injury and cobalt chloride-induced cardiomyocyte injury. *Int J Immunopathol Pharmacol,* 36**,** 20587384211051993.

LIU, M., WANG, X., WANG, L., MA, X., GONG, Z., ZHANG, S. & LI, Y. 2018a. Targeting the IDO1 pathway in cancer: from bench to bedside. *Journal of Hematology & Oncology,* 11**,** 100.

LIU, Q., CAI, P., GUO, S., SHI, J. & SUN, H. 2020a. Identification of a lathyrane-type diterpenoid EM-E-11-4 as a novel paclitaxel resistance reversing agent with multiple mechanisms of action. *Aging (Albany NY),* 12**,** 3713-3729.

LIU, R., QU, Z., LIN, Y., LEE, C. S., TAI, W. C. & CHEN, S. 2019b. Brevilin A Induces Cell Cycle Arrest and Apoptosis in Nasopharyngeal Carcinoma. *Front Pharmacol,* 10**,** 594.

LIU, S., LACHAPELLE, J., LEUNG, S., GAO, D., FOULKES, W. D. & NIELSEN, T. O. 2012b. CD8+ lymphocyte infiltration is an independent favorable prognostic indicator in basal-like breast cancer. *Breast Cancer Res,* 14**,** R48.

LIU, W. C., ZHOU, S. H., BALASUBRAMANIAN, B., ZENG, F. Y., SUN, C. B. & PANG, H. Y. 2020b. Dietary seaweed (Enteromorpha) polysaccharides improves growth performance involved in regulation of immune responses, intestinal morphology and microbial community in banana shrimp Fenneropenaeus merguiensis. *Fish Shellfish Immunol,* 104**,** 202-212.

LIU, Y., LU, S., ZHAO, L., DONG, X., ZHU, Z., JIN, Y., CHEN, H., LU, F., HONG, Z. & CHAI, Y. 2018b. Effects of glaucocalyxin A on human liver cancer cells as revealed by GC/MS- and LC/MS-based metabolic profiling. *Anal Bioanal Chem,* 410**,** 3325-3335.

LIVAK, K. J. & SCHMITTGEN, T. D. 2001. Analysis of relative gene expression data using real-time quantitative PCR and the 2(-Delta Delta C(T)) Method. *Methods,* 25**,** 402-8.

LO, Y. C., LIN, C. L., FANG, W. Y., LŐRINCZI, B., SZATMÁRI, I., CHANG, W. H., FÜLÖP, F. & WU, S. N. 2021. Effective Activation by Kynurenic Acid and Its Aminoalkylated Derivatives on M-Type K(+) Current. *Int J Mol Sci,* 22.

LOBIKIN, M., CHERNET, B., LOBO, D. & LEVIN, M. 2012. Resting potential, oncogene-induced tumorigenesis, and metastasis: the bioelectric basis of cancer in vivo. *Phys Biol,* 9**,** 065002.

LOI, S., GIOBBIE-HURDER, A., GOMBOS, A., BACHELOT, T., HUI, R., CURIGLIANO, G., CAMPONE, M., BIGANZOLI, L., BONNEFOI, H., JERUSALEM, G., BARTSCH, R., RABAGLIO-PORETTI, M., KAMMLER, R., MAIBACH, R., SMYTH, M. J., DI LEO, A., COLLEONI, M., VIALE, G., REGAN, M. M. & ANDRÉ, F. 2019. Pembrolizumab plus trastuzumab in trastuzumab-resistant, advanced, HER2-positive breast cancer (PANACEA): a single-arm, multicentre, phase 1b-2 trial. *Lancet Oncol,* 20**,** 371-382.

LOIBL, S., SCHNEEWEISS, A., HUOBER, J., BRAUN, M., REY, J., BLOHMER, J. U., FURLANETTO, J., ZAHM, D. M., HANUSCH, C., THOMALLA, J., JACKISCH, C., STAIB, P., LINK, T., RHIEM, K., SOLBACH, C., FASCHING, P. A., NEKLJUDOVA, V., DENKERT, C. & UNTCH, M. 2022. Neoadjuvant durvalumab improves survival in early triple-negative breast cancer independent of pathological complete response. *Ann Oncol,* 33**,** 1149-1158.

LOPACHEV, A. V., LOPACHEVA, O. M., OSIPOVA, E. A., VLADYCHENSKAYA, E. A., SMOLYANINOVA, L. V., FEDOROVA, T. N., KOROLEVA, O. V. & AKKURATOV, E. E. 2016. Ouabain-induced changes in MAP kinase phosphorylation in primary culture of rat cerebellar cells. *Cell Biochem Funct,* 34**,** 367-77.

LOPINA, O. D., TVERSKOI, A. M., KLIMANOVA, E. A., SIDORENKO, S. V. & ORLOV, S. N. 2020a. Ouabain-Induced Cell Death and Survival. Role of α1-Na,K-ATPase-Mediated Signaling and [Na(+)](i)/[K(+)](i)-Dependent Gene Expression. *Front Physiol,* 11**,** 1060.

LOPINA, O. D., TVERSKOI, A. M., KLIMANOVA, E. A., SIDORENKO, S. V. & ORLOV, S. N. 2020b. Ouabain-Induced Cell Death and Survival. Role of α1-Na,K-ATPase-Mediated Signaling and [Na+]i/[K+]i-Dependent Gene Expression. *Frontiers in Physiology,* 11.

LORETO, F., FÖRSTER, A., DÜRR, M., CSIKY, O. & SEUFERT, G. 1998. On the monoterpene emission under heat stress and on the increased thermotolerance of leaves of Quercus ilex L. fumigated with selected monoterpenes. *Plant, Cell & Environment,* 21**,** 101-107.

LOU, C., CHEN, Y., ZHANG, J., YANG, B. & ZHAO, H. 2019. Eupalinolide J Suppresses the Growth of Triple-Negative Breast Cancer Cells via Targeting STAT3 Signaling Pathway. *Front Pharmacol,* 10**,** 1071.

LOWE, D. A., RICHARDSON, N. P., TAYLOR, P. & DONATSCH, P. 1976. Increasing intracellular sodium triggers calcium release from bound pools. *Nature,* 260**,** 337-8.

LU, B. W., BAUM, L., SO, K. F., CHIU, K. & XIE, L. K. 2019. More than anti-malarial agents: therapeutic potential of artemisinins in neurodegeneration. *Neural Regen Res,* 14**,** 1494-1498.

LU, H., FORBES, R. A. & VERMA, A. 2002. Hypoxia-inducible factor 1 activation by aerobic glycolysis implicates the Warburg effect in carcinogenesis. *J Biol Chem,* 277**,** 23111-5.

LU, S. C. 2013. Glutathione synthesis. *Biochim Biophys Acta,* 1830**,** 3143-53.

LUAN, B., YOON, Y. S., LE LAY, J., KAESTNER, K. H., HEDRICK, S. & MONTMINY, M. 2015. CREB pathway links PGE2 signaling with macrophage polarization. *Proc Natl Acad Sci U S A,* 112**,** 15642-7.

ŁUKASIEWICZ, S., CZECZELEWSKI, M., FORMA, A., BAJ, J., SITARZ, R. & STANISŁAWEK, A. 2021. Breast Cancer-Epidemiology, Risk Factors, Classification, Prognostic Markers, and Current Treatment Strategies-An Updated Review. *Cancers (Basel),* 13.

LUKE, J. J., TABERNERO, J., JOSHUA, A., DESAI, J., VARGA, A. I., MORENO, V., GOMEZ-ROCA, C. A., MARKMAN, B., BRAUD, F. G. D., PATEL, S. P., CARLINO, M. S., SIU, L. L., CURIGLIANO, G., LIU, Z., ISHII, Y., WIND-ROTOLO, M., BASCIANO, P. A., AZRILEVICH, A. & GELMON, K. A. 2019. BMS-986205, an indoleamine 2, 3-dioxygenase 1 inhibitor (IDO1i), in combination with nivolumab (nivo): Updated safety across all tumor cohorts and efficacy in advanced bladder cancer (advBC). *Journal of Clinical Oncology,* 37**,** 358-358.

LUNDHOLT, B. K., SCUDDER, K. M. & PAGLIARO, L. 2003. A simple technique for reducing edge effect in cell-based assays. *J Biomol Screen,* 8**,** 566-70.

LUO, Y., SONG, L., WANG, X., HUANG, Y., LIU, Y., WANG, Q., HONG, M. & YUAN, Z. 2020. Uncovering the Mechanisms of Cryptotanshinone as a Therapeutic Agent Against Hepatocellular Carcinoma. *Front Pharmacol,* 11**,** 1264.

LV, C., QU, H., ZHU, W., XU, K., XU, A., JIA, B., QING, Y., LI, H., WEI, H. J. & ZHAO, H. Y. 2017. Low-Dose Paclitaxel Inhibits Tumor Cell Growth by Regulating Glutaminolysis in Colorectal Carcinoma Cells. *Front Pharmacol,* 8**,** 244.

MA, F., OUYANG, Q., LI, W., JIANG, Z., TONG, Z., LIU, Y., LI, H., YU, S., FENG, J., WANG, S., HU, X., ZOU, J., ZHU, X. & XU, B. 2019. Pyrotinib or Lapatinib Combined With Capecitabine in HER2-Positive Metastatic Breast Cancer With Prior Taxanes, Anthracyclines, and/or Trastuzumab: A Randomized, Phase II Study. *J Clin Oncol,* 37**,** 2610-2619.

MA, J., CHEN, P., DENG, B. & WANG, R. 2023. Kynurenic acid promotes osteogenesis via the Wnt/β-catenin signaling. *In Vitro Cell Dev Biol Anim,* 59**,** 356-365.

MA, L., XU, B., WANG, W., DENG, W. & DING, M. 2009. Analysis of tryptophan catabolism in HBV patients by HPLC with programmed wavelength ultraviolet detection. *Clin Chim Acta,* 405**,** 94-6.

MACHAMER, C. E. & CRESSWELL, P. 1984. Monensin prevents terminal glycosylation of the N- and O-linked oligosaccharides of the HLA-DR-associated invariant chain and inhibits its dissociation from the alpha-beta chain complex. *Proc Natl Acad Sci U S A,* 81**,** 1287-91.

MĄCZKA, W., DUDA-MADEJ, A., GRABARCZYK, M. & WIŃSKA, K. 2022. Natural Compounds in the Battle against Microorganisms-Linalool. *Molecules,* 27.

MADELIN, G. & REGATTE, R. R. 2013. Biomedical applications of sodium MRI in vivo. *J Magn Reson Imaging,* 38**,** 511-29.

MAGNUS, C. J., LEE, P. H., ATASOY, D., SU, H. H., LOOGER, L. L. & STERNSON, S. M. 2011. Chemical and genetic engineering of selective ion channel-ligand interactions. *Science,* 333**,** 1292-6.

MAGNUS, C. J., LEE, P. H., BONAVENTURA, J., ZEMLA, R., GOMEZ, J. L., RAMIREZ, M. H., HU, X., GALVAN, A., BASU, J., MICHAELIDES, M. & STERNSON, S. M. 2019. Ultrapotent chemogenetics for research and potential clinical applications. *Science,* 364.

MAGRO, F., FRAGA, S., RIBEIRO, T. & SOARES-DA-SILVA, P. 2004. Intestinal Na+-K+-ATPase activity and molecular events downstream of interferon-gamma receptor stimulation. *British journal of pharmacology,* 142**,** 1281-1292.

MAHTAL, N., WU, Y., CINTRAT, J. C., BARBIER, J., LEMICHEZ, E. & GILLET, D. 2020. Revisiting Old Ionophore Lasalocid as a Novel Inhibitor of Multiple Toxins. *Toxins (Basel),* 12.

MAILANKOT, M. & NAGARAJ, R. H. 2010. Induction of indoleamine 2,3-dioxygenase by interferon-gamma in human lens epithelial cells: apoptosis through the formation of 3-hydroxykynurenine. *The international journal of biochemistry & cell biology,* 42**,** 1446-1454.

MAJOROS, A., PLATANITIS, E., KERNBAUER-HÖLZL, E., ROSEBROCK, F., MÜLLER, M. & DECKER, T. 2017. Canonical and Non-Canonical Aspects of JAK-STAT Signaling: Lessons from Interferons for Cytokine Responses. *Front Immunol,* 8**,** 29.

MAKKI, J. 2015. Diversity of Breast Carcinoma: Histological Subtypes and Clinical Relevance. *Clin Med Insights Pathol,* 8**,** 23-31.
MALHOTRA, G. K., ZHAO, X., BAND, H. & BAND, V. 2010. Histological, molecular and functional subtypes of breast cancers. *Cancer biology & therapy,* 10**,** 955-960.
MANSFIELD, A. S., HEIKKILA, P. S., VAARA, A. T., VON SMITTEN, K. A., VAKKILA, J. M. & LEIDENIUS, M. H. 2009. Simultaneous Foxp3 and IDO expression is associated with sentinel lymph node metastases in breast cancer. *BMC Cancer,* 9**,** 231.
MANSOURY, M., HAMED, M., KARMUSTAJI, R., AL HANNAN, F. & SAFRANY, S. T. 2021. The edge effect: A global problem. The trouble with culturing cells in 96-well plates. *Biochemistry and Biophysics Reports,* 26**,** 100987.
MANU, K. A. & KUTTAN, G. 2009. Anti-metastatic potential of Punarnavine, an alkaloid from Boerhaavia diffusa Linn. *Immunobiology,* 214**,** 245-55.
MANUNTA, P., FERRANDI, M., BIANCHI, G. & HAMLYN, J. M. 2009. Endogenous ouabain in cardiovascular function and disease. *J Hypertens,* 27**,** 9-18.
MAO, Y., QU, Q., CHEN, X., HUANG, O., WU, J. & SHEN, K. 2016. The Prognostic Value of Tumor-Infiltrating Lymphocytes in Breast Cancer: A Systematic Review and Meta-Analysis. *PLoS One,* 11**,** e0152500.
MARKS, M. J. & SEEDS, N. W. 1978. A heterogeneous ouabain-ATPase interaction in mouse brain. *Life Sci,* 23**,** 2735-44.
MARSTERS, S. A., AYRES, T. M., SKUBATCH, M., GRAY, C. L., ROTHE, M. & ASHKENAZI, A. 1997. Herpesvirus entry mediator, a member of the tumor necrosis factor receptor (TNFR) family, interacts with members of the TNFR-associated factor family and activates the transcription factors NF-kappaB and AP-1. *J Biol Chem,* 272**,** 14029-32.
MARUHASHI, T., OKAZAKI, I. M., SUGIURA, D., TAKAHASHI, S., MAEDA, T. K., SHIMIZU, K. & OKAZAKI, T. 2018. LAG-3 inhibits the activation of CD4(+) T cells that recognize stable pMHCII through its conformation-dependent recognition of pMHCII. *Nat Immunol,* 19**,** 1415-1426.
MATIN, A., STREETE, I. M., JAMIE, I. M., TRUSCOTT, R. J. & JAMIE, J. F. 2006. A fluorescence-based assay for indoleamine 2,3-dioxygenase. *Anal Biochem,* 349**,** 96-102.
MCGUIRE, A., BROWN, J. A., MALONE, C., MCLAUGHLIN, R. & KERIN, M. J. 2015. Effects of age on the detection and management of breast cancer. *Cancers (Basel),* 7**,** 908-29.
MEAD, K. I., ZHENG, Y., MANZOTTI, C. N., PERRY, L. C., LIU, M. K., BURKE, F., POWNER, D. J., WAKELAM, M. J. & SANSOM, D. M. 2005. Exocytosis of CTLA-4 is dependent on phospholipase D and ADP ribosylation factor-1 and stimulated during activation of regulatory T cells. *J Immunol,* 174**,** 4803-11.
MELLOR, A. L., CHANDLER, P., BABAN, B., HANSEN, A. M., MARSHALL, B., PIHKALA, J., WALDMANN, H., COBBOLD, S., ADAMS, E. & MUNN, D. H. 2004. Specific subsets of murine dendritic cells acquire potent T cell regulatory functions following CTLA4-mediated induction of indoleamine 2,3 dioxygenase. *Int Immunol,* 16**,** 1391-401.
MERCER, R. W., BIEMESDERFER, D., BLISS, D. P., JR., COLLINS, J. H. & FORBUSH, B., 3RD 1993. Molecular cloning and immunological characterization of the gamma polypeptide, a small protein associated with the Na,K-ATPase. *J Cell Biol,* 121**,** 579-86.
MERCER, R. W. & DUNHAM, P. B. 1981. Membrane-bound ATP fuels the Na/K pump. Studies on membrane-bound glycolytic enzymes on inside-out vesicles from human red cell membranes. *J Gen Physiol,* 78**,** 547-68.
METZ, R., RUST, S., DUHADAWAY, J. B., MAUTINO, M. R., MUNN, D. H., VAHANIAN, N. N., LINK, C. J. & PRENDERGAST, G. C. 2012. IDO inhibits a tryptophan sufficiency signal that stimulates mTOR: A novel IDO effector pathway targeted by D-1-methyl-tryptophan. *OncoImmunology,* 1**,** 1460-1468.

MEYER, D. J., DÍAZ-GARCÍA, C. M., NATHWANI, N., RAHMAN, M. & YELLEN, G. 2022. The Na(+)/K(+) pump dominates control of glycolysis in hippocampal dentate granule cells. *Elife,* 11.

MEZRICH, J. D., FECHNER, J. H., ZHANG, X., JOHNSON, B. P., BURLINGHAM, W. J. & BRADFIELD, C. A. 2010. An interaction between kynurenine and the aryl hydrocarbon receptor can generate regulatory T cells. *Journal of immunology (Baltimore, Md. : 1950),* 185**,** 3190-3198.

MICHELET, X., DYCK, L., HOGAN, A., LOFTUS, R. M., DUQUETTE, D., WEI, K., BEYAZ, S., TAVAKKOLI, A., FOLEY, C., DONNELLY, R., O'FARRELLY, C., RAVERDEAU, M., VERNON, A., PETTEE, W., O'SHEA, D., NIKOLAJCZYK, B. S., MILLS, K. H. G., BRENNER, M. B., FINLAY, D. & LYNCH, L. 2018. Metabolic reprogramming of natural killer cells in obesity limits antitumor responses. *Nat Immunol,* 19**,** 1330-1340.

MILES, D., GLIGOROV, J., ANDRÉ, F., CAMERON, D., SCHNEEWEISS, A., BARRIOS, C., XU, B., WARDLEY, A., KAEN, D., ANDRADE, L., SEMIGLAZOV, V., REINISCH, M., PATEL, S., PATRE, M., MORALES, L., PATEL, S. L., KAUL, M., BARATA, T. & O'SHAUGHNESSY, J. 2021. Primary results from IMpassion131, a double-blind, placebo-controlled, randomised phase III trial of first-line paclitaxel with or without atezolizumab for unresectable locally advanced/metastatic triple-negative breast cancer. *Ann Oncol,* 32**,** 994-1004.

MIN, H. Y., CHUNG, H. J., KIM, E. H., KIM, S., PARK, E. J. & LEE, S. K. 2010. Inhibition of cell growth and potentiation of tumor necrosis factor-α (TNF-α)-induced apoptosis by a phenanthroindolizidine alkaloid antofine in human colon cancer cells. *Biochem Pharmacol,* 80**,** 1356-64.

MINTA, A. & TSIEN, R. 1989. Fluorescent indicators for cytosolic sodium. *The Journal of biological chemistry,* 264 32**,** 19449-57.

MINTZ, M. A., FELCE, J. H., CHOU, M. Y., MAYYA, V., XU, Y., SHUI, J. W., AN, J., LI, Z., MARSON, A., OKADA, T., WARE, C. F., KRONENBERG, M., DUSTIN, M. L. & CYSTER, J. G. 2019. The HVEM-BTLA Axis Restrains T Cell Help to Germinal Center B Cells and Functions as a Cell-Extrinsic Suppressor in Lymphomagenesis. *Immunity,* 51**,** 310-323.e7.

MITCHELL, J. A., ARONSON, A. R., MORK, J. G., FOLK, L. C., HUMPHREY, S. M. & WARD, J. M. 2003. Gene indexing: characterization and analysis of NLM's GeneRIFs. *AMIA Annu Symp Proc,* 2003**,** 460-4.

MO, B., ZHAO, X., WANG, Y., JIANG, X., LIU, D. & CAI, H. 2023. Pan-cancer analysis, providing a reliable basis for IDO2 as a prognostic biomarker and target for immunotherapy. *Oncologie,* 25**,** 17-35.

MOHAMMADI, K., KOMETIANI, P., XIE, Z. & ASKARI, A. 2001. Role of protein kinase C in the signal pathways that link Na+/K+-ATPase to ERK1/2. *J Biol Chem,* 276**,** 42050-6.

MOHAMMED, F. H., KHAJAH, M. A., YANG, M., BRACKENBURY, W. J. & LUQMANI, Y. A. 2016. Blockade of voltage-gated sodium channels inhibits invasion of endocrine-resistant breast cancer cells. *Int J Oncol,* 48**,** 73-83.

MOLLENHAUER, H. H., MORRÉ, D. J. & ROWE, L. D. 1990. Alteration of intracellular traffic by monensin; mechanism, specificity and relationship to toxicity. *Biochim Biophys Acta,* 1031**,** 225-46.

MONDAL, A., GANDHI, A., FIMOGNARI, C., ATANASOV, A. G. & BISHAYEE, A. 2019. Alkaloids for cancer prevention and therapy: Current progress and future perspectives. *Eur J Pharmacol,* 858**,** 172472.

MONTEITH, G. R., PREVARSKAYA, N. & ROBERTS-THOMSON, S. J. 2017. The calcium-cancer signalling nexus. *Nat Rev Cancer,* 17**,** 367-380.

MONTRUCCHIO, D. P., CÓRDOVA, M. M. & SANTOS, A. R. 2013. Plant derived aporphinic alkaloid S-(+)-dicentrine induces antinociceptive effect in both acute and chronic

inflammatory pain models: evidence for a role of TRPA1 channels. *PLoS One,* 8**,** e67730.

MORAD, H. O. J., LUQMAN, S., PINTO, L. G., CUNNINGHAM, K. P., VILAR, B., CLAYTON, G., SHANKAR-HARI, M. & MCNAUGHTON, P. A. 2022. Artemisinin inhibits neutrophil and macrophage chemotaxis, cytokine production and NET release. *Sci Rep,* 12**,** 11078.

MOREIRA SOUZA, A. C., GRABE-GUIMARÃES, A., CRUZ, J. D. S., SANTOS-MIRANDA, A., FARAH, C., TEIXEIRA OLIVEIRA, L., LUCAS, A., AIMOND, F., SICARD, P., MOSQUEIRA, V. C. F. & RICHARD, S. 2020. Mechanisms of artemether toxicity on single cardiomyocytes and protective effect of nanoencapsulation. *Br J Pharmacol,* 177**,** 4448-4463.

MORETTI, S., MENICALI, E., NUCCI, N., VOCE, P., COLELLA, R., MELILLO, R. M., LIOTTI, F., MORELLI, S., FALLARINO, F., MACCHIARULO, A., SANTORO, M., AVENIA, N. & PUXEDDU, E. 2017. Signal Transducer and Activator of Transcription 1 Plays a Pivotal Role in RET/PTC3 Oncogene-induced Expression of Indoleamine 2,3-Dioxygenase 1. *Journal Of Biological Chemistry,* 292**,** 1785-1797.

MORTH, J. P., PEDERSEN, B. P., TOUSTRUP-JENSEN, M. S., SØRENSEN, T. L., PETERSEN, J., ANDERSEN, J. P., VILSEN, B. & NISSEN, P. 2007. Crystal structure of the sodium-potassium pump. *Nature,* 450**,** 1043-9.

MOTZER, R. J., ESCUDIER, B., MCDERMOTT, D. F., GEORGE, S., HAMMERS, H. J., SRINIVAS, S., TYKODI, S. S., SOSMAN, J. A., PROCOPIO, G., PLIMACK, E. R., CASTELLANO, D., CHOUEIRI, T. K., GURNEY, H., DONSKOV, F., BONO, P., WAGSTAFF, J., GAULER, T. C., UEDA, T., TOMITA, Y., SCHUTZ, F. A., KOLLMANNSBERGER, C., LARKIN, J., RAVAUD, A., SIMON, J. S., XU, L. A., WAXMAN, I. M. & SHARMA, P. 2015. Nivolumab versus Everolimus in Advanced Renal-Cell Carcinoma. *N Engl J Med,* 373**,** 1803-13.

MOTZER, R. J., TANNIR, N. M., MCDERMOTT, D. F., ARÉN FRONTERA, O., MELICHAR, B., CHOUEIRI, T. K., PLIMACK, E. R., BARTHÉLÉMY, P., PORTA, C., GEORGE, S., POWLES, T., DONSKOV, F., NEIMAN, V., KOLLMANNSBERGER, C. K., SALMAN, P., GURNEY, H., HAWKINS, R., RAVAUD, A., GRIMM, M. O., BRACARDA, S., BARRIOS, C. H., TOMITA, Y., CASTELLANO, D., RINI, B. I., CHEN, A. C., MEKAN, S., MCHENRY, M. B., WIND-ROTOLO, M., DOAN, J., SHARMA, P., HAMMERS, H. J. & ESCUDIER, B. 2018. Nivolumab plus Ipilimumab versus Sunitinib in Advanced Renal-Cell Carcinoma. *N Engl J Med,* 378**,** 1277-1290.

MOULDER, S. L., BORGES, V. F., BAETZ, T., MCSPADDEN, T., FERNETICH, G., MURTHY, R. K., CHAVIRA, R., GUTHRIE, K., BARRETT, E. & CHIA, S. K. 2017. Phase I Study of ONT-380, a HER2 Inhibitor, in Patients with HER2(+)-Advanced Solid Tumors, with an Expansion Cohort in HER2(+) Metastatic Breast Cancer (MBC). *Clin Cancer Res,* 23**,** 3529-3536.

MOYER, B. J., ROJAS, I. Y., MURRAY, I. A., LEE, S., HAZLETT, H. F., PERDEW, G. H. & TOMLINSON, C. R. 2017. Indoleamine 2,3-dioxygenase 1 (IDO1) inhibitors activate the aryl hydrocarbon receptor. *Toxicol Appl Pharmacol,* 323**,** 74-80.

MULLER, A. J., DUHADAWAY, J. B., DONOVER, P. S., SUTANTO-WARD, E. & PRENDERGAST, G. C. 2005. Inhibition of indoleamine 2,3-dioxygenase, an immunoregulatory target of the cancer suppression gene Bin1, potentiates cancer chemotherapy. *Nat Med,* 11**,** 312-9.

MUNN, D. H. & MELLOR, A. L. 2007. Indoleamine 2,3-dioxygenase and tumor-induced tolerance. *J Clin Invest,* 117**,** 1147-54.

MUNN, D. H., SHARMA, M. D., BABAN, B., HARDING, H. P., ZHANG, Y., RON, D. & MELLOR, A. L. 2005. GCN2 Kinase in T Cells Mediates Proliferative Arrest and Anergy Induction in Response to Indoleamine 2,3-Dioxygenase. *Immunity,* 22**,** 633-642.

MUNN, D. H., SHARMA, M. D., LEE, J. R., JHAVER, K. G., JOHNSON, T. S., KESKIN, D. B., MARSHALL, B., CHANDLER, P., ANTONIA, S. J., BURGESS, R., SLINGLUFF, C. L. & MELLOR, A. L. 2002. Potential Regulatory Function of Human Dendritic Cells Expressing Indoleamine 2,3-Dioxygenase. *Science,* 297**,** 1867-1870.

MUNN, D. H., SHARMA, M. D. & MELLOR, A. L. 2004. Ligation of B7-1/B7-2 by human CD4+ T cells triggers indoleamine 2,3-dioxygenase activity in dendritic cells. *J Immunol,* 172**,** 4100-10.

MUÑOZ-MONTESINO, C., BURGOS, C. F., LARA, C. O., RIQUELME, C. R., FLAIG, D., SAN MARTIN, V. P., AGUAYO, L. G., FUENTEALBA, J., CASTRO, P. A., GUZMÁN, L., YÉVENES, G. E. & MORAGA-CID, G. 2020. Inhibition of the Glycine Receptor alpha 3 Function by Colchicine. *Front Pharmacol,* 11**,** 1143.

NAFISI, S., BONSAII, M., MAALI, P., KHALILZADEH, M. A. & MANOUCHEHRI, F. 2010. Beta-carboline alkaloids bind DNA. *J Photochem Photobiol B,* 100**,** 84-91.

NAGY, I. Z., LUSTYIK, G., NAGY, V. Z., ZARÁNDI, B. & BERTONI-FREDDARI, C. 1981. Intracellular Na+:K+ ratios in human cancer cells as revealed by energy dispersive x-ray microanalysis. *The Journal of cell biology,* 90**,** 769-777.

NAIR, J. S., DAFONSECA, C. J., TJERNBERG, A., SUN, W., DARNELL, J. E., JR., CHAIT, B. T. & ZHANG, J. J. 2002. Requirement of Ca2+ and CaMKII for Stat1 Ser-727 phosphorylation in response to IFN-gamma. *Proc Natl Acad Sci U S A,* 99**,** 5971-6.

NAKAMURA, K., SHIOZAKI, A., KOSUGA, T., SHIMIZU, H., KUDOU, M., OHASHI, T., ARITA, T., KONISHI, H., KOMATSU, S., KUBOTA, T., FUJIWARA, H., OKAMOTO, K., KISHIMOTO, M., KONISHI, E. & OTSUJI, E. 2021. The expression of the alpha1 subunit of Na+/K+-ATPase is related to tumor development and clinical outcomes in gastric cancer. *Gastric Cancer,* 24**,** 1278-1292.

NAKAYAMA, M., AKIBA, H., TAKEDA, K., KOJIMA, Y., HASHIGUCHI, M., AZUMA, M., YAGITA, H. & OKUMURA, K. 2009. Tim-3 mediates phagocytosis of apoptotic cells and cross-presentation. *Blood,* 113**,** 3821-30.

NAKAZATO, K. & HATANO, Y. 1991. Monensin-mediated antiport of Na+ and H+ across liposome membrane. *Biochim Biophys Acta,* 1064**,** 103-10.

NATARAJAN, K., SINGH, S., BURKE, T. R., JR., GRUNBERGER, D. & AGGARWAL, B. B. 1996. Caffeic acid phenethyl ester is a potent and specific inhibitor of activation of nuclear transcription factor NF-kappa B. *Proc Natl Acad Sci U S A,* 93**,** 9090-5.

NAUJOKAT, C. & STEINHART, R. 2012. Salinomycin as a drug for targeting human cancer stem cells. *J Biomed Biotechnol,* 2012**,** 950658.

NEAVIN, D. R., LIU, D., RAY, B. & WEINSHILBOUM, R. M. 2018. The Role of the Aryl Hydrocarbon Receptor (AHR) in Immune and Inflammatory Diseases. *International Journal of Molecular Sciences,* 19**,** 3851.

NEGULESCU, P. A. & MACHEN, T. E. 1990. [4] Intracellular ion activities and membrane transport in parietal cells measured with fluorescent dyes. *Methods in Enzymology.* Academic Press.

NEGULYAEV, Y. A., VEDERNIKOVA, E. A. & MAXIMOV, A. V. 1996. Disruption of actin filaments increases the activity of sodium-conducting channels in human myeloid leukemia cells. *Mol Biol Cell,* 7**,** 1857-64.

NELSON, M., YANG, M., DOWLE, A. A., THOMAS, J. R. & BRACKENBURY, W. J. 2015a. The sodium channel-blocking antiepileptic drug phenytoin inhibits breast tumour growth and metastasis. *Mol Cancer,* 14**,** 13.

NELSON, M., YANG, M., MILLICAN-SLATER, R. & BRACKENBURY, W. J. 2015b. Nav1.5 regulates breast tumor growth and metastatic dissemination in vivo. *Oncotarget,* 6**,** 32914-32929.

NEWMAN, A. C., FALCONE, M., HUERTA URIBE, A., ZHANG, T., ATHINEOS, D., PIETZKE, M., VAZQUEZ, A., BLYTH, K. & MADDOCKS, O. D. K. 2021. Immune-regulated IDO1-

dependent tryptophan metabolism is source of one-carbon units for pancreatic cancer and stellate cells. *Mol Cell,* 81**,** 2290-2302.e7.
NGUYEN, P. T., DEISL, C., FINE, M., TIPPETTS, T. S., UCHIKAWA, E., BAI, X. C. & LEVINE, B. 2022. Structural basis for gating mechanism of the human sodium-potassium pump. *Nat Commun,* 13**,** 5293.
NI, D., MADDEN, T. L., JOHANSEN, M., FELIX, E., HO, D. H. & NEWMAN, R. A. 2002. Murine pharmacokinetics and metabolism of oleandrin, a cytotoxic component of Nerium oleander. *J Exp Ther Oncol,* 2**,** 278-85.
NIN, V., HERNÁNDEZ, J. A. & CHIFFLET, S. 2009. Hyperpolarization of the plasma membrane potential provokes reorganization of the actin cytoskeleton and increases the stability of adherens junctions in bovine corneal endothelial cells in culture. *Cell Motil Cytoskeleton,* 66**,** 1087-99.
NISHIMURA, R., OSAKO, T., OKUMURA, Y., HAYASHI, M., TOYOZUMI, Y. & ARIMA, N. 2010. Ki-67 as a prognostic marker according to breast cancer subtype and a predictor of recurrence time in primary breast cancer. *Exp Ther Med,* 1**,** 747-754.
NOLAN, E., SAVAS, P., POLICHENI, A. N., DARCY, P. K., VAILLANT, F., MINTOFF, C. P., DUSHYANTHEN, S., MANSOUR, M., PANG, J. B., FOX, S. B., PEROU, C. M., VISVADER, J. E., GRAY, D. H. D., LOI, S. & LINDEMAN, G. J. 2017. Combined immune checkpoint blockade as a therapeutic strategy for BRCA1-mutated breast cancer. *Sci Transl Med,* 9.
NOONEPALLE, S. K., GU, F., LEE, E. J., CHOI, J. H., HAN, Q., KIM, J., OUZOUNOVA, M., SHULL, A. Y., PEI, L., HSU, P. Y., KOLHE, R., SHI, F., CHOI, J., CHIOU, K., HUANG, T. H., KORKAYA, H., DENG, L., XIN, H. B., HUANG, S., THANGARAJU, M., SREEKUMAR, A., AMBS, S., TANG, S. C., MUNN, D. H. & SHI, H. 2017. Promoter Methylation Modulates Indoleamine 2,3-Dioxygenase 1 Induction by Activated T Cells in Human Breast Cancers. *Cancer Immunol Res,* 5**,** 330-344.
NOVIKOV, O., WANG, Z., STANFORD, E. A., PARKS, A. J., RAMIREZ-CARDENAS, A., LANDESMAN, E., LAKLOUK, I., SARITA-REYES, C., GUSENLEITNER, D., LI, A., MONTI, S., MANTEIGA, S., LEE, K. & SHERR, D. H. 2016. An Aryl Hydrocarbon Receptor-Mediated Amplification Loop That Enforces Cell Migration in ER[−]/PR[−]/Her2[−] Human Breast Cancer Cells. *Molecular Pharmacology,* 90**,** 674-688.
NURGALI, K., JAGOE, R. T. & ABALO, R. 2018. Editorial: Adverse Effects of Cancer Chemotherapy: Anything New to Improve Tolerance and Reduce Sequelae? *Front Pharmacol,* 9**,** 245.
NUTI, R., GARGARO, M., MATINO, D., DOLCIAMI, D., GROHMANN, U., PUCCETTI, P., FALLARINO, F. & MACCHIARULO, A. 2014. Ligand binding and functional selectivity of L-tryptophan metabolites at the mouse aryl hydrocarbon receptor (mAhR). *J Chem Inf Model,* 54**,** 3373-83.
O'NEILL, P. M., BARTON, V. E. & WARD, S. A. 2010. The molecular mechanism of action of artemisinin--the debate continues. *Molecules,* 15**,** 1705-21.
OH, S. Y., KIM, S., KEAM, B., KIM, T. M., KIM, D. W. & HEO, D. S. 2021. Soluble PD-L1 is a predictive and prognostic biomarker in advanced cancer patients who receive immune checkpoint blockade treatment. *Sci Rep,* 11**,** 19712.
OKAMOTO, M., TAKEMORI, H. & KATOH, Y. 2004. Salt-inducible kinase in steroidogenesis and adipogenesis. *Trends Endocrinol Metab,* 15**,** 21-6.
OMAR, A. K., AHMED, K. A., HELMI, N. M., ABDULLAH, K. T., QARII, M. H., HASAN, H. E., ASHWAG, A., NABIL, A. M., ABDU, A. M. & SALAMA, M. S. 2017. The sensitivity of Na(+), K(+) ATPase as an indicator of blood diseases. *Afr Health Sci,* 17**,** 262-269.
ONG, S. T., NG, A. S., NG, X. R., ZHUANG, Z., WONG, B. H. S., PRASANNAN, P., KOK, Y. J., BI, X., SHIM, H., WULFF, H., CHANDY, K. G. & VERMA, N. K. 2019. Extracellular K(+)

Dampens T Cell Functions: Implications for Immune Suppression in the Tumor Microenvironment. *Bioelectricity,* 1**,** 169-179.
ONG, W. Y., FAROOQUI, T., KOH, H. L., FAROOQUI, A. A. & LING, E. A. 2015. Protective effects of ginseng on neurological disorders. *Front Aging Neurosci,* 7**,** 129.
ONGANER, P. U. & DJAMGOZ, M. B. 2005. Small-cell lung cancer (human): potentiation of endocytic membrane activity by voltage-gated Na(+) channel expression in vitro. *J Membr Biol,* 204**,** 67-75.
ONO, K., FOZZARD, H. A. & HANCK, D. A. 1995. A direct effect of forskolin on sodium channel bursting. *Pflugers Arch,* 429**,** 561-9.
OOPPACHAI, C., LIMTRAKUL DEJKRIENGKRAIKUL, P. & YODKEEREE, S. 2019. Dicentrine Potentiates TNF-α-Induced Apoptosis and Suppresses Invasion of A549 Lung Adenocarcinoma Cells via Modulation of NF-κB and AP-1 Activation. *Molecules,* 24.
OPITZ, C. A., LITZENBURGER, U. M., SAHM, F., OTT, M., TRITSCHLER, I., TRUMP, S., SCHUMACHER, T., JESTAEDT, L., SCHRENK, D., WELLER, M., JUGOLD, M., GUILLEMIN, G. J., MILLER, C. L., LUTZ, C., RADLWIMMER, B., LEHMANN, I., VON DEIMLING, A., WICK, W. & PLATTEN, M. 2011. An endogenous tumour-promoting ligand of the human aryl hydrocarbon receptor. *Nature,* 478**,** 197-203.
OSHI, M., ASAOKA, M., TOKUMARU, Y., YAN, L., MATSUYAMA, R., ISHIKAWA, T., ENDO, I. & TAKABE, K. 2020. CD8 T Cell Score as a Prognostic Biomarker for Triple Negative Breast Cancer. *Int J Mol Sci,* 21.
OUWERKERK, R., JACOBS, M., MACURA, K., WOLFF, A., STEARNS, V., MEZBAN, S., KHOURI, N., BLUEMKE, D. & BOTTOMLEY, P. 2007. Elevated tissue sodium concentration in malignant breast lesions detected with non-invasive 23 Na MRI. *Breast Cancer Research and Treatment,* 106**,** 151-160.
OVERMAN, M. J., MCDERMOTT, R., LEACH, J. L., LONARDI, S., LENZ, H. J., MORSE, M. A., DESAI, J., HILL, A., AXELSON, M., MOSS, R. A., GOLDBERG, M. V., CAO, Z. A., LEDEINE, J. M., MAGLINTE, G. A., KOPETZ, S. & ANDRÉ, T. 2017. Nivolumab in patients with metastatic DNA mismatch repair-deficient or microsatellite instability-high colorectal cancer (CheckMate 142): an open-label, multicentre, phase 2 study. *Lancet Oncol,* 18**,** 1182-1191.
OXENKRUG, G. 2013. Serotonin-kynurenine hypothesis of depression: historical overview and recent developments. *Curr Drug Targets,* 14**,** 514-21.
OZ, M., LOZON, Y., SULTAN, A., YANG, K. H. & GALADARI, S. 2015. Effects of monoterpenes on ion channels of excitable cells. *Pharmacol Ther,* 152**,** 83-97.
OZAKI, Y., NICHOL, C. A. & DUCH, D. S. 1987. Utilization of dihydroflavin mononucleotide and superoxide anion for the decyclization of L-tryptophan by murine epididymal indoleamine 2,3-dioxygenase. *Arch Biochem Biophys,* 257**,** 207-16.
PAGE, D. B., BEAL, K., LINCH, S. N., SPINELLI, K. J., RODINE, M., HALPENNY, D., MODI, S., PATIL, S., YOUNG, R. J., KALEY, T., MERGHOUB, T., REDMOND, D., WONG, P., BARKER, C. A., DIAB, A., NORTON, L. & MCARTHUR, H. L. 2022. Brain radiotherapy, tremelimumab-mediated CTLA-4-directed blockade +/- trastuzumab in patients with breast cancer brain metastases. *NPJ Breast Cancer,* 8**,** 50.
PAJOT, A., HAO HUYNH, G., PICOT, L., MARCHAL, L. & NICOLAU, E. 2022. Fucoxanthin from Algae to Human, an Extraordinary Bioresource: Insights and Advances in up and Downstream Processes. *Mar Drugs,* 20.
PALLOTTA, M. T., ORABONA, C., VOLPI, C., GROHMANN, U., PUCCETTI, P. & FALLARINO, F. 2010. Proteasomal Degradation of Indoleamine 2,3-Dioxygenase in CD8 Dendritic Cells is Mediated by Suppressor of Cytokine Signaling 3 (SOCS3). *Int J Tryptophan Res,* 3**,** 91-7.

PALLOTTA, M. T., ROSSINI, S., SUVIERI, C., COLETTI, A., ORABONA, C., MACCHIARULO, A., VOLPI, C. & GROHMANN, U. 2022. Indoleamine 2,3-dioxygenase 1 (IDO1): an up-to-date overview of an eclectic immunoregulatory enzyme. *Febs j,* 289**,** 6099-6118.

PALTY, R., SILVERMAN, W. F., HERSHFINKEL, M., CAPORALE, T., SENSI, S. L., PARNIS, J., NOLTE, C., FISHMAN, D., SHOSHAN-BARMATZ, V., HERRMANN, S., KHANANSHVILI, D. & SEKLER, I. 2010. NCLX is an essential component of mitochondrial Na+/Ca2+ exchange. *Proc Natl Acad Sci U S A,* 107**,** 436-41.

PANFILI, E., MONDANELLI, G., ORABONA, C., GARGARO, M., VOLPI, C., BELLADONNA, M. L., ROSSINI, S., SUVIERI, C. & PALLOTTA, M. T. 2023. The catalytic inhibitor epacadostat can affect the non-enzymatic function of IDO1. *Front Immunol,* 14**,** 1134551.

PANG, Z., SCHAFROTH, M. A., OGASAWARA, D., WANG, Y., NUDELL, V., LAL, N. K., YANG, D., WANG, K., HERBST, D. M., HA, J., GUIJAS, C., BLANKMAN, J. L., CRAVATT, B. F. & YE, L. 2022. In situ identification of cellular drug targets in mammalian tissue. *Cell,* 185**,** 1793-1805.e17.

PARDO, L. A. & STÜHMER, W. 2014. The roles of K(+) channels in cancer. *Nat Rev Cancer,* 14**,** 39-48.

PARK, K. H., PARK, H. J., SHIN, K. S., CHOI, H. S., KAI, M. & LEE, M. K. 2012. Modulation of PC12 cell viability by forskolin-induced cyclic AMP levels through ERK and JNK pathways: an implication for L-DOPA-induced cytotoxicity in nigrostriatal dopamine neurons. *Toxicol Sci,* 128**,** 247-57.

PATANAPHAN, V., SALAZAR, O. M. & RISCO, R. 1988. Breast cancer: metastatic patterns and their prognosis. *South Med J,* 81**,** 1109-12.

PATEL, S., VYAS, V. K. & MEHTA, P. J. 2023. A Review on Forced Degradation Strategies to Establish the Stability of Therapeutic Peptide Formulations. *International Journal of Peptide Research and Therapeutics,* 29**,** 22.

PEANA, A. T., D'AQUILA, P. S., PANIN, F., SERRA, G., PIPPIA, P. & MORETTI, M. D. 2002. Anti-inflammatory activity of linalool and linalyl acetate constituents of essential oils. *Phytomedicine,* 9**,** 721-6.

PENG, M., HUANG, L., XIE, Z., HUANG, W. H. & ASKARI, A. 1996. Partial inhibition of Na+/K+-ATPase by ouabain induces the Ca2+-dependent expressions of early-response genes in cardiac myocytes. *J Biol Chem,* 271**,** 10372-8.

PENG, Y. H., UENG, S. H., TSENG, C. T., HUNG, M. S., SONG, J. S., WU, J. S., LIAO, F. Y., FAN, Y. S., WU, M. H., HSIAO, W. C., HSUEH, C. C., LIN, S. Y., CHENG, C. Y., TU, C. H., LEE, L. C., CHENG, M. F., SHIA, K. S., SHIH, C. & WU, S. Y. 2016. Important Hydrogen Bond Networks in Indoleamine 2,3-Dioxygenase 1 (IDO1) Inhibitor Design Revealed by Crystal Structures of Imidazoleisoindole Derivatives with IDO1. *J Med Chem,* 59**,** 282-93.

PERNE, A., MUELLNER, M. K., STEINRUECK, M., CRAIG-MUELLER, N., MAYERHOFER, J., SCHWARZINGER, I., SLOANE, M., URAS, I. Z., HOERMANN, G., NIJMAN, S. M. & MAYERHOFER, M. 2009. Cardiac glycosides induce cell death in human cells by inhibiting general protein synthesis. *PLoS One,* 4**,** e8292.

PEROU, C. M., SØRLIE, T., EISEN, M. B., VAN DE RIJN, M., JEFFREY, S. S., REES, C. A., POLLACK, J. R., ROSS, D. T., JOHNSEN, H., AKSLEN, L. A., FLUGE, O., PERGAMENSCHIKOV, A., WILLIAMS, C., ZHU, S. X., LØNNING, P. E., BØRRESEN-DALE, A. L., BROWN, P. O. & BOTSTEIN, D. 2000. Molecular portraits of human breast tumours. *Nature,* 406**,** 747-52.

PHILIPP, S., SOSNA, J., PLENGE, J., KALTHOFF, H. & ADAM, D. 2015. Homoharringtonine, a clinically approved anti-leukemia drug, sensitizes tumor cells for TRAIL-induced necroptosis. *Cell Commun Signal,* 13**,** 25.

PHILLIPS, R. S. 2014. Structure and mechanism of kynureninase. *Archives of Biochemistry and Biophysics,* 544**,** 69-74.
PICCART, M., HORTOBAGYI, G. N., CAMPONE, M., PRITCHARD, K. I., LEBRUN, F., ITO, Y., NOGUCHI, S., PEREZ, A., RUGO, H. S., DELEU, I., BURRIS, H. A., 3RD, PROVENCHER, L., NEVEN, P., GNANT, M., SHTIVELBAND, M., WU, C., FAN, J., FENG, W., TARAN, T. & BASELGA, J. 2014. Everolimus plus exemestane for hormone-receptor-positive, human epidermal growth factor receptor-2-negative advanced breast cancer: overall survival results from BOLERO-2†. *Ann Oncol,* 25**,** 2357-2362.
PINKERTON, M. & STEINRAUF, L. K. 1970. Molecular structure of monovalent metal cation complexes of monensin. *J Mol Biol,* 49**,** 533-46.
PISIBON, C., OUERTANI, A., BERTOLOTTO, C., BALLOTTI, R. & CHELI, Y. 2021. Immune Checkpoints in Cancers: From Signaling to the Clinic. *Cancers (Basel),* 13.
PLATTEN, M., NOLLEN, E. A. A., RÖHRIG, U. F., FALLARINO, F. & OPITZ, C. A. 2019. Tryptophan metabolism as a common therapeutic target in cancer, neurodegeneration and beyond. *Nat Rev Drug Discov,* 18**,** 379-401.
PLATTEN, M., WICK, W. & VAN DEN EYNDE, B. J. 2012. Tryptophan catabolism in cancer: beyond IDO and tryptophan depletion. *Cancer Res,* 72**,** 5435-40.
PLITMAN, E., IWATA, Y., CARAVAGGIO, F., NAKAJIMA, S., CHUNG, J. K., GERRETSEN, P., KIM, J., TAKEUCHI, H., CHAKRAVARTY, M. M., REMINGTON, G. & GRAFF-GUERRERO, A. 2017. Kynurenic Acid in Schizophrenia: A Systematic Review and Meta-analysis. *Schizophr Bull,* 43**,** 764-777.
PLITZKO, B. & LOESGEN, S. 2018. Measurement of Oxygen Consumption Rate (OCR) and Extracellular Acidification Rate (ECAR) in Culture Cells for Assessment of the Energy Metabolism. *Bio Protoc,* 8**,** e2850.
POPOV, S., VENETSANOU, K., CHEDRESE, P., PINTO, V., TAKEMORI, H., FRANCO-CERECEDA, A., ERIKSSON, P., MOCHIZUKI, N., SOARES-DA-SILVA, P. & BERTORELLO, A. 2012. Increases in intracellular sodium activate transcription and gene expression via the salt-inducible kinase 1 network in an atrial myocyte cell line. *American Journal Of Physiology. Heart And Circulatory Physiology,* 303**,** H57-H65.
POST, R. L., KUME, S., TOBIN, T., ORCUTT, B. & SEN, A. K. 1969. Flexibility of an active center in sodium-plus-potassium adenosine triphosphatase. *J Gen Physiol,* 54**,** 306-26.
PRASSAS, I. & DIAMANDIS, E. P. 2008. Novel therapeutic applications of cardiac glycosides. *Nat Rev Drug Discov,* 7**,** 926-35.
PRENDERGAST, G. C., MALACHOWSKI, W. J., MONDAL, A., SCHERLE, P. & MULLER, A. J. 2018. Indoleamine 2,3-Dioxygenase and Its Therapeutic Inhibition in Cancer. *Int Rev Cell Mol Biol,* 336**,** 175-203.
PU, Y. & JI, Q. 2022. Tumor-Associated Macrophages Regulate PD-1/PD-L1 Immunosuppression. *Front Immunol,* 13**,** 874589.
QI, T., FU, J., ZHANG, W., CUI, W., XU, X., YUE, J., WANG, Q. & TIAN, X. 2020. Mutation of PD-1 immune receptor tyrosine-based switch motif (ITSM) enhances the antitumor activity of cytotoxic T cells. *Transl Cancer Res,* 9**,** 6811-6819.
QIN, H., YEH, W.-I., DE SARNO, P., HOLDBROOKS, A. T., LIU, Y., MULDOWNEY, M. T., REYNOLDS, S. L., YANAGISAWA, L. L., FOX, T. H., 3RD, PARK, K., HARRINGTON, L. E., RAMAN, C. & BENVENISTE, E. N. 2012. Signal transducer and activator of transcription-3/suppressor of cytokine signaling-3 (STAT3/SOCS3) axis in myeloid cells regulates neuroinflammation. *Proceedings of the National Academy of Sciences of the United States of America,* 109**,** 5004-5009.
QIU, B., KLINE, C. & MUELLER, S. 2021. Radiation in Combination With Targeted Agents and Immunotherapies for Pediatric Central Nervous System Tumors - Progress, Opportunities, and Challenges. *Front Oncol,* 11**,** 674596.

QUINTANS, J. S. S., SHANMUGAM, S., HEIMFARTH, L., ARAÚJO, A. A. S., ALMEIDA, J., PICOT, L. & QUINTANS-JÚNIOR, L. J. 2019. Monoterpenes modulating cytokines - A review. *Food Chem Toxicol,* 123**,** 233-257.

QURESHI, O. S., ZHENG, Y., NAKAMURA, K., ATTRIDGE, K., MANZOTTI, C., SCHMIDT, E. M., BAKER, J., JEFFERY, L. E., KAUR, S., BRIGGS, Z., HOU, T. Z., FUTTER, C. E., ANDERSON, G., WALKER, L. S. & SANSOM, D. M. 2011. Trans-endocytosis of CD80 and CD86: a molecular basis for the cell-extrinsic function of CTLA-4. *Science,* 332**,** 600-3.

RAKER, V. K., BECKER, C. & STEINBRINK, K. 2016. The cAMP Pathway as Therapeutic Target in Autoimmune and Inflammatory Diseases. *Front Immunol,* 7**,** 123.

RAMANA, C. V., CHATTERJEE-KISHORE, M., NGUYEN, H. & STARK, G. R. 2000. Complex roles of Stat1 in regulating gene expression. *Oncogene,* 19**,** 2619-27.

RAVISHANKAR, B., LIU, H., SHINDE, R., CHAUDHARY, K., XIAO, W., BRADLEY, J., KORITZINSKY, M., MADAIO, M. P. & MCGAHA, T. L. 2015a. The amino acid sensor GCN2 inhibits inflammatory responses to apoptotic cells promoting tolerance and suppressing systemic autoimmunity. *Proc Natl Acad Sci U S A,* 112**,** 10774-9.

RAVISHANKAR, B., LIU, H., SHINDE, R., CHAUDHARY, K., XIAO, W., BRADLEY, J., KORITZINSKY, M., MADAIO, M. P. & MCGAHA, T. L. 2015b. The amino acid sensor GCN2 inhibits inflammatory responses to apoptotic cells promoting tolerance and suppressing systemic autoimmunity. *Proceedings of the National Academy of Sciences,* 112**,** 10774-10779.

REARDON, D. A., DESJARDINS, A., RIXE, O., CLOUGHESY, T., ALEKAR, S., WILLIAMS, J. H., LI, R., TAYLOR, C. T. & LASSMAN, A. B. 2020. A phase 1 study of PF-06840003, an oral indoleamine 2,3-dioxygenase 1 (IDO1) inhibitor in patients with recurrent malignant glioma. *Invest New Drugs,* 38**,** 1784-1795.

RECK, M., RODRÍGUEZ-ABREU, D., ROBINSON, A. G., HUI, R., CSŐSZI, T., FÜLÖP, A., GOTTFRIED, M., PELED, N., TAFRESHI, A., CUFFE, S., O'BRIEN, M., RAO, S., HOTTA, K., LEIBY, M. A., LUBINIECKI, G. M., SHENTU, Y., RANGWALA, R. & BRAHMER, J. R. 2016. Pembrolizumab versus Chemotherapy for PD-L1-Positive Non-Small-Cell Lung Cancer. *N Engl J Med,* 375**,** 1823-1833.

REDONDO, J. M., RIVAS, A. L. & FRESNO, M. 1986. Activation of the Na+/K+-ATPase by interleukin-2. *FEBS Letters,* 206**,** 199-202.

REN, Y., ZHENG, G., YOU, L., WEN, L., LI, C., FU, X. & ZHOU, L. 2017. Structural characterization and macrophage immunomodulatory activity of a polysaccharide isolated from Gracilaria lemaneiformis. *Journal of Functional Foods,* 33**,** 286-296.

RIDGWAY, N. D. 2013. The role of phosphatidylcholine and choline metabolites to cell proliferation and survival. *Crit Rev Biochem Mol Biol,* 48**,** 20-38.

RIGHINI, H., BARALDI, E., GARCÍA FERNÁNDEZ, Y., MARTEL QUINTANA, A. & ROBERTI, R. 2019. Different Antifungal Activity of Anabaena sp., Ecklonia sp., and Jania sp. against Botrytis cinerea. *Mar Drugs,* 17.

RIMOLA, V., HAHNEFELD, L., ZHAO, J., JIANG, C., ANGIONI, C., SCHREIBER, Y., OSTHUES, T., PIERRE, S., GEISSLINGER, G., JI, R. R., SCHOLICH, K. & SISIGNANO, M. 2020. Lysophospholipids Contribute to Oxaliplatin-Induced Acute Peripheral Pain. *J Neurosci,* 40**,** 9519-9532.

RITTMEYER, A., BARLESI, F., WATERKAMP, D., PARK, K., CIARDIELLO, F., VON PAWEL, J., GADGEEL, S. M., HIDA, T., KOWALSKI, D. M., DOLS, M. C., CORTINOVIS, D. L., LEACH, J., POLIKOFF, J., BARRIOS, C., KABBINAVAR, F., FRONTERA, O. A., DE MARINIS, F., TURNA, H., LEE, J. S., BALLINGER, M., KOWANETZ, M., HE, P., CHEN, D. S., SANDLER, A. & GANDARA, D. R. 2017. Atezolizumab versus docetaxel in patients with previously treated non-small-cell lung cancer (OAK): a phase 3, open-label, multicentre randomised controlled trial. *Lancet,* 389**,** 255-265.

ROBERT, C., RIBAS, A., WOLCHOK, J. D., HODI, F. S., HAMID, O., KEFFORD, R., WEBER, J. S., JOSHUA, A. M., HWU, W. J., GANGADHAR, T. C., PATNAIK, A., DRONCA, R., ZAROUR, H., JOSEPH, R. W., BOASBERG, P., CHMIELOWSKI, B., MATEUS, C., POSTOW, M. A., GERGICH, K., ELASSAISS-SCHAAP, J., LI, X. N., IANNONE, R., EBBINGHAUS, S. W., KANG, S. P. & DAUD, A. 2014. Anti-programmed-death-receptor-1 treatment with pembrolizumab in ipilimumab-refractory advanced melanoma: a randomised dose-comparison cohort of a phase 1 trial. *Lancet,* 384**,** 1109-17.

ROBERTS, K. M. & FITZPATRICK, P. F. 2013. Mechanisms of tryptophan and tyrosine hydroxylase. *IUBMB Life,* 65**,** 350-7.

ROBINSON, C. M., HALE, P. T. & CARLIN, J. M. 2005. The role of IFN-gamma and TNF-alpha-responsive regulatory elements in the synergistic induction of indoleamine dioxygenase. *J Interferon Cytokine Res,* 25**,** 20-30.

ROBINSON, C. M., SHIREY, K. A. & CARLIN, J. M. 2003. Synergistic transcriptional activation of indoleamine dioxygenase by IFN-gamma and tumor necrosis factor-alpha. *J Interferon Cytokine Res,* 23**,** 413-21.

ROBINSON, P. K. 2015. Enzymes: principles and biotechnological applications. *Essays Biochem,* 59**,** 1-41.

ROGER, S., ROLLIN, J., BARASCU, A., BESSON, P., RAYNAL, P. I., IOCHMANN, S., LEI, M., BOUGNOUX, P., GRUEL, Y. & LE GUENNEC, J. Y. 2007. Voltage-gated sodium channels potentiate the invasive capacities of human non-small-cell lung cancer cell lines. *Int J Biochem Cell Biol,* 39**,** 774-86.

RONG, G., WENG, W., HUANG, J., CHEN, Y., YU, X., YUAN, R., GU, X., WU, X., CAI, Y., HAN, P., SHAO, M., SUN, H. & GE, N. 2022. Artemether Alleviates Diabetic Kidney Disease by Modulating Amino Acid Metabolism. *Biomed Res Int,* 2022**,** 7339611.

ROSSI, A., PIZZO, P. & FILADI, R. 2019. Calcium, mitochondria and cell metabolism: A functional triangle in bioenergetics. *Biochimica et Biophysica Acta (BBA) - Molecular Cell Research,* 1866**,** 1068-1078.

ROY, A. & TALUKDAR, P. 2021. Recent Advances in Bioactive Artificial Ionophores. *Chembiochem,* 22**,** 2925-2940.

ROYCE, M., OSGOOD, C. L., AMATYA, A. K., FIERO, M. H., CHANG, C. J. G., RICKS, T. K., SHETTY, K. A., KRAFT, J., QIU, J., SONG, P., CHARLAB, R., YU, J., KING, K. E., RASTOGI, A., JANELSINS, B., WEINBERG, W. C., CLOUSE, K., BORDERS-HEMPHILL, V., BROWN, L., GOMEZ-BROUGHTON, C., LI, Z., NGUYEN, T. T., QIU, Z., LY, A. T., CHANG, S., GAO, T., TU, C. M., KING-KALLIMANIS, B., PIERCE, W. F., CHIANG, K., LEE, C., GOLDBERG, K. B., LEIGHTON, J. K., TANG, S., PAZDUR, R., BEAVER, J. A. & AMIRI-KORDESTANI, L. 2022. FDA Approval Summary: Margetuximab plus Chemotherapy for Advanced or Metastatic HER2-Positive Breast Cancer. *Clin Cancer Res,* 28**,** 1487-1492.

RUDD, C. E., TAYLOR, A. & SCHNEIDER, H. 2009. CD28 and CTLA-4 coreceptor expression and signal transduction. *Immunol Rev,* 229**,** 12-26.

RUDDICK, J. P., EVANS, A. K., NUTT, D. J., LIGHTMAN, S. L., ROOK, G. A. & LOWRY, C. A. 2006. Tryptophan metabolism in the central nervous system: medical implications. *Expert Rev Mol Med,* 8**,** 1-27.

RUSHING, B. R., SCHRODER, M. & SUMNER, S. C. J. 2022. Comparison of Lysis and Detachment Sample Preparation Methods for Cultured Triple-Negative Breast Cancer Cells Using UHPLC-HRMS-Based Metabolomics. *Metabolites,* 12.

RUSSO-ABRAHÃO, T., LACERDA-ABREU, M. A., GOMES, T., COSENTINO-GOMES, D., CARVALHO-DE-ARAÚJO, A. D., RODRIGUES, M. F., OLIVEIRA, A. C. L. D., RUMJANEK, F. D., MONTEIRO, R. D. Q. & MEYER-FERNANDES, J. R. 2018. Characterization of inorganic phosphate transport in the triple-negative breast cancer cell line, MDA-MB-231. *PLOS ONE,* 13**,** e0191270.

SAADANE, A., MASTERS, S., DIDONATO, J., LI, J. & BERGER, M. 2007. Parthenolide inhibits IkappaB kinase, NF-kappaB activation, and inflammatory response in cystic fibrosis cells and mice. *Am J Respir Cell Mol Biol,* 36**,** 728-36.

SALIMI ELIZEI, S., POORMASJEDI-MEIBOD, M. S., WANG, X., KHEIRANDISH, M. & GHAHARY, A. 2017. Kynurenic acid downregulates IL-17/1L-23 axis in vitro. *Mol Cell Biochem,* 431**,** 55-65.

SALVADORI, M. L., DA CUNHA BIANCHI, P. K., GEBRIM, L. H., SILVA, R. S. & KFOURY, J. R., JR. 2015. Effect of the association of 1-methyl-DL-tryptophan with paclitaxel on the expression of indoleamine 2,3-dioxygenase in cultured cancer cells from patients with breast cancer. *Med Oncol,* 32**,** 248.

SANDERSON, S. M., XIAO, Z., WISDOM, A. J., BOSE, S., LIBERTI, M. V., REID, M. A., HOCKE, E., GREGORY, S. G., KIRSCH, D. G. & LOCASALE, J. W. 2020. The Na⁺/K⁺ ATPase Regulates Glycolysis and Modifies Immune Metabolism in Tumors. *bioRxiv***,** 2020.03.31.018739.

SANKARANARAYANAN, R., SWAMINATHAN, R., BRENNER, H., CHEN, K., CHIA, K. S., CHEN, J. G., LAW, S. C., AHN, Y. O., XIANG, Y. B., YEOLE, B. B., SHIN, H. R., SHANTA, V., WOO, Z. H., MARTIN, N., SUMITSAWAN, Y., SRIPLUNG, H., BARBOZA, A. O., ESER, S., NENE, B. M., SUWANRUNGRUANG, K., JAYALEKSHMI, P., DIKSHIT, R., WABINGA, H., ESTEBAN, D. B., LAUDICO, A., BHURGRI, Y., BAH, E. & AL-HAMDAN, N. 2010. Cancer survival in Africa, Asia, and Central America: a population-based study. *Lancet Oncol,* 11**,** 165-73.

SAUTER, M., TSHISUAKA, B., FETZNER, S. & LINGENS, F. 1993. Microbial metabolism of quinoline and related compounds. XX. Quinaldic acid 4-oxidoreductase from Pseudomonas sp. AK-2 compared to other procaryotic molybdenum-containing hydroxylases. *Biol Chem Hoppe Seyler,* 374**,** 1037-46.

SAVITZ, J. 2017. Role of Kynurenine Metabolism Pathway Activation in Major Depressive Disorders. *Curr Top Behav Neurosci,* 31**,** 249-267.

SBODIO, J. I., SNYDER, S. H. & PAUL, B. D. 2018. Golgi stress response reprograms cysteine metabolism to confer cytoprotection in Huntington's disease. *Proc Natl Acad Sci U S A,* 115**,** 780-785.

SCALISE, M., GALLUCCIO, M., CONSOLE, L., POCHINI, L. & INDIVERI, C. 2018. The Human SLC7A5 (LAT1): The Intriguing Histidine/Large Neutral Amino Acid Transporter and Its Relevance to Human Health. *Front Chem,* 6**,** 243.

SCHELLENBERG, K. A. & COATNEY, G. R. 1961. The influence of antimalarial drugs on nucleic acid synthesis in Plasmodium gallinaceum and Plasmodium berghei. *Biochem Pharmacol,* 6**,** 143-52.

SCHLAM, I. & SWAIN, S. M. 2021. HER2-positive breast cancer and tyrosine kinase inhibitors: the time is now. *NPJ Breast Cancer,* 7**,** 56.

SCHMID, P., ADAMS, S., RUGO, H. S., SCHNEEWEISS, A., BARRIOS, C. H., IWATA, H., DIÉRAS, V., HEGG, R., IM, S. A., SHAW WRIGHT, G., HENSCHEL, V., MOLINERO, L., CHUI, S. Y., FUNKE, R., HUSAIN, A., WINER, E. P., LOI, S. & EMENS, L. A. 2018. Atezolizumab and Nab-Paclitaxel in Advanced Triple-Negative Breast Cancer. *N Engl J Med,* 379**,** 2108-2121.

SCHMID, P., RUGO, H. S., ADAMS, S., SCHNEEWEISS, A., BARRIOS, C. H., IWATA, H., DIÉRAS, V., HENSCHEL, V., MOLINERO, L., CHUI, S. Y., MAIYA, V., HUSAIN, A., WINER, E. P., LOI, S. & EMENS, L. A. 2020. Atezolizumab plus nab-paclitaxel as first-line treatment for unresectable, locally advanced or metastatic triple-negative breast cancer (IMpassion130): updated efficacy results from a randomised, double-blind, placebo-controlled, phase 3 trial. *Lancet Oncol,* 21**,** 44-59.

SCHMIDT, S. V. & SCHULTZE, J. L. 2014. New Insights into IDO Biology in Bacterial and Viral Infections. *Front Immunol,* 5**,** 384.

SCHMIEDEKNECHT, K., KAUFMANN, A., BAUER, S. & VENEGAS SOLIS, F. 2022. L-lactate as an indicator for cellular metabolic status: An easy and cost-effective colorimetric L-lactate assay. *PLoS One,* 17**,** e0271818.
SCHÖNFELD, W., WEILAND, J., LINDIG, C., MASNYK, M., KABAT, M. M., KUREK, A., WICHA, J. & REPKE, K. R. 1985. The lead structure in cardiac glycosides is 5 beta, 14 beta-androstane-3 beta 14-diol. *Naunyn Schmiedebergs Arch Pharmacol,* 329**,** 414-26.
SCHULTHEISS, O. C. & STANTON, S. J. 2009. Assessment of salivary hormones. *Methods in social neuroscience.* New York, NY, US: Guilford Press.
SCHWARTZBERG, L. S. & KIEDROWSKI, L. A. 2021. Olaparib in hormone receptor-positive, HER2-negative metastatic breast cancer with a somatic BRCA2 mutation. *Ther Adv Med Oncol,* 13**,** 17588359211006962.
SECA, A. M. L. & PINTO, D. 2018. Plant Secondary Metabolites as Anticancer Agents: Successes in Clinical Trials and Therapeutic Application. *Int J Mol Sci,* 19.
SEDLMAYR, P., BLASCHITZ, A. & STOCKER, R. 2014. The role of placental tryptophan catabolism. *Front Immunol,* 5**,** 230.
SEDY, J. R., GAVRIELI, M., POTTER, K. G., HURCHLA, M. A., LINDSLEY, R. C., HILDNER, K., SCHEU, S., PFEFFER, K., WARE, C. F., MURPHY, T. L. & MURPHY, K. M. 2005. B and T lymphocyte attenuator regulates T cell activation through interaction with herpesvirus entry mediator. *Nat Immunol,* 6**,** 90-8.
SEEGERS, N., VAN DOORNMALEN, A. M., UITDEHAAG, J. C., DE MAN, J., BUIJSMAN, R. C. & ZAMAN, G. J. 2014. High-throughput fluorescence-based screening assays for tryptophan-catabolizing enzymes. *J Biomol Screen,* 19**,** 1266-74.
SEIGLER, D. S. 1998. Phenylpropanoids. *In:* SEIGLER, D. S. (ed.) *Plant Secondary Metabolism.* Boston, MA: Springer US.
SELDEN, R. & SMITH, T. W. 1972. Ouabain pharmacokinetics in dog and man. Determination by radioimmunoassay. *Circulation,* 45**,** 1176-82.
SEOL, G.-H., KANG, P., LEE, H. S. & SEOL, G. H. 2016. Antioxidant activity of linalool in patients with carpal tunnel syndrome. *BMC Neurology,* 16**,** 17.
SERTER KOCOGLU, S., SECME, M., OY, C., KORKUSUZ, G. & ELMAS, L. 2023. Monensin, an Antibiotic Isolated from Streptomyces Cinnamonensis, Regulates Human Neuroblastoma Cell Proliferation via the PI3K/AKT Signaling Pathway and Acts Synergistically with Rapamycin. *Antibiotics (Basel),* 12.
SHAJIB, M. S. & KHAN, W. I. 2015. The role of serotonin and its receptors in activation of immune responses and inflammation. *Acta Physiol (Oxf),* 213**,** 561-74.
SHANDELL, M. A., CAPATINA, A. L., LAWRENCE, S. M., BRACKENBURY, W. J. & LAGOS, D. 2022. Inhibition of the Na(+)/K(+)-ATPase by cardiac glycosides suppresses expression of the IDO1 immune checkpoint in cancer cells by reducing STAT1 activation. *J Biol Chem,* 298**,** 101707.
SHAPIRO, L. & DINARELLO, C. A. 1995. Osmotic regulation of cytokine synthesis in vitro. *Proc Natl Acad Sci U S A,* 92**,** 12230-4.
SHARMA, R. 2021. Global, regional, national burden of breast cancer in 185 countries: evidence from GLOBOCAN 2018. *Breast Cancer Research and Treatment,* 187**,** 557-567.
SHARMA, S., YANG, S. C., ZHU, L., RECKAMP, K., GARDNER, B., BARATELLI, F., HUANG, M., BATRA, R. K. & DUBINETT, S. M. 2005. Tumor cyclooxygenase-2/prostaglandin E2-dependent promotion of FOXP3 expression and CD4+ CD25+ T regulatory cell activities in lung cancer. *Cancer Res,* 65**,** 5211-20.
SHARMNI VISHNU, K., WIN, T. T., AYE, S. N. & BASAVARAJ, A. K. 2022. Combined atezolizumab and nab-paclitaxel in the treatment of triple negative breast cancer: a meta-analysis on their efficacy and safety. *BMC Cancer,* 22**,** 1139.

SHAYDA, H., MAHMOOD, J. T., EBRAHIM, T., JAMILEH, G., GOLNAZ ENSIEH, K. S., PARIVASH, D., LEILA, B. Y., MOHAMMAD MEHDI, A. & AMIR HASSAN, Z. 2009. Indoleamine 2,3-dioxygenase (IDO) is expressed at feto-placental unit throughout mouse gestation: An immunohistochemical study. *J Reprod Infertil,* 10**,** 177-83.

SHEN, J.-J., ZHAN, Y.-C., LI, H.-Y. & WANG, Z. 2020a. Ouabain impairs cancer metabolism and activates AMPK-Src signaling pathway in human cancer cell lines. *Acta Pharmacologica Sinica,* 41**,** 110-118.

SHEN, J. J., ZHAN, Y. C., LI, H. Y. & WANG, Z. 2020b. Ouabain impairs cancer metabolism and activates AMPK-Src signaling pathway in human cancer cell lines. *Acta Pharmacol Sin,* 41**,** 110-118.

SHIM, H., DOLDE, C., LEWIS, B. C., WU, C. S., DANG, G., JUNGMANN, R. A., DALLA-FAVERA, R. & DANG, C. V. 1997. c-Myc transactivation of LDH-A: implications for tumor metabolism and growth. *Proc Natl Acad Sci U S A,* 94**,** 6658-63.

SHINDO-OKADA, N., TAKEUCHI, K., HAN, B. S. & NAGAMACHI, Y. 2002. Establishment of cell lines with high and low metastatic potential from A549 human lung adenocarcinoma. *Jpn J Cancer Res,* 93**,** 50-60.

SHULL, M. M., PUGH, D. G. & LINGREL, J. B. 1990. The human Na, K-ATPase alpha 1 gene: characterization of the 5'-flanking region and identification of a restriction fragment length polymorphism. *Genomics,* 6**,** 451-60.

SIEGEL, R. L., MILLER, K. D., WAGLE, N. S. & JEMAL, A. 2023. Cancer statistics, 2023. *CA Cancer J Clin,* 73**,** 17-48.

SILVA-GARCÍA, O., VALDEZ-ALARCÓN, J. J. & BAIZABAL-AGUIRRE, V. M. 2014. The Wnt/β-catenin signaling pathway controls the inflammatory response in infections caused by pathogenic bacteria. *Mediators Inflamm,* 2014**,** 310183.

SILVA, C. I. D., GONÇALVES-DE-ALBUQUERQUE, C. F., MORAES, B. P. T. D., GARCIA, D. G. & BURTH, P. 2021. Na/K-ATPase: Their role in cell adhesion and migration in cancer. *Biochimie,* 185**,** 1-8.

SILVA, N. M., RODRIGUES, C. V., SANTORO, M. M., REIS, L. F., ALVAREZ-LEITE, J. I. & GAZZINELLI, R. T. 2002. Expression of indoleamine 2,3-dioxygenase, tryptophan degradation, and kynurenine formation during in vivo infection with Toxoplasma gondii: induction by endogenous gamma interferon and requirement of interferon regulatory factor 1. *Infect Immun,* 70**,** 859-68.

SILVER, I. A. & ERECIŃSKA, M. 1997. Energetic demands of the Na+/K+ ATPase in mammalian astrocytes. *Glia,* 21**,** 35-45.

SIMAN, F. D., SILVEIRA, E. A., FERNANDES, A. A., STEFANON, I., VASSALLO, D. V. & PADILHA, A. S. 2015. Ouabain induces nitric oxide release by a PI3K/Akt-dependent pathway in isolated aortic rings from rats with heart failure. *J Cardiovasc Pharmacol,* 65**,** 28-38.

SIMEONOV, A. & DAVIS, M. I. 2004. Interference with Fluorescence and Absorbance. *In:* MARKOSSIAN, S., GROSSMAN, A., BRIMACOMBE, K., ARKIN, M., AULD, D., AUSTIN, C., BAELL, J., CHUNG, T. D. Y., COUSSENS, N. P., DAHLIN, J. L., DEVANARAYAN, V., FOLEY, T. L., GLICKSMAN, M., GORSHKOV, K., HAAS, J. V., HALL, M. D., HOARE, S., INGLESE, J., IVERSEN, P. W., KALES, S. C., LAL-NAG, M., LI, Z., MCGEE, J., MCMANUS, O., RISS, T., SARADJIAN, P., SITTAMPALAM, G. S., TARSELLI, M., TRASK, O. J., JR., WANG, Y., WEIDNER, J. R., WILDEY, M. J., WILSON, K., XIA, M. & XU, X. (eds.) *Assay Guidance Manual.* Bethesda (MD): Eli Lilly & Company and the National Center for Advancing Translational Sciences.

SIMEONOV, A., JADHAV, A., SAYED, A. A., WANG, Y., NELSON, M. E., THOMAS, C. J., INGLESE, J., WILLIAMS, D. L. & AUSTIN, C. P. 2008. Quantitative high-throughput screen identifies inhibitors of the Schistosoma mansoni redox cascade. *PLoS Negl Trop Dis,* 2**,** e127.

SIMON, S. & LABARRIERE, N. 2017. PD-1 expression on tumor-specific T cells: Friend or foe for immunotherapy? *Oncoimmunology,* 7**,** e1364828.

SINCLAIR, L. V., NEYENS, D., RAMSAY, G., TAYLOR, P. M. & CANTRELL, D. A. 2018. Single cell analysis of kynurenine and System L amino acid transport in T cells. *Nat Commun,* 9**,** 1981.

SIU, L., GELMON, K., CHU, Q., PACHYNSKI, R., ALESE, O., BASCIANO, P., WALKER, J., MITRA, P., ZHU, L., PHILLIPS, P., HUNT, J. & DESAI, J. 2017. Abstract CT116: BMS-986205, an optimized indoleamine 2,3-dioxygenase 1 (IDO1) inhibitor, is well tolerated with potent pharmacodynamic (PD) activity, alone and in combination with nivolumab (nivo) in advanced cancers in a phase 1/2a trial. *Cancer Research,* 77**,** CT116-CT116.

SJÖSTRÖM, M., STENSTRÖM, K., ENELING, K., ZWILLER, J., KATZ, A. I., TAKEMORI, H. & BERTORELLO, A. M. 2007. SIK1 is part of a cell sodium-sensing network that regulates active sodium transport through a calcium-dependent process. *Proc Natl Acad Sci U S A,* 104**,** 16922-7.

SLAMON, D. J., LEYLAND-JONES, B., SHAK, S., FUCHS, H., PATON, V., BAJAMONDE, A., FLEMING, T., EIERMANN, W., WOLTER, J., PEGRAM, M., BASELGA, J. & NORTON, L. 2001. Use of chemotherapy plus a monoclonal antibody against HER2 for metastatic breast cancer that overexpresses HER2. *N Engl J Med,* 344**,** 783-92.

SMALLRIDGE, R. C., GIST, I. D. & KIANG, J. G. 1992. Na+-H+ antiport and monensin effects on cytosolic pH and iodide transport in FRTL-5 rat thyroid cells. *Am J Physiol,* 262**,** E834-9.

SMITH, C. A., WANT, E. J., O'MAILLE, G., ABAGYAN, R. & SIUZDAK, G. 2006. XCMS: processing mass spectrometry data for metabolite profiling using nonlinear peak alignment, matching, and identification. *Anal Chem,* 78**,** 779-87.

SMITH, T. W. 1985. Pharmacokinetics, bioavailability and serum levels of cardiac glycosides. *J Am Coll Cardiol,* 5**,** 43a-50a.

SOLIMAN, H. H., JACKSON, E., NEUGER, T., DEES, E. C., HARVEY, R. D., HAN, H., ISMAIL-KHAN, R., MINTON, S., VAHANIAN, N. N., LINK, C., SULLIVAN, D. M. & ANTONIA, S. 2014. A first in man phase I trial of the oral immunomodulator, indoximod, combined with docetaxel in patients with metastatic solid tumors. *Oncotarget,* 5**,** 8136-46.

SOLIMAN, H. H., MINTON, S. E., HAN, H. S., ISMAIL-KHAN, R., NEUGER, A., KHAMBATI, F., NOYES, D., LUSH, R., CHIAPPORI, A. A., ROBERTS, J. D., LINK, C., VAHANIAN, N. N., MAUTINO, M., STREICHER, H., SULLIVAN, D. M. & ANTONIA, S. J. 2016. A phase I study of indoximod in patients with advanced malignancies. *Oncotarget,* 7**,** 22928-38.

SOLIMAN, N. A. & YUSSIF, S. M. 2016. Ki-67 as a prognostic marker according to breast cancer molecular subtype. *Cancer Biol Med,* 13**,** 496-504.

SOLTOFF, S. P. & HEDDEN, L. 2008. Regulation of ERK1/2 by ouabain and Na-K-ATPase-dependent energy utilization and AMPK activation in parotid acinar cells. *Am J Physiol Cell Physiol,* 295**,** C590-9.

SONG, I. H., HEO, S. H., BANG, W. S., PARK, H. S., PARK, I. A., KIM, Y. A., PARK, S. Y., ROH, J., GONG, G. & LEE, H. J. 2017a. Predictive Value of Tertiary Lymphoid Structures Assessed by High Endothelial Venule Counts in the Neoadjuvant Setting of Triple-Negative Breast Cancer. *Cancer Res Treat,* 49**,** 399-407.

SONG, M. M. & SHUAI, K. 1998. The suppressor of cytokine signaling (SOCS) 1 and SOCS3 but not SOCS2 proteins inhibit interferon-mediated antiviral and antiproliferative activities. *J Biol Chem,* 273**,** 35056-62.

SONG, P., RAMPRASATH, T., WANG, H. & ZOU, M. H. 2017b. Abnormal kynurenine pathway of tryptophan catabolism in cardiovascular diseases. *Cell Mol Life Sci,* 74**,** 2899-2916.

SØRENSEN, R. B., HADRUP, S. R., SVANE, I. M., HJORTSØ, M. C., THOR STRATEN, P. & ANDERSEN, M. H. 2011. Indoleamine 2,3-dioxygenase specific, cytotoxic T cells as immune regulators. *Blood,* 117**,** 2200-10.

SORRELL, T. C. & FORBES, I. J. 1975. Depression of immune competence by phenytoin and carbamazepine. Studies in vivo and in vitro. *Clin Exp Immunol,* 20**,** 273-85.

SOULTOUKIS, G. A. & PARTRIDGE, L. 2016. Dietary Protein, Metabolism, and Aging. *Annu Rev Biochem,* 85**,** 5-34.

SOUSA, L., GARCIA, I. J., COSTA, T. G., SILVA, L. N., RENÓ, C. O., OLIVEIRA, E. S., TILELLI, C. Q., SANTOS, L. L., CORTES, V. F., SANTOS, H. L. & BARBOSA, L. A. 2015. Effects of Iron Overload on the Activity of Na,K-ATPase and Lipid Profile of the Human Erythrocyte Membrane. *PLoS One,* 10**,** e0132852.

SPARKS, R. L., POOL, T. B., SMITH, N. K. & CAMERON, I. L. 1983. Effects of amiloride on tumor growth and intracellular element content of tumor cells in vivo. *Cancer Res,* 43**,** 73-7.

SPIGSET, O., KLEPP, O., HAUX, J. & TRETLI, S. 2001. Digitoxin medication and cancer; case control and internal dose-response studies. *BMC Cancer,* 1**,** 11.

STANIETSKY, N., SIMIC, H., ARAPOVIC, J., TOPORIK, A., LEVY, O., NOVIK, A., LEVINE, Z., BEIMAN, M., DASSA, L., ACHDOUT, H., STERN-GINOSSAR, N., TSUKERMAN, P., JONJIC, S. & MANDELBOIM, O. 2009. The interaction of TIGIT with PVR and PVRL2 inhibits human NK cell cytotoxicity. *Proc Natl Acad Sci U S A,* 106**,** 17858-63.

STAVRUM, A. K., HEILAND, I., SCHUSTER, S., PUNTERVOLL, P. & ZIEGLER, M. 2013. Model of tryptophan metabolism, readily scalable using tissue-specific gene expression data. *J Biol Chem,* 288**,** 34555-66.

STINGL, J. & CALDAS, C. 2007. Molecular heterogeneity of breast carcinomas and the cancer stem cell hypothesis. *Nat Rev Cancer,* 7**,** 791-9.

STONE, T. W. & WILLIAMS, R. O. 2023. Interactions of IDO and the Kynurenine Pathway with Cell Transduction Systems and Metabolism at the Inflammation–Cancer Interface. *Cancers,* 15**,** 2895.

SUGI, K., MUSCH, M. W., FIELD, M. & CHANG, E. B. 2001. Inhibition of Na+,K+-ATPase by interferon gamma down-regulates intestinal epithelial transport and barrier function. *Gastroenterology,* 120**,** 1393-403.

SUGIMOTO, H., ODA, S., OTSUKI, T., HINO, T., YOSHIDA, T. & SHIRO, Y. 2006. Crystal structure of human indoleamine 2,3-dioxygenase: catalytic mechanism of O2 incorporation by a heme-containing dioxygenase. *Proc Natl Acad Sci U S A,* 103**,** 2611-6.

SUN, G. C., CHEN, H. H., LIANG, W. Z. & JAN, C. R. 2019. Exploration of the effect of the alkaloid colchicine on Ca(2+) handling and its related physiology in human oral cancer cells. *Arch Oral Biol,* 102**,** 179-185.

SUN, S., FEI, X., MAO, Y., WANG, X., GARFIELD, D. H., HUANG, O., WANG, J., YUAN, F., SUN, L., YU, Q., JIN, X., WANG, J. & SHEN, K. 2014. PD-1(+) immune cell infiltration inversely correlates with survival of operable breast cancer patients. *Cancer Immunol Immunother,* 63**,** 395-406.

SUN, X., LI, L., MA, H. G., SUN, P., WANG, Q. L., ZHANG, T. T., SHEN, Y. M., ZHU, W. M. & LI, X. 2017. Bisindolylmaleimide alkaloid BMA-155Cl induces autophagy and apoptosis in human hepatocarcinoma HepG-2 cells through the NF-κB p65 pathway. *Acta Pharmacol Sin,* 38**,** 524-538.

SUN, Z., JIANG, Q., LI, J. & GUO, J. 2020. The potent roles of salt-inducible kinases (SIKs) in metabolic homeostasis and tumorigenesis. *Signal Transduction and Targeted Therapy,* 5**,** 150.

SUNG, H., FERLAY, J., SIEGEL, R. L., LAVERSANNE, M., SOERJOMATARAM, I., JEMAL, A. & BRAY, F. 2021. Global Cancer Statistics 2020: GLOBOCAN Estimates of Incidence

and Mortality Worldwide for 36 Cancers in 185 Countries. *CA Cancer J Clin,* 71**,** 209-249.

SUZUKI, T., MATSUZAKI, T., HAGIWARA, H., AOKI, T., TAJIKA-TAKAHASHI, Y. & TAKATA, K. 2006. Apical localization of sodium-dependent glucose transporter SGLT1 is maintained by cholesterol and microtubules. *Acta Histochem Cytochem,* 39**,** 155-61.

SWAIN, R. J., KEMP, S. J., GOLDSTRAW, P., TETLEY, T. D. & STEVENS, M. M. 2010. Assessment of cell line models of primary human cells by Raman spectral phenotyping. *Biophys J,* 98**,** 1703-11.

SWEADNER, K. J. 1989. Isozymes of the Na+/K+-ATPase. *Biochim Biophys Acta,* 988**,** 185-220.

SZÁSZI, K., SIROKMÁNY, G., DI CIANO-OLIVEIRA, C., ROTSTEIN, O. D. & KAPUS, A. 2005. Depolarization induces Rho-Rho kinase-mediated myosin light chain phosphorylation in kidney tubular cells. *Am J Physiol Cell Physiol,* 289**,** C673-85.

TAHERIAN-FARD, A., SRIHARI, S. & RAGAN, M. A. 2015. Breast cancer classification: linking molecular mechanisms to disease prognosis. *Brief Bioinform,* 16**,** 461-74.

TAKAISHI, M., UCHIDA, K., FUJITA, F. & TOMINAGA, M. 2014. Inhibitory effects of monoterpenes on human TRPA1 and the structural basis of their activity. *J Physiol Sci,* 64**,** 47-57.

TAKI, A. C., BYRNE, J. J., BOAG, P. R., JABBAR, A. & GASSER, R. B. 2021. Practical High-Throughput Method to Screen Compounds for Anthelmintic Activity against Caenorhabditis elegans. *Molecules,* 26.

TAKIKAWA, O., KUROIWA, T., YAMAZAKI, F. & KIDO, R. 1988. Mechanism of interferon-gamma action. Characterization of indoleamine 2,3-dioxygenase in cultured human cells induced by interferon-gamma and evaluation of the enzyme-mediated tryptophan degradation in its anticellular activity. *J Biol Chem,* 263**,** 2041-8.

TALEB, O., MAAMMAR, M., BRUMARU, D., BOURGUIGNON, J. J., SCHMITT, M., KLEIN, C., KEMMEL, V., MAITRE, M. & MENSAH-NYAGAN, A. G. 2012. Xanthurenic acid binds to neuronal G-protein-coupled receptors that secondarily activate cationic channels in the cell line NCB-20. *PLoS One,* 7**,** e48553.

TANG, K., WU, Y. H., SONG, Y. & YU, B. 2021. Indoleamine 2,3-dioxygenase 1 (IDO1) inhibitors in clinical trials for cancer immunotherapy. *J Hematol Oncol,* 14**,** 68.

TAPPER, H. & SUNDLER, R. 1990. Role of lysosomal and cytosolic pH in the regulation of macrophage lysosomal enzyme secretion. *Biochem J,* 272**,** 407-14.

TAUB, M. 2018. Gene Level Regulation of Na,K-ATPase in the Renal Proximal Tubule Is Controlled by Two Independent but Interacting Regulatory Mechanisms Involving Salt Inducible Kinase 1 and CREB-Regulated Transcriptional Coactivators. *Int J Mol Sci,* 19.

TAUB, M. 2019. Salt Inducible Kinase Signaling Networks: Implications for Acute Kidney Injury and Therapeutic Potential. *International Journal of Molecular Sciences,* 20**,** 3219.

TAUB, M., GARIMELLA, S., KIM, D., RAJKHOWA, T. & CUTULI, F. 2015. Renal proximal tubule Na,K-ATPase is controlled by CREB-regulated transcriptional coactivators as well as salt-inducible kinase 1. *Cell Signal,* 27**,** 2568-78.

TAUB, M., SPRINGATE, J. E. & CUTULI, F. 2010. Targeting of renal proximal tubule Na,K-ATPase by salt-inducible kinase. *Biochem Biophys Res Commun,* 393**,** 339-44.

TAURIN, S., DULIN, N. O., PCHEJETSKI, D., GRYGORCZYK, R., TREMBLAY, J., HAMET, P. & ORLOV, S. N. 2002. c-Fos expression in ouabain-treated vascular smooth muscle cells from rat aorta: evidence for an intracellular-sodium-mediated, calcium-independent mechanism. *J Physiol,* 543**,** 835-47.

TAUTENHAHN, R., BÖTTCHER, C. & NEUMANN, S. 2008. Highly sensitive feature detection for high resolution LC/MS. *BMC Bioinformatics,* 9**,** 504.

TEICHMANN, M., KRETSCHY, N., KOPF, S., JARUKAMJORN, K., ATANASOV, A. G., VIOLA, K., GIESSRIGL, B., SAIKO, P., SZEKERES, T., MIKULITS, W., DIRSCH, V. M., HUTTARY, N., KRIEGER, S., JÄGER, W., GRUSCH, M., DOLZNIG, H. & KRUPITZA, G. 2014. Inhibition of tumour spheroid-induced prometastatic intravasation gates in the lymph endothelial cell barrier by carbamazepine: drug testing in a 3D model. *Arch Toxicol,* 88**,** 691-9.

TERNESS, P., BAUER, T., ROESE, L., DUFTER, C., WATZLIK, A., SIMON, H. & OPELZ, G. 2002. Inhibition of Allogeneic T Cell Proliferation by Indoleamine 2,3-Dioxygenase-expressing Dendritic Cells: Mediation of Suppression by Tryptophan Metabolites. *Journal of Experimental Medicine,* 196**,** 447-457.

THAKER, A. I., RAO, M. S., BISHNUPURI, K. S., KERR, T. A., FOSTER, L., MARINSHAW, J. M., NEWBERRY, R. D., STENSON, W. F. & CIORBA, M. A. 2013. IDO1 metabolites activate β-catenin signaling to promote cancer cell proliferation and colon tumorigenesis in mice. *Gastroenterology,* 145**,** 416-25.e1-4.

THÉATE, I., VAN BAREN, N., PILOTTE, L., MOULIN, P., LARRIEU, P., RENAULD, J. C., HERVÉ, C., GUTIERREZ-ROELENS, I., MARBAIX, E., SEMPOUX, C. & VAN DEN EYNDE, B. J. 2015. Extensive profiling of the expression of the indoleamine 2,3-dioxygenase 1 protein in normal and tumoral human tissues. *Cancer Immunol Res,* 3**,** 161-72.

THOMAS, S. R., TERENTIS, A. C., CAI, H., TAKIKAWA, O., LEVINA, A., LAY, P. A., FREEWAN, M. & STOCKER, R. 2007. Post-translational regulation of human indoleamine 2,3-dioxygenase activity by nitric oxide. *J Biol Chem,* 282**,** 23778-87.

THOMPSON, D., EASTON, D. F. & CONSORTIUM, T. B. C. L. 2002. Cancer Incidence in BRCA1 Mutation Carriers. *JNCI: Journal of the National Cancer Institute,* 94**,** 1358-1365.

TIAN, J., CAI, T., YUAN, Z., WANG, H., LIU, L., HAAS, M., MAKSIMOVA, E., HUANG, X. Y. & XIE, Z. J. 2006. Binding of Src to Na+/K+-ATPase forms a functional signaling complex. *Mol Biol Cell,* 17**,** 317-26.

TOLEDO, M. M., DE SOUZA GONÇALVES, B., COLODETTE, N. M., CHAVES, A. L. F., MUNIZ, L. V., DE, A. R. R. I. M., DOS SANTOS, H. B., CORTES, V. F., SOARES, J. M. A., DE LIMA SANTOS, H. & BARBOSA, L. A. 2021. Tumor Tissue Oxidative Stress Changes and Na, K-ATPase Evaluation in Head and Neck Squamous Cell Carcinoma. *J Membr Biol,* 254**,** 475-486.

TOMBLIN, J. K., ARTHUR, S., PRIMERANO, D. A., CHAUDHRY, A. R., FAN, J., DENVIR, J. & SALISBURY, T. B. 2016. Aryl hydrocarbon receptor (AHR) regulation of L-Type Amino Acid Transporter 1 (LAT-1) expression in MCF-7 and MDA-MB-231 breast cancer cells. *Biochem Pharmacol,* 106**,** 94-103.

TOMEK, P., PALMER, B. D., KENDALL, J. D., FLANAGAN, J. U. & CHING, L. M. 2015. Formation of fluorophores from the kynurenine pathway metabolite N-formylkynurenine and cyclic amines involves transamidation and carbon-carbon bond formation at the 2-position of the amine. *Biochim Biophys Acta,* 1850**,** 1772-80.

TORIELLI, L., TIVODAR, S., MONTELLA, R. C., IACONE, R., PADOANI, G., TARSINI, P., RUSSO, O., SARNATARO, D., STRAZZULLO, P., FERRARI, P., BIANCHI, G. & ZURZOLO, C. 2008. alpha-Adducin mutations increase Na/K pump activity in renal cells by affecting constitutive endocytosis: implications for tubular Na reabsorption. *Am J Physiol Renal Physiol,* 295**,** F478-87.

TOY, W., SHEN, Y., WON, H., GREEN, B., SAKR, R. A., WILL, M., LI, Z., GALA, K., FANNING, S., KING, T. A., HUDIS, C., CHEN, D., TARAN, T., HORTOBAGYI, G., GREENE, G., BERGER, M., BASELGA, J. & CHANDARLAPATY, S. 2013. ESR1 ligand-binding domain mutations in hormone-resistant breast cancer. *Nat Genet,* 45**,** 1439-45.

TSUBOKURA, S., SAKAMOTO, Y. & ICHIHARA, K. 1961. The Bacterial Decomposition of Indoleacetic Acid*. *The Journal of Biochemistry,* 49**,** 38-42.

TSUCHIDA, K., HIROSE, H., OZAWA, S., ISHIDA, H., IWATANI, T. & MATSUMOTO, U. 2021. Monensin-Induced Increase in Intracellular Na+ Induces Changes in Na+ and Ca2+ Currents and Regulates Na+-K+ and Na+-Ca2+ Transport in Cardiomyocytes. *Pharmacology,* 106**,** 91-105.

TSUJI, A., IKEDA, Y., YOSHIKAWA, S., TANIGUCHI, K., SAWAMURA, H., MORIKAWA, S., NAKASHIMA, M., ASAI, T. & MATSUDA, S. 2023. The Tryptophan and Kynurenine Pathway Involved in the Development of Immune-Related Diseases. *International Journal of Molecular Sciences,* 24**,** 5742.

TURNER, D. L. 1995. The conformation of the monensin-A-sodium complex in solution determined from self-consistent NOE distance constraints. *J Magn Reson B,* 108**,** 137-42.

ULBRICHT, W. 1998. Effects of veratridine on sodium currents and fluxes. *Rev Physiol Biochem Pharmacol,* 133**,** 1-54.

URBAN, D. J., ZHENG, W., GOKER-ALPAN, O., JADHAV, A., LAMARCA, M. E., INGLESE, J., SIDRANSKY, E. & AUSTIN, C. P. 2008. Optimization and validation of two miniaturized glucocerebrosidase enzyme assays for high throughput screening. *Comb Chem High Throughput Screen,* 11**,** 817-24.

VALK, E., LEUNG, R., KANG, H., KANEKO, K., RUDD, C. E. & SCHNEIDER, H. 2006. T cell receptor-interacting molecule acts as a chaperone to modulate surface expression of the CTLA-4 coreceptor. *Immunity,* 25**,** 807-21.

VAN DER GOOT, A. T., ZHU, W., VÁZQUEZ-MANRIQUE, R. P., SEINSTRA, R. I., DETTMER, K., MICHELS, H., FARINA, F., KRIJNEN, J., MELKI, R., BUIJSMAN, R. C., RUIZ SILVA, M., THIJSSEN, K. L., KEMA, I. P., NERI, C., OEFNER, P. J. & NOLLEN, E. A. 2012. Delaying aging and the aging-associated decline in protein homeostasis by inhibition of tryptophan degradation. *Proc Natl Acad Sci U S A,* 109**,** 14912-7.

VAN DER MERWE, P. A., BODIAN, D. L., DAENKE, S., LINSLEY, P. & DAVIS, S. J. 1997. CD80 (B7-1) binds both CD28 and CTLA-4 with a low affinity and very fast kinetics. *J Exp Med,* 185**,** 393-403.

VAN DER VEEN, J. N., KENNELLY, J. P., WAN, S., VANCE, J. E., VANCE, D. E. & JACOBS, R. L. 2017. The critical role of phosphatidylcholine and phosphatidylethanolamine metabolism in health and disease. *Biochim Biophys Acta Biomembr,* 1859**,** 1558-1572.

VAN HAASTEREN, G., LI, S., MUDA, M., SUSINI, S. & SCHLEGEL, W. 1999. Calcium signalling and gene expression. *J Recept Signal Transduct Res,* 19**,** 481-92.

VANDER HEIDEN, M. G., CANTLEY, L. C. & THOMPSON, C. B. 2009. Understanding the Warburg effect: the metabolic requirements of cell proliferation. *Science,* 324**,** 1029-33.

VANGEEL, L. & VOETS, T. 2019. Transient Receptor Potential Channels and Calcium Signaling. *Cold Spring Harb Perspect Biol,* 11.

VANNEMAN, M. & DRANOFF, G. 2012. Combining immunotherapy and targeted therapies in cancer treatment. *Nat Rev Cancer,* 12**,** 237-51.

VANNESTE, M., HUANG, Q., LI, M., MOOSE, D., ZHAO, L., STAMNES, M. A., SCHULTZ, M., WU, M. & HENRY, M. D. 2019. High content screening identifies monensin as an EMT-selective cytotoxic compound. *Sci Rep,* 9**,** 1200.

VASAN, N., BASELGA, J. & HYMAN, D. M. 2019. A view on drug resistance in cancer. *Nature,* 575**,** 299-309.

VASAS, A. & HOHMANN, J. 2014. Euphorbia diterpenes: isolation, structure, biological activity, and synthesis (2008-2012). *Chem Rev,* 114**,** 8579-612.

VAUPEL, P., BRIEST, S. & HÖCKEL, M. 2002. Hypoxia in breast cancer: pathogenesis, characterization and biological/therapeutic implications. *Wien Med Wochenschr,* 152**,** 334-42.

VELLANKI, P. J., MULKEY, F., JAIGIRDAR, A. A., RODRIGUEZ, L., WANG, Y., XU, Y., ZHAO, H., LIU, J., HOWE, G., WANG, J., CHOO, Q., GOLDING, S. J., MANSELL, V., KORSAH, K., SPILLMAN, D., DE CLARO, R. A., PAZDUR, R., BEAVER, J. A. & SINGH, H. 2021. FDA Approval Summary: Nivolumab with Ipilimumab and Chemotherapy for Metastatic Non-small Cell Lung Cancer, A Collaborative Project Orbis Review. *Clin Cancer Res,* 27**,** 3522-3527.

VENKATESWARAN, N., LAFITA-NAVARRO, M. C., HAO, Y. H., KILGORE, J. A., PEREZ-CASTRO, L., BRAVERMAN, J., BORENSTEIN-AUERBACH, N., KIM, M., LESNER, N. P., MISHRA, P., BRABLETZ, T., SHAY, J. W., DEBERARDINIS, R. J., WILLIAMS, N. S., YILMAZ, O. H. & CONACCI-SORRELL, M. 2019. MYC promotes tryptophan uptake and metabolism by the kynurenine pathway in colon cancer. *Genes Dev,* 33**,** 1236-1251.

VENUSOVA, E., KOLESAROVA, A., HORKY, P. & SLAMA, P. 2021. Physiological and Immune Functions of Punicalagin. *Nutrients,* 13.

VIEIRA-COELHO, M. A., SERRÃO, P., GUIMARÃES, J. T., PESTANA, M. & SOARES-DA-SILVA, P. 2000. Concerted action of dopamine on renal and intestinal Na(+)-K(+)-ATPase in the rat remnant kidney. *Am J Physiol Renal Physiol,* 279**,** F1033-44.

VILA-CARRILES, W. H., KOVACS, G. G., JOVOV, B., ZHOU, Z.-H., PAHWA, A. K., COLBY, G., ESIMAI, O., GILLESPIE, G. Y., MAPSTONE, T. B., MARKERT, J. M., FULLER, C. M., BUBIEN, J. K. & BENOS, D. J. 2006. Surface expression of ASIC2 inhibits the amiloride-sensitive current and migration of glioma cells. *J. Biol. Chem.,* 281**,** 19220-19232.

VILLALOBO, A. & BERCHTOLD, M. W. 2020. The Role of Calmodulin in Tumor Cell Migration, Invasiveness, and Metastasis. *Int J Mol Sci,* 21.

VISVADER, J. E. 2009. Keeping abreast of the mammary epithelial hierarchy and breast tumorigenesis. *Genes & development,* 23**,** 2563-2577.

WAGNER, E. F. & NEBREDA, Á. R. 2009. Signal integration by JNK and p38 MAPK pathways in cancer development. *Nature Reviews Cancer,* 9**,** 537-549.

WALCZAK, K., TURSKI, W. A. & RAJTAR, G. 2014. Kynurenic acid inhibits colon cancer proliferation in vitro: effects on signaling pathways. *Amino Acids,* 46**,** 2393-401.

WALCZAK, K., WNOROWSKI, A., TURSKI, W. A. & PLECH, T. 2020. Kynurenic acid and cancer: facts and controversies. *Cellular and Molecular Life Sciences,* 77**,** 1531-1550.

WAN, M., DING, L., WANG, D., HAN, J. & GAO, P. 2020. Serotonin: A Potent Immune Cell Modulator in Autoimmune Diseases. *Front Immunol,* 11**,** 186.

WANG, G., KAWAKAMI, K. & GICK, G. 2007a. Divergent signaling pathways mediate induction of Na,K-ATPase alpha1 and beta1 subunit gene transcription by low potassium. *Mol Cell Biochem,* 294**,** 73-85.

WANG, G., KAWAKAMI, K. & GICK, G. 2007b. Regulation of Na,K-ATPase alpha1 subunit gene transcription in response to low K(+): role of CRE/ATF- and GC box-binding proteins. *J Cell Physiol,* 213**,** 167-76.

WANG, G. K. & WANG, S. Y. 2003. Veratridine block of rat skeletal muscle Nav1.4 sodium channels in the inner vestibule. *J Physiol,* 548**,** 667-75.

WANG, H., FRANCO, F., TSUI, Y. C., XIE, X., TREFNY, M. P., ZAPPASODI, R., MOHMOOD, S. R., FERNÁNDEZ-GARCÍA, J., TSAI, C. H., SCHULZE, I., PICARD, F., MEYLAN, E., SILVERSTEIN, R., GOLDBERG, I., FENDT, S. M., WOLCHOK, J. D., MERGHOUB, T., JANDUS, C., ZIPPELIUS, A. & HO, P. C. 2020a. CD36-mediated metabolic adaptation supports regulatory T cell survival and function in tumors. *Nat Immunol,* 21**,** 298-308.

WANG, H., LOU, C. & MA, N. 2019a. Forskolin exerts anticancer roles in non-Hodgkin's lymphomas via regulating Axin/β-catenin signaling pathway. *Cancer Manag Res,* 11**,** 1685-1696.

WANG, J., CHEN, Z., XIAO, Z., WENG, Y., YANG, M., YANG, L., TU, Y., ZHOU, H., WU, L., SHUN, F., LI, P., HUANG, G. & ZHAO, S. 2020b. Estrogen induces IDO expression via TGF-β in chorionic villi and decidua during early stages of pregnancy. *Int J Mol Med,* 46**,** 1186-1196.

WANG, J., CUI, L., FENG, L., ZHANG, Z., SONG, J., LIU, D. & JIA, X. 2016. Isoalantolactone inhibits the migration and invasion of human breast cancer MDA-MB-231 cells via suppression of the p38 MAPK/NF-κB signaling pathway. *Oncol Rep,* 36**,** 1269-76.

WANG, K. S., LI, J., WANG, Z., MI, C., MA, J., PIAO, L. X., XU, G. H., LI, X. & JIN, X. 2017. Artemisinin inhibits inflammatory response via regulating NF-κB and MAPK signaling pathways. *Immunopharmacol Immunotoxicol,* 39**,** 28-36.

WANG, N., FENG, Y., ZHU, M., TSANG, C. M., MAN, K., TONG, Y. & TSAO, S. W. 2010a. Berberine induces autophagic cell death and mitochondrial apoptosis in liver cancer cells: the cellular mechanism. *J Cell Biochem,* 111**,** 1426-36.

WANG, Q., LI, S. H., WANG, H., XIAO, Y., SAHIN, O., BRADY, S. W., LI, P., GE, H., JAFFEE, E. M., MULLER, W. J., HORTOBAGYI, G. N. & YU, D. 2012a. Concomitant targeting of tumor cells and induction of T-cell response synergizes to effectively inhibit trastuzumab-resistant breast cancer. *Cancer Res,* 72**,** 4417-28.

WANG, R. Q., GENG, J., SHENG, W. J., LIU, X. J., JIANG, M. & ZHEN, Y. S. 2019b. The ionophore antibiotic gramicidin A inhibits pancreatic cancer stem cells associated with CD47 down-regulation. *Cancer Cell Int,* 19**,** 145.

WANG, S., LI, H., LIU, D., ZHAO, Q., YANG, T., LI, R. & CHEN, X. 2020c. Diterpenoids from the Seeds of Euphorbia lathyris and their in Vitro Anti-HIV Activity. *Chemistry of Natural Compounds,* 56**,** 78-85.

WANG, W., FU, C., LIN, M., LU, Y., LIAN, S., XIE, X., ZHOU, G., LI, W., ZHANG, Y., JIA, L., ZHONG, C. & HUANG, M. 2022a. Fucoxanthin prevents breast cancer metastasis by interrupting circulating tumor cells adhesion and transendothelial migration. *Front Pharmacol,* 13**,** 960375.

WANG, X., HE, M. J., CHEN, X. J., BAI, Y. T. & ZHOU, G. 2022b. Glaucocalyxin A impairs tumor growth via amplification of the ATF4/CHOP/CHAC1 cascade in human oral squamous cell carcinoma. *J Ethnopharmacol,* 290**,** 115100.

WANG, X., WU, X., ZHANG, Z., MA, C., WU, T., TANG, S., ZENG, Z., HUANG, S., GONG, C., YUAN, C., ZHANG, L., FENG, Y., HUANG, B., LIU, W., ZHANG, B., SHEN, Y., LUO, W., WANG, X., LIU, B., LEI, Y., YE, Z., ZHAO, L., CAO, D., YANG, L., CHEN, X., HAYDON, R. C., LUU, H. H., PENG, B., LIU, X. & HE, T. C. 2018. Monensin inhibits cell proliferation and tumor growth of chemo-resistant pancreatic cancer cells by targeting the EGFR signaling pathway. *Sci Rep,* 8**,** 17914.

WANG, X., ZHANG, X., DONG, X. P., SAMIE, M., LI, X., CHENG, X., GOSCHKA, A., SHEN, D., ZHOU, Y., HARLOW, J., ZHU, M. X., CLAPHAM, D. E., REN, D. & XU, H. 2012b. TPC proteins are phosphoinositide- activated sodium-selective ion channels in endosomes and lysosomes. *Cell,* 151**,** 372-83.

WANG, Y., GAO, D., JIN, L., REN, X., OUYANG, Y., ZHOU, Y., HE, X., JIA, L., TIAN, Z., WU, D. & YANG, Z. 2022c. NADPH Selective Depletion Nanomedicine-Mediated Radio-Immunometabolism Regulation for Strengthening Anti-PDL1 Therapy against TNBC. *Adv Sci (Weinh)***,** e2203788.

WANG, Y., LAWSON, M. A., DANTZER, R. & KELLEY, K. W. 2010b. LPS-induced indoleamine 2,3-dioxygenase is regulated in an interferon-gamma-independent manner by a JNK signaling pathway in primary murine microglia. *Brain Behav Immun,* 24**,** 201-9.

WANG, Y., LONARD, D. M., YU, Y., CHOW, D.-C., PALZKILL, T. G., WANG, J., QI, R., MATZUK, A. J., SONG, X., MADOUX, F., HODDER, P., CHASE, P., GRIFFIN, P. R., ZHOU, S., LIAO, L., XU, J. & O'MALLEY, B. W. 2014. Bufalin is a potent small-molecule inhibitor of the steroid receptor coactivators SRC-3 and SRC-1. *Cancer research,* 74**,** 1506-1517.

WANG, Y., QIU, Q., SHEN, J. J., LI, D. D., JIANG, X. J., SI, S. Y., SHAO, R. G. & WANG, Z. 2012c. Cardiac glycosides induce autophagy in human non-small cell lung cancer cells through regulation of dual signaling pathways. *Int J Biochem Cell Biol,* 44**,** 1813-24.

WANG, Y., ZHANG, H., LIU, C., WANG, Z., WU, W., ZHANG, N., ZHANG, L., HU, J., LUO, P., ZHANG, J., LIU, Z., PENG, Y., LIU, Z., TANG, L. & CHENG, Q. 2022d. Immune checkpoint modulators in cancer immunotherapy: recent advances and emerging concepts. *J Hematol Oncol,* 15**,** 111.

WARBURG, O. 1956. On the origin of cancer cells. *Science,* 123**,** 309-14.

WARBURG, O., GAWEHN, K. & GEISSLER, A. W. 1958. [Metabolism of leukocytes]. *Z Naturforsch B,* 13b**,** 515-6.

WEBB, B. A., CHIMENTI, M., JACOBSON, M. P. & BARBER, D. L. 2011. Dysregulated pH: a perfect storm for cancer progression. *Nat Rev Cancer,* 11**,** 671-7.

WEBER, J. S., D'ANGELO, S. P., MINOR, D., HODI, F. S., GUTZMER, R., NEYNS, B., HOELLER, C., KHUSHALANI, N. I., MILLER, W. H., JR., LAO, C. D., LINETTE, G. P., THOMAS, L., LORIGAN, P., GROSSMANN, K. F., HASSEL, J. C., MAIO, M., SZNOL, M., ASCIERTO, P. A., MOHR, P., CHMIELOWSKI, B., BRYCE, A., SVANE, I. M., GROB, J. J., KRACKHARDT, A. M., HORAK, C., LAMBERT, A., YANG, A. S. & LARKIN, J. 2015. Nivolumab versus chemotherapy in patients with advanced melanoma who progressed after anti-CTLA-4 treatment (CheckMate 037): a randomised, controlled, open-label, phase 3 trial. *Lancet Oncol,* 16**,** 375-84.

WEI, L., ZHU, S., LI, M., LI, F., WEI, F., LIU, J. & REN, X. 2018. High Indoleamine 2,3-Dioxygenase Is Correlated With Microvessel Density and Worse Prognosis in Breast Cancer. *Frontiers in Immunology,* 9.

WEISS, J. N., QU, Z. & SHIVKUMAR, K. 2017. Electrophysiology of Hypokalemia and Hyperkalemia. *Circ Arrhythm Electrophysiol,* 10.

WEN, H., LIU, Y., WANG, S., WANG, T., ZHANG, G., CHEN, X., LI, Y., CUI, H., LAI, F. & SHENG, L. 2019. Design and Synthesis of Indoleamine 2,3-Dioxygenase 1 Inhibitors and Evaluation of Their Use as Anti-Tumor Agents. *Molecules,* 24.

WENG, T., QIU, X., WANG, J., LI, Z. & BIAN, J. 2018. Recent discovery of indoleamine-2,3-dioxygenase 1 inhibitors targeting cancer immunotherapy. *Eur J Med Chem,* 143**,** 656-669.

WHAN HAN, J., GON LEE, B., KEE KIM, Y., WOO YOON, J., KYOUNG JIN, H., HONG, S., YOUNG LEE, H., RO LEE, K. & WOO LEE, H. 2001. Ergolide, sesquiterpene lactone from Inula britannica, inhibits inducible nitric oxide synthase and cyclo-oxygenase-2 expression in RAW 264.7 macrophages through the inactivation of NF-kappaB. *Br J Pharmacol,* 133**,** 503-12.

WHERRY, E. J. 2011. T cell exhaustion. *Nat Immunol,* 12**,** 492-9.

WHITE, N. J., VAN VUGT, M. & EZZET, F. 1999. Clinical pharmacokinetics and pharmacodynamics and pharmacodynamics of artemether-lumefantrine. *Clin Pharmacokinet,* 37**,** 105-25.

WIDNER, B., LAICH, A., SPERNER-UNTERWEGER, B., LEDOCHOWSKI, M. & FUCHS, D. 2002. Neopterin production, tryptophan degradation, and mental depression--what is the link? *Brain Behav Immun,* 16**,** 590-5.

WILHOIT, T., PATRICK, J. M. & MAY, M. B. 2020. Alpelisib: A Novel Therapy for Patients With PIK3CA-Mutated Metastatic Breast Cancer. *J Adv Pract Oncol,* 11**,** 768-775.

WILLIAMS, R. O. 2013. Exploitation of the IDO Pathway in the Therapy of Rheumatoid Arthritis. *Int J Tryptophan Res,* 6**,** 67-73.

WILSCHEFSKI, S. C. & BAXTER, M. R. 2019. Inductively Coupled Plasma Mass Spectrometry: Introduction to Analytical Aspects. *Clin Biochem Rev,* 40**,** 115-133.

WILSON, T. R., FRIDLYAND, J., YAN, Y., PENUEL, E., BURTON, L., CHAN, E., PENG, J., LIN, E., WANG, Y., SOSMAN, J., RIBAS, A., LI, J., MOFFAT, J., SUTHERLIN, D. P., KOEPPEN, H., MERCHANT, M., NEVE, R. & SETTLEMAN, J. 2012. Widespread potential for growth-factor-driven resistance to anticancer kinase inhibitors. *Nature,* 487**,** 505-9.

WINER, E. P., LIPATOV, O., IM, S. A., GONCALVES, A., MUÑOZ-COUSELO, E., LEE, K. S., SCHMID, P., TAMURA, K., TESTA, L., WITZEL, I., OHTANI, S., TURNER, N., ZAMBELLI, S., HARBECK, N., ANDRE, F., DENT, R., ZHOU, X., KARANTZA, V., MEJIA, J. & CORTES, J. 2021. Pembrolizumab versus investigator-choice chemotherapy for metastatic triple-negative breast cancer (KEYNOTE-119): a randomised, open-label, phase 3 trial. *Lancet Oncol,* 22**,** 499-511.

WINNICKA, K., BIELAWSKI, K., BIELAWSKA, A. & MILTYK, W. 2007. Apoptosis-mediated cytotoxicity of ouabain, digoxin and proscillaridin A in the estrogen independent MDA-MB-231 breast cancer cells. *Archives of Pharmacal Research,* 30**,** 1216-1224.

WIRTHGEN, E., HOEFLICH, A., REBL, A. & GÜNTHER, J. 2017. Kynurenic Acid: The Janus-Faced Role of an Immunomodulatory Tryptophan Metabolite and Its Link to Pathological Conditions. *Front Immunol,* 8**,** 1957.

WISE, W. C. & ARCHDEACON, J. W. 1969. Accumulation of iron in the rabbit erythroid cell as affected by ouabain, sodium and potassium ions, and temperature. *J Gen Physiol,* 53**,** 487-97.

WISHART, D. S., TZUR, D., KNOX, C., EISNER, R., GUO, A. C., YOUNG, N., CHENG, D., JEWELL, K., ARNDT, D., SAWHNEY, S., FUNG, C., NIKOLAI, L., LEWIS, M., COUTOULY, M. A., FORSYTHE, I., TANG, P., SHRIVASTAVA, S., JERONCIC, K., STOTHARD, P., AMEGBEY, G., BLOCK, D., HAU, D. D., WAGNER, J., MINIACI, J., CLEMENTS, M., GEBREMEDHIN, M., GUO, N., ZHANG, Y., DUGGAN, G. E., MACINNIS, G. D., WELJIE, A. M., DOWLATABADI, R., BAMFORTH, F., CLIVE, D., GREINER, R., LI, L., MARRIE, T., SYKES, B. D., VOGEL, H. J. & QUERENGESSER, L. 2007. HMDB: the Human Metabolome Database. *Nucleic Acids Res,* 35**,** D521-6.

WOLFF, A. C., LAZAR, A. A., BONDARENKO, I., GARIN, A. M., BRINCAT, S., CHOW, L., SUN, Y., NESKOVIC-KONSTANTINOVIC, Z., GUIMARAES, R. C., FUMOLEAU, P., CHAN, A., HACHEMI, S., STRAHS, A., CINCOTTA, M., BERKENBLIT, A., KRYGOWSKI, M., KANG, L. L., MOORE, L. & HAYES, D. F. 2013. Randomized phase III placebo-controlled trial of letrozole plus oral temsirolimus as first-line endocrine therapy in postmenopausal women with locally advanced or metastatic breast cancer. *J Clin Oncol,* 31**,** 195-202.

WRIGHT, E. M., HIRSCH, J. R., LOO, D. D. & ZAMPIGHI, G. A. 1997. Regulation of Na+/glucose cotransporters. *J Exp Biol,* 200**,** 287-93.

WU, C. M., YANG, C. W., LEE, Y. Z., CHUANG, T. H., WU, P. L., CHAO, Y. S. & LEE, S. J. 2009. Tylophorine arrests carcinoma cells at G1 phase by downregulating cyclin A2 expression. *Biochem Biophys Res Commun,* 386**,** 140-5.

WU, J., AKKURATOV, E. E., BAI, Y., GASKILL, C. M., ASKARI, A. & LIU, L. 2013a. Cell signaling associated with Na(+)/K(+)-ATPase: activation of phosphatidylinositide 3-kinase IA/Akt by ouabain is independent of Src. *Biochemistry,* 52**,** 9059-67.

WU, J., AKKURATOV, E. E., BAI, Y., GASKILL, C. M., ASKARI, A. & LIU, L. 2013b. Cell signaling associated with Na(+)/K(+)-ATPase: activation of phosphatidylinositide 3-kinase IA/Akt by ouabain is independent of Src. *Biochemistry,* 52**,** 9059-9067.

WU, J., LI, D., DU, L., BALDAWI, M., GABLE, M. E., ASKARI, A. & LIU, L. 2015. Ouabain prevents pathological cardiac hypertrophy and heart failure through activation of phosphoinositide 3-kinase α in mouse. *Cell Biosci,* 5**,** 64.

WU, X., GU, Z., CHEN, Y., CHEN, B., CHEN, W., WENG, L. & LIU, X. 2019. Application of PD-1 Blockade in Cancer Immunotherapy. *Comput Struct Biotechnol J,* 17**,** 661-674.
WU, Y., SHEN, D., CHEN, Z., CLAYTON, S. & VADGAMA, J. V. 2007. Taxol induced apoptosis regulates amino acid transport in breast cancer cells. *Apoptosis,* 12**,** 593-612.
XIAO, L. D., LUO, X. B., PI, L. G. & TANG, A. G. 2008. Simultaneous determination of kynurenine and kynurenic acid concentrations in human serum by HPLC with dual wavelengths fluorescence detection. *Clin Chim Acta,* 395**,** 178-80.
XIAO, X., CAO, W., JIANG, X., ZHANG, W., ZHANG, Y., LIU, B., CHENG, J., HUANG, H., HUO, J. & ZHANG, X. 2013. Glaucocalyxin A, a negative Akt regulator, specifically induces apoptosis in human brain glioblastoma U87MG cells. *Acta Biochim Biophys Sin (Shanghai),* 45**,** 946-52.
XIE, B., WATERS, M. J. & SCHIRRA, H. J. 2012. Investigating potential mechanisms of obesity by metabolomics. *J Biomed Biotechnol,* 2012**,** 805683.
XIE, Z. & ASKARI, A. 2002. Na + /K + -ATPase as a signal transducer. Oxford, UK.
XIN, L., LIU, C., LIU, Y., MANSEL, R. E., RUGE, F., DAVIES, E., JIANG, W. G. & MARTIN, T. A. 2021. SIKs suppress tumor function and regulate drug resistance in breast cancer. *Am J Cancer Res,* 11**,** 3537-3557.
XIN, W. K. 2005. A Functional Interaction of Sodium and Calcium in the Regulation of NMDA Receptor Activity by Remote NMDA Receptors. *Journal of Neuroscience,* 25**,** 139-148.
XU, F., LIU, J., LIU, D., LIU, B., WANG, M., HU, Z., DU, X., TANG, L. & HE, F. 2014. LSECtin expressed on melanoma cells promotes tumor progression by inhibiting antitumor T-cell responses. *Cancer Res,* 74**,** 3418-28.
XU, G., LIANG, Q., GONG, Z., YU, W., HE, S. & XI, L. 2006. Antitumor activities of the four sesquiterpene lactones from Elephantopus scaber L. *Exp Oncol,* 28**,** 106-9.
XU, J., CAO, K., LIU, X., ZHAO, L., FENG, Z. & LIU, J. 2021. Punicalagin Regulates Signaling Pathways in Inflammation-Associated Chronic Diseases. *Antioxidants (Basel),* 11.
XU, Q., LI, M., YANG, M., YANG, J., XIE, J., LU, X., WANG, F. & CHEN, W. 2018a. α-pinene regulates miR-221 and induces G(2)/M phase cell cycle arrest in human hepatocellular carcinoma cells. *Biosci Rep,* 38.
XU, W., HIẾU, T., MALARKANNAN, S. & WANG, L. 2018b. The structure, expression, and multifaceted role of immune-checkpoint protein VISTA as a critical regulator of anti-tumor immunity, autoimmunity, and inflammation. *Cell Mol Immunol,* 15**,** 438-446.
XU, X., HOU, B., FULZELE, A., MASUBUCHI, T., ZHAO, Y., WU, Z., HU, Y., JIANG, Y., MA, Y., WANG, H., BENNETT, E. J., FU, G. & HUI, E. 2020. PD-1 and BTLA regulate T cell signaling differentially and only partially through SHP1 and SHP2. *J Cell Biol,* 219.
XU, Y., WANG, W., WANG, M., LIU, X., LEE, M.-H., WANG, M., ZHANG, H., LI, H. & CHEN, W. 2018c. High Salt Intake Attenuates Breast Cancer Metastasis to Lung. *Journal of Agricultural and Food Chemistry,* 66**,** 3386-3392.
YANG, B., ZHAO, Y., LOU, C. & ZHAO, H. 2016a. Eupalinolide O, a novel sesquiterpene lactone from Eupatorium lindleyanum DC., induces cell cycle arrest and apoptosis in human MDA-MB-468 breast cancer cells. *Oncol Rep,* 36**,** 2807-2813.
YANG, I. H., WONG, J. H., CHANG, C. M., CHEN, B. K., TSAI, Y. T., CHEN, W. C., WANG, E. T., HSU, W. L. & CHANG, W. C. 2015a. Involvement of intracellular calcium mobilization in IL-8 activation in human retinal pigment epithelial cells. *Invest Ophthalmol Vis Sci,* 56**,** 761-9.
YANG, M. & BRACKENBURY, W. J. 2013. Membrane potential and cancer progression. *Front Physiol,* 4**,** 185.
YANG, M., KOZMINSKI, D. J., WOLD, L. A., MODAK, R., CALHOUN, J. D., ISOM, L. L. & BRACKENBURY, W. J. 2012. Therapeutic potential for phenytoin: targeting Na(v)1.5

sodium channels to reduce migration and invasion in metastatic breast cancer. *Breast Cancer Res Treat,* 134**,** 603-15.

YANG, S., SUN, J., LU, H., MA, H. & ZHANG, Y. 2015b. Bioactivity-guided isolation of anticancer compounds from Euphorbia lathyris. *Analytical Methods,* 7**,** 9568-9576.

YANG, S. L., TAN, H. X., NIU, T. T., LIU, Y. K., GU, C. J., LI, D. J., LI, M. Q. & WANG, H. Y. 2021. The IFN-γ-IDO1-kynureine pathway-induced autophagy in cervical cancer cell promotes phagocytosis of macrophage. *Int J Biol Sci,* 17**,** 339-352.

YANG, T.-H., HSU, P.-Y., MENG, M. & SU, C.-C. 2015c. Supplement of 5-hydroxytryptophan before induction suppresses inflammation and collagen-induced arthritis. *Arthritis Research & Therapy,* 17**,** 364.

YANG, W., BAI, Y., XIONG, Y., ZHANG, J., CHEN, S., ZHENG, X., MENG, X., LI, L., WANG, J., XU, C., YAN, C., WANG, L., CHANG, C. C., CHANG, T. Y., ZHANG, T., ZHOU, P., SONG, B. L., LIU, W., SUN, S. C., LIU, X., LI, B. L. & XU, C. 2016b. Potentiating the antitumour response of CD8(+) T cells by modulating cholesterol metabolism. *Nature,* 531**,** 651-5.

YANG, X., LONG, F., JIA, W., ZHANG, M., SU, G., LIAO, M., ZENG, Z., CHEN, W. & CHEN, J. 2023. Artesunate inhibits PDE4 leading to intracellular cAMP accumulation, reduced ERK/MAPK signaling, and blockade of influenza A virus vRNP nuclear export. *Antiviral Research,* 215**,** 105635.

YAO, W., QIU, H. M., CHEONG, K. L. & ZHONG, S. 2022. Advances in anti-cancer effects and underlying mechanisms of marine algae polysaccharides. *Int J Biol Macromol,* 221**,** 472-485.

YARDLEY, D. A., MCCLEOD, M., SCHREIBER, F., MURPHY, P., PATTON, J., THOMPSON, D. S., SHASTRY, M., RUBIN, M., MELNIK, M., BURRIS, H. A. & HAINSWORTH, J. D. 2010. A phase II trial of vinflunine as monotherapy or in combination with trastuzumab as first-line treatment of metastatic breast cancer. *Cancer Invest,* 28**,** 925-31.

YE, Z., YUE, L., SHI, J., SHAO, M. & WU, T. 2019. Role of IDO and TDO in Cancers and Related Diseases and the Therapeutic Implications. *J Cancer,* 10**,** 2771-2782.

YILDIRIM, S., ALTUN, S., GUMUSHAN, H., PATEL, A. & DJAMGOZ, M. B. A. 2012. Voltage-gated sodium channel activity promotes prostate cancer metastasis in vivo. *Cancer Lett,* 323**,** 58-61.

YODKEEREE, S., OOPPACHAI, C., POMPIMON, W. & LIMTRAKUL DEJKRIENGKRAIKUL, P. 2018. O-Methylbulbocapnine and Dicentrine Suppress LPS-Induced Inflammatory Response by Blocking NF-κB and AP-1 Activation through Inhibiting MAPKs and Akt Signaling in RAW264.7 Macrophages. *Biol Pharm Bull,* 41**,** 1219-1227.

YOUNG, M. L., SU, M. J., WU, M. H. & CHEN, C. C. 1994. The electrophysiological effects of dicentrine on the conduction system of rabbit heart. *Br J Pharmacol,* 113**,** 69-76.

YU, X., HARDEN, K., GONZALEZ, L. C., FRANCESCO, M., CHIANG, E., IRVING, B., TOM, I., IVELJA, S., REFINO, C. J., CLARK, H., EATON, D. & GROGAN, J. L. 2009. The surface protein TIGIT suppresses T cell activation by promoting the generation of mature immunoregulatory dendritic cells. *Nat Immunol,* 10**,** 48-57.

YU, X. M., GROVEMAN, B. R., FANG, X. Q. & LIN, S. X. 2010. THE ROLE OF INTRACELLULAR SODIUM (Na) IN THE REGULATION OF CALCIUM (Ca)-MEDIATED SIGNALING AND TOXICITY. *Health (Irvine Calif),* 2**,** 8-15.

YU, Y., CHEN, C., HUO, G., DENG, J., ZHAO, H., XU, R., JIANG, L., CHEN, S. & WANG, S. 2019. ATP1A1 Integrates AKT and ERK Signaling via Potential Interaction With Src to Promote Growth and Survival in Glioma Stem Cells. *Frontiers in Oncology,* 9**,** 320.

ZAHAVI, D. & WEINER, L. 2020. Monoclonal Antibodies in Cancer Therapy. *Antibodies (Basel),* 9.

ZAHRAN, A. M., EL-BADAWY, O., KAMEL, L. M., RAYAN, A., REZK, K. & ABDEL-RAHIM, M. H. 2021. Accumulation of Regulatory T Cells in Triple Negative Breast Cancer Can Boost Immune Disruption. *Cancer Manag Res,* 13**,** 6019-6029.

ZAPPASODI, R., MERGHOUB, T. & WOLCHOK, J. D. 2018. Emerging Concepts for Immune Checkpoint Blockade-Based Combination Therapies. *Cancer Cell,* 33**,** 581-598.

ZHAI, L., SPRANGER, S., BINDER, D. C., GRITSINA, G., LAUING, K. L., GILES, F. J. & WAINWRIGHT, D. A. 2015. Molecular Pathways: Targeting IDO1 and Other Tryptophan Dioxygenases for Cancer Immunotherapy. *Clin Cancer Res,* 21**,** 5427-33.

ZHANG, D., DENG, T., YUAN, W., CHEN, T. & JIANG, S. 2022a. Glaucocalyxin A induces apoptosis of non-small cell lung carcinoma cells by inhibiting the PI3K/Akt/GSK3β pathway. *Clin Exp Pharmacol Physiol,* 49**,** 797-804.

ZHANG, D., ZHANG, P., YANG, P., HE, Y., WANG, X., YANG, Y., ZHU, H., XU, N. & LIANG, S. 2017a. Downregulation of ATP1A1 promotes cancer development in renal cell carcinoma. *Clin Proteomics,* 14**,** 15.

ZHANG, H., QIAN, D. Z., TAN, Y. S., LEE, K., GAO, P., REN, Y. R., REY, S., HAMMERS, H., CHANG, D., PILI, R., DANG, C. V., LIU, J. O. & SEMENZA, G. L. 2008. Digoxin and other cardiac glycosides inhibit HIF-1 synthesis and block tumor growth. *Proceedings of the National Academy of Sciences,* 105**,** 19579-19586.

ZHANG, H., RYU, D., WU, Y., GARIANI, K., WANG, X., LUAN, P., D'AMICO, D., ROPELLE, E. R., LUTOLF, M. P., AEBERSOLD, R., SCHOONJANS, K., MENZIES, K. J. & AUWERX, J. 2016. NAD^+ repletion improves mitochondrial and stem cell function and enhances life span in mice. *Science,* 352**,** 1436-43.

ZHANG, Q., ZHU, S., CHENG, X., LU, C., TAO, W., ZHANG, Y., WILLIAM, B. C., CAO, X., YI, S., LIU, Y., ZHAO, Y. & LUO, Y. 2018a. Euphorbia factor L2 alleviates lipopolysaccharide-induced acute lung injury and inflammation in mice through the suppression of NF-κB activation. *Biochem Pharmacol,* 155**,** 444-454.

ZHANG, Y., DONG, Y., MELKUS, M. W., YIN, S., TANG, S. N., JIANG, P., PRAMANIK, K., WU, W., KIM, S., YE, M., HU, H., LU, J. & JIANG, C. 2018b. Role of P53-Senescence Induction in Suppression of LNCaP Prostate Cancer Growth by Cardiotonic Compound Bufalin. *Mol Cancer Ther,* 17**,** 2341-2352.

ZHANG, Y., KURUPATI, R., LIU, L., ZHOU, X. Y., ZHANG, G., HUDAIHED, A., FILISIO, F., GILES-DAVIS, W., XU, X., KARAKOUSIS, G. C., SCHUCHTER, L. M., XU, W., AMARAVADI, R., XIAO, M., SADEK, N., KREPLER, C., HERLYN, M., FREEMAN, G. J., RABINOWITZ, J. D. & ERTL, H. C. J. 2017b. Enhancing CD8(+) T Cell Fatty Acid Catabolism within a Metabolically Challenging Tumor Microenvironment Increases the Efficacy of Melanoma Immunotherapy. *Cancer Cell,* 32**,** 377-391.e9.

ZHANG, Z., ZHANG, K., ZHANG, M., ZHANG, X. & ZHANG, R. 2022b. Parthenolide Suppresses T Helper 17 and Alleviates Experimental Autoimmune Encephalomyelitis. *Front Immunol,* 13**,** 856694.

ZHAO, Y., FU, L., CHEN, J., ZHOU, J., TIAN, C., ZHOU, D. & ZHU, R. 2022. Eupalinolide O Induces Apoptosis in Human Triple-Negative Breast Cancer Cells via Modulating ROS Generation and Akt/p38 MAPK Signaling Pathway. *J Oncol,* 2022**,** 8802453.

ZHELJAZKOV, V. D., GAWDE, A., CANTRELL, C. L., ASTATKIE, T. & SCHLEGEL, V. 2015. Distillation Time as Tool for Improved Antimalarial Activity and Differential Oil Composition of Cumin Seed Oil. *PLoS One,* 10**,** e0144120.

ZHENG, J. 2013. Molecular mechanism of TRP channels. *Compr Physiol,* 3**,** 221-42.

ZHOU, Y., WONG, C. O., CHO, K. J., VAN DER HOEVEN, D., LIANG, H., THAKUR, D. P., LUO, J., BABIC, M., ZINSMAIER, K. E., ZHU, M. X., HU, H., VENKATACHALAM, K. & HANCOCK, J. F. 2015. SIGNAL TRANSDUCTION. Membrane potential modulates plasma membrane phospholipid dynamics and K-Ras signaling. *Science,* 349**,** 873-6.

ZHU, J., SUN, Y., LU, Y., JIANG, X., MA, B., YU, L., ZHANG, J., DONG, X. & ZHANG, Q. 2018. Glaucocalyxin A exerts anticancer effect on osteosarcoma by inhibiting GLI1 nuclear translocation via regulating PI3K/Akt pathway. *Cell Death Dis,* 9**,** 708.

ZHU, W. H., LU, C. Z., HUANG, Y. M., LINK, H. & XIAO, B. G. 2007. A putative mechanism on remission of multiple sclerosis during pregnancy: estrogen-induced indoleamine 2,3-dioxygenase by dendritic cells. *Mult Scler,* 13**,** 33-40.

ZONG, S., LI, C., LUO, C., ZHAO, X., LIU, C., WANG, K., JIA, W., BAI, M., YIN, M., BAO, S., GUO, J., KANG, J., DUAN, T. & ZHOU, Q. 2016. Dysregulated expression of IDO may cause unexplained recurrent spontaneous abortion through suppression of trophoblast cell proliferation and migration. *Sci Rep,* 6**,** 19916.

ZOU, L., BAO, W., GAO, Y., CHEN, M., WU, Y., WANG, S., LI, C., ZHANG, J., ZHANG, D., WANG, Q. & ZHU, A. 2022. Integrated Analysis of Transcriptome and microRNA Profile Reveals the Toxicity of Euphorbia Factors toward Human Colon Adenocarcinoma Cell Line Caco-2. *Molecules,* 27.